Etude de l'hépatolyse induite par les cellules immunitaires dans des modèles murins d'hépatites : rôles des protéines RIPK1 et PARP1/2

Aveline Filliol

ANNÉE 2016

THÈSE / UNIVERSITÉ DE RENNES 1
sous le sceau de l'Université Bretagne Loire

pour le grade de

DOCTEUR DE L'UNIVERSITÉ DE RENNES 1

Mention : Biologie et Sciences de la santé

Ecole doctorale Vie Agro Santé

présentée par

Aveline Filliol

Préparée à l'unité de recherche Inserm U.1085 IRSET
Institut de Recherche en Santé Environnement et Travail
UFR Sciences de la Vie et de l'Environnement

Etude de l'hépatolyse induite par les cellules immunitaires dans des modèles murins d'hépatites : rôles des protéines RIPK1 et PARP1/2

Thèse soutenue à Rennes le 16 novembre 2016

devant le jury composé de :

Catherine BRENNER JAN
DR, Université de Paris Sud
Rapporteur

Violaine MOREAU
DR, Université de Bordeaux
Rapporteur

Laurent CORCOS
DR, Université de Bretagne Occidentale
Examinateur

Luc PAILLARD
Pr, Université de Rennes1
Examinateur

Lucie LAMONTAGNE
Pr, Université de Québec à Montréal
Co-directrice de thèse

Michel SAMSON
DR, Université de Rennes1
Co-directeur de thèse

Ce travail n'aurait jamais pu être réalisé sans toutes les personnes qui m'ont entourée et soutenue, au cours de ces trois années, je souhaite tous vous remercier profondément.

Je souhaite tout d'abord remercier la région Bretagne ainsi que l'IRSET qui par leurs financements ont permis la réalisation de ce travail.

Je tiens à remercier le Pr Luc Paillard d'avoir accepté de présider ce jury de thèse.

Je tiens à remercier le Dr Catherine Brenner Jan ainsi que le Dr Violaine Moreau d'avoir accepté de lire et de juger de mon travail en tant que rapporteur.

Je tiens à remercier le Dr Laurent Corcos d'avoir accepté de siéger à ce jury de soutenance de thèse en tant qu'examinateur.

Je tiens à remercier le Dr Dominique Lagadic-Gossman pour m'avoir accueillie au sein de l'IRSET et permise de réaliser ma thèse au sein de l'institut.

Je souhaite remercier nos différents collaborateurs le Pr Peter Vandenabeele et le Pr Mathieu Bertrand, ainsi que leur équipe pour nous avoir permis de travailler sur les souris *Ripk1*$^{LPC\text{-}KO}$, merci également pour votre aide et votre accueil lors de nos différents séjours à Gand.

Je souhaite également remercier le Dr Françoise Dantzer pour nous avoir fourni les souris *Parp1*$^{-/-}$ et *Parp2*$^{-/-}$.

Je tiens à remercier le Dr Michel Samson pour m'avoir accueillie dans son équipe et permis de réaliser ma thèse dans de très bonnes conditions. Michel, je tiens à t'exprimer toute ma reconnaissance pour toutes les choses que tu m'as apportées au cours de ces trois années. Merci de m'avoir dès le début accordé ta confiance et de m'avoir soutenue tout au long de mon doctorat. Ce fut un plaisir de travailler avec toi et de partager nos réflexions scientifiques.

Je souhaite remercier le Pr Lucie Lamontagne, j'ai été heureuse de travailler et collaborer avec toi sur plusieurs de tes projets de recherche. Je te remercie de m'avoir chaleureusement accueillie lors de mon séjour à Montréal et de m'avoir aidée pour l'ensemble des expériences réalisées sur le MHV3.

Je souhaite remercier le Dr Claire Piquet-Pellorce, pour tes nombreux conseils scientifiques, de m'avoir formée à l'analyse de la cytométrie en flux et pour ton soutien tout au long de cette thèse. Un grand merci également d'être venue tard ou beaucoup trop tôt pour toi le matin pour les injections en iv (les résultats en valaient le coup ! ;))

Je souhaite également remercier le Dr Jacques Le Seyec pour ta rigueur scientifique, ton aide avec Farooq dans la préparation des hépatocytes en culture et les nombreuses heures que tu as passées à corriger mes manuscrits d'articles.

Je tiens à remercier Céline Raguenes-Nicol pour m'avoir aidée à la préparation des liposomes.

Un grand grand merci à tous les membres de l'équipe, Grégory, Virginie, Elise, Fidaa, Benjamin, François, Cristina, Farooq, Sarah, Charlotte, Sorya, Valentine, Nicolas, Arnaud, Laurence et Michel vous contribuez tous à ce bel esprit d'équipe, et cette ambiance qui m'ont aidée à venir travailler dans les moments les plus durs. Resteront de bons souvenirs au moment du café, et des nombreuses dégustations de vos talents culinaires. Merci aussi pour votre aide dans les manips *in vivo*, en A1, en A3 ou dans la préparation des cellules immunes votre présence était indispensable.

Un merci tout particulier à Grégory, Virginie et Anne, pour nos discussions diverses et enrichissantes le midi, votre gentillesse et votre soutien.

Merci à mes deux libanaises préférées, Fidaa et Elise, pour avoir mis de l'ambiance dans le labo, pour votre soutien, votre énergie, votre sourire et pour l'organisation des week-ends extra labo.

Je souhaite également remercier nos deux futurs médecins François et Benjamin pour avoir partagé vos connaissances médicales, ainsi que pour votre gentillesse et votre ouverture au monde de la recherche. Benjamin, tes compétences artistiques (entre autres) m'ont bien fait rire au cours de cette dernière année.

También, quiero dar las gracias a Cristina, eras muy voluntaria y el fin de tesis habría sido mucho más duro sin ti. Gracias por los excellente western-blot, tu rigor, tu energía y tu dinamismo.

I would like to thank Farooq for the primary hepatocytes isolation and culture.

Merci également à Sarah, ton aide pour les dernières manips m'a été très précieuse.

Valentine, merci pour ton aide dans les manips au début de ma thèse et pour ton excellente mémoire de toutes les choses "rangées" dans le labo.

Merci également à Christian pour son aide dans mes différentes expériences réalisées sur le MHV3 à Montréal.

Je souhaite également remercier Brigitte, ton aide est indispensable à la vie de l'institut, merci pour ton efficacité dans toutes les taches administrative et la gestion des commandes.

Je souhaite remercier tous les membres des plateformes H2P2, l'animalerie Arche et de cytométrie en flux qui m'ont aidée et formée à de nombreuses techniques. Un merci particulier à Pascale, Roselyne, Marine et Alain, pour m'avoir formée aux différentes techniques d'histologie et votre gentillesse. Je tiens à remercier aussi Laurence et toute son équipe pour la gestion de l'animalerie. Un merci également à Laurent et Gersende pour l'acquisition des données de cytométrie en flux.

Enfin je souhaite remercier l'ensemble de mes proches Normands, Bretons et Québécois, merci 1000 fois pour votre soutien et d'avoir été là pour me permettre de me changer les idées. Un merci particulier à Hugues et Laureen, même loin, vous avez toujours été là pour moi et notamment dans les moments les plus durs, merci pour votre gentillesse et votre écoute.

Merci à toutes les personnes que j'ai pu rencontrer au sein de l'AMAP de Villejean. Un merci tout particulier pour Louise, Maëlig, Maelenn, Téo, Mathilde et Baptiste. Merci pour votre bonne humeur, votre optimisme, votre dynamisme et vos discussions toujours intéressantes. Les soirées à la théière et les mardis soirs à l'AMAP, ainsi que les cinés du dimanche soir ont été à chaque fois un bol d'air frais me permettant de me changer les idées.

Je tiens également à remercier Xavier, merci pour ton soutien ta gentillesse et ton écoute.

Je remercie également Mélodie, nos échanges (scientifiques mais pas que !) et partage de nos expériences doctoralesques étaient importantes pour moi. Merci pour ton soutien.

Je souhaite également remercier toute la colocation d'Hochelaga où l'on y fait de belles rencontres, un merci tout particulier à Rachel, Etienne et Valentin, merci pour votre énergie et votre gentillesse.

Je remercie Michel Provost pour la lecture et la correction de mon introduction de thèse.

Je tiens à remercier également mes parents Monique et Alain pour leur soutien et leur participation à la correction de l'introduction de ma thèse.

Abréviations

J'ai choisi dans ce travail de presenter les abréviations de termes anglais et français

ACD : Accidental Cell Death
ACLF : Acute on Chronic Liver Failure
ADH : Alcool Déshydrogénase
α-GalCer : α-Galactosylceramide
AIF : Apoptosis Inducing Factor
AIH : Auto-Immune Hepatitis
ALAT : Alanine aminotransferase
ALD : Alcoholic Liver Disease
ALF : Acute Liver Failure
ALI : Acute Liver Injury
APAP : Acetyl-Para-Aminophenol
APC : Antigen Presentating Cells
ARH3 : ADP-ribosyl-hydrolase 3
ASAT : Aspartate aminotransferase
ASK1 : Apoptosis Signal Related Kinase

BBB : Blood Brain Barrier
Bid : BH3 Interacting Domain death agonist
BMECs : Brain Microvascular Endothelial Cells

cFLIP : cellular FLICE like Inhibitory protein
CHC : Carcinome hépatocellulaire
cIAP : cellular Inhibitor of Apoptosis Protein
CMH : Complexe Majeur d'Histocompatibilité
ConA : Concanavaline A
CpG : Cytosine-phosphate Guanine
CYLD : Cylindromatosis

DAI : DNA-dependent activator of IFN regulatory factors
DAMPs : Damage Associated Molecular Patterns
DAPK1 : Death Associated Protein Kinase 1
DC : Dendritic Cells
DD : Death Domain

D-GalN : D-Galactosamine
DILI : Drug Induced Liver Injury
DISC : Death Inducing Signaling Complex
DR : Death Receptor

EGFR : Epithelial Growth factor ;
ERK : Extracellular Signal-Regulated Kinase

FADD : FAS Associated Death Domain
FasL : Ligand Fas
FGF : Fibroblast Growth Factor

GSH : Glutathion Hépatique

HMGB1 : High Mobility Group protein B1
HSC : Hepatic Stellate Cell

IAP : Inhibitor of Apoptosis Protein
ID : Intermediate Domain
IDO : Indoleamine-pyrrole 2,3-dioxygenase
IFN : Interféron
IHC : Immunohistochimie
IKK : Inhibitor of NF-κB Kinase
IL-1RAcP : IL-1 Receptor Accessory Protein
ILCs : Innate Lymphoïd Cells
iNKT : invariant-NKT
IPS : IFN-β Promoter Stimulator
IRF : Interferon Regulatory Factor
IκBα : Inhibitor of κB-alpha

JNK : c-Jun N-terminal Kinase

KC : Kupffer Cells
KD : Kinase Dead
KO : Knockout

LB : Lymphocytes B

LPC : Liver Parenchymal Cells
LPS : Lipopolysaccharide
LSEC : Liver Sinusoidal Endothelial Cells
LT : Lymphocytes T
LUBAC : Linear Ubiquitin Chain Assembly Complex

MAPK : Mitogen Activated Kinases
MDC : Cellules Myéloïdes
Mda5 : Melanoma differentiation-associate Gene 5
MHV : Murine Hepatitis Virus
MLKL : Mixed Lineage Kinase Domain Like
MOMP : Mitochondrial Outer Membrane Permeabilization

NAFLD : Non-Alcoholic Fat Liver Disease
NAPQI : N-acétyl-p-benzoquinone imine
NASH : Non-Alcoholic Steatosis Hepatitis
NETs : Neutrophil Extracellular Traps
NF-κB : Nuclear Factor-κB
NIK : NF-κB Inducing Kinase
NK : Natural Killer
NKT : Natural Killer T

PAMPs : Pathogen Associated Molecular Patterns
PAR : Polymères d'ADP Riboses
PARG : Poly(ADP-Ribose) Glycohydrolase
PARP : Poly(ADP-Ribose) Polymerase
PGAM5 : Phosphoglycerate Mutase Family Member 5
PP2A : Protein Phosphatase 2A
Poly(I:C) : Polyinosine-polycytidylique
PRR : Pattern Recognition Receptor

RAGE : Receptor for Advanced Glycation Endoproducts
RCD : Regulated Cell Death
RHIM : RIP Homotypic Interaction Motif
RIG1 : RNA helicase retinoic acid Inducible Gene I
RIPK : Receptor Inducing Protein Kinase
ROCK1 : Rho-associated Coiled-coil containing protein Kinase 1

ROS : Reactive Oxygen Species

Smac : Second mitochondrial activator of caspases

TACE : TNF-Converting Enzyme
TAK1 : TGF-β Activated Kinase 1
TCR: Récepteurs des cellules T
TGF : Transforming Growth Factor
TIR : Toll-IL-1 Receptor
TLR : Toll Like Receptor
TNF : Tumor Necrosis Factor
TNFR : TNF-Receptor
TRADD : TNFR1-Associated Death Domain
TRAF2 : TNFR Associated Factor 2
TRAIL : TNF-Related Apoptosis Inducing Ligand
TRIF : TIR- domain-containing adapter inducing IFN-β

VEGF : Vascular Endothelial Growth Factor
VHA : Virus de l'Hépatite A
VHB : Virus de l'Hépatite B
VHC : Virus de l'Hépatite C
VHD : Virus de l'Hépatite D
VHE : Virus de l'Hépatite E

WHO : World Health Organisation
WT : Wild Type

XIAP : X-linked Inhibitor of Apoptosis

ZO-1 : Zona occludens-1

SOMMAIRE

TABLE DES FIGURES

TABLE DES TABLEAUX

I. INTRODUCTION

I.1. Introduction générale sur le foie

I.1.1. Anatomie du foie

Situé sous le diaphragme, dans la cavité abdominale, le foie est le plus gros organe du corps humain et représente 2 % de sa masse totale. Il présente quatre lobes asymétriques et est entouré par la capsule de Glisson, un tissu conjonctif qui, contrairement au foie lui-même, est innervé.

La vascularisation du foie est particulière et dite mixte. Environ 20-25 % du sang hépatique provient du flux de la circulation systémique, via l'artère hépatique. Les 75-80 % restant arrivent par la veine porte et transportent un sang riche en éléments provenant de l'intestin (Malhi et al., 2010; Robinson et al., 2016). Les sangs veineux et artériel se mélangent au niveau des sinusoïdes hépatiques, formés par les travées d'hépatocytes, jusqu'à atteindre la veine centrolobulaire. Le foie est organisé en plusieurs sous-unités répétées, appelées lobules hépatiques (**Figure 1**). Au niveau des sinusoïdes hépatiques, le sang circule avec une faible pression et l'endothélium, qui est fenestré, assure une communication directe entre les hépatocytes et le sang, permettant la détoxification et l'élimination du matériel indésirable provenant de l'intestin.

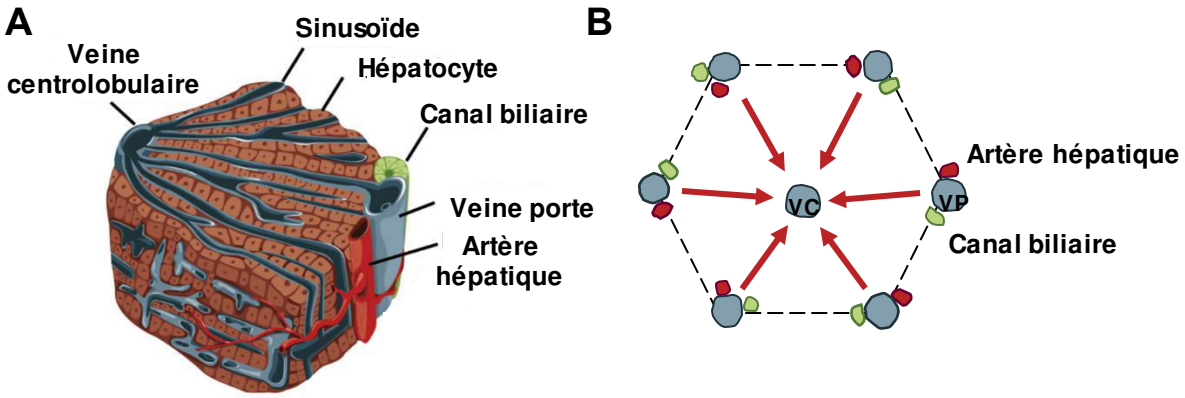

Figure 1. Représentation du lobule hépatique. *Abréviations : VP : veine porte, VC : veine centrolobulaire (inspiré de Si-Tayeb et al., 2010).*

I.1.2. Rôles du foie

Le foie exerce de nombreux rôles dans :

- le métabolisme des glucides, des lipides et des protéines,
- la synthèse de protéines et de la bile,
- la détoxification et l'élimination de substances indésirables dans la circulation sanguine.

Le foie est ainsi considéré comme une glande exocrine par son rôle d'excrétion de la bile vers l'intestin mais également comme une glande endocrine par sa fonction de filtration du sang du système digestif vers la circulation sanguine (MacSween et al., 1994) .

Les fonctions du foie sont assurées par les cellules parenchymateuses du foie (LPC pour "Liver Parenchymal Cells"). Ces cellules, de type épithélial, proviennent d'un précurseur commun: l'hépatoblaste qui, à J16 de gestation chez la souris et au bout de 8 semaines de grossesse chez la femme va former les hépatocytes et les cholangiocytes (appelés également cellules biliaires). Par leur importante capacité métabolique les hépatocytes vont être responsables des rôles présentés ci-dessus alors que les cholangiocytes vont former les canaux biliaires et assurer la sécrétion de la bile vers l'intestin (MacSween et al., 1994).

I.1.3. Prévalence et étiologie des maladies hépatiques

L'hépatite est définie comme une inflammation aiguë ou chronique du foie, pouvant résulter d'un dommage porté au parenchyme hépatique. On distingue trois formes d'hépatites :

- **L'hépatite aiguë ou fulminante** (ALI pour "Acute Liver Injury" ou ALF pour "Acute Liver Failure") qui est une destruction massive du parenchyme hépatique et peut conduire à une insuffisance hépatique. Dans 90 % des cas, les patients se rétablissent spontanément. Cependant, l'incapacité du foie à assurer ses fonctions peut conduire à des complications telle que l'encéphalopathie hépatique qui peut entraîner la mort des individus (Saliba and Samuel, 2013).
- **L'hépatique chronique** qui se caractérise par une inflammation et une hépatolyse continue ou répétée dans le temps. Ses conséquences sont le développement de la fibrose, de la cirrhose voire de la survenue d'un carcinome hépatocellulaire (CHC) (Luedde et al., 2014).
- **L'insuffisance hépatique aiguë sur une maladie chronique du foie** (ACLF pour "Acute on Chronic Liver Failure") qui correspond à une mort massive des hépatocytes survenant dans un foie présentant une cirrhose ou une fibrose préexistante. L'ACLF s'avère un très mauvais pronostic et peut entraîner rapidement la mort des patients (Sarin and Choudhury, 2016).

Majoritairement chroniques, les hépatites représentent un problème de santé publique. Induites par une grande diversité de facteurs, elles peuvent être réparties en quatre catégories : infectieuses (virales, parasitaires), toxiques (médicamenteuses, alcoolique ou d'autres substances toxiques telles que des toxines de champignons), métaboliques ou enfin auto-immunes. Les hépatites sont majoritairement virales mais la diminution de la prévalence des hépatites B et C ainsi que l'augmentation de l'obésité ont rapidement placé la stéatose-hépatite non induite par l'alcool (NASH pour "Non-Alcoholic Steatosis Hepatitis") comme un des facteurs principaux d'hépatite. Les caractéristiques ainsi que l'épidémiologie et la prévalence des hépatites sont présentées dans le Tableau 1.

Tableau 1. Etiologies, caractéristiques et épidémiologie des hépatites.

Etiologies		Causes/caractéristiques	Epidémiologie et prévalence	Références
Virales	Hépatite A	VHA, Picornaviridae - sb-ARN, groupe IV – Transmission par voie orale	Hépatite fulminante mais pas chronique. Rarement mortelle	OMS, 2016 www.who.int
	Hépatite B	VHB Hepadnaviridae - ds-ADN, groupe VII – Transmission par voie sexuelle et/ou sanguine.	Hépatite fulminante mais majoritairement chronique : 240 millions de personnes chroniquement infectées dans le monde ; 13 millions en Europe.	OMS, 2016 www.who.int ; www.euro.who.int/
	Hépatite C	VHC, Flaviviridae - sb-ARN, groupe IV – Transmission par voie sexuelle et/ou sanguine.	Hépatite chronique. 150 millions de personnes chroniquement infectées dans le monde ; 15 millions en Europe.	OMS, 2016 www.who.int ; www.euro.who.int/
	Hépatite D	VHD, Deltavirus - sb-ARN, groupe V	Virus dit satellite, nécessité d'une coinfection avec le VHB	Flodgren et al., 2000
	Hépatite E	VHE, Hepeviridae - sb-ARN, groupe IV. Transmission par ingestion.	Hépatite aiguë principalement, chronique chez les immunodéprimés : 20 millions de personnes infectées et 3 millions présentant une hépatite aiguë.	OMS, 2016 (http://www.who.int)
Toxiques	Alcool	La stéatose alcoolique est la forme la plus sévère. Effets cytotoxiques en partie dus à sa métabolisation en acétaldéhyde entraînant un stress oxydatif, une peroxydation lipidique, un dommage mitochondrial et une mort cellulaire.	Les pathologies liées à la consommation d'alcool sont nombreuses : parmi elles, la cirrhose et le cancer du foie sont les causes majeures de décès.	Gao and Bataller, 2011; Rehm et al., 2009
	Intoxication par toxines de champignons	Anatoxines provenant d'*Amanita phalloides* ou Aflatoxin B1 d'*Aspergillus- flavus,* or A. *parasiticus*.	Rares - Hépatites fulminantes	El-Serag, 2012; Panaro et al., 2006
	Médicamenteuses	Principalement provoquées par le paracétamol. Sa métabolisation conduit à la production de NAPQI, induisant une déplétion en glutathion, un stress oxydatif et une hépatolyse.	Hépatite aiguë majoritairement mais pouvant conduire à une hépatite chronique.	Ichai and Samuel, 2011
Métaboliques : NAFLD/NASH		Un régime riche en lipides et glucides peut conduire à une stéatose du foie. NAFLD regroupe l'ensemble des stéatoses de forme plus ou moins sévère. NASH : inflammation et stéatose du foie	Hépatite chronique : 20 % d'individus présentent les symptômes d'une stéatose et 3 % souffrent d'une NASH.	Iyer et al., 2015
Auto-immunes (AIH)		Caractérisées par la présence d'anticorps anti-muscle lisse (anti-SMA) et anti-nucléaires (anti-ANA) (type I) ou des anticorps anti-LKM1 ou anti-CYP2D6 (type II)	Maladies rares : prévalence de 11-24/10^5 personnes et une incidence annuelle de 0.8-3 /10^5 personnes. Provoque majoritairement une hépatite chronique.	van Gerven et al., 2016
Maladie de Wilson		Maladie génétique. Absence ou non-fonctionnalité de la protéine ATP7B conduisant à l'accumulation de cuivre au niveau du foie provoquant un stress oxydatif et la formation de radicaux libres	Insuffisance hépatique aiguë ou maladie hépatique chronique, peut être associée à des désordres neurologiques. Maladie rare, incidence de 1/30 000-40 000 habitants	Bandmann et al., 2015; Patil et al., 2013
Hémochromatose		Maladie génétique. Dans 90 % des cas, mutation du gène HFE conduisant à une hyperabsorption de fer et l'activation d'un processus de fibrose hépatique.	Cirrhose hépatique. Prévalence de 1-4/ 10^3 personnes mais incidence de 10 % chez ces personnes.	Powell et al., 2016

Abréviations : NAFLD : Non Alcoholic Fat Liver disease ; NASH : Non-Alcoholic Steatosis Hepatitis

I.1.4. Physiopathologie

Quelle que soit l'étiologie de l'hépatite, l'inflammation et l'hépatolyse sont les deux composantes principales conduisant au développement de l'hépatite. Ces deux acteurs se trouvent étroitement liés et peuvent chacun contribuer à l'amplification de l'autre. Ceci nécessite donc une fine régulation.

L'hépatolyse peut être induite de manière passive, par un stress physicochimique ou des agressions néfastes (c'est le cas au cours des hépatites toxiques) mais aussi de manière active par

l'induction de voies de mort cellulaire régulées (RCD pour "regulated cell death") (Luedde et al., 2014). Au cours des hépatites virales ou auto-immunes, la mort de l'hépatocyte est induite par le système immunitaire via une cascade d'interactions protéines/protéines conduisant à une RCD. L'augmentation des transaminases alanine-aminotransférase et aspartate-aminotransférase (respectivement ALAT et ASAT) reflète la lyse des hépatocytes et est utilisé en test de première intention pour diagnostiquer une maladie hépatique. Ces enzymes, essentielles dans le métabolisme, sont libérées dans le sang lors de la lyse des cellules. Contrairement aux ASAT qui sont exprimées dans plusieurs organes tels que le foie, le cœur, les muscles et les reins, le niveau des ALAT sériques reflète plus précisément la lyse des hépatocytes et corrèle avec la gravité de l'hépatite (Luedde et al., 2014).

Quel que soit la cause du dommage, la mort de l'hépatocyte conduit à la libération passive ou à l'exposition de molécules intracellulaires regroupées sous le terme de Damage Associated Molecular Patterns (DAMPs) et d'alarmines. Ces molécules de nature diverse participent à la régulation de l'inflammation et de l'immunité. La réponse immunitaire a tout d'abord un rôle hépatoprotecteur par sa contribution dans l'induction d'une réponse anti-infectieuse (antivirale, antiparasitaire, ou antimicrobienne), ou dans la réparation tissulaire suite à un dommage et a pour but de rétablir l'homéostasie hépatique (Brenner et al., 2013). Cependant, une inflammation excessive va avoir des conséquences délétères pouvant conduire à l'induction ou à l'amplification de l'hépatolyse et entraîner à court terme des altérations métaboliques (insuffisance hépatique) ou une ischémie mais aussi, à plus long terme, conduire à des effets irréversibles tels la fibrose ou le développement d'un CHC (Brenner et al., 2013; Luedde et al., 2014).

Ainsi, une mauvaise régulation de l'inflammation ou de l'hépatolyse va contribuer au développement d'une hépatite chronique via deux mécanismes principaux : d'une part la stimulation des cellules étoilées du foie (HSC pour Hepatic Stellate Cell) conduisant à la production de matrice extracellulaire, composée notamment de collagène, constituant la fibrose et, d'autre part, à l'induction d'une prolifération des hépatocytes. Ces deux mécanismes ont pour but de restaurer l'architecture et les fonctions hépatiques. Cependant, une activation des HSC et une prolifération des hépatocytes durant plusieurs dizaines d'années peuvent conduire à une insuffisance hépatique, par l'incapacité du foie à exercer ses fonctions ou induire le développement d'un CHC résultant de la prolifération incontrôlée des hépatocytes (Figure 2).

Bien que l'hépatite puisse être une des causes du développement d'un CHC, cette pathologie est plus fréquemment observée sur des foies atteints de fibrose ou cirrhotiques présentant une hépatolyse chronique. Les données sur les modèles animaux ainsi qu'une corrélation entre un taux élevé de transaminases et le développement d'un CHC chez les patients atteints d'hépatites

chroniques étayent l'idée qu'une mort cellulaire chronique est suffisante pour le développement d'un CHC et placent l'hépatolyse comme un déclencheur-clef du développement des maladies hépatiques (Luedde et al., 2014).

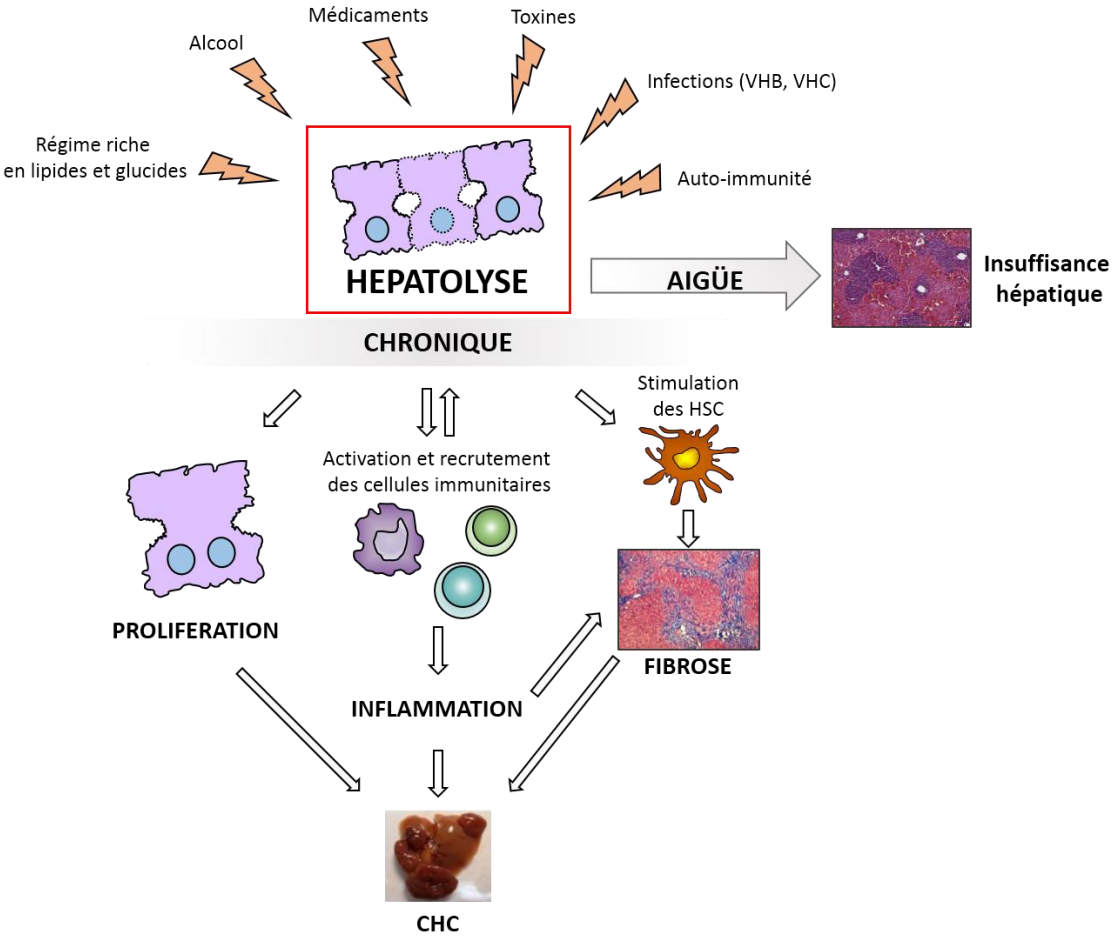

Figure 2. L'hépatolyse, un déclencheur de la progression des maladies hépatiques. *Quelle que soit l'étiologie, une mort massive des hépatocytes va conduire à une hépatite aiguë et provoquer une insuffisance hépatique. Une hépatolyse à plus bas bruit mais persistante va activer la prolifération hépatocytaire, stimuler les HSCs responsables de la fibrose par une production excessive de collagène et recruter le système immunitaire qui développera alors une réponse inflammatoire. Cette dernière peut également contribuer à l'hépatolyse. La somme de ces quatre phénomènes : la mort hépatocytaire, l'inflammation, la prolifération des hépatocytes et la production de fibrose vont contribuer au developpement de l'hépatite chronique et au développement d'un CHC (inspiré de Luedde et al., 2014).*

I.2. Immunologie et homéostasie hépatiques

En plus de ses importantes activités métaboliques et de détoxification, le foie est également considéré comme un organe immunologique central par sa composition comprenant de nombreuses cellules immunitaires qui lui permettent de produire une diversité de molécules inflammatoires telles que des cytokines, des chimiokines et des protéines de phase aiguë. Constamment exposé à des protéines du « non-soi » dérivées de l'alimentation, du microbiote ou provenant de l'environnement, le foie doit instaurer une tolérance immunitaire vis-à-vis de ces

molécules mais également pouvoir induire une réponse immunitaire efficace lors d'infections par des pathogènes hépatotropes (virus, parasites, bactéries, etc.) néfastes pour l'individu. Ce double rôle nécessite donc la mise en place de mécanismes finement régulés par les cellules immunitaires résidentes du foie.

I.2.1. Natures et caractéristiques des cellules hépatiques

Majoritairement composé de LPC, et plus particulièrement des hépatocytes qui représentent 70 à 80 % du volume du foie, celui-ci présente une diversité de cellules immunitaires spécialisées (**Figure 3**). Le système réticulo-endothélial hépatique composé des cellules endothéliales sinusoïdales (LSEC pour Liver Sinusoidal Endothelial Cells), des cellules de Kupffer (KC pour Kupffer Cells), qui sont les macrophages résidents du foie, et des cellules dendritiques (DC pour

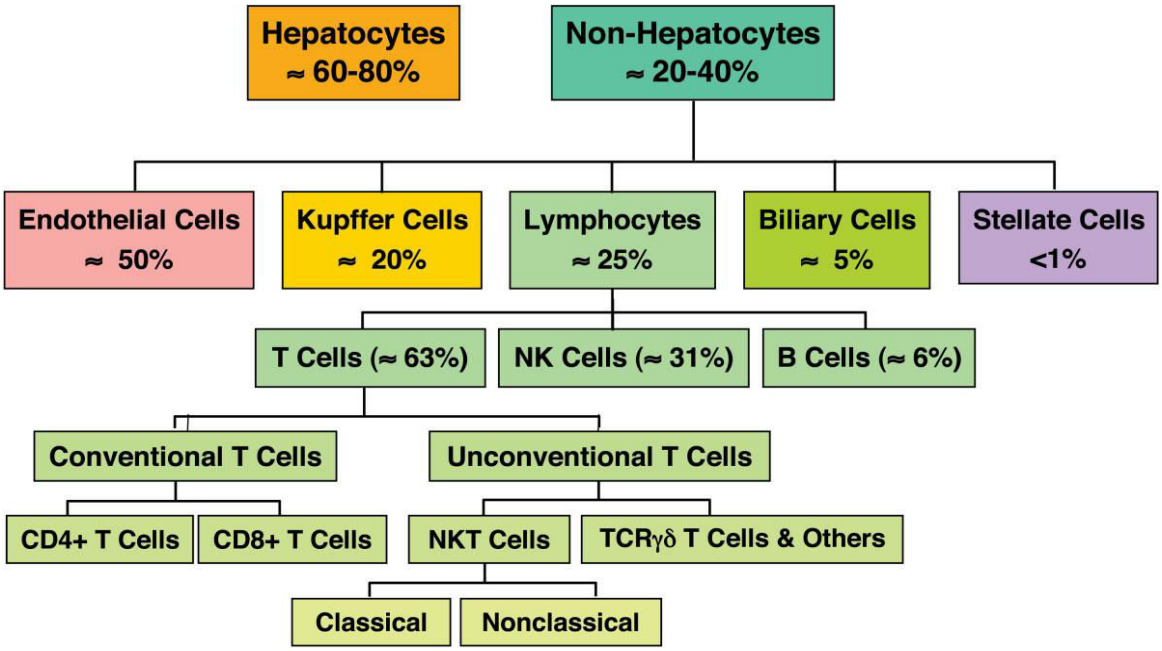

Dendritic Cells). Ce système assure l'élimination des antigènes et leur présentation aux cellules de

Figure 3. Composition des cellules du foie *(Issu de Racanelli and Rehermann, Hepatology, 2006).*

l'immunité adaptative ainsi que la dégradation de produits et toxines provenant du sang sinusoïdal, lesquels peuvent être transférés aux hépatocytes pour être éliminés (Thomson and Knolle, 2010). Par ailleurs, le foie est composé de lymphocytes B (LB) et T (LT), enrichi en lymphocytes NK et NKT et présente également une population de lymphocytes appelées Innate Lymphoïd Cells (ILCs). Alors que les premiers font partie de l'immunité adaptative, les derniers appartiennent à l'immunité innée par leurs capacités inflammatoires et cytolytiques induites rapidement lors d'une infection, sans reconnaissance d'un antigène spécifique. Enfin, le foie comporte également des HSC et des neutrophiles (**Figure 3**).

Les cellules non-parenchymateuses sont majoritairement localisées dans les sinusoïdes hépatiques mais on retrouve au sein de l'espace de Disse (qui sépare les hépatocytes des LSEC) des HSC et des protéines de matrice extracellulaire (**Figure 4**).

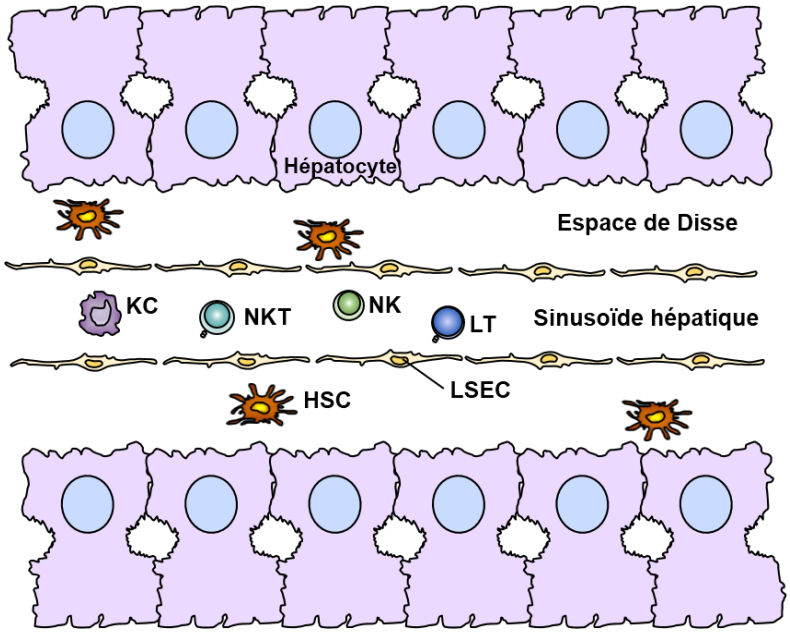

Figure 4. Représentation des cellules composant un sinusoïde hépatique.
Les cellules de Kupffer (KC), les Natural Killer T (NKT), les Natural Killer (NK) et les Lymphocytes T sont majoritairement retrouvés dans le sinusoïde hépatique qui est délimité par les cellules endothéliales sinusoïdales hépatiques (LSECs). Entre les LSECs et les hépatocytes se trouve l'espace de Disse, composé de matrice extracellulaire et des cellules étoilées du foie (HSC) (inspiré de Racanelli and Rehermann, Hepatology, 2006).

Les cellules des immunités innée et adaptative vont participer à la réponse immunitaire lors d'une infection mais le système immunitaire inné agit comme première ligne de défense contre les pathogènes et permet au système immunitaire adaptatif de développer une réponse effectrice spécifique et de garder une mémoire immunologique. Son étroite relation avec le tractus gastro-intestinal explique la forte tolérance des cellules immunitaires vis-à-vis d'éléments étrangers provenant de l'environnement. Cependant, la reconnaissance d'éléments pathogènes tels que les Pathogen Associated Molecular Patterns (PAMPs) par les cellules de l'immunité innée va conduire à une réponse immunitaire. Ces cellules ont également un rôle important dans la détection d'un dommage hépatique via la reconnaissance des DAMPs qui permettent la mise en place de la réponse immunitaire innée. Ces cellules vont moduler la réponse inflammatoire et jouer un rôle majeur dans la progression des maladies hépatiques, d'une part via la sécrétion de médiateurs chimiques tels que les cytokines et les chimiokines permettant la communication entre les cellules hépatiques et d'autre part, dans l'expression et/ou la libération de ligands induisant la mort cellulaire, dont les membres de la superfamille du Tumor Necrosis Factor (TNF) tels que le TNF-α, le ligand Fas (FasL/ CD95L ou APO-1L) et le TNF-Related Apoptosis Inducing Ligand

(TRAIL) jouent un rôle majeur. La régulation de ces différents effecteurs dans le foie déterminera la progression des maladies hépatiques.

I.2.1.1. Les cellules de Kupffer

Les KC sont les macrophages résidents du foie et représentent 80 % de l'ensemble des macrophages de l'individu. Ils exercent des fonctions critiques dans l'homéostasie du foie par leur capacité à induire une tolérance hépatique dans des conditions physiologiques, mais également par l'initiation d'une réponse inflammatoire en cas d'infection ou de dommages cellulaires. Sujet longtemps débattu, il est aujourd'hui admis que les KC se renouvellent à partir d'un précurseur résident et non de la moelle osseuse (Tacke and Zimmermann, 2014). Cependant, au cours des hépatopathies, des monocytes circulants sont recrutés au niveau du foie et jouent également un rôle dans la réponse inflammatoire (Tacke and Zimmermann, 2014). Contrairement à d'autres organes où les macrophages sont caractérisés en type M1 (plutôt pro-inflammatoire) ou M2 (plutôt anti-inflammatoire), selon la nature des cytokines qu'ils produisent, les KC peuvent exprimer simultanément des marqueurs de type M1 et M2, rendant difficile la caractérisation des macrophages hépatiques (Tacke and Zimmermann, 2014). Principalement localisés au sein des sinusoïdes hépatiques, ils peuvent traverser l'espace de Disse pour se trouver en contact avec les hépatocytes. Ils ont donc un rôle majeur dans la réponse immunitaire et dans la tolérance hépatique. En effet, comme les DC, ce sont d'importantes cellules présentatrices d'antigènes (APC pour "Antigen Presentating Cells") qui possèdent une forte activité de phagocytose permettant l'élimination des éléments étrangers à l'individu. De plus, la stimulation des KC par le lipopolysaccharide (LPS), un élément de la paroi des bactéries à Gram négatif, conduit à la sécrétion d'IL-10, une cytokine anti-inflammatoire, responsable de l'inhibition de l'activation des lymphocytes T et de la stimulation des lymphocytes T régulateurs (Heymann and Tacke, 2016). Malgré un rôle anti-inflammatoire important pour le maintien de la tolérance hépatique, les KC vont également être capables de sécréter rapidement des cytokines et chimiokines pro-inflammatoires telles que le TNF-α, l'IL-6, l'IL-1β, le CCL2 et le CCL5, suite à la reconnaissance de DAMPs ou de PAMPs. Ainsi, elles contribuent au recrutement des cellules immunitaires mais peuvent aussi favoriser une activité antimicrobienne et l'activation de la mort des hépatocytes infectés (Heymann and Tacke, 2016; Racanelli and Rehermann, 2006; Tacke and Zimmermann, 2014). De plus la production d'IL-1β, d'IL-12 et d'IL-18 par les KC va permettre de réguler la différenciation des cellules NK et promouvoir leur activité cytolytique (Heymann and Tacke, 2016; Lauwerys et al., 2000).

I.2.1.2. Les cellules dendritiques

Les DC hépatiques ont une faible capacité de phagocytose mais possèdent des fonctions immuno-régulatrices. Comme les KC et les LSECs, les DC hépatiques ont un important rôle tolérogénique en conditions physiologiques (Thomson and Knolle, 2010). En effet, en comparaison avec les DC dérivées de la rate, les DC du foie produiraient des quantités plus importantes d'IL-10 et seraient moins puissants pour activer des LT (Robinson, 2016). Cependant, au cours des hépatites chroniques, les DC produisent du TNF-α permettant l'activation des lymphocytes T et NK mais auraient également un rôle dans la régénération hépatique (Heymann and Tacke, 2016).

I.2.1.3 Les cellules Natural Killer et les Innate Lymphoïd Cells

Chez l'Homme, les cellules NK conventionnelles représentent la population majoritaire des lymphocytes du foie et constituent la sous-population lymphocytaire la plus importante. Majoritairement dérivées de la moelle osseuse, les cellules NK sont classées comme des cellules de l'immunité innée par l'absence de récepteurs reconnaissant des antigènes spécifiques. Elles ont des fonctions cytolytiques principalement induites par l'expression de ligands de mort tels que FasL et TRAIL. Elles sont également considérées comme de puissants producteurs d'IFN-γ leur permettant d'avoir une forte activité antivirale mais aussi de promouvoir l'inflammation par l'induction de chimiokines, telles que CXCL9, et de molécules d'adhésion, favorisant le recrutement des LT dans le foie (Gao et al., 2012; Racanelli and Rehermann, 2006). Alors que l'IL-10 va inhiber l'activation des cellules NK, l'IL-18 et l'IL-12 vont augmenter leurs capacités cytolytiques (Lauwerys et al., 2000). Les cellules NK résidentes du foie sont à distinguer des cellules NK conventionnelles par leur origine, leurs fonctions et leurs marqueurs de surface qui se rapprochent d'une population lymphoïde récemment identifiée et appelée ILCs (Peng and Tian, 2015). Ces ILCs auraient de faibles capacités cytolytiques mais sont capables de secréter de l'IFN-γ et du TNF-α (Heymann and Tacke, 2016).

I.2.1.4 Les cellules Natural Killer T

En comparaison avec d'autres organes, le foie est particulièrement riche en cellules NKT. Ces cellules de l'immunité innée sont des LT partageant certaines caractéristiques avec les cellules NK (marqueur NK1.1 chez la souris et CD56 chez l'Homme) et jouent un rôle important d'immunorégulateur dans différentes conditions inflammatoires telles que dans le cancer, les maladies auto-immunes ou infectieuses. Contrairement aux LT, les cellules NKT expriment un répertoire restreint de récepteurs T (TCR) qui leur permet de reconnaître des antigènes lipidiques endogènes présentés par le CD1d, une molécule analogue aux protéines du complexe majeur

d'histocompatibilité (CMH) de classe 1 (Slauenwhite and Johnston, 2015). Cette reconnaissance ainsi que le réarrangement du TCR permet de distinguer deux classes de cellules NKT, d'une part les NKT de type I ou NKT invariants (iNKT) qui expriment une chaîne alpha du TCR composée du réarrangement Vα14-Jα18 chez la souris et Vα24-Jα18 chez l'Homme associée à une chaîne bêta restreinte (Vβ8.2, Vβ7 ou Vβ2 chez la souris et Vβ11 chez l'Homme) et qui reconnaissent spécifiquement l'α-galactosylceramide (α-GalCer) présenté par le CD1d. D'autre part, les cellules NKT de type II présentent un TCR oligoclonal restreint mais plus varié que les cellules iNKT et reconnaissent des lipides présentés par le CD1d autres que l'α-GalCer (Slauenwhite and Johnston, 2015). La souris et l'Homme présentent quelques différences au niveau de l'immunité innée et notamment vis-à-vis des proportions de cellules NK et NKT. En effet, chez la souris les cellules NK représentent environ 10 % des cellules immunitaires hépatiques et les cellules NKT 20 à 40 % avec une forte proportion de cellules iNKT (70 à 80 % des NKT totaux). Chez l'humain, ce ratio est inversé et les cellules NKT de type II sont prédominantes parmi les cellules NKT totales (Bandyopadhyay et al., 2016; Klugewitz et al., 2004; Robinson et al., 2016). Les rôles des lymphocytes NKT dans les hépatopathies résultent majoritairement des expérimentations sur des modèles murins mais sont peu connues chez leurs homologues humains (Heymann and Tacke, 2016).

Suite à leur activation, les cellules NKT vont être capables de polariser la réponse immunitaire par la production rapide d'importantes quantités de cytokines de type Th1 (TNF-α et IFN-γ), Th2 (IL-4 et IL-13) et Th17 (IL-17 et IL-23) (Swain, 2008). En parallèle, les cellules NKT vont être capables, comme les cellules NK, d'induire la mort des hépatocytes via l'expression et/ou la libération de FasL, de TRAIL ainsi que via le système perforine/granzyme (Swain, 2008). Les lymphocytes NKT sont impliqués dans de nombreuses maladies hépatiques mais présentent des fonctions différentes selon l'étiologie. Ainsi, ils auraient un effet délétère par l'induction d'un dommage hépatique dans la NASH ou au cours des hépatites auto-immunes, virales et alcooliques, mais un effet protecteur au cours des hépatites induites par un toxique ou un médicament (Bandyopadhyay et al., 2016).

I.2.1.5. Les neutrophiles

Quelle que soit l'étiologie de l'hépatite, les neutrophiles vont être recrutés en réponse au dommage hépatique. Ils vont contribuer à l'aggravation du dommage hépatique par la production d'espèces réactives à l'oxygène (ROS) et de cytokines pro-inflammatoires telles que l'IL-1β et le TNFα (Heymann and Tacke, 2016). Les neutrophiles jouent un rôle important en réponse à l'infection par la phagocytose des bactéries et la production de Neutrophil Extracellular Traps (NETs). Ces derniers sont composés d'ADN et de nucléosomes permettant de piéger et de tuer les

bactéries et les virus, et conduisent à une mort cellulaire appelée NETose ou ETose (traduction littérale de NETosis et ETosis). Cependant la formation de NETs peut diminuer le débit sanguin du foie, qui peut être la cause d'une ischémie et contribuer au dommage hépatique (Heymann and Tacke, 2016).

I.2.1.6. Les lymphocytes B et T

Contrairement aux lymphocytes NK et NKT, les LB et les LT vont avoir un rôle dans l'immunité adaptative face à une infection. Produits à partir de la moelle osseuse, les LB sont peu nombreux dans le foie; leur activation et leur différenciation sont déclenchées dans les organes lymphoïdes secondaires (Burrows and Cooper, 1997). C'est pourquoi le rôle des LB au niveau du foie et dans les maladies hépatiques est peu connu (Racanelli and Rehermann, 2006).

Suite à leur différenciation dans le thymus, les LT CD4+ et CD8+ présentent un répertoire varié de TCR qui va leur permettre de reconnaître les antigènes présentés par les APC. Les CD8+ ou LT cytolytiques reconnaissent des peptides présentés par le CMH de classe I et vont avoir un rôle majeur contre la plupart des pathogènes hépatotropes tels que le VHB et le VHC. Suite à la reconnaissance d'un antigène spécifique les LT doivent, pour être pleinement activés, recevoir un signal de costimulation. Leurs fonctions effectrices sont réalisées par la sécrétion de cytokines pro-inflammatoires, telles que l'IFN-γ et le TNF-α, et des mécanismes cytolytiques par la libération des molécules perforine/granzyme et l'induction de l'apoptose par l'activation de Fas (Berke, 1995; Guidotti and Chisari, 1996). Le système réticulo-endothélial et les HSC modulent la réponse immunitaire induite par les LT (Thomson and Knolle, 2010) et au cours des hépatites chroniques plusieurs mécanismes conduisant à l'inhibition, l'anergie, voire la mort des LT conventionnels ou à l'activation des LT régulateurs ont été observés et démontrés comme contribuant au développement des maladies hépatiques (Heymann and Tacke, 2016).

I.2.1.7. Les Liver Sinusoidal Endothelial Cells

Les LSECs sont morphologiquement très différentes des cellules endothéliales classiques et vont former un endothélium fenestré dont les espaces vont varier selon la localisation des LSEC au niveau du sinusoïde hépatique (DeLeve, 2013). Les LSECs vont présenter une forte activité d'endocytose permettant l'élimination des produits indésirables provenant de l'environnement via l'expression de différents récepteurs tels que le récepteur au mannose ou "scavenger". Elles vont également présenter des antigènes via les molécules des CMH de classe I et II et être aussi efficaces que les DC dans l'endocytose et la présentation des antigènes aux cellules immunitaires (Racanelli and Rehermann, 2006).

I.2.2. Inflammation et tolérance hépatique

Le foie est constamment au contact de produits bactériens ou dérivés de l'alimentation qui présentent un potentiel inflammatoire. Ces diverses molécules provenant de l'intestin doivent être tolérées par le foie mais cette tolérance ne doit pas empêcher le développement d'une réponse immunitaire efficace face à une infection par des pathogènes. Le microenvironnement hépatique va déterminer la balance entre tolérance et inflammation (Robinson et al., 2016). Le système réticulo-endothélial hépatique joue un rôle majeur dans la mise en place de la tolérance immunitaire par de nombreux mécanismes tels que :

a) la prévention de l'activation de la réponse adaptative par la diminution de l'expression des molécules de costimulation, nécessaires à la différenciation efficace des lymphocytes T par les APC (Heymann and Tacke, 2016; Robinson et al., 2016),
b) la sécrétion de prostaglandines qui va promouvoir l'activation des LT régulateurs (Heymann and Tacke, 2016; Robinson et al., 2016),
c) la sécrétion, par le système réticulo-endothélial hépatique ainsi que les LT régulateurs, d'IL-10 et de TGF-β, de puissants immunosuppresseurs par leurs capacités à diminuer l'expression du CMH de classe II sur les LSECs et les DC et à réduire l'activation des LT (Groux et al., 1996; Robinson et al., 2016),
d) l'expression d'indoleamine-pyrrole 2,3-dioxygenase (IDO) et d'arginase qui restreint la production d'acides aminés essentiels tel que le tryptophane requis pour l'activation des LT (Robinson et al., 2016; Thomson and Knolle, 2010),
e) l'expression de différentes molécules telle que "Programmed Death Ligand 1" (PD-L1) induisant la tolérance et l'anergie des LT (Heymann and Tacke, 2016).

Cette tolérance hépatique est majeure pour maintenir l'homéostasie hépatique dans des conditions physiologiques, cependant le foie doit être capable de promouvoir une rapide réaction immunitaire en réponse à une infection ou à un dommage tissulaire (Heymann and Tacke, 2016).

Un ensemble de récepteurs de l'immunité innée appelés Pattern Recognition Receptors (PRRs) permet la détection des PAMPs et des DAMPs reflétant la présence d'un pathogène ou d'un dommage tissulaire. Sont regroupés sous le terme de PAMP un ensemble d'éléments de structure bactérienne, parasitaire ou virale, contrairement aux DAMPs qui sont des molécules provenant de l'individu lui-même et induites ou libérées lors d'un dommage permettant d'alerter le système immunitaire. Dans le foie, "High mobility group protein B1" (HMGB1) et l'IL-33 sont des alarmines classiques libérées lors de la mort des hépatocytes. De plus, l'accumulation hépatique

d'acide biliaire peut également déclencher la production de cytokines pro-inflammatoires (Heymann and Tacke, 2016).

La reconnaissance des PAMPs et DAMPs par les PRRs va conduire, dans la cellule cible, à l'activation de facteurs de transcription communs tels que "Nuclear Factor-κB" (NF-κB), Fos-Jun et "Interferon Regulatory Factor" (IRF), conduisant à la production de cytokines et de chimiokines inflammatoires (Silke et al., 2015) qui vont orchestrer la réponse immunitaire et le rétablissement de l'homéostasie hépatique. Parmi ces PRRs, les membres de la famille des Toll like receptors (TLRs) jouent un rôle clef dans cette reconnaissance et sont constitutivement exprimés par les cellules parenchymateuses et non-parenchymateuses hépatiques. Selon la nature des molécules, les TLRs et les voies de signalisation impliquées vont être différents et permettre une réponse immunitaire adaptée à la cause de l'hépatite (Tableau 2).

Une diversité de cytokines et de chimiokines sera sécrétée lors de cette réponse immunitaire et agira sur l'ensemble des cellules du foie de manière autocrine ou paracrine tout en étant impliquée dans de nombreux processus biologiques tels que la prolifération, l'inflammation, l'immunité, la migration, la fibrose, la réparation et l'angiogenèse (Oppenheim, 2001; Vilcek and Feldmann, 2004). La reconnaissance du danger va conduire à la production de nombreuses cytokines et chimiokines.

Tableau 2. Localisation, ligands et caractéristiques des TLR (adapté de Kesar and Odin, 2014)

Récepteurs	Ligands naturels et caractéristiques	Localisation et expression cellulaire
TLR1	Le complexe TLR1/TLR2 reconnaît des peptidoglycanes et lipoprotéines bactériens. Reconnaissance d'éléments de la paroi des bactéries à Gram positif.	Membranaire H, NK, LT, DC, LB
TLR2		Membranaire H, NK, LT, KC, DC, HSC ; C
TLR3	ARN double brin	Intracellulaire H, NK, KC, C
TLR4	Lipopolysaccharide (paroi des bactéries à Gram négatif), DAMPs	Membranaire H, NK, LT, LSEC, KC, DC, HSC, C
TLR5	Flagelline monomérique	Membranaire H, LT, NK, DC, C
TLR6	Diacyl lipopeptides	Membranaire H, NK,
TLR7	ARN simple brin, imidazoquinolines	Intracellulaire H, NK, LB, DC
TLR8	ARN simple brin, imidazoquinolines	Intracellulaire H, NK, DC
TLR9	Motifs non méthylés CpG présents dans l'ADN bactérien	Intracellulaire H, NK, LT, KC, LB, HSC
TLR10	Lipopeptides triacylés	Membranaire NK, LB

Abréviations : H : hépatocyte, NK : cellule Natural Killer, LT : Lymphocyte T, DC : cellule dendritique, LB : lymphocyte B, HSC : cellule étoilée du foie, C : cholangiocyte.

La reconnaissance du danger va conduire à la production de nombreuses cytokines et chimiokines. La libération des cytokines pro-inflammatoires telles que le TNF-α, l'IFN-γ, l'IL-1β,

l'IL-12 et l'IL-18 va promouvoir l'inflammation par l'activation des KC et des lymphocytes NK et NKT et la libération des chimiokines telles que les CCL1, CCL2, CCL3, CCL4 et CCL5 impliquées dans le recrutement des monocytes et lymphocytes au niveau du foie (Ajuebor et al., 2006; Heymann and Tacke, 2016). En parallèle, une réponse plutôt anti-inflammatoire va être induite et principalement régulée par l'IL-10 et le TGF-β qui va moduler la réponse inflammatoire dans le but de rétablir l'homéostasie hépatique. De plus, la libération d'IL-4, d'IL-5 et d'IL-13 va être induite lors d'infections par des pathogènes extracellulaires ou des parasites mais va être également impliquée dans la régénération hépatique (Heymann and Tacke, 2016). Celle-ci passe notamment par l'induction d'une réponse pro-fibrotique, via la stimulation des HSCs en myofibroblastes et par l'induction de signaux anti-apoptotiques hépatocytaires. Cette réponse va être modulée par le TGF-β, l'IL-6, le TNF-a, l'IL-4 et l'IL-13 (Robinson et al., 2016). Des facteurs de croissance tels que le "Vascular Endothelial Growth Factor" (VEGF), l'"Hepatocyte Growth Factor (HGF) ou le "Fibroblast Growth Factor" (FGF) vont également être produits pour contribuer à la réparation du parenchyme hépatique (Heymann and Tacke, 2016).

I.3. Mécanismes moléculaires et cellulaires de l'hépatolyse.

I.3.1 Différents modes de mort cellulaire

Le mécanisme de mort conduisant à l'hépatolyse peut différer selon l'étiologie de l'hépatite. En effet, alors qu'au cours des hépatites métaboliques ou induites par un toxique, la mort de l'hépatocyte est directement causée par le toxique lui-même, les cellules immunitaires sont les premiers effecteurs conduisant à la mort de l'hépatocyte au cours des hépatites auto-immunes ou virales. Cependant, au cours des hépatites induites par un toxique, l'hépatolyse va conduire à la libération de facteurs activant le système immunitaire qui peut alors dans un second temps participer au dommage du parenchyme hépatique.

Depuis 150 ans, la mort cellulaire était décrite en fonction de ses caractéristiques morphologiques distinguant ainsi deux types de mort cellulaire : l'apoptose et la nécrose (Ziegler and Groscurth, 2004). La nécrose, caractérisée comme une mort « accidentelle », se distingue de l'apoptose qui est une mort régulée par la cellule. Cependant, cette dichotomie n'est pas aussi simple et l'évolution des techniques biochimiques a permis de découvrir d'autres voies de RCD qui, morphologiquement, ressemblent à la nécrose mais ne partagent pas forcément les mêmes partenaires protéiques. Aujourd'hui on distingue donc deux types de mort, classées sur le plan opérationnel : accidentelle (ACD pour Accidental Cell Death) ou régulée (RCD) (Galluzzi et al., 2015). L'ACD peut être causée par différents facteurs physiques, chimiques ou mécaniques qui conduisent à une mort de la cellule quasi-immédiate et est insensible à une intervention génétique

ou pharmacologique puisque ne faisant pas intervenir une machinerie moléculaire spécifique (Galluzzi et al., 2015). A l'inverse, les RCD sont aujourd'hui très diverses et ont été référenciées par le comité de la mort cellulaire qui a établi une nomenclature regroupant onze formes différentes de RCD (Galluzzi et al., 2012) (**Tableau *3***).

Ces RCD présentent très souvent les mêmes caractéristiques morphologiques et vont donc être classifiées selon le signal et les protéines effectrices conduisant à la mort de la cellule. L'induction des différentes RCD est dépendante de plusieurs critères tels que : le type cellulaire, le contexte environnemental de la cellule, son niveau d'énergie métabolique et les différents stimuli reçus par la cellule.

Tableau 3. Modes de RCD défini par le comité de mort cellulaire (Adapté de Galluzi et al., 2012).

Mode de mort cellulaire régulé	Caractéristiques biochimiques
Anoïkis	Sous-expression de l'EGFR Inhibition de la signalisation d'ERK1 Absence d'engagement de l'intégrine β1 Surexpression de Bim Activation des caspases 3, 6, et 7
Autophagie	La mort par autophagie correspond en réalité à la mort de la cellule induite par une inhibition de l'activation de l'autophagie
Apoptose intrinsèque dépendante des caspases	Perméabilisation de la membrane externe mitochondriale Dissipation du potentiel mitochondrial irréversible Libération du cytochrome c Activation des caspases 9 et 3
Apoptose extrinsèque induite par des récepteurs de mort	Induite par l'activation des récepteurs de mort de la superfamille du TNF Activation des caspases 8 et 10 Activation des caspases 3, 6 et 7
Apoptose extrinsèque par une dépendance de récepteurs	Dépendance de la signalisation de récepteurs (autres que récepteurs de mort) : PP2A, DAPK1 Activation de la caspase 9 ou des caspases 3, 6 et 7
Cornification	Activation de transglutaminases Activation de la caspase 14
Entose	Activation de Rho-GTPase Activation de ROCK1
Catastrophe mitotique	Activation de la caspase 2 dans certaines conditions Activation de TP53 et TP73 dans certaines conditions Arrêt de la mitose
Necroptose	Induit par l'activation de récepteurs de mort et Activation de RIPK3, MLKL et dans certains cas de RIPK1
NETose	Inhibition des caspases Activation de la NADPH oxydase Libération de NET (dans certaines conditions)
Parthanatos	Accumulation de PAR Dissipation du potentiel mitochondrial irréversible Déplétion de l'ATP et du NADH Translocation de AIF au niveau nucléaire par l'intervention des PAR
Pyroptose	Activation de la caspase 1 Activation de la caspase 7 Sécrétion d'IL-1β et d'IL-18

Abréviations : EGFR : Epithelial Growth factor ; ERK : Extracellular Signal-Regulated Kinase ; PP2A : Protein Phosphatase 2A ; DAPK1 : Death Associated Protein Kinase 1 ; ROCK1 : Rho-associated coiled-coil containing protein Kinase 1 ; RIPK : Receptor Interacting Protein Kinase ; MLKL : Mixed Lineage Kinase domain Like ; NET : Neutrophil Extracellular Traps ; PAR : Poly-(ADP-ribose).

I.3.2. L'apoptose et la nécroptose, deux voies de mort cellulaire induites par les récepteurs de mort

Alors qu'il a été largement décrit que l'activation des récepteurs de mort (DR pour "Death Receptor") de la cellule conduisait à l'activation de l'apoptose, il est aujourd'hui reconnu qu'elle peut également, sous certaines conditions, activer une autre voie de RCD, la nécroptose (Galluzzi et al., 2012).

I.3.2.1 Définitions, caractéristiques et mécanismes de l'apoptose

Le terme d'apoptose fut proposé par Kerr en 1972 pour définir l'aspect morphologique spécifique de la cellule au cours de sa mort, caractérisée par le bourgeonnement de la membrane, le rétrécissement de la cellule, la condensation de la chromatine et la fragmentation nucléaire (Kerr et al., 1972). L'apoptose peut être déclenchée par de nombreux stimuli : externes par l'activation des DR ou internes, par des facteurs de stress, un changement majeur de l'homéostasie cellulaire ou un dommage important de l'intégrité de l'ADN (Ziegler and Groscurth, 2004). Ces phénomènes conduisent à l'activation d'enzymes intracellulaires appelées caspases, contraction de "cysteine dependent aspartate specific protease". Ces enzymes vont provoquer le clivage des protéines vitales à l'intégrité de la structure cellulaire : protéines responsables du maintien, de l'organisation et de l'attachement du cytosquelette ainsi que celles impliquées dans le maintien de l'appareil mitotique nucléaire permettant l'intégrité structurale du noyau (Ziegler and Groscurth, 2004).

Deux voies distinctes régulent l'apoptose : la voie extrinsèque et la voie intrinsèque :

- La voie extrinsèque est activée par des ligands extracellulaires appartenant principalement à la superfamille du TNF, tels que le TNF-α, le FasL et le TRAIL, qui conduisent à la formation du complexe IIa appelé également "Death Inducing Signaling Complex" (DISC) amenant à l'activation de la caspase 8.
- La voie intrinsèque peut être activée par différents stimuli de dommage intracellulaire ou de signal de stress, convergeant vers une perméabilisation de la membrane externe mitochondriale (MOMP pour "Mitochondrial Outer Membrane Permeabilization") et une libération du cytochrome c, ce qui conduit à la formation de l'apoptosome par sa liaison avec la protéine Apaf1 permettant l'activation de la caspase 9. Cette voie est finement régulée par des protéines pro-apoptotiques et anti-apoptotiques appartenant à la famille Bcl2. Dans certains types de cellules, dites de type II, tels que les hépatocytes, les DRs peuvent conduire à l'activation de la voie intrinsèque par le clivage de la protéine "BH3 Interacting Domain death agonist" (Bid) par la caspase 8 conduisant à une translocation de sa forme active tBid vers la mitochondrie provoquant une MOMP et les évènements décrits

ci-dessus. L'engagement de la voie intrinsèque en parallèle de la voie extrinsèque, conduit à une amplification du signal pro-apoptotique. Ces deux voies se rejoignent par l'activation *in fine* de la caspase 3, ce qui constitue un évènement de non-retour et entraîne la mort de la cellule par apoptose (**Figure 5**).

Ainsi, l'apoptose est considérée comme une voie dépendante de l'activation des caspases. Cependant, il faut distinguer les caspases effectrices de l'apoptose de celles impliquées dans

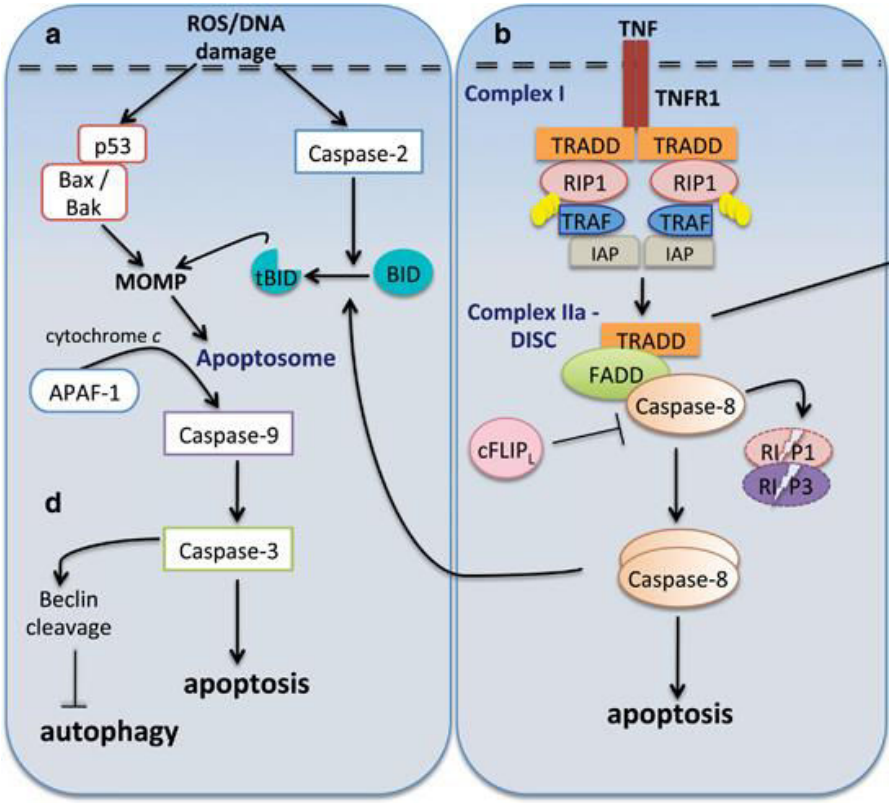

Figure 5. Voies intrinsèque (a) et extrinsèque (b) de l'apoptose. *(modifié à partir de Shalini et al., 2015)*

l'inflammation. Ainsi, les caspases 2, 3, 7, 8, 9 et 10 agissent chacune à un niveau différent dans l'induction de la voie apoptotique alors que les caspases 1, 4, 5, 11 et 12 régulent l'inflammation, par exemple par la maturation de certaines cytokines pro-inflammatoires tel que l'IL-1β (Shalini et al., 2015). Ceci explique pourquoi certaines voies de mort sont dépendantes des caspases et ne sont pas considérées comme apoptotiques (Tableau 3).

Contrairement à la nécrose, la formation des corps apoptotiques empêche le déversement du contenu intracellulaire dans le milieu extracellulaire et évite, en théorie, une inflammation massive du tissu. La cellule va exposer des signaux « find me » ou « eat me », par exemple par l'externalisation de la phosphatidyl-sérine, sur les corps apoptotiques qui vont permettre leur reconnaissance et leur élimination par les cellules voisines. Dans le foie, les HSC et les KC vont être majoritairement responsables de la phagocytose des corps apoptotiques (Canbay et al., 2003, 2004). Cependant si ces corps apoptotiques persistent dans l'environnement, par exemple

lorsqu'ils sont trop nombreux, la membrane plasmique va se dégrader et entraîner la libération du contenu cellulaire et provoquer ce qu'on appelle une nécrose secondaire, conduisant à une inflammation du foie. De plus, il a été montré que la phagocytose des corps apoptotiques par les KC ou les HSC va entraîner leur activation et la production de TNF-α, de FasL et de TRAIL pouvant amplifier la mort des hépatocytes et aggraver l'inflammation du foie (Malhi et al., 2010). Bien qu'il fut décrit que la formation des corps apoptotiques empêchait l'activation de l'inflammation, il est aujourd'hui admis que l'induction de l'apoptose n'est pas forcément synonyme d'absence d'inflammation et contribue donc largement au développement des hépatopathies (Malhi et al., 2010).

I.3.2.2 Nécroptose

Suite à une infection virale, les cellules sont capables d'induire leur apoptose afin de diminuer la réplication et la dissémination du virus. Cependant certains de ces virus ont pu développer des stratégies d'évasion via la production de protéines inhibant l'activation des caspases. L'évolution a conduit l'hôte à s'adapter à ce mécanisme par le développement d'un autre mode de mort cellulaire, la nécroptose (Humphries et al., 2015; Silke et al., 2015). La nécroptose peut également être induite par le TNF-α, lorsque les caspases, et plus particulièrement la caspase 8 sont inhibées et en présence de molécules appelées Second mitochondrial activator of caspases (Smac) mimétiques qui ont la capacité de bloquer les protéines "cellular inhibitor of apoptosis" (cIAP)1 et 2 et "X-linked Inhibitor of Apoptosis" (XIAP). Depuis, l'utilisation d'inhibiteurs chimiques et de souris knockout a permis d'associer la nécroptose à diverses pathologies. Ces observations expliquent également l'étroite relation entre l'apoptose et la nécroptose.

Bien qu'elle soit largement étudiée dans la signalisation du TNF-α, la nécroptose peut être activée par différents stimuli tels que l'activation des récepteurs de mort TRAIL et FasL, des TLR3 et 4, le récepteur des lymphocytes T, la voie des interférons, les stress génotoxique ou oxydatifs ou les DAI (pour "DNA-dependent activator of IFN regulatory factors") (Jouan-Lanhouet et al., 2014a). Selon le stimulus, les effecteurs induisant la nécroptose vont être différents mais converger à l'activation des protéines "Receptor Inducing Protein Kinase" (RIPK) 1 et 3 qui suite à leur phosphorylation vont former le nécrosome (appelé également nécroptosome) et activer des substrats tels que les protéines "Mixed Lineage Kinase Domain Like" (MLKL) et "Phosphoglycerate Mutase Family Member 5" (PGAM5) conduisant à la mort de la cellule (Liu et al., 2016). Bien que le rôle de PGAM5 dans l'activation de la nécroptose soit débattu, celui de MLKL est largement admis et sa phosphorylation en fait un marqueur de la nécroptose. L'activation de MLKL conduit à la formation d'un oligomère qui interagit avec la membrane plasmique et conduit à l'influx d'ions Ca^{2+} et de Na^{+} dans la cellule, entraînant une augmentation

de la pression osmotique et la rupture de la membrane (Cai et al., 2014; Chen et al., 2014). Les principaux médiateurs et les voies de signalisation conduisant au déclenchement de la nécroptose sont présentés dans la Figure 6. Morphologiquement, les cellules nécroptotiques présentent les mêmes caractéristiques que les cellules nécrotiques soit un gonflement du cytoplasme et des organelles suivi par une rupture de l'intégrité membranaire et la libération du contenu cytoplasmique dans le milieu extracellulaire (Vanden Berghe et al., 2015).

I.3.2.3. Outils pour l'étude des voies apoptotiques et nécroptotiques

L'apoptose, définie comme dépendante de la voie des caspases, peut donc être étudiée par l'utilisation d'inhibiteurs pan-caspases, tel que le Z-VAD-fmk ou le QVD-OPh ou par une délétion

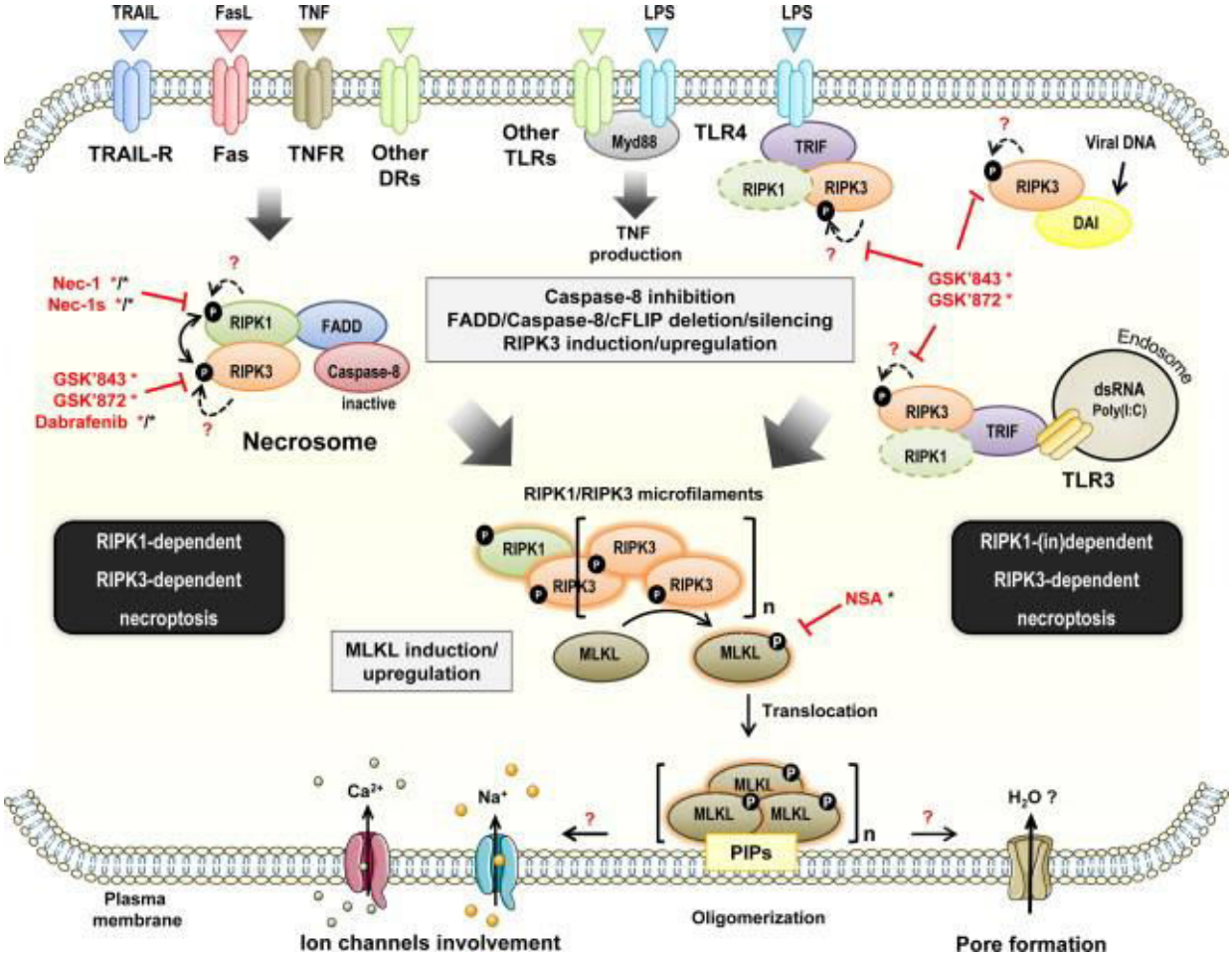

Figure 6. Voies de signalisation conduisant à l'activation de la nécroptose. *(Jouan-Lanhouet et al., 2014)*

des gènes codant pour la caspase 8 ou la caspase 3, les deux caspases effectrices conduisant à l'apoptose. L'activation de l'une ou de l'autre peut également être déterminée par l'identification de la protéine clivée par western-blot (WB), ou par immunohistochimie (IHC), ou par un test d'activité de ces caspases.

Due à sa plus récente identification, l'activation de la nécroptose est plus difficile a démontrer que l'apoptose mais les outils immunologiques et chimiques s'avèrent de plus en plus nombreux.

Tout d'abord, la surexpression des protéines RIPK1, RIPK3 ou MLKL ne constitue pas un marqueur suffisant pour démontrer l'activation de cette voie. De plus, alors que l'inhibition de la mort cellulaire lors de l'emploi des nécrostatines tels que le Nec-1 ou le Nec-1s pouvait être utilisé comme un marqueur de la nécroptose, ces inhibiteurs chimiques bloquant l'activité kinase de RIPK1 ne sont plus suffisants. Il est aujourd'hui admis que le blocage de la mort cellulaire par l'inhibition génétique de RIPK3 et plus particulièrement de MLKL ou le blocage de l'activité de RIPK3 peuvent permettre l'identification de la nécroptose. Cependant, aucun inhibiteur n'est encore disponible et fonctionnel pour bloquer l'activité kinase de RIPK3 chez la souris. Enfin, il a très récemment était mis au point un anticorps reconnaissant la protéine murine MLKL phosphorylée qui est considérée comme un marqueur de la nécroptose.

Cependant, il est important de noter que l'étude des voies de mort cellulaire est complexe, de par leur diversité mais également parce que l'inhibition d'une voie de RCD peut ne pas avoir de véritable effet protecteur mais conduire à l'activation d'une autre voie de mort cellulaire, dû au changement du statut biochimique de la cellule (Galluzzi et al., 2015). L'apoptose et la nécroptose partagent plusieurs protéines effectrices et l'inhibition d'une des voies peut donc conduire à l'activation de l'autre.

I.3.3. Mort cellulaire et inflammation.

Suite à l'hépatolyse, un ensemble de molécules chimiques tels que les DAMPs et les alarmines va être libéré dans le microenvironnement et contribuer à l'inflammation. Ces effecteurs vont alerter le système immunitaire d'un dommage. HMGB1 et l'IL-33 représentent deux alarmines classiques retrouvées au cours d'un dommage hépatique. La HMGB1 est une protéine nucléaire qui lors de sa libération dans le milieu extracellulaire va se fixer sur les TLR2 et TLR4 ainsi que sur le récepteur "Receptor for advanced glycation endoproducts" (RAGE) (Heymann and Tacke, 2016). Libérée par les cellules nécrotiques au cours de l'hépatite induite par l'acétaminophène, la HMGB1 active le recrutement des neutrophiles et amplifie le dommage hépatique (Huebener et al., 2015). L'IL-33 est une protéine nucléaire, membre de la famille de l'IL-1 et interagit avec un récepteur dimérique composé du ST2, spécifique à l'IL-33, et de "l'IL-1 receptor accessory protein" (IL-1RAcP). Exprimée au niveau basal par les cellules sinusoïdales hépatiques, l'IL-33 est produit par les hépatocytes dans certaines étiologies d'hépatite chez la souris et chez l'Homme (Arshad et al., 2012) et aurait un effet protecteur au cours de l'hépatite (Noel et al., 2016; Volarevic et al., 2012). Ces deux alarmines représentent deux exemples importants de molécules libérées au cours d'un dommage hépatique et qui contribue à la modulation de l'inflammation.

Après la présentation des différents modèles d'hépatite utilisés chez la souris, les voies de signalisation induites par l'activation des récepteurs présents sur l'hépatocyte seront décrites plus en détail.

I.4. Modèles d'hépatites chez la souris

L'utilisation des modèles d'hépatites animaux, majoritairement sur la souris, ont permis de mieux comprendre ces mécanismes de mort cellulaire au cours des maladies hépatiques. Nous caractérisons ici le type de modèle d'hépatite en fonction de l'agent induisant l'hépatolyse tel que hépatotoxique, métabolique ou dépendant du système immunitaire.

I.4.1. Modèles d'hépatite induit par un hépatotoxique

Chez l'humain, l'ingestion de certains champignons (amanite phalloïde), et l'excès de médicament (paracétamol), de certains produits chimiques tels que le tétrachlorure de carbone (CCl_4) ou la consommation chronique et abusive d'alcool peuvent entraîner une atteinte aiguë ou chronique du foie. Ces atteintes sont mimées par plusieurs modèles d'hépatites chez la souris et résultent principalement d'un stress oxydatif.

I.4.1.1. Hépatite induite par le paracétamol/acétaminophène

Le paracétamol et l'acétaminophène sont composés d'acetyl-para-aminophenol (APAP) dont une surdose conduit à une insuffisance hépatique aiguë chez l'Homme et la souris qui peut aller jusqu'à la mort (Dargan and Jones, 2002). La souris est le modèle le plus utilisé pour étudier l'effet d'une surdose d'APAP et reproduit la physiopathologie retrouvée chez l'Homme. Dans les hépatocytes, l'APAP est principalement métabolisé en une forme non toxique, mais une petite fraction se trouve transformée par le cytochrome P450 en N-acetyl-p-benzoquinone imine (NAPQI) (Dahlin et al., 1984; Mitchell et al., 1973) qui est détoxifié par la forme réduite du glutathion hépatique (GSH). Une forte accumulation de NAPQI entraine donc une diminution de la disponibilité du GSH et rend les hépatocytes sensibles au stress oxydatif (Malhi et al., 2010). De plus, en l'absence de GSH, le NAPQI va alors interagir avec des protéines mitochondriales, conduisant à une déplétion en ATP et un stress oxydatif déclenchant la mort des hépatocytes (Kaplowitz et al., 2015). Le rôle de la nécroptose dans la mort des hépatocytes induite par l'APAP est également débattu. Tout d'abord, l'observation de la phosphorylation de la MLKL dans le foie de patients atteints d'hépatite induite par les médicaments (DILI pour "Drug Induced Liver Injury") suggère le rôle de la nécroptose dans l'induction de l'hépatolyse et conduit à l'étude de cette voie (Wang et al., 2014). De plus, l'inhibition chimique de l'activité kinase de RIPK1 par les

nécrostatines (Dara et al., 2015; Deutsch et al., 2015; Takemoto et al., 2014) et la diminution de l'expression de RIPK3 (Ramachandran et al., 2013) ou de RIPK1 (Dara et al., 2015) par des siRNA réduisent l'hépatolyse induite par l'APAP chez la souris. Cependant, alors que Deutsch et al. ont montré que l'utilisation de souris déficientes en RIPK3 révélait une réduction de l'hépatolyse (Deutsch et al., 2015), Dara et al. ont démontré que la délétion génétique de RIPK3 ou MLKL ne permettait pas de protéger de l'hépatite induite par l'APAP (Dara et al., 2015). De plus, la déficience en RIPK1 spécifiquement dans les LPC n'était pas suffisante pour inhiber l'hépatolyse (Schneider et al., 2016). Des études plus précises sont donc nécessaires pour clarifier le rôle de la nécroptose dans ce modèle.

I.4.1.2. Hépatite induite par le CCl_4

Le tétrachlorure de carbone a largement été utilisé comme solvant industriel conduisant à la découverte de ses effets hépatotoxiques et carcinogènes chez l'Homme. L'intoxication au CCl_4 est aujourd'hui utilisé pour étudier certains effets hépatotoxiques (Weber et al., 2003) et comme modèle expérimental de fibrose hépatique (Iredale, 2007). L'ingestion par voie orale chez la souris de CCl_4 induit une hépatite aiguë ou chronique et s'avère dose-dépendante. La métabolisation du CCl_4 par les cytochromes conduit à la formation d'un radical trichloromethyl (CCl_3), provoquant la production d'espèces réactives de l'oxygène (ROS) qui initient une peroxydation lipidique affectant la perméabilité des organelles cellulaires et une mort cellulaire par nécrose (Weber et al., 2003). Bien que l'hépatolyse soit considérée comme accidentelle (nécrotique), elle induit la production de cytokines pro-inflammatoires telles que le TNF-α qui contribue au dommage du parenchyme (Sato et al., 2014).

I.4.1.2.3. Hépatite induite par l'alcool

Au niveau du foie, l'éthanol est principalement métabolisé en acétaldéhyde par trois systèmes enzymatiques : l'alcool déshydrogénase (ADH), les cytochromes (plus particulièrement la CYP2E1) et les catalases. L'acétaldéhyde va ensuite être métabolisé dans la mitochondrie en acétate par l'aldéhyde déshydrogénase. La métabolisation de l'éthanol va conduire à la formation de métabolites réactifs entraînant un stress oxydatif par la formation de ROS, une déplétion du GSH mitochondrial, un changement de l'équilibre redox et la mort cellulaire (Beier and McClain, 2010). La mort des hépatocytes a premièrement été décrite comme apoptotique (McVicker et al., 2007; Roychowdhury et al., 2012) et serait en partie induite par le stress oxydatif. Les ligands de mort TNF-α et FasL pourraient être également impliqués puisqu'il a été observé qu'ils étaient induits au cours des hépatites alcooliques (McVicker et al., 2007) et prennent part à l'hépatolyse car des souris déficientes en TNFR1 ou en Fas (CD95/ APO-1) sont protégées du dommage hépatique induit par une ingestion chronique d'alcool (Minagawa et al., 2004; Yin et al., 1999).

En parallèle de l'apoptose, des études récentes se sont intéressées à l'implication de la nécroptose dans l'hépatite induite par l'ingestion d'alcool. Ces travaux ont montré que la délétion génétique de RIPK3 conduisait à une réduction de l'hépatolyse (Roychowdhury et al., 2013; Wang et al., 2016).

I.4.2. Modèles d'hépatite immuno-induites

I.4.2.1. Hépatite induite par la Concanavaline A (ConA)

La ConA est une lectine, extraite du haricot *Canavalia brasiliensis*, qui lie les résidus mannose de différentes glycoprotéines. Suite à une injection chez la souris, son affinité pour les sinusoïdes hépatiques conduit à une activation des lymphocytes, des KC et des LSEC entraînant en quelques heures la libération massive de cytokines pro-inflammatoires, suivie par un recrutement des cellules immunitaires au niveau du foie. L'environnement inflammatoire produit par la ConA conduit à une hépatite aiguë avec un pic des ASAT/ALAT vers 10-12 h p.i. (Trautwein et al., 1998). Développé depuis les années 1990, ce modèle d'hépatite a largement été utilisé pour comprendre les mécanismes immunitaires, inflammatoires et de mort des hépatocytes au cours des hépatites immuno-induites (Tiegs et al., 1992). La libération de TNF-α et d'IFN-γ contribue à l'hépatolyse puisque leur blocage ou leur absence par l'utilisation de souris knockout protège du dommage hépatique (Gantner et al., 1995; Küsters et al., 1997; Mizuhara et al., 1994; Tagawa et al., 1997; Watanabe et al., 1996; Wolf et al., 2001). Bien que le rôle du TNF-α dans ce modèle soit encore discuté, l'IFN-γ intervient dans l'activation des cellules NKT.

Plusieurs travaux montrent que la mort des hépatocytes dans l'hépatite induite par la ConA est dépendante des lymphocytes T et plus particulièrement conduite par les cellules NKT (Kaneko et al., 2000; Takeda et al., 2000; Tiegs et al., 1992). Ces cellules tueraient les hépatocytes par différents mécanismes, à la fois via le système perforine/granzyme B (Arshad et al., 2012; Watanabe et al., 1996) mais aussi par la fixation des ligands de mort tels que FasL (Leist et al., 1996; Seino et al., 1997; Tagawa et al., 1997; Takeda et al., 2000) et TRAIL (Arshad et al., 2012; Beraza et al., 2009; Zheng et al., 2004) sur leur récepteurs respectifs, Fas et DR5, présents à la surface des hépatocytes. La signalisation conduisant à la mort des hépatocytes dans le modèle ConA est encore débattue. L'absence d'observation de cellules apoptotiques (caspase 8 ou 3 positives), d'activité caspase dans les foies des souris traitées avec la ConA, ainsi que l'absence de protection par le prétraitement avec un inhibiteur pan-caspases, ou encore l'utilisation de souris conditionnellement déficientes pour la caspase 8 dans les hépatocytes (Caspase8$^{Hepa\text{-}KO}$) (Jouan-Lanhouet et al., 2012; Künstle et al., 1999; Liedtke et al., 2011), suggèrent que l'hépatolyse serait indépendante des caspases et non apoptotique. Bien qu'il soit aujourd'hui admis l'existence de différents modes de mort cellulaire (voir précédemment), seule l'apoptose et la nécroptose seraient

activées par les récepteurs de mort, suggérant qu'au cours de l'hépatite induite par la ConA l'hépatolyse dépendrait de la nécroptose. Dans ce sens, l'utilisation d'un inhibiteur de l'activité de RIPK1, le Nec-1, a montré une protection de l'hépatolyse (Jouan-Lanhouet et al., 2012; Zhou et al., 2013a). En revanche, les études utilisant des souris RIPK3 KO ont révélé des résultats controversés (Deutsch et al., 2015; Kang et al., 2015; Weinlich et al., 2013) et l'une d'entre elle, décrivant une réduction de l'hépatolyse induite par la ConA, suggère une contribution de RIPK3 dans l'activation des cellules NKT (Kang et al., 2015).

I.4.2.2. Hépatite induite par les virus de l'hépatite murine (MHV)

Les virus de l'hépatite murine appartiennent à la famille des *coronaviridae* et sont responsables de désordres hépatiques et neurologiques chez la souris (Virelizier et al., 1975). Le MHV de type 3 (MHV3) est connu comme le plus virulent puisque son injection chez les souris de souche C57BL/6 conduit à une hépatite fulminante, caractérisée par plusieurs plages de nécrose dans le parenchyme hépatique 72 h post-injection et la mort des souris dans les 3 à 5 jours post-infection (Prévost et al., 1975). Comme les souris ne développent pas naturellement une hépatite lors de leur inoculation avec le VHB ou le VHC, l'infection par le MHV3 est donc considérée comme un bon modèle pour étudier les désordres inflammatoires induits par les virus au cours de l'hépatite aiguë (Lamontagne and Dupuy, 1984; Lamontagne et al., 1989). Le MHV3 présente un tropisme pour différentes cellules immunitaires et plus particulièrement pour les macrophages péritonéaux et hépatiques, les hépatocytes, les LSECs et les HSCs (Godfraind and Coutelier, 1998; Martin et al., 1994). Afin de comprendre les mécanismes inflammatoires provoqués par le MHV3, différents variants atténués ont été produits. Parmi eux, le MHV3 51.6 n'a pas la capacité de se répliquer dans les LSECs et provoque une mort retardée des souris, 5 à 9 jours après son inoculation (Martin et al., 1994). Le variant MHV-A59 est beaucoup moins virulent car il induit une hépatite modérée et se trouve contrôlé puis rapidement éliminé par le système immunitaire (Jacques et al., 2008).

Quelle que soit la souche, l'infection par le MHV passe par l'interaction de la protéine virale S avec le récepteur cellulaire CEACAM1a permettant son entrée dans la cellule par endocytose ou fusion (Godfraind and Coutelier, 1998; Godfraind et al., 1995). De plus, cette interaction serait responsable de la formation de larges syncitia qui caractérisent l'effet cytopathique du virus en déclenchant la fusion des cellules entre elles (Frana et al., 1985; Sturman et al., 1985), induisant leur mort cellulaire par l'activation de l'apoptose (Xu et al., 2014).

Les macrophages, les LSECs et les lymphocytes NK et NKT sont les principaux contributeurs de la réponse anti-virale contre le MHV3 par la libération de cytokines et de chimiokines. Cependant, la déplétion en macrophages ainsi que l'inhibition immunologique du TNF-α réduit l'hépatolyse, suggérant que la réponse inflammatoire aggrave l'hépatite induite par le MHV3 (Schindler et al., 1984; Xu et al., 2014; Yang et al., 2013).

I.4.2.3. Hépatite induite par l'injection de LPS et de D-GalN

L'injection de LPS mène à l'activation du TLR4, présent majoritairement sur la membrane des KC et conduit à une libération rapide et massive de cytokines telles que le TNF-α, l'IL-6 et l'IL-10. L'injection seule de LPS n'est pas suffisante pour induire un dommage hépatique mais une dose trop importante peut entraîner la mort des souris par choc septique (Galanos et al., 1979). La D-Galactosamine (D-GalN) est un hépatotoxique, métabolisé uniquement par les hépatocytes, qui va conduire à une déplétion en uridine et une inhibition de la transcription (Decker and Keppler, 1974). Dans ce contexte, le TNF-α induit par le LPS va se fixer sur son récepteur TNFR1 présent à la surface de l'hépatocyte et conduire à l'activation du complexe II, à l'activation de la caspase 8 et à l'apoptose des cellules conduisant à un dommage aigu du tissu hépatique quelques heures après l'injection (Galanos et al., 1979; Liedtke et al., 2011; Wroblewski et al., 2016). Tout comme pour le LPS, les administrations de polyinosine-polycytidylique [poly(I:C)] ou d'ADN cytosine-phosphate guanine (CpG) qui miment respectivement l'ADN viral et l'ADN bactérien, conduisent à la production de TNF-α qui déclenche une hépatite aiguë lorsque les souris sont traitées avec la D-GalN (Dejager and Libert, 2008).

I.4.2.4. Hépatite induite par l'injection de poly(I:C)

Le poly(I:C) est un analogue de l'ARN double brin, et s'utilise pour mimer certains mécanismes retrouvés au cours d'une infection virale. Il est reconnu par le TLR3 (Alexopoulou et al., 2001) ainsi que par les protéines cytoplasmiques "RNA helicase retinoic acid inducible gene I" (RIGI) (Yoneyama et al., 2004) et "Melanoma differentiation-associate Gene 5" (Mda5) (Kato et al., 2006) et va activer un ensemble de cellules immunitaires, tels les macrophages et les cellules NK, et induire la production de cytokines parmi lesquelles le TNF-α, l'IFN-γ, l'IL-6 et l'IL-12 ainsi que les IFN de type 1 (IFN-α et IFN-β) jouent un rôle clef dans la réponse inflammatoire anti-virale (Alexopoulou et al., 2001; Dejager and Libert, 2008; Schwabe et al., 2006). L'activation du TLR3 par le poly(I:C) active la protéine "Toll-IL-1 receptor (TIR) domain-containing adapter inducing IFN-β" (TRIF), puis le facteur de transcription IRF3 ainsi que la voie NF-κB, conduisant à la production d'IL-12, et de TNF-α (Alexopoulou et al., 2001; Kumar et al., 2008). En parallèle, la fixation du poly(I:C) sur les RIG1 et Mda5 active la protéine "IFN-β Promoter Stimulator 1" (IPS-1) entraînant la production des IFN-α et β ainsi que d'IL-6 (Kumar et al., 2008). L'injection de poly(I:C) induit une faible hépatolyse largement aggravée sous la dépendance du TNF-α en présence de D-GalN (Dejager and Libert, 2008).

I.4.2.5. Hépatite induite par l'α-GalCer

L'α-GalCer est un glycolipide, initialement isolé de l'éponge marine (*Agelas mauritianus*), qui active spécifiquement les cellules iNKT par sa présentation sur le CD1d (Kawano et al., 1997; Natori et al., 1993) et induit une hépatite aiguë absente chez des souris déficientes en cellules NKT ou iNKT (Cao et al., 2010; Osman et al., 2000). Suite à l'injection d'α-GalCer, les cellules NKT vont rapidement être activées et éliminées par l'induction de leur propre apoptose qui est concomitante avec la mort des hépatocytes (Osman et al., 2000; Subramanian et al., 2014). L'activation des cellules iNKT est associée à la production rapide de nombreuses cytokines de types Th1 et Th2 telles que le TNF-α, l'IFN-γ, l'IL-12, l'IL-2, l'IL-4 et l'IL-6 et à l'activation des autres cellules de l'immunité (Biburger and Tiegs, 2005; Van Kaer, 2005). Cette hépatite serait dépendante du FasL et du TNF-α mais indépendante de l'IFN-γ, des KC et des cellules NK. En effet, le FasL est surexprimé à la surface des lymphocytes NKT activés quelques heures après l'injection d'α-GalCer (Subramanian et al., 2014). De plus, son inhibition par des anticorps ainsi que celle du TNF-α protègent de l'hépatite (Biburger and Tiegs, 2005; Nakashima et al., 2008). Cependant la délétion des KC ou des cellules NK ainsi que le blocage de l'IFN-γ n'interfèrent pas dans l'induction de l'hépatolyse induite par l'α-GalCer (Biburger and Tiegs, 2005; Nakashima et al., 2008). Le mode de mort cellulaire a été peu étudié dans ce modèle et bien qu'une corrélation entre l'activité caspase 3 et l'élévation des transaminases hépatiques sériques ait été observée, le prétraitement des souris avec un inhibiteur pan-caspase avant l'injection d' α-GalCer ne permet pas de protéger du dommage hépatique (Biburger and Tiegs, 2005).

Tableau 4. Cellules et protéines effectrices de la mort cellulaire et voies de mort cellulaire régulées dans les différents modèles d'hépatites murines.

Modèle	Cellules, métabolites et protéines effectrices de la mort cellulaire	Mort cellulaire	Références
APAP	Formation NAPQI, déplétion glutathion, production de ROS	Nécrose médié par la MOMP Necroptose ?	Dara et al., 2015; Kaplowitz et al., 2015
Alcool	Déplétion en glutathion, production de ROS FasL et TNF-α	Nécrose médié par la MOMP Apoptosis Necroptose	McVicker et al., 2007; Roychowdhury et al., 2013; Wang et al., 2016
CCl_4	CCl4 transformé en CCl3, production de ROS	Nécrose	Weber, 2003
ConA	NKT et KC IFN-γ, TNF-α, FasL, TRAIL	Caspase indépendant Necroptose ?	Deutsch, 2015 ; Jouan-Lanhouet ; 2012, Kang, 2015 ; Liedtke, 2011
MHV3	Virus cytolytique, FasL, TNF-α	Apoptose	Xu, 2014 ; Yang, 2013
Alpha-GalCer	NKT TNF-α, FasL	Apoptose ? Autres ?	Biburger, 2005 ; Subramanian, 2014 ; Nakashima, 2008
PolyIC/D-GalN	TLR3, TNF-α	Apoptose ?	Dejager and Libert, 2008
CpG/D-GalN	TLR9, TNF-α	Apoptose ?	Dejager and Libert, 2008
LPS/DGalN	KC/TLR4 TNF-α	Apoptose	Dejager, 2008 ; Liedtke, 2011

I.5. Mécanismes moléculaires de l'hépatolyse induite par les membres de la superfamille du TNF-α

La superfamille du TNF regroupe 19 membres capables d'activer 29 récepteurs (Aggarwal, 2003) dont, parmi les plus étudiés, le TNF-α, le FasL et le TRAIL qui sont connus comme étant de puissants inducteurs de la mort cellulaire et responsables de l'hépatolyse induite par les cellules immunitaires (principalement par les KC et les lymphocytes T CD8+, NK et NKT). Cette mort cellulaire survient lors des hépatites auto-immunes, des hépatites virales, mais peut également aggraver une hépatite préexistante par l'amplification de l'inflammation et de l'hépatolyse (Brenner et al., 2013).

I.5.1. Le TNF-α

Le TNF-α a premièrement été décrit comme induisant la nécrose de cellules tumorales mais il a depuis été révélé pouvant agir comme une cytokine pro-inflammatoire maitresse avec d'importantes fonctions pléiotropiques. Exprimé principalement par les KC et les LT au cours d'une infection ou en réponse à des produits bactériens tels que le LPS, le TNF-α est tout d'abord produit comme une protéine transmembranaire (tm-TNF) qui peut être libérée sous une forme soluble (s-TNF) après clivage par la "TNF-converting enzyme" (TACE) (Black et al., 1997). Le TNF-α peut interagir avec deux récepteurs : le TNFR1, constitutivement exprimé dans la plupart des tissus, ou le TNFR2 qui est hautement régulé, se trouve à la surface des cellules immunitaires et qui est activé uniquement par la forme transmembranaire (Wajant et al., 2003). Le TNFR1 joue un rôle prédominant dans le foie (Liedtke and Trautwein, 2012). Finement régulé à différents niveaux, la signalisation du TNFR1 est complexe et dépendante de la cellule cible (l'activation au niveau de l'hépatocyte ou de la cellule immunitaire n'induira pas les mêmes réponses), du stade de la pathologie (avant ou après l'induction de l'hépatolyse par exemple) mais également dépendant des autres signaux reçus par la cellule et qui vont influencer son comportement. Ces différents facteurs expliquent les effets pléiotropiques du TNF-α qui est capable d'induire la survie cellulaire par l'induction de protéines anti-apoptotiques, l'inflammation par l'induction de cytokines, chimiokines et de molécules d'adhésion, la prolifération de la cellule ou la mort cellulaire par apoptose ou nécroptose. Depuis les dix dernières années, l'utilisation des souris conditionnellement déficientes a largement permis de mieux comprendre la signalisation du TNF-α au niveau hépatique.

Au niveau de la membrane de l'hépatocyte, l'interaction du TNF-α avec le TNFR1 conduit à la formation du complexe I composé des protéines "TNFR1-Associated Death Domain" (TRADD), RIPK1 et des E3 ubiquitine ligase "TNFR Associated Factor 2" (TRAF2), "Cellular Inhibitor of

Apoptosis Protein" 1 (cIAP1) et 2 (cIAP2). Ces dernières vont ubiquitinyler (par des chaines d'ubiquitines liées au niveau de la lysine 63 [K63-linked chain]) plusieurs protéines au niveau de ce complexe, tel que RIPK1. Ce réseau de chaines de polyubiquitine régule finement l'assemblage du complexe et permet le recrutement des protéines "Linear Ubiquitin Chain Assembly Complex" (LUBAC), "TGF-β Activated Kinase 1" (TAK1) lié à ses protéines adaptatrices TAB1 et TAB2, ainsi qu'au recrutement du complexe "Inhibitor of NF-κB kinase" (IKK) composé des protéines IKK-α, IKK-β et IKK-γ/NEMO. L'ensemble de ces protéines va permettre l'activation des voies "Mitogen Activated Kinases" (MAPK) et NF-κB. Cette dernière est régulée par le complexe IKK qui, suite à son activation, phosphoryle la protéine "Inhibitor of κB-alpha" (IκBα), induisant son ubiquitinylation et sa dégradation par le protéasome. La protéine IκBα a pour rôle de séquestrer l'hétérodimère p50/p65 NF-κB dans le cytoplasme. Son élimination conduit ainsi à la translocation de NF-κB dans le noyau, lui permettant d'induire de nombreux gènes cibles impliqués dans l'inflammation (cytokines et chimiokines) ainsi que dans l'inhibition de l'apoptose, telles les protéines "cellular FLICE like Inhibitory protein" (cFLIP [FLICE désigne la caspase 8]) ou Bcl2 (Liedtke and Trautwein, 2012; Ofengeim and Yuan, 2013; Ting and Bertrand, 2016). Cette dynamique va être rapidement réprimée par les déubiquitinylases A20 et "Cylindromatosis" (CYLD) (Ting and Bertrand, 2016) (**Figure 7**).

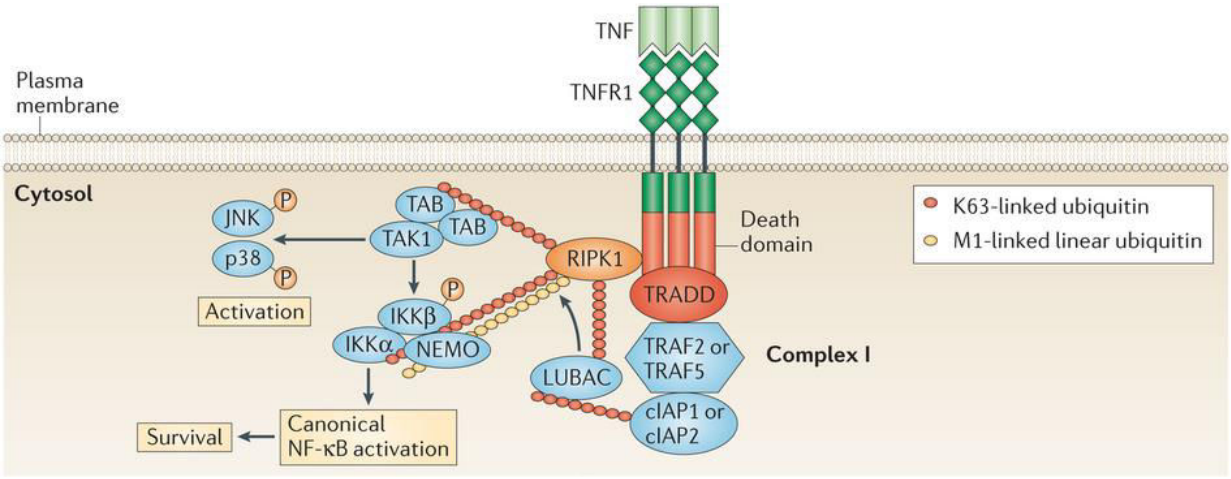

Figure 7. Formation du complexe I suite à l'activation du TNFR1 (issu de Brenner et al., 2015)

Dans certaines conditions, le complexe I peut être internalisé et conduire à la formation du complexe IIa composé des protéines TRADD, "FAS Associated Death Domain" (FADD) caspase 8, IIb (appelé également ripoptosome) composé des protéines FADD, caspase 8, cFLIP, RIPK1 et RIPK3 ou du nécrosome caractérisé par les protéines RIPK1, RIPK3 et MLKL. La formation des complexes IIa et IIb déclenche l'apoptose alors que l'activation du nécrosome va conduire à la nécroptose de la cellule. Parallèlement à ces complexes, les protéines TRADD et TRAF2 peuvent activer la voie "c-Jun N-terminal kinases" (JNK) menant à l'activation de l'apoptose. Les

mécanismes conduisant à la phosphorylation de JNK1 et JNK2, et donc leur activation, sont encore peu connus et feraient intervenir les protéines "Apoptosis Signal Related Kinase" (ASK1) et les MAPK MKK4 et MKK7 (Liedtke and Trautwein, 2012). L'activation de JNK1 déclencherait la dégradation de cFLIP et celle de JNK2 activerait la caspase 8, ces deux voies permettant l'induction de l'apoptose (Schwabe and Brenner, 2006) (**Figure 8**).

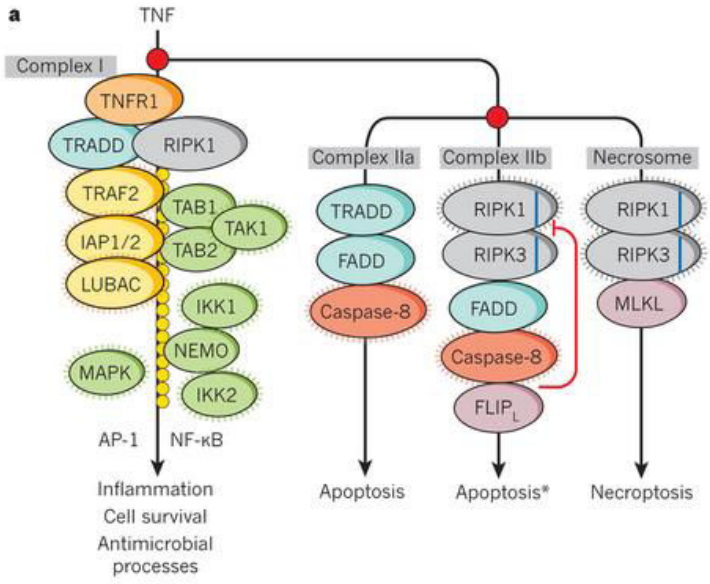

Figure 8. Schéma représentant les protéines principales formant les complexes I, IIa, IIb ou le nécrosome suite à la fixation du TNF-α sur le TNFR1 *(issu de Pasparakis et Vandenabeele, Nature, 2015).*

Dans la majorité des types cellulaires, incluant les hépatocytes, l'activation du TNFR1 entraîne la survie de la cellule et les conditions conduisant à l'induction des complexes IIa et IIb sont encore débattues. Des études suggèrent qu'une production trop faible de protéines anti-apoptotiques par le complexe I favoriserait l'induction de l'hépatolyse (Zhang et al., 2010). Physiologiquement, cette faible expression pourrait résulter d'une inhibition de l'activité NF-κB observée dans certaines étiologies d'hépatites. Les causes sont encore débattues mais plusieurs études suggèrent qu'un haut niveau de ROS pourrait conduire à cette inhibition (Han et al., 2009). En l'absence d'activité NF-κB, le TNF-α conduirait à l'activation de la voie JNK qui, lorsqu'elle est persistante, favoriserait l'activation de l'apoptose (Schwabe and Brenner, 2006). L'oxydation des phosphatases, dans des conditions de stress oxydatif (production de ROS), inhiberait la déphosphorylation des protéines JNK conduisant au maintien de son activation et à l'induction de l'apoptose (Kamata et al., 2005). Des études *in vitro* ont permis de montrer que les protéines cIAP1/2 ont un rôle majeur dans la survie de la cellule dépendante du TNF-α. En effet, leur inhibition par des molécules pharmacologiques telles que les « *Smac-mimétic* », induit la formation du complexe IIb et donc l'apoptose. L'addition d'un inhibiteur pan-caspase ne bloque pas la mort de la cellule mais conduit à la formation du nécrosome et une mort nécroptotique. Deux études

récentes ont montré que l'inhibition chimique des IAPs par les *Smac mimetic* ou la délétion génétique des protéines cIAP1/2 (souris cIAP1^{LPC-KO}/cIAP2$^{-/-}$) augmente l'élimination du VHB en augmentant la mort des hépatocytes médiée par le TNF-α, démontrant que ces protéines protègent de l'hépatolyse tout en contribuant à la persistance de l'infection par le VHB (Ebert et al., 2015a, 2015b).

La compréhension de la signalisation du TNF-α permet de comprendre pourquoi son injection, n'induit pas la mort des hépatocytes, puisqu'il active préférentiellement la voie NF-κB (Chaisson et al., 2002) et donc la survie de la cellule. Par contre, l'inhibition spécifique de la transcription hépatocytaire par la D-GalN sensibilise les hépatocytes à l'apoptose induite par le TNF-α (Decker and Keppler, 1974) par le blocage de l'expression des protéines anti-apoptotiques induites par NF-κB (Maeda et al., 2003). De plus, plusieurs travaux ont montré que la délétion génétique de plusieurs effecteurs tels que NEMO, TAK1 ou p65/RelA, spécifiquement dans les LPC, sensibilise à l'hépatolyse induite par le TNF-α dans plusieurs modèles d'hépatite aiguë, via une inhibition de l'activation de la voie NF-κB (Tableau 5). Cependant, une simple délétion de NEMO ou de TAK1 dans les LPC (respectivement NEMO^{LPC-KO} et TAK1^{LPC-KO}) conduit à une hépatolyse spontanée suivie d'une stéatohépatite et d'un CHC (Bettermann et al., 2010; Luedde et al., 2007). Ce phénotype n'est pas retrouvé chez les souris RelA^{LPC-KO} (Geisler et al., 2007) ce qui suggère que ces protéines sont impliquées dans d'autres voies que celles conduisant à l'activation de NF-κB. Ces observations sont aussi supportées par les travaux d'Inokuchi et al. qui ont montré que TAK1 avait un important rôle dans la régulation du métabolisme et de l'autophagie et que sa délétion génétique conduit à une stéatohépatite suite à une inhibition de l'autophagie (Inokuchi-Shimizu et al., 2014). En revanche, toutes ces études mettent en évidence le rôle majeur de la régulation de la voie du TNF-α au sein des hépatocytes pour le maintien de l'homéostasie hépatique.

Lors d'hépatites induites par différents facteurs étiologiques chez l'Homme, des niveaux sériques de TNF-α et de la forme soluble du TNFR1 ont été retrouvés positivement corrélés à la gravité de la pathologie (Marinos et al., 1995; Nagaki et al., 2000; Tokushige et al., 2000; Trebicka et al., 2011). De plus, son inhibition par des anticorps ou génétique a permis de protéger de l'hépatolyse, tel qu'observé dans différents modèles d'hépatites dépendantes de l'immunité, comme celles induites par la ConA (Gantner et al., 1995; Küsters et al., 1997; Mizuhara et al., 1994; Seino et al., 1997; Trautwein et al., 1998), par le MHV3 (Xu et al., 2014; Yang et al., 2013), par le LPS/D-GalN (Olleros et al., 2010; Wroblewski et al., 2016), par l'α-GalCer (Biburger and Tiegs, 2005; Nakashima et al., 2008) ou par le VHB ou le VHC chez des souris humanisées (Chyuan et al., 2015; Sekiguchi et al., 2012).

Tableau 5. Etude des protéines impliquées dans la voie NF-κB au cours de l'hépatite par l'utilisation de souris conditionnellement déficientes.

Protéines	Déficience	Hépatolyse basale	Hépatolyse induite (comparaison avec WT)	Références
TNFR1	LPC-KO	Non	ConA : pas de différence TNF-α /D-GalN : protection	Wroblewski, 2016
	TC-KO	Non	ConA : pas de différence	Wroblewski, 2016
	EC-KO	Non	ConA : pas de différence	Wroblewski, 2016
	MDC-KO	Non	ConA : protection	Wroblewski, 2016
NEMO/ IKK-γ/ IKK1	LPC-KO Hepa-KO	oui et développement d'un CHC à 6-12 mois	LPS : aggravée TNF-α : aggravée ConA : aggravée	Luedde, 2007 Beraza, 2007 Beraza, 2009 Ehlker, 2014
Mécanismes	Hépatolyse induite par une inhibition de la voie NF-κB hépatocytaire et diminution de l'expression protéines anti-apoptotiques Bcl2 et cFLIP Suractivation et prolongement de l'activité JNK Hépatolyse induite et spontanée caspase dépendante Hépatolyse spontanée partiellement dépendante du TNFR1 et de FADD			
IKK-β/ IKK2	Hepa-KO	Non	LPS : pas de différence TNF-α : pas de différence ConA : pas de différence	Maeda, 2005
Remarques	Contrairement aux $NEMO^{LPC-KO}$ pas d'inhibition de la voie NF-κB			
TAK1	LPC-KO	Oui + CHC et cholestase à 6 semaines	LPS : aggravée	Inokuchi, 2014 Bettermann, 2010 Vucur, 2013 Morioka, 2014
Mécanismes	Inhibition de la voie NF-κB Hépatolyse induite et spontanée dépendante de la caspase 8 mais indépendante de RIPK3 (sauf quand caspase 8 est bloquée) Hépatolyse spontanée partiellement dépendante du TNFR1			
RelA /p65	LPC-KO	Non	LPS : aggravée TNF-α : aggravée	Geisler, 2007
Mécanismes	Hépatolyse induite par une inhibition de la voie NF-κB hépatocytaire et une diminution de l'expression de cFLIP Hépatolyse dépendante du stress oxydatif et de l'activation de JNK			
FLIP	Hepa-KO	Non	D/GalN : aggravée ConA : aggravée	Schattenberg, 2011

Abréviations : LPC : Liver Parenchymal Cells, TC : T-cells ; EC : Endothelial Cells ; MDC : Cellules myéloïdes ; Hepa : Hepatocytes.

Par conséquent, en fonction du microenvironnement inflammatoire hépatique, ces différents résultats supportent le rôle du TNF-α dans l'induction ou l'amplification de l'hépatolyse. Bien qu'il soit largement admis que, dans des conditions physiologiques, le TNF-α favorise l'induction de la survie de l'hépatocyte, son rôle est en revanche débattu dans des conditions d'hépatite, où les hépatocytes se situent dans un microenvironnement inflammatoire qui peut conduire à une modification dans l'induction des voies de signalisation. De plus, l'activation de la voie NF-κB par le TNF-α conduit également à une réponse pro-inflammatoire qui peut donc amplifier l'inflammation déjà sous-jacente dans le foie et par conséquent amplifier la destruction du parenchyme hépatique. Ainsi, selon la nature des facteurs étiologiques de l'hépatite, le TNF-α pourrait être un facteur aggravant de l'hépatolyse, de manière directe sur l'hépatocyte, ou indirecte en promouvant l'amplification de l'inflammation.

Des travaux étayent la première hypothèse en suggérant que le stress oxydatif induirait une réduction de l'activation de la voie NF-κB, ainsi qu'une activation soutenue de la voie JNK,

lesquels conduiraient mutuellement à l'induction de l'apoptose de l'hépatocyte par le TNF-α (Han et al., 2009). De plus, dans le modèle d'hépatite induite par la D-GalN et le LPS, l'absence du TNFR1 spécifiquement dans les LPC protège complétement de l'hépatolyse. Dans ce modèle de souris TNFR1^{LPC-KO}, le blocage de la transcription conduit à la formation du complexe IIa par le TNF-α et l'apoptose (Wroblewski et al., 2016). Cependant, cette même souche de souris n'est pas protégée de l'hépatite à ConA. En revanche, la déficience spécifique du TNFR1 dans les cellules myéloïdes (MDC), protège ces souris de l'hépatolyse induite par la ConA (Wroblewski et al., 2016). Ces données démontrent qu'au cours de l'hépatite induite par la ConA, le TNF-α agirait de manière indirecte dans l'induction de l'hépatolyse en permettant la mise en place d'un microenvironnement inflammatoire.

I.5.2. FasL

Le FasL est une protéine transmembranaire qui, suite à son clivage, peut être libéré sous forme soluble. Ces deux formes de FasL (membranaire et soluble) peuvent interagir avec le récepteur Fas présent à la surface des cellules cibles, conduisant à sa trimérisation et l'induction de l'apoptose. Cependant, la forme soluble serait beaucoup moins active que la forme membranaire et nécessiterait donc un certain niveau d'agrégation pour induire un signal (Huang et al., 1999; Schneider et al., 1998). Dans le foie, le FasL est principalement exprimé par les lymphocytes T cytolytiques, les cellules NK et NKT et régulé positivement au cours de l'hépatite. Des niveaux élevés de FasL solubles ont été retrouvés chez des patients atteints d'hépatites virales ou auto-immunes suggérant son rôle dans la mort des hépatocytes au cours de ces hépatopathies. Le FasL interagit avec son récepteur Fas, constitutivement exprimé au niveau des hépatocytes et des LSEC (Luedde et al., 2002) et chez la souris, l'injection d'anticorps agonistes de Fas (Ogasawara et al., 1993), ou de FasL (Huang et al., 1999) a conduit à une mort massive des hépatocytes et des LSEC provoquant une hépatite fulminante et une hémorragie, pouvant entraîner, selon la dose injectée, à la mort de l'animal. (Huang et al., 1999; Ogasawara et al., 1993; Wanner et al., 1999). Ce modèle a largement été utilisé pour étudier les mécanismes de l'hépatolyse induite par Fas au cours de l'hépatite.

L'activation de Fas conduit au recrutement du DISC, composé de FADD, de la caspase 8 et de cFLIP, entraînant l'activation de l'auto-protéolyse de la caspase 8. Le niveau de caspase 8 clivée ainsi que la force du signal induite par le récepteur Fas va réguler l'activation ou non de l'apoptose. En effet, bien que les hépatocytes soient considérés comme des cellules de type II, une forte activation du Fas, par exemple via l'utilisation du MegaFasL (un FasL hexamérique), conduit directement à l'activation de la voie extrinsèque de l'apoptose et à la mort des cellules, sans une amplification par la voie intrinsèque. Par ailleurs, alors que des souris déficientes en Bid sont

protégées de l'hépatite induite par l'agoniste de Fas, l'anticorps monoclonal Jo2 (mAb-Jo2), elles présentent la même sensibilité que leurs homologues sauvages (WT) suite à une injection du MegaFasL, (Schüngel et al., 2009). L'activation de cette voie intrinsèque par cet agoniste serait modulée par la protéine XIAP puisque, chez des souris knockout pour Bid, l'ajout d'une déficience en XIAP les resensibilise à l'hépatite (Jost et al., 2009). Les membres de la famille Bcl2 vont réguler l'activation de l'apoptose par Fas. En effet, une surexpression des protéines Bcl2 (Lacronique et al., 1996; Rodriguez et al., 1996), Bcl-xL (Kanda et al., 2002) et Mcl-1 (Chen et al., 2015) chez la souris va protéger ou retarder l'apoptose hépatocytaire et les dommages dans le parenchyme hépatique. De plus, la délétion de MCl-1 spécifiquement dans les hépatocytes conduit à une apoptose spontanée, à la formation de fibrose chez des souris âgées de 10 semaines, et les sensibilisent à l'hépatite induite par la ConA ou le FasL (Vick et al., 2009). La protéine cFLIP aurait également un rôle important dans la régulation de l'apoptose induite par le FasL. En effet, les souris conditionnellement déficientes en cFLIP dans les hépatocytes sont plus sensibles à l'hépatite dépendante de FasL (Schattenberg et al., 2011). Cette protection serait induite par la forme longue de cFLIP ($cFLIP_L$). Ainsi, la régulation de cFLIP au niveau post-transcriptionnel conduit à la formation des isoformes $cFLIP_L$, $cFLIP_S$ et $cFLIP_R$ (chez la souris, seules les formes L et R sont exprimées) (Tsuchiya et al., 2015). La similarité entre les protéines cFLIP et la pro-caspase 8 leur permet d'interagir entre elles. Cependant, l'absence de domaine catalytique au sein de la protéine cFLIP en fait donc un inhibiteur de l'apoptose en entrant en compétition avec les pro-caspase 8 de la cellule. Toutefois, dans la signalisation du TNF-α, les niveaux d'expression des isoformes de cFLIP réguleraient l'activation de l'apoptose. En effet, la forme longue préviendrait la formation du complexe IIb alors qu'une surexpression de la forme S et potentiellement R faciliterait sa formation (Brenner et al., 2015; Nagaki et al., 2000). Récemment, une étude a montré un différentiel dans l'expression de la forme $cFLIP_L$ entre les souris de souche C57BL/6 et MSM/Ms : ces dernières, résistantes à l'hépatite induite par le FasL, présentaient des niveaux de $cFLIP_L$ plus élevés que les souris C57BL/6 qui exprimaient plus favorablement la forme $cFLIP_R$ (Ram et al., 2016). De plus, les souris conditionnellement déficientes en cFLIP dans les hépatocytes étaient plus sensibles à l'hépatite dépendante de FasL (Schattenberg et al., 2011).

I.5.3. TRAIL

Le TRAIL est principalement exprimé à la surface des cellules de l'immunité innée telles que les cellules NK et NKT, les DC et les KC. Cependant, le TRAIL peut être exprimé sur la plupart des cellules après une activation par des cytokines pro-inflammatoires telles que le TNF-α et les interférons (Saitou et al., 2005). Ce ligand de mort peut interagir avec 5 récepteurs : TRAIL-R1/DR4, TRAIL-R2/DR5, TRAIL-R3/DcR1, TRAIL-R4/DcR2 et "Osteoprotegerin" (OPG)

(LeBlanc and Ashkenazi, 2003). Néanmoins, seuls DR4 et DR5 contiennent un domaine de mort (DD pour "Death Domain") et peuvent induire la mort de la cellule. Contrairement à l'Homme, seule la forme DR5 est exprimée chez la souris (Wu et al., 1999). Initialement moins étudié que le FasL et le TNF-α, TRAIL a gagné de l'intérêt dans les études s'intéressant aux traitements contre le cancer. En effet, ce ligand a la particularité de pouvoir induire sélectivement la mort de différentes cellules tumorales ou transformées mais pas la plupart des cellules normales telles que les hépatocytes. En accord avec ces données, l'injection de TRAIL chez la souris, contrairement à un agoniste de Fas, n'induit pas d'hépatolyse (Walczak et al., 1999). Cependant l'infection par le VHB *in vivo* et *in vitro* sensibilise les hépatocytes à l'apoptose induite par TRAIL (Liang et al., 2007; Mundt et al., 2003). Cette sensibilité s'expliquerait par une modulation de l'expression des protéines impliquées dans la voie de signalisation de TRAIL. En effet, les protéines DR4 et DR5, ainsi que TRAIL ont été montrées comme surexprimées dans des conditions inflammatoires et d'infections par le VHB ou le VHC (Janssen et al., 2003; Liu et al., 2007; Mundt et al., 2003; Saitou et al., 2005). De plus, la protéine virale Hbx, exprimée par le VHB, s'est avérée capable de déréguler les voies intracellulaires, notamment par une surexpression des protéines Bax (Liang et al., 2007)et A20 (Zhang et al., 2015) et une sous-expression des protéines cIAP et cFLIP, ce qui déclencherait une mort dépendante de TRAIL (Shepard and Badley, 2009).

La présence de TRAIL soluble ainsi que la surexpression de ses récepteurs chez des patients infectés par le VHB ou le VHC suggèrent son implication au cours de l'hépatite virale. De même au cours de l'hépatite à ConA, les protéines TRAIL et DR5 sont rapidement surexprimées et le blocage de la signalisation de TRAIL, par l'utilisation d'un récepteur soluble ou de souris déficientes pour TRAIL, permettent de réduire l'hépatolyse induite par la ConA (Arshad et al., 2012; Zheng et al., 2004) ou celle induite lors de l'infection par le VHB de souris humanisées (Liang et al., 2007). De plus, la réduction de l'hépatolyse suite à une déficience en cellules NKT au cours de l'hépatite à ConA peut être restaurée par l'injection de TRAIL recombinante (Arshad et al., 2012). Les mécanismes conduisant à une sensibilité des cellules cancéreuses ou transformées mais non à celle des cellules primaires, dans des conditions physiologiques, sont peu connues. Cependant, ces données montrent que l'environnement pro-inflammatoire induit par le VHB ou le VHC ou encore par la ConA permet de promouvoir cette sensibilité. De plus, des études ont montré que les souris déficientes en TRAIL étaient protégées de l'hépatite induite par le FasL. TRAIL permettrait d'amplifier le signal induit par Fas grâce à l'activation de JNK et Bim (Corazza et al., 2006).

I.6. RIPK1 et PARP1/2

I.6.1. Travaux antérieurs de l'équipe

En 2012, Jouan-Lanhouet et al. ont montré que dans le modèle d'hépatite à ConA, où l'hépatolyse est essentiellement dépendante des récepteurs de mort, le prétraitement des souris avec le Nec-1, un inhibiteur de l'activité de RIPK1, ou avec le PJ-34, un inhibiteur de l'activité de polyADPribolsylation (PAR) des protéines PARP1 et 2, réduisait fortement l'hépatolyse. De plus, les auteurs ont montré que ces inhibiteurs chimiques ne semblaient pas inhiber l'environnement inflammatoire induit par la ConA puisque aucune différence n'avait été observée entre les groupes traités et non traités au niveau de l'induction des gènes et de la libération sérique des cytokines inflammatoires tels que le TNF-α, l'IFN-γet l'IL-1β , ni dans l'activation et le recrutement des cellules immunitaires au niveau hépatique (Arshad et al., 2015; Jouan-Lanhouet et al., 2012). Ces données suggéraient donc que l'activité enzymatique des protéines RIPK1 et PARP1/2 joueraient un rôle clef au cours de l'hépatite induite par la ConA.

I.6.2. Caractéristiques et rôles généraux de la protéine RIPK1

I.6.2.1. Caractéristiques moléculaires de RIPK1

La protéine RIPK1 appartient à une famille d'enzymes contenant 7 membres dont le domaine kinase (KD) est la signature de cette famille (Zhang et al., 2010). En plus de son domaine kinase en N-terminal, RIPK1 présente différents modules, tel qu'un DD en C-terminal, un "RIP Homotypic Interaction Motif" (RHIM) et un "Intermediate Domain" (ID) (**Figure 9**).

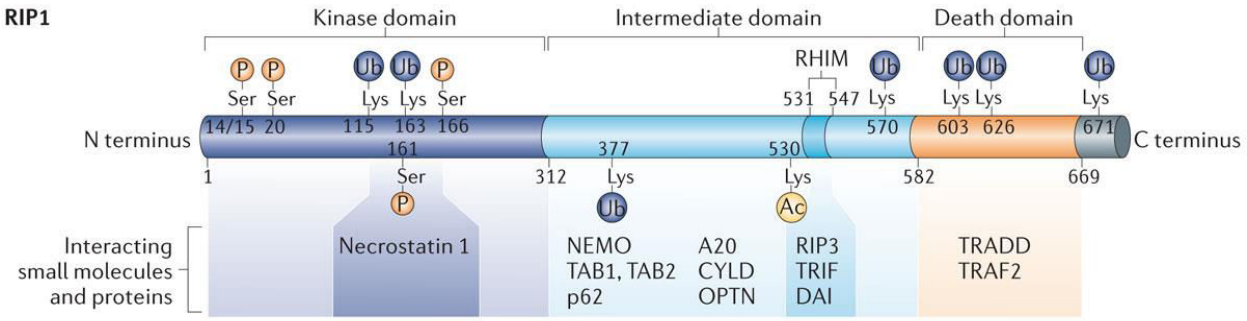

Figure 9. Domaines et modifications post-traductionnelles de RIPK1 *(issu d' Ofengeim and Yuan, 2013).*

En plus de présenter une activité kinase, RIPK1 va interagir, via ses domaines, avec de nombreuses protéines et permettre, selon l'environnement cellulaire, l'activation de la voie NF-κB par sa fonction d'échafaudage, ou de la mort de la cellule via sa fonction kinase, par l'induction de l'apoptose ou de la nécroptose. Au carrefour de plusieurs voies de signalisation conduisant à la survie ou à la mort de la cellule, RIPK1 est donc considérée comme une protéine clef du contrôle décidant du destin de la cellule. La signalisation induite par RIPK1 doit donc être finement régulée

pour maintenir l'homéostasie tissulaire. La mort des souris *Ripk1* knockout 1 à 3 jours après leur naissance souligne son importance dans ce maintien et des effets délétères lorsque sa signalisation est dérégulée. RIPK1 a premièrement été identifiée lors de l'activation du Fas (Stanger et al., 1995), par la suite caractérisée comme impliquée dans la signalisation du TNF-α (Hsu et al., 1996) et du TRAIL (Chaudhary et al., 1997; Lin et al., 2000), mais également activée par la stimulation des TLR 3 et 4 (Meylan et al., 2004; Youn et al., 2005).

I.6.2.2. Rôle de RIPK1 dans la survie cellulaire et l'inflammation

L'observation de la mort prématurée des souris *Ripk1-/-* (Kelliher et al., 1998) démontre le rôle important de RIPK1 dans la survie cellulaire et le maintien de l'homéostasie qui se fait indépendamment de son activité kinase puisque les souris dont l'activité de RIPK1 est inactive sont viables jusqu'à l'âge adulte (Berger et al., 2014; Kaiser et al., 2014).

Principalement étudiée dans la signalisation du TNF-α, de nombreux travaux ont montré que l'absence de RIPK1 sensibilise des cellules primaires ou transformées à une mort apoptotique induite par le TNF-α. (Dillon et al., 2014; Rickard et al., 2014; Takahashi et al., 2014). Ces quinze dernières années ont ainsi fait l'objet de nombreuses publications disséquant le rôle de RIPK1 dans la signalisation de la cellule. Ces travaux ont permis de montrer que RIPK1, via sa fonction d'échafaudage, est nécessaire à la survie de la cellule, en partie par l'activation de la voie NF-κB canonique, par le recrutement du complexe IKK au niveau du TNFR1, et par la voie non-canonique, via la stabilisation des protéines cIAP1 et TRAF2 au niveau du récepteur. En effet, certains travaux ont montré que l'absence de RIPK1 inhibe le recrutement du complexe IKK au niveau du TNFR1 et l'activation de la voie NF-κB (Dillon et al., 2014; Kelliher et al., 1998; Vanlangenakker et al., 2011). De plus, des cellules exprimant une protéine mutée de RIPK1 ne pouvant être polyubiquitiné sur sa lysine 377 (*Ripk1*^{K377R}), présentent un défaut d'activation de la voie NF-κB et une sensibilité à l'apoptose, toutes deux induites par le TNF-α (Ea et al., 2006). Cependant, dans certaines cellules déficientes en RIPK1, bien que le TNF-α déclenche l'apoptose, l'absence de RIPK1 n'empêche pas l'activation de la voie NF-κB. Ceci suggère à la fois la présence de mécanismes alternatifs permettant l'activation de la voie NF-κB, ainsi qu'un rôle de RIPK1 dans la survie des cellules indépendamment de NF-κB. Ces études proposent un rôle majeur de RIPK1 dans la stabilisation des protéines cIAP1 et TRAF2 permettant la survie cellulaire et une stabilisation de cFLIP$_L$ (Gentle et al., 2011; Wong et al., 2010). De plus, la sensibilité des cellules *Traf2*$^{-/-}$ à l'apoptose induite par le TNF-α (Vince et al., 2009) ainsi que le fait que des souris déficientes pour des protéines essentielles à l'activation de la voie NF-κB (**Tableau 5**) meurent au cours de l'embryogenèse contrairement au souris *Ripk1*$^{-/-}$ qui survivent jusqu'à la naissance (Vanden Berghe et al., 2015), corroborent ces résultats. La déficience en

RIPK1 conduirait également à l'activation de la voie non-canonique NF-κB induite par une surexpression de la protéine " NF-κB Inducing Kinase" (NIK) et un clivage de la sous-unité p100 de NF-κB en p52 (Gentle et al., 2011). Cependant le rôle de cette voie dans l'induction de la mort des cellules n'est pas élucidé puisque la voie NF-κB non canonique est décrite pour induire l'expression des mêmes gènes que la voie canonique, soit des gènes anti-inflammatoires et pro-apoptotiques. Par conséquent, RIPK1 aurait un rôle majeur dans la prévention de l'apoptose induite par le TNF-α, via une stabilisation de la protéine FLIP-L, soit par l'activation de la voie canonique NF-κB soit par la stabilisation des protéines cIAP1 et TRAF2 (Ting and Bertrand, 2016).

In vivo, il a été observé que les souris *Ripk1*$^{-/-}$ mourraient suite à une mort cellulaire excessive dans de nombreux tissus et notamment lymphoïdes, adipeux et hépatiques ainsi que d'une inflammation systémique (Kelliher et al., 1998; Rickard et al., 2014). Cependant, la délétion supplémentaire du gène codant pour le *Tnf* ou le *Tnfr1* n'est pas suffisante pour préserver la vie des souris *Ripk1*$^{-/-}$, suggérant que d'autres facteurs, que le TNF-α, sont impliqués dans la mort des cellules déficientes en Ripk1. De plus, l'absence de la caspase 8 ou de RIPK3 ne permet pas d'éviter la létalité des nouveau-nés *Ripk1*$^{-/-}$. En effet, l'inhibition d'une des deux voies conduit à l'activation de l'autre et provoque *in fine* la mort des souris *Ripk1*$^{-/-}$. Seul le blocage de l'apoptose et de la nécroptose par la délétion de la caspase 8 et de RIPK3 permet au souris *Ripk1*$^{-/-}$ de survivre jusqu'à l'âge adulte (Dillon et al., 2014; Rickard et al., 2014). Ces mêmes données ont été retrouvées chez des souris déficientes en RIPK1 spécifiquement dans les cellules hématopoïétique ou épithéliales de l'intestin ou de la peau, chez lesquels ces cellules présentent, *in vivo*, une apoptose spontanée quelques semaines après la naissance (Dannappel et al., 2014; Rickard et al., 2014; Takahashi et al., 2014).

I.6.2.3. Rôle de RIPK1 dans la mort cellulaire.

RIPK1 joue un rôle central dans le destin de la cellule par sa capacité de contrôle sur la survie ou la mort cellulaire. Sous certaines conditions, RIPK1 est également capable d'induire l'apoptose ou la nécroptose de la cellule via son activité kinase. Le statut d'ubiquitylation de RIPK1 joue un rôle majeur dans ce contrôle en prévenant la formation des complexes IIa et IIb, par l'inhibition de la voie NF-κB, mais également de manière indépendante de cette voie (Ea et al., 2006; O'Donnell et al., 2007). Il a été observé que l'absence des protéines cIAP1 et cIAP2 induisait une réduction voire une absence d'ubiquitinylation de RIPK1 conduisant à la formation du complexe IIb et à l'activation de l'apoptose dépendant de l'activité kinase de RIPK1, ce qui démontre également son rôle dans l'induction de la mort de la cellule (Brenner et al., 2015; Wang et al., 2008). Ainsi, l'utilisation des *« Smac mimétic »* permet d'induire une apoptose dépendante de

l'activité kinase de RIPK1. En revanche, lorsque les caspases sont bloquées, le complexe IIb se dissocie pour former le nécroptosome et induire l'activation de MLKL et la nécroptose de la cellule.

I.6.3. Caractéristiques et rôles généraux des protéines PARP1 et PARP2

Les poly(ADP-ribose) polymérases (PARP) forment une large famille d'enzymes, composée de 17 membres partageant un domaine catalytique et un site actif conservé qui constituent la signature de la famille (Amé et al., 2004). Ces enzymes sont capables de synthétiser des monomères ou polymères d'ADP riboses (PAR) à partir du NAD+, tout en libérant de la nicotinamide et des protons. Ces PARs sont synthétisés sur les résidus Glu, Asp et Lys des protéines (Aredia and Scovassi, 2014), conduisant au recrutement de partenaires protéiques et à la formation de complexes jouant un rôle dans la réparation/réplication de l'ADN et dans la transcription (Aredia and Scovassi, 2014). Cette modification post-traductionnelle est transitoire car les poly(ADP-ribose) glycohydrolase (PARG) et l'ADP-ribosyl-hydrolase 3 (ARH3) assurent la dégradation des PAR (De Vos et al., 2012; Lautier et al., 1993).

L'activation des PARP peut s'effectuer par différents stimuli telles que des cassures simple ou double brin ainsi que des structures particulières de l'ADN, des ROS, des agents alkylants, des modifications post-traductionnelles ou la voie calcique (Vanden Berghe et al., 2014), conduisant à leur implication dans plusieurs processus cellulaires tels que la réparation de l'ADN, l'inflammation ou la mort cellulaire (Bai et al., 2012). Les protéines PARP1 et PARP2 (PARP1/2) vont partager des partenaires et des fonctions similaires mais également distinctes (Isabelle et al., 2010; Oliver et al., 2004; Troiani et al., 2011).

I.6.3.1. Rôles des protéines PARP1/2 dans la réparation de l'ADN

Parmi les enzymes de cette famille, seules les protéines PARP1/2 vont présenter une activité de poly-ADP-rybosylation suite à leur activation causée par un dommage de l'ADN (Amé et al., 1999; Shieh et al., 1998). Cependant, PARP2 est moins active et contribue à 5-10 % de cette activité (Yélamos et al., 2008). C'est pourquoi les rôles de la protéine PARP1 ont été largement étudiés et elle joue un rôle clef dans le processus de résolution du dommage de l'ADN (De Vos et al., 2012).

Localisées au niveau nucléaire, l'activation des protéines PARP1/2 par des structures particulières ou des cassures doubles ou simples brins de l'ADN conduit à la synthèse de PAR sur des partenaires protéiques tels que les histones et des enzymes impliquées dans le remodelage de la chromatine, permettant ainsi le recrutement de la machinerie de réparation de l'ADN (De Vos et al., 2012). Ainsi, elles jouent un rôle clef dans de nombreux processus de réparation de l'ADN

et sont des cibles importantes dans les stratégies thérapeutiques contre le cancer (De Vos et al., 2012).

I.6.3.2. Rôles des protéines PARP1/2 dans l'inflammation

Depuis plus d'une décennie, l'inhibition des PARP a mis en évidence ses propriétés anti-inflammatoire (Weltin et al., 1995). Ce rôle a été démontré dans de nombreux modèles de maladies inflammatoires de nature et de localisation variées suite à l'utilisation de souris KO et d'inhibiteurs chimiques (Bai et al., 2012). Par leur localisation nucléaire et leur interaction avec l'ADN, les protéines PARP1/2 joueraient un rôle :

- dans la maturation des cellules immunitaires, et notamment au cours de la recombinaison VDJ et dans la maturation des lymphocytes T,
- dans les voies de signalisation impliquées dans l'inflammation par l'interaction avec différents facteurs de transcription tels que NF-κB,
- dans la régulation de l'expression de cytokines, chimiokines, molécules d'adhésion et médiateurs de l'inflammation.

I.6.3.3. Rôles des protéines PARP1/2 dans la mort cellulaire

Alors que le blocage de l'activité PARP entraine un délai dans la réparation de l'ADN et la mort de la cellule, il a été observé dès les années 80 qu'une activation excessive de PARP, suite à un stress génotoxique sévère, pouvait déclencher la mort cellulaire (Berger et al., 1983). Il fut tout d'abord suggéré que la suractivation de PARP et donc une activité de parylation excessive entrainerait une catastrophe métabolique, induite par une déplétion du NAD+, le substrat de PARP, ou une catastrophe énergétique par une réduction des taux d'ATP. En effet, le NAD+ nécessite 4 molécules d'ATP pour être re-synthétisé. Plusieurs études supportent ces deux hypothèses dans la mort induite par PARP. Cependant, plus récemment, un autre mécanisme alternatif a également émergé et prend le nom de parthanatos, une mort indépendante de l'activation des caspases. Dans certaines conditions, les PAR synthétisées au niveau nucléaire pourraient migrer dans la mitochondrie et conduire à la translocation de la protéine "Apoptosis Inducing Factor" (AIF) vers le noyau de la cellule. La présence d'AIF au niveau nucléaire entraînerait une condensation et une fragmentation de la chromatine donc la mort de la cellule (Virág et al., 2013).

II. CONTEXTE ET OBJECTIFS

L'objectif de ce travail de thèse était d'étudier le rôle des protéines RIPK1 et PARP1/2 dans le déclenchement de l'hépatolyse induite par les cellules de l'immunité innée dans des modèles d'hépatites aiguës chez la souris. La mort des hépatocytes est considérée comme l'élément déclencheur dans la majorité des maladies hépatiques. Activées suite à un dommage cellulaire ou par la reconnaissance d'éléments étrangers à l'organisme, les cellules de l'immunité innée induisent rapidement une réponse inflammatoire dans le but de restaurer l'homéostasie hépatique. Cependant si cette réponse immunitaire n'est pas efficacement contrôlée et par conséquent devient excessive ou chronique, elle contribuera à l'amplification du dommage hépatique.

Les ligands de mort de la superfamille du TNF-α dont principalement TNF-α, FasL et TRAIL sont exprimés et libérés par les cellules immunes ou les cellules épithéliales et sont connus pour induire la mort des hépatocytes. L'administration de Concanavaline A (ConA) chez la souris conduit à une hépatite aiguë, associée à une inflammation et une hépatolyse induite par les cellules de Kupffer et les lymphocytes NKT. Cette mort hépatocytaire est connue pour être dépendante du TNF-α, de l'IFN-γ, du FasL et de TRAIL. L'utilisation d'inhibiteurs chimiques : Nec-1 et PJ-34 bloquant respectivement l'activité kinase de RIPK1 et l'activité de poly(ADP)-ribosylation des protéines PARP1/2 ont préalablement été démontrés comme inhibant l'hépatolyse induite suite à l'administration de ConA. Mon travail de thèse s'est donc intéressé aux rôles de ces protéines afin de mieux connaître leurs fonctions, leurs partenaires protéiques et *in fine* mieux caractériser les mécanismes moléculaires impliqués dans la mort des hépatocytes.

Rôle de RIPK1 dans la mort des hépatocytes

La protéine RIPK1 présente une fonction double, puisqu'elle est capable d'induire la mort des cellules via son activité kinase mais peut également contribuer à leur survie via le recrutement de partenaires protéiques. Ces deux fonctions étant reliées à des domaines structurels différents, nous nous sommes donc intéressés d'une part au rôle de l'activité kinase de RIPK1 par l'utilisation de Nec-1s, un inhibiteur chimique de RIPK1 plus stable et plus spécifique que Nec-1 et de souris dont l'activité kinase est inactive (*Ripk1*^{K45A}) ; d'autre part à son rôle dans la survie cellulaire par l'utilisation de souris conditionnellement déficientes pour RIPK1 dans les cellules parenchymateuses hépatiques (LPC) (*Ripk1*$^{LPC\text{-}KO}$). Ce travail a été réalisé en collaboration avec l'équipe du Pr Peter Vandenabeele (Université de Gand, VIB) qui a généré ces souris.

Dans un premier temps, le rôle de RIPK1 a été étudié dans l'hépatite induite par la ConA. L'objectif de ce travail a été : *i)* d'évaluer la mort hépatocytaire et l'inflammation induite par la ConA lorsque RIPK1 était inhibé ou absent, *ii)* de caractériser la nature de cette mort cellulaire, *iii)* de déterminer les facteurs responsables de la mort des hépatocytes chez les souris *Ripk1*$^{LPC\text{-}KO}$. Ces travaux sont présentés dans un article récemment accepté dans *Cell Death and Disease*.

Les Pathogens Associated Molecular Patterns (PAMPs) sont des motifs qui sont reconnus par les cellules de l'immunité innée et déclenchent l'induction d'une réponse inflammatoire, connue pour être responsable de complications au cours de la stéatohépatite ou des hépatites alcooliques chroniques. Nous nous sommes intéressés, dans un deuxième temps, au rôle de RIPK1 suite à l'administration de deux types de PAMPs bactériens : le lipopolysaccharide (LPS) et les motifs CpG chez les souris *Ripk1*$^{LPC\text{-}KO}$. L'objectif de ce travail a été : *i)* d'évaluer la mort cellulaire et l'inflammation dans ces deux modèles, *ii)* de déterminer la nature de cette mort cellulaire, *iii)* de caractériser le rôle des cellules de Kupffer et du TNF-α, chez les souris *Ripk1*$^{LPC\text{-}KO}$ dans l'induction de l'hépatolyse. Ces travaux sont présentés dans un article actuellement en cours de révision à *Journal of Hepatology*.

Les données cliniques suggèrent le rôle des ligands de mort FasL et TRAIL dans les hépatites auto-immunes et virales. Au cours de ces hépatites, ces protéines sont exprimées ou libérées sous forme soluble majoritairement par les lymphocytes cytotoxiques, NK et NKT. RIPK1 est connu pour interagir avec les récepteurs de mort Fas et TRAIL-R2 (DR5). Nous nous sommes intéressés dans un troisième temps au rôle de RIPK1 dans la voie de signalisation de ces récepteurs, par l'utilisation d'un modèle d'hépatite induite par un agoniste de Fas (mAb-Jo2) ou par la co-administration d'IFN-γ et de TRAIL recombinantes. Les objectifs étaient : *i)* de quantifier et d'évaluer la nature de l'hépatolyse induite par ces facteurs chez les souris *Ripk1*$^{LPC\text{-}KO}$, *ii)* de déterminer le rôle du TNF-α dans ces modèles. Ces travaux font l'objet d'un article en cours de préparation.

Rôle de PARP1/2 dans l'hépatite induite par la ConA

En parallèle de ces travaux, nous nous sommes intéressés aux rôles des protéines PARP1/2 dans l'hépatite induite par la ConA, en utilisant des souris déficientes pour *Parp1* ou *Parp2*. Ce travail a été réalisé en collaboration avec l'équipe du Dr Françoise Dantzer (Université de Strasbourg, IREBS, Illkirch) qui nous a fourni ces souris. L'objectif de ce travail a été : *i)* de quantifier la mort des hépatocytes chez ces souris et, *ii)* de caractériser les populations immunitaires dans le foie, la rate, le thymus et la moelle osseuse des souris déficientes en *Parp2*. Ces travaux font l'objet d'un article actuellement soumis dans *Journal of Hepatology*.

Par ailleurs, au cours de mon doctorat qui s'est effectué en co-direction avec le Prof Lucie Lamontagne (Université UQAM, Montréal), j'ai été amenée à réaliser un séjour dans son

laboratoire canadien. Mon implication dans ces travaux de recherche s'est concrétisée dans ma participation à des publications listées ci-dessous et jointes en annexe.

- Christian Bleau, Mélanie Burnette, **Aveline Filliol**, Claire Piquet-Pellorce, Michel Samson, and Lucie Lamontagne. "Toll-like Receptor-2 Exacerbates Murine Acute Viral Hepatitis." *Immunology* 149, no. 2 (October 2016): 204–24. doi:10.1111/imm.12627.

- Christian Bleau, **Aveline Filliol**, Michel Samson, and Lucie Lamontagne. "Mouse Hepatitis Virus Infection Induces a Toll-Like Receptor 2-Dependent Activation of Inflammatory Functions in Liver Sinusoidal Endothelial Cells during Acute Hepatitis." *Journal of Virology* 90, no. 20 (October 15, 2016): 9096–9113. doi:10.1128/JVI.01069-16.

- Christian Bleau, **Aveline Filliol**, Michel Samson, and Lucie Lamontagne. "Brain Invasion by Mouse Hepatitis Virus Depends on Impairment of Tight Junctions and Beta Interferon Production in Brain Microvascular Endothelial Cells." *Journal of Virology* 89, no. 19 (October 2015): 9896–9908. doi:10.1128/JVI.01501-15.

III. RESULTATS

III.1. ARTICLE I : RIPK1 protège du dommage hépatique induit par le TNF-α au cours de l'hépatite.

Aveline Filliol, Claire Piquet-Pellorce, Jacques Le Seyec, Muhammad Farooq, Valentine Genet, Catherine Lucas-Clerc, John Bertin, Peter J. Gough, Marie-Thérèse Dimanche-Boitrel, Peter Vandenabeele, Mathieu JM Bertrand* and Michel Samson*.

* These authors contributed equally to this work.

Article accepté dans *Cell Death and Disease*.

Introduction de l'article.

La mort des hépatocytes est considérée comme un facteur clef dans le déclenchement et la progression des maladies hépatiques. En effet, lorsqu'elle est excessive, l'hépatolyse risque de compromettre les fonctions hépatiques et quand elle persiste, elle induit une inflammation et des processus de régénération chroniques favorisant le développement de la fibrose et du CHC. Par conséquent, l'étude de la mort des hépatocytes dans les hépatopathies et la recherche d'inhibiteurs de l'hépatolyse est une des approches thérapeutiques utilisée pour réduire l'évolution des maladies hépatiques. Notre équipe s'intéresse aux mécanismes moléculaires et cellulaires impliqués dans le processus de mort des hépatocytes par l'utilisation de différents modèles d'hépatite. La tolérance des souris face au VHB et au VHC qui déclenche, chez l'Homme, une hépatolyse médiée principalement par les lymphocytes cytolytiques CD8+, NK et NKT, conduit à l'utilisation de modèles alternatifs d'hépatite immuno-induite. L'hépatite induite par la Concanavaline A permet de mimer des caractéristiques présentes au cours des AIH et des hépatites virales et dont l'hépatolyse est dépendante des NKT et des ligands de mort tels que TNF-α, FasL et TRAIL. Les travaux antérieurs, réalisés par l'équipe du Dr MT Dimanche Boitrel et en collaboration avec notre équipe, ont montré que l'inhibition de l'activité kinase de RIPK1, par l'utilisation de la Nec-1, conduisait à une réduction de l'hépatolyse au cours de l'hépatite induite par la ConA, suggérant un rôle de RIPK1 dans ce processus de mort.

Dans ce travail, nous avons caractérisé le rôle de RIPK1 dans le foie au cours de l'hépatite induite par la ConA par deux approches : pharmacologique et génétique, via l'utilisation de la Nec-1s, décrite comme plus stable et plus spécifique que la Nec-1 et de souris génétiquement modifiées, dont l'activité kinase de RIPK1 est inactive ($Ripk1^{K45A}$) ou conditionnellement déficientes pour RIPK1 dans les LPC ($Ripk1^{LPC\text{-}KO}$). L'utilisation de TNF-α recombinant et de l'Etanercept (un

anti-TNF-α utilisé en clinique) nous a permis d'étudier l'implication de cette cytokine dans ce modèle.

Plusieurs techniques ont été utilisées pour évaluer le dommage hépatique (niveaux des transaminases hépatiques et coloration H&E des coupes de foie), l'inflammation (transcrits hépatique et niveaux sériques de cytokines pro-inflammatoire, infiltration cellulaire hépatique, mesure de l'activation des cellules immunitaires par FACS) et les voies de signalisation impliquées dans la survie via NF-κB et TRAF2 ou dans la mort cellulaire apoptotique et nécroptotique autant *in vivo* et *in vitro* dans les deux génotypes.

Cette étude a permis de démontrer que RIPK1 : *i)* n'est pas indispensable au maintien de l'homéostasie du foie, *ii)* induit la mort des hépatocytes dans l'hépatite à ConA via sa fonction kinase, *iii)* protège les hépatocytes de la mort induite par le TNF-α, indépendamment de sa fonction kinase et sans empêcher l'activation du facteur NF-κB mais via la stabilisation de la protéine TRAF2. Ces résultats suggèrent que RIPK1 pourrait être une cible thérapeutique pertinente afin de bloquer l'hépatolyse au cours des maladies hépatiques mais que la préservation de sa fonction d'échafaudage est primordiale à la survie des hépatocytes.

OPEN

Citation: Cell Death and Disease (2016) 7, e●; doi:10.1038/cddis.2016.362
Official journal of the Cell Death Differentiation Association

www.nature.com/cddis

RIPK1 protects from TNF-α-mediated liver damage during hepatitis

Aveline Filliol[1,2,3], Claire Piquet-Pellorce[1,2,3], Jacques Le Seyec[1,2,3], Muhammad Farooq[1,2,3], Valentine Genet[1,2,3], Catherine Lucas-Clerc[2,4], John Bertin[5], Peter J Gough[5], Marie-Thérèse Dimanche-Boitrel[1,2,3], Peter Vandenabeele[6,7], Mathieu JM Bertrand[6,7,8] and Michel Samson*[,1,2,3,8]

Cell death of hepatocytes is a prominent characteristic in the pathogenesis of liver disease, while hepatolysis is a starting point of inflammation in hepatitis and loss of hepatic function. However, the precise molecular mechanisms of hepatocyte cell death, the role of the cytokines of hepatic microenvironment and the involvement of intracellular kinases, remain unclear. Tumor necrosis factor alpha (TNF-α) is a key cytokine involved in cell death or survival pathways and the role of RIPK1 has been associated to the TNF-α-dependent signaling pathway. We took advantage of two different deficient mouse lines, the RIPK1 kinase dead knock-in mice (Ripk1^{K45A}) and the conditional knockout mice lacking RIPK1 only in liver parenchymal cells (Ripk1^{LPC-KO}), to characterize the role of RIPK1 and TNF-α in hepatitis induced by concanavalin A (ConA). Our results show that RIPK1 is dispensable for liver homeostasis under steady-state conditions but in contrast, RIPK1 kinase activity contributes to caspase-independent cell death induction following ConA injection and RIPK1 also serves as a scaffold, protecting hepatocytes from massive apoptotic cell death in this model. In the Ripk1^{LPC-KO} mice challenged with ConA, TNF-α triggers apoptosis, responsible for the observed severe hepatitis. Mechanism potentially involves both TNF-independent canonical NF-κB activation, as well as TNF-dependent, but canonical NF-κB-independent mechanisms. In conclusion, our results suggest that RIPK1 kinase activity is a pertinent therapeutic target to protect liver against excessive cell death in liver diseases.

Cell Death and Disease (2016) **7,** e●; doi:10.1038/cddis.2016.362; published online xx xxx 2016

Contemporary liver diseases result from chronic conditions, such as chronic viral hepatitis, nonalcoholic fatty liver hepatitis (NASH) and alcoholic liver hepatitis.[1] The global pandemic of chronic viral hepatitis (hepatitis B and C virus infections) affects a significant proportion of the world population, currently estimated at around 500 million people.[2] In parallel, the prevalence of NASH rises especially in Western countries because of lifestyle evolution. Untreated, chronic hepatitis predispose to the development of cirrhosis and hepatocellular carcinoma (HCC).[3] The progression of these diseases is triggered by hepatocyte death,[3,4] and the cell death processes are starting to emerge. Immune cells, including liver resident macrophages (Kupffer cells) or infiltrating natural killer (NK) cells and T cells (natural killer T (NKT) and T lymphocytes), produce molecules that induce hepatic parenchyma damage. Immune cells secrete or expressed at their surface tumor necrosis factor alpha (TNF-α), FAS ligand (FasL) and TNF-related apoptosis-inducing ligand (TRAIL). These ligands induce cell death by engaging their respective receptors (TNFR, Fas and death receptors 4 and 5 (DR4, DR5)) present at the surface of hepatocytes.[5] Receptor interacting protein kinase 1 (RIPK1) is a key protein regulating signaling downstream of these DRs, and is best characterized for its roles downstream of TNFR1.[6] Clinical studies have underlined the crucial role of TNF-α in several liver diseases. Indeed, serum TNF-α levels increase in patients with fulminant hepatic failure[7] and is correlated with poor prognostic.[8] TNF-α is a master pro-inflammatory cytokine that binds TNFR1 and TNFR2, but most of its biological activities have been associated with TNFR1 signaling. Downstream of TNFR1, RIPK1 functions as a signaling node driving cell survival as well as caspase-8-dependent apoptosis or RIPK3/mixed lineage kinase domain-like pseudokinase (MLKL)-dependent necroptosis.[9] These opposed cellular fates are regulated by two different faces of RIPK1, it functions as a scaffold to promote cell survival, in part via NF-κB activation, and as a kinase to induce cell death.[6] The perinatal lethality of RIPK1-deficient mice has long hampered the *in vivo* study of the dual faces of RIPK1.[10] Recently, the publication of viable and healthy RIPK1

[1]Institut National de la Santé et de la Recherche Médicale (Inserm), U1085, Institut de Recherche Santé Environnement et Travail (IRSET), Rennes, France; [2]Université de Rennes 1, Rennes, France; [3]Structure Fédérative BioSit UMS 3480 CNRS-US18 Inserm, Rennes, France; [4]Service de Biochimie CHU Rennes, Université de Rennes 1, Rennes, France; [5]Pattern Recognition Receptor Discovery Performance Unit, Immuno-inflammation Therapeutic Area, GlaxoSmithKline, Collegeville, PA, USA; [6]Inflammation Research Center, VIB, Zwijnaarde-Ghent, Belgium and [7]Department of Biomedical Molecular Biology, Ghent University, Zwijnaarde-Ghent, Belgium
*Corresponding author: M Samson, INSERM-U1085, IRSET, Université de Rennes 1, 2, Avenue du Professeur Léon Bernard, 35043 RENNES Cedex, France. Tel: +33 22 323 5927; Fax: +33 22 323 4794; E-mail: michel.samson@inserm.fr
[8]These authors contributed equally to this work.

Abbreviations: AST, aspartate amino-transferase; ALT, alanine amino-transferase; ConA, concanavalin A; DR, death receptor; ETA, etanercept; HCC, hepatocellular carcinoma; H&E, hematoxylin and eosin coloration; i.v, intravenous; i.p, intraperitoneal; NASH, nonalcoholic fatty liver hepatitis; Nec-1, necrostatin-1; P.I, post-injection; RIPK, receptor interacting protein kinase; Q-VD-OPh, quinoline-Val-Asp-CH_2-Ph; TNF, tumor necrosis factor; TRAF2, TNF receptor-associated factor 2; TRAIL, TNF-related apoptosis-inducing ligand

Received 16.5.16; revised 26.9.16; accepted 29.9.16; Edited by J Zhang

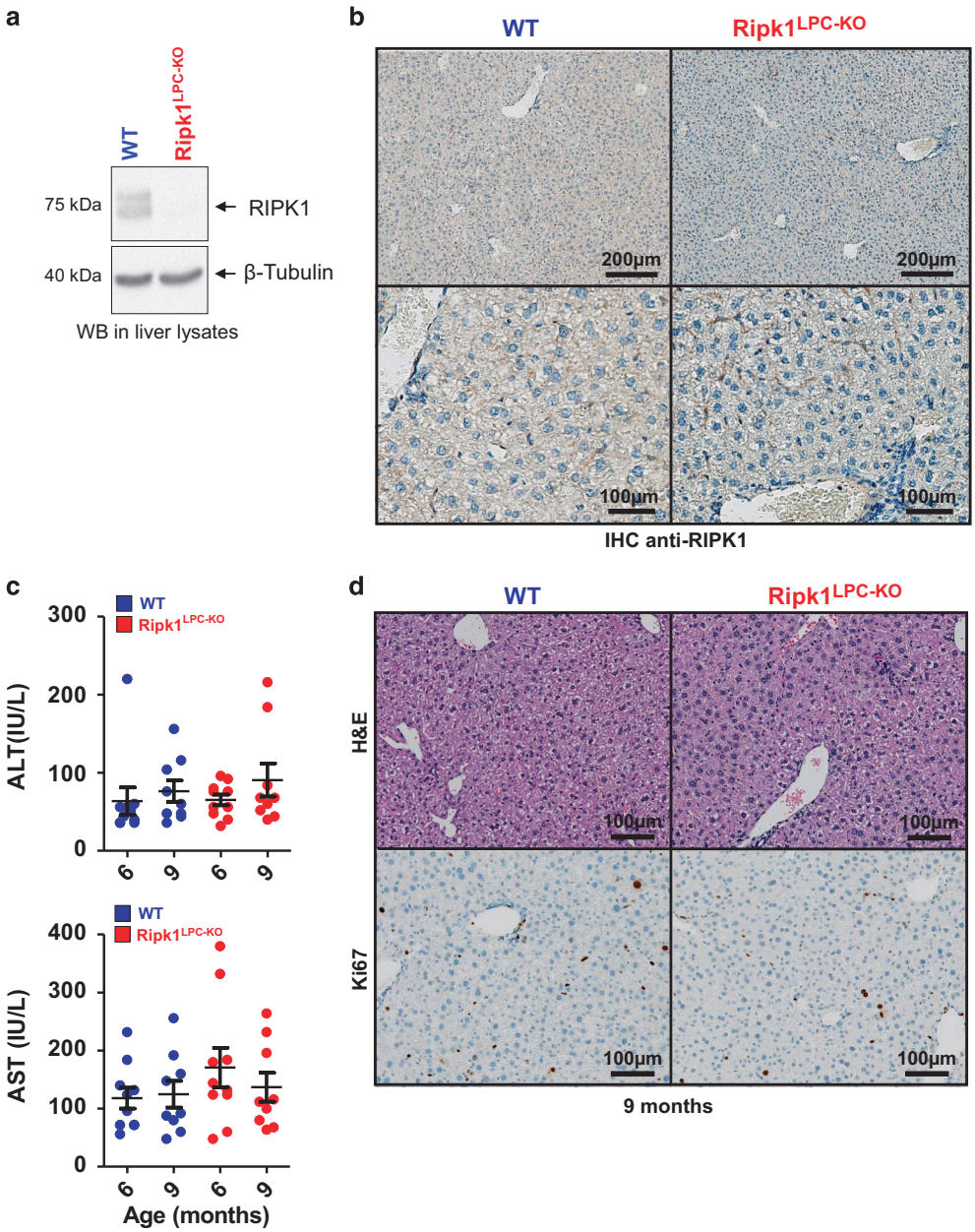

Figure 1 RIPK1 is dispensable for liver homeostasis under steady-state conditions. (**a**) Western blot analysis of RIPK1 and β-tubulin in protein extracts issued from the livers of WT and *Ripk1*$^{LPC\text{-}KO}$ mice. (**b**) Pictures of liver tissue sections analyzed by IHC for RIPK1 issued from WT and *Ripk1*$^{LPC\text{-}KO}$ mice challenged with PBS. (**c**) Levels of serum ALT and AST in unchallenged animals aged 6 and 9 months. (**d**) Pictures of liver tissue sections, stained by H&E or analyzed by IHC for Ki67, issued from WT and *Ripk1*$^{LPC\text{-}KO}$ mice aged of 9 months

Figure 2 RIPK1 has pro-necroptotic and anti-apoptotic hepatocyte cell death functions during ConA-mediated hepatitis. (**a**) Levels of serum ALT 10 h after ConA injection, in WT mice pretreated or not by Nec-1 S (left panel), or in WT or *Ripk1*^{K45A} mice (right panel). (**b**) Survival curve: all WT mice ($n=23$) treated with ConA (12 mg/kg) survived and 7 *Ripk1*$^{LPC\text{-}KO}$ mice on 33 died 12 h after ConA injection: kinetics of weight and serum ALT of WT and *Ripk1*$^{LPC\text{-}KO}$ mice after PBS or ConA injection. (**c**) Pictures of liver tissue sections, analyzed by IHC for cleaved-caspase-3, issued from mice 7 h after ConA injection (upper panels). Signal quantification of cleaved-caspase-3 (lower panel). (**d**) Western blot analysis of cleaved-caspase-3 and β-actin in protein extracts issued from the livers of WT and *Ripk1*$^{LPC\text{-}KO}$ mice, collected 7 h after ConA injection. Positions of molecular weight markers (kDa) and of studied proteins are respectively indicated on the left and right sides of the gel. (**e**) Cleaved-caspase-3 staining and (**f**) amounts of serum ALT in WT and *Ripk1*$^{LPC\text{-}KO}$ mice, 11 h after ConA challenge with an eventual pre-treatment with a pan-caspase inhibitor (Q-VD-OPh) or only with its vehicle (Cont). For all graphs, each dot represent an individual and errors bars are expressed as means $\pm$S.E.M. (*, $^{\#}$, $^{\$}P<0.05$; **, $^{\#\#}$, $^{\$\$}P<0.01$; ***, $^{\#\#\#}$, $^{\$\$\$}P<0.001$; NS, nonsignificant)

kinase dead knock-in mice (*Ripk1*^{K45A}) revealed that only RIPK1 scaffolding function, and not its kinase activity, is crucial for homeostasis and viability.[11] The generation of conditional RIPK1-deficient mouse lines also demonstrated the crucial pro-survival role of RIPK1 in intestinal and epidermal epithelia and in hematopoietic cells.[12–14]

RIPK1 functions in the liver, especially under pathological conditions, have so far remained unclear. The hepatic

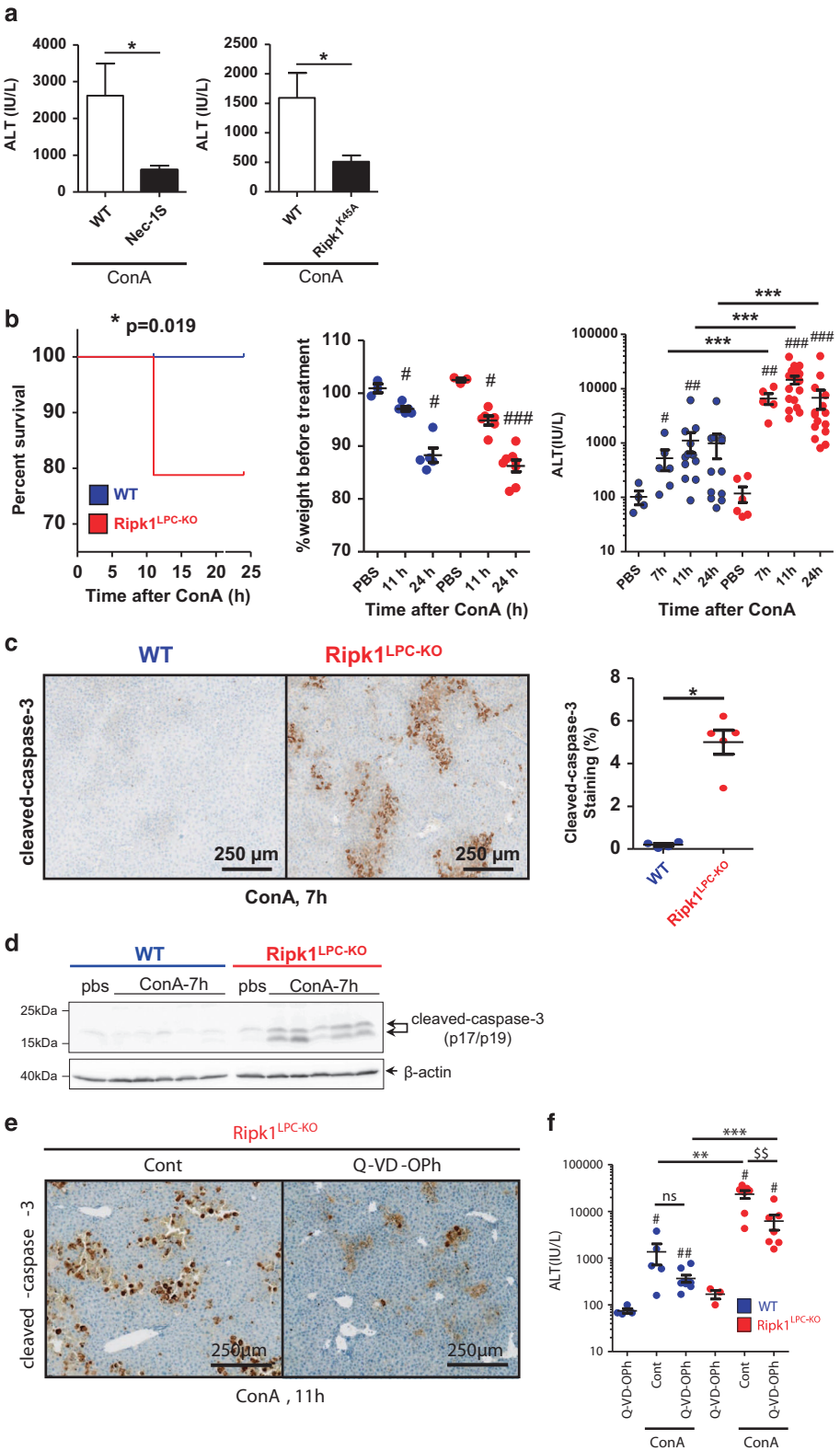

inflammation induced in mice by concanavalin A (ConA) injection reflects the overall physiopathological conditions observed in human viral or autoimmune hepatitis.[15] In this model, the combined occurrence of usual cytotoxic effectors (perforin, granzyme B, TNF-*α*, FasL and TRAIL) triggers hepatocyte death and takes part in hepatitis development.[16] Indeed, artificial impairment of one effector, or of its cognate receptor, is sufficient to prevent hepatitis in ConA-challenged animals.[5,17–19] Data suggest implication of RIPK1 kinase activity in the DR-induced death of hepatocytes in this model. Indeed, chemical inhibition of RIPK1 seems to protect the organ from ConA-induced T-cell-mediated injuries.[20–22] However, genetic evidence for the implication of RIPK1 kinase activity in the death process is still lacking. In addition, whether RIPK1 also functions as a scaffold maintaining liver homeostasis under physiological condition and/or protecting hepatocytes from death under challenged conditions is currently unknown. Thus, to characterize the role of RIPK1 in hepatitis, we took advantage of two genetically modified mouse lines, the RIPK1 kinase dead knock-in mice (*Ripk1*^{K45A}) and the conditional knockout mice lacking RIPK1 only in liver parenchymal cells (*Ripk1*$^{LPC\text{-}KO}$).

Results

RIPK1 is dispensable for liver homeostasis under steady-state conditions. In order to evaluate the role of RIPK1 in liver homeostasis, we generated mice specifically deficient for RIPK1 in liver parenchymal cell (hepatocytes and cholangiocytes) (*Ripk1*$^{LPC\text{-}KO}$) by crossing RIPK1 conditional mice (*Ripk1*$^{fl/fl}$)[12] with transgenic mice expressing the Cre recombinase under the control of the mouse albumin regulatory elements and *α*-fetoprotein enhancers (Alfp-Cre).[23,24] *Ripk1*$^{LPC\text{-}KO}$ mice were viable and reached adulthood without morphological liver alteration. Western blot and IHC analyses confirmed RIPK1 expression in the liver parenchymal cells of the *Ripk1*$^{fl/fl}$ wild-type (WT) animals but not of the *RipK1*$^{LPC\text{-}KO}$ littermates (Figures 1a and b). Monitoring of *RipK1*$^{LPC\text{-}KO}$ mice over a period 9 months did not revealed occurrence of any obvious abnormality. Even if liver histology of mature *Ripk1*$^{LPC\text{-}KO}$ mice revealed few infiltrated immune cells, no inflammation settled. Indeed, serum transaminase (aspartate amino-transferase (AST) and alanine amino-transferase (ALT)) levels remained stable and similar to those of WT littermates (Figure 1c). No changes in the expression levels of inflammatory cytokines (TNF-*α*, IFN-*γ* and IL-6) were similarly detected (Supplementary Figure 2A). Finally, Ki67 labeling of liver tissues did not show any modification in basal cell proliferation rate between the two genotypes (Figure 1d). Together, these results showed that, contrary to its role in other tissues,[12,13] RIPK1 is dispensable for proper liver development and homeostasis.

RIPK1 has pro-cell death and anti-apoptotic functions in hepatocyte during ConA-mediated hepatitis. Next, we evaluated the role of RIPK1 in liver parenchymal cells under challenged conditions. We, and others, have previously reported that ConA injection in mice induces TRAIL-mediated caspase-independent cell death of hepatocytes, which can be partially prevented by co-injection of the RIPK1 kinase inhibitor necrostatin-1 (Nec-1), suggestive of necroptosis induction.[20] This inhibitor has, however, later been demonstrated not to be so specific for RIPK1.[25,26] We therefore re-evaluate the implication of RIPK1 enzymatic activity to ConA-induced hepatocyte death by inhibiting RIPK1 with Nec-1S, a RIPK1 kinase inhibitor more stable and specific than Nec-1, and by making use of the RIPK1 kinase dead (*Ripk1*^{K45A}) mice. Importantly, both approaches confirmed that RIPK1 kinase activity drives liver injury induced by ConA, as shown by reduced levels of serum transaminase in Nec-1S pretreated mice and in *Ripk1*^{K45A} mice (Figure 2a).

In order to explore the pro-survival role of RIPK1 in the ConA-induced acute-hepatitis model, we used the *Ripk1*$^{LPC\text{-}KO}$ mice that are fully deficient for both RIPK1 scaffold and kinase functions. Although injection of a low dose (12 mg/kg) of ConA in WT mice provoked a non-lethal moderate hepatitis, it elicited a fulminant hepatitis in *Ripk1*$^{LPC\text{-}KO}$ mice leading to 21% lethality (Figure 2b, left). In both genotypes, the illness induced weight loss because of poor appetite (Figure 2b, middle) but liver damage were more pronounced in *Ripk1*$^{LPC\text{-}KO}$ mice, as shown by wider necrotic areas (Supplementary Figure 1A), higher number of TUNEL-positive cells (Supplementary Figure 1A) and higher levels of serum transaminases (Figure 2b,Supplementary Figure 1B). Cell death in *Ripk1*$^{LPC\text{-}KO}$ mice was apoptosis, as demonstrated by the important cleaved-caspase-3 staining detected by histological and western blot analysis (Figures 2c and d). This active caspase-3 staining was not observed in the WT littermate. To evaluate the importance of apoptosis in the fulminant ConA-induced hepatitis observed in *Ripk1*$^{LPC\text{-}KO}$ mice, we treated mice 1 h before ConA injection with Q-VD-OPh hydrate (Q-VD-OPh), a pan-caspase inhibitor. Q-VD-OPh greatly decreased the number of cleaved-caspase-3-positive cells (Figure 2e) and significantly reduced hepatolysis, as shown by reduced injured areas in the liver (Supplementary Figure 1C) and the limited serum levels of transaminases (Figure 2f,Supplementary Figure 1D). In conclusion, our results indicated that RIPK1 kinase activity drives hepatocyte necroptosis following ConA injection but also serves as a scaffold protecting hepatocytes from massive apoptosis in the same model.

RIPK1 limits inflammation in ConA-mediated hepatitis. The lack of RIPK1 in liver parenchymal cells not only induced apoptotic cell death but also clearly exacerbated inflammation in ConA-challenged mice. Indeed, the induced mRNA levels of the inflammatory cytokines IFN-*γ*, TNF-*α* and IL-6 were comparable between the two genotypes 11 h after ConA injection, but significantly more abundant in the liver of *Ripk1*$^{LPC\text{-}KO}$ mice 24 h after challenge (Figure 3a). Moreover, IFN-*γ* concentrations were significantly higher in the serum of *Ripk1*$^{LPC\text{-}KO}$ mice at 11 and 24 h post-ConA injection (Supplementary Figure 2A). Although not statistically significant, a similar trend was also observed for TNF-*α* and IL-6 (Supplementary Figure 2A). In addition, immunolabeling of liver sections revealed higher hepatic recruitment of CD45- and CD11b-positive immune cells in *Ripk1*$^{LPC\text{-}KO}$ individuals (Figure 3b,Supplementary Figure 2B). Sustained

inflammation in *Ripk1*$^{LPC\text{-}KO}$ mice was also demonstrated by the fact that hepatic mRNA levels of IL-6, a marker of liver injury involved in tissue repair, continued to increase at 24 h post-injection (P.I.) only in these animals (Figure 3a). In line with this, the number of CD69-positive lymphocytes remained more elevated in the spleen of *Ripk1*$^{LPC\text{-}KO}$ mice at 24 h,

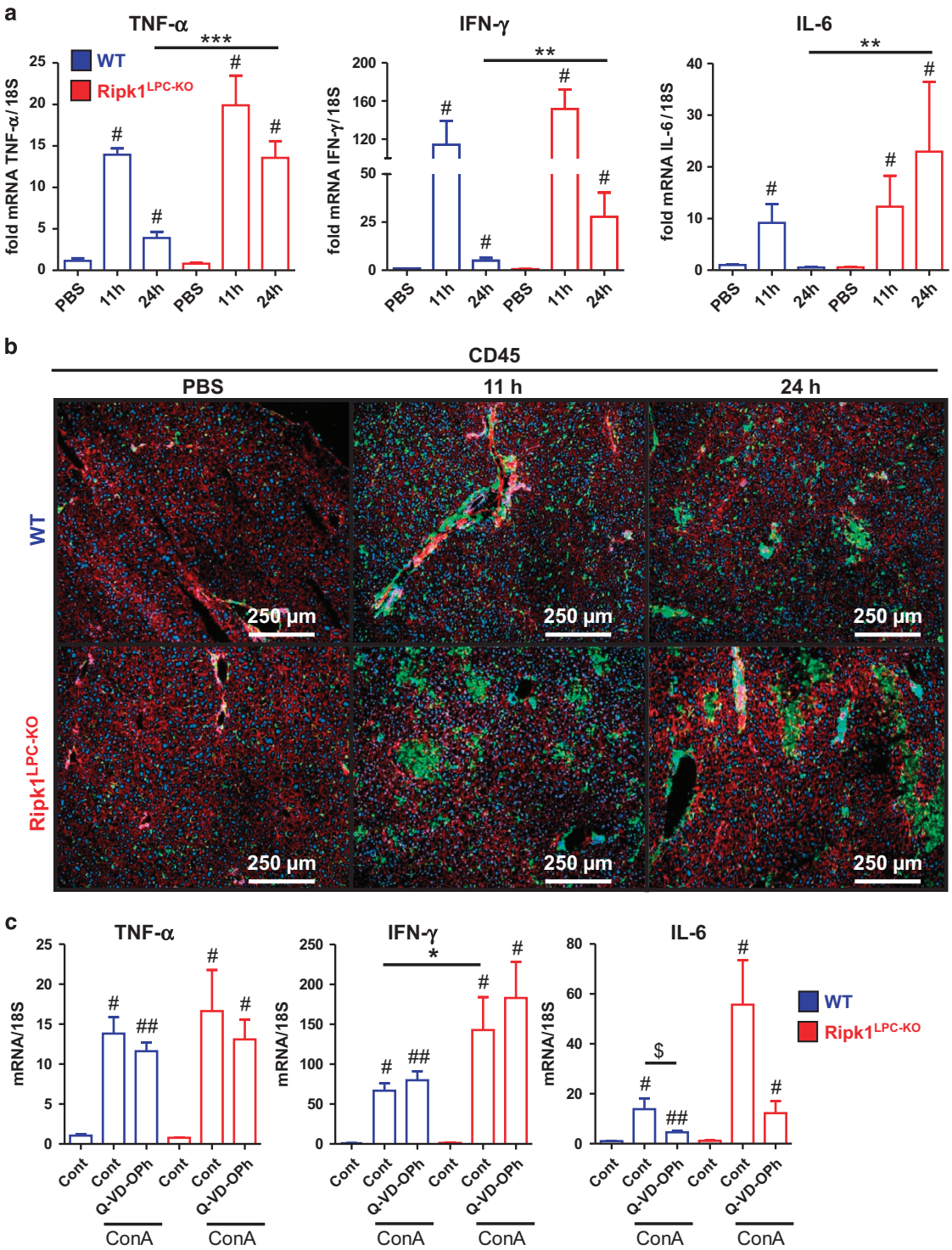

Figure 3 RIPK1 limits inflammation in ConA-mediated hepatitis. (**a**) Levels of hepatic TNF-α, IFN-γ and IL-6 transcripts in WT or *Ripk1*$^{LPC\text{-}KO}$ mice 11 or 24 h after PBS or ConA injection. (**b**) CD45 immunofluorescence staining (green) on liver sections collected at the indicated times P.I. and issued from WT or *Ripk1*$^{LPC\text{-}KO}$ mice challenged by PBS or ConA. Nucleus were stained by Hoechst (blue) and actin by fluorescent phalloidin (red). (**c**) Levels of hepatic TNF-α, IFN-γ and IL-6 transcripts in WT and *Ripk1*$^{LPC\text{-}KO}$ mice, 11 h after ConA challenge with an eventual pre-treatment with a pan-caspase inhibitor (Q-VD-OPh) or only with its vehicle (Cont). For all graphs, errors bars are expressed as means $\pm$S.E.M. (*, $^{\#}P<0.05$; **, $^{\#\#}P<0.01$; ***, $^{\#\#\#}P<0.001$)

reflecting prolonged activation of T lymphocytes promoted by the inflammatory microenvironment (Supplementary Figure 2C). Importantly, the occurrence of hepatocyte apoptosis in the liver of *Ripk1*$^{LPC-KO}$ mice mostly contributed to the exacerbation of inflammation in these mice, and only to a limited extent to the establishment of the initial inflammatory

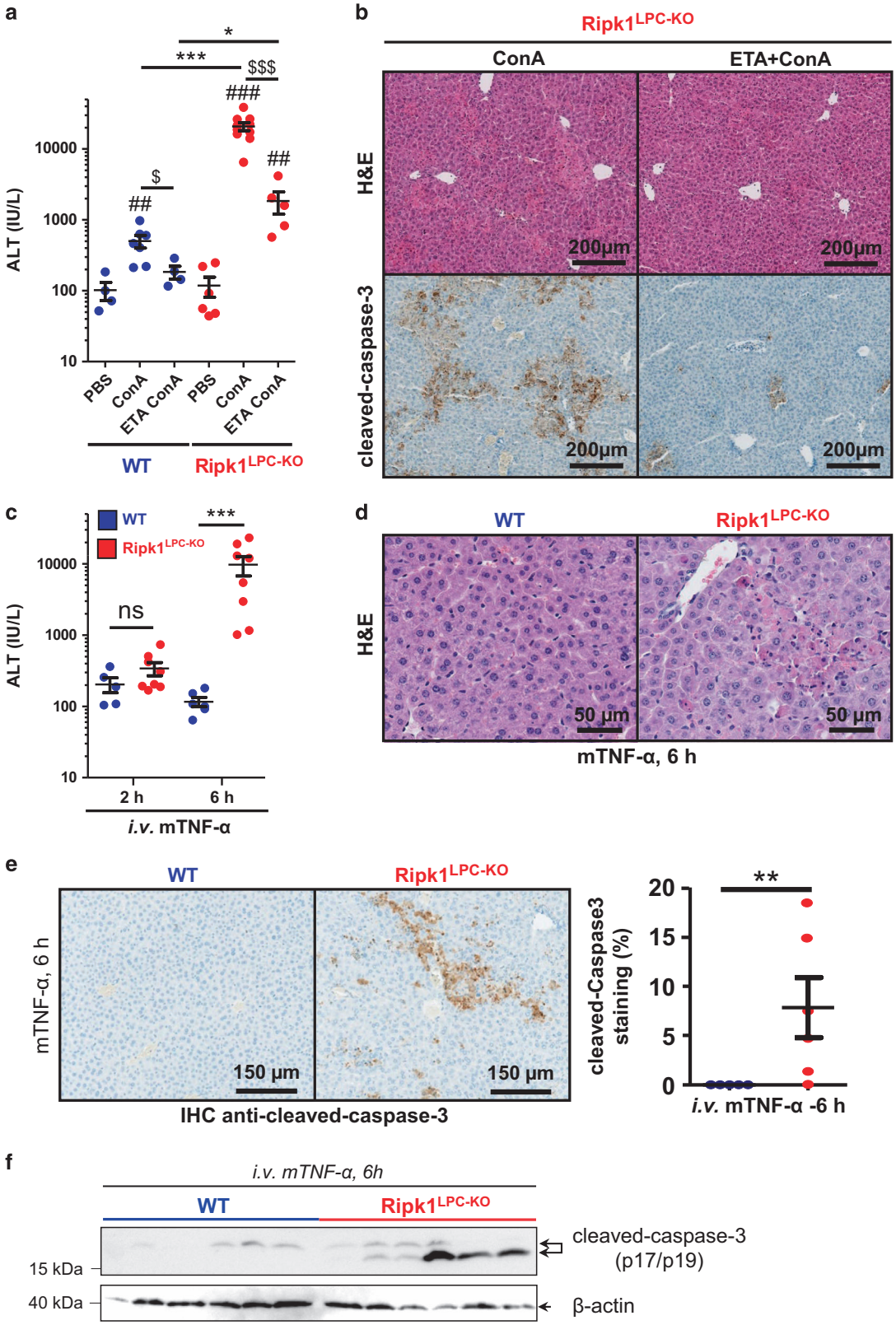

microenvironment. Indeed, blocking apoptosis by Q-VD-OPh did not alter the early (11 h) induction of the hepatic TNF-*α* and IFN-*γ* transcripts (Figure 3c), nor the immune cell recruitment and activity (Supplementary Figures 3A and B). Nevertheless, Q-VD-OPh still prevented the 11-h induction of IL-6 mRNA in *Ripk1*$^{LPC\text{-}KO}$ mice (Figure 3c), probably due to the fact that IL-6 has a key biological function in the liver regeneration and repair, and therefore lower hepatic damage induced less of IL-6 transcription. Together, these observations suggest that the protective effect of Q-VD-OPh on ConA-treated *Ripk1*$^{LPC\text{-}KO}$ mice was due to the inhibition of caspase-mediated cell death and not to a major modification of the inflammatory microenvironment.

The enhanced sensitivity of *Ripk1*$^{LPC\text{-}KO}$ mice to ConA-induced hepatitis is mediated by TNF-*α*-promoted apoptosis. Our data demonstrated that, contrary to WT littermates, ConA injection resulted in a fulminant hepatitis in *Ripk1*$^{LPC\text{-}KO}$ mice, in part caused by the sensitization of RIPK1-deficient liver parenchymal cells to apoptosis. Previous *in vitro* and *in vivo* studies have reported sensitization of RIPK1-deficient cells to TNF-mediated apoptosis.[27,28] Liver expression of TNF-*α*, and of its receptors TNFR1/2, is rapidly induced in the ConA-induced hepatitis model (Figures 3a and c,Supplementary Figures 2A and 4A). To investigate the role of TNF-*α* in the apoptosis of *Ripk1*$^{LPC\text{-}KO}$ during ConA hepatitis, we neutralized TNF-*α* by injection of etanercept (ETA), a TNF-*α* decoy receptor. TNF-*α* blockade greatly protected *Ripk1*$^{LPC\text{-}KO}$ mice from the exacerbated ConA-induced liver damage, as demonstrated by highly reduced serum levels of transaminases (Figure 4a, Supplementary Figure 4B), associated with a decrease of necrotic area and less apoptotic hepatocytes (Figure 4b). Of note, ETA also reduced the moderate liver damage in the similarly challenged WT littermates, indicative of a general role for TNF-*α* in the establishment of the ConA-induced hepatitis model (Figure 4a,Supplementary Figure 4B), as previously reported.[17,29,30] To further assess the *in vivo* role of RIPK1 in the TNF-*α* signaling pathway in hepatocytes, soluble mTNF-*α* was injected in WT and *Ripk1*$^{LPC\text{-}KO}$ littermates. Single mTNF-*α* injection had no effect on the liver of WT mice, but induced hepatolysis, already detected 6 h after injection, in *Ripk1*$^{LPC\text{-}KO}$ mice. Hepatolysis was demonstrated by the analyses of serum transaminases (Figure 4c,Supplementary Figure 4C), liver infiltrate of immune cells (data not shown) and necrotic areas (Figure 4d,Supplementary Figure 4D). Hepatocytes died of apoptosis, as revealed by cleaved-caspase-3 staining (Figures 4e and f) and absence of phosphorylated MLKL immunodetection in the liver lysates (Supplementary Figure 5), a marker of necroptosis. Together, these experiments demonstrated that TNF-*α* contributes to ConA-induced hepatitis, and is responsible for the apoptosis and hepatitis severity observed in the *Ripk1*$^{LPC\text{-}KO}$ mice.

RIPK1 protects hepatocytes from ConA-mediated apoptosis independently of TNF-*α*-induced canonical NF-*κ*B activation. In the TNFR1 signaling pathway, RIPK1 functions as a scaffold protein protecting cells from apoptosis by activating canonical NF-*κ*B-dependent and -independent responses.[10,12,13,27] Canonical NF-*κ*B activation is known to induce expression of various pro-survival molecules that prevent caspase activation. As a consequence, NF-*κ*B inhibition is often used to sensitize cells to TNF-*α*-induced apoptosis.[31] The canonical NF-*κ*B-independent pro-survival function of RIPK1 is on the other hand far less understood, but suggested to rely on TNF receptor-associated factor 2 (TRAF2) stabilization, which prevents non-canonical NF-*κ*B activation and caspase-8 processing.[12,13,27] We observed that the nuclear translocation of the p65 NF-*κ*B subunit was significantly reduced in *Ripk1*$^{LPC\text{-}KO}$ hepatocytes 7 h following ConA injection, indicative of defective canonical NF-*κ*B activation (Figure 5a). Accordingly, induction of NF-*κ*B-target gene transcripts (IKK-*γ*/NEMO, CXCL1, SAA1 and CCL20) was repressed in the liver of *Ripk1*$^{LPC\text{-}KO}$ mice (Figure 5b). The role of RIPK1 in ConA-induced canonical NF-*κ*B activation was independent of its kinase activity, as no difference was observed in the Nec-1S treated mice or the *Ripk1*^{K45A} mice (Supplementary Figure 6). Surprisingly, although TNF-*α* greatly contributed to apoptosis in RIPK1-deficient hepatocytes during ConA hepatitis (Figures 4a and b), no defect in p65 nuclear translocation or NF-*κ*B-dependent gene transcription (SAA1, CXCL1 and CCL20) was observed in the liver of *Ripk1*$^{LPC\text{-}KO}$ mice 30 min after mTNF-*α* challenge (Figure 5c,Supplementary Figure 7). By contrast, TNF-*α* stimulation led to TRAF2 degradation only in *Ripk1*$^{LPC\text{-}KO}$ animals, supporting a defect in the canonical NF-*κ*B-independent pro-survival pathway (Figure 5d).

In contrast to primary hepatocytes isolated from WT mice, RIPK1-deficient hepatocytes died spontaneously after liver perfusion. Importantly, the death was prevented by seeding the cells in presence of ETA or with the pan-caspase inhibitor z-VAD-fmk (data not shown), demonstrating higher sensitivity of primary RIPK1-deficient hepatocytes to TNF-*α*-induced apoptosis. In line with this, TNF-*α* also only induced apoptosis in RIPK1-deficient primary hepatocytes when ETA was used only for seeding but removed before TNF-*α* stimulation, as revealed by active caspase-3 staining (Figure 6a). Consistent with our *in vivo* results, TRAF2 levels were also reduced in primary RIPK1-deficient hepatocytes stimulated with TNF-*α* (Figures 6a and b). The fact that

Figure 4 Sensitization of *Ripk1*$^{LPC\text{-}KO}$ mice to ConA-induced hepatitis is triggered by TNF-*α*-mediated apoptosis. (**a**) Levels of serum ALT and (**b**) Pictures of liver tissue sections, stained by H&E (upper panel) or analyzed by IHC for cleaved-caspase-3 (lower panel), issued from mice in WT and *Ripk1*$^{LPC\text{-}KO}$ mice, 11 h after ConA or PBS challenge with an eventual pre-treatment with ETA. (**c**) Levels of serum ALT in WT and *Ripk1*$^{LPC\text{-}KO}$ mice, 2 and 6 h after mTNF-*α* injection. (**d**) Pictures of liver tissue sections stained by H&E and (**e**) analyzed by IHC for cleaved-caspase-3 (left panel) issued from WT and *Ripk1*$^{LPC\text{-}KO}$ mice, 6 h after mTNF-*α* injection. Signal quantification of cleaved-caspase-3 (right panel). (**f**) Western blot analysis of cleaved-caspase-3 and *β*-actin in protein extracts issued from the liver of WT or *Ripk1*$^{LPC\text{-}KO}$ mice, collected 6 h after mTNF-*α* injection. For all graphs, each dot represent an individual and errors bars are expressed as means ± S.E.M. (*, #, $^{\$}P<0.05$; **, ##, $^{\$\$}P<0.01$; ***, ###, $^{\$\$\$}P<0.001$; NS, nonsignificant)

z-VAD-fmk did not block TRAF2 degradation suggests that TRAF2 acts upstream of caspase activation (Figures 6a and b). Finally, we observed that RIPK1 deficiency did not affect canonical NF-κB activation in primary hepatocytes stimulated with TNF-α in absence or presence of z-VAD-fmk, as shown by the kinetics of IκBα phosphorylation

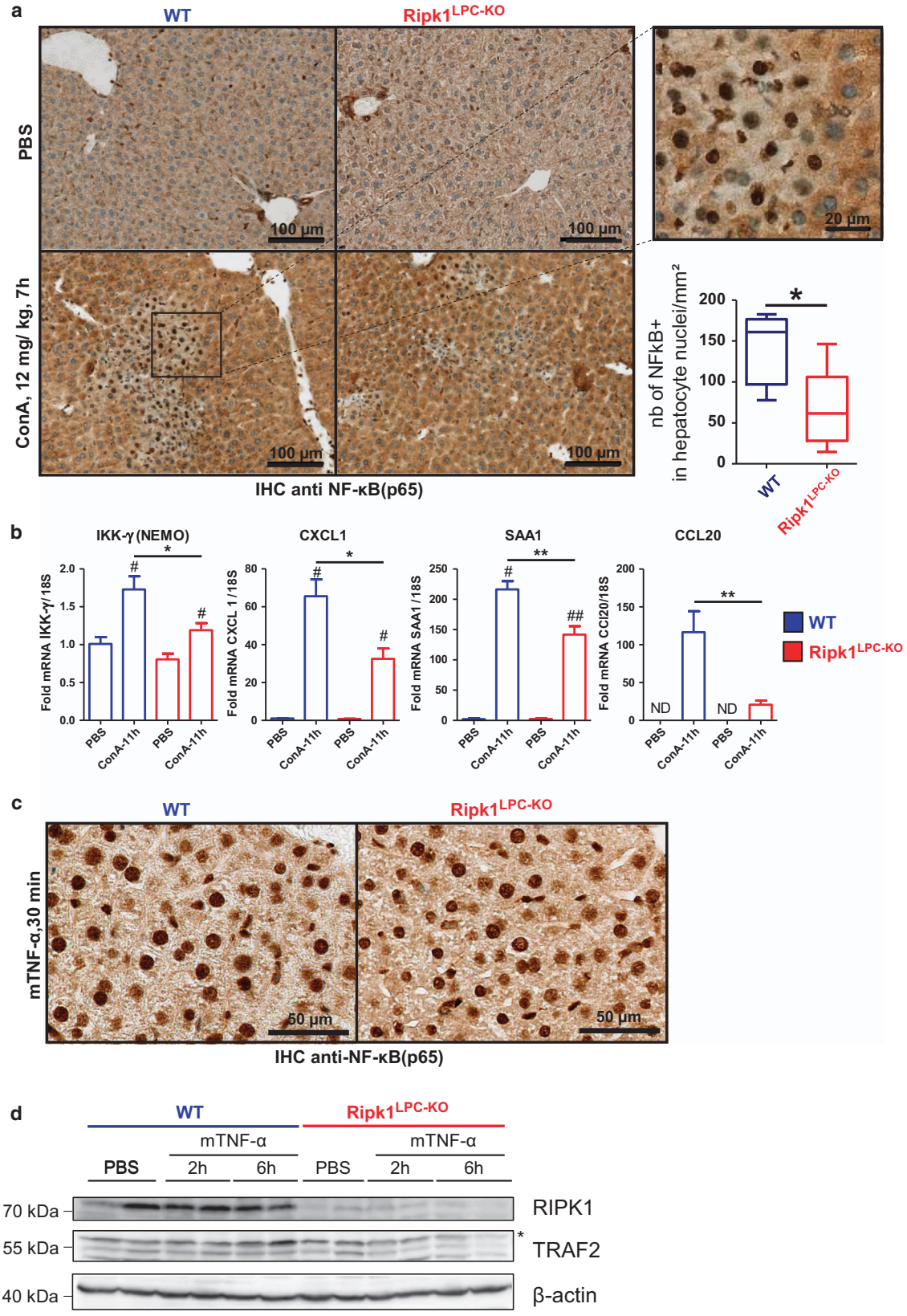

and degradation and by the induction of CCL20, a NF-κB-responsive gene (Figures 6c and d). Taken together, our results suggest that the protective role of RIPK1 against ConA-induced hepatocytes apoptosis may involve both TNF-independent canonical NF-κB activation, as well as TNF-dependent, but canonical NF-κB-independent mechanisms.

Discussion

TNF-α has a key role in the initiation of the inflammatory response during acute or chronic hepatitis caused by viral infections, steatosis, autoimmunity, alcohol or acetaminophen consumptions.[4,32] The production of TNF-α by liver Kupffer cells promotes expression of other cytokines and adhesion molecules that mediates the recruitment and the activation of

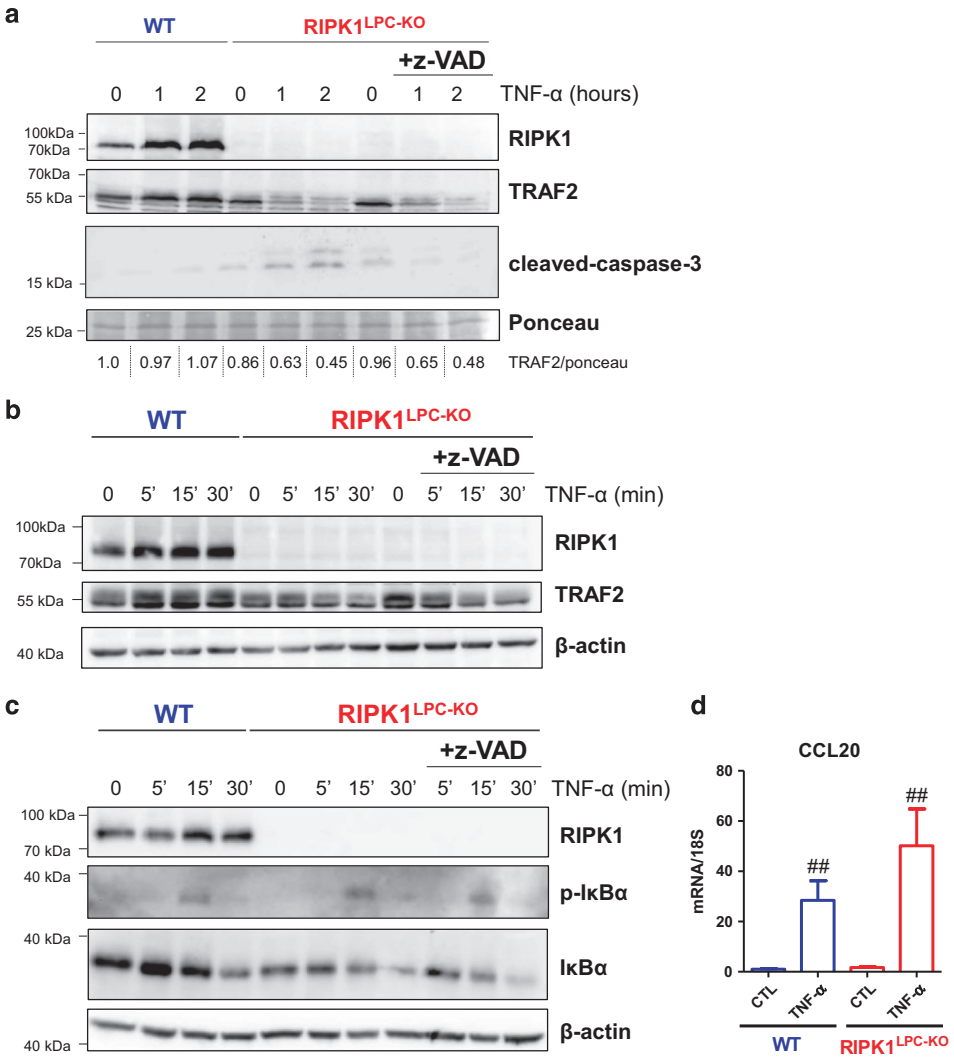

Figure 6 TNF-α induced primary hepatocyte death and TRAF2 destabilization in a NF-κB-independent manner in absence of RIPK1. (**a**) Western blot analysis of RIPK1, TRAF2 and cleaved-caspase-3 in protein extracts of primary WT or RIPK1-deficient hepatocytes treated or not with TNF-α with or without z-VAD-fmk, during 1 h or 2 h. (**b** and **c**) Western blot analysis of RIPK1, TRAF2, P-IκBα and β-actin in protein extracts of primary WT or RIPK1-deficient hepatocytes treated or not with TNF-α during 5, 15, 30 min. (**d**) Levels of CCL20 transcripts 2 h after or not (CTL) TNF-α stimulation in primary WT or RIPK1-deficient hepatocytes seeded with z-VAD-fmk before treatment. Errors bars are expressed as means ± S.D. ($^{\#}P<0.05$; $^{\#\#}P<0.01$; $^{\#\#\#}P<0.001$) and is based on the duplicate of primary hepatocyte cultures and triplicate for qPCR experiment

Figure 5 RIPK1 protects hepatocytes from ConA-mediated apoptosis independently of TNF-induced canonical NF-κB activation. (**a**) Pictures of liver tissue sections, analyzed by IHC for NF-κB-(p65), issued from WT or *Ripk1*$^{LPC-KO}$ mice 7 h after ConA or PBS injection. Quantifications of hepatocyte nuclear signals are depicted in the bottom right inset. (**b**) Levels of hepatic IKK-γ/NEMO, CXCL1, SAA1 and CCL20 transcripts in WT and *Ripk1*$^{LPC-KO}$ mice 11 h after ConA injection. (**c**) Pictures of liver tissue sections analyzed by IHC for NF-κB-(p65) issued from mice 30 min after mTNF-α injection. (**d**) Western blot analysis of RIPK1, TRAF2 and β-actin in protein extracts issued from the liver of WT or *Ripk1*$^{LPC-KO}$ mice, collected 2 h or 6 h after mTNF-α or PBS injection the star shows a nonspecific band. Errors bars are expressed as means ± S.E.M. ($^{*}P<0.05$; $^{**}P<0.01$; $^{***}P<0.001$)

immune cells involved in hepatocyte death.[33,34] A specific pro-inflammatory context is needed for the induction of hepatolysis by TNF-*α* as injection of TNF-*α* alone in mice is insufficient to induce hepatitis. Inhibition of transcription by D-galactosamine or inactivation of canonical NF-*κ*B signaling is often required to drive TNF-*α*-mediated hepatocyte apoptosis.[35,36] In the ConA hepatitis mouse model, which mimics human dysimmune hepatitis, immune cells activated by the lectin rapidly release TNF-*α* that is one of the first cytokines detected in the mouse serum.[29] We found that neutralizing TNF-*α* with ETA reduced ConA-induced hepatitis, confirming previous studies indicating that genetic or chemical inactivation of TNF-*α* or TNFR1 protects ConA-treated animals from hepatitis.[17,29,30] Together, these results underline the key role played by TNF-*α* in hepatitis induction. However, a recent publication reported that TNF-*α* does not directly induce hepatocyte death in ConA hepatitis in contrast to the D-GalN/LPS model. Indeed, specific deficiency for TNFR1 in myeloid derived cells (TNFR1$^{MDC\text{-}KO}$), but not in liver parenchymal cells (TNFR1$^{LPC\text{-}KO}$), protected mice from ConA hepatitis.[37] These results indicate that TNF-*α* promotes inflammatory conditions to provoke liver damage in the ConA model, but that TNF-*α* is not a direct inductor of hepatocyte death. In the TNF-*α* signaling pathway, RIPK1 governs cell fate.[6,38] Our work highlights a dual role of RIPK1 during ConA hepatitis. First, and in accordance with previous studies,[20,39] we found that RIPK1 functions as a kinase inducing cell death. Indeed, inactivation of RIPK1 activity either by Nec-1S or genetic modification greatly protected ConA-challenged mice from hepatitis, demonstrating a key role of RIPK1 kinase activity in ConA-induced hepatocyte death. Depending on the cellular conditions, the enzymatic activity of RIPK1 has been reported capable of mediating apoptosis or necroptosis, a regulated form of necrosis with RIPK3 and MLKL as core components.[40,41] We found that WT mice with ConA-induced liver injuries exhibited only few caspase-3-positive hepatocytes, and that pan-caspase inhibition by Q-VD-OPh failed to protect these mice from ConA-induced hepatitis, supportive of necroptosis induction. Nevertheless, because a switch from apoptosis to necroptosis has been reported in hepatocytes upon caspases inactivation,[42,43] future works using hepatocytes-deficient RIPK3 or MLKL mice will help ruling out the occurrence of RIPK1 kinase-dependent apoptosis during ConA hepatitis. Next to its pro-death role, RIPK1 also appeared as a pro-survival scaffold for hepatocytes. In accordance with a recently published article, we found that RIPK1 is nonessential to maintain liver homeostasis under physiological condition.[44] Nevertheless, mice with liver parenchymal cells lacking RIPK1 developed fulminant hepatitis associated with hepatocyte apoptosis when low doses of ConA or TNF-*α* were administrated. This phenotype partly contrasts with those observed in mice in which RIPK1 deficiency was limited to intestinal epithelial cells or to keratinocytes.[12,13] In these tissues, spontaneous apoptosis and inflammation arise, likely due to their direct interaction with commensal bacteria that trigger *de novo* TNF-*α* secretion. The role of TNF-*α* as a direct mediator of hepatocyte apoptosis in *Ripk1*$^{LPC\text{-}KO}$ mice is highlighted by the reduction of ConA hepatitis by ETA or Q-VD-OPh, the induction of liver apoptosis by a single injection of TNF-*α* in *Ripk1*$^{LPC\text{-}KO}$ mice, and the susceptibility of primary RIPK1-deficient hepatocytes to TNF-*α*-induced apoptosis. Activation of the canonical NF-*κ*B pathway may contribute to the protective role of RIPK1 in hepatocytes but would not be sufficient, and would occur independently of TNF-*α* signaling. Indeed, ConA-induced hepatitis in *Ripk1*$^{LPC\text{-}KO}$ mice was associated with a partial defect in NF-*κ*B activation, as shown by reduced nuclear p65 labeling and by the lower expression of NF-*κ*B-dependent genes. However, hepatitis was also detected despite a widespread activation of the NF-*κ*B signaling pathway in hepatocytes of TNF-*α*-treated *Ripk1*$^{LPC\text{-}KO}$ mice. This may be explained by the quick destabilization of TRAF2, observed *in vivo and in vitro* after TNF-*α* treatment. Accordingly, published data described different mechanisms by which RIPK1 may protect cells from TNF-induced death. In mouse embryonic fibroblasts lacking RIPK1, TNF-*α*-induced apoptosis is correlated to defective canonical NF-*κ*B activation and consequent c-FLIP dysregulation.[12] Besides, RIPK1 would contribute to cell survival regardless of canonical NF-*κ*B, by its capacity to stabilize cIAPs and TRAF2 proteins, precluding non-canonical NF-*κ*B activation, c-FLIP destabilization and caspase recruitment.[12,13,27,45] Of note, the discrepancy between the defect, or not, in canonical NF-*κ*B activation following ConA or TNF-*α* injection could still be explained by the amount of circulating TNF-*α* provided in both systems, or RIPK1-dependent activation of NF-*κ*B by other stimulus than TNF. Anyway, our results still show TNF-*α*-induced apoptosis in RIPK1-deficient hepatocytes despite the ability of NF-*κ*B to translocate in nucleus, demonstrating a canonical NF-*κ*B-independent protective role of RIPK1 in these cells, as previously reported in other cells.[12,13,27,45]

Figure 7 proposes a schematic model of TNF-*α* signaling in hepatocytes of mice challenged with ConA. The lectin activates T lymphocytes (LT), Kupffer (KC), NK and NKT cells, which result in the release by these cells of cytokines, such as TNF-*α* and IFN-*γ*. Activation of NKT cells induces hepatocyte death mediated by TRAIL/DR5 signaling, and potentially also by TNFR1, which depends on RIPK1 kinase activity. TNF/TNFR1 binding also induces assembly of complex I by recruitment of TRADD, RIPK1 and TRAF2 preventing caspase activation and limiting cell death. RIPK1 deficiency induces TRAF2 destabilization upon stimulation and promotes formation of complex II, caspase-8 activation and apoptosis induction.

This work underlines the interest to focus studies on RIPK1 in other hepatitis models, and especially in acetaminophen (APAP) liver toxicity, where the role attributed to RIPK1 is not yet fully understood. Whereas most studies reveal a protective role of kinase inhibition by Nec-1[46–48] or RIPK1 knockdown.[49] Schneider *et al.*[50] recently suggest that RIPK1 deletion in hepatocytes has no effect in this hepatitis model. According to our demonstrated dual role of RIPK1 in hepatocytes, the kinase pro-death role of RIPK1 should be dissociated from his scaffolding pro-survival function in these studies by challenging RIPK1 kinase dead (*Ripk1*^{K45A}) mice with APAP.

Moreover, our data could explain recent results obtained with of NEMO$^{LPC\text{-}KO}$ mice, which presented spontaneous hepatocyte death.[44,51,52] Surprisingly, apoptosis is strongly prevented by crossing NEMO$^{LPC\text{-}KO}$ mice with RIPK1 kinase dead mice while poorly with *Ripk1*$^{LPC\text{-}KO}$.[44] As NEMO$^{LPC\text{-}KO}$ mice presented elevated TNF-*α* in the liver compared with WT

mice,[51] additional RIPK1 deficiency could induce hepatocyte apoptosis in a TNF-α-dependent manner.

In conclusion, our results underline the protective role of RIPK1 in dysimmune hepatitis and the risks of potential defects in the RIPK1 scaffolding function that would sensitize hepatocyte to the death, risking to worsen hepatitis and even to the increase of HCC onset. Furthermore, our data pointed out the importance of studying the potential relationship between the genetic polymorphism of *Ripk1* gene and the predisposition to more severe liver damage in hepatic infectious or autoimmune diseases. Finally, our results support also that RIPK1 kinase activity is a pertinent therapeutic target to protect liver against excessive cell death in liver diseases.

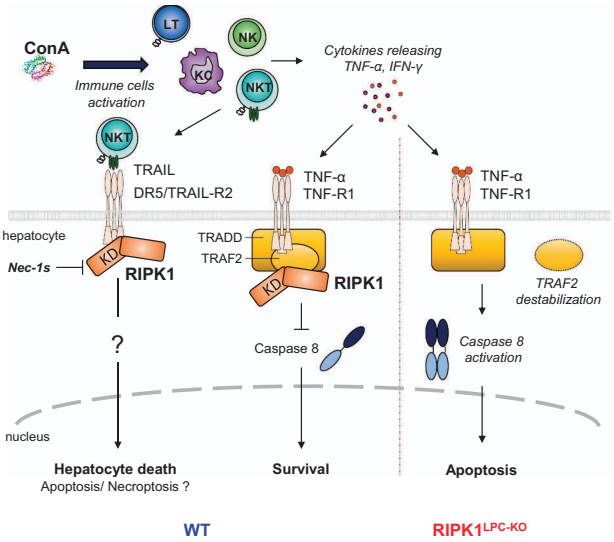

Figure 7 Role of RIPK1 in ConA hepatitis model. Schema of cell death pathway during ConA hepatitis in WT and *Ripk1*$^{LPC-KO}$ mice. The lectin activates LT, KC, NK and NKT cells, which result in the release by these cells of cytokines, such as TNF-α and IFN-γ. Activation of NKT cells induces hepatocyte death mediated by TRAIL/DR5 signaling, and potentially also by TNFR1, which depends on RIPK1 kinase activity. TNF/TNFR1 binding also induces assembly of complex I by recruitment of TRADD, RIPK1 and TRAF2 preventing caspase activation and limiting cell death. RIPK1 deficiency induces TRAF2 destabilization upon stimulation and promotes formation of complex II by caspase-8 and apoptosis induction

Materials and Methods

Animals and treatment protocols. *Ripk1*$^{LPC-KO}$ mice were generated by crossing *Ripk1*$^{fl/fl}$ strain[11] with Alfp-Cre transgenic mice having a Cre recombinase driven by the serum albumin gene promoter completed with albumin and α-fetoprotein enhancers.[21] RIPK1 kinase dead knock-in (*Ripk1*^{K45A}) mice have been already described.[10] In all experiments, genetically modified mice were systematically compared with their littermates. Animals were housed in individually ventilated cages at the VIB Inflammation Research Center in conventional animal facilities. All experiments on mice were conducted according to Institutional, National and European animal regulations. *In vivo* protocols were approved by the ethics committee of Ghent University. Homogeneous groups of male and female mice at 7–13 weeks of age were used for each experiment. ConA (C2010 Sigma-Aldrich, St. Louis, MO, USA) diluted at 3 mg/ml in PBS supplemented with $MnCl_2$ 0.31 mM and $CaCl_2$ 0.75 mM, was administered by intravenous (i.v.) injection at a dose of 10 or 12 mg/kg body weight. Q-VD-OPh hydrate (Sigma-Aldrich, SML0063) was injected in mice via the intraperitoneal (i.p.) route (20 mg/kg and 10 μl/g of body weight) 1 h before ConA injection. Nec-1 s (Biovision Inc., #2263) was administered by i.v. injection (6.25 mg/kg and 4 μl/g body weight) 15 min before the ConA challenge. An i.p. injection was used to deliver ETA (Enbrel, Pfizer) to mice (10 mg/kg and 10 μl/g body weight) 1 h before ConA injection. Mice were given a single i.v. injection of murine TNF-α (mTNF-α, Peprotech, 315-01A, 40 μg/ml, at a dose of 10 μg/kg body weight). The control mice received similar volumes of vehicle in each treatment group. Times of killing are indicated for each experiment.

RNA analysis. Total RNA was extracted, from mice livers tissues using TRIzol reagent (Invitrogen) and from primary hepatocytes by using the RNeasy mini kit (Qiagen, #74106). First-strand cDNA was synthesized using the SuperScript™ II Reverse Transcriptase (Invitrogen). Real-time quantitative PCR was performed using the fluorescent dye SYBR Green with the double-strand specific SYBR® Green system (Applied Biosystems) and the ABI 7000 Prism sequence detector (Applied Biosystems) or the CFX384 Touch™ Real-Time PCR Detection System (Bio-Rad). cDNA was used as template for amplification with specific primer pairs (Table 1). Each measurement was performed in triplicate. The relative gene expression was normalized against the 18S gene expression. The control mice in each treatment group served as a reference for messenger RNA (mRNA) expression (control mRNA level was arbitrarily set at 1).

Histopathological and biochemical studies. Fragments of mouse livers were fixed in 4% paraformaldehyde and embedded in paraffin for IHC and hematoxylin and eosin (H&E), or frozen in isopentane cooled with liquid nitrogen for immunofluorescence studies. For histopathology, H&E staining of liver tissues was carried out to investigate liver injury. Serum ALT and AST transaminases was measured according to the IFCC primary reference procedures using Olympus AU2700 Autoanalyser® (Olympus Optical, Tokyo, Japan).

Immunolocalization in liver tissues. For immunolocalization of cleaved-caspase-3, RIPK1, NF-κB-p65 and Ki67 in liver tissues, paraffin-embedded mouse liver sections (4–5 μm) were dried 1 h at 58 °C, followed by antigen retrieval and incubated with primary antibody (Cell Signaling, 9661S; 3493; Santa Cruz Biotechnology, sc-372, respectively) in a Ventana automated machine (Ventana Medical Systems, USA). Revelation of primary antibody was carried out using horseradish peroxidase (HRP)-conjugated secondary antibody (Dako, USA) and

Table 1 Sequence of primers used for qPCR

Gene	Forward	Reverse
Mouse 18S	5′-CGCCGCTAGAGGTGAAATTC-3′	5′-TTGGCAAATGCTTTCGCTC-3′
Mouse TNF-α	5′-TAGCTCCCAGAAAAGCAAGC-3′	5′-TTTTCTGGAGGGAGATGTGG-3′
Mouse IL-6	5′-CCGGAGAGGAGACTTCACAG-3′	5′-CAGAATTGCCATTGCACAAC-3′
Mouse IFN-γ	5′-AGGTCAACAACCCACAGGTC-3′	5′-ATCAGCAGCGACTCCTTTTC-3′
Mouse-CXCL1	5′-CGCCTATCGCCAATGAGC-3′	5′-GAACCAAGGGAGCTTCAGG-3′
Mouse TNFR1	5′-CAGAACACCGTGTGTAACTGC-3′	5′-GCAAGCGGAGGAGGTAGG-3′
Mouse TNFR2	5′-CGCTGGTCTTCGAACTGC-3′	5′-CAGGAGGACACTTAGCACAGC-3′
SAA1	5′-TGTTCACGAGGCTTTCCAAG-3′	5′-GTCCTCTGCCGAAGAATTCC-3′
CCL20	5′-TCTGCTCTTCCTTGCTTTGG-3′	5′-TCACCCAGTTCTGCTTTGG-3′
Mouse-IKK-γ/NEMO	5′-GGTGGAGAGACTGAGCTTGG-3′	5′-CCTCTAAAGCTTGCCGATCC-3′

DAB substrate kit (Ventana Medical Systems, #760-124). Slides were then counterstained with hematoxylin. TUNEL analysis was performed on mouse liver sections incubated after antigen retrieval with a mix composed of terminal transferase (Roche, 3333566 011) and digoxigenin-11-UTP (Roche, #1558706) followed by biotinylated anti-digoxigenin (Sigma, #B7405) and counterstained with hematoxylin.

For immunolocalization of CD11b and CD45 in liver tissues, cryosections of mouse liver tissues (8 μm) were successively fixed with paraformaldehyde 4%, treated with NH_4Cl 0.1 M, blocked with 2–4% BSA and incubated with primary antibody (BD Pharmingen, #552850 and #553079; respectively) at 4 °C overnight. Revelation of primary antibody was carried out using DyLight 649-conjugated donkey anti-rat IgG secondary antibody (Jackson ImmunoResearch Laboratories). Nuclei were stained with Hoechst (Invitrogen, H3570) and F-actin with Phalloïdine FluoProbes-547H (Interchim, BZ9620). Image analysis and merged were performed with SpotAdvanced software. Quantification of cleaved-caspase-3 positive-signal was performed with image analysis software (NIS-Element AR analysis) and measured to cover an area of 4.3–6 mm^2. The quantification hepatocytes with nuclear NF-κB, labeled nuclei were counted on 3–4 independent fields to cover an area of 3.54–4.72 mm^2.Pictures presented in the figures are issued from animals with ALT or quantified staining values close to the average obtained for the membership group.

Protein extraction and western blotting. Primary hepatocytes and mouse liver specimens were lysed in RIPA buffer (50 mM Tris-HCl pH 7.4; 1% Triton X-100; 25 mM HEPES; 150 mM NaCl; 0,2% SDS; 5 mM $MgCl_2$; 1 mM Na_3VO_4; 1 mM NaF and proteases inhibitors (Roche, #04 693 132 001)), and liver were crushed with UltraTurax. After 40 min in ice, samples were centrifuged at 13 000 *g*. Proteins from supernatant were assayed with the Bradford method (Bio-Rad). Proteins were separated by SDS-PAGE and transferred onto nitrocellulose membrane. Membranes were blocked with non-fat milk or BSA 3–5% in TBS (20 mM Tris, 137 mM NaCl) during 1–2 h and incubated overnight with primary antibody anti-cleaved-caspase-3, anti-RIPK1 (Cell Signaling) anti-actin (Sigma A3854), anti-TRAF2 (Santa Cruz Biotechnology, sc-876), anti-phospho-IκBα (Cell Signaling, #2859) or anti-IκBα (Santa Cruz Biotechnology, sc-371) at 4 °C, and then with secondary goat anti-rabbit immunoglobulins/HRP (Dako, P0448). Protein–antibody complexes were revealed by enhanced chemiluminescence (Millipore) and ImageQuant LAS-4000 mini imager analysis (GE Healthcare).

Primary hepatocyte isolation and culture. Hepatocytes were isolated from adult C57BL/6 WT and *Ripk1*$^{LPC\text{-}KO}$ mice by the retrograde perfusion approach.[23] Mice were previously anesthetized by i.p injection of a ketamine (Imalgene^{TM}, supplier) and xylazine (Rompun^{TM}, supplier) cocktail (60 and 10 mg/kg of live body weight, respectively) diluted in PBS. After laparotomy, the liver, perfused through *inferior vena cava*, was first washed with solution I (8 g/l NaCl, 0.2 g/l KCl, 0.1 g/l Na_2HPO_4. 12 H_2O and 2.38 g/l Hepes, pH 7.6) at a 5.5 ml/min flow rate for 8–10 min. Then, the perfusion solution I was supplemented with 5 mM $CaCl_2.2H_2O$ and 0.01% collagenases (Liberase^{TM} TM Research Grade, Roche) for 5–7 min. Hepatocytes were harvested after three centrifugations at 90 g for 1 min and an additional purification of viable cells on a percoll cushion. Cell suspensions, with over 90% viability, were seeded at a density of 0.1×10^6 cells/cm^2 in 24-well plates, previously coated with collagen type I (BD Biosciences, Le Pont de Claix, France), in Williams' E medium supplemented with 10% (vol/vol) fetal calf serum, 2 mM glutamine, 10 IU/ml penicillin, 10 μg/ml streptomycin and 5 μg/ml insulin. Seeding medium was removed after a 4-h period and replaced by a similar supplemented Williams' E medium, without fetal calf serum but with 1 mg/ml bovine serum albumin, but with 1 μg/ml of ETA and optionally with 10 μM of z-VAD-fmk. After two or three washes, cells were stimulated with 10 ng/ml of mTNF-α (Peprotech, 315-01A), and used for RNA or protein extraction. Experimental protocol was conducted in compliance with French laws and the institution's guidelines for animal welfare (agreement of M Samson # A3523840).

Serum cytokine immunoassays by flow cytometry. Murine TNF-α, IFN-γ and IL-6 cytokines were quantified by bead-based immunoassays according to the manufacturer protocol, using a filter plate and a vacuum filtration system for washing steps (BioLegend's LEGENDPLEX, multi-analyte flow assay kit). Samples were analyzed on FC500 cytometer (Beckman Coulter).

Immune cells analysis by flow cytometry. Immune cells were prepared from spleen or liver crushed on a 70 μm filter. Liver immune cells were isolated after sedimentation and cell fractionation on a 35% Percoll layer. For each organ, red blood cells were lysed with the ammonium-chloride-potassium (ACK) buffer. To exclude dead cells from analysis, cell suspensions were labeled for 30 min with LIVE/DEAD fixable yellow stain (Life Technologies, L34959). Cells were also pre-incubated with an anti-CD16/32 antibody (BD Pharmingen) to block nonspecific binding, before the incubation with the appropriate fluorochrome-conjugated antibodies (BD Pharmingen, eBioscience): anti-CD3-FITC (clone 17A2), anti-TCRβ-V450 (clone H57-597), anti-CD69-PE (clone H1.2F3), anti-CD19-APC (clone 1D3), anti-NK1.1-PerCP-Cy-5.5 (clone PK136), anti-CD4-PE-Cy7 (clone RM4-5), anti-CD8-APC-Cy7 (clone 53-6.7), anti-GR1-eFluor450 (clone FB6-8C5) or anti-CD11b-PE-Cy7 (clone M1/70). The stained cells were analyzed on FACSAria™ II flow cytometer using BD FACSDiva software (BD Bioscience), and data were analyzed with the CXP software (Beckman Coulter). Doublet and dead cells were excluded, respectively, on the basis of forward/side scatter and with the LIVE/DEAD labeling. The used immuno-phenotyping was as followed: Lymphocyte B (LyB): CD19+/CD3- cells; Lymphocyte T (LyT): CD3+/TCRVβ+/NK1.1-; NKT cells: CD3+/ TCRVβ+/NK1.1+; NK cells: CD3-/NK1.1+; granulocytes: GR1+CD11b+. Lymphoid activation was studied by analyzing the expression of CD69. To calculate percentage of each immune cell population, we considered as 100% of immune cells the sum of events of each immune cell population analyzed (sum of LyT, LyB, NK cells, NKT cells and granulocytes).

Statistical analysis. Data were expressed as means $\pm$S.E.M. for all mice treated similarly. Kruskal–Wallis one-way analysis of variance (ANOVA) was performed, and mean differences between experimental groups were assessed using the non-parametric Mann–Whitney *U*-test with the GraphPad Prism5 software. The significance is shown as follows: $^{*}P<0.05$, $^{**}P<0.01$, $^{***}P<0.001$, WT versus RIPK1 mice. $^{\#}P<0.05$, $^{\#\#}P<0.01$, $^{\#\#\#}P<0.001$, mice treated with ConA, or TNF-α versus mice treated with PBS. $^{\$}P<0.05$, $^{\$\$}P<0.01$, $^{\$\$\$}P<0.001$ mice treated with ConA, or TNF-α at an indicated time versus mice treated with ConA, or TNF-α at another time in same genotype.

Conflict of Interest

The authors declare no conflict of interest.

Acknowledgements. This work was supported by Inserm, The Ministère de l'Education Nationale de la Recherche et de la Technologie, the University of Rennes 1, the Région Bretagne, the INCa (Institut national du cancer), and the 'Ligue contre le cancer, comités du grand Ouest'. Research in the Vandenabeele group is supported by Belgian grants (Interuniversity Attraction Poles, IAP 7/32), Flemish grants (Research Foundation Flanders: FWO G.0875.11, FWO G.0973.11, FWO G.0A45.12N, FWO G.0172.12, FWO G.0787.13N, FWO G.0607.13N, FWO KAN 31528711, FWO KAN 1504813N, FWO G0E04.16N), Methusalem grant (BOF16/MET_V/007), Ghent University grants (MRP, GROUP-ID consortium, BOF-GOA2014000702), grant from the Foundation against Cancer (F94), and grants from VIB. AF was supported by a PhD fellowship from the Région Bretagne. MF was supported by a PhD fellowship from the Government of Pakistan (Higher Education Commission, University of Agriculture, Lahore). PV is senior full professor at Ghent University and holds a Methusalem grant (BOF09/01M00709). For immunohistochemistry analysis and animal house facilities, we would like to thank dedicated platforms (i.e., H2P2 and animal house platforms) of SFR BIOSIT, University of Rennes 1, France. We would also like to thank Barbara Gilbert and Cristina Ulecia Morón for technical assistance.

1. Friedman SL. Liver fibrosis – from bench to bedside. *J Hepatol* 2003; **38**: S38–S53.
2. Luedde T, Kaplowitz N, Schwabe RF. Cell death and cell death responses in liver disease: mechanisms and clinical relevance. *Gastroenterology* 2014; **147**: 765–783 e764.
3. Brenner C, Galluzzi L, Kepp O, Kroemer G. Decoding cell death signals in liver inflammation. *J Hepatol* 2013; **59**: 583–594.
4. Arshad MI, Piquet-Pellorce C, L'Helgoualc'h A, Rauch M, Patrat-Delon S, Ezan F *et al.* TRAIL but not FasL and TNFalpha, regulates IL-33 expression in murine hepatocytes during acute hepatitis. *Hepatology* 2012; **56**: 2353–2362.
5. Pasparakis M, Vandenabeele P. Necroptosis and its role in inflammation. *Nature* 2015; **517**: 311–320.
6. Muto Y, Nouri-Aria KT, Meager A, Alexander GJ, Eddleston AL, Williams R. Enhanced tumour necrosis factor and interleukin-1 in fulminant hepatic failure. *Lancet* 1988; **2**: 72–74.
7. Bird GL, Sheron N, Goka AK, Alexander GJ, Williams RS. Increased plasma tumor necrosis factor in severe alcoholic hepatitis. *Ann Intern Med* 1990; **112**: 917–920.

8. Morioka S, Broglie P, Omori E, Ikeda Y, Takaesu G, Matsumoto K *et al.* TAK1 kinase switches cell fate from apoptosis to necrosis following TNF stimulation. *J Cell Biol* 2014; **204**: 607–623.
9. Kelliher MA, Grimm S, Ishida Y, Kuo F, Stanger BZ, Leder P. The death domain kinase RIP mediates the TNF-induced NF-kappaB signal. *Immunity* 1998; **8**: 297–303.
10. Berger SB, Kasparcova V, Hoffman S, Swift B, Dare L, Schaeffer M *et al.* Cutting edge: RIP1 kinase activity is dispensable for normal development but is a key regulator of inflammation in SHARPIN-deficient mice. *J Immunol* 2014; **192**: 5476–5480.
11. Takahashi N, Vereecke L, Bertrand MJ, Duprez L, Berger SB, Divert T *et al.* RIPK1 ensures intestinal homeostasis by protecting the epithelium against apoptosis. *Nature* 2014; **513**: 95–99.
12. Dannappel M, Vlantis K, Kumari S, Polykratis A, Kim C, Wachsmuth L *et al.* RIPK1 maintains epithelial homeostasis by inhibiting apoptosis and necroptosis. *Nature* 2014; **513**: 90–94.
13. Roderick JE, Hermance N, Zelic M, Simmons MJ, Polykratis A, Pasparakis M *et al.* Hematopoietic RIPK1 deficiency results in bone marrow failure caused by apoptosis and RIPK3-mediated necroptosis. *Proc Natl Acad Sci USA* 2014; **111**: 14436–14441.
14. Tiegs G, Hentschel J, Wendel AA. T cell-dependent experimental liver injury in mice inducible by concanavalin A. *J Clin Invest* 1992; **90**: 196–203.
15. Arshad MI, Rauch M, L'Helgoualc'h A, Julia V, Leite-de-Moraes MC, Lucas-Clerc C *et al.* NKT cells are required to induce high IL-33 expression in hepatocytes during ConA-induced acute hepatitis. *Eur J Immunol* 2011; **41**: 2341–2348.
16. Watanabe Y, Morita M, Akaike T. Concanavalin A induces perforin-mediated but not Fas-mediated hepatic injury. *Hepatology* 1996; **24**: 702–710.
17. Tagawa Y, Kakuta S, Iwakura Y. Involvement of Fas/Fas ligand system-mediated apoptosis in the development of concanavalin A-induced hepatitis. *Eur J Immunol* 1998; **28**: 4105–4113.
18. Kusters S, Tiegs G, Alexopoulou L, Pasparakis M, Douni E, Kunstle G *et al. In vivo* evidence for a functional role of both tumor necrosis factor (TNF) receptors and transmembrane TNF in experimental hepatitis. *Eur J Immunol* 1997; **27**: 2870–2875.
19. Jouan-Lanhouet S, Arshad MI, Piquet-Pellorce C, Martin-Chouly C, Le Moigne-Muller G, Van Herreweghe F *et al.* TRAIL induces necroptosis involving RIPK1/RIPK3-dependent PARP-1 activation. *Cell Death Differ* 2012; **19**: 2003–2014.
20. Zhou Y, Dai W, Lin C, Wang F, He L, Shen M *et al.* Protective effects of necrostatin-1 against concanavalin A-induced acute hepatic injury in mice. *Mediators Inflamm* 2013; **2013**: 1–15.
21. Kellendonk C, Opherk C, Anlag K, Schütz G, Tronche F. Hepatocyte-specific expression of Cre recombinase. *Genesis (New York, NY: 2000)* 2000; **26**: 151–153.
22. Arshad MI, Piquet-Pellorce C, Filliol A, L'Helgoualc'h A, Lucas-Clerc C, Jouan-Lanhouet S *et al.* The chemical inhibitors of cellular death, PJ34 and Necrostatin-1, down-regulate IL-33 expression in liver. *J Mol Med (Berl)* 2015; **93**: 867–878.
23. Houseman L, Edwards M, Phillips IR, Shephard EA. Isolation and culture of mouse hepatocytes: gender-specific gene expression responses to chemical treatments. *Methods Mol Biol* 2015; **1250**: 3–12.
24. Sato M, Tanigawa M. Production of CETD transgenic mouse line allowing ablation of any type of specific cell population. *Mol Reprod Dev* 2005; **72**: 54–67.
25. Degterev A, Maki JL, Yuan J. Activity and specificity of necrostatin-1, small-molecule inhibitor of RIP1 kinase. *Cell Death Differ* 2013; **20**: 366.
26. Takahashi N, Duprez L, Grootjans S, Cauwels A, Nerinckx W, DuHadaway JB *et al.* Necrostatin-1 analogues: critical issues on the specificity, activity and in vivo use in experimental disease models. *Cell Death Dis* 2012; **3**: e437.
27. Gentle IE, Wong WW, Evans JM, Bankovacki A, Cook WD, Khan NR *et al.* In TNF-stimulated cells, RIPK1 promotes cell survival by stabilizing TRAF2 and cIAP1, which limits induction of non-canonical NF-kappaB and activation of caspase-8. *J Biol Chem* 2011; **286**: 13282–13291.
28. Estornes Y, Aguileta MA, Dubuisson C, De Keyser J, Goossens V, Kersse K *et al.* RIPK1 promotes death receptor-independent caspase-8-mediated apoptosis under unresolved ER stress conditions. *Cell Death Dis* 2014; **5**: e1555.
29. Mizuhara H, O'Neill E, Seki N, Ogawa T, Kusunoki C, Otsuka K *et al.* T cell activation-associated hepatic injury: mediation by tumor necrosis factors and protection by interleukin 6. *J Exp Med* 1994; **179**: 1529–1537.
30. Gantner F, Leist M, Lohse AW, Germann PG, Tiegs G. Concanavalin A-induced T-cell-mediated hepatic injury in mice: the role of tumor necrosis factor. *Hepatology (Baltimore, MD)* 1995; **21**: 190–198.
31. Van Antwerp DJ, Martin SJ, Kafri T, Green DR, Verma IM. Suppression of TNF-alpha-induced apoptosis by NF-kappaB. *Science* 1996; **274**: 787–789.
32. Liedtke C, Trautwein C. The role of TNF and Fas dependent signaling in animal models of inflammatory liver injury and liver cancer. *Eur J Cell Biol* 2012; **91**: 582–589.
33. Kawasuji A, Hasegawa M, Horikawa M, Fujita T, Matsushita Y, Matsushita T *et al.* L-selectin and intercellular adhesion molecule-1 regulate the development of concanavalin A-induced liver injury. *J Leukoc Biol* 2006; **79**: 696–705.
34. Wolf D, Hallmann R, Sass G, Sixt M, Kusters S, Fregien B *et al.* TNF-alpha-induced expression of adhesion molecules in the liver is under the control of TNFR1–relevance for concanavalin A-induced hepatitis. *J Immunol* 2001; **166**: 1300–1307.
35. Tiegs G, Wolter M, Wendel A. Tumor necrosis factor is a terminal mediator in galactosamine/endotoxin-induced hepatitis in mice. *Biochem Pharmacol* 1989; **38**: 627–631.
36. Geisler F, Algül H, Paxian S, Schmid RM. Genetic inactivation of RelA/p65 sensitizes adult mouse hepatocytes to TNF-induced apoptosis *in vivo and in vitro. Gastroenterology* 2007; **132**: 2489–2503.
37. Wroblewski R, Armaka M, Kondylis V, Pasparakis M, Walczak H, Mittrucker HW *et al.* Opposing role of tumor necrosis factor receptor 1 signaling in T cell-mediated hepatitis and bacterial infection in mice. *Hepatology* 2016.
38. Festjens N, Vanden Berghe T, Cornelis S, Vandenabeele P. RIP1, a kinase on the crossroads of a cell's decision to live or die. *Cell Death Differ* 2007; **14**: 400–410.
39. Kunstle G, Hentze H, Germann PG, Tiegs G, Meergans T, Wendel A. Concanavalin A hepatotoxicity in mice: tumor necrosis factor-mediated organ failure independent of caspase-3-like protease activation. *Hepatology* 1999; **30**: 1241–1251.
40. Dondelinger Y, Aguileta MA, Goossens V, Dubuisson C, Grootjans S, Dejardin E *et al.* RIPK3 contributes to TNFR1-mediated RIPK1 kinase-dependent apoptosis in conditions of cIAP1/2 depletion or TAK1 kinase inhibition. *Cell Death Differ* 2013; **20**: 1381–1392.
41. Ting AT, Bertrand MJ. More to life than NF-kappaB in TNFR1 signaling. *Trends Immunol* 2016; **37**: 535–545.
42. Liedtke C, Bangen JM, Freimuth J, Beraza N, Lambertz D, Cubero FJ *et al.* Loss of caspase-8 protects mice against inflammation-related hepatocarcinogenesis but induces non-apoptotic liver injury. *Gastroenterology* 2011; **141**: 2176–2187.
43. Vucur M, Reisinger F, Gautheron J, Janssen J, Roderburg C, Cardenas DV *et al.* RIP3 inhibits inflammatory hepatocarcinogenesis but promotes cholestasis by controlling caspase-8- and JNK-dependent compensatory cell proliferation. *Cell Rep* 2013; **4**: 776–790.
44. Kondylis V, Polykratis A, Ehlken H, Ochoa-Callejero L, Straub BK, Krishna-Subramanian S *et al.* NEMO prevents steatohepatitis and hepatocellular carcinoma by inhibiting RIPK1 kinase activity-mediated hepatocyte apoptosis. *Cancer Cell* 2015; **28**: 582–598.
45. Wong WW, Gentle IE, Nachbur U, Anderton H, Vaux DL, Silke J. RIPK1 is not essential for TNFR1-induced activation of NF-kappaB. *Cell Death Differ* 2010; **17**: 482–487.
46. An J, Mehrhof F, Harms C, Lattig-Tunnemann G, Lee SL, Endres M *et al.* ARC is a novel therapeutic approach against acetaminophen-induced hepatocellular necrosis. *J Hepatol* 2013; **58**: 297–305.
47. Takemoto K, Hatano E, Iwaisako K, Takeiri M, Noma N, Ohmae S *et al.* Necrostatin-1 protects against reactive oxygen species (ROS)-induced hepatotoxicity in acetaminophen-induced acute liver failure. *FEBS Open Bio* 2014; **4**: 777–787.
48. Zhang YF, He W, Zhang C, Liu XJ, Lu Y, Wang H *et al.* Role of receptor interacting protein (RIP)1 on apoptosis-inducing factor-mediated necroptosis during acetaminophen-evoked acute liver failure in mice. *Toxicol Lett* 2014; **225**: 445–453.
49. Dara L, Johnson H, Suda J, Win S, Gaarde W, Han D *et al.* Receptor interacting protein kinase 1 mediates murine acetaminophen toxicity independent of the necrosome and not through necroptosis. *Hepatology* 2015; **62**: 1847–1857.
50. Schneider AT, Gautheron J, Tacke F, Vucur M, Luedde T. Receptor interacting protein kinase-1 (RIPK1) in hepatocytes does not mediate murine acetaminophen toxicity. *Hepatology* 2015.
51. Luedde T, Beraza N, Kotsikoris V, van Loo G, Nenci A, De Vos R *et al.* Deletion of NEMO/IKKgamma in liver parenchymal cells causes steatohepatitis and hepatocellular carcinoma. *Cancer Cell* 2007; **11**: 119–132.
52. Ehlken H, Krishna-Subramanian S, Ochoa-Callejero L, Kondylis V, Nadi NE, Straub BK *et al.* Death receptor-independent FADD signalling triggers hepatitis and hepatocellular carcinoma in mice with liver parenchymal cell-specific NEMO knockout. *Cell Death Differ* 2014; **21**: 1721–1732.

Supplementary Information accompanies this paper on Cell Death and Disease website (http://www.nature.com/cddis)

Suplementary Figure 1

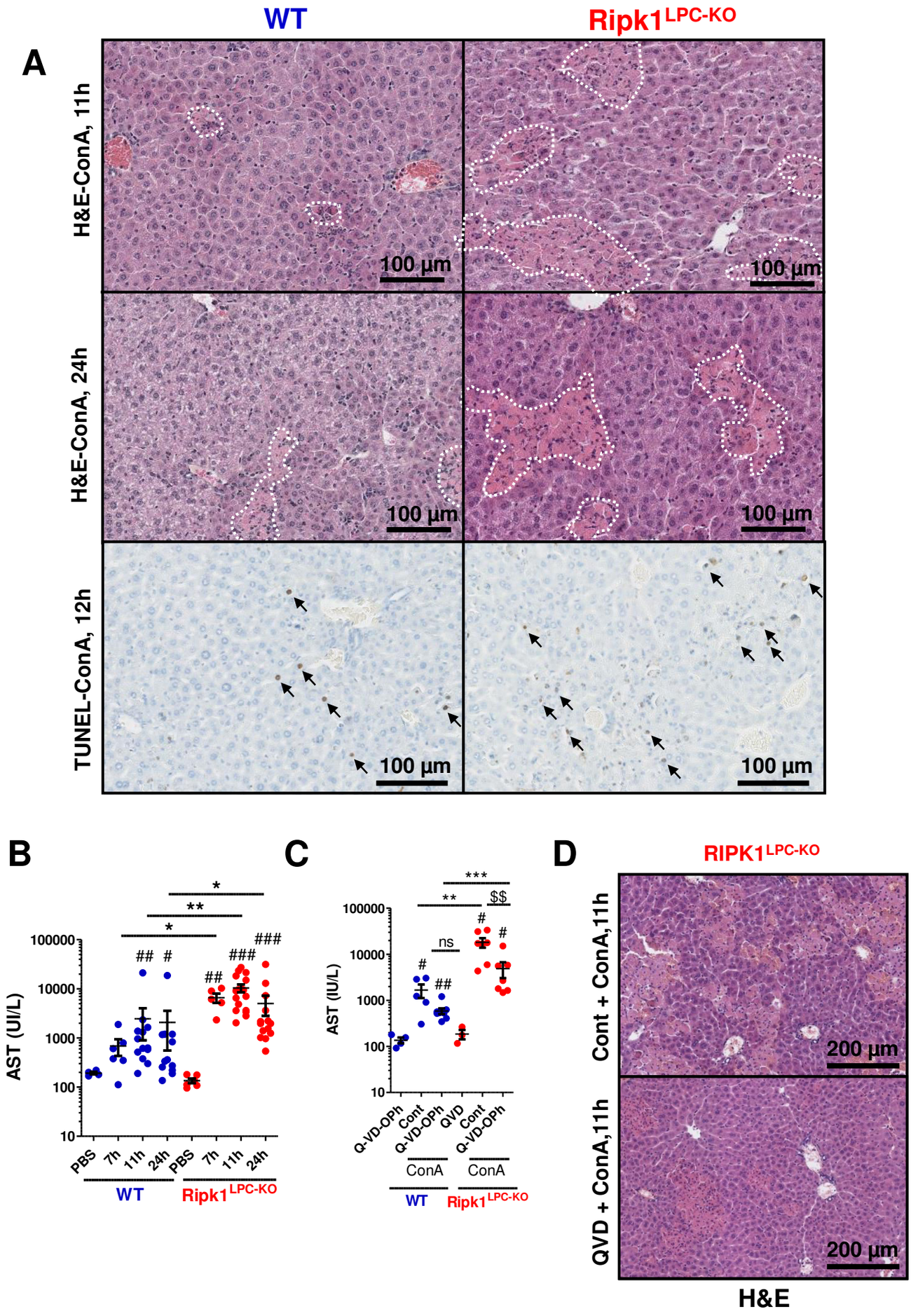

Suplementary Figure 2

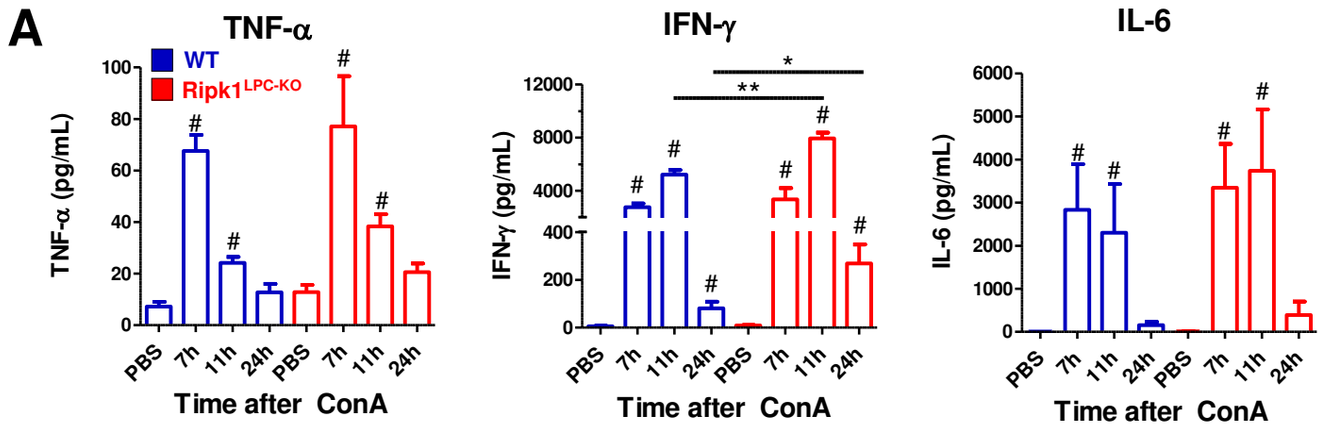

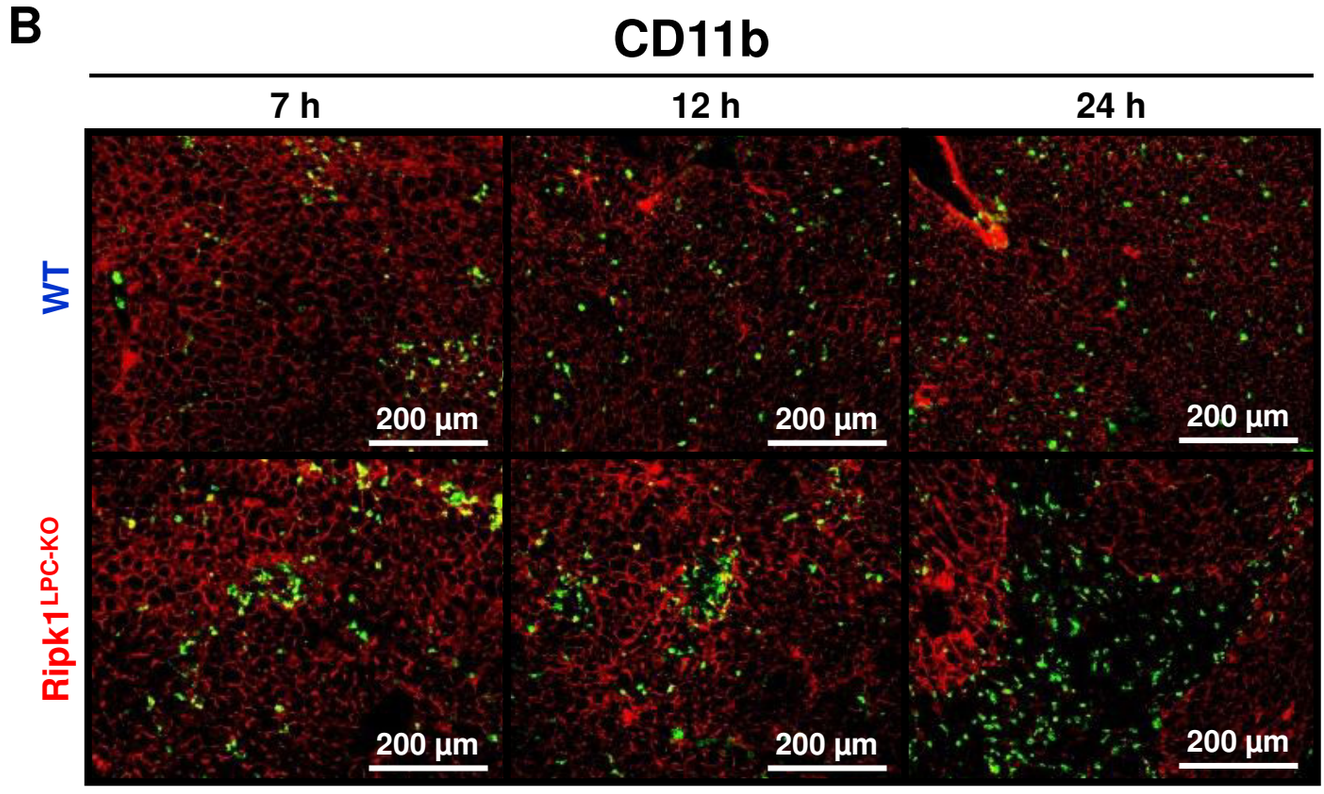

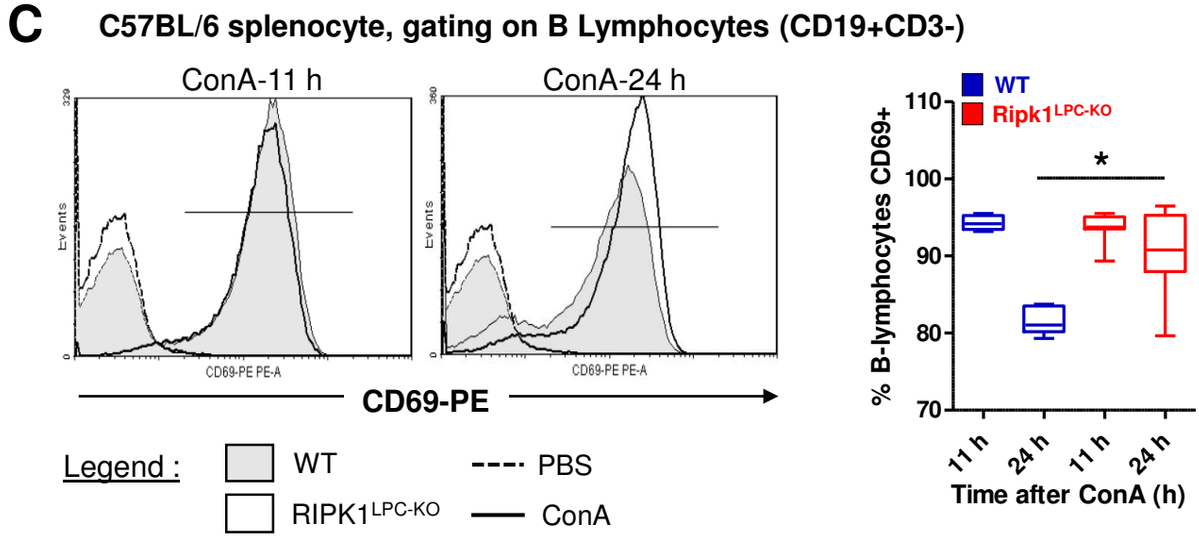

Suplementary Figure 3

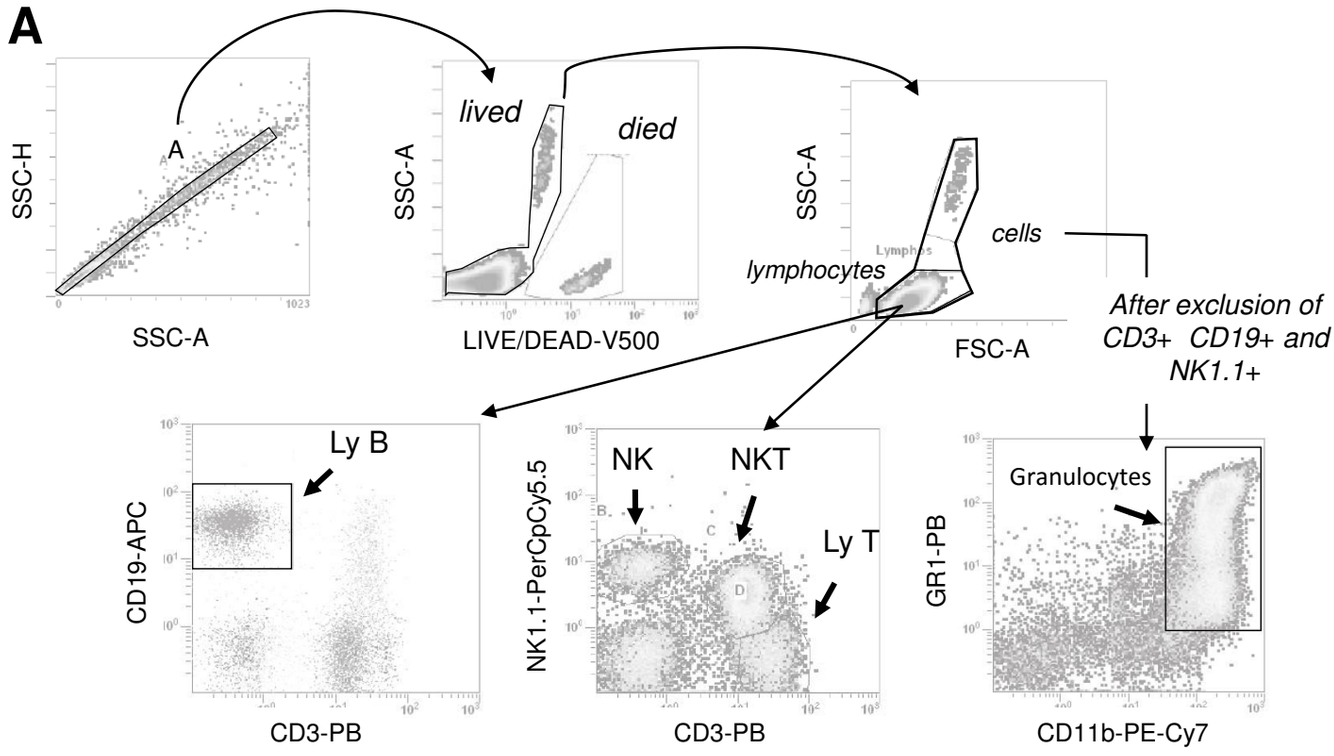

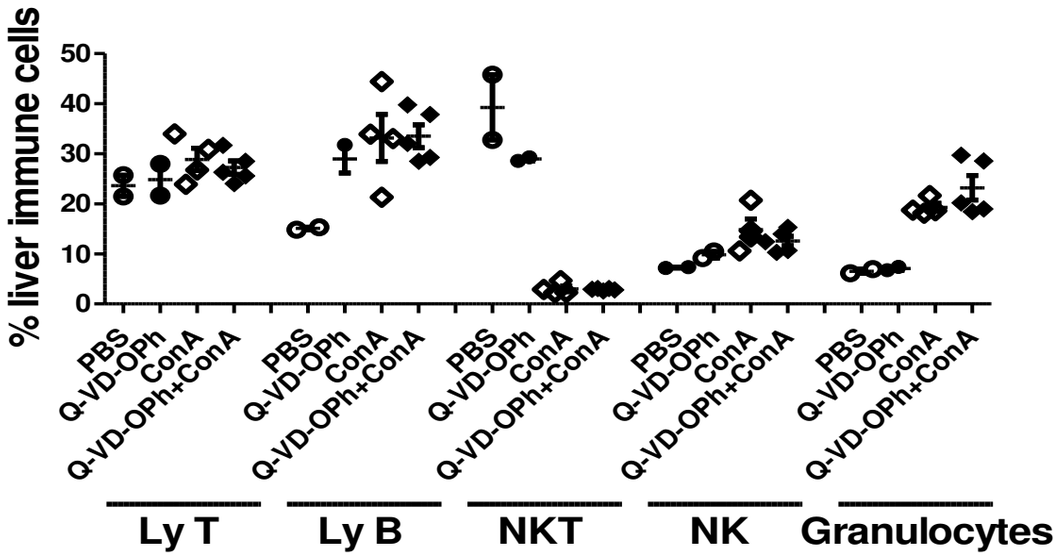

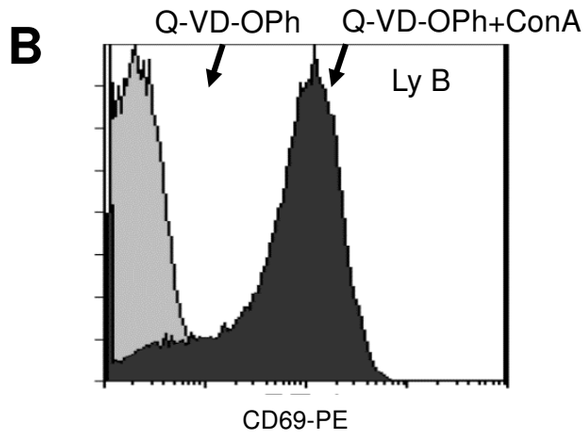

Suplementary Figure 4

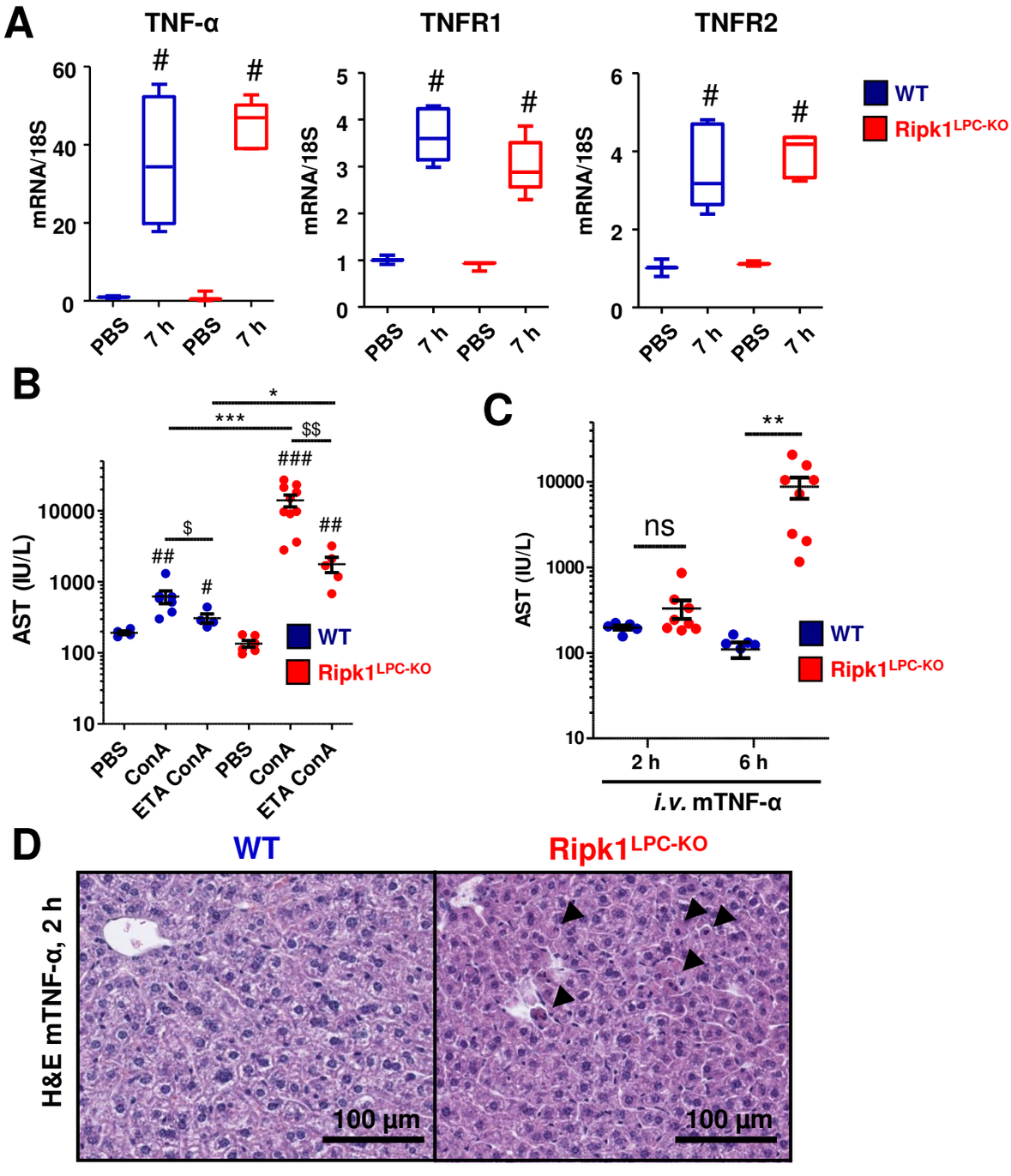

Suplementary Figure 5

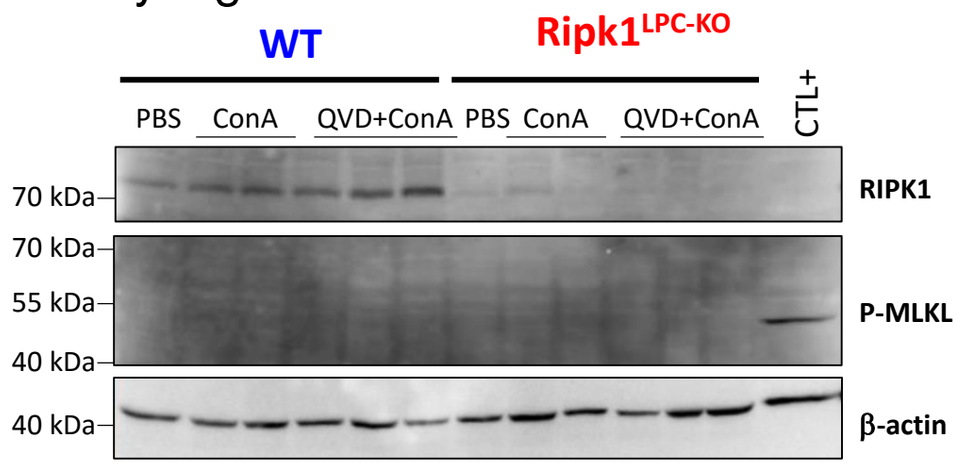

Supplementary Figure 6

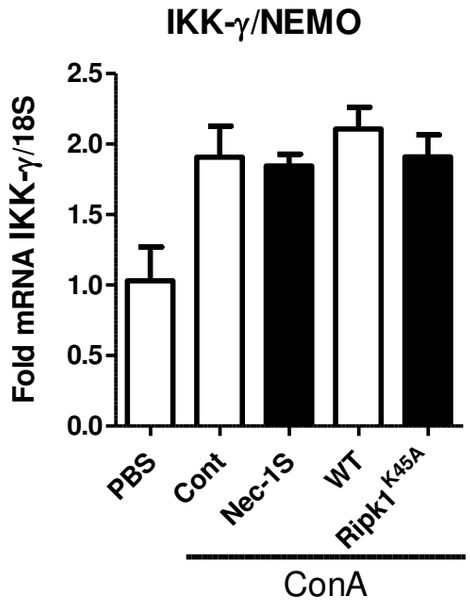

Supplementary Figure 7

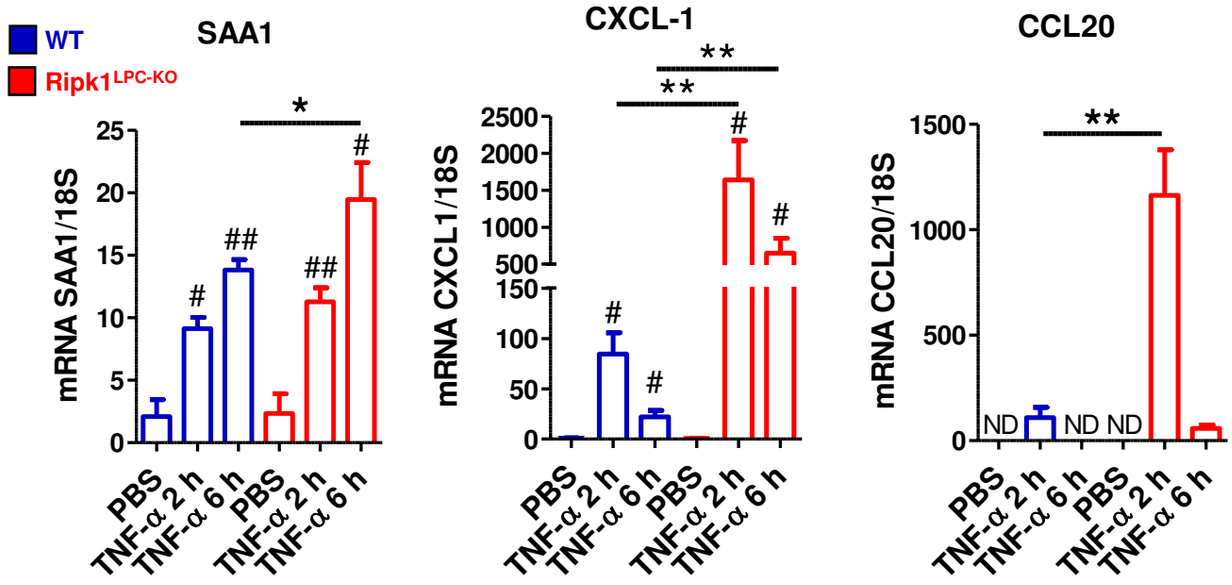

III.2. ARTICLE II : RIPK1 protège les hépatocytes de l'apoptose déclenché par le TNF-α induit par les cellules de Kupffer dans des modèles d'hépatites dépendant de PAMP

Aveline Filliol, Claire Piquet-Pellorce, Céline Raguénès-Nicol, Muhammad Farooq, Catherine Lucas-Clerc, Peter Vandenabeele, Mathieu JM Bertrand, Jacques Le Seyec and Michel Samson.

Article actuellement en révision dans *Journal of Hepatology*.

Introduction de l'article.

La sensibilité des souris *Ripk1*$^{LPC\text{-}KO}$ à l'hépatite induite par la ConA et le TNF-α (article I) nous a conduit à étudier cette protéine dans un autre contexte physiopathologique. Au cours de la stéatohépatite non alcoolique (NASH) ou des hépatites alcooliques (ALD) chroniques, les prises d'un régime riche en lipides ou glucides ou d'alcool conduisent à une hépatite chronique mais aussi à une perméabilisation de la paroi intestinale. Cette dernière conduit à une augmentation de la translocation de débris microbiens, regroupés sous le terme de "Pathogen Associated Molecular Patterns" (PAMPs), au niveau du foie. La reconnaissance des PAMPs par les "Toll Like Receptors" (TLRs), récepteurs de l'immunité innée présents à la surface des cellules immunitaires et principalement des cellules de Kupffer (KC), déclenche une réaction inflammatoire qui contribuerait à la destruction du parenchyme hépatique au cours des maladies chroniques du foie. Ce processus serait impliqué dans le déclenchement de l' "Acute on Chronic Liver Failure" (ACLF) qui est aujourd'hui un domaine d'étude important en hépatologie puisqu'il conduit brusquement à une insuffisance hépatique voire la mort des patients. Afin d'étudier le rôle de RIPK1 dans la mort des hépatocytes induite par les PAMPs, nous avons dans cette étude utilisée la lignée de souris *Ripk1*$^{LPC\text{-}KO}$, et induit des hépatites par l'injection de deux types différents de PAMPs : le LPS et les motifs CpG. Nous avons également étudié le rôle du TNF-α par l'utilisation de l'Etanercept (inhibiteur du TNF-α) et le rôle des macrophages par l'utilisation de clodronate encapsulé dans des liposomes. Le clodronate est une molécule toxique qui, protégée par le liposome, va tuer les macrophages systémiques suite à leur phagocytose. Nos résultats ont permis de montrer : *i)* une sensibilité accrue des souris *Ripk1*$^{LPC\text{-}KO}$ aux PAMPs qui induisent une hépatolyse aiguë, *ii)* le rôle important des KC dans l'induction de cette lyse, par leur forte capacité à produire du TNF-α et *iii)* le fait que le TNF-α semble être le seul élément déclencheur de l'hépatolyse dans ce modèle. Nos résultats ont permis de montrer le rôle clef de RIPK1 dans la protection des hépatocytes contre le TNF-α exprimé par les cellules de KC suite à la reconnaissance de PAMPs.

Title: RIPK1 protects hepatocytes from Kupffer cells-mediated TNF-induced apoptosis in models of PAMP-dependent hepatitis

Short title: Protective role of RIPK1 in PAMP-dependent hepatitis

Aveline Filliol[1,2,3], Claire Piquet-Pellorce[1,2,3], Céline Raguénès-Nicol[1,2,3,7], Muhammad Farooq[1,2,3], Catherine Lucas-Clerc[2,4], Peter Vandenabeele[5,6], Mathieu JM Bertrand[5,6], Jacques Le Seyec[1,2,3] and Michel Samson[1,2,3].

[1]Institut National de la Santé et de la Recherche Médicale (Inserm), U.1085, Institut de Recherche Santé Environnement et Travail (IRSET), F-35043 Rennes, France.
[2]Université de Rennes 1, F-35043 Rennes, France.
[3]Structure Fédérative BioSit UMS3480 CNRS-US18 Inserm, F-35043 Rennes, France.
[4]Service de Biochimie CHU Rennes, Université de Rennes 1; F-35043 Rennes, France.
[5]Inflammation Research Center, VIB, Technologiepark 927, Zwijnaarde-Ghent, 9052, Belgium.
[6]Department of Biomedical Molecular Biology, Ghent University, Technologiepark 927, Zwijnaarde-Ghent, 9052, Belgium.
[7] Centre National de la Recherche Scientifique (CNRS), UMR 6290, Institut de Génétique et Développement de Rennes (IGDR), F-35043 Rennes, France.

Financial support: This work was supported by INSERM, the Ministère de l'Education Nationale de la Recherche et de la Technologie, the University of Rennes 1, the Région Bretagne, the "Ligue contre le cancer, comités du grand Ouest".

Keywords: Cytokine, Acute Hepatitis, RIP kinase, RIPK1, TNF-α, LPS, CpG, PAMPs, DAMPs.

List of abbreviations: ACLF: Acute on chronic liver failure, AST: aspartate amino-transferase, ALT: alanine amino-transferase, Cl_2MBP: dichloromethylene bisphosphonate, Cl-Caspase3: Cleaved-Caspase3, DAMP: Damage Associated Molecular Pattern, DC: dendritic cells, D-GalN: D-Galactosamine, ETA: Etanercept, H&E: hematoxylin and eosin coloration, IHC: Immunohistochemistry, i.p: Intraperitoneal, KC: kupffer cells, LPS: lipopolysaccharide, LSEC: Liver sinusoïdal endothelial cells, NASH: nonalcoholic fatty liver hepatitis, ODN: oligodeoxynucleotide, PAMP: Pathogen associated molecular patterns, p.i.: Post injection, RIPK: receptor interacting protein kinase, TLR: toll like receptor, TNF: tumor necrosis factor.

ABSTRACT (212 words)

Background and aims: The severity of liver diseases is exacerbated by the death of hepatocytes, which can be induced by the sensing of Pathogen Associated Molecular Patterns (PAMPs) derived from the gut microbiota. The molecular mechanisms regulating these cell death pathways are poorly documented. In this study, we investigated the role of RIPK1, a protein known to regulate cell fate decisions, in the death of hepatocytes using two *in vivo* models of PAMP-induced hepatitis. **Materiels and methods:** Hepatitis was induced in mice by independent injections of two different bacterial PAMPs: LPS and CpG DNA motifs. The role of RIPK1 was evaluated by making use of mice specifically lacking RIPK1 in liver parenchymal cells ($RIPK1^{LPC\text{-}KO}$). Administration of lipsome-encapusated Cl_2MBP served to investigate the role of Kupffer cells in the establishment of the disease. Etanercept, a TNF-decoy receptor, was used to study the contribution of TNF-α during LPS-mediated liver injury. **Results:** Whereas RIPK1 deficiency in liver parenchymal cells did not trigger basal hepatolysis, it greatly sensitized to hepatocyte apoptosis and liver damage following single injection of LPS or CpG. Importantly, hepatocyte death was prevented by macrophage depletion or TNF inhibition. **Conclusion:** Our data highlight the pivotal function of RIPK1 in maintaining liver homeostasis in conditions of macrophage-induced TNF burst in response to PAMPs sensing.

INTRODUCTION

The liver is constantly exposed to bacterial Pathogen Associated Molecular Patterns (PAMPs) such as unmethylated CpG DNA motifs or lipopolysaccharides (LPS) originating from the microbiota of the gastrointestinal tract. In physiological condition, the intestinal barrier prevents the translocation of large amount of bacterial products to the liver [1]. The low quantities of products reaching the liver are efficiently cleared due to the high immune tolerance of the liver, which avoids induction of inflammation and harmful response [2]. During chronic liver diseases induced by alcohol or fat diet exposure, the intestine barrier is damaged [3] [4] resulting in an abnormal elevation of PAMPs in the liver and impairing liver homeostasis [5]. PAMPs increase in the liver is one of the most common factor responsible for the outbreak of acute hepatitis on chronic liver failure background (ACLF for acute on chronic liver failure) [6]. According to *the European Association for the Study of Liver Disease* (EASL) and the *Asian Pacific Association for the Study of the Liver* (APASL), ACLF is an acute deterioration of pre-existing chronic liver diseases, and as a consequence, can provoke high short-term mortality. Thus, ACLF is, today, one of the most challenging fields in hepatology [7]. However, the molecular mechanisms responsible for the liver failure are incompletely understood.

Due to its anatomical link with the gut, the liver plays a key role in the bacterial clearance, which explains why ~80% of macrophages are in the liver [5] [8]. These liver resident macrophages, named Kupffer cells (KC) efficiently phagocytose bacteria and eliminate endotoxins in order to avoid systemic bacterial infection [5]. In addition to phagocytosis, KC are among the first cells to initiate the inflammatory response through the sensing of microbial products by the toll like receptors (TLRs) expressed at their surface or within their endosomes [8]. For example CpG and LPS respectively activate TLR9 and TLR4. Activation of TLRs contributes to ACLF by triggering an inflammatory response. Thus, LPS has been shown to contribute to cirrhosis, autoimmune hepatitis, primary biliary cirrhosis, alcoholic and fatty liver diseases both in humans and mouse models [9] [10] [11] [5]. Among pro-inflammatory cytokines released by LPS-activated-KC, TNF-α has emerged as a key factor in the inflammatory process, as levels of soluble TNF receptors correlate with endotoxin influx and liver injury [12] [13]. In mice, LPS intraperitoneal administration induces a systemic inflammatory response that can lead to death by septic shock, without inducing liver injury [14]. However, administration of LPS in a dietary NASH model or in combination with the hepatotoxic D-Galactosamine (D-GalN) in mice induces hepatocyte apoptosis in a TNF-α -dependent manner [15] [16]. D-GalN is metabolized into an active metabolite exclusively in hepatocytes and inhibits transcription by hepatic uridine nucleotide depletion [17]. Thus, it has been widely described that in the liver, NF-κB or transcription inhibition sensitizes hepatocytes to TNF-α -mediated apoptosis [18] [16] [19]. However, due to the pleiotropic role of TNF-α, anti-TNF-α therapeutic strategies in patients with alcoholic hepatitis are associated with an increased risk of infection and mortality [20] [21]. The Receptor Interacting Protein Kinase 1 (RIPK1) plays key roles in the signaling of several death receptors such as TNFR1 by deciding the cell fate between survival and death [22]. It has been recently reported that RIPK1 is implicated in epithelial cell death in intestine in TNF and bacterial dependent manner [23]. As its role in the liver is poorly understood, we address here the potential role of RIPK1 in hepatocyte death induced by PAMPs and relayed by TNF-α, taking advantage of a knockout mouse line invalidated for the RIPK1 expressed in liver parenchymal cells ($RIPK1^{LPC\text{-}KO}$).

MATERIAL AND METHODS

Animals and treatment protocols

RIPK1$^{LPC\text{-}KO}$ mice were generated by crossing $RIPK1^{fl/fl}$ strain [23] with Alfp-Cre transgenic mice [24]. LPS (Sigma-Aldrich, #L6761) diluted at 2 µg/mL in PBS was administrated by intraperitoneal (i.p.) route (20 µg/kg body weight and 200 µL/20 g). Unmethylated CpG oligodeoxynucleotide (ODN) (Invivogen, ODN 2395) diluted at 3.5 mg/mL in PBS was administrated by i.p. route (2 mg/kg body

weight and 200 µL/20 g). Etanercept (Pfizer) was administrated by i.p. route 1 h before LPS injection (10 mg/kg body weight and 200 µL/20g). Two injections of liposomes-encapsulated dichloromethylene bisphosphonate (Cl_2MBP) (see below for the preparation) were administrated by i.p. route in mice. The first injection was given with 200 µL/20 g body weight, and the second, 24 h after the first, with 100 µL/20 g body weight. Mice were administrated with LPS or control (PBS) 48 h after first injection of liposomes encapsulated Cl_2MBP and sacrificed 8.5 h after LPS injection. In all experiments, genetically modified mice were systematically compared to their littermates. Mature mice at 10-12 weeks of age were used for each experiments. Animals were housed in individually ventilated cages at the VIB Inflammation Research Center (Ghent, Belgium) in conventional animal facilities. All experiments on mice were conducted according to institutional, national and European animal regulations. *In vivo* protocols were approved by the ethics committee of Ghent University.

Genotyping

Genotyping was routinely performed using DNA extracted from tails with Nucleospin Tissue kit (Macherey Nagel, #740952), and PCR with couple of primers for Alfp-Cre gene. Forward and reverse primers sequences were GCC TGC ATT ACC GGT CGA TGC AAC GA and GTG GCA GAT GGC GCG GCA ACA CCA TT, respectively.

Preparation of liposomes-encapsulated Cl_2MBP (Lip-Cl_2MBP)

Liposomes-encapsulated Cl_2MBP were prepared according to Rooijen [25]. In brief, 86 mg of phosphatidylcholine (Sigma-Aldrich) and 9 mg of cholesterol (Sigma-Aldrich) were dissolved in chloroform in a round bottom flask. After 4 h on a gentle rotation on a rotary evaporator at 37°C and under reduced pressure, the thin film formed was resuspended with 10 mL of PBS, and 1 g of Cl_2MBP (Sigma-Aldrich). After vigorous shaking for 1 min, liposomes in the saturated Cl_2MBP solution were extruded through 1 µm diameter pores, followed by centrifugation at 10,000 g for 1 h. The Lip-Cl_2MBP were washed 3 times with PBS with centrifugations at 22,000 g during 30 min, and resuspended with 4 mL of PBS. The size measurement of Lip-Cl_2MBP was checked by Dynamic Light Scattering (DLS) technology (Zeta Sizer Nanoseries, Malvern) and as expected, 95 % of the liposome had 1 µm diameter. The Lip-Cl_2MBP solution was diluted by half in PBS just before injection.

Histopathological and biochemical studies

Fragments of mouse livers were fixed in 4% paraformaldehyde and embedded in paraffin for IHC and hematoxylin and eosin (H&E). For histopathology, H&E staining of liver tissues was carried out to investigate liver injury. Serum ALT and AST transaminases were measured according to the IFCC primary reference procedures using Olympus AU2700 Autoanalyser® (Olympus Optical, Tokyo, Japan).

Immunolocalization in liver tissues

For immunolocalization of cleaved caspase-3 in liver tissues, paraffin-embedded mouse liver sections (5 µm) were dried 1 h at 58°C, followed by antigen retrieval and incubated with primary antibody (Cell Signaling, 9661S) in a Ventana automated instrument (Ventana Medical Systems, USA). Revelation of primary antibody was carried out using horseradish peroxidase (HRP)-conjugated secondary antibody (Dako, USA) and DAB substrate kit (Ventana, #760-124). Slides were then counterstained with hematoxylin.

TUNEL analysis was performed on paraffin-embedded mouse liver sections (5 µm), incubated after antigen retrieval with a mix, composed of terminal transferase (Roche, #3333566011) and digoxigenin-11-UTP (Roche, #1558706) followed by HRP-anti-digoxigenin (Ventana, #760-4822). Revelation was used according to the manufacturer with the Discovery Rhodamine kit (Ventana #760-233) followed by nucleus labelling with DAPI.

All paraffin-embedded mouse liver sections were scanned with a digital slide scanner (Hamamatsu, Nanozoomer 2.0-RS) and files were analysis with the NDP viewer software.

TNF-α and F4/80 immunofluorescence staining were performed on cryosections of mouse liver tissues (7 µm). After fixation with 4 % paraformaldehyde and NH_4Cl treatment, liver slides were blocked with 4 % of BSA and then

incubated with rabbit-anti-murine TNF-α (Abcam, #ab6671) and rat-anti-murine-F4/80 (eBioscience, #47-4801-80) at 4°C overnight. Revelation of primary antibodies was carried out using DyLight 649-conjugated anti-Rabbit and DyLight 549 anti-rat IgG secondary antibodies (Jackson ImmunoResearch Laboratories). Nuclei were stained with Hoechst (Invitrogen, H3570). Slides were observed with a fluorescence microscope (Nikon's Eclipse Ni-E).

Primary hepatocytes Isolation and culture

Hepatocytes were isolated from adult C57BL/6 mice by the retrograde perfusion approach [26]. Mice were previously anesthetized by i.p injection of a ketamine (Imalgene^{TM}, *supplier*) and xylazine (Rompun^{TM}, *supplier*) cocktail (60 and 10 mg/kg of live body weight, respectively) diluted in PBS. After laparotomy, the liver, perfused through *inferior vena cava*, was first washed with solution I (8 g/L NaCl, 0.2 g/L KCl, 0.1 g/L Na_2HPO_4. $12H_2O$ and 2.38 g/L Hepes, pH 7.6) at a 5.5 ml/min flow rate for 8-10 min. Then, the perfusion solution I was supplemented with 5 mM $CaCl_2.2H_2O$ and 0.01% collagenases (Liberase^{TM} TM Research Grade, Roche) for 5-7 minutes. Hepatocytes were harvested after 3 centrifugations at 90 g for 1 min and an additional purification of viable cells on a percoll cushion. Cell suspensions, with over 90% viability, were seeded at a density of 0.1 x 10^6 cells/cm^2 in 24-well plates, previously coated with collagen type I (BD Biosciences, Le Pont de Claix, France), in Williams' E medium supplemented with 10% (vol/vol) fetal calf serum, 2 mM glutamine, 10 IU/mL penicillin, 10 µg/mL streptomycin and 5 µg/mL insulin. Seeding medium was removed after a 4 h-period and replaced by a similar supplemented Williams' E medium, except that fetal calf serum was replaced by 1 mg/mL bovine serum albumin, but with 1 µg/mL of Etanercept. Experimental protocol was conducted in compliance with French laws and the institution's guidelines for animal welfare (agreement of M. Samson # A3523840).

Protein extraction and western blotting

Mouse liver specimens were lysed in RIPA buffer (50 mM Tris-HCl pH 7.4; 1 % Triton X-100; 25 mM HEPES; 150 mM NaCl; 0,2 % SDS; 5 mM $MgCl_2$), complemented with 1 mM Na_3VO_4; 1 mM NaF and proteases inhibitors (Roche, #04 693 132 001), using UltraTurax. For protein extraction from primary hepatocyte, cell cultures were lysed with RIPA complemented with proteases and phosphatases inhibitors one day after seeding. After 40 min in ice, samples were centrifuged at 13,000 g. Proteins from supernatant were assayed with the Bradford method (BioRad) and then separated by SDS-PAGE and transferred onto nitrocellulose membrane. Membranes were blocked with non-fat milk or BSA 3-5 % in TBS (20 mM Tris, 137 mM NaCl) during 1-2 h and incubated overnight with primary antibody anti-cleaved Caspase-3 (Cell Signaling 9661S), anti-actin (Sigma A3854), anti- TNF-α (Abcam, ab6671) or anti-RIPK1 (Cell Signaling, 3493) at 4°C, and then with secondary goat anti-rabbit immunoglobulins/HRP antibody (Dako, P0448). Protein-antibody complexes were revealed by enhanced chemiluminescence (Millipore) and ImageQuant LAS-4000 mini imager analysis (GE-Healthcare).

Serum cytokine immunoassay by flow cytometry

Murine TNF-α, IL-6 and MIP-1α/CCL3 cytokines were quantified by bead-based immunoassays according to manufacturer protocol, using a filter plate and a vacuum filtration system for washing steps (BioLegend's LEGENDPLEX, multi-analyte flow assay kit). Samples were analyzed on a LSR Fortessa cytometer (BD Biosciences).

Statistical analysis

Data were expressed as means +/- SEM for all mice treated similarly. Kruskal–Wallis one-way analysis of variance (ANOVA) was performed, and mean differences between experimental groups were assessed using the non-parametric Mann–Whitney *U*-test with the GraphPad Prism5 software. The significance is shown as follows: * $p<0.05$, ** $p<0.01$, *** $p<0.001$, $RIPK1^{fl/fl\ mice}$ versus $RIPK1^{LPC\text{-}KO}$ mice. # $p<0.05$, ## $p<0.01$, ### $p<0.001$, mice treated with LPS or CpG versus mice treated with PBS.

RESULTS

Deficiency of RIPK1 in liver parenchymal cells sensitizes to liver damage induced by unmethylated CpG DNA

To investigate the role of RIPK1 in the liver, we generated RIPK1^{LPC-KO} mice by crossing RIPK1$^{fl/fl}$ with transgenic mice expressing the Cre-recombinase under the control of the mouse albumin regulatory elements and α-fetoprotein enhancers (Alfp-Cre). Western-blot on liver lysates and on hepatocytes from primary cultures confirmed the expression of RIPK1 in liver parenchymal cells in adult RIPK1$^{fl/fl}$ mice but not in RIPK1^{LPC-KO} mice (Supplementary Fig. 1). Serum transaminases levels (AST and ALT) were similar and normal between mature RIPK1$^{fl/fl}$ and RIPK1^{LPC-KO} mice suggested that deficiency of RIPK1 in steady state does not induce hepatolysis (Fig. 1A). Next, we evaluated acute effects on the liver of CpG DNA administration in RIPK1$^{fl/fl}$ and RIPK1^{LPC-KO} mice by monitoring serum levels of ALT and AST transaminases, as well as liver histology by H&E and TUNEL staining. Whereas WT mice did not exhibit increase in serum transaminase levels, sera from RIPK1^{LPC-KO} mice revealed significant increase of ALT and AST (Fig. 1A). In line with these results, liver sections of RIPK1$^{fl/fl}$ did not reveal any damage while necrotic areas associated with TUNEL positive cells and cleaved caspase-3 (Cl-caspase 3) staining, a marker of apoptosis induction, were observed in liver sections from the RIPK1^{LPC-KO} mice exposed to CpG DNA (Fig. 1B).

Deficiency of RIPK1 in liver parenchyma cells strongly sensitizes to LPS-induced liver damage

Next, we analyzed the response of RIPK1^{LPC-KO} mice to LPS, another important PAMP involved in chronic liver failure. Administration of low dose of LPS (0.4 μg/20 g of body weight) did not induce liver damage 8.5 h post injection in RIPK1$^{fl/fl}$ but resulted in severe induction of apoptosis in the liver of RIPK1^{LPC-KO} mice, as monitored by serum transaminase levels, H&E coloration, TUNEL staining and Cl-caspase 3 labeling (Fig. 2A and 2B). In order to evaluate whether RIPK1 deficiency had any impact on the systemic inflammatory response induced by LPS, we measured the levels of TNF-α, IL-6 and MIP-1α/CCL3 in the serum of the injected mice. Interestingly, absence of RIPK1 did not affect the early (1.5 h p.i.) induction of these cytokines, but led to a sustained (8.5 h p.i.) expression of TNF-α and MIP-1α/CCL3 at the time of apoptosis induction (Fig. 2C). Thus, deficiency of RIPK1 in liver parenchymal cells does not affect the early TLR4 signaling induced by LPS but leads to more extended pro-inflammatory cytokine expression.

Depletion of Kupffer cells reduces LPS-mediated hepatitis in RIPK1^{LPC-KO} mice

Kupffer cells are widely involved in LPS-mediated inflammation [8]. In order to evaluate their contribution to the severe liver damage induced by LPS in RIPK1^{LPC-KO} mice, we depleted the mice of their macrophages by treating them for two days with liposome-encapsulated Cl_2MBP (Lip-Cl_2MBP), which specifically induces macrophage cell death [27]. Depletion was confirmed by F4/80 staining of liver sections, either with or without LPS injection. While LPS challenge led to the recruitment of F4/80 positive cells in the liver of sham RIPK1^{LPC-KO} mice (controls pretreated with vehicle [PBS] in place of Lip-Cl_2MBP), the labelling was dramatically reduced in the liver of LPS challenged animals pretreated with Lip-Cl_2MBP. This proved the effectiveness of the pretreatment defined to deplete the systemic macrophages (Fig. 3A). According to the F4/80 labeling, the early LPS-mediated increased in serum levels of CCL3, a cytokine mainly produced by macrophages, was significantly reduced in mice pretreated with Lip-Cl_2MBP (Fig. 3B). Interestingly, macrophage depletion greatly rescued the liver damage induced by LPS in RIPK1^{LPC-KO} mice. Indeed, Lip-Cl_2MBP pre-treatment massively reduced LPS-induced serum transaminase levels (Fig. 3C), which was associated with a reduction of necrosis areas, TUNEL positive cells as well as apoptotic cells (Fig. 3D and 3E).

TNF-α produced by Kupffer cells mediates LPS-induced liver damage in RIPK1^{LPC-KO} mice

Our results demonstrate a key role of Kupffer cells during LPS-mediated liver injury in RIPK1^{LPC-KO} mice. Macrophages are the main source of the TNF-α produced in the body and RIPK1 deficient cells such as embryonic fibroblasts, thymocytes or keratinocytes [28] [29], as well as intestinal organoids [23] are reportedly sensitized to TNF-α -mediated apoptosis. We therefore speculated that the TNF-α, known to be produced mainly by

Kupffer cells in response to LPS sensing [30] [31] was responsible for the apoptotic death of the RIPK1 deficient hepatocytes. In accordance with this idea, we found that TNF-α was quickly released in RIPK1^{LPC-KO} and RIPK1$^{fl/fl}$ littermates following LPS injection (Fig. 2C), and that depletion of macrophages reduced by more than 90% the serum concentration of TNF-α, 1.5 h after LPS administration in RIPK1^{LPC-KO} mice (Fig. 4A). In addition, cellular staining of TNF-α and F4/80 on liver sections of RIPK1^{LPC-KO} mice treated or not with Lip-Cl_2MBP demonstrated that Kupffer cells are the major source of TNF-α produced in the liver after LPS challenge (Fig. 4B, orange arrows), but it is also expressed by few sinusoidal liver cells (Fig. 4B, white arrows).

As we demonstrated that macrophage depletion in RIPK1^{LPC-KO} mice prevented from both a TNF-α burst and severe liver damage, we investigated the role of TNF-α in our model by pre-treating RIPK1^{LPC-KO} mice for 1 h with Etanercept, a TNF-α decoy receptor widely used clinically in humans, before LPS injection. Remarkably, we found that TNF-α blockade fully protected RIPK1^{LPC-KO} mice from LPS-induced liver injury, as demonstrated by the dramatic reduction of serum transaminase levels (Fig. 5A), the absence of necrotic areas, and the reduction of TUNEL and Cl-caspase 3 positive cells in the livers of RIPK1^{LPC-KO} mice (Fig. 5B). Western blot analysis confirmed the presence of TNF-α release and Caspase 3 activation in the livers from WT and RIPK1^{LPC-KO} mice after LPS injection, which were avoided by the Etanercept pre-treatment (Fig. 5C).

DISCUSSION

Hepatocyte death is a key trigger of liver disease progression [32]. During chronic hepatitis, acute hepatocyte death can occur and causes ACLF, and induces quick and high mortality rate in patients [7]. One of the main cause is the elevation of gut-derived-microbacterial products in the liver [6]. PAMPs activate TLR receptors, expressed at the surface of innate immune cells, such as KC, inducing cytokines release which promote liver inflammation and hepatocyte death, eventually leading to liver failure [8]. Elevation of bacterial products in the liver can be mimic by LPS or CpG DNA injection in mice. In healthy liver, their administration induce a quick delivery of cytokines without triggering liver injury. However, during ACLF, inflammatory context of chronic hepatitis sensitizes hepatocytes, and elevation of PAMPs in the liver triggers acute hepatocyte death and liver failure [9] [5] [10] [11]. In many studies, treatment with D-GalN is used to study endotoxin mediated liver injury. D-GalN leads to uridine depletion that sensitizes hepatocyte to LPS-induced apoptosis by inhibiting survival proteins transcription [17]. Here, we shown that in RIPK1^{LPC-KO} mice, administration of LPS or DNA-CpG, without adding D-GalN, induced a strong acute liver injury associated with hepatocyte apoptosis. Previously, an identical phenotype was observed in conditional or inducible LPC-KO mice for NEMO, TAK1 or RelA [33] [34] [19]. However, whereas these mice presented hepatolysis in steady state, RIPK1 seemed dispensable for liver homeostasis. Indeed, according to Kondylis et *al* [33], we showed that 10 weeks old RIPK1^{LPC-KO} mice do not present basal hepatolysis. LPS treatment induced a quick release of cytokines in the blood that was not affected by RIPK1 deficiency in LPC. However, whereas at latter time, serum cytokine levels were almost back to their basal levels in WT mice, their RIPK1^{LPC-KO} littermates presented a sustained inflammation, which possibly resulted from hepatocyte death observed at the same time. As KC are important source of cytokine delivery after LPS administration, and as it was observed that PAMP recognition by KC is a key step in the induction of liver injury during chronic alcoholic, NASH or acute hepatitis induced by D-GalN in mice [35] [36] [37] [10] [38], we next investigated the role of KC in LPS-mediated liver damage in RIPK1^{LPC-KO} mice. Liposome-encapsulated Cl_2MBP is an efficient method to deplete macrophages and to study the role of cytokines induced by LPS stimulation [27]. Indeed, in contrast to other methods (such as gadolinium chloride, silica or dextran sulfate), liposomes do not stimulate production of cytokines by macrophages [27]. Depletion of KC in the liver was associated with a strong reduction of hepatolysis in RIPK1^{LPC-KO} mice challenged with LPS. Whereas RIPK1 has been shown to regulate TLR signaling [39], our data

revealed an indirect role of LPS to induce hepatocyte death in RIPK1^{LPC-KO} mice. Thus, we suggest that, in RIPK1^{LPC-KO} mice, LPS activated TLR4, mainly present on KC, which induced the release of cytokines deleterious for hepatocytes. In accordance with others, we found an important reduction of serum TNF-α level in mice depleted of macrophages after LPS challenge [30] [31], suggesting a deleterious role of TNF-α in RIPK1^{LPC-KO} mice. Moreover TNF-α release by LPS-activated KC has been shown to play a key role during acute and chronic liver diseases in different mice models, where it was shown to promote fibrosis and hepatolysis [15] [16] [40]. In the same way, we showed that TNF-α inhibition with Etanercept fully protected hepatocytes from the apoptosis induced by LPS in RIPK1^{LPC-KO}. The low hepatolysis observed after LPS treatment in RIPK1^{LPC-KO} mice previously depleted from their macrophages can be probably attributed to the small detected quantities of TNF-α, which may originate from the few surviving macrophages which escaped from Lip-Cl$_2$MBP pretreatment, and/or from other liver cells such as liver sinusoidal endothelial cells.

Thus, our data showed that physiological TNF-α quantities mainly produced by KC after LPS administration induce hepatocyte apoptosis in RIPK1^{LPC-KO} mice. Moreover, TNF-α seemed to be the main cell death effector in RIPK1^{LPC-KO} mice after LPS injection. In the Figure 6, we proposed a schematic model on the vital role played by RIPK1 to maintain liver homeostasis under elevated PAMPs conditions.

In conclusion, the sensitivity of RIPK1^{LPC-KO} mice to PAMPs such as LPS and CpG-DNA, could be used as a model to test some TLR inhibitors or probiotics and antibiotics which are currently investigated to reduce inflammatory response induced by high bacterial translocation in the liver [5]. Moreover, this sensitivity of RIPK1 $^{LPC-KO}$ mice to PAMPs highlights the importance of the preservation of the RIPK1 function to maintain the liver homeostasis. Thus, analysis of *Ripk1* gene polymorphism or RIPK1 expression could be helpful in the management of patients with chronic hepatitis and their risk to develop ACLF.

ACKNOWLEDGEMENTS

This work was supported by INSERM, The Ministère de l'Education Nationale de la Recherche et de la Technologie, the University of Rennes 1, the Région Bretagne and the "Ligue contre le cancer, comités du grand Ouest". Research in the Vandenabeele unit is supported by Belgian grants (IAP 7/32), Flemish grants (FWO G087511, G097311, G0A4512N, G078713N, G017212N, G013715N; Methusalem BOF09/01M00709), Ghent University grants (MRP, GROUP-ID consortium), grants from the Foundation against Cancer (F94 and 2010-162) and grants from the VIB. AF was supported by a PhD fellowship from the Région Bretagne. MF was supported by a Ph.D. fellowship from the Government of Pakistan (Higher Education Commission, University of Agriculture, Lahore). MJMB has a tenure track position within the Multidisciplinary Research Program of Ghent University (GROUP-ID). For immunohistochemistry analysis and animal house facilities, we would like to thank dedicated platforms (i.e. H2P2 and animal house platforms) of SFR BIOSIT, University of Rennes 1, France. For experimental help, we would like to thank the student Cristina Ulecia Morón.

REFERENCES

[1] Wiest R, Garcia-Tsao G. Bacterial translocation (BT) in cirrhosis. Hepatology 2005;41:422-433.

[2] Crispe IN. The liver as a lymphoid organ. Annu Rev Immunol 2009;27:147-163.

[3] Louvet A, Mathurin P. Alcoholic liver disease: mechanisms of injury and targeted treatment. Nat Rev Gastroenterol Hepatol 2015;12:231-242.

[4] Ilan Y. Leaky gut and the liver: a role for bacterial translocation in nonalcoholic steatohepatitis. World J Gastroenterol 2012;18:2609-2618.

[5] Mencin A, Kluwe J, Schwabe RF. Toll-like receptors as targets in chronic liver diseases. Gut 2009;58:704-720.

[6] Jalan R, Fernandez J, Wiest R, Schnabl B, Moreau R, Angeli P, et al. Bacterial infections in cirrhosis: a position statement based on the

EASL Special Conference 2013. J Hepatol 2014;60:1310-1324.
[7] Sarin SK, Choudhury A. Acute-on-chronic liver failure: terminology, mechanisms and management. Nat Rev Gastroenterol Hepatol 2016;13:131-149.
[8] Heymann F, Tacke F. Immunology in the liver - from homeostasis to disease. Nat Rev Gastroenterol Hepatol 2016;13:88-110.
[9] Jirillo E, Caccavo D, Magrone T, Piccigallo E, Amati L, Lembo A, et al. The role of the liver in the response to LPS: experimental and clinical findings. J Endotoxin Res 2002;8:319-327.
[10] Rivera CA, Adegboyega P, van Rooijen N, Tagalicud A, Allman M, Wallace M. Toll-like receptor-4 signaling and Kupffer cells play pivotal roles in the pathogenesis of non-alcoholic steatohepatitis. J Hepatol 2007;47:571-579.
[11] Inokuchi S, Tsukamoto H, Park E, Liu ZX, Brenner DA, Seki E. Toll-like receptor 4 mediates alcohol-induced steatohepatitis through bone marrow-derived and endogenous liver cells in mice. Alcohol Clin Exp Res 2011;35:1509-1518.
[12] Trebicka J, Krag A, Gansweid S, Appenrodt B, Schiedermaier P, Sauerbruch T, et al. Endotoxin and tumor necrosis factor-receptor levels in portal and hepatic vein of patients with alcoholic liver cirrhosis receiving elective transjugular intrahepatic portosystemic shunt. Eur J Gastroenterol Hepatol 2011;23:1218-1225.
[13] Spahr L, Giostra E, Frossard JL, Bresson-Hadni S, Rubbia-Brandt L, Hadengue A. Soluble TNF-R1, but not tumor necrosis factor alpha, predicts the 3-month mortality in patients with alcoholic hepatitis. J Hepatol 2004;41:229-234.
[14] Galanos C, Freudenberg MA, Reutter W. Galactosamine-induced sensitization to the lethal effects of endotoxin. Proc Natl Acad Sci U S A 1979;76:5939-5943.
[15] Kudo H, Takahara T, Yata Y, Kawai K, Zhang W, Sugiyama T. Lipopolysaccharide triggered TNF-alpha-induced hepatocyte apoptosis in a murine non-alcoholic steatohepatitis model. J Hepatol 2009;51:168-175.
[16] Tiegs G, Wolter M, Wendel A. Tumor necrosis factor is a terminal mediator in galactosamine/endotoxin-induced hepatitis in mice. Biochem Pharmacol 1989;38:627-631.
[17] Decker K, Keppler D. Galactosamine hepatitis: key role of the nucleotide deficiency period in the pathogenesis of cell injury and cell death. Rev Physiol Biochem Pharmacol 1974:77-106.
[18] Leist M, Gantner F, Bohlinger I, Germann PG, Tiegs G, Wendel A. Murine hepatocyte apoptosis induced in vitro and in vivo by TNF-alpha requires transcriptional arrest. J Immunol 1994;153:1778-1788.
[19] Geisler F, Algul H, Paxian S, Schmid RM. Genetic inactivation of RelA/p65 sensitizes adult mouse hepatocytes to TNF-induced apoptosis in vivo and in vitro. Gastroenterology 2007;132:2489-2503.
[20] Naveau S, Chollet-Martin S, Dharancy S, Mathurin P, Jouet P, Piquet MA, et al. A double-blind randomized controlled trial of infliximab associated with prednisolone in acute alcoholic hepatitis. Hepatology 2004;39:1390-1397.
[21] Boetticher NC, Peine CJ, Kwo P, Abrams GA, Patel T, Aqel B, et al. A randomized, double-blinded, placebo-controlled multicenter trial of etanercept in the treatment of alcoholic hepatitis. Gastroenterology 2008;135:1953-1960.
[22] Pasparakis M, Vandenabeele P. Necroptosis and its role in inflammation. Nature 2015;517:311-320.
[23] Takahashi N, Vereecke L, Bertrand MJ, Duprez L, Berger SB, Divert T, et al. RIPK1 ensures intestinal homeostasis by protecting the epithelium against apoptosis. Nature 2014;513:95-99.
[24] Kellendonk C, Opherk C, Anlag K, Schutz G, Tronche F. Hepatocyte-specific expression of Cre recombinase. Genesis 2000;26:151-153.
[25] Van Rooijen N, Sanders A. Liposome mediated depletion of macrophages: mechanism of action, preparation of liposomes and applications. J Immunol Methods 1994;174:83-93.
[26] Houseman L, Edwards M, Phillips IR, Shephard EA. Isolation and Culture of Mouse Hepatocytes:Gender-Specific Gene Expression Responses to Chemical Treatments. Methods Mol Biol 2015;1250:3-12.

[27] van Rooijen N, Sanders A. Elimination, blocking, and activation of macrophages: three of a kind? J Leukoc Biol 1997;62:702-709.
[28] Kelliher MA, Grimm S, Ishida Y, Kuo F, Stanger BZ, Leder P. The death domain kinase RIP mediates the TNF-induced NF-kappaB signal. Immunity 1998;8:297-303.
[29] Gentle IE, Wong WW, Evans JM, Bankovacki A, Cook WD, Khan NR, et al. In TNF-stimulated cells, RIPK1 promotes cell survival by stabilizing TRAF2 and cIAP1, which limits induction of non-canonical NF-kappaB and activation of caspase-8. J Biol Chem 2011;286:13282-13291.
[30] Bautista AP, Skrepnik N, Niesman MR, Bagby GJ. Elimination of macrophages by liposome-encapsulated dichloromethylene diphosphonate suppresses the endotoxin-induced priming of Kupffer cells. J Leukoc Biol 1994;55:321-327.
[31] Luster MI, Germolec DR, Yoshida T, Kayama F, Thompson M. Endotoxin-induced cytokine gene expression and excretion in the liver. Hepatology 1994;19:480-488.
[32] Luedde T, Kaplowitz N, Schwabe RF. Cell death and cell death responses in liver disease: mechanisms and clinical relevance. Gastroenterology 2014;147:765-783 e764.
[33] Kondylis V, Polykratis A, Ehlken H, Ochoa-Callejero L, Straub BK, Krishna-Subramanian S, et al. NEMO Prevents Steatohepatitis and Hepatocellular Carcinoma by Inhibiting RIPK1 Kinase Activity-Mediated Hepatocyte Apoptosis. Cancer Cell 2015;28:582-598.
[34] Bettermann K, Vucur M, Haybaeck J, Koppe C, Janssen J, Heymann F, et al. TAK1 suppresses a NEMO-dependent but NF-kappaB-independent pathway to liver cancer. Cancer Cell 2010;17:481-496.
[35] Adachi E, Maeda T, Matsumata T, Shirabe K, Kinukawa N, Sugimachi K, et al. Risk factors for intrahepatic recurrence in human small hepatocellular carcinoma. Gastroenterology 1995;108:768-775.
[36] Ben Ari Z, Avlas O, Pappo O, Zilbermints V, Cheporko Y, Bachmetov L, et al. Reduced hepatic injury in Toll-like receptor 4-deficient mice following D-galactosamine/lipopolysaccharide-induced fulminant hepatic failure. Cell Physiol Biochem 2012;29:41-50.
[37] Spruss A, Kanuri G, Wagnerberger S, Haub S, Bischoff SC, Bergheim I. Toll-like receptor 4 is involved in the development of fructose-induced hepatic steatosis in mice. Hepatology 2009;50:1094-1104.
[38] Uesugi T, Froh M, Arteel GE, Bradford BU, Thurman RG. Toll-like receptor 4 is involved in the mechanism of early alcohol-induced liver injury in mice. Hepatology 2001;34:101-108.
[39] Meylan E, Burns K, Hofmann K, Blancheteau V, Martinon F, Kelliher M, et al. RIP1 is an essential mediator of Toll-like receptor 3-induced NF-kappa B activation. Nat Immunol 2004;5:503-507.
[40] Miura K, Yang L, van Rooijen N, Ohnishi H, Seki E. Hepatic recruitment of macrophages promotes nonalcoholic steatohepatitis through CCR2. Am J Physiol Gastrointest Liver Physiol 2012;302:G1310-1321.

LEGENDS OF FIGURES

Figure 1. RIPK1 deficiency sensitized mice to unmethylated CpG DNA motifs.
(A) Levels of serum ALT and AST in WT and RIPK1^{LPC-KO} mice, 8.5 h after PBS or CpG ODN injection (each dot represents an individual and errors bars are expressed as means +/- SEM. (*, # $p<0.05$; **, ## $p<0.01$; ***, ### $p<0.001$, ns: non-significant). (B) Pictures of liver tissue sections, stained by H&E (upper panel), analyzed by TUNEL (in red) and DAPI (in blue) immunofluorescence (middle panel) or analyzed by IHC for cleaved caspase-3 (lower panel), issued from WT or *RIPK1*$^{LPC-KO}$ mice, 8.5 h after CpG ODN challenge. Black arrows show the dead cells.

Figure 2. RIPK1 deficiency sensitized mice to LPS.
(A) Levels of serum ALT and AST in WT and RIPK1^{LPC-KO} mice, 8.5 h after PBS or LPS injection. (B) Pictures of liver tissue sections, stained by H&E (left panel), analyzed by TUNEL (in red) and DAPI (in blue) immunofluorescence (middle panel) or analyzed by IHC for cleaved caspase-3 (right panel), issued from WT and *RIPK1*$^{LPC-KO}$ mice, 8.5 h after LPS challenge. (C) Levels of

serum TNF-α, IL-6 and MIP-1α/CCL3 from WT and RIPK1^{LPC-KO} mice, 1.5 h or 8.5 h after LPS injection. On dot plots, each dot represents an individual and errors bars are expressed as means +/- SEM. (*, # $p<0.05$; **, ## $p<0.01$; ***, ### $p<0.001$, ns: non-significant).

Figure 3. Depletion of Kupffer cells reduced LPS mediated hepatitis in RIPK1^{LPC-KO} mice.
(A) Pictures of liver tissue sections, analyzed by IHC for F4/80, issued from RIPK1^{LPC-KO} mice 8.5 h after LPS or PBS injection with an eventual pre-treatment during 48 h with liposomes encapsulated Cl_2MBP (Lip- Cl_2MBP). (B) Serum levels of MIP-1α/CCL3 collected 1.5 h after LPS injection and (C) of AST and ALT, collected 8.5 h after LPS injection in RIPK1^{LPC-KO} mice pre-treated or not with Lip-Cl_2MBP. (D) Pictures of liver tissue sections, stained by H&E (upper panel), analyzed by TUNEL (dead cells in red) and DAPI (nuclei in blue) immunofluorescence (middle panel) or analyzed by IHC for cleaved caspase-3 (lower panel), issued from RIPK1^{LPC-KO} mice, 8.5 h after LPS injection with an eventual pre-treatment with Lip-Cl_2MBP. (E) Western-blot analysis of β-actin and cleaved-caspase 3 in protein extracts issued from the liver of WT or RIPK1^{LPC-KO} mice, collected 8.5 h after LPS injection with an eventual pre-treatment with Lip-Cl_2MBP. On dot plots, each dot represents an individual and errors bars are expressed as means +/- SEM. (* $p<0.05$; ** $p<0.01$; *** $p<0.001$).

Figure 4. Kupffer cells induced LPS mediated liver damage in RIPK1 mice in a TNF-dependent manner.
(A) Serum levels of TNF-α collected 1.5 h after LPS injection in RIPK1^{LPC-KO} mice pre-treated or not with Lip-Cl_2MBP. Each dot represents an individual and errors bars are expressed as means +/- SEM. (* $p<0.05$; ** $p<0.01$; *** $p<0.001$). (B) TNF-α (red) and F4/80 (green) immunofluorescence staining on liver sections from RIPK1^{LPC-KO} mice, collected 8.5 h after LPS injection with an eventual pre-treatment with Lip-Cl_2MBP. Nuclei were stained by Hoechst (blue). White and orange arrows show TNF positive cells, and TNF and F4/80 positive cells, respectively.

Figure 5. LPS induced TNF mediated liver damage in RIPK1^{LPC-KO} mice.
(A) Levels of serum ALT and AST and (B) pictures of liver tissue sections, stained by H&E (left panel), analyzed by TUNEL (dead cells in red) and DAPI (nuclei in blue) immunofluorescence (middle panel), or analyzed by IHC for cleaved caspase-3 (right panel), issued from RIPK1^{LPC-KO} mice, 8.5 h after PBS or LPS injection with an eventual pre-treatment with Etanercept (ETA) injection (each dot represents an individual and errors bars are expressed as means +/- SEM. (*, # $p<0.05$; **, ## $p<0.01$; ***, ### $p<0.001$, ns: non-significant). (C) Western-blot analysis of RIPK1, β-actin, transmembrane (tm) and soluble (s) forms of TNF-α and cleaved-caspase 3 in protein extracts issued from the liver of WT or *RIPK1*$^{LPC-KO}$ mice, collected 8.5 h after LPS injection with an eventual pre-treatment with ETA.

Figure 6. Role of RIPK1 in PAMPs mediated hepatitis.
During some chronic liver diseases, such as acute on chronic liver failure, different factors such as gut permeabilization induce elevated PAMPs translocation in the liver. LPS and CpG are recognize respectively by TLR4 and 9 carried by Kupffer cells (KC) which promote inflammatory cytokine production such as TNF-α. Transmembrane (tm-) or (s-) soluble TNF can be inhibited by Etanercept (ETA), if not, they bind the TNFR1 on hepatocyte and promote recruitment of RIPK1 under the receptor which plays a protective role by inhibition of caspase activation.

Supplementary Figure1.
Western-blot analysis of RIPK1 and β-actin, in protein extracts issued (A) from the liver, (B) or from primary hepatocyte cultures (PH) of WT or *RIPK1*$^{LPC-KO}$ mice.

Figure 1

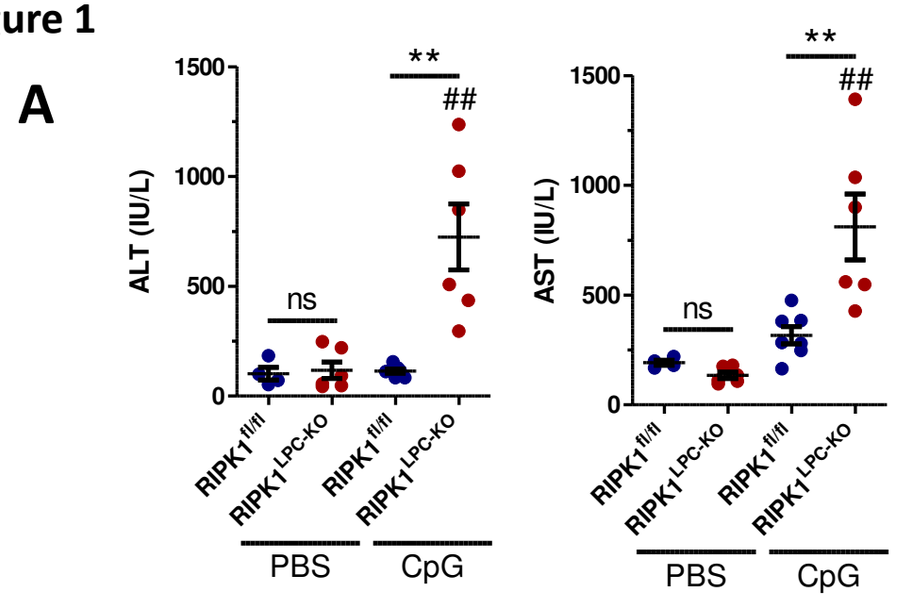
A
ALT (IU/L)
AST (IU/L)
1500
1000
500
0
**
##
ns
RIPK1fl/fl
RIPK1LPC-KO
PBS
CpG

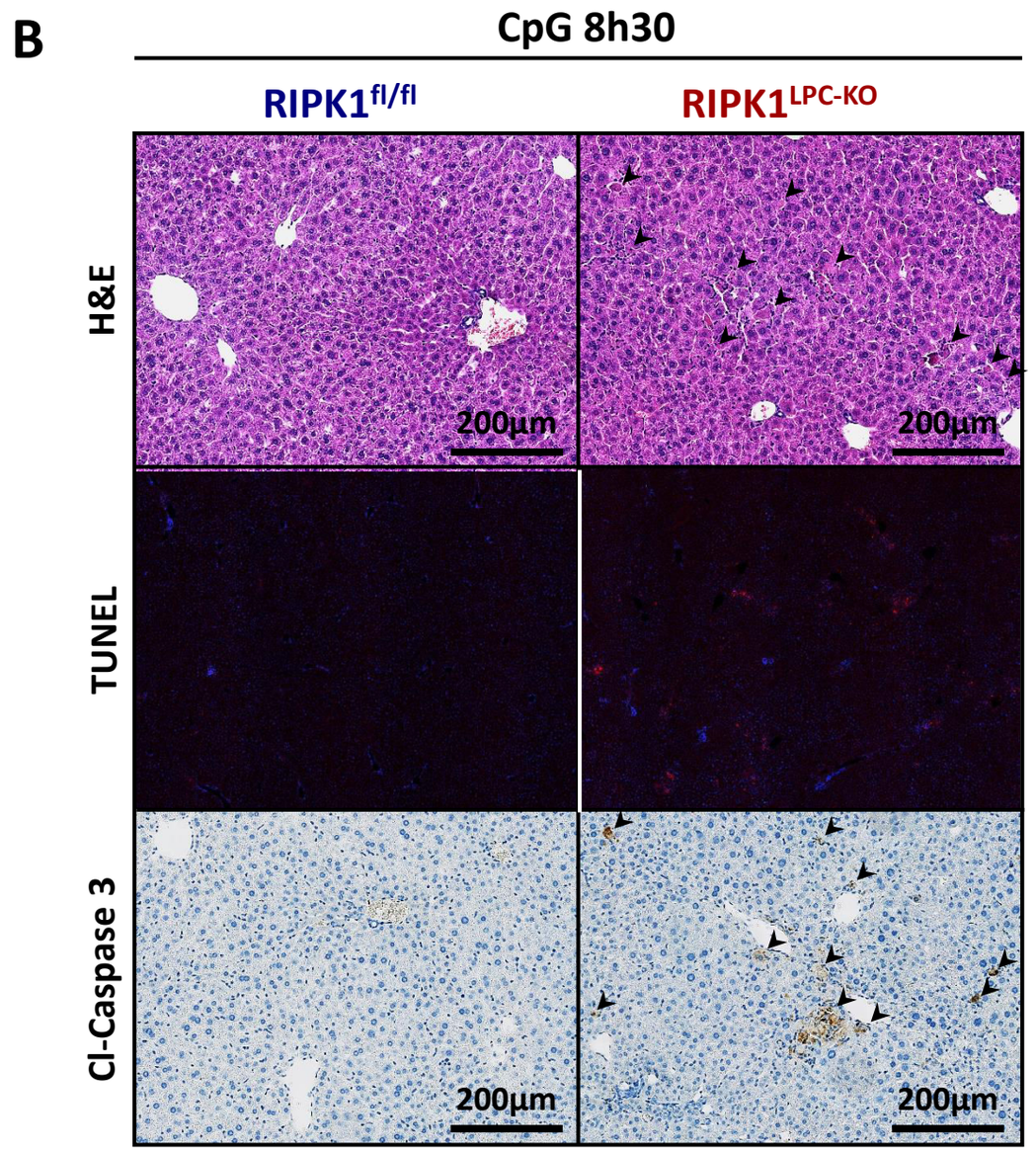
B
CpG 8h30
RIPK1fl/fl
RIPK1LPC-KO
H&E
TUNEL
Cl-Caspase 3
200µm

Figure 2

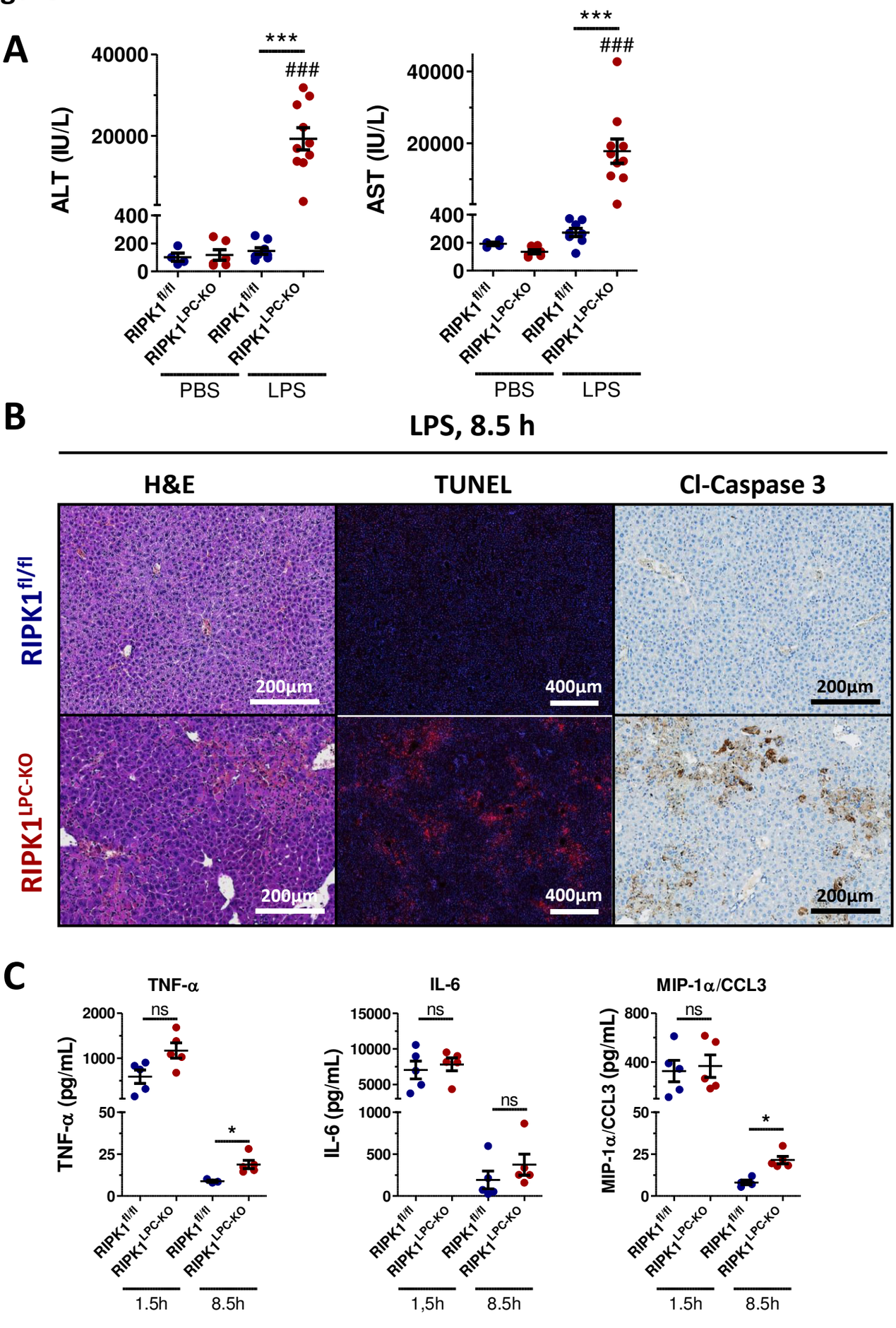
A
ALT (IU/L)
AST (IU/L)
40000
20000
400
200
0
***
###
RIPK1fl/fl
RIPK1LPC-KO
PBS
LPS
B
LPS, 8.5 h
H&E
TUNEL
Cl-Caspase 3
RIPK1fl/fl
RIPK1LPC-KO
200µm
400µm
C
TNF-α
IL-6
MIP-1α/CCL3
TNF-α (pg/mL)
IL-6 (pg/mL)
MIP-1α/CCL3 (pg/mL)
2000
1000
50
25
0
15000
10000
5000
500
800
ns
*
1.5h
8.5h
1,5h

Figure 3

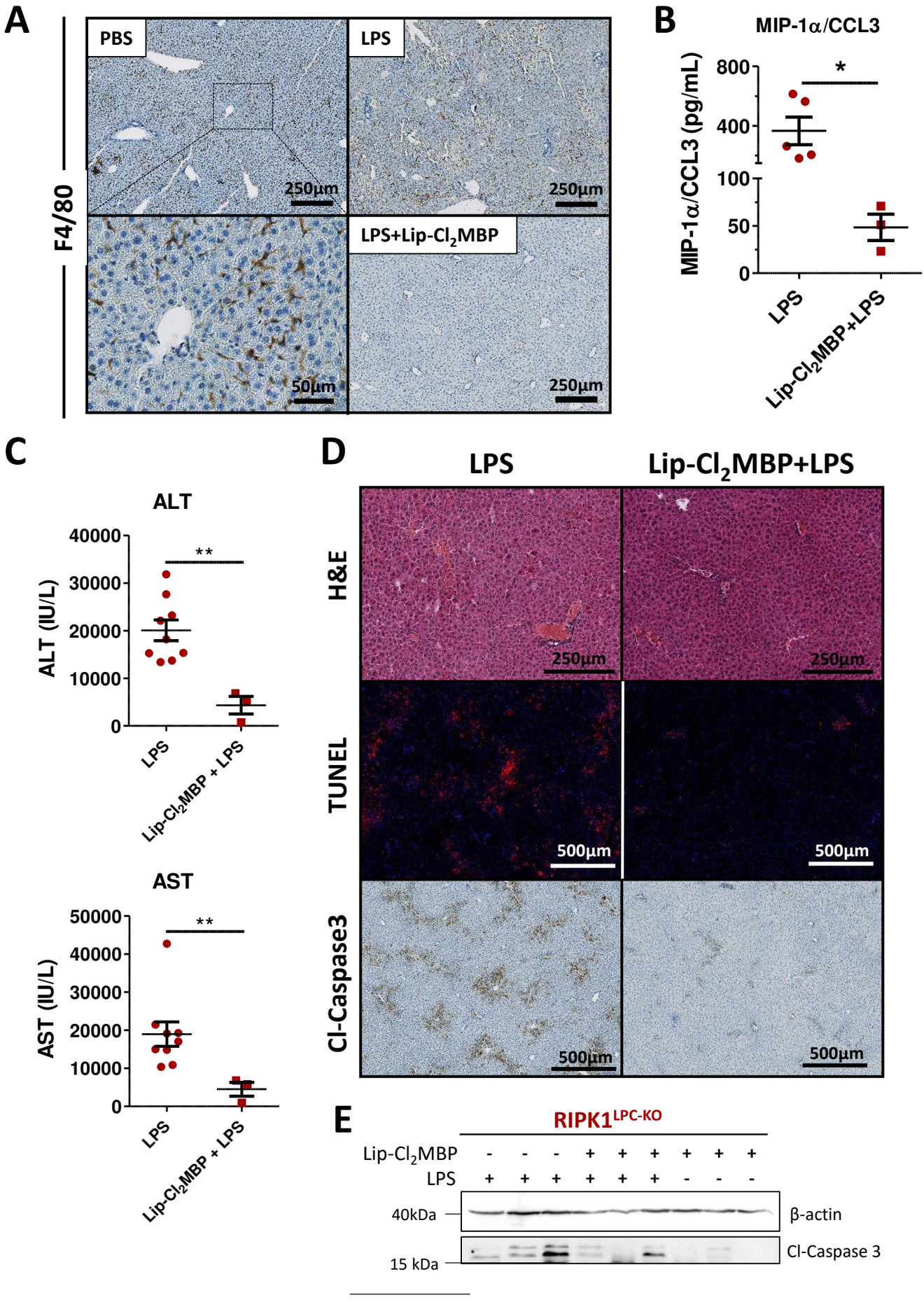
A
PBS
LPS
LPS+Lip-Cl2MBP
F4/80
250μm
250μm
50μm
250μm
B
MIP-1α/CCL3
MIP-1α/CCL3 (pg/mL)
800
400
100
50
0
*
LPS
Lip-Cl2MBP+LPS
C
ALT
ALT (IU/L)
40000
30000
20000
10000
0
**
LPS
Lip-Cl2MBP + LPS
AST
AST (IU/L)
50000
40000
30000
20000
10000
0
**
LPS
Lip-Cl2MBP + LPS
D
LPS
Lip-Cl2MBP+LPS
H&E
TUNEL
Cl-Caspase3
250μm
250μm
500μm
500μm
500μm
500μm
E
RIPK1LPC-KO
Lip-Cl2MBP - - - + + + + + +
LPS + + + + + + - - -
40kDa
β-actin
15 kDa
Cl-Caspase 3

Figure 4

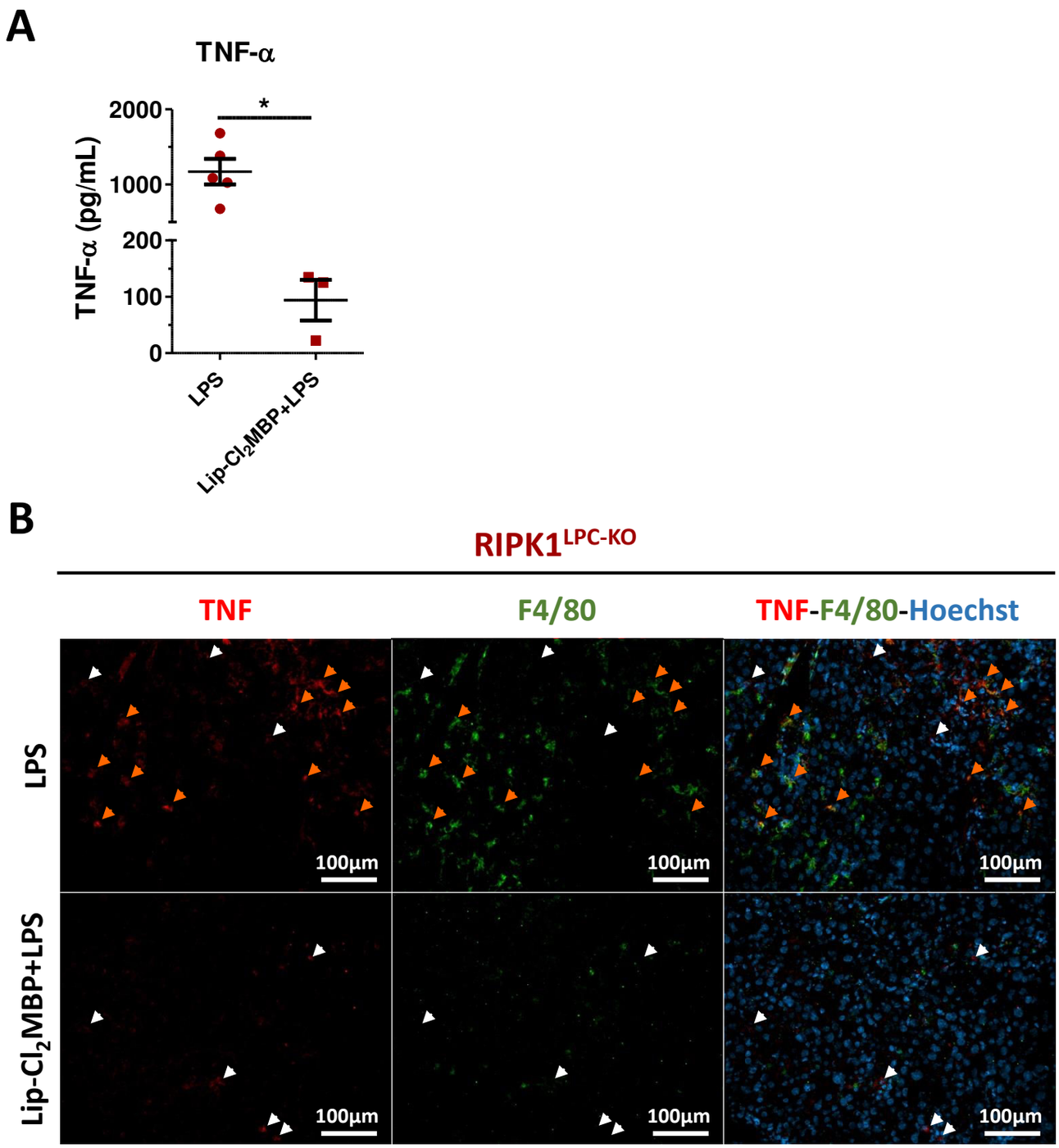
A
TNF-α
TNF-α (pg/mL)
2000
1000
200
100
0
*
LPS
Lip-Cl2MBP+LPS
B
RIPK1LPC-KO
TNF
F4/80
TNF-F4/80-Hoechst
LPS
Lip-Cl2MBP+LPS
100μm

Figure 5

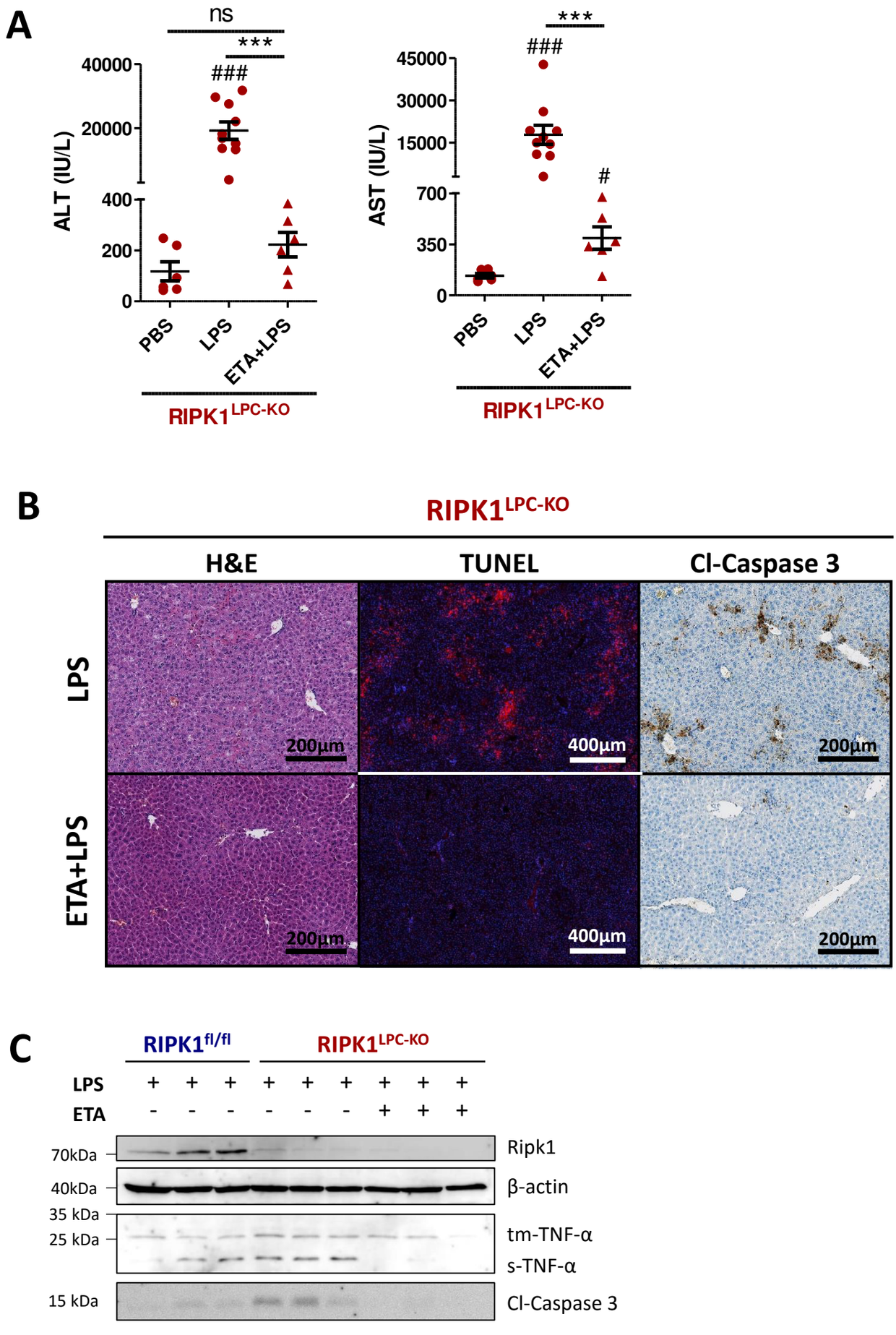
A
ns
***
###
ALT (IU/L)
40000
20000
400
200
0
PBS
LPS
ETA+LPS
RIPK1LPC-KO
***
###
#
AST (IU/L)
45000
30000
15000
700
350
0
PBS
LPS
ETA+LPS
RIPK1LPC-KO
B
RIPK1LPC-KO
H&E
TUNEL
Cl-Caspase 3
LPS
ETA+LPS
200μm
400μm
200μm
200μm
400μm
200μm
C
RIPK1fl/fl
RIPK1LPC-KO
LPS + + + + + + + + +
ETA - - - - - - + + +
70kDa
40kDa
35 kDa
25 kDa
15 kDa
Ripk1
β-actin
tm-TNF-α
s-TNF-α
Cl-Caspase 3

Figure 6

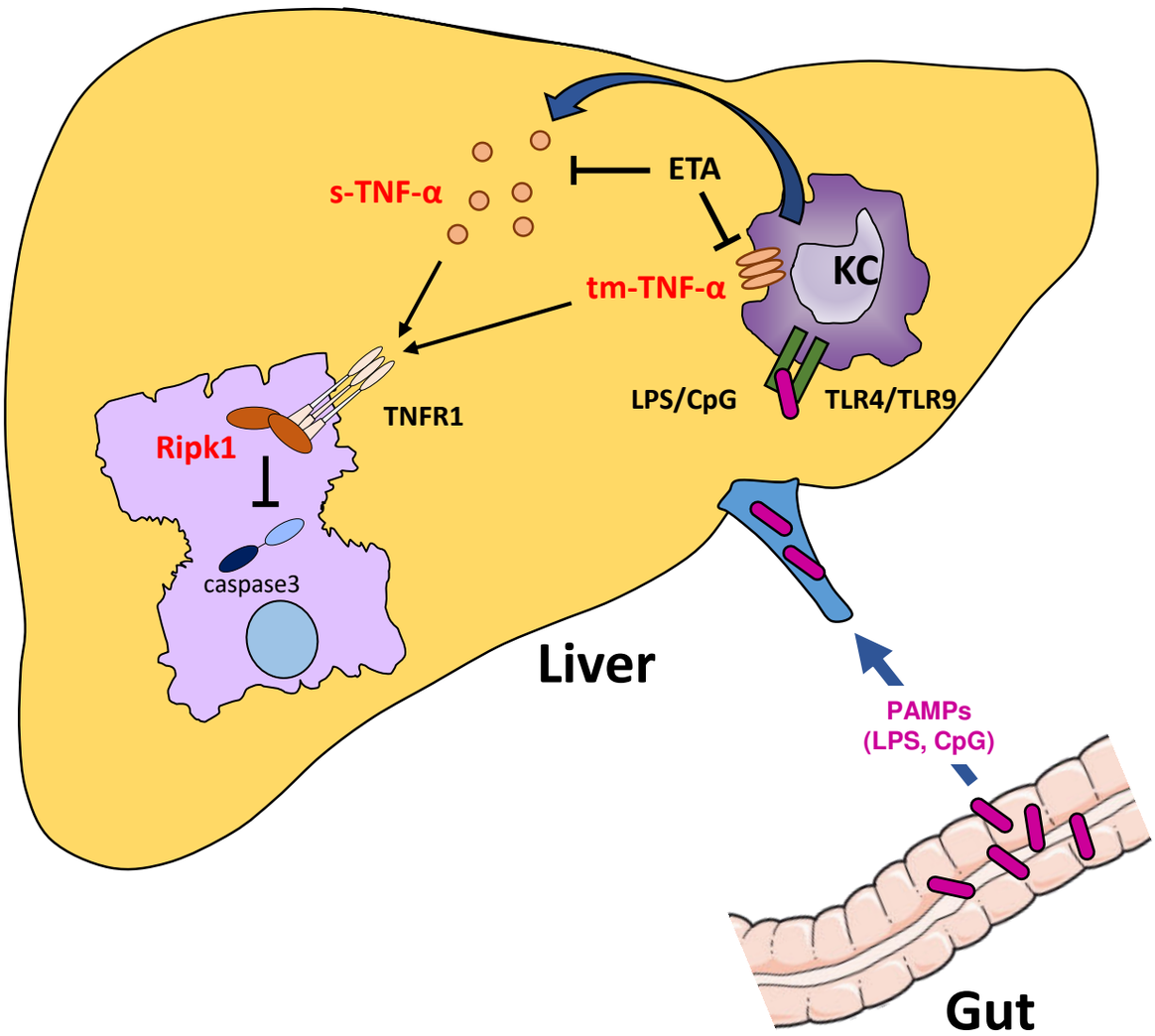
s-TNF-α
ETA
KC
tm-TNF-α
TNFR1
LPS/CpG
TLR4/TLR9
Ripk1
caspase3
Liver
PAMPs
(LPS, CpG)
Gut

Supplementary Figure 1

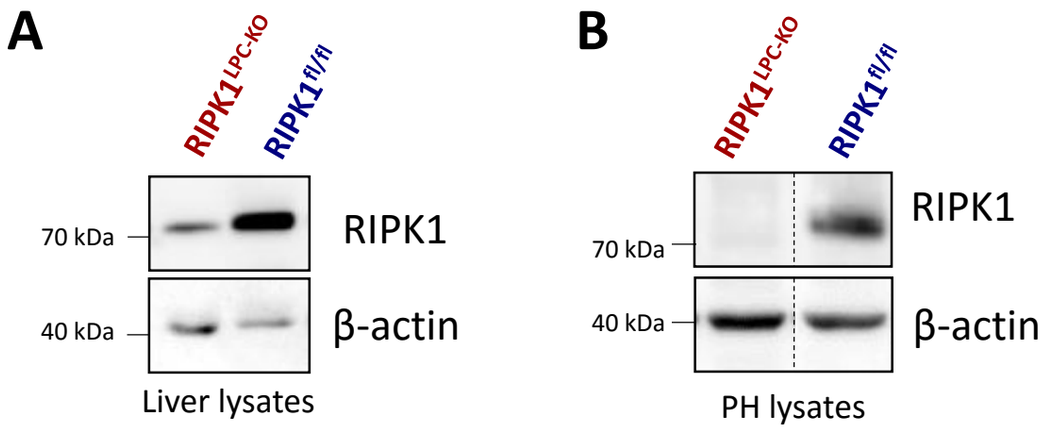

III.3. ARTICLE III : RIPK1 protège contre le dommage hépatique induit par l'activation de Fas et TRAIL-R2

Aveline Filliol, Claire Piquet-Pellorce, Valentine Genet, Catherine Lucas-Clerc, Peter Vandenabeele, Mathieu JM Bertrand, Jacques Le Seyec and Michel Samson.

Article en préparation

Introduction de l'article.

La mort des hépatocytes est considérée comme un facteur initiateur du déclenchement et de la progression des maladies hépatiques. En effet, lorsqu'elle est excessive, l'hépatolyse risque de compromettre les fonctions hépatiques et quand elle persiste, elle induit une inflammation et des processus de régénération chroniques favorisant le développement de la fibrose et du CHC. Les cellules immunitaires jouent un rôle majeur dans l'induction de l'hépatolyse via l'expression et la libération de facteurs de mort appartenant à la superfamille du TNF. En effet les données cliniques suggèrent un important rôle du TNF-α, de FasL et de TRAIL dans l'induction de la mort des hépatocytes. La protéine RIPK1 est capable d'interagir avec plusieurs récepteurs de mort tels que le TNFR1, Fas et TRAIL-R2/DR5. Ces ligands de mort sont également impliqués dans l'hépatolyse induite par l'administration de Concanavaline A (ConA) chez la souris et nous avons précédemment montré, dans l'article I, le rôle de RIPK1 dans la survie des hépatocytes induite par le TNF-α dans ce modèle. Cependant, le blocage du TNF-α chez des souris conditionnellement déficientes pour RIPK1 dans les cellules parenchymateuses du foie (*Ripk1*$^{LPC\text{-}KO}$) n'inhibe pas totalement la mort des hépatocytes induite par la ConA. Afin d'étudier le rôle de RIPK1 en aval des récepteurs du FasL et de TRAIL (respectivement Fas et TRAIL-R2/DR5), nous avons dans ce travail étudié l'hépatolyse induite par un agoniste de Fas (mAb-Jo2) ainsi que par une co-administration d'IFN-γ et de TRAIL recombinantes chez les souris *Ripk1*$^{LPC\text{-}KO}$. Comme cette souche de souris est très sensible à l'hépatolyse induite par le TNF-α, nous avons également vérifié l'implication du TNF-α dans ces deux modèles par sa neutralisation via l'administration d'Etanercept. Cette étude a permis de montrer que *i)* l'absence de RIPK1 dans les LPC sensibilise les souris à l'hépatite induite par le mAb-Jo2, *ii)* que l'hépatolyse induite par Fas chez les souirs *Ripk1*$^{LPC\text{-}KO}$ est dépendante des caspases et indépendante du TNF-α, *iii)* la co-administration d'IFN-γ et de TRAIL mais pas des cytokines seules induit une mort des hépatocytes uniquement chez les souris *Ripk1*$^{LPC\text{-}KO}$ qui est dépendante des caspases et totalement inhibée par le blocage du TNF-α.

Nos résultats mettent en évidence le rôle protecteur de RIPK1 dans la signalisation du TNF-α et suggère que la sensibilité accrue des souris *Ripk1*$^{LPC\text{-}KO}$ à l'hépatite à ConA est dépendante de l'activation de Fas. De plus nos données, en association avec ceux de l'article I et II démontrant le rôle crucial de RIPK1 dans la signalisation du TNF-α et renforcent l'importance de la préservation de la fonction d'échafaudage de RIPK1 dans la survie des hépatocytes au cours des maladies hépatiques.

RIPK1 protects against liver injuries induced by Fas and TRAIL-R2 activation.

Aveline Filliol[1,2,3], Claire Piquet-Pellorce[1,2,3], Valentine Genet[1,2,3], Catherine Lucas-Clerc[2,4], Peter Vandenabeele[5,6], Mathieu JM Bertrand[5,6], Jacques Le Seyec[1,2,3] and Michel Samson[1,2,3].

[1]Institut National de la Santé et de la Recherche Médicale (Inserm), U.1085, Institut de Recherche Santé Environnement et Travail (IRSET), F-35043 Rennes, France.
[2]Université de Rennes 1, F-35043 Rennes, France.
[3]Structure Fédérative BioSit UMS 3480 CNRS-US18 Inserm, F-35043 Rennes, France.
[4]Service de Biochimie CHU Rennes, Université de Rennes 1; F-35043 Rennes, France.
[5]Inflammation Research Center, VIB, Technologiepark 927, Zwijnaarde-Ghent, 9052, Belgium.
[6]Department of Biomedical Molecular Biology, Ghent University, Technologiepark 927, Zwijnaarde-Ghent, [9]052, Belgium.

Financial support: This work was supported by INSERM, the Ministère de l'Education Nationale de la Recherche et de la Technologie, the University of Rennes 1, the Région Bretagne, the "Ligue contre le cancer, comités du grand Ouest".

Keywords: Fas, FasL, RIP kinase, RIPK1, Acute Hepatitis, Hepatocyte death, TRAIL, IFN-γ

ABSTRACT (227 words)

In liver diseases, hepatocyte death is a starting point of liver disease progression. Immune cells play a key role in this process, mainly by activation of the death receptors belonging to the Tumor Necrosis Factor (TNF) superfamily. The Receptor Interacting Protein Kinase 1 (RIPK1) is able to interact with the death domain of TNFR1, Fas or TRAIL-R2. Scaffold function of RIPK1 is involved in the maintenance of hepatocyte survival under TNF signaling. However its role under TRAIL and Fas receptors is poorly understood. In this work we used conditional knockout mice for RIPK1 in liver parenchymal cells (*Ripk1*$^{LPC\text{-}KO}$) and studied the role of Fas and TRAIL signaling by administration of the Fas-agonist (mAb-Jo2) in mice or by a treatment with recombinants INF-γ and TRAIL. As *Ripk1*$^{LPC\text{-}KO}$ mice are highly susceptible from TNF-α-induced hepatocyte death, we studied the role of TNF-α in these models by using Etanercept, a TNF-α decoy receptor. Our data showed that *i) Ripk1*$^{LPC\text{-}KO}$ mice were susceptible from Fas-mediated hepatocyte death, *ii)* this death was apoptotic and independent of TNF-α signaling, *iii)* recombinants INF-γ and TRAIL co-treatment but not the cytokines alone triggered apoptotic hepatocyte death only in *Ripk1*$^{LPC\text{-}KO}$ in a TNF-α dependent manner. As a consequence, our data highlight the protective role of RIPK1 under the Fas receptor in mice, and suggest the important protective role of RIPK1 in hepatocytes during human liver diseases.

INTRODUCTION

The Receptor Interacting protein kinase 1 (RIPK1) is a regulator of cellular responses induced by the Tumor Necrosis Factor (TNF) receptor superfamily such as TNF-α, Fas (or Apo1L/CD95L) [1] and TNF-Related Apoptosis Inducing Ligand (TRAIL) [2, 3]. RIPK1 roles has been actively studied this last decade, but mainly for TNFR1 signaling [4]. These works highlighted the key role of RIPK1 as a cell-fate switch engaging cells either in survival or death pathways [5, 6]. While the scaffold function of RIPK1 promotes cell survival through NF-kB activation or TRAF2 stabilization [7-10], its kinase activity initiates apoptotic or necroptotic signaling [5, 11].

We and others have recently demonstrated that RIPK1 protects hepatocytes from massive death during an acute hepatitis experimentally induced by the Concanavalin A lectin (ConA) [12, 13]. During liver diseases, members of the TNF superfamily such as TNF-α, FasL and TRAIL are expressed and released by immune cells, playing a key role in directly or indirectly triggering hepatocyte death [14, 15]. The ConA carbohydrate-binding protein is known to induce both activation and recruitment of hepatic immune cells such as natural killer T (NKT) –cell involved in inflammation and hepatocyte death. Thus, depletion of NKT-lymphocytes or of the invariant-NKT subpopulation avoids the liver injury normally induced by ConA [16-18]. In this hepatitis context, cytokines, such as TNF-α and IFN-γ, participate in liver injury by promoting favorable inflammatory conditions dependent of non-parenchymal cells. Indeed, specific deletion of TNFR1 in myeloid-derived cells, but not in liver parenchymal cells, protects from ConA hepatitis [19], while IFN-γ have been shown to promote NKT-activation [20]. Besides, TRAIL and FasL, mainly expressed by the hepatic NK- and NKT-cells, are most likely responsible for the direct induction of hepatocyte death since their inhibition or deletion prevents ConA-induced liver damage [17, 21-25].

Since RIPK1 has been described to interact with TRAIL-Receptor 2 (TRAIL-R2 or DR5) and Fas (or Apo1/CD95), we hypothesized that RIPK1 would step in downstream of these two receptors during hepatitis. These death receptors share some signaling effectors and their activation allows the recruitment of the death inducing signaling complex (DISC) which triggers caspase activation and ultimately apoptosis [26, 27]. The mouse liver is highly sensitive to a single injection of a Fas agonist [28] or of FasL [29]. Indeed, it induces fulminant hepatitis by triggering acute hepatocyte and liver sinusoidal endothelial cell (LSEC) death in a dose dependent manner, which lead to liver hemorrhages and death of the mice [28-30]. In contrast, a single injection of TRAIL does not induce hepatolysis. However, co-injection of soluble-DR5 or the use of TRAIL knockout (KO) mice have been shown to protect the animals from liver damage, suggesting that inflammatory conditions induced by ConA sensitized hepatocytes to death induced by TRAIL.

In this study, we addressed the role of RIPK1 during FasL or TRAIL signaling by taking advantage of conditional mice specifically deficient in RIPK1 in liver parenchymal cells (*Ripk1*$^{LPC\text{-}KO}$).

MATERIALS AND METHODS

Animals and treatment protocols

Ripk1$^{LPC\text{-}KO}$ mice were generated by crossing *Ripk1*$^{fl/fl}$ strain [31] with Alfp-Cre transgenic mice having a Cre recombinase driven by the serum albumin gene promoter completed with albumin and α-fetoprotein enhancers [32]. In all experiments, genetically modified mice were systematically compared to their littermates. Homogeneous groups of male and female mice at 7 to 13 weeks of age were used for each experiment. Mice fasted for 24 h received Fas agonist (mAb, Jo2) antibody (BD Pharmingen, #554255) via intraperitoneal (i.p.) route at a dose of 0.15 mg/kg body weight (10 µL/g body weight). Recombinant-murine TRAIL (rm-TRAIL) (Peprotech, 315-19) was injected in intravenous (i.v) route at a dose of 1.5 mg/kg body weight (4 µL/g body weight), 2 h after i.v. injection of IFN-γ (Peprotech, AF-315-05) at a dose of 0,35 mg/kg body weight or of PBS, as control. An i.p. injection was used to deliver Etanercept (Enbrel, Pfizer) to mice at a dose of 10 mg/kg body weight (10 µL/g body weight),

1 h before mAb-Jo2 or recombinant murine IFN-γ (rm-IFN-γ) injection. Mice were sacrificed at the indicated time.

Histopathological and biochemical studies

Fragments of mouse livers were fixed in 4% paraformaldehyde and embedded in paraffin for IHC and hematoxylin and eosin (H&E). For histopathology, H&E staining of liver tissues was carried out to investigate liver injury. Serum aspartate and alanine transaminases (ALT and AST, respectively) was measured according to the IFCC primary reference procedures using Olympus AU2700 Autoanalyser® (Olympus Optical, Tokyo, Japan).

Immunolocalization in liver tissues

For immunolocalization of cleaved caspase-3 in liver tissues, paraffin-embedded mouse liver sections (5 µm) were dried 1 h at 58°C, followed by antigen retrieval and incubated with primary antibody (Cell Signaling, 9661S) in a Ventana automated machine (Ventana Medical Systems, USA). Revelation of primary antibody was carried out using horseradish peroxidase (HRP)-conjugated secondary antibody (Dako, USA) and DAB substrate kit (Ventana, #760-124). Slides were then counterstained with hematoxylin. TUNEL analysis was performed on paraffin-embedded mouse liver sections (5 µm), incubated after antigen retrieval with a mix, composed of terminal transferase (Roche, #3333566011) and digoxigenin-11-UTP (Roche, #1558706) followed by HRP-anti-digoxigenin (Ventana, #760-4822). Revelation was used according to the manufacturer with the Discovery Rhodamine kit (Ventana #760-233) followed by nucleus labelling with DAPI.

All paraffin-embedded mouse liver sections were scanned with a digital slide scanner (Hamamatsu, Nanozoomer 2.0-RS) and files were analysis with the NDP viewer software.

RNA analysis

Fragments of liver from mice were collected after sacrifices and frozen in liquid nitrogen and conserved at -80°C. Total RNA was extracted from mice livers using TRIzol reagent (Invitrogen). First-strand cDNA was synthesized using the SuperScript™ II Reverse Transcriptase (Invitrogen). Real-time quantitative PCR was performed using the fluorescent dye SYBR Green with the double-strand specific SYBR® Green system (Applied Biosystems) and the ABI 7000 Prism sequence detector (Applied Biosystems) or the CFX384 Touch™ Real-Time PCR Detection System (Bio-Rad). cDNA was used as template for amplification with specific primer pairs (Table 1). Each measurement was performed in triplicate. The relative gene expression was normalized against the 18S gene expression. The control mice in each treatment group served as a reference for messenger RNA (mRNA) expression (control mRNA level was arbitrarily set at 1).

Protein extraction and western blotting

Mouse liver specimens were lysed in RIPA buffer (50 mM Tris-HCl pH 7.4; 1 % Triton X-100; 25 mM HEPES; 150 mM NaCl; 0,2 % SDS; 5 mM $MgCl_2$; 1 mM Na_3VO_4; 1 mM NaF) containing proteases inhibitors (Roche, #04 693 132 001) using UltraTurax. After 40 min in ice, samples were centrifuged at 15,000 g. Proteins from diluted supernatant were assayed with the Bradford method (BioRad). Proteins were separated by SDS-PAGE and transferred onto nitrocellulose membrane. Membranes were blocked with non-fat milk in TBS (20 mM Tris, 137 mM NaCl) during 1-2 h and incubated overnight with primary antibody anti-cleaved Caspase-3, anti-RIPK1 (Cell Signaling, 3493) anti-actin (Sigma A3854), anti-phospho-Thr183/Tyr185-JNK (Cell Signaling, 9251), anti-JNK (Calbiochem, 559304) or anti-TNF-α (Abcam, ab6671) at 4°C, and then with secondary goat anti-rabbit immunoglobulins/HRP (Dako, P0448). Protein-antibody complexes were revealed by enhanced chemiluminescence (Millipore) and ImageQuant LAS-4000 mini imager analysis (GE-Healthcare).

Serum cytokine dosage

Murine TNF-α was quantified by ELISA (Peprotech, 900-M54) or bead-based immunoassays according to manufacturer protocol, using a filter plate and a vacuum filtration system for washing steps (BioLegend's LEGENDPLEX, multi-analyte flow assay kit). Samples were analyzed on a LSR Fortessa cytometer (BD Biosciences).

Statistical analysis

Data were expressed as means +/- SEM for all mice treated similarly. Kruskal–Wallis one-way analysis of variance (ANOVA) was performed, and mean differences between experimental groups were assessed using the non-parametric Mann–Whitney *U*-test with the GraphPad Prism5 software. The significance is shown as follows: * $p<0.05$, ** $p<0.01$, *** $p<0.001$, $Ripk1^{fl/fl}$ mice versus $RIPK1^{LPC\text{-}KO}$ mice. # $p<0.05$, ## $p<0.01$, ### $p<0.001$, mice treated with ConA, mAb-Jo2, rm-IFN-γ or rm-TRAIL versus mice treated with PBS.

RESULTS AND DISCUSSION

We have previously described the susceptibility of conditional RIPK1 deficiency in liver parenchymal cells to TNF-α- and ConA-induced liver injury [13]. Even if the use of Etanercept (ETA), a TNF-α decoy receptor, significantly reduced liver injury, it did not fully protect animals from ConA-hepatitis (Fig. 1A). This suggested that other factors may take part in the hepatocyte death process, such as FasL and/or TRAIL which have been shown to be involved during ConA-induced liver injury [17, 21-25]. Thus, FasL, Fas and DR5 transcripts were significantly up-regulated in $Ripk1^{LPC\text{-}KO}$ mice and their WT littermate ($Ripk1^{fl/fl}$) after ConA treatment. The TRAIL transcripts tend to also be induced at a lesser extent, in both WT and $Ripk1^{LPC\text{-}KO}$ groups but only significantly for WT mice (Fig 1B). As Fas activation with the Fas-agonist mAb-Jo2 has been shown to induce acute liver injury [28], we used this hepatitis model to explore the role of RIPK1 under Fas signaling. While injection of a low dose (0,15 mg/kg) of mAb-Jo2 provoked a mild hepatitis in WT mice, the same treatment elicited more important liver damage in $Ripk1^{LPC\text{-}KO}$ mice, as shown by higher levels of serum transaminases (Fig. 2A) and by the increase number of necrotic areas and of TUNEL positive cells, 6 h after mAb-Jo2 injection (Fig. 2B). In this model, it has been stated that hepatocytes die by caspase-dependent apoptotic pathway as demonstrated by the resistance of hepatocyte-specific caspase-8 deficient mice to Fas agonist induced liver injury [33]. Activation of c-Jun N-terminal kinases (JNKs) is also known to take part in the apoptotic death process of hepatocytes in different murine hepatitis models [34], including those induced by Fas [35]. Therefore, we decided to investigate the apoptosis signaling by assessing the rate of cleaved-caspase-3 and of JNK activation in the livers of $Ripk1^{fl/fl}$ and $Ripk1^{LPC\text{-}KO}$ mice. As expected, the cleaved-caspase-3 labelling of hepatic tissues issued from WT mice revealed positive hepatocytes around the portal veins. Moreover, an activation of JNK1/2 was found 6 h after mAb-Jo2 treatment as revealed by their enhanced phosphorylation status. However, the activation of these both apoptotic markers proved to be more important in the $Ripk1^{LPC\text{-}KO}$ mice (Fig. 2C and Fig. 2D). Altogether, these data showed that RIPK1 deficiency in liver parenchymal cells sensitized mice to liver injury induced by the Fas agonist, which resulted from an increasing caspase activation, itself under the dependence of JNK activation. The observed hepatocyte death was also associated with an increase of the liver inflammation, as shown by the upregulation of TNF-α, IL-1β and IL-6 transcripts in $Ripk1^{fl/fl}$ after mAb-Jo2 treatment, which were even more substantial in the liver of $Ripk1^{LPC\text{-}KO}$ mice (Fig. 2E).

To investigate the protective role of RIPK1 in the hepatocyte death process induced by Fas, we next evaluated transcription of some genes whose proteins are known to be involved in cell survival such as A20, the inhibitor of apoptosis proteins (IAP) XIAP and cIAP2, and the Bcl-xL, cFLIP and Bcl2 anti-apoptotic proteins. Indeed, hepatocyte specific Bcl-xL KO and A20 total KO mice developed both liver inflammation and injury [36, 37], suggesting their important hepatoprotective role. Moreover Bcl-xL specific anti-sense oligonucleotides have been shown to sensitized mice from Fas-induced liver injury [38]. Thus, analysis were performed in $Ripk1^{fl/fl}$ and $Ripk1^{LPC\text{-}KO}$ mice, 6 h after mAb-Jo2 injection. Transcription rates of XIAP, cIAP2, cFLIP and Bcl-2 were never significantly modified after treatment in both strain mice (Fig. 3A). In contrast, A20 and Bcl-xL transcripts were up-regulated in $Ripk1^{fl/fl}$ and $Ripk1^{LPC\text{-}KO}$ mice. Moreover, A20 mRNA was significantly higher in the $Ripk1^{LPC\text{-}KO}$ mice livers. Although not statistically significant, a similar trend was also observed for Bcl-xL (Fig. 3A). These observations did not support the hypothesis that RIPK1 could protect

hepatocytes from Fas-induced apoptosis by transcriptional upregulation of anti-apoptotic pathways. The surprising up-regulation of these genes in *Ripk1*$^{LPC\text{-}KO}$ mice after Fas-agonist treatment however suggests a RIPK1-independent induction of a hepatoprotective process dedicated to the repair of liver damage. Indeed, as IL-6, a well-known cytokine involved in the liver repair [1, 39, 40] and that was also more upregulated in Fas-agonist *Ripk1*$^{LPC\text{-}KO}$ treated mice (Fig. 2E), the production of A20 may be stimulated rather for liver repair purpose since its role in the regenerative response has already been suggested [41]. Accordingly, when the correlation between the expression levels of IL-6, A20 and Bcl-xL transcripts with the serum transaminase levels in *Ripk1*$^{fl/fl}$ and *Ripk1*$^{LPC\text{-}KO}$ mice was analyzed, it appeared that these mRNA were positively and significantly correlated with the hepatolysis severity (Fig. 3B), suggesting that their up-regulation result from the induction of liver damage by the Fas-agonist.

Although induced by different cues, the transcription of the A20 gene is well known to also result from TNF-α stimulation. Moreover, we observed that TNF-α transcripts were up-regulated during Fas-agonist-induced-hepatitis in both tested murine strains (Fig. 2E). Since we previously showed that, unlike their WT counterparts, *Ripk1*$^{LPC\text{-}KO}$ mice are susceptible to TNF-α-induced liver damage, we next investigated the potential contribution played by TNF-α during the Fas-agonist induced hepatitis. TNF-α could not be detected in the serum of challenged *Ripk1*$^{fl/fl}$ and *Ripk1*$^{LPC\text{-}KO}$ mice (data not shown), because their levels were below the detection threshold of the ELISA test. However, the cytokine could be detected in liver extracts by western-blot analysis. Even if the used anti-TNF-α antibody has been described as being able to recognize both soluble and transmembrane TNF-α forms, only its transmembrane form was detected in mouse livers, with weaker signals in *Ripk1*$^{LPC\text{-}KO}$ specimens (Fig. 3A). In parallel, we found that TNF-α neutralization by prior ETA injection never improved liver injury induced by the Fas-agonist whatsoever in *Ripk1*$^{fl/fl}$ or *Ripk1*$^{LPC\text{-}KO}$ mice, as assessed by serum transaminase releasing (Fig. 3B). Accordingly, liver from *Ripk1*$^{LPC\text{-}KO}$ mice which received ETA and the mAb-Jo2 displayed large necrosis areas, and a large number of cleaved-caspase-3 positive cells, similar to those revealed for *Ripk1*$^{LPC\text{-}KO}$ mouse livers only receiving the Fas-agonist (Fig. 3C). All these data demonstrate that the susceptibility of *Ripk1*$^{LPC\text{-}KO}$ mice to Fas-induced liver injury is TNF-α independent and thus strongly suggest the protective role played by RIPK1 during the Fas signaling. Apparent contradictory data were recently published [12]. In this article, authors showed that the *in vivo* Ripk1 knockdown did not affect Fas-induced liver injury. This discrepancy may be explained by their approach using antisense oligonucleotide which reduced but not completely abolished the expression of RIPK1. Thus, one cannot exclude that remaining RIPK1 was sufficient to protect hepatocyte from the liver injury induced by Fas agonist. Moreover, in contrast to our model, Ripk1 knockdown affected not only liver parenchymal cells but also most probably the immune hepatic microenvironment triggered by mAb-Jo2 injection.

During ConA hepatitis, TRAIL has been shown to contribute in the liver injury process [21, 24], but implied mechanisms are not fully understood. Indeed, unlike Fas-agonist, *in vivo* treatment with TRAIL never induces hepatolysis [42]. Zheng *et al.* have proposed that the microenvironment induced by ConA sensitizes hepatocytes to TRAIL-induced cell death [24]. As IFN-γ has been shown to be implied during ConA hepatitis [43]; [25, 44] and since this cytokine also sensitized some cells to TRAIL-induced apoptosis [45, 46], we decided to investigate the *in vivo* role of RIPK1 under TRAIL and IFN-γ stimulation. Whereas single injections of TRAIL or IFN-γ did not induced hepatolysis in *Ripk1*$^{fl/fl}$ and *Ripk1*$^{LPC\text{-}KO}$ mice, their co-injection was able to trigger hepatocyte apoptosis only in *Ripk1*$^{LPC\text{-}KO}$ mice, as assessed by the observed moderate levels of serum transaminase, and necrotic and cleaved-caspase 3 positive cells in the liver of these mice (Fig. 5A and 5B). However, this hepatolysis could be completely prevented by the use of ETA. As we previously showed that *Ripk1*$^{LPC\text{-}KO}$ mice are susceptible to TNF-α induced liver injury, this strongly suggested that IFN-γ and TRAIL co-stimulation triggered TNF-α release

which in turn induced hepatocyte death due to the lack of RIPK1. Accordingly, low levels of serum TNF-α were detected 8 h after TRAIL injection in *Ripk1*$^{LPC\text{-}KO}$ mice pre-treated with IFN-γ (9.23 ± 2.17 pg/mL).

Finally, our data showed that RIPK1 in hepatocytes is able to limit the hepatic injuries induced by FasL which is independent of TNF-α. Consequently, this suggested that the remaining hepatolysis observed in *Ripk1*$^{LPC\text{-}KO}$ mice treated with ETA and ConA (Fig. 1A) was most likely dependent of FasL. In order to confirm this hypothesis, experiments blocking both FasL and TNF-α signaling during ConA hepatitis in *Ripk1*$^{LPC\text{-}KO}$ mice would be informative. Like for TNF-α, FasL is known to be involved in several liver diseases. As a consequence, our data consolidate the protective role of RIPK1 in dysimmune hepatitis and the risks of potential defects in the RIPK1 scaffolding function that would sensitize hepatocyte to the death, risking to worsen hepatitis and even to increase HCC onset.

ACKNOWLEDGEMENTS

This work was supported by INSERM, The "Ministère de l'Education Nationale de la Recherche et de la Technologie", the University of Rennes 1, the "Région Bretagne" and the "Ligue contre le cancer, comités du grand Ouest", the Institut national du cancer « INCA ». Research in the Vandenabeele group is supported by Belgian grants (Interuniversity Attraction Poles, IAP 7/32), Flemish grants (Research Foundation Flanders: FWO G.0875.11, FWO G.0973.11, FWO G.0A45.12N, FWO G.0172.12, FWO G.0787.13N, FWO G.0607.13N, FWO KAN 31528711, FWO KAN 1504813N, FWO G0E04.16N), Methusalem grant (BOF16/MET_V/007), Ghent University grants (MRP, GROUP-ID consortium, BOFGOA2014000702), grant from the Foundation against Cancer (F94), and grants from VIB. AF was supported by a PhD fellowship from the "Région Bretagne". PV is senior full professor at Ghent University and holds a Methusalem grant (BOF09/01M00709). For immunohistochemistry analysis and animal house facilities, we would like to thank dedicated platforms (i.e. H2P2 and animal house platforms) of SFR BIOSIT, University of Rennes 1, France. We would also like to thank Barbara Gilbert and Cristina Ulecia Morón for technical assistance.

REFERENCES

[1] Stanger BZ, Leder P, Lee TH, Kim E, Seed B. RIP: a novel protein containing a death domain that interacts with Fas/APO-1 (CD95) in yeast and causes cell death. Cell 1995;81:513-523.

[2] Chaudhary PM, Eby M, Jasmin A, Bookwalter A, Murray J, Hood L. Death receptor 5, a new member of the TNFR family, and DR4 induce FADD-dependent apoptosis and activate the NF-kappaB pathway. Immunity 1997;7:821-830.

[3] Lin Y, Devin A, Cook A, Keane MM, Kelliher M, Lipkowitz S, et al. The death domain kinase RIP is essential for TRAIL (Apo2L)-induced activation of IkappaB kinase and c-Jun N-terminal kinase. Mol Cell Biol 2000;20:6638-6645.

[4] Pasparakis M, Vandenabeele P. Necroptosis and its role in inflammation. Nature 2015;517:311-320.

[5] Ofengeim D, Yuan J. Regulation of RIP1 kinase signalling at the crossroads of inflammation and cell death. Nat Rev Mol Cell Biol 2013;14:727-736.

[6] Silke J, Rickard JA, Gerlic M. The diverse role of RIP kinases in necroptosis and inflammation. Nat Immunol 2015;16:689-697.

[7] Dillon CP, Weinlich R, Rodriguez DA, Cripps JG, Quarato G, Gurung P, et al. RIPK1 blocks early postnatal lethality mediated by caspase-8 and RIPK3. Cell 2014;157:1189-1202.

[8] Gentle IE, Wong WW, Evans JM, Bankovacki A, Cook WD, Khan NR, et al. In TNF-stimulated cells, RIPK1 promotes cell survival by stabilizing TRAF2 and cIAP1, which limits induction of non-canonical NF-kappaB and activation of caspase-8. J Biol Chem 2011;286:13282-13291.

[9] Vanlangenakker N, Bertrand MJ, Bogaert P, Vandenabeele P, Vanden Berghe T. TNF-induced necroptosis in L929 cells is tightly regulated by multiple TNFR1 complex I and II members. Cell Death Dis 2011;2:e230.

[10] Wong WW, Gentle IE, Nachbur U, Anderton H, Vaux DL, Silke J. RIPK1 is not essential for TNFR1-induced activation of NF-kappaB. Cell Death Differ 2010;17:482-487.
[11] Wang L, Du F, Wang X. TNF-alpha induces two distinct caspase-8 activation pathways. Cell 2008;133:693-703.
[12] Suda J, Dara L, Yang L, Aghajan M, Song Y, Kaplowitz N, et al. Knockdown of RIPK1 Markedly Exacerbates Murine Immune-Mediated Liver Injury through Massive Apoptosis of Hepatocytes, Independent of Necroptosis and Inhibition of NF-kappaB. J Immunol 2016.
[13] Filliol A, Piquet-Pellorce C, Le Seyec J, Farooq M, Genet V, Lucas-Clerc C, et al. RIPK1 protects from TNF-α mediated liver damage during hepatitis. Cell Death & Diseases 2017.
[14] Brenner C, Galluzzi L, Kepp O, Kroemer G. Decoding cell death signals in liver inflammation. J Hepatol 2013;59:583-594.
[15] Malhi H, Guicciardi ME, Gores GJ. Hepatocyte death: a clear and present danger. Physiol Rev 2010;90:1165-1194.
[16] Kaneko Y, Harada M, Kawano T, Yamashita M, Shibata Y, Gejyo F, et al. Augmentation of Valpha14 NKT cell-mediated cytotoxicity by interleukin 4 in an autocrine mechanism resulting in the development of concanavalin A-induced hepatitis. J Exp Med 2000;191:105-114.
[17] Takeda K, Hayakawa Y, Van Kaer L, Matsuda H, Yagita H, Okumura K. Critical contribution of liver natural killer T cells to a murine model of hepatitis. Proc Natl Acad Sci U S A 2000;97:5498-5503.
[18] Trautwein C, Rakemann T, Brenner DA, Streetz K, Licato L, Manns MP, et al. Concanavalin A-induced liver cell damage: activation of intracellular pathways triggered by tumor necrosis factor in mice. Gastroenterology 1998;114:1035-1045.
[19] Wroblewski R, Armaka M, Kondylis V, Pasparakis M, Walczak H, Mittrucker HW, et al. Opposing role of tumor necrosis factor receptor 1 signaling in T cell-mediated hepatitis and bacterial infection in mice. Hepatology 2016;64:508-521.
[20] Hong F, Jaruga B, Kim WH, Radaeva S, El-Assal ON, Tian Z, et al. Opposing roles of STAT1 and STAT3 in T cell-mediated hepatitis: regulation by SOCS. J Clin Invest 2002;110:1503-1513.
[21] Arshad MI, Piquet-Pellorce C, L'Helgoualc'h A, Rauch M, Patrat-Delon S, Ezan F, et al. TRAIL but not FasL and TNFalpha, regulates IL-33 expression in murine hepatocytes during acute hepatitis. Hepatology 2012;56:2353-2362.
[22] Leist M, Gantner F, Kunstle G, Bohlinger I, Tiegs G, Bluethmann H, et al. The 55-kD tumor necrosis factor receptor and CD95 independently signal murine hepatocyte apoptosis and subsequent liver failure. Mol Med 1996;2:109-124.
[23] Seino K, Kayagaki N, Takeda K, Fukao K, Okumura K, Yagita H. Contribution of Fas ligand to T cell-mediated hepatic injury in mice. Gastroenterology 1997;113:1315-1322.
[24] Zheng SJ, Wang P, Tsabary G, Chen YH. Critical roles of TRAIL in hepatic cell death and hepatic inflammation. J Clin Invest 2004;113:58-64.
[25] Tagawa Y, Sekikawa K, Iwakura Y. Suppression of concanavalin A-induced hepatitis in IFN-gamma(-/-) mice, but not in TNF-alpha(-/-) mice: role for IFN-gamma in activating apoptosis of hepatocytes. J Immunol 1997;159:1418-1428.
[26] Krammer PH. CD95(APO-1/Fas)-mediated apoptosis: live and let die. Adv Immunol 1999;71:163-210.
[27] Zender L, Hutker S, Liedtke C, Tillmann HL, Zender S, Mundt B, et al. Caspase 8 small interfering RNA prevents acute liver failure in mice. Proc Natl Acad Sci U S A 2003;100:7797-7802.
[28] Ogasawara J, Watanabe-Fukunaga R, Adachi M, Matsuzawa A, Kasugai T, Kitamura Y, et al. Lethal effect of the anti-Fas antibody in mice. Nature 1993;364:806-809.
[29] Huang DC, Hahne M, Schroeter M, Frei K, Fontana A, Villunger A, et al. Activation of Fas by FasL induces apoptosis by a mechanism that cannot be blocked by Bcl-2 or Bcl-x(L). Proc Natl Acad Sci U S A 1999;96:14871-14876.
[30] Wanner GA, Mica L, Wanner-Schmid E, Kolb SA, Hentze H, Trentz O, et al. Inhibition of caspase activity prevents CD95-mediated hepatic microvascular perfusion failure and restores Kupffer cell clearance capacity. FASEB J 1999;13:1239-1248.

[31] Takahashi N, Vereecke L, Bertrand MJ, Duprez L, Berger SB, Divert T, et al. RIPK1 ensures intestinal homeostasis by protecting the epithelium against apoptosis. Nature 2014;513:95-99.
[32] Kellendonk C, Opherk C, Anlag K, Schutz G, Tronche F. Hepatocyte-specific expression of Cre recombinase. Genesis 2000;26:151-153.
[33] Liedtke C, Bangen JM, Freimuth J, Beraza N, Lambertz D, Cubero FJ, et al. Loss of caspase-8 protects mice against inflammation-related hepatocarcinogenesis but induces non-apoptotic liver injury. Gastroenterology 2011;141:2176-2187.
[34] Seki E, Brenner DA, Karin M. A liver full of JNK: signaling in regulation of cell function and disease pathogenesis, and clinical approaches. Gastroenterology 2012;143:307-320.
[35] Corazza N, Jakob S, Schaer C, Frese S, Keogh A, Stroka D, et al. TRAIL receptor-mediated JNK activation and Bim phosphorylation critically regulate Fas-mediated liver damage and lethality. J Clin Invest 2006;116:2493-2499.
[36] Lee EG, Boone DL, Chai S, Libby SL, Chien M, Lodolce JP, et al. Failure to regulate TNF-induced NF-kappaB and cell death responses in A20-deficient mice. Science 2000;289:2350-2354.
[37] Takehara T, Tatsumi T, Suzuki T, Rucker EB, 3rd, Hennighausen L, Jinushi M, et al. Hepatocyte-specific disruption of Bcl-xL leads to continuous hepatocyte apoptosis and liver fibrotic responses. Gastroenterology 2004;127:1189-1197.
[38] Zhang H, Taylor J, Luther D, Johnston J, Murray S, Wyatt JR, et al. Antisense oligonucleotide inhibition of Bcl-xL and Bid expression in liver regulates responses in a mouse model of Fas-induced fulminant hepatitis. J Pharmacol Exp Ther 2003;307:24-33.
[39] Luedde T, Trautwein C. Intracellular survival pathways in the liver. Liver Int 2006;26:1163-1174.
[40] Taub R. Hepatoprotection via the IL-6/Stat3 pathway. J Clin Invest 2003;112:978-980.
[41] Studer P, da Silva CG, Revuelta Cervantes JM, Mele A, Csizmadia E, Siracuse JJ, et al. Significant lethality following liver resection in A20 heterozygous knockout mice uncovers a key role for A20 in liver regeneration. Cell Death Differ 2015;22:2068-2077.
[42] Walczak H, Miller RE, Ariail K, Gliniak B, Griffith TS, Kubin M, et al. Tumoricidal activity of tumor necrosis factor-related apoptosis-inducing ligand in vivo. Nat Med 1999;5:157-163.
[43] Mizuhara H, Uno M, Seki N, Yamashita M, Yamaoka M, Ogawa T, et al. Critical involvement of interferon gamma in the pathogenesis of T-cell activation-associated hepatitis and regulatory mechanisms of interleukin-6 for the manifestations of hepatitis. Hepatology 1996;23:1608-1615.
[44] Watanabe Y, Morita M, Akaike T. Concanavalin A induces perforin-mediated but not Fas-mediated hepatic injury. Hepatology 1996;24:702-710.
[45] Fulda S, Debatin KM. IFNgamma sensitizes for apoptosis by upregulating caspase-8 expression through the Stat1 pathway. Oncogene 2002;21:2295-2308.
[46] Hacker S, Dittrich A, Mohr A, Schweitzer T, Rutkowski S, Krauss J, et al. Histone deacetylase inhibitors cooperate with IFN-gamma to restore caspase-8 expression and overcome TRAIL resistance in cancers with silencing of caspase-8. Oncogene 2009;28:3097-3110.

LEGENDS OF FIGURES

Figure 1. TNF-α inhibition partially protects from ConA-induced liver injuries in *Ripk1*$^{LPC-KO}$ mice, role of the FasL and TRAIL signaling.
(A) Levels of serum ALT, 11 h after ConA or PBS injection in *Ripk1*$^{LPC-KO}$ mice, eventually pre-treated with Etanercept. Number of mice for each group: PBS (n=6), ConA (n=10) and ETA+ConA (n=5) (B) Levels of hepatic TNF-α, IL-1β and IL-6 transcripts in *Ripk1*$^{fl/fl}$ or *Ripk1*$^{LPC-KO}$ mice treated with ConA or PBS (n=3-5). (*, #p<0.05; **, ## p<0.01; ***, ### p<0.001).

Figure 2. RIPK1 sensitizes mice to Fas-mediated liver injuries
(A) Levels of serum ALT and AST, 6 h after mAb-Jo2 injection in *Ripk1*$^{fl/fl}$ and *Ripk1*$^{LPC\text{-}KO}$ mice. (B) Pictures of liver tissue sections, stained by H&E (upper panel) or analyzed by TUNEL (in red) and DAPI (in blue) immunofluorescence (lower panel) issued from *Ripk1*$^{fl/fl}$ and *Ripk1*$^{LPC\text{-}KO}$ mice, 6 h after mAb-Jo2 injection. White arrows shown necrotic areas or apoptotic hepatocytes. (C) Immunostaining of cleaved-caspase-3 in the livers of *Ripk1*$^{fl/fl}$ and *Ripk1*$^{LPC\text{-}KO}$ mice, 6 h after mAb-Jo2 injection. The graph represents signal quantification of cleaved-caspase-3 measured on these livers (each dot represents an individual). (D) Western-blot analysis of cleaved-caspase-3 and β-actin (upper panel) or phosphorylated and total form of JNK1/2 proteins (lower panel) in protein extracts issued from the livers of *Ripk1*$^{fl/fl}$ and *Ripk1*$^{LPC\text{-}KO}$ mice, collected 6 h after mAb-Jo2 injection. Studied proteins are respectively indicated on the bottom of the gel. (E) Levels of hepatic TNF-α, IL-1β and IL-6 transcripts in *Ripk1*$^{fl/fl}$ or *Ripk1*$^{LPC\text{-}KO}$ mice 6 h after mAb-Jo2 injection. Data are expressed ± SEM (*, # $p<0.05$; **, ## $p<0.01$; ***, ### $p<0.001$, ns: non-significant).

Figure 3. Up-regulation of pro-survival genes in *Ripk1*$^{LPC\text{-}KO}$ mice after Fas-agonist stimulation correlates with liver injury.
(A) Levels of hepatic A20, XIAP, cIAP2, Bcl-xl, cFLIP and Bcl-2 transcripts in *Ripk1*$^{fl/fl}$ or *Ripk1*$^{LPC\text{-}KO}$ mice 6 h after mAb-Jo2 injection (n=4-7 mice). Data are expressed ± SEM (*, # $p<0.05$; **, ## $p<0.01$; ***, ### $p<0.001$, ns: non-significant). (B) Correlation analysis between measured serum ALT with levels of hepatic IL-6, A20 or Bcl-xl transcripts in liver tissues of the *Ripk1*$^{fl/fl}$ and *Ripk1*$^{LPC\text{-}KO}$ was performed using Pearson's and Spearman's correlation coefficient.

Figure 4. Liver injury in *Ripk1*$^{LPC\text{-}KO}$ mice is independent of TNF-α
(A) Western-blot analysis of RIPK1, TNF-α and β-actin in protein extracts issued from the livers of *Ripk1*$^{fl/fl}$ and *Ripk1*$^{LPC\text{-}KO}$ mice, collected 3 h or 6 h after mAb-Jo2 injection. Studied proteins are respectively indicated on right of the gels (tm-TNF correspond to the transmembrane form). (B) Levels of serum ALT and AST and (C) pictures of liver tissue sections, stained by H&E (upper panel) or analyzed by IHC for cleaved-caspase-3 (lower panel), issued from *Ripk1*$^{fl/fl}$ and *Ripk1*$^{\text{LPC-KO}}$ mice, 6 h after mAb-Jo2 injection.

Figure 5: Co-injection of IFN-γ and TRAIL promotes liver injury in *Ripk1*$^{LPC\text{-}KO}$ mice in a TNF-α dependent manner.
(A) Levels of serum ALT, 8 h after TRAIL or PBS injection with an eventual pre-treatment with IFN-γ and/or ETA in *Ripk1*$^{fl/fl}$ and *Ripk1*$^{LPC\text{-}KO}$ mice. (B) Pictures of liver tissue sections, stained by H&E (upper panel) or analyzed by IHC for cleaved-caspase-3 (lower panel), issued from *Ripk1*$^{fl/fl}$ and *Ripk1*$^{\text{LPC-KO}}$ mice, 8 h after TRAIL injection, pre-treated 2 h before with IFN-γ and with an eventual pre-treatment with ETA. White arrows show necrotic areas and apoptotic hepatocytes.

Table 1. Sequence of primers used for qPCR

Gene	Forward	Reverse
Mouse 18S	5′-CGCCGCTAGAGGTGAAATTC-3′	5′-TTGGCAAATGCTTTCGCTC-3′
Mouse TNFα	5′-TAGCTCCCAGAAAAGCAAGC-3′	5′-TTTTCTGGAGGGAGATGTGG-3′
Mouse IL-6	5′-CCGGAGAGGAGACTTCACAG-3’	5′-CAGAATTGCCATTGCACAAC-3′
Mouse IL-1β	5’-GAAGAAGTGCCCATCCTCTG-3’	AGCTCATATGGGTCCGACAG-3’
Mouse FasL	5′-GCAGCAGCCCATGAATTACC-3′	5′-AGATGAAGTGGCACTGCTGTCTAC-3′
Mouse Fas	5′-CTCCGAGTTTAAAGCTGAGG-3′	5′-TGTACTCCTTCCCTTCTGTGC-3′
Mouse TRAIL	5′-CCCTGCTTGCAGGTTAAGAG-3′	5′-GGCCTAAGGTCTTTCCATCC-3′
Mouse DR5	5′-TGACGGGGAAGAGGAACTGA-3′	5′-GGCTTTGACCATTTGGATCT-3′
Mouse Bcl-xl	5’- TGGAGTCAGTTTAGTGATGTCGAAG -3’	5’- AGTTTACTCCATCCCGAAAGAGTTC -3’
Mouse cIAP2	5′-TCA GTG ACC TCG TTA TAG GCT T-3′	5′-TCA CAC ACG TCA AAT GTT GGA A-3′
Mouse XIAP	5’-TGGGAAATAGAAATCCTTTTGC-3’	5’-TGG AGAGTTTGTTGAATTTGGG-3’
Mouse A20	5′-AAACCAATGGTGATGGAAACTG-3′	5′-GTTGTCCCATTCGTCATTCC-3′
Mouse cFLIP	5′-GGATTACAAGGGATTACACAGGC-3′	5′-CTGGTACTCCATACACTGGCT-3′
Mouse Bcl-2	5’-TTATAAGCTGTCACAGAGGGGCTAC-3’	5’-GAACTCAAAGAAGGCCACAATCCTC-3’

Figure 1

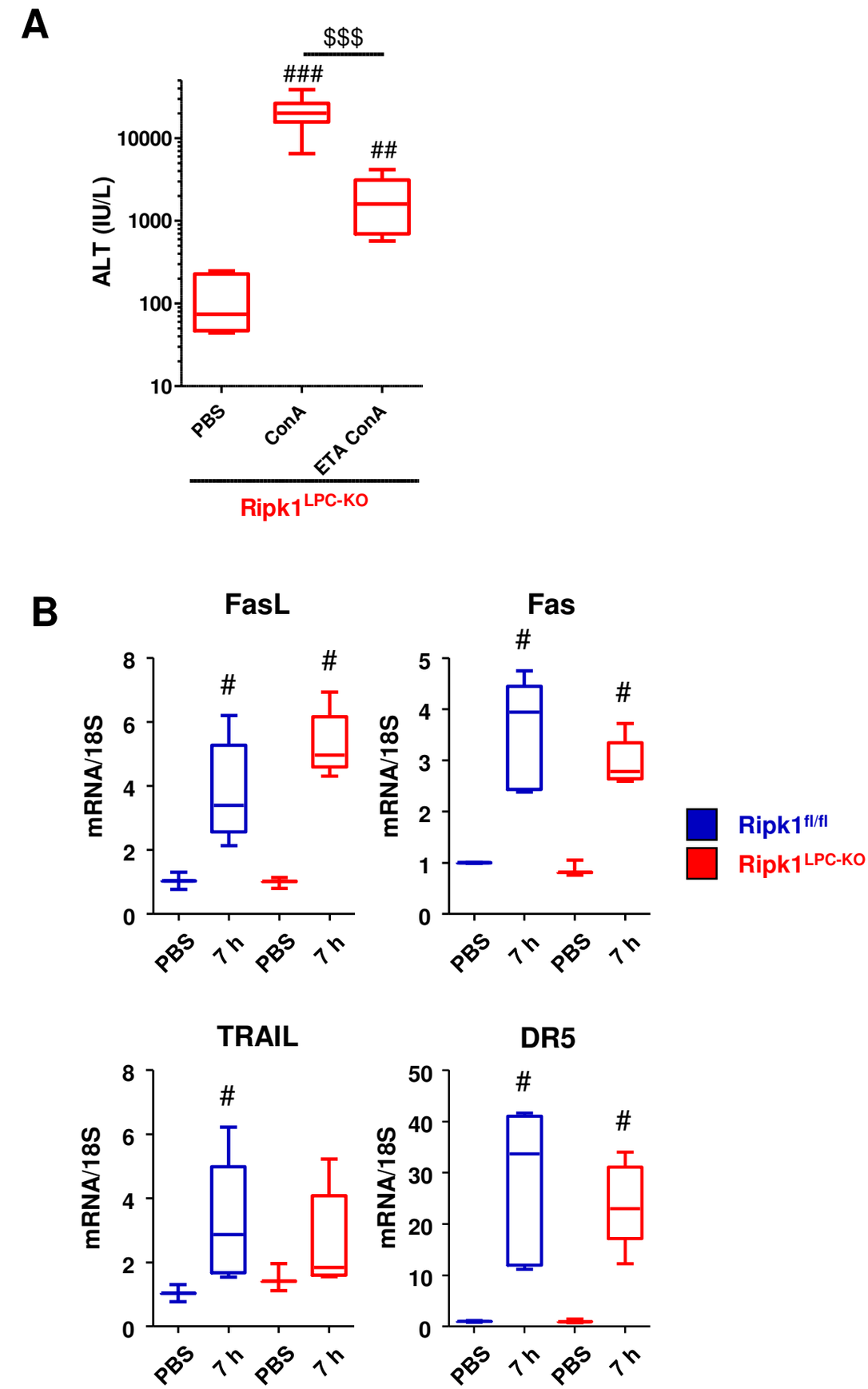
A
$$$
###
##
10000
1000
100
10
ALT (IU/L)
PBS
ConA
ETA ConA
Ripk1LPC-KO
B
FasL
Fas
TRAIL
DR5
mRNA/18S
PBS
7 h
Ripk1fl/fl
Ripk1LPC-KO

Figure 2

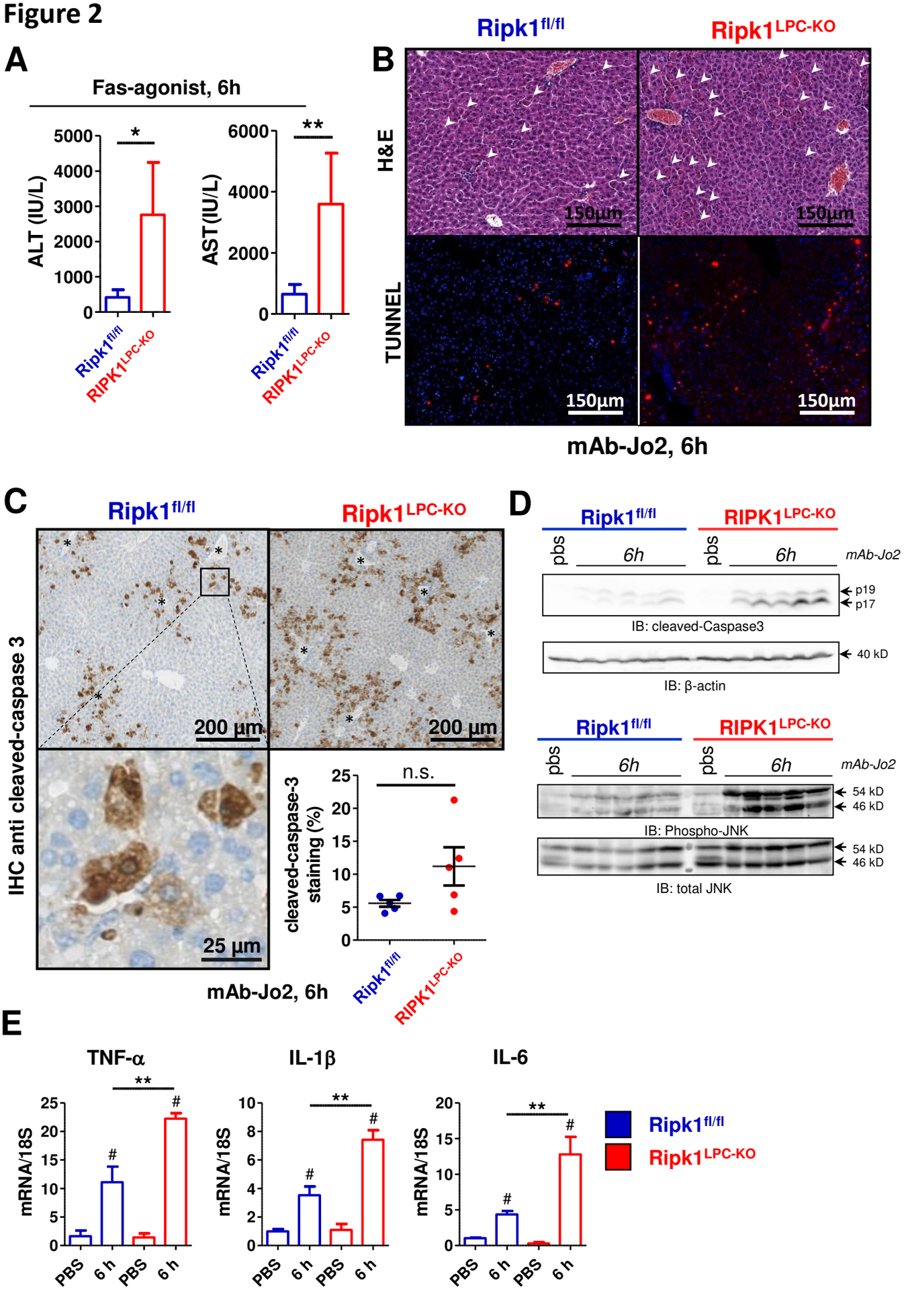
A
Fas-agonist, 6h
ALT (IU/L)
AST (IU/L)
Ripk1fl/fl
RIPK1LPC-KO
B
Ripk1fl/fl
Ripk1LPC-KO
H&E
TUNNEL
150μm
mAb-Jo2, 6h
C
Ripk1fl/fl
Ripk1LPC-KO
IHC anti cleaved-caspase 3
200 μm
25 μm
cleaved-caspase-3 staining (%)
n.s.
mAb-Jo2, 6h
D
Ripk1fl/fl
RIPK1LPC-KO
pbs
6h
mAb-Jo2
p19
p17
IB: cleaved-Caspase3
40 kD
IB: β-actin
54 kD
46 kD
IB: Phospho-JNK
IB: total JNK
E
TNF-α
IL-1β
IL-6
mRNA/18S
PBS
6 h

Figure 3

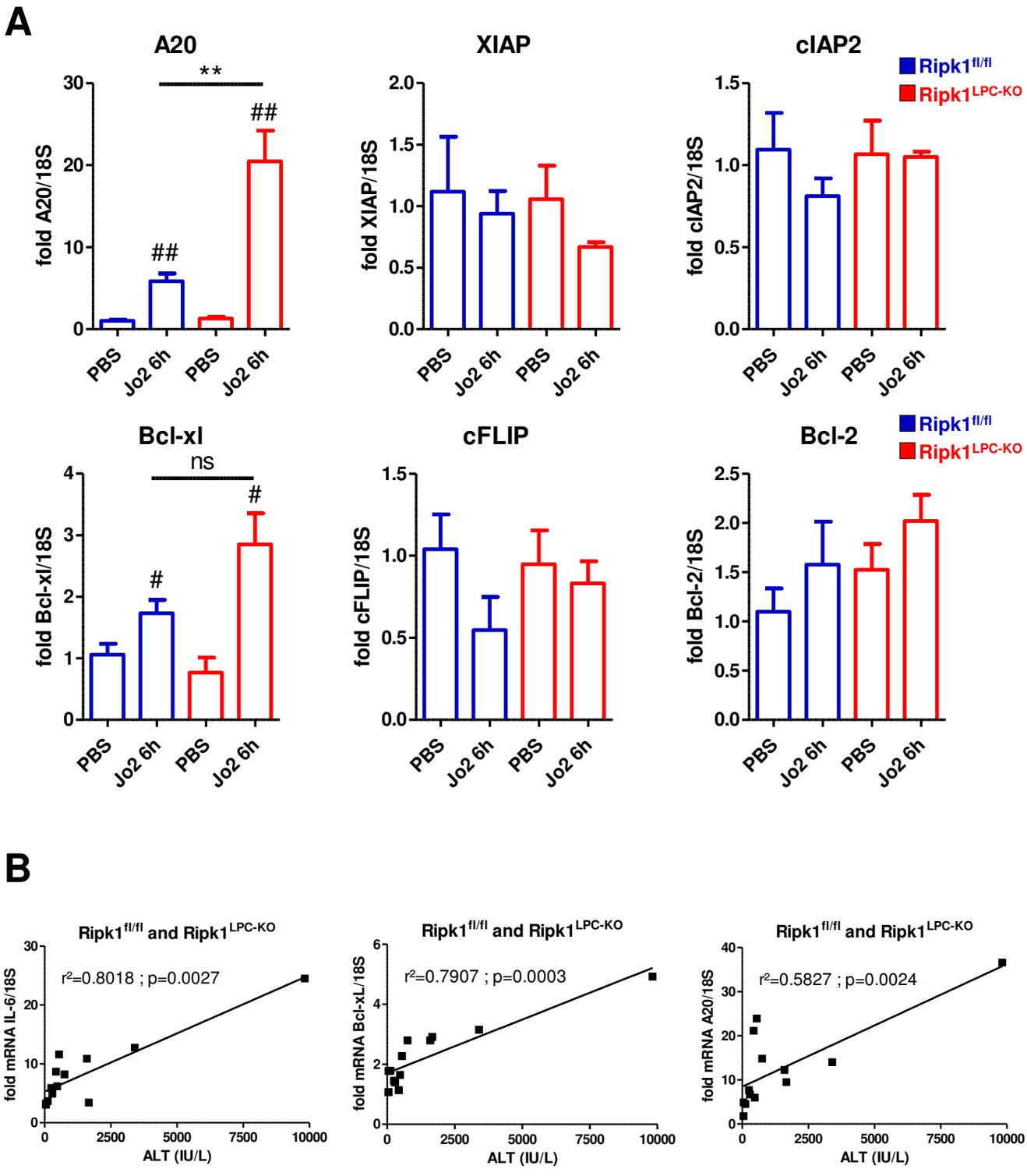
A
A20
**
##
##
fold A20/18S
XIAP
fold XIAP/18S
cIAP2
fold cIAP2/18S
Ripk1fl/fl
Ripk1LPC-KO
Bcl-xl
ns
#
#
fold Bcl-xl/18S
cFLIP
fold cFLIP/18S
Bcl-2
fold Bcl-2/18S
PBS
Jo2 6h
PBS
Jo2 6h

B
Ripk1fl/fl and Ripk1LPC-KO
r2=0.8018 ; p=0.0027
fold mRNA IL-6/18S
ALT (IU/L)
Ripk1fl/fl and Ripk1LPC-KO
r2=0.7907 ; p=0.0003
fold mRNA Bcl-xL/18S
ALT (IU/L)
Ripk1fl/fl and Ripk1LPC-KO
r2=0.5827 ; p=0.0024
fold mRNA A20/18S
ALT (IU/L)

Figure 4

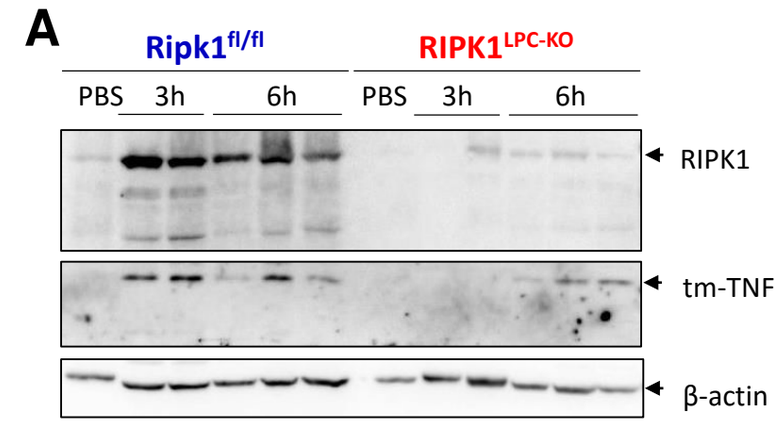
A
Ripk1fl/fl
RIPK1LPC-KO
PBS
3h
6h
PBS
3h
6h
RIPK1
tm-TNF
β-actin

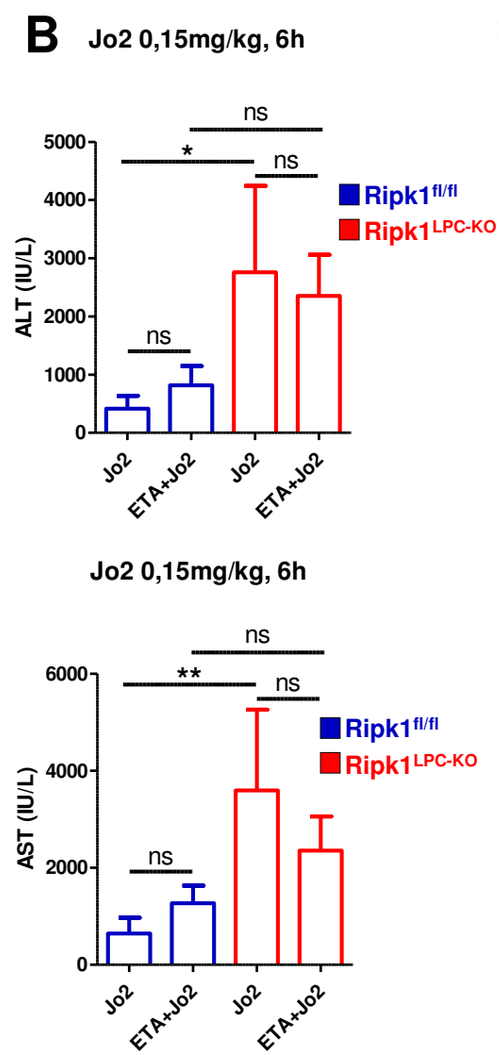
B
Jo2 0,15mg/kg, 6h
ALT (IU/L)
5000
4000
3000
2000
1000
0
ns
*
ns
ns
Ripk1fl/fl
Ripk1LPC-KO
Jo2
ETA+Jo2
Jo2
ETA+Jo2
Jo2 0,15mg/kg, 6h
AST (IU/L)
6000
4000
2000
0
ns
**
ns
ns
Ripk1fl/fl
Ripk1LPC-KO
Jo2
ETA+Jo2
Jo2
ETA+Jo2

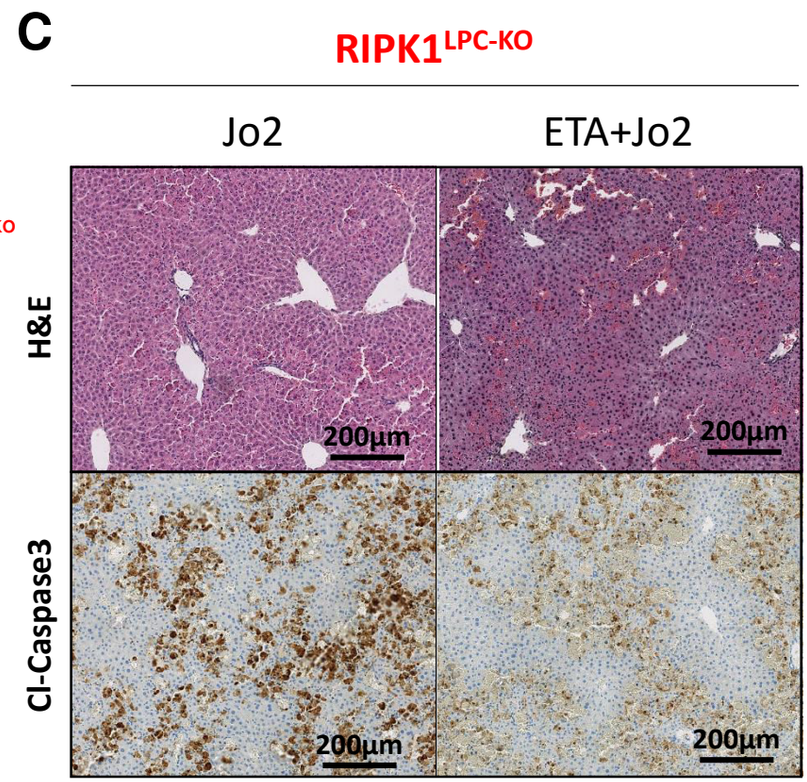
C
RIPK1LPC-KO
Jo2
ETA+Jo2
H&E
Cl-Caspase3
200µm
200µm
200µm
200µm

Figure 5

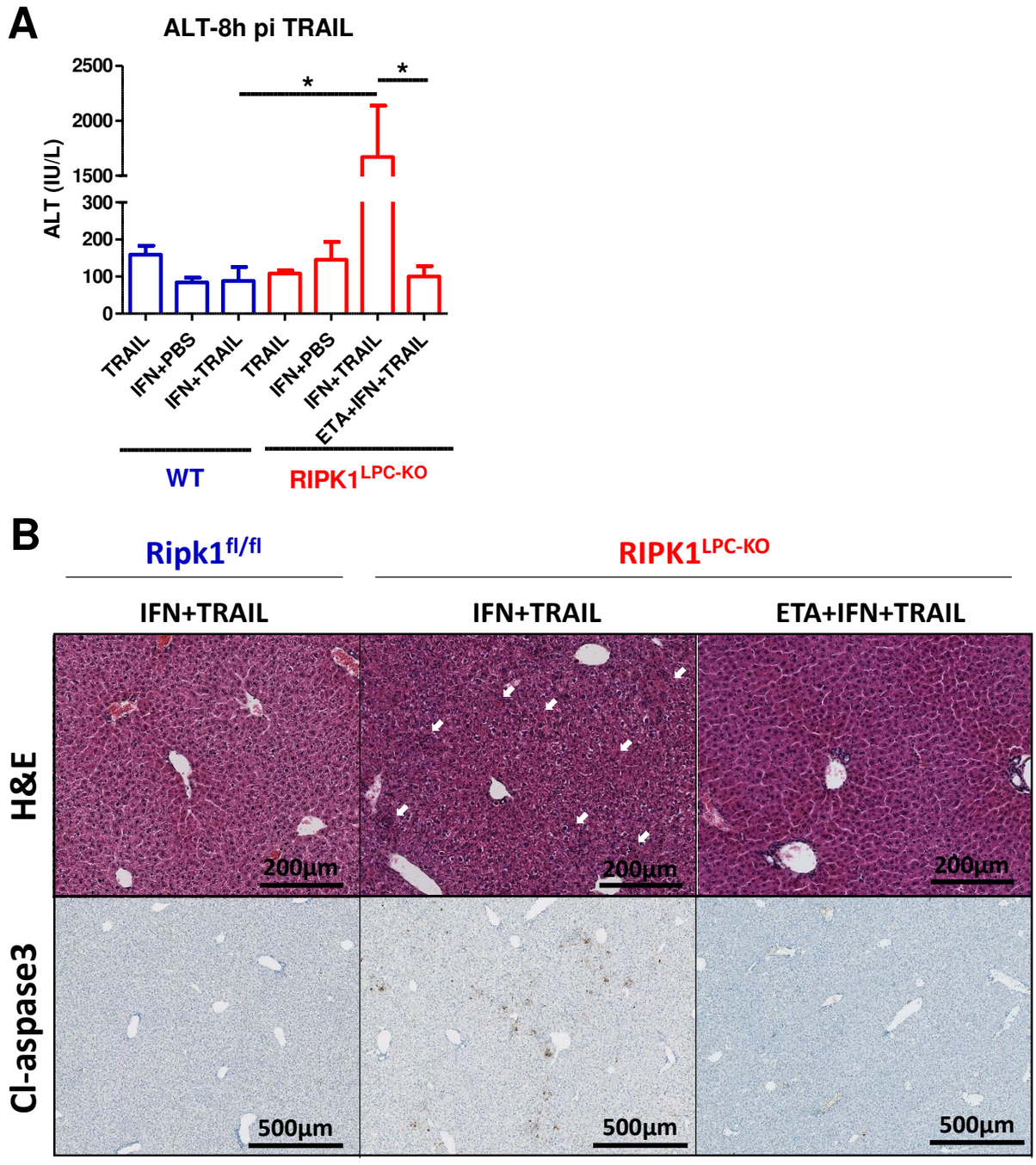
A
ALT-8h pi TRAIL
ALT (IU/L)
2500
2000
1500
300
200
100
0
*
*
TRAIL
IFN+PBS
IFN+TRAIL
TRAIL
IFN+PBS
IFN+TRAIL
ETA+IFN+TRAIL
WT
RIPK1LPC-KO
B
Ripk1fl/fl
RIPK1LPC-KO
IFN+TRAIL
IFN+TRAIL
ETA+IFN+TRAIL
H&E
Cl-aspase3
200μm
200μm
200μm
500μm
500μm
500μm

III.4. ARTICLE IV : La déficience en PARP2 affecte la maturation des iNKT et protège les souris du dommage hépatique induit par la Concanavaline A

Aveline Filliol, Claire Piquet-Pellorce, Valentine Genet, Catherine Lucas-Clerc, Françoise Dantzer, and Michel Samson.

Article actuellement en soumission dans *Journal of Hepatology*.

Introduction de l'article.

Nos observations précédentes montraient que le PJ-34 (inhibiteur de l'activité des protéines PARP) inhibait l'hépatolyse induite par la Concanavaline A (ConA) (travaux réalisés par l'équipe du Dr MT Dimanche Boitrel et en collaboration avec notre équipe). Les protéines PARP sont décrites pour jouer un rôle dans l'inflammation et la mort cellulaire, et plus particulièrement la parthanatos. Elles sont connues pour activer la mort des cellules suite à une surproduction de poly(ADP)-ribosylation et donc indépendante de l'activation des caspases. Bien qu'encore mal compris, l'hépatolyse induite par la ConA est décrite comme non-apoptotique et suggère donc l'induction d'un autre type de mort cellulaire régulée (RCD). De plus, bien que les protéines PARP soient également impliquées dans l'induction de l'inflammation et que notre équipe a montré que le PJ-34 ne semble pas modifier le microenvironnement inflammatoire induit par la ConA, ces observations suggèrent donc fortement un rôle de l'activité des protéines PARP dans l'induction de la mort hépatocytaire au cours de l'hépatite induite par la ConA.

Dans cette large famille composée de 17 membres, seul PARP1 et PARP2 ont été identifiées comme présentant une activité enzymatique. Nous avons donc choisi d'étudier ces deux protéines au cours de l'hépatite à ConA par l'utilisation de souris *Parp1* et *Parp2* knockout (*Parp1*$^{-/-}$ et *Parp2*$^{-/-}$ respectivement). Nos résultats ont permis de montrer que l'absence de PARP2 mais pas de PARP1 réduisait l'hépatolyse induite par la ConA. L'analyse des populations immunitaires du foie, de la rate, du thymus et de la moelle osseuse révèle chez les souris Parp2-/- une déficience systémique en cellules NKT invariant (iNKT). Les lymphocytes NKT et plus particulièrement les iNKT sont les cellules effectrices conduisant à la mort des hépatocytes au cours de l'hépatite à ConA. Nos résultats suggèrent donc que le défaut de maturation des iNKT entraîne sa réduction au niveau systémique et donc au niveau du foie conduisant à la réduction de l'hépatolyse induite par la ConA et à la diminution de la gravité de l'hépatite.

PARP2 deficiency affects invariant-NKT-cell maturation and protects mice from Concanavalin A-induced liver injury.

Aveline Filliol[1,2,3], Claire Piquet-Pellorce[1,2,3], Valentine Genet[1,2,3], Catherine Lucas-Clerc[2,4], Françoise Dantzer[5], and Michel Samson[1,2,3].

[1]Institut National de la Santé et de la Recherche Médicale (Inserm), U.1085, Institut de Recherche Santé Environnement et Travail (IRSET), F-35043 Rennes, France.
[2]Université de Rennes 1, F-35043 Rennes, France.
[3]Structure Fédérative BioSit UMS 3480 CNRS-US18 Inserm, F-35043 Rennes, France.
[4]Service de Biochimie CHU Rennes, Université de Rennes 1; F-35043 Rennes, France.
[5]Université de Strasbourg, Biotechnologie et Signalisation Cellulaire, UMR7242 CNRS, Laboratoire d'Excellence Medalis, ESBS, 300, Boulevard Sébastien-Brant, CS 10413, 67412 Illkirch, France.

Financial support: This work was supported by INSERM, the Ministère de l'Education Nationale, de l'Enseignement Supérieur et de la Recherche, the Université de Rennes 1, the Région Bretagne, the "Ligue Contre le Cancer, Comités du Grand Ouest".

Conflict of interest: The authors declare no financial or commercial conflict of interest.

Keywords: Hepatitis, Parp, Liver, NKT cells, Autoimmune hepatitis

List of abbreviations:
α-GalCer: α-Galactosylceramide, ConA: Concanavalin A, DAMPs: Damage Associated Molecular Patterns, DN: double negative, DR: death receptors, NKT: Natural Killer-T, NK: Natural Killer, PARP: poly(ADP) ribose polymerase.

Abstract (208 words)

Background and aims: Excessive or persistent inflammation and hepatocyte death are the key triggers of liver diseases. The poly(ADP-ribose) polymerase (PARP) proteins induce cell death and inflammation. Chemical inhibition of PARP activity protects against liver injury during Concanavalin A (ConA)-induced hepatitis. In this mice model, ConA activates immune cells which promote inflammation and induce hepatocyte death, mediated by the activated invariant NKT-(iNKT) lymphocyte population. **Materials and methods:** We analyzed immune cell populations in the liver and several lymphoid organs such as spleen, thymus, and bone marrow in *Parp2* deficient mice to better define the role of PARP proteins in liver immunity and inflammation at steady state and during ConA-induced hepatitis. **Results:** We show that *i)* the genetic inactivation of *Parp2*, but not *Parp1*, protected mice from ConA hepatitis without deregulating cytokine expression and leucocyte recruitment; *ii)* cellularity was lower in the thymus, but not in spleen, liver, or bone marrow of *Parp2*$^{-/-}$ mice; *iii)* spleen and liver iNKT lymphocytes, as well as thymic T and NKT lymphocytes were reduced in *Parp2* knockout mice. **Conclusion:** Our results suggest that the defect of T-lymphocyte maturation in *Parp2* knockout mice leads to a systemic reduction of iNKT cells, reducing hepatocyte death during ConA-mediated liver damage, thus protecting the mice from hepatitis.

INTRODUCTION

Hepatitis can be caused by various insults such as alcohol, a high fat diet, food-derived toxins, or infections, and is characterized by hepatocyte death and inflammation [1]. Acute hepatitis is associated with massive hepatolysis which can lead to liver failure, whereas in chronic hepatitis, unresolved hepatolysis triggers the release of Damage Associated Molecular Patterns (DAMPs) which promote inflammation. This process induces an inflammation and cell death amplification loop that contributes to the progression of liver diseases [1, 2]. Blocking the pro-inflammatory hepatocyte death response could be beneficial to in treating liver diseases.

During viral or auto-immune hepatitis, innate and adaptive lymphocytes kill hepatocytes which present proteins recognized as non-self-antigens, by the activation of death receptors (DR). In mice, Concanavalin A (ConA)-induced liver injury mimics immune cell-mediated hepatitis in humans [3] and is dependent on innate Natural Killer T (NKT) lymphocytes. NKT cells are involved in numerous immune responses and are particularly abundant in the liver and spleen of mice. They have the ability to recognize lipids presented by CD1d which allows there distinction into two categories of NKT cells. Type I or invariant-NKT (iNKT) cells express an invariant T-cell receptor α-chain (TCRα; Vα14-Jα18) and are able to recognize the α-Galactosylceramide (α-GalCer) presented by CD1d. Type II NKT cells express more diverse TCR Vα chains that cannot recognize α-GalCer and are characterized as CD4/CD8 double negative (DN). The iNKT are the major NKT subset in the liver and $CD1d^{-/-}$ (NKT deficient) mice as well as $V\alpha14^{-/-}$ (iNKT deficient) mice are protected from ConA-induced hepatitis [3-6]. ConA activates liver immune cells which promote hepatocyte death in two ways. First, activated immune cells release large amounts of cytokines, such as TNF-α [7, 8], IFN-γ [9, 10], and IL-4 [11] which play key roles in the hepatocyte death process [3, 8, 12]. Second, activated NKT cells, potent producers of IFN-γ, kill hepatocytes by activation of the TNF-superfamily DR [5, 13-15] and the perforin/granzyme B system [16]. Our group has extensively investigated the mechanisms of hepatocyte death during hepatitis. We and others have demonstrated a key role for PARP proteins in the liver. We have shown that inhibition of poly(ADP) ribose polymerase (PARP) 1 and 2 activity with the PJ-34-inhibitor protects mice from ConA-mediated hepatolysis [17, 18]. Mukhopadhyay *et al.* have shown that genetic or chemical inhibition of PARP1 also prevents liver inflammation and fibrosis induced by the hepatotoxic carbon tetrachloride (CCl_4) or bile duct ligation [19]. PARP1 and PARP2 are activated by DNA strand breaks and use NAD^+ as a substrate to synthetize chains of poly(ADPribose) onto various acceptor proteins, thereby inducing chromatin remodeling and the recruitment of DNA repair complexes [20]. In the last decades, PARP1 and PARP2 have also been found to play an important role in inflammation [21] and cell death [22]. In this study, we aimed to better define the roles of PARP1 and PARP2 proteins in ConA-induced hepatitis using the *Parp1* and *Parp2* knockout mouse models.

MATERIAL AND METHODS

Animals and treatment protocols

C57BL/6 *Parp1* and *Parp2* genetically modified mice ($Parp1^{-/-}$ and $Parp2^{-/-}$, respectively) were provided by Dr. F. Dantzer and generated as described previously [23, 24]. Heterozygous mice were crossed to obtain knockout and littermate WT mice. Adult male and female mice, of 10 to 12 weeks of age, were used for each experiment with the ConA model. ConA (C2010 Sigma-Aldrich, St. Louis, MO) was prepared at 3 mg/mL in PBS supplemented with 0.31 mM $MnCl_2$ and 0.75 mM $CaCl_2$ and administered by intravenous (i.v.) injection at a dose of 10 or 12 mg/kg body weight. For histopathological and biochemical studies, mice treated with ConA were compared to mice which received PBS supplemented with 0.31 mM $MnCl_2$ and 0.75 mM $CaCl_2$. For all phenotypic immune cell analyses, adult (10 to 12 weeks old) or early adult (five- week-old) mice were either not treated, to analyze the population at steady state, or treated with ConA. Animals were housed in individual cages and bred in specific pathogen-free conditions in the local animal house facilities. All treatment protocols were in accordance with the French

laws and the institution's guidelines for animal welfare (agreement of M. Samson # R-2012-CPP-01).

Histopathological and biochemical studies

Mouse liver biopsies were fixed in 4% paraformaldehyde and embedded in paraffin for IHC and hematoxylin and eosin (H&E) staining. For histopathology, H&E staining of liver tissues was carried out to investigate liver injury. Serum ALT and AST transaminases were measured according to the IFCC primary reference procedures using an Olympus AU2700 Autoanalyser® (Olympus Optical, Tokyo, Japan).

RNA analysis

Total RNA was extracted from mouse livers using TRIzol reagent (Invitrogen). First-strand cDNA was synthesized using the SuperScript™ II Reverse Transcriptase (Invitrogen). Real-time quantitative PCR was performed using the fluorescent dye SYBR Green with the double-strand specific SYBR® Green system (Applied Biosystems) and the ABI 7000 Prism sequence detector (Applied Biosystems) or the CFX384 Touch™ Real-Time PCR Detection System (Bio-Rad). cDNA was used as template for amplification using specific primer pairs (Table 1). Each measurement was performed in triplicate. The relative gene expression was normalized against 18S rRNA gene expression. The control mice in each treatment group served as a reference for messenger RNA (mRNA) expression (the control mRNA level was arbitrarily set to 1).

Immune cell analysis by flow cytometry

Immune cells were prepared from spleen, thymus, or liver crushed on a 70 µm filter. Liver immune cells were isolated after sedimentation and cell fractionation on a 35% Percoll layer. For each organ, red blood cells were lysed using ammonium-chloride-potassium (ACK) buffer. Bone marrow immune cells were isolated by flushing two femurs with RPMI medium (Gibco). The number of immune cells was determined by counting in a Malassez counting chamber.

Cell suspensions were labeled for 30 min with LIVE/DEAD fixable yellow stain (Life technologies, L34959) to exclude dead cells from the analysis. Cells were also pre-incubated with an anti-CD16/32 antibody (BD Pharmingen) to block non-specific binding before incubation with the appropriate fluorochrome-conjugated antibodies (BD Pharmingen, eBioscience): anti-CD3-FITC (clone 17A2), anti- TCRβ-V450 (clone H57-597), anti-CD69-PE (clone H1.2F3), anti-CD19-APC or anti-CD19-PE (clone 1D3), anti-NK1.1-PerCP-Cy-5.5 (clone PK136), anti-CD4-PE-Cy7 (clone RM4-5), anti-CD8-APC-Cy7 (clone 53-6.7), anti-GR1-eFluor450 (clone FB6-8C5), anti-CD11b-PE-Cy7 (clone M1/70), anti-Sca1-PE (clone D7), anti-c-kit-PerCP-eFluor710 (clone 2B8), anti-Ter119-eFluor780 (clone Ter119), and empty CD1d tetramer or CD1d tetramer loaded with α-galactosylceramide (GalCer)-PE (provided by Dr. M. Leite de Morales). The stained cells were analyzed on a FACSAria™ II flow cytometer and data were analyzed using CXP software (Beckman Coulter). Doublets and dead cells were excluded on the basis of forward/side scatter and LIVE/DEAD labeling, respectively. The immuno-phenotyping used was as follows: B-lymphocytes: CD19+/CD3- cells; T-lymphocytes: CD3+/TCRVβ+/NK1.1-; NKT cells: CD3+/TCRVβ+/NK1.1+; NK cells: CD3-/NK1.1+; and granulocytes: GR1+CD11b+. Lymphoid activation was studied by analyzing the expression of CD69. We calculated the percentage of each immune cell population, by considering the sum of events of all immune cell populations analyzed (sum of T, NK, NKT, B cells and myeloid cells) as 100% of the total immune cells. The absolute number in each immune cell population was calculated by multiplying the percentage of each population by the total number of immune cells.

Statistical analysis

Data are expressed as the means +/- SEM for all mice treated similarly. Kruskal–Wallis one-way analysis of variance (ANOVA) was performed, and mean differences between experimental groups were assessed using the non-parametric Mann–Whitney *U*-test using GraphPad Prism5 software. The significance is shown as follows: * $p < 0.05$, ** $p < 0.01$, *** $p < 0.001$ for WT versus *Parp2*$^{-/-}$ or *Parp1*$^{-/-}$ mice. # $p < 0.05$, ## $p < 0.01$, ### $p < 0.001$ for mice treated with ConA, *versus* mice treated with PBS. \$ $p < 0.05$, \$\$ $p < 0.01$, \$\$\$ $p < 0.001$ for early adult mice *versus* adult mice.

RESULTS

PARP2 but not PARP1 deficiency protects mice from ConA-induced hepatitis

We investigated the role of PARP1 and PARP2 proteins in hepatitis using adult knockout mice for PARP1 (*Parp1*$^{-/-}$) and PARP2 (*Parp2*$^{-/-}$) and comparing the results to those obtained using wild-type mice (WT). We challenged mice with ConA to induce hepatitis, or with PBS as a control, and evaluated liver damage using serum transaminase (ALT and AST) levels and hematoxylin coloration. In ConA induced-hepatitis, the peak of hepatolysis occurs 11 h after ConA treatment [12]. *Parp1*$^{-/-}$ mice displayed visibly, but non-significantly, lower ALT and AST transaminase levels than WT mice at this time point. In contrast, *Parp2*$^{-/-}$ mice were highly protected from ConA-induced hepatitis as they had significantly lower (4-fold) levels of both AST and ALT than WT mice (Fig. 1A). Accordingly, H&E coloration of liver slides from Con A-treated WT and *Parp2*$^{-/-}$ mice, revealed fewer areas of necrosis in *Parp2* deficient mice than in WT mice (Fig. 1B). Moreover, the absence of PARP2 appeared to protect mice from hepatolysis and did not simply delay liver injury as serum transaminase levels remained significantly lower in *Parp2*$^{-/-}$ mice than in WT mice, even 24 h after ConA administration (Fig. 1C). We next evaluated the level of inflammation induced by ConA, by measuring the mRNA levels of TNF-α, IFN-γ, IL-1β, and IL-4, all known to play key roles during ConA-induced hepatitis. TNF-α, IFN-γ, IL-1β, and IL-4 transcript levels were higher in all genotypes after ConA treatment. However, we observed no significant differences between the IFN-γ or IL-4 mRNA levels in *Parp1*$^{-/-}$, *Parp2*$^{-/-}$, or WT mice, whereas TNF-α transcript levels were significantly lower in *Parp2*$^{-/-}$ mice than in the other two mouse strains. In contrast, IL-1β mRNA levels were higher in both *Parp2*$^{-/-}$ and *Parp1*$^{-/-}$ mice than in WT mice.

Parp2$^{-/-}$ mice display a substantial reduction in the number of liver iNKT cells

We performed all further experiments using only the *Parp2*$^{-/-}$ mouse model, as PARP2 protein deficiency protected mice from ConA-induced liver damage, whereas that of PARP1 did not. ConA induces liver injury in an immune cell-dependent manner. Thus we next measured the steady-state, basal levels of the different liver immune cell subsets in *Parp2*$^{-/-}$ mice of two different ages: early adult (five weeks) and adult (10 to 12 weeks) by flow cytometry. Cell doublets and dead cells were excluded as depicted in Supplementary Figure 1 and the phenotypic analysis of liver immune cells was determined using the gating strategy presented in Supplementary Figure 2.

Parp2$^{-/-}$ mice displayed a similar number of liver immune cells as WT mice at the two different ages (Fig. 2A). The absolute number of total T lymphocytes and the ratio of CD4:CD8 T-lymphocytes were also similar in the livers of both genotypes (Fig. 2B). We next analyzed the NKT-lymphocyte population, defined as CD3, TCRVβ, and NK1.1 positive cells. We used the CD1d tetramer loaded with αGalCer to analyze the invariant-NKT (iNKT) subset (CD3+ TCRVβ+ NK1.1+ αGalCer+) and the anti-CD4 antibody to study NKT DN cells (CD3+ TCRVβ+ NK1.1+ αGalCer- CD4-). *Parp2*$^{-/-}$ mice displayed a reduction in the percentage of total liver NKT cells of two fold in five-week-old mice and of 1.5 fold in 10-12-week-old mice (Fig. 2C). However, PARP2 deficiency did not impair the increase in the percentage of liver NKT cells as the mice aged (Fig 2C). We also observed that only the percentage of iNKT cells, but not NKT DN cells, was significantly lower in the *Parp2*$^{-/-}$ mice at both ages (Fig. 2D). The absolute number of liver immune cells was similar between both genotypes, whereas the number of iNKT cells was lower in *Parp2*$^{-/-}$ mice. We thus aimed to determine which immune cell subsets compensated this reduction. The percentage of NK-cells (NK1.1+ CD3-) and B-lymphocytes (CD19+ CD11b-) were higher in five-week-old *Parp2*$^{-/-}$ mice, but only the percentage of NK-cells was higher in adult Parp2 $^{-/-}$ mice (Fig. 2E and 2F). The liver myeloid compartment, based on GR1 and CD11b labelling, also appeared to be similar in *Parp2*$^{-/-}$ and WT mice, regardless of age (Fig. 2G). In conclusion, PARP2 deficiency induced a significant reduction in the number of iNKT cells in the liver which was not compensated by an increase of all immune cell subsets, but by a gain of B and NK-lymphocytes.

PARP2 deficiency does not affect the recruitment and activation of immune cells during ConA-induced hepatitis.

We next examined the impact of PARP2 deficiency on ConA-induced cell recruitment and activation. ConA-induced inflammation and cell death induced a similarly high level of leucocyte recruitment to the liver in mice of both genotypes as seen by the large increase in the absolute number of liver immune cells 11 h after injection, which then decreased with the resolution of the hepatitis 24 h after ConA treatment (Fig. 3A). We evaluated the NKT-cell subset and found a reduction in the number of NKT cells in the livers of mice of both genotypes upon ConA treatment. However, this reduction was 3.7 fold in WT mice, relative to untreated mice, but only 1.7 fold in *Parp2*$^{-/-}$ mice, (Fig. 3B). The absence of PARP2 protein did not seem to affect the recruitment of other leucocyte populations, as T, B, and NK-lymphocytes, and myeloid cells were similarly recruited for both genotypes 11 h after ConA administration (Fig. 3C). Finally, we analyzed the early activation marker CD69 on lymphocytes and observed that more than 90% of T-lymphocytes in both *Parp2*$^{-/-}$ and WT mice were activated after ConA treatment (Fig. 3D).

***Parp2*$^{-/-}$ mice have fewer spleen iNKT cells than WT mice**

We demonstrated that *Parp2*$^{-/-}$ mice were protected from ConA-hepatitis and had fewer hepatic NKT cells, without affecting ConA-induced inflammation. We next analyzed the immune cell subsets in the various lymphoid compartments such as spleen, bone marrow, and thymus. Gating strategies used for splenocyte analysis are depicted in Supplementary Figures 1 and 2. PARP2 deficiency did not affect the absolute number of splenocytes in mature mice but they were slightly, but not significantly, higher in number in early adult mice (Fig 4A). We then evaluated the percentage cells in each immune cell subset in the spleen. The number of T-lymphocytes (CD3+ NK1.1- TCRVβ+) were lower only in early adult *Parp2*$^{-/-}$ mice (Fig. 4B) and was compensated by an increase in the number of B-lymphocytes (CD19+ CD11b-) (Fig. 4C). Similar to our observations in the liver, the spleens of five- and 10-12-week-old *Parp2*$^{-/-}$ mice had significantly fewer NKT cells than those of WT mice, and only the iNKT cells were affected (Fig. 4D). In contrast to the liver, the number of spleen NK cells was only slightly, but not significantly, higher in Parp2 $^{-/-}$ than in WT mice (Fig. 4E).

***Parp2*$^{-/-}$ mice have fewer thymus iNKT cells than WT mice.**

We next investigated the thymocyte population of five-week-old mice to understand the cause of the reduction in NKT-cell number in the liver and spleen of *Parp2*$^{-/-}$ mice. The absolute number of thymocytes was lower in *Parp2*$^{-/-}$ mice than in WT mice, and was associated with a reduction in the absolute number of immature CD4/CD8 double positive (DP) and CD4 or CD8 simple positive (SP) thymocytes (Fig. 5A and 5B). The absolute number of iNKT cells (αGalCer^{+}) was also lower in *Parp2*$^{-/-}$ mice (Fig. 5C). However, the remaining iNKT cells expressed wild-type levels of mature T lymphocyte markers such as CD3 and TCRVβ (Fig. 5D).

***Parp2*$^{-/-}$ mice have more Ter119^{+}-cells than WT mice.**

Finally, we investigated the immune cell subsets in the bone marrow (BM) of *Parp2*$^{-/-}$ mice. As observed in the spleen and the liver, BM cellularity was similar between *Parp2*$^{-/-}$ and WT adult mice (Fig. 6A). We eliminated doublets and dead cells and analyzed BM immune cells by flow cytometry to analyze the different immune cell subsets, as depicted in Supplementary Figure 3. The absolute numbers of the different mature BM cell subsets (CD19+, GR1high CD11b+, GR1high CD11b+ and CD3^{+}) were similar with slight variations between the two genotypes, except for Ter119 positive cells which were significantly more numerous in *Parp2*$^{-/-}$ mice (Fig. 6B). Similarly, the number of Lin^{-} cells (Ter119- CD19- CD3- GR1- CD11b-) was slightly, but not significantly higher in the *Parp2*$^{-/-}$ mice, and was associated with a small increase in the number of the myeloid progenitor (MP) (Lin- ckit+ Sca-) and LSK populations (Lin- ckit+ Sca+).

DISCUSSION

We previously reported that inhibition of PARP protein activity with the PJ-34 inhibitor protected mice from ConA-induced hepatolysis [17, 18]. PARP proteins mediate the activation

of various transcription factors, such as NF-κB, to promote inflammation in several inflammatory diseases, including CCl4 induced chronic liver injury. Inactivation or inhibition of PARP proteins prevents inflammation-induced tissue damage [21]. Inflammation induced by ConA plays a key role in the induction of hepatolysis [7-11]. However, we previously demonstrated that PJ-34 does not inhibit inflammation during ConA-induced hepatitis, as cytokine release and liver leucocyte recruitment occurred efficiently, suggesting a more direct role for PARP proteins in the induction of hepatocyte death [17, 18]. Here, we show that the genetic inactivation of *Parp2*, but not *Parp1*, protects mice from ConA-induced hepatitis without deregulating inflammation, as leucocyte recruitment and pro-inflammatory cytokine expression were not affected. Analysis of liver and spleen immune populations revealed a substantial reduction in the percentage of iNKT cells, normally enriched in both organs [25]. The reduction in the number of iNKT in *Parp2*$^{-/-}$ mice may explain the reduced hepatolysis and protection from ConA-induced hepatitis observed in these mice. Indeed, rapid elimination of NKT cells after ConA treatment is a marker of NKT-induced liver injury following their activation [5]. We also observed the elimination of NKT cells after ConA treatment in both *Parp2*$^{-/-}$ and WT mice, but as fewer NKT cells were present in the untreated *Parp2*$^{-/-}$ mice relative to WT mice, there were fewer NKT cells available to induce hepatocyte cell death after ConA treatment in these mice. In the liver, the reduction of NKT-cell number was compensated by an increase in the number of NK cells. While this may explain the absence of a decrease in the induction of IFN-γ expression during ConA-induced hepatitis, the increase in NK-cell number was not sufficient to restore hepatocyte cell death, as ConA-induced liver injury is strictly NKT-dependent and NK-independent [4, 5]. Our study using *Parp1* and *Parp2* knockout mice did not allow us to clarify the effect of the PJ-34 inhibitor. Moreover, the fact that *Parp1*$^{-/-}$ mice were not protected against ConA-induced hepatitis, suggests that PARP2 participates in ConA-mediated liver injury, as the two proteins share common functions [20, 26]. *Parp1* and *Parp2* double knockout mice are lethal [27]. It may be informative to use conditional knockout mice to further decipher the role of both proteins in the liver.

We analyzed the thymus and bone marrow of *Parp2*$^{-/-}$ mice to identify the cause of the systemic reduction of iNKT cells detected in these mice. As previously described, *Parp2*$^{-/-}$ mice displayed an increase of the erythroid subset [28], but no T-lymphocyte deregulation. iNKT cells mature in the thymus and are derived from the DP population [29]. In agreement with others, we observed a reduction in the number of DP-thymocytes in the absence of PARP2 protein [24] and revealed a substantial reduction in the number of thymic iNKT cells. PARP2 deficiency leads to inefficient Vα to Jα rearrangement inducing the death of DP-thymocytes [24], resulting in a decrease in the number of mature SP T-lymphocytes and iNKT cells. However, only iNKT-cell numbers were lower in the liver and spleens of adult mice, but not those of conventional T-lymphocytes.

In conclusion, previous phenotypic investigations of *Parp2*$^{-/-}$ mice revealed an important role of the PARP2 protein in the regulation of lipid metabolism [30], erythropoiesis [31], thymopoiesis [24], and spermatogenesis [32]. Here, we highlight a new phenotype in *Parp2*$^{-/-}$ mice associated with the deregulation of thymopoiesis, resulting in a systemic iNKT deficiency, leading to protection against ConA-induced liver injury.

ACKNOWLEDGEMENTS

This work was supported by INSERM, The Ministère de l'Education Nationale de la Recherche et de la Technologie, the University of Rennes 1, the Région Bretagne and the "Ligue Contre le Cancer, Comités du Grand Ouest". AF was supported by a PhD fellowship from the Région Bretagne. We would like to thank the dedicated platforms for immunohistochemistry analysis and animal house facilities (i.e. H2P2 and animal house platforms) of SFR BIOSIT, University of Rennes 1, France.

References

[1] Brenner C, Galluzzi L, Kepp O, Kroemer G. Decoding cell death signals in liver inflammation. J Hepatol 2013;59:583-594.

[2] Luedde T, Kaplowitz N, Schwabe RF. Cell death and cell death responses in liver disease: mechanisms and clinical relevance. Gastroenterology 2014;147:765-783 e764.
[3] Tiegs G, Hentschel J, Wendel A. A T cell-dependent experimental liver injury in mice inducible by concanavalin A. J Clin Invest 1992;90:196-203.
[4] Toyabe S, Seki S, Iiai T, Takeda K, Shirai K, Watanabe H, et al. Requirement of IL-4 and liver NK1+ T cells for concanavalin A-induced hepatic injury in mice. J Immunol 1997;159:1537-1542.
[5] Takeda K, Hayakawa Y, Van Kaer L, Matsuda H, Yagita H, Okumura K. Critical contribution of liver natural killer T cells to a murine model of hepatitis. Proc Natl Acad Sci U S A 2000;97:5498-5503.
[6] Kaneko Y, Harada M, Kawano T, Yamashita M, Shibata Y, Gejyo F, et al. Augmentation of Valpha14 NKT cell-mediated cytotoxicity by interleukin 4 in an autocrine mechanism resulting in the development of concanavalin A-induced hepatitis. J Exp Med 2000;191:105-114.
[7] Mizuhara H, O'Neill E, Seki N, Ogawa T, Kusunoki C, Otsuka K, et al. T cell activation-associated hepatic injury: mediation by tumor necrosis factors and protection by interleukin 6. J Exp Med 1994;179:1529-1537.
[8] Kusters S, Tiegs G, Alexopoulou L, Pasparakis M, Douni E, Kunstle G, et al. In vivo evidence for a functional role of both tumor necrosis factor (TNF) receptors and transmembrane TNF in experimental hepatitis. Eur J Immunol 1997;27:2870-2875.
[9] Hong F, Jaruga B, Kim WH, Radaeva S, El-Assal ON, Tian Z, et al. Opposing roles of STAT1 and STAT3 in T cell-mediated hepatitis: regulation by SOCS. J Clin Invest 2002;110:1503-1513.
[10] Tagawa Y, Sekikawa K, Iwakura Y. Suppression of concanavalin A-induced hepatitis in IFN-gamma(-/-) mice, but not in TNF-alpha(-/-) mice: role for IFN-gamma in activating apoptosis of hepatocytes. J Immunol 1997;159:1418-1428.
[11] Jaruga B, Hong F, Sun R, Radaeva S, Gao B. Crucial role of IL-4/STAT6 in T cell-mediated hepatitis: up-regulating eotaxins and IL-5 and recruiting leukocytes. J Immunol 2003;171:3233-3244.
[12] Trautwein C, Rakemann T, Brenner DA, Streetz K, Licato L, Manns MP, et al. Concanavalin A-induced liver cell damage: activation of intracellular pathways triggered by tumor necrosis factor in mice. Gastroenterology 1998;114:1035-1045.
[13] Zheng SJ, Wang P, Tsabary G, Chen YH. Critical roles of TRAIL in hepatic cell death and hepatic inflammation. J Clin Invest 2004;113:58-64.
[14] Arshad MI, Piquet-Pellorce C, L'Helgoualc'h A, Rauch M, Patrat-Delon S, Ezan F, et al. TRAIL but not FasL and TNFalpha, regulates IL-33 expression in murine hepatocytes during acute hepatitis. Hepatology 2012;56:2353-2362.
[15] Seino K, Kayagaki N, Takeda K, Fukao K, Okumura K, Yagita H. Contribution of Fas ligand to T cell-mediated hepatic injury in mice. Gastroenterology 1997;113:1315-1322.
[16] Watanabe Y, Morita M, Akaike T. Concanavalin A induces perforin-mediated but not Fas-mediated hepatic injury. Hepatology 1996;24:702-710.
[17] Jouan-Lanhouet S, Arshad MI, Piquet-Pellorce C, Martin-Chouly C, Le Moigne-Muller G, Van Herreweghe F, et al. TRAIL induces necroptosis involving RIPK1/RIPK3-dependent PARP-1 activation. Cell Death Differ 2012;19:2003-2014.
[18] Arshad MI, Piquet-Pellorce C, Filliol A, L'Helgoualc'h A, Lucas-Clerc C, Jouan-Lanhouet S, et al. The chemical inhibitors of cellular death, PJ34 and Necrostatin-1, down-regulate IL-33 expression in liver. J Mol Med (Berl) 2015;93:867-878.
[19] Mukhopadhyay P, Rajesh M, Cao Z, Horvath B, Park O, Wang H, et al. Poly (ADP-ribose) polymerase-1 is a key mediator of liver inflammation and fibrosis. Hepatology 2014;59:1998-2009.
[20] De Vos M, Schreiber V, Dantzer F. The diverse roles and clinical relevance of PARPs in DNA damage repair: current state of the art. Biochem Pharmacol 2012;84:137-146.
[21] Bai P, Virag L. Role of poly(ADP-ribose) polymerases in the regulation of inflammatory processes. FEBS Lett 2012;586:3771-3777.
[22] Virag L, Robaszkiewicz A, Rodriguez-Vargas JM, Oliver FJ. Poly(ADP-ribose) signaling in cell death. Mol Aspects Med 2013;34:1153-1167.

[23] de Murcia JM, Niedergang C, Trucco C, Ricoul M, Dutrillaux B, Mark M, et al. Requirement of poly(ADP-ribose) polymerase in recovery from DNA damage in mice and in cells. Proc Natl Acad Sci U S A 1997;94:7303-7307.
[24] Yelamos J, Monreal Y, Saenz L, Aguado E, Schreiber V, Mota R, et al. PARP-2 deficiency affects the survival of CD4+CD8+ double-positive thymocytes. EMBO J 2006;25:4350-4360.
[25] Matsuda JL, Naidenko OV, Gapin L, Nakayama T, Taniguchi M, Wang CR, et al. Tracking the response of natural killer T cells to a glycolipid antigen using CD1d tetramers. J Exp Med 2000;192:741-754.
[26] Ame JC, Spenlehauer C, de Murcia G. The PARP superfamily. Bioessays 2004;26:882-893.
[27] Menissier de Murcia J, Ricoul M, Tartier L, Niedergang C, Huber A, Dantzer F, et al. Functional interaction between PARP-1 and PARP-2 in chromosome stability and embryonic development in mouse. EMBO J 2003;22:2255-2263.
[28] Farres J, Martin-Caballero J, Martinez C, Lozano JJ, Llacuna L, Ampurdanes C, et al. Parp-2 is required to maintain hematopoiesis following sublethal gamma-irradiation in mice. Blood 2013;122:44-54.
[29] Gapin L, Matsuda JL, Surh CD, Kronenberg M. NKT cells derive from double-positive thymocytes that are positively selected by CD1d. Nat Immunol 2001;2:971-978.
[30] Szanto M, Brunyanszki A, Marton J, Vamosi G, Nagy L, Fodor T, et al. Deletion of PARP-2 induces hepatic cholesterol accumulation and decrease in HDL levels. Biochim Biophys Acta 2014;1842:594-602.
[31] Farres J, Llacuna L, Martin-Caballero J, Martinez C, Lozano JJ, Ampurdanes C, et al. PARP-2 sustains erythropoiesis in mice by limiting replicative stress in erythroid progenitors. Cell Death Differ 2015;22:1144-1157.
[32] Dantzer F, Mark M, Quenet D, Scherthan H, Huber A, Liebe B, et al. Poly(ADP-ribose) polymerase-2 contributes to the fidelity of male meiosis I and spermiogenesis. Proc Natl Acad Sci U S A 2006;103:14854-14859.

Table 1. Sequence of primers used for qPCR.

Gene	Forward	Reverse
Mouse 18S	5′-CGCCGCTAGAGGTGAAATTC-3′	5′-TTGGCAAATGCTTTCGCTC-3′
Mouse TNFα	5′-TAGCTCCCAGAAAAGCAAGC-3′	5′-TTTTCTGGAGGGAGATGTGG-3′
Mouse IFN-γ	5'AGGTCAACAACCCACAGGTC3'	5'ATCAGCAGCGACTCCTTTTC3'
Mouse IL-1β	5'-GAAGAAGTGCCCATCCTCTG-3'	5'-AGCTCATATGGGTCCGACAG-3'
Mouse IL-4	5'-GGCTTCCAAGGTGCTTGG-3'	5'-GGACTTGGACTCATTCATGG-3'

LEGENDS OF FIGURES

Figure 1: The absence of PARP2 but not PARP1 protects mice from ConA induced-hepatitis. (A) Serum levels of serum AST and ALT in WT, *Parp1*$^{-/-}$, and *Parp2*$^{-/-}$ mice, 11 h after PBS (n = 4 to 6) or ConA injection (n =1 3 for WT, 8 for *Parp1*$^{-/-}$, and 24 for *Parp2*$^{-/-}$). (B) Representative images of H&E stained liver tissue sections, necrosis areas are outlined by the white dotted line. (C) Serum levels of ALT of WT or *Parp2*$^{-/-}$ mice 24 h after ConA treatment. (D) Levels of liver TNF-α, IFN-γ, IL-1β and IL-4 transcripts from WT, *Parp1*$^{-/-}$, and *Parp2*$^{-/-}$ mice 11 h after ConA administration. Errors bars in the histograms represent + SEM. (* #$p < 0.05$; ** ## $p < 0.01$; *** ### $p < 0.001$; ns: non-significant).

Figure 2: PARP2 deficiency results in a decrease in the number of liver iNKT cells.

(A) Absolute number of liver immune cells. (B) Absolute number of T lymphocytes (CD3+ TCRVb+NK1.1-), CD4-positive cells (in black) and CD8-positive cells (in white). (C) Absolute number of NKT cells (CD3+ TCRVb+NK1.1-) in the liver (D) Representative dot plot showing NKT subsets in the liver (left panel) and absolute number of liver iNKT cells (corresponding to aGalCer+CD4+ and aGalCer+CD4- cells) (middle panel) and liver NKT DN-cells (aGalCer-CD4-) (right panel). (E) Representative dot plot showing liver NK-cell population (left part) and absolute number of liver NK cells (NK1.1+CD3-) (right panel). (F) Absolute number of liver B-lymphocytes (CD19+CD11b) and (G) myeloid cells ($GR1^{int}$CD11b+ and $GR1^{high}$CD11b+). All suspensions of liver immune cells from non-treated mice, aged 5 or 10 to 12 weeks, were obtained from the livers of WT or *Parp2*$^{-/-}$ mice. Each dot in the graph represents the number of cells recovered from one liver. The line and error bars represent the mean +/- SEM. For the histograms, the errors bars represent + SD. (* #p < 0.05; ** ## p < 0.01; *** ### p < 0.001; ns: non-significant).

Figure 3: PARP2 deficiency does not affect ConA-induced liver-leucocyte recruitment or activation.

(A) Absolute number of liver immune cells from WT or *Parp2*$^{-/-}$ adult mice, non-treated (Ctl) or treated with ConA. Immune cells were isolated 11 or 24 h after ConA treatment. (B) Absolute number of NKT-cells from the livers of WT or *Parp2*$^{-/-}$ mice at steady state (Ctl) or 11 h after ConA treatment. (C) Absolute number of lymphocytes: T cells, B cells, and NK cells (upper panel) and myeloid cells (lower part) from liver of WT or *Parp2*$^{-/-}$ mice at steady state or 11 h after ConA treatment. (D) Representation of the activation marker (CD69) of T-lymphocytes CD8+ (NK1.1-TCRVb+CD3+CD8+) in the liver of WT or *Parp2*$^{-/-}$ mice treated or not with ConA. The line and error bars represent the mean + SD (* #p < 0.05; ** ## p < 0.01; *** ### p < 0.001; ns: non-significant).

Figure 4: PARP2 deficiency results in a reduction in the number of iNKT cells in the spleen.

(A) Number of splenocytes of non-treated WT and *Parp2*$^{-/-}$ mice, aged 5 (early adult mice) or 10 at 12 weeks (adult mice). (B) Percentage of T lymphocytes (CD3+), TCRVb+NK1.1-), (C) B-ymphocytes (CD19+CD11b-), (D) total NKT cells (CD3+TCRVb+NK1.1+) (left panel), and NKT subsets: iNKT (NKT, α-GalCer+) (midle panel) and NKT-DN (NKT, α-GalCer- CD4-) (right panel), (E) NK cells (CD3-NK1.1+) determined by flow cytometry analysis from spleens of early-adult or adult WT and *Parp2*$^{-/-}$ mice. Each dot in the graph represents the number of cells recovered from one liver. The lines and error bars represent the mean +/- SEM. (* p <0.05; ** p < 0.01; *** p < 0.001; ns: non-significant).

Figure 5: PARP2 deficiency results in a decreased number of CD4/CD8 DP and SP cells as well as iNKT cells.

(A) Representative staining profiles of CD4 and CD8 single or double positive cells from the thymus of non-treated five-week-old WT or *Parp2*$^{-/-}$ mice. (B) Graph showing total number and the number of $CD4^+CD8^+$ double positive thymocytes. (C) Representative staining profile of αGalCer positive thymocytes. (D) Representation of mature T-cell markers (CD3 and TCRVβ) of αGalCer positive thymocytes. Each dot in the graph represent the number of cells recovered from one liver. The lines and errors bars represent the mean +/- SEM. (* p<0.05; ** p<0.01; *** p<0.001; ns: non-significant).

Figure 6: *Parp2*$^{-/-}$ mice display an increased number of Ter119+-cells but not of other mature or immature subsets.

(A) Absolute number of cells recovered from two femurs of WT or *Parp2*$^{-/-}$ adult (10 at 12 weeks old) mice. (B) Absolute cell number for each mature bone marrow immune cells subset: $Ter119^+$, $CD19^+$, $CD3^+$, $GR1^{high}CD11b^+$, and $GR1^{int}CD11b^+$. (C) Absolute number of immature Lin- bone marrow immune cells ($Ter119^-$ $CD19^-$ $CD3^-$ $GR1^-$ $CD11b^-$) (left panel) and the specific MP (Lin-ckit+Sca-) and LSK (Lin-ckit+Sca+) subsets (right panel). In graph, Each dot in the graph represents the number of cells recovered from one liver. The lines and errors bars represent the mean +/- SEM. (* p<0.05; ** p<0.01; *** p<0.001; ns: non-significant).

Supplementary Figure 1.
Gating strategy used for each organ (liver, spleen, thymus, and bone marrow) to exclude doublets and dead cells before the analysis of each immune cell subsets. A representative gating strategy is presented for immune cells recovered from the livers of mice 11 h after ConA treatment.

Supplementary Figure 2.
Gating strategy used to analyze lymphocyte subpopulations (NKT, NK, T cells, B cells) and myeloid cells in the liver and spleen. The gating strategy for liver immune cells is presented.

Supplementary Figure 3.
Gating strategy used to analyze bone marrow immune cell subsets.

Figure 1

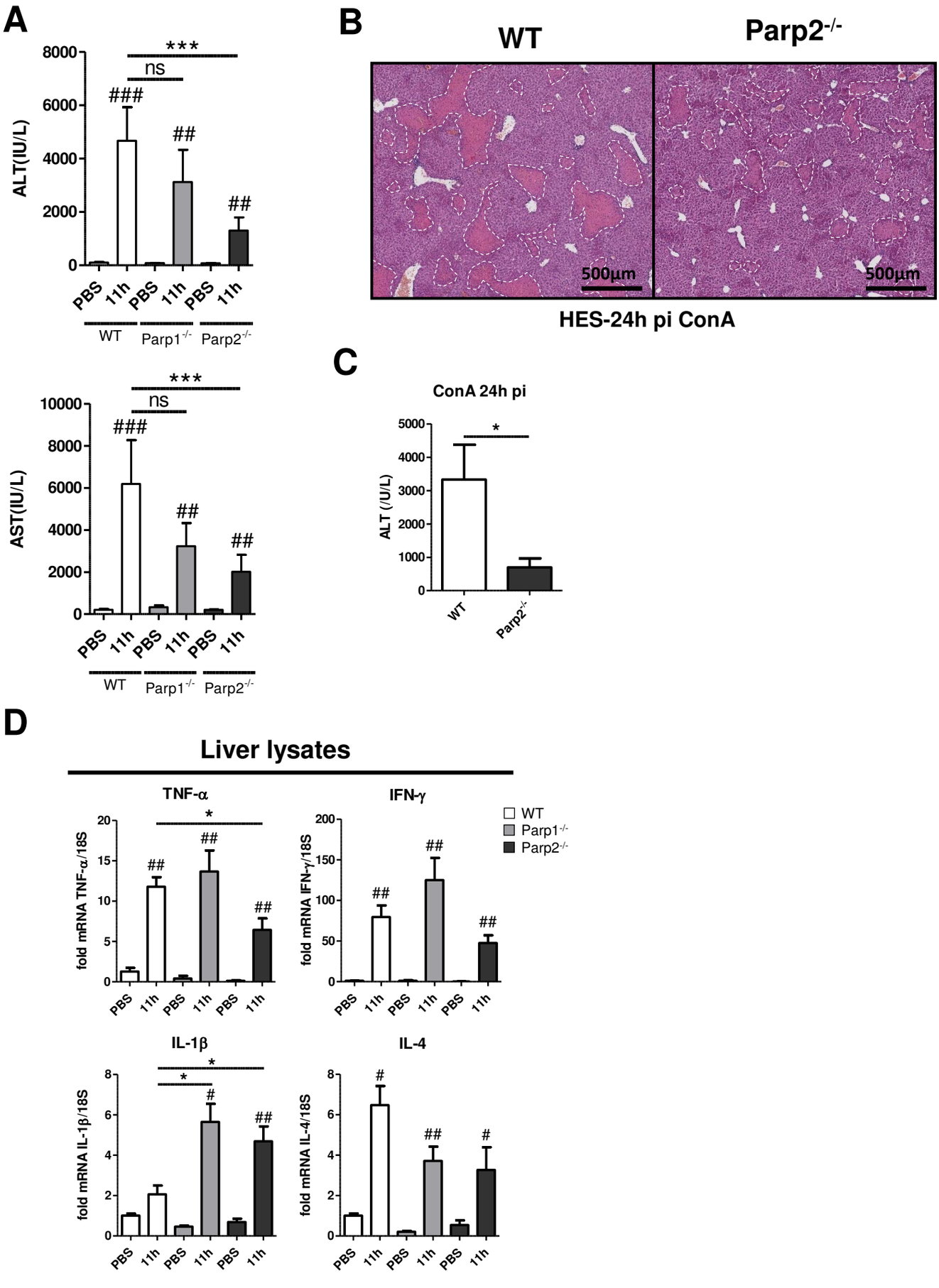
A
ALT(IU/L)
AST(IU/L)
***
ns
###
##
PBS
11h
WT
Parp1-/-
Parp2-/-
B
WT
Parp2-/-
500µm
HES-24h pi ConA
C
ConA 24h pi
ALT (/U/L)
*
D
Liver lysates
TNF-α
IFN-γ
IL-1β
IL-4
fold mRNA TNF-α/18S
fold mRNA IFN-γ/18S
fold mRNA IL-1β/18S
fold mRNA IL-4/18S

Figure 2

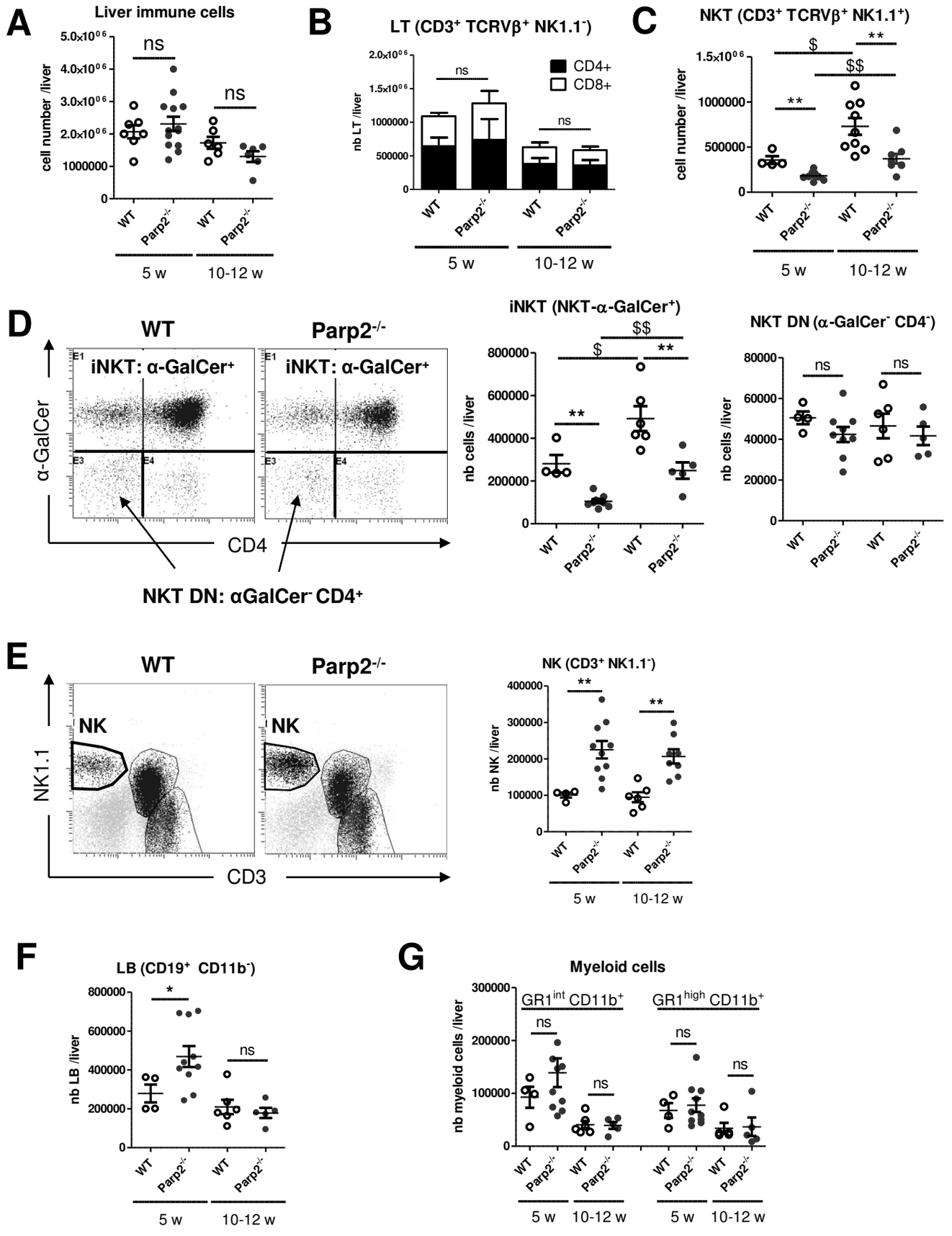
A
Liver immune cells
cell number /liver
ns
ns
WT
Parp2-/-
WT
Parp2-/-
5 w
10-12 w
B
LT (CD3+ TCRVβ+ NK1.1-)
nb LT /liver
CD4+
CD8+
ns
ns
C
NKT (CD3+ TCRVβ+ NK1.1+)
cell number /liver
$
$$
**
**
D
WT
Parp2-/-
iNKT: α-GalCer+
α-GalCer
CD4
NKT DN: αGalCer- CD4+
iNKT (NKT-α-GalCer+)
nb cells /liver
NKT DN (α-GalCer- CD4-)
E
NK
NK1.1
CD3
NK (CD3+ NK1.1-)
nb NK /liver
F
LB (CD19+ CD11b-)
nb LB /liver
*
ns
G
Myeloid cells
GR1int CD11b+
GR1high CD11b+
nb myeloid cells /liver

Figure 3

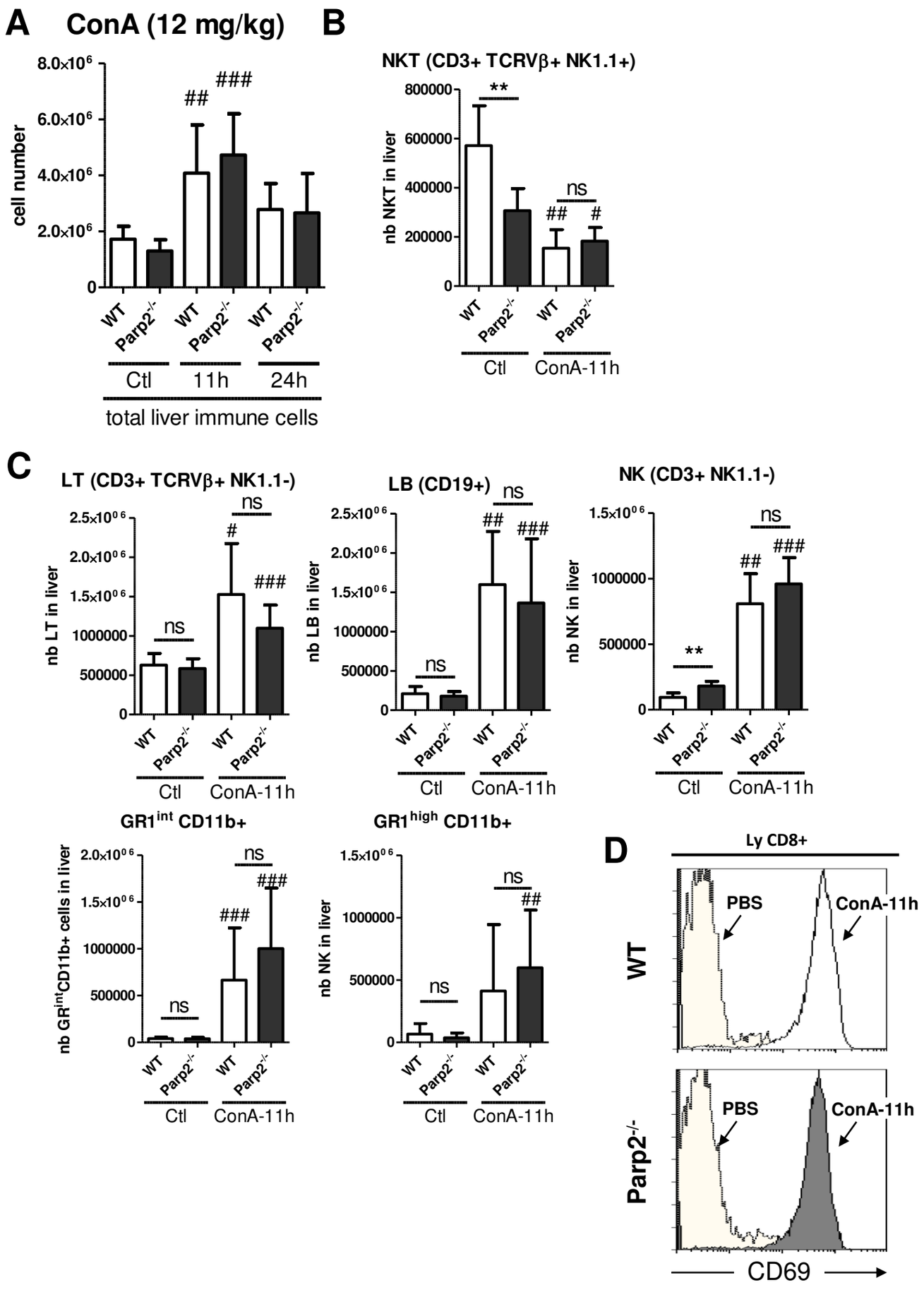
A
ConA (12 mg/kg)
cell number
8.0x10^6
6.0x10^6
4.0x10^6
2.0x10^6
0
##
###
WT
Parp2-/-
Ctl
11h
24h
total liver immune cells
B
NKT (CD3+ TCRVβ+ NK1.1+)
nb NKT in liver
800000
600000
400000
200000
**
ns
##
#
Ctl
ConA-11h
C
LT (CD3+ TCRVβ+ NK1.1-)
nb LT in liver
2.5x10^06
2.0x10^06
1.5x10^06
1000000
500000
LB (CD19+)
nb LB in liver
NK (CD3+ NK1.1-)
nb NK in liver
GR1int CD11b+
nb GRintCD11b+ cells in liver
GR1high CD11b+
D
Ly CD8+
PBS
ConA-11h
WT
Parp2-/-
CD69

Figure 4

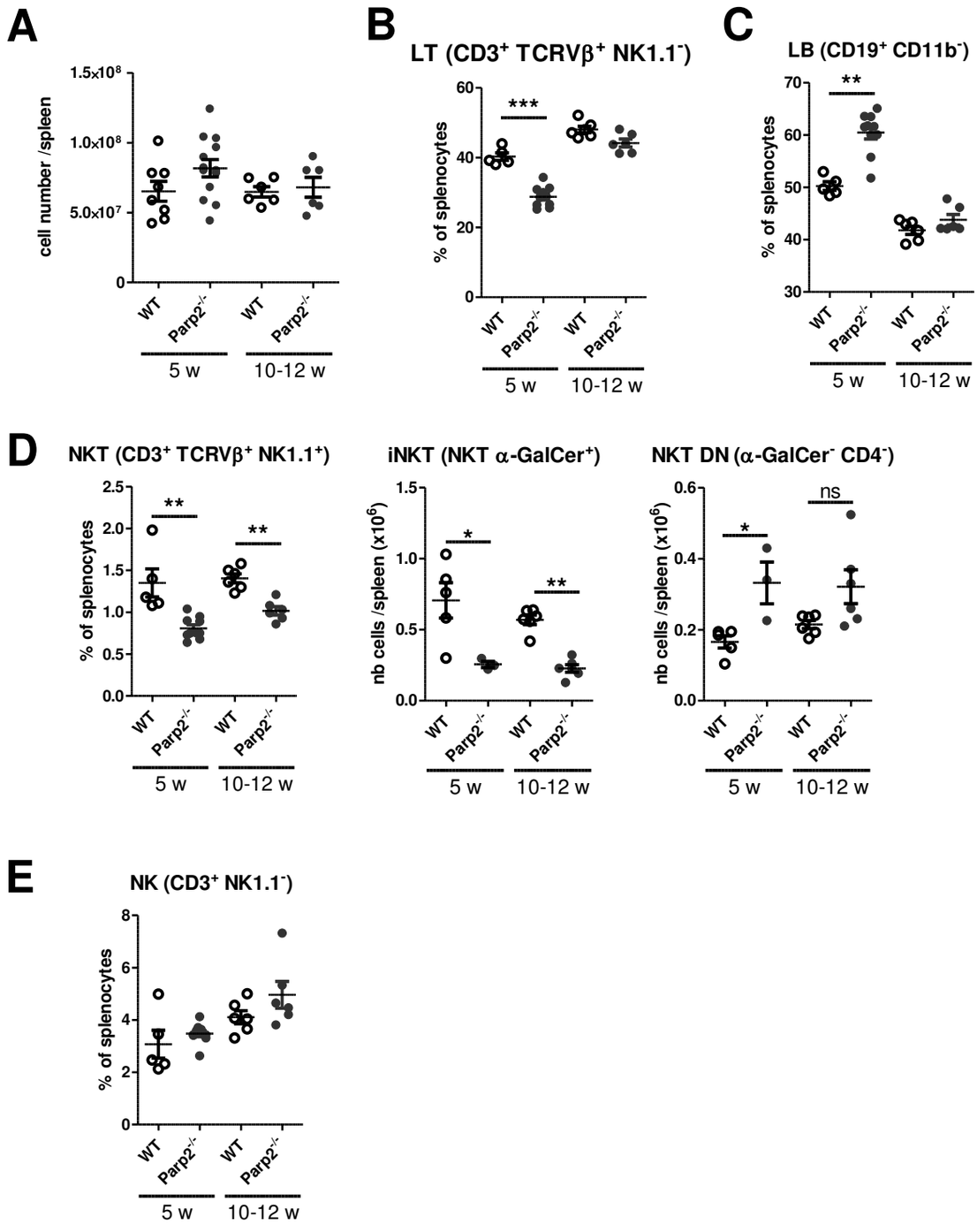
A
cell number /spleen
1.5x10^8
1.0x10^8
5.0x10^7
0
WT
Parp2^-/-
WT
Parp2^-/-
5 w
10-12 w
B
LT (CD3+ TCRVβ+ NK1.1-)
% of splenocytes
60
40
20
0
***
C
LB (CD19+ CD11b-)
% of splenocytes
70
60
50
40
30
**
D
NKT (CD3+ TCRVβ+ NK1.1+)
% of splenocytes
2.5
2.0
1.5
1.0
0.5
0.0
**
**
iNKT (NKT α-GalCer+)
nb cells /spleen (x10^6)
1.5
1.0
0.5
0.0
*
**
NKT DN (α-GalCer- CD4-)
nb cells /spleen (x10^6)
0.6
0.4
0.2
0.0
*
ns
E
NK (CD3+ NK1.1-)
% of splenocytes
8
6
4
2
0

Figure 5

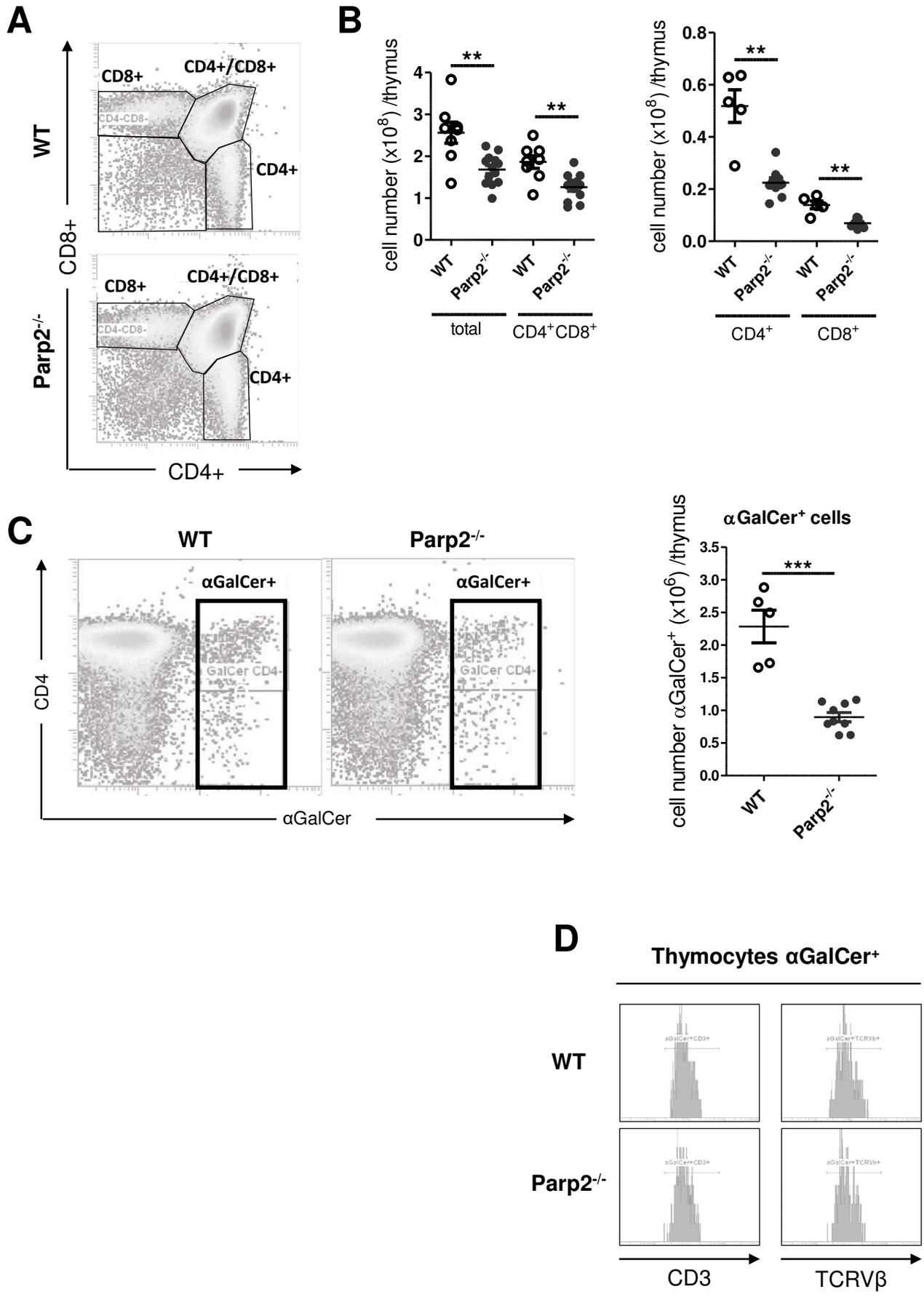
A
WT
Parp2-/-
CD8+
CD4+/CD8+
CD4-CD8-
CD4+
CD8+
CD4+
B
cell number (x10^8) /thymus
**
**
WT
Parp2-/-
WT
Parp2-/-
total
CD4+CD8+
cell number (x10^8) /thymus
**
**
WT
Parp2-/-
WT
Parp2-/-
CD4+
CD8+
C
WT
Parp2-/-
αGalCer+
αGalCer+
GalCer CD4-
GalCer CD4-
CD4
αGalCer
αGalCer+ cells
cell number αGalCer+ (x10^6) /thymus
***
WT
Parp2-/-
D
Thymocytes αGalCer+
WT
Parp2-/-
CD3
TCRVβ

Figure 6

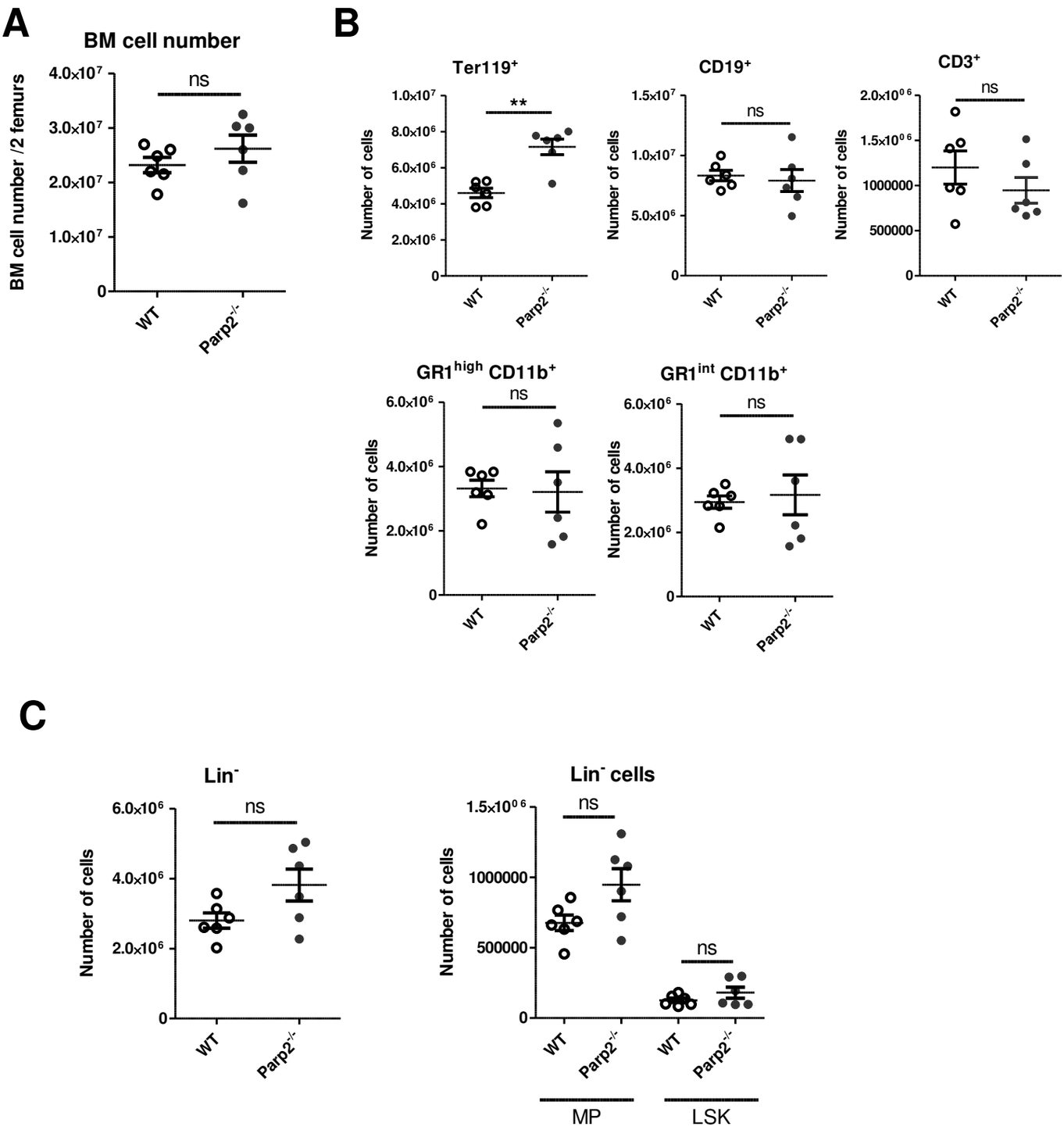
A
BM cell number
BM cell number /2 femurs
4.0x10^7
3.0x10^7
2.0x10^7
1.0x10^7
0
ns
WT
Parp2-/-
B
Ter119+
Number of cells
1.0x10^7
8.0x10^6
6.0x10^6
4.0x10^6
2.0x10^6
0
**
WT
Parp2-/-
CD19+
Number of cells
1.5x10^7
1.0x10^7
5.0x10^6
0
ns
WT
Parp2-/-
CD3+
Number of cells
2.0x10^06
1.5x10^06
1000000
500000
0
ns
WT
Parp2-/-
GR1high CD11b+
Number of cells
6.0x10^6
4.0x10^6
2.0x10^6
0
ns
WT
Parp2-/-
GR1int CD11b+
Number of cells
6.0x10^6
4.0x10^6
2.0x10^6
0
ns
WT
Parp2-/-
C
Lin-
Number of cells
6.0x10^6
4.0x10^6
2.0x10^6
0
ns
WT
Parp2-/-
Lin- cells
Number of cells
1.5x10^06
1000000
500000
0
ns
ns
WT
Parp2-/-
WT
Parp2-/-
MP
LSK

Supplementary Figure 1

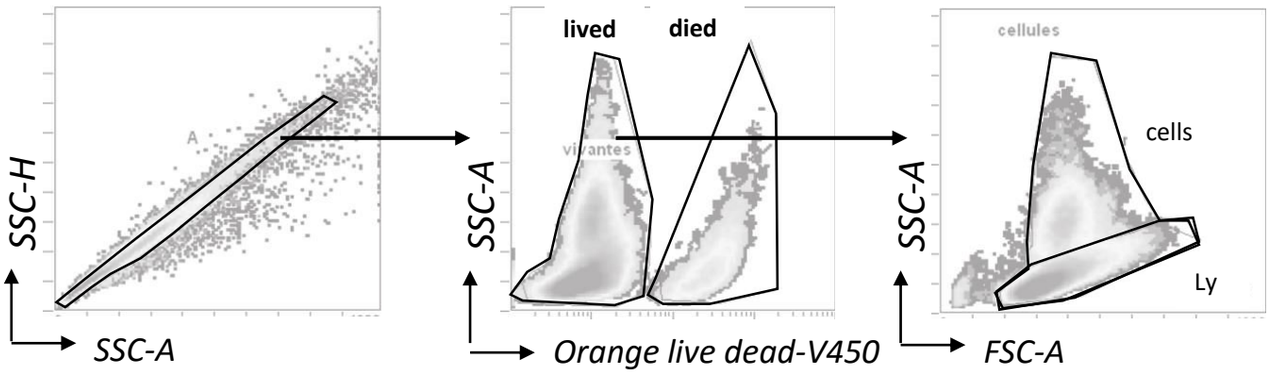

Supplementary Figure 2

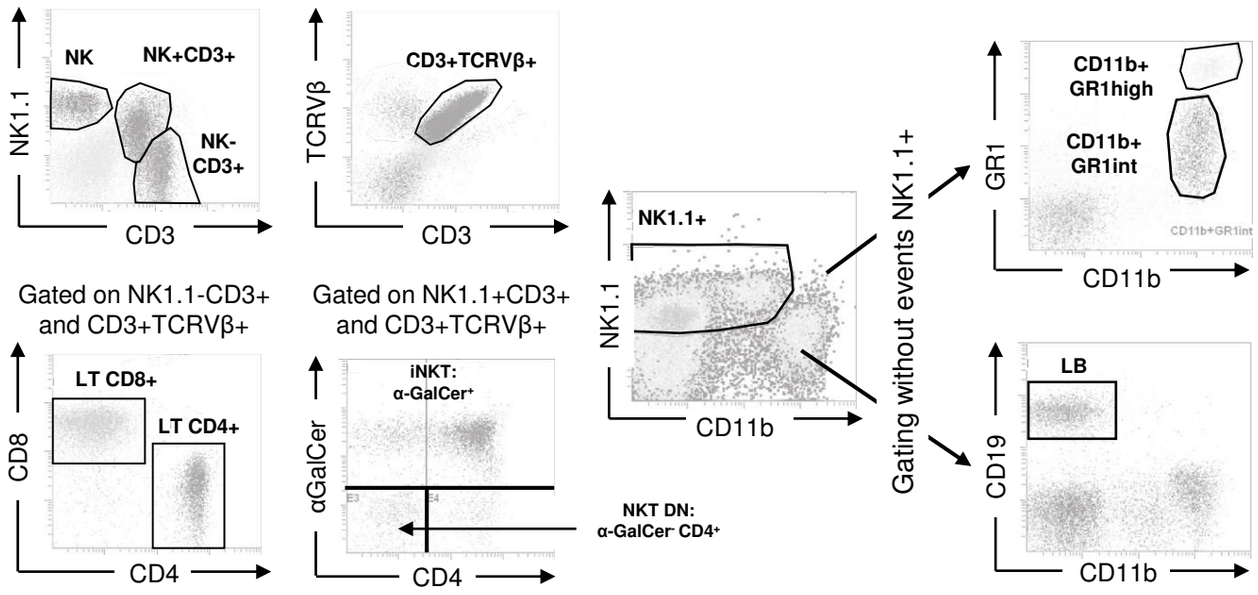

Supplementary Figure 3

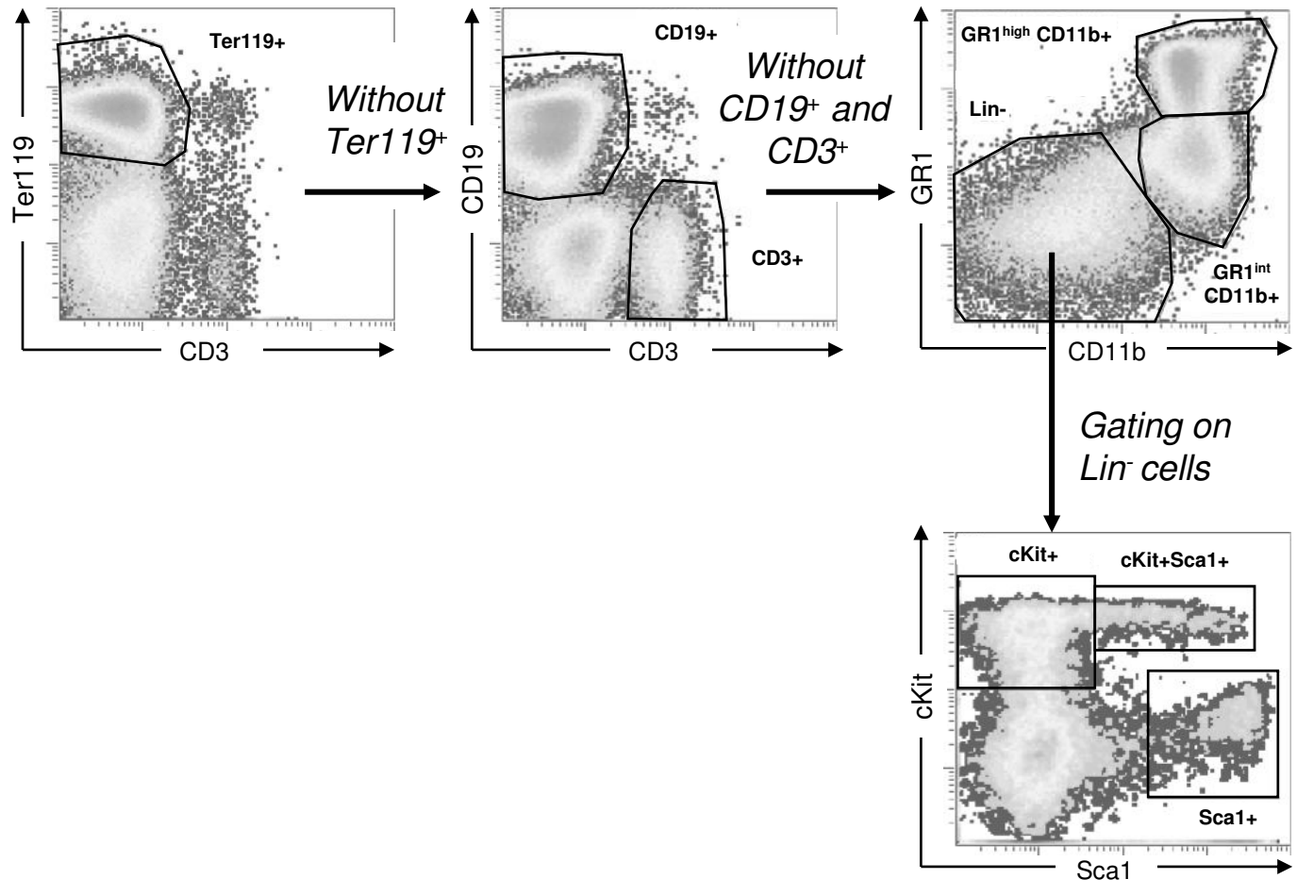

IV. DISCUSSION GENERALE ET PERSPECTIVES

Le déclenchement de la mort des hépatocytes au cours des différentes maladies hépatiques induit des processus de régénération. Toutefois, si la mort excède la prolifération compensatoire des hépatocytes, des mécanismes pro-fibrotiques se mettent en place. Ces mécanismes ont un rôle fondamental dans la réparation du tissu mais lorsqu'ils ne sont pas contrôlés et persistent, ils favorisent le développement de la fibrose et du CHC. La libération des DAMPs (déclenchés par une mort nécrotique, nécroptotique ou une nécrose secondaire), ainsi que la formation des corps apoptotiques dans le microenvironnement du foie, contribuent à ces processus par le recrutement et l'activation des cellules immunitaires. Ainsi, l'ensemble de ces événements place la mort des hépatocytes comme un élément initiateur dans la progression des maladies hépatiques et a conduit à la recherche de son inhibition pharmacologique comme une potentielle approche thérapeutique (Luedde et al., 2014).

Que ce soit par son induction directe ou secondaire, la réponse inflammatoire joue un rôle clef dans l'induction de l'hépatolyse, principalement par la libération ou l'expression des ligands de mort de la superfamille du TNF (dont majoritairement le TNF-α, TRAIL et FasL) sous leur forme soluble ou portés par les cellules immunitaires. En effet, de nombreuses données cliniques, chez des patients atteints d'hépatites aiguës ou chroniques de diverses étiologies, corrèlent la gravité de la pathologie avec les niveaux hépatiques ou sériques de ces ligands ou de leurs récepteurs (cf Introduction, section 5). De plus, dans de nombreux modèles hépatiques, une réduction de l'hépatolyse et une amélioration de la maladie a été observée lorsque ces facteurs étaient inhibés. Plusieurs études se sont donc intéressées à la recherche d'inhibiteurs pour le traitement des hépatites. Le TNF-α a été la cible de plusieurs études cliniques, cependant bien que les anti-TNF-α soient utilisés dans le traitement de plusieurs maladies auto-immunes, leur utilisation au cours des AIH, des hépatites virales, de l'ALD, des DILI ou de la NASH a montré d'importants effets indésirables et peu d'effets bénéfiques. En effet ces différents travaux ont montré un risque de réactivation du VHB ou du VHC, d'augmentation du dommage hépatique, voire de provoquer, de manière significativement plus importante, la mort des patients (Boetticher et al., 2008; Coffin et al., 2011; Wree et al., 2016).

D'autres études se sont intéressées à cibler les inducteurs de la mort cellulaire en aval de ces récepteurs, tels que les caspases. Plusieurs inhibiteurs pan-caspases ont été testés, tels que l'IDN-6556 (ou Emricasan) et le GS-9450 qui semblent avoir des effets bénéfiques par leur capacité à réduire les niveaux de transaminases hépatiques sériques chez des patients atteints d'hépatites chroniques induites par le VHC ou la NASH et sont actuellement en essai clinique de phase II (Luedde et al., 2014; Wree et al., 2016). Ces deux inhibiteurs ont la capacité de bloquer des caspases pro-apoptotiques et pro-inflammatoires dont la caspase 1 qui a un important rôle dans la

promotion de l'inflammation hépatique lors de ces hépatites. La réduction des transaminases sériques peut donc être le reflet de l'inhibition de la mort apoptotique des hépatocytes ainsi que celle de l'inflammation.

La découverte de nouvelles voies de mort cellulaire, impliquant des membres de la superfamille du TNF-α à induire la nécroptose, ainsi que l'interconnexion entre l'apoptose et la nécroptose, a conduit à la recherche de nouvelles molécules inhibant la mort hépatocytaire. De par sa capacité à induire l'apoptose et la nécroptose via son activité enzymatique, RIPK1 apparaît comme une cible thérapeutique intéressante. De plus, l'utilisation de la Nec-1, une molécule capable de bloquer l'activité kinase de RIPK1, a montré des effets bénéfiques au cours des hépatites aiguë induites par la ConA (Jouan-Lanhouet et al., 2012; Zhou et al., 2013b) ou l'APAP (An et al., 2013; Takemoto et al., 2014; Zhang et al., 2014). Cependant, des travaux ont montré que cette molécule pouvait également bloquer l'activité d'autres kinases tels que PAK1 et PKAcα (Biton and Ashkenazi, 2011; Jouan-Lanhouet et al., 2014b) et présente une structure identique à la methyl-thiohydantoin-tryptophan, un inhibiteur de la protéine IDO. Cette dernière serait également bloquée par la molécule Nec-1i, utilisée habituellement comme contrôle inactif de la Nec-1. Au cours de son travail de thèse, Sandrine Jouan-Lanhouet et al. ont montré que les molécules Nec-1 et Nec-1i réduisaient toutes les deux l'hépatolyse induite par la ConA (Jouan-Lanhouet, 2011). La protéine IDO ayant un rôle important dans la production d'acides aminés essentiels à l'activation des lymphocytes (Robinson et al., 2016; Thomson and Knolle, 2010), son inhibition par la Nec-1 ou la Nec-1i pourrait donc contribuer à l'inhibition de l'hépatolyse induite par la ConA. Au cours de mes travaux de doctorat, l'utilisation d'une nécrostatine de seconde génération, la 7-Cl-O-Nec-1 (Nec-1s), décrite comme présentant une activité plus stable et plus spécifique que la Nec-1 (EC50 de 206 nM pour la Nec-1s vs 494 nM pour la Nec-1) et prédite comme n'interagissant pas avec la protéine IDO (Jouan-Lanhouet et al., 2014b; Takahashi et al., 2012) a permis de confirmer le rôle de l'activité kinase de RIPK1 dans l'induction de l'hépatolyse. En effet le traitement des souris avec la Nec-1s conduit à une réduction de la mort des hépatocytes induite par la ConA. De plus, des souris, dont l'activité de RIPK1 est inactive (*Ripk1*^{K45A}), ont répondu de manière similaire à l'injection de la lectine, corroborant le rôle de RIPK1 dans le processus de mort de l'hépatocyte. Par ailleurs, en association avec le Dr MT. Dimanche-Boitrel, nous avons étudié l'effet d'une nouvelle molécule ciblant l'activité kinase de RIPK1 *in vivo* dans l'hépatite à ConA qui conduit également à une diminution significative de l'hépatolyse (données non présentées). La découverte d'un nouvel inhibiteur de RIPK1 a donc permis d'avancer dans la recherche de molécules permettant de bloquer l'hépatolyse au cours de l'hépatite. Il serait intéressant dans de futures études d'étudier l'impact de Nec-1s dans d'autres modèles d'hépatite et tirer avantage de sa demi-vie plus importante que la Nec-1 (Teng et al., 2005) pour l'étudier dans des modèles d'hépatites

chroniques, qui sont d'un haut intérêt au niveau clinique. Comme observé dans des modèles animaux d'hépatite, les essais cliniques chez l'Homme utilisant des inhibiteurs de caspases dans le traitement des maladies hépatiques semblent conduire à une réduction de l'hépatolyse. L'étude des voies conduisant à l'apoptose et la nécroptose a montré qu'elles partageaient de nombreux effecteurs, provoquant parfois le changement d'une voie au profit d'une autre lors de l'inhibition de l'une d'entre elle. Par conséquent, il est fortement probable qu'une situation similaire survienne chez les patients atteints d'hépatites et l'utilisation d'inhibiteurs de l'apoptose et de la nécroptose permettrait le blocage de l'hépatolyse et la réduction de l'évolution de la pathologie.

Plusieurs éléments suggèrent très fortement l'activation de la nécroptose au cours de l'hépatite à ConA. En effet, l'hépatolyse est dépendante des récepteurs de mort et indépendante de l'activation des caspases. Cependant, nous ne pouvons pas exclure le rôle de l'activité kinase de RIPK1 dans les cellules non parenchymateuses du foie, puisque les deux approches utilisées dans nos travaux (chimique par l'utilisation de la Nec-1s, et génétique par l'utilisation des souris *Ripk1*^{K45A}) ne nous permettent pas de cibler spécifiquement les hépatocytes. De plus une étude récente a montré le rôle de l'activité kinase de RIPK1 au sein de macrophages dans l'induction de cytokines pro-inflammatoires (Shutinoski et al., 2016). L'activité de RIPK1 pourrait donc avoir à la fois un rôle dans l'induction de la mort des hépatocytes et la promotion de l'inflammation. Afin d'étayer cette hypothèse, l'utilisation de souris exprimant la Cre-recombinase sous la dépendance d'un promoteur spécifiquement exprimé dans les macrophages permettrait d'étudier le rôle de RIPK1 dans ces cellules.

En plus d'avoir montré que le blocage de l'activité de RIPK1 réduisait l'hépatolyse induite par la ConA, les travaux antérieurs à l'équipe avaient également démontré que l'inhibition des protéines PARP1/2 par l'utilisation du PJ-34 produisait le même effet. Mes travaux de doctorat ont cherché à mieux comprendre le rôle de ces deux protéines dans le processus de mort des hépatocytes induits par la ConA, en ciblant spécifiquement ces deux protéines par l'utilisation de souris déficientes en *Parp1* ou *Parp2*. Cependant bien qu'on ait observé une réduction de la mort hépatocytaire chez les souris déficientes en *Parp2*, ce modèle présente des limites. En effet, l'étude des souris *Parp2*$^{-/-}$ a préalablement montré le rôle de PARP2 dans la régulation du métabolisme des lipides (Bai et al., 2007; Szántó et al., 2014), l'érythropoïèse (Farrés et al., 2015), la thymopoïese (Yélamos et al., 2006) et la spermatogenèse (Dantzer et al., 2006). Les effets de PARP2 sur plusieurs processus physiologiques conduisent au changement de nombreux facteurs et rendent difficile l'interprétation des résultats sur un phénomène particulier. Nous avons montré que l'absence de PARP2 provoquait un défaut de maturation des NKT invariants conduisant à une diminution de leur nombre au niveau systémique et également hépatique. Les iNKT étant les cellules effectrices

de la mort des hépatocytes au cours de l'hépatite à ConA, ces effets ne nous ont donc pas permis de déterminer l'implication de PARP2 en aval de l'induction de la lyse.

Comme pour la Nec-1 décrite précédemment, les inhibiteurs chimiques de PARP2 sont des molécules pouvant interagir et interférer avec d'autres protéines que celles d'intérêt. Bien que les souris déficientes en *Parp1* ou *Parp2* ne nous ont pas permis de mieux comprendre les effets retrouvés avec le PJ-34, ils n'excluent pas l'implication des deux protéines dans l'induction de l'hépatolyse. L'utilisation d'autres inhibiteurs que le PJ-34 pourrait être envisagée dans le but de mieux caractériser l'effet enzymatique de ces protéines dans ce processus. L'utilisation de siRNA ou de souris dont la délétion du gène d'intérêt est inductible permettrait de s'affranchir des modifications physiologiques telles que l'altération de la thymopoïèse provoquée par l'absence de PARP2. De même, l'utilisation de souris déficientes spécifiquement dans les hépatocytes ou les LPC permettrait d'étudier plus spécifiquement l'implication de PARP1 et PARP2 dans les voies de signalisation conduisant à la mort des hépatocytes.

Ces travaux de doctorat apportent également une meilleure compréhension de la physiopathologie hépatique au cours des maladies du foie. En effet, le TNF-α est une cytokine pléïotrope qui, dépendant de sa dose, de sa cellule cible et des autres signaux reçus par cette cellule, a des effets pro-inflammatoires, anti-apoptotiques ou au contraire peut induire leur mort par apoptose ou nécroptose. Ainsi, le TNF-α est associé à plusieurs étiologies d'hépatites aigües ou chroniques telles que celles induite par l'alcool, l'infection par le VHB ou le VHC ou au cours de l'AIH ou la NASH. Suite à sa fixation sur le TNFR1, le TNF-α, dans des conditions physiologiques, active la voie pro-inflammatoire et anti-apoptotique NF-κB. Cependant, lorsque l'activation de cette voie est bloquée ou lorsque la transcription est inhibée, le TNF-α déclenche la formation du complexe IIa (indépendant de RIPK1) ou IIb (dépendant de RIPK1) entraînant l'apoptose de la cellule. Si les caspases sont inhibées, le nécrosome, composé des protéines RIPK1, RIPK3 et MLKL, peut se former et activer la nécroptose de la cellule. Ainsi, le microenvironnement du foie va déterminer l'effet du TNF-α entre la mort et la survie des hépatocytes. L'administration de TNF-α ou de LPS, qui conduit à la production de TNF-α par les cellules immunitaires chez la souris, ne déclenche pas d'hépatolyse mais l'activation de la voie NF-κB, qui maintient les hépatocytes en vie. Cependant lorsque cette voie est inhibée, par exemple via l'utilisation de souris déficientes pour les protéines du complexe IKK (IKKα, IKKβ et IKKγ/NEMO), qui permettent la translocation de NF-κB au noyau, le TNF-α va conduire à l'apoptose des hépatocytes et à une hépatite aigüe. Les mêmes effets sont retrouvés lorsque le TNF-α ou le LPS sont co-administrés avec la D-GalN, un inhibiteur de la transcription hépatocytaire. Au cours de l'hépatite induite par la ConA, le TNF-α a également un rôle dans

l'induction de l'hépatolyse. Cependant les données récentes suggèrent que le TNF-α aurait un effet indirect en instaurant un environnement favorable à l'induction de la mort des hépatocytes par les NKT en agissant sur les cellules dérivées des myéloïdes (cf Introduction, section 5.1).

RIPK1 joue un rôle majeur dans la survie cellulaire puisque sa délétion chez la souris conduit à une inflammation et une mort cellulaire systémique et la létalité périnatale des souris. En parallèle, plusieurs travaux ont montré la capacité de RIPK1 à induire la mort cellulaire, via sa fonction kinase, dans plusieurs pathologies, dont l'hépatite. Activé par plusieurs récepteurs dont les DR de la superfamille du TNF-α, son rôle dans le contrôle du destin cellulaire a majoritairement été étudié dans la signalisation du TNF-α. L'ensemble de ces travaux a permis de montrer une sensibilité des cellules au TNF-α en l'absence de RIPK1. Cependant les voies conduisant à la survie de la cellule semblent dépendant et indépendant de la voie NF-kB, en fonction de la cinétique et du type cellulaire. L'utilisation récente des souris conditionnellement déficientes a permis de montrer que l'absence de RIPK1 dans les cellules hématopoïétiques ou les cellules épithéliales de la peau ou de l'intestin conduit à une apoptose spontanée de ces cellules chez la souris (Dannappel et al., 2014; Roderick et al., 2014; Takahashi et al., 2014). A l'inverse, RIPK1 ne semble pas être important dans le maintien de l'homéostasie des LPC dans des conditions physiologiques. En effet comme il a été rapporté récemment par Kondylis et al. (Kondylis et al., 2015) et comme nous l'avons également observé, aucune hépatolyse, ni induction d'une prolifération hépatocytaire différentielle en l'absence ou non de RIPK1 dans les LPC, n'a été observée au cours du vieillissement des souris, jusqu'à l'âge d'un an.

Majoritairement étudié dans la signalisation du TNF-α, RIPK1 est un facteur impliqué dans les voies induites par les TLR, et des DR tels que Fas et DR4/5. Par l'utilisation de différents modèles d'hépatite nos travaux ont permis de montrer une sensibilité des souris *Ripk1*$^{LPC\text{-}KO}$ aux dommages hépatiques induits par la ConA, le LPS, les motifs CpG, le TNF-α, l'agoniste de Fas (mAb-Jo2), ainsi qu'une co-administraion d'IFN-γ et de TRAIL recombinantes, dont les résultats sont résumés dans le Tableau 6.

Excepté l'hépatite induite par l'agoniste de Fas, nous avons montré que la sensibilité des souris *Ripk1*$^{LPC\text{-}KO}$ était dépendante du TNF-α dans ces différents modèles. Tout d'abord puisqu'une simple administration de TNF-α recombinant provoquait la lyse des hépatocytes et que sa neutralisation par l'Etanercept protégeait les souris de l'hépatolyse induite par les PAMPs ou une co-administration d'IFN-γ et de TRAIL recombinants et réduisait celle induite par la ConA. En revanche l'inhibition du TNF-α ne semble pas être impliquée dans l'hépatite induite par l'agoniste de Fas, suggérant un rôle direct de RIPK1 dans la signalisation de Fas. L'activation de Fas a été démontrée comme jouant un rôle dans l'hépatite à ConA. Nos données suggèrent que l'hépatolyse

qui persiste chez les souris *Ripk1*$^{LPC\text{-}KO}$ co-traitées avec l'Etanercept et la ConA (ALT = 1838 +/- 1427 UI/L) pourrait être induite par l'activation de la signalisation de Fas. En effet, RIPK1 est connu pour intéragir avec le récepteur Fas et son absence spécifique dans les LPC sensibilisait les souris à l'hépatite induite par Fas et indépendamment de la voie du TNF-α. Afin de confirmer cette hypothèse, il serait intéressant d'inhiber la signalisation de Fas, par l'utilisation d'un anti-FasL ou d'un récepteur Fas soluble, en combinaison avec l'Etanercept avant l'injection de ConA.

Tableau 6. Quantification et analyse de l'hépatolyse induite chez les souris *Ripk1*$^{LPC\text{-}KO}$ dans différents modèles d'hépatites aiguës chez la souris.

Modèles d'hépatite	Moyenne ALAT (UI/L) (+/- SD)	Moyenne ALAT (UI/L) après prétraitement à l'ETA (+/- SD)	Activation de la caspase 3
Concanavaline A	**20 754** +/- 8596	**1838** +/-1427	Oui
LPS	**19 253** +/- 8625	**222,7** +/- 117,8	Oui
CpG	**724,7** +/- 368,9	ND	Oui
TNF-α	**9698** +/- 8404	ND	Oui
rmIFN-γ + rmTRAIL	**1671** +/- 1141	**314** +/- 429,8	Oui
Agoniste de Fas	**2758** +/- 3625	**2353** +/- 1580	Oui

Abréviation : ND : non déterminé

Comme présenté dans le Tableau 6, les différents modèles d'hépatites que nous avons utilisés ont montré que l'absence de RIPK1 dans les LPC sensibilisait les souris à l'hépatite par l'activation de l'apoptose. Plusieurs études ont montré que la sensibilité au TNF-α des cellules déficientes en RIPK1 pouvait être la conséquence d'une inhibition de la voie NF-κB qui conduirait à une diminution des protéines anti-apoptotiques tel que cFLIP et constituerait un signal de mort pour la cellule. L'activation de NF-κB pourrait participer à l'effet protecteur de RIPK1, puisque nous avons montré qu'elle était moins activée au cours de l'hépatite à ConA. Cependant, cet effet serait indépendant du TNF-α, puisque nous avons montré que cette voie était activée *in vitro* et *in vivo* dans les hépatocytes en l'absence de RIPK1. Des études suggèrent que RIPK1 empêche l'activation de l'apoptose induite par le TNF-α en stabilisant les protéines TRAF2 et cIAP1/2 (Gentle et al., 2011; Wong et al., 2010). Bien que les mécanismes en aval de la dégradation de TRAF2 ne soient pas encore bien compris, ces protéines sont reconnues comme étant responsables de l'induction de l'apoptose par le TNF-α lorsque RIPK1 est absent (Ting and Bertrand, 2016). Nos résultats ont permis de montrer que RIPK1 protège les hépatocytes de la mort induite par le TNF-α via sa fonction d'échafaudage en empêchant la dégradation de TRAF2 (et certainement des cIAP1/2) et indépendamment de la voie canonique de NF-κB. Ces données permettent d'expliquer la sensibilité des souris *Ripk1*$^{LPC\text{-}KO}$ à l'hépatite induite par la ConA, les PAMPs et l'administration d'IFN-g et de TRAIL recombinantes, que nous avons montré dépendantes du TNF-α. Elles ajoutent également un élément à la complexité du rôle du TNF-α dans le foie. En effet, sa capacité à induire la survie des hépatocytes est caractérisée comme dépendant de l'activation de la voie NF-

κB. Ici nous montrons qu'elle peut également être indépendant de NF-κB mais dépendante de la présence de RIPK1.

Le TNF-α et le FasL, ainsi que l'induction de l'apoptose sont des facteurs associés à de nombreuses maladies hépatiques aiguës, mais également chroniques. La compréhension des mécanismes en aval de leurs récepteurs est donc d'un intérêt clinique important et nos travaux ont permis de révéler l'implication de RIPK1 dans différents modèles d'hépatite chez la souris. Comme décrit précédemment, l'activité kinase de RIPK1 pourrait être utilisée comme une cible thérapeutique intéressante dans le traitement des maladies hépatiques. De plus, nos données sur les souris *Ripk1*$^{LPC\text{-}KO}$ soulignent que de potentielles modifications dans la structure de RIPK1 pourraient sensibiliser les hépatocytes à la mort et aggraver l'hépatite. Ces données ouvrent la porte à des études de RIPK1 dans des modèles d'hépatites chroniques et notamment au cours de la NASH ou l'hépatite alcoolique qui sont les principales causes d'hépatites dans les pays occidentaux. Il existe plusieurs modèles pour étudier la NASH *in vivo,* soit suite à une délétion génétique soit par un régime alimentaire riche en lipides et glucides (Ibrahim et al., 2016). Ce dernier serait le plus approprié pour étudier le rôle de RIPK1, puisque comme l'alcool, des hauts niveaux de lipides conduisent à une perméabilisation de la barrière intestinale entrainant une augmentation des débris bactériens au niveau hépatique et une inflammation (Ilan, 2012; Louvet and Mathurin, 2015). Plusieurs travaux ont montré l'implication des macrophages, des TLR et plus particulièrement le TLR4 ainsi que du TNF-α dans des modèles de NASH et d'hépatites induites par l'alcool chez la souris (Rivera et al., 2007; Spruss et al., 2009; Uesugi et al., 2001). Nos travaux montrant que l'injection de PAMPs, majoritairement détectés par les macrophages, sensibilisent les souris *Ripk1*$^{LPC\text{-}KO}$ à l'hépatolyse induite par le TNF-α, démontrent le rôle protecteur de RIPK1 dans ces conditions et suggèrent son implication possible au cours de la NASH.

La survenue du CHC est la 3ème cause de mortalité par cancer (Forner et al., 2012) et donc une des complications majeure de l'évolution des hépatites chroniques. Des études récentes se sont intéressées au rôle de RIPK1 dans un modèle de cancer génétiquement induit par la délétion spécifique de NEMO dans les LPC (*Nemo*$^{LPC\text{-}KO}$). Ces souris présentent une hépatolyse spontanée suivi du développement d'un CHC. Ce phénotype ferait intervenir des processus dépendant et indépendant de l'activation de la voie NF-kB. RIPK1 interviendrait dans l'induction de la lyse de manière indépendante de NF-kB. En effet, l'absence de *Nemo* dans les LPC provoque la formation du complexe IIb et l'induction de l'apoptose par RIPK1. Cette hépatolyse serait prévenue par l'utilisation de souris présentant une activité kinase de RIPK1 inactive (*Ripk1*^{D138N}) (Kondylis et al., 2015). En revanche, l'absence spécifique de RIPK1 dans les LPC n'inhiberait pas l'hépatolyse

spontanée provoquée par l'absence de NEMO mais serait induite par la formation du complexe IIa (Kondylis et al., 2015). Bien que la délétion spécifique du *Tnfr1* dans les LPC n'empêche pas l'hépatolyse spontanée qui survient chez les souris $Nemo^{LPC\text{-}KO}$ (Ehlken et al., 2014), nos données montrant la sensibilité des souris $Ripk1^{LPC\text{-}KO}$ au TNF-α suggèrent que l'hépatolyse spontanée observée chez les souris $Nemo/Ripk1^{LPC\text{-}KO}$ est dépendante du TNF-α.

Ces données soulignent l'importance de la préservation de la fonction d'échafaudage de RIPK1 dans l'inhibition de l'hépatolyse pour le maintien des fonctions hépatiques et suggèrent l'implication de RIPK1 dans le processus de mort des hépatocytes via sa fonction kinase au cours des maladies hépatiques chez l'Homme. Par conséquent, l'analyse de l'expression transcriptionnelle, traductionnelle ainsi que des polymorphismes de *Ripk1* pourrait aider à la prise en charge des patients présentant une hépatite chronique ou une ACLF.

Dans le foie, la mort des hépatocytes est un des facteurs conduisant à plusieurs caractéristiques des maladies hépatiques. L'atteinte des cholangiocytes est également responsable de pathologie hépatique. En effet, leur mort est connue pour entrainer une détérioration du flux biliaire et une cholestase. Les souris spécifiquement déficientes pour IKKα/β dans les LPC ($Ikk\alpha/\beta^{LPCKO}$) développent une hépatolyse spontanée associée à une cholestase. De manière intéressante, une étude a démontré un rôle clef de RIPK1 dans l'induction de la cholestase dans ce modèle. En effet, bien que les mécanismes soient peu compris l'absence supplémentaire de *Ripk1* chez les $Ikk\alpha/\beta^{LPCKO}$ inhiberait le développement de la cholestase mais induirait le développement d'un CHC. Dans cette étude, les auteurs ont étudié ces protéines dans une cohorte de 19 patients atteints de CHC. Ils ont révélé que 5 d'entre eux, présentaient une forte réduction d'IKKα/β associée à une diminution de RIPK1. Ces données appuient l'implication potentielle de RIPK1 dans le développement des maladies hépatiques et du CHC. L'utilisation de différents modèles de CHC pourrait permettre de mieux comprendre le rôle de RIPK1 dans le processus de tumorigenèse et ouvre également la porte à son étude dans les cholangiocytes.

Les LSECs jouent un rôle majeur dans l'intégrité du foie. En effet leur atteinte au cours de l'hépatite induite par un agoniste de Fas ou du FasL conduit à une hémorragie, qui est une des causes de la mort des souris. De même, il existe des hémorragies hépatiques spontanées chez l'Homme. Il serait donc intéressant d'étudier le rôle de RIPK1 dans la survie de ces cellules. Bien qu'il n'existe pas de lignée de souris exprimant spécifiquement la Cre-recombinase dans les LSECs, la lignée "VE-Cadherin-PAC-$CreER^{T2}$" permet l'expression de cette enzyme spécifiquement dans les cellules endothéliales et de manière inductible par l'administration de tamoxifène (Greenhalgh et al., 2015). Le croisement de ces souris, dont la lignée est déjà existante (Ding et al., 2014), avec les souris $Ripk1^{fl/fl}$ conduirait à la délétion de RIPK1 dans les cellules

endothéliales. La ConA ayant une affinité pour les sinusoïdes hépatiques, (Trautwein et al., 1998), les LSECs seraient les premières atteintes par le TNF-α produit par les cellules immunes activées par la ConA et serait donc un bon modèle pour étudier le rôle de RIPK1 dans ces cellules.

En conclusion, mon travail de thèse a permis de préciser un peu mieux le rôle de la kinase RIP1 et de PARP2 dans les hépatites aiguës. Toutefois, la position de RIPK1 dans un carrefour des voies de survie et de mort mérite d'être éclaircies et de nouvelles fonctions et partenaires protéiques seront dans un futur proche peut-être découvertes. Cette thèse a posé les bases de la fonction de RIPK1 dans les hépatocytes, mais son rôle dans les cellules non-parenchymateuses dont les cellules immunitaires, les cellules endothéliales ou les cellules étoilées hépatiques demeure de nouvelles orientations de grand intérêt. De même, le rôle de la protéine RIPK1 dans les maladies chroniques du foie reste à investir comme modèle chez la souris et bien entendu chez l'Homme.

V. REFERENCES

Aggarwal, B.B. (2003). Signalling pathways of the TNF superfamily: a double-edged sword. Nat. Rev. Immunol. *3*, 745–756.

Ajuebor, M.N., Carey, J.A., and Swain, M.G. (2006). CCR5 in T cell-mediated liver diseases: what's going on? J. Immunol. Baltim. Md 1950 *177*, 2039–2045.

Alexopoulou, L., Holt, A.C., Medzhitov, R., and Flavell, R.A. (2001). Recognition of double-stranded RNA and activation of NF-kappaB by Toll-like receptor 3. Nature *413*, 732–738.

Amé, J.C., Rolli, V., Schreiber, V., Niedergang, C., Apiou, F., Decker, P., Muller, S., Höger, T., Ménissier-de Murcia, J., and de Murcia, G. (1999). PARP-2, A novel mammalian DNA damage-dependent poly(ADP-ribose) polymerase. J. Biol. Chem. *274*, 17860–17868.

Amé, J.-C., Spenlehauer, C., and de Murcia, G. (2004). The PARP superfamily. BioEssays News Rev. Mol. Cell. Dev. Biol. *26*, 882–893.

An, J., Mehrhof, F., Harms, C., Lättig-Tünnemann, G., Lee, S.L.L., Endres, M., Li, M., Sellge, G., Mandić, A.D., Trautwein, C., et al. (2013). ARC is a novel therapeutic approach against acetaminophen-induced hepatocellular necrosis. J. Hepatol. *58*, 297–305.

Aredia, F., and Scovassi, A.I. (2014). Poly(ADP-ribose): a signaling molecule in different paradigms of cell death. Biochem. Pharmacol. *92*, 157–163.

Arshad, M.I., Piquet-Pellorce, C., L'Helgoualc'h, A., Rauch, M., Patrat-Delon, S., Ezan, F., Lucas-Clerc, C., Nabti, S., Lehuen, A., Cubero, F.J., et al. (2012). TRAIL but not FasL and TNFα, regulates IL-33 expression in murine hepatocytes during acute hepatitis. Hepatol. Baltim. Md *56*, 2353–2362.

Arshad, M.I., Piquet-Pellorce, C., Filliol, A., L'Helgoualc'h, A., Lucas-Clerc, C., Jouan-Lanhouet, S., Dimanche-Boitrel, M.-T., and Samson, M. (2015). The chemical inhibitors of cellular death, PJ34 and Necrostatin-1, down-regulate IL-33 expression in liver. J. Mol. Med. Berl. Ger. *93*, 867–878.

Bai, P., Houten, S.M., Huber, A., Schreiber, V., Watanabe, M., Kiss, B., de Murcia, G., Auwerx, J., and Ménissier-de Murcia, J. (2007). Poly(ADP-ribose) polymerase-2 [corrected] controls adipocyte differentiation and adipose tissue function through the regulation of the activity of the retinoid X receptor/peroxisome proliferator-activated receptor-gamma [corrected] heterodimer. J. Biol. Chem. *282*, 37738–37746.

Bai, Y., Zhou, T., Fu, H., Sun, H., and Huang, B. (2012). 14-3-3 interacts with LKB1 via recognizing phosphorylated threonine 336 residue and suppresses LKB1 kinase function. FEBS Lett. *586*, 1111–1119.

Bandmann, O., Weiss, K.H., and Kaler, S.G. (2015). Wilson's disease and other neurological copper disorders. Lancet Neurol. *14*, 103–113.

Bandyopadhyay, K., Marrero, I., and Kumar, V. (2016). NKT cell subsets as key participants in liver physiology and pathology. Cell. Mol. Immunol. *13*, 337–346.

Beier, J.I., and McClain, C.J. (2010). Mechanisms and cell signaling in alcoholic liver disease. Biol. Chem. *391*, 1249–1264.

Beraza, N., Malato, Y., Sander, L.E., Al-Masaoudi, M., Freimuth, J., Riethmacher, D., Gores, G.J., Roskams, T., Liedtke, C., and Trautwein, C. (2009). Hepatocyte-specific NEMO deletion promotes NK/NKT cell- and TRAIL-dependent liver damage. J. Exp. Med. *206*, 1727–1737.

Berger, N.A., Sims, J.L., Catino, D.M., and Berger, S.J. (1983). Poly(ADP-ribose) polymerase mediates the suicide response to massive DNA damage: studies in normal and DNA-repair defective cells. Princess Takamatsu Symp. *13*, 219–226.

Berger, S.B., Kasparcova, V., Hoffman, S., Swift, B., Dare, L., Schaeffer, M., Capriotti, C., Cook, M., Finger, J., Hughes-Earle, A., et al. (2014). Cutting Edge: RIP1 Kinase Activity Is Dispensable for Normal Development but Is a Key Regulator of Inflammation in SHARPIN-Deficient Mice. J. Immunol. *192*, 5476–5480.

Berke, G. (1995). The CTL's kiss of death. Cell *81*, 9–12.

Bettermann, K., Vucur, M., Haybaeck, J., Koppe, C., Janssen, J., Heymann, F., Weber, A., Weiskirchen, R., Liedtke, C., Gassler, N., et al. (2010). TAK1 suppresses a NEMO-dependent but NF-kappaB-independent pathway to liver cancer. Cancer Cell *17*, 481–496.

Biburger, M., and Tiegs, G. (2005). Alpha-galactosylceramide-induced liver injury in mice is mediated by TNF-alpha but independent of Kupffer cells. J. Immunol. Baltim. Md 1950 *175*, 1540–1550.

Biton, S., and Ashkenazi, A. (2011). NEMO and RIP1 Control Cell Fate in Response to Extensive DNA Damage via TNF-α Feedforward Signaling. Cell *145*, 92–103.

Black, R.A., Rauch, C.T., Kozlosky, C.J., Peschon, J.J., Slack, J.L., Wolfson, M.F., Castner, B.J., Stocking, K.L., Reddy, P., Srinivasan, S., et al. (1997). A metalloproteinase disintegrin that releases tumour-necrosis factor-alpha from cells. Nature *385*, 729–733.

Boetticher, N.C., Peine, C.J., Kwo, P., Abrams, G.A., Patel, T., Aqel, B., Boardman, L., Gores, G.J., Harmsen, W.S., McClain, C.J., et al. (2008). A Randomized, Double-Blinded, Placebo-Controlled Multicenter Trial of Etanercept in the Treatment of Alcoholic Hepatitis. Gastroenterology *135*, 1953–1960.

Brenner, C., Galluzzi, L., Kepp, O., and Kroemer, G. (2013). Decoding cell death signals in liver inflammation. J. Hepatol. *59*, 583–594.

Brenner, D., Blaser, H., and Mak, T.W. (2015). Regulation of tumour necrosis factor signalling: live or let die. Nat. Rev. Immunol. *15*, 362–374.

Burrows, P.D., and Cooper, M.D. (1997). B cell development and differentiation. Curr. Opin. Immunol. *9*, 239–244.

Cai, Z., Jitkaew, S., Zhao, J., Chiang, H.-C., Choksi, S., Liu, J., Ward, Y., Wu, L.-G., and Liu, Z.-G. (2014). Plasma membrane translocation of trimerized MLKL protein is required for TNF-induced necroptosis. Nat. Cell Biol. *16*, 55–65.

Canbay, A., Taimr, P., Torok, N., Higuchi, H., Friedman, S., and Gores, G.J. (2003). Apoptotic body engulfment by a human stellate cell line is profibrogenic. Lab. Investig. J. Tech. Methods Pathol. *83*, 655–663.

Canbay, A., Feldstein, A., Baskin-Bey, E., Bronk, S.F., and Gores, G.J. (2004). The caspase inhibitor IDN-6556 attenuates hepatic injury and fibrosis in the bile duct ligated mouse. J. Pharmacol. Exp. Ther. *308*, 1191–1196.

Cao, Z., Dhupar, R., Cai, C., Li, P., Billiar, T.R., and Geller, D.A. (2010). A critical role for IFN regulatory factor 1 in NKT cell-mediated liver injury induced by alpha-galactosylceramide. J. Immunol. Baltim. Md 1950 *185*, 2536–2543.

Chaisson, M.L., Brooling, J.T., Ladiges, W., Tsai, S., and Fausto, N. (2002). Hepatocyte-specific inhibition of NF-κB leads to apoptosis after TNF treatment, but not after partial hepatectomy. J. Clin. Invest. *110*, 193–202.

Chaudhary, P.M., Eby, M., Jasmin, A., Bookwalter, A., Murray, J., and Hood, L. (1997). Death receptor 5, a new member of the TNFR family, and DR4 induce FADD-dependent apoptosis and activate the NF-kappaB pathway. Immunity *7*, 821–830.

Chen, W., Han, C., Zhang, J., Song, K., Wang, Y., and Wu, T. (2015). Deletion of Mir155 prevents Fas-induced liver injury through up-regulation of Mcl-1. Am. J. Pathol. *185*, 1033–1044.

Chen, X., Li, W., Ren, J., Huang, D., He, W.-T., Song, Y., Yang, C., Li, W., Zheng, X., Chen, P., et al. (2014). Translocation of mixed lineage kinase domain-like protein to plasma membrane leads to necrotic cell death. Cell Res. *24*, 105–121.

Chyuan, I.-T., Tsai, H.-F., Tzeng, H.-T., Sung, C.-C., Wu, C.-S., Chen, P.-J., and Hsu, P.-N. (2015). Tumor necrosis factor-alpha blockage therapy impairs hepatitis B viral clearance and enhances T-cell exhaustion in a mouse model. Cell. Mol. Immunol. *12*, 317–325.

Coffin, C.S., Fraser, H.F., Panaccione, R., and Ghosh, S. (2011). Liver diseases associated with anti-tumor necrosis factor-alpha (TNF-α) use for inflammatory bowel disease: Inflamm. Bowel Dis. *17*, 479–484.

Corazza, N., Jakob, S., Schaer, C., Frese, S., Keogh, A., Stroka, D., Kassahn, D., Torgler, R., Mueller, C., Schneider, P., et al. (2006). TRAIL receptor-mediated JNK activation and Bim phosphorylation critically regulate Fas-mediated liver damage and lethality. J. Clin. Invest. *116*, 2493–2499.

Dahlin, D.C., Miwa, G.T., Lu, A.Y., and Nelson, S.D. (1984). N-acetyl-p-benzoquinone imine: a cytochrome P-450-mediated oxidation product of acetaminophen. Proc. Natl. Acad. Sci. U. S. A. *81*, 1327–1331.

Dannappel, M., Vlantis, K., Kumari, S., Polykratis, A., Kim, C., Wachsmuth, L., Eftychi, C., Lin, J., Corona, T., Hermance, N., et al. (2014). RIPK1 maintains epithelial homeostasis by inhibiting apoptosis and necroptosis. Nature *513*, 90–94.

Dantzer, F., Mark, M., Quenet, D., Scherthan, H., Huber, A., Liebe, B., Monaco, L., Chicheportiche, A., Sassone-Corsi, P., de Murcia, G., et al. (2006). Poly(ADP-ribose) polymerase-2 contributes to the fidelity of male meiosis I and spermiogenesis. Proc. Natl. Acad. Sci. *103*, 14854–14859.

Dara, L., Johnson, H., Suda, J., Win, S., Gaarde, W., Han, D., and Kaplowitz, N. (2015). Receptor interacting protein kinase 1 mediates murine acetaminophen toxicity independent of the necrosome and not through necroptosis. Hepatol. Baltim. Md *62*, 1847–1857.

Dargan, P.I., and Jones, A.L. (2002). Acetaminophen poisoning: an update for the intensivist. Crit. Care Lond. Engl. *6*, 108–110.

De Vos, M., Schreiber, V., and Dantzer, F. (2012). The diverse roles and clinical relevance of PARPs in DNA damage repair: current state of the art. Biochem. Pharmacol. *84*, 137–146.

Decker, K., and Keppler, D. (1974). Galactosamine hepatitis: key role of the nucleotide deficiency period in the pathogenesis of cell injury and cell death. Rev. Physiol. Biochem. Pharmacol. 77–106.

Dejager, L., and Libert, C. (2008). Tumor necrosis factor alpha mediates the lethal hepatotoxic effects of poly(I:C) in D-galactosamine-sensitized mice. Cytokine *42*, 55–61.

DeLeve, L.D. (2013). Liver sinusoidal endothelial cells and liver regeneration. J. Clin. Invest. *123*, 1861–1866.

Deutsch, M., Graffeo, C.S., Rokosh, R., Pansari, M., Ochi, A., Levie, E.M., Van Heerden, E., Tippens, D.M., Greco, S., Barilla, R., et al. (2015). Divergent effects of RIP1 or RIP3 blockade in murine models of acute liver injury. Cell Death Dis. *6*, e1759.

Dillon, C.P., Weinlich, R., Rodriguez, D.A., Cripps, J.G., Quarato, G., Gurung, P., Verbist, K.C., Brewer, T.L., Llambi, F., Gong, Y.-N., et al. (2014). RIPK1 blocks early postnatal lethality mediated by caspase-8 and RIPK3. Cell *157*, 1189–1202.

Ding, B.-S., Cao, Z., Lis, R., Nolan, D.J., Guo, P., Simons, M., Penfold, M.E., Shido, K., Rabbany, S.Y., and Rafii, S. (2014). Divergent angiocrine signals from vascular niche balance liver regeneration and fibrosis. Nature *505*, 97–102.

Ea, C.-K., Deng, L., Xia, Z.-P., Pineda, G., and Chen, Z.J. (2006). Activation of IKK by TNFalpha requires site-specific ubiquitination of RIP1 and polyubiquitin binding by NEMO. Mol. Cell *22*, 245–257.

Ebert, G., Allison, C., Preston, S., Cooney, J., Toe, J.G., Stutz, M.D., Ojaimi, S., Baschuk, N., Nachbur, U., Torresi, J., et al. (2015a). Eliminating hepatitis B by antagonizing cellular inhibitors of apoptosis. Proc. Natl. Acad. Sci. U. S. A. *112*, 5803–5808.

Ebert, G., Preston, S., Allison, C., Cooney, J., Toe, J.G., Stutz, M.D., Ojaimi, S., Scott, H.W., Baschuk, N., Nachbur, U., et al. (2015b). Cellular inhibitor of apoptosis proteins prevent clearance of hepatitis B virus. Proc. Natl. Acad. Sci. U. S. A. *112*, 5797–5802.

Ehlken, H., Krishna-Subramanian, S., Ochoa-Callejero, L., Kondylis, V., Nadi, N.E., Straub, B.K., Schirmacher, P., Walczak, H., Kollias, G., and Pasparakis, M. (2014). Death receptor-independent FADD signalling triggers hepatitis and hepatocellular carcinoma in mice with liver parenchymal cell-specific NEMO knockout. Cell Death Differ. *21*, 1721–1732.

El-Serag, H.B. (2012). Surveillance for hepatocellular carcinoma: long way to achieve effectiveness. Dig. Dis. Sci. *57*, 3050–3051.

Farrés, J., Llacuna, L., Martin-Caballero, J., Martínez, C., Lozano, J.J., Ampurdanés, C., López-Contreras, A.J., Florensa, L., Navarro, J., Ottina, E., et al. (2015). PARP-2 sustains erythropoiesis in mice by limiting replicative stress in erythroid progenitors. Cell Death Differ. *22*, 1144–1157.

Flodgren, E., Bengtsson, S., Knutsson, M., Strebkova, E.A., Kidd, A.H., Alexeyev, O.A., and Kidd-Ljunggren, K. (2000). Recent high incidence of fulminant hepatitis in Samara, Russia: molecular analysis of prevailing hepatitis B and D virus strains. J. Clin. Microbiol. *38*, 3311–3316.

Forner, A., Llovet, J.M., and Bruix, J. (2012). Hepatocellular carcinoma. Lancet Lond. Engl. *379*, 1245–1255.

Frana, M.F., Behnke, J.N., Sturman, L.S., and Holmes, K.V. (1985). Proteolytic cleavage of the E2 glycoprotein of murine coronavirus: host-dependent differences in proteolytic cleavage and cell fusion. J. Virol. *56*, 912–920.

Galanos, C., Freudenberg, M.A., and Reutter, W. (1979). Galactosamine-induced sensitization to the lethal effects of endotoxin. Proc. Natl. Acad. Sci. U. S. A. *76*, 5939–5943.

Galluzzi, L., Vitale, I., Abrams, J.M., Alnemri, E.S., Baehrecke, E.H., Blagosklonny, M.V., Dawson, T.M., Dawson, V.L., El-Deiry, W.S., Fulda, S., et al. (2012). Molecular definitions of cell death subroutines: recommendations of the Nomenclature Committee on Cell Death 2012. Cell Death Differ. *19*, 107–120.

Galluzzi, L., Bravo-San Pedro, J.M., Vitale, I., Aaronson, S.A., Abrams, J.M., Adam, D., Alnemri, E.S., Altucci, L., Andrews, D., Annicchiarico-Petruzzelli, M., et al. (2015). Essential versus accessory aspects of cell death: recommendations of the NCCD 2015. Cell Death Differ. *22*, 58–73.

Gantner, F., Leist, M., Lohse, A.W., Germann, P.G., and Tiegs, G. (1995). Concanavalin A-induced T-cell-mediated hepatic injury in mice: the role of tumor necrosis factor. Hepatol. Baltim. Md *21*, 190–198.

Gao, B., and Bataller, R. (2011). Alcoholic liver disease: pathogenesis and new therapeutic targets. Gastroenterology *141*, 1572–1585.

Gao, B., Wang, H., Lafdil, F., and Feng, D. (2012). STAT proteins - key regulators of anti-viral responses, inflammation, and tumorigenesis in the liver. J. Hepatol. *57*, 430–441.

Geisler, F., Algül, H., Paxian, S., and Schmid, R.M. (2007). Genetic Inactivation of RelA/p65 Sensitizes Adult Mouse Hepatocytes to TNF-induced Apoptosis In Vivo and In Vitro. Gastroenterology *132*, 2489–2503.

Gentle, I.E., Wong, W.W.-L., Evans, J.M., Bankovacki, A., Cook, W.D., Khan, N.R., Nachbur, U., Rickard, J., Anderton, H., Moulin, M., et al. (2011). In TNF-stimulated cells, RIPK1 promotes cell survival by stabilizing TRAF2 and cIAP1, which limits induction of non-canonical NF-kappaB and activation of caspase-8. J. Biol. Chem. *286*, 13282–13291.

van Gerven, N.M., de Boer, Y.S., Mulder, C.J., van Nieuwkerk, C.M., and Bouma, G. (2016). Auto immune hepatitis. World J. Gastroenterol. *22*, 4651–4661.

Godfraind, C., and Coutelier, J.P. (1998). Morphological analysis of mouse hepatitis virus A59-induced pathology with regard to viral receptor expression. Histol. Histopathol. *13*, 181–199.

Godfraind, C., Langreth, S.G., Cardellichio, C.B., Knobler, R., Coutelier, J.P., Dubois-Dalcq, M., and Holmes, K.V. (1995). Tissue and cellular distribution of an adhesion molecule in the carcinoembryonic antigen family that serves as a receptor for mouse hepatitis virus. Lab. Investig. J. Tech. Methods Pathol. *73*, 615–627.

Greenhalgh, S.N., Conroy, K.P., and Henderson, N.C. (2015). Cre-ativity in the liver: transgenic approaches to targeting hepatic nonparenchymal cells. Hepatol. Baltim. Md *61*, 2091–2099.

Groux, H., Bigler, M., de Vries, J.E., and Roncarolo, M.G. (1996). Interleukin-10 induces a long-term antigen-specific anergic state in human CD4+ T cells. J. Exp. Med. *184*, 19–29.

Guidotti, L.G., and Chisari, F.V. (1996). To kill or to cure: options in host defense against viral infection. Curr. Opin. Immunol. *8*, 478–483.

Han, D., Ybanez, M.D., Ahmadi, S., Yeh, K., and Kaplowitz, N. (2009). Redox regulation of tumor necrosis factor signaling. Antioxid. Redox Signal. *11*, 2245–2263.

Heymann, F., and Tacke, F. (2016). Immunology in the liver--from homeostasis to disease. Nat. Rev. Gastroenterol. Hepatol. *13*, 88–110.

Hsu, H., Huang, J., Shu, H.B., Baichwal, V., and Goeddel, D.V. (1996). TNF-dependent recruitment of the protein kinase RIP to the TNF receptor-1 signaling complex. Immunity *4*, 387–396.

Huang, D.C., Hahne, M., Schroeter, M., Frei, K., Fontana, A., Villunger, A., Newton, K., Tschopp, J., and Strasser, A. (1999). Activation of Fas by FasL induces apoptosis by a mechanism that cannot be blocked by Bcl-2 or Bcl-x(L). Proc. Natl. Acad. Sci. U. S. A. *96*, 14871–14876.

Huebener, P., Pradere, J.-P., Hernandez, C., Gwak, G.-Y., Caviglia, J.M., Mu, X., Loike, J.D., Jenkins, R.E., Antoine, D.J., and Schwabe, R.F. (2015). The HMGB1/RAGE axis triggers neutrophil-mediated injury amplification following necrosis. J. Clin. Invest. *125*, 539–550.

Humphries, F., Yang, S., Wang, B., and Moynagh, P.N. (2015). RIP kinases: key decision makers in cell death and innate immunity. Cell Death Differ. *22*, 225–236.

Ibrahim, S.H., Hirsova, P., Malhi, H., and Gores, G.J. (2016). Animal Models of Nonalcoholic Steatohepatitis: Eat, Delete, and Inflame. Dig. Dis. Sci. *61*, 1325–1336.

Ichai, P., and Samuel, D. (2011). Epidemiology of liver failure. Clin. Res. Hepatol. Gastroenterol. *35*, 610–617.

Ilan, Y. (2012). Leaky gut and the liver: a role for bacterial translocation in nonalcoholic steatohepatitis. World J. Gastroenterol. *18*, 2609–2618.

Inokuchi-Shimizu, S., Park, E.J., Roh, Y.S., Yang, L., Zhang, B., Song, J., Liang, S., Pimienta, M., Taniguchi, K., Wu, X., et al. (2014). TAK1-mediated autophagy and fatty acid oxidation prevent hepatosteatosis and tumorigenesis. J. Clin. Invest. *124*, 3566–3578.

Iredale, J.P. (2007). Models of liver fibrosis: exploring the dynamic nature of inflammation and repair in a solid organ. J. Clin. Invest. *117*, 539–548.

Isabelle, M., Moreel, X., Gagné, J.-P., Rouleau, M., Ethier, C., Gagné, P., Hendzel, M.J., and Poirier, G.G. (2010). Investigation of PARP-1, PARP-2, and PARG interactomes by affinity-purification mass spectrometry. Proteome Sci. *8*, 22.

Iyer, S., Upadhyay, P.K., Majumdar, S.S., and Nagarajan, P. (2015). Animal Models Correlating Immune Cells for the Development of NAFLD/NASH. J. Clin. Exp. Hepatol. *5*, 239–245.

Jacques, A., Bleau, C., Martin, J.-P., and Lamontagne, L. (2008). Intrahepatic endothelial and Kupffer cells involved in immunosuppressive cytokines and natural killer (NK)/NK T cell disorders in viral acute hepatitis. Clin. Exp. Immunol. *152*, 298–310.

Janssen, H.L.A., Higuchi, H., Abdulkarim, A., and Gores, G.J. (2003). Hepatitis B virus enhances tumor necrosis factor-related apoptosis-inducing ligand (TRAIL) cytotoxicity by increasing TRAIL-R1/death receptor 4 expression. J. Hepatol. *39*, 414–420.

Jost, P.J., Grabow, S., Gray, D., McKenzie, M.D., Nachbur, U., Huang, D.C.S., Bouillet, P., Thomas, H.E., Borner, C., Silke, J., et al. (2009). XIAP discriminates between type I and type II FAS-induced apoptosis. Nature *460*, 1035–1039.

Jouan-Lanhouet, S. (2011). Modèles de nécroptose induite par TRAIL (TNF-Related Apoptosis Inducing Ligand) in vitro et in vivo. Université de Rennes1.

Jouan-Lanhouet, S., Arshad, M.I., Piquet-Pellorce, C., Martin-Chouly, C., Le Moigne-Muller, G., Van Herreweghe, F., Takahashi, N., Sergent, O., Lagadic-Gossmann, D., Vandenabeele, P., et al. (2012). TRAIL induces necroptosis involving RIPK1/RIPK3-dependent PARP-1 activation. Cell Death Differ. *19*, 2003–2014.

Jouan-Lanhouet, S., Riquet, F., Duprez, L., Vanden Berghe, T., Takahashi, N., and Vandenabeele, P. (2014a). Necroptosis, in vivo detection in experimental disease models. Semin. Cell Dev. Biol. *35*, 2–13.

Jouan-Lanhouet, S., Riquet, F., Duprez, L., Vanden Berghe, T., Takahashi, N., and Vandenabeele, P. (2014b). Necroptosis, in vivo detection in experimental disease models. Semin. Cell Dev. Biol. *35*, 2–13.

Kaiser, W.J., Daley-Bauer, L.P., Thapa, R.J., Mandal, P., Berger, S.B., Huang, C., Sundararajan, A., Guo, H., Roback, L., Speck, S.H., et al. (2014). RIP1 suppresses innate immune necrotic as well as apoptotic cell death during mammalian parturition. Proc. Natl. Acad. Sci. U. S. A. *111*, 7753–7758.

Kamata, H., Honda, S.-I., Maeda, S., Chang, L., Hirata, H., and Karin, M. (2005). Reactive oxygen species promote TNFalpha-induced death and sustained JNK activation by inhibiting MAP kinase phosphatases. Cell *120*, 649–661.

Kanda, D., Takagi, H., Toyoda, M., Horiguchi, N., Nakajima, H., Otsuka, T., and Mori, M. (2002). Transforming growth factor alpha protects against Fas-mediated liver apoptosis in mice. FEBS Lett. *519*, 11–15.

Kaneko, Y., Harada, M., Kawano, T., Yamashita, M., Shibata, Y., Gejyo, F., Nakayama, T., and Taniguchi, M. (2000). Augmentation of Valpha14 NKT cell-mediated cytotoxicity by interleukin 4 in an autocrine mechanism resulting in the development of concanavalin A-induced hepatitis. J. Exp. Med. *191*, 105–114.

Kang, Y.J., Bang, B.-R., Han, K.H., Hong, L., Shim, E.-J., Ma, J., Lerner, R.A., and Otsuka, M. (2015). Regulation of NKT cell-mediated immune responses to tumours and liver inflammation by mitochondrial PGAM5-Drp1 signalling. Nat. Commun. *6*, 8371.

Kaplowitz, N., Win, S., Than, T.A., Liu, Z.-X., and Dara, L. (2015). Targeting signal transduction pathways which regulate necrosis in acetaminophen hepatotoxicity. J. Hepatol. *63*, 5–7.

Kato, H., Takeuchi, O., Sato, S., Yoneyama, M., Yamamoto, M., Matsui, K., Uematsu, S., Jung, A., Kawai, T., Ishii, K.J., et al. (2006). Differential roles of MDA5 and RIG-I helicases in the recognition of RNA viruses. Nature *441*, 101–105.

Kawano, T., Cui, J., Koezuka, Y., Toura, I., Kaneko, Y., Motoki, K., Ueno, H., Nakagawa, R., Sato, H., Kondo, E., et al. (1997). CD1d-restricted and TCR-mediated activation of valpha14 NKT cells by glycosylceramides. Science *278*, 1626–1629.

Kelliher, M.A., Grimm, S., Ishida, Y., Kuo, F., Stanger, B.Z., and Leder, P. (1998). The death domain kinase RIP mediates the TNF-induced NF-kappaB signal. Immunity *8*, 297–303.

Kerr, J.F., Wyllie, A.H., and Currie, A.R. (1972). Apoptosis: a basic biological phenomenon with wide-ranging implications in tissue kinetics. Br. J. Cancer *26*, 239–257.

Klugewitz, K., Adams, D.H., Emoto, M., Eulenburg, K., and Hamann, A. (2004). The composition of intrahepatic lymphocytes: shaped by selective recruitment? Trends Immunol. *25*, 590–594.

Kondylis, V., Polykratis, A., Ehlken, H., Ochoa-Callejero, L., Straub, B.K., Krishna-Subramanian, S., Van, T.-M., Curth, H.-M., Heise, N., Weih, F., et al. (2015). NEMO Prevents Steatohepatitis and Hepatocellular Carcinoma by Inhibiting RIPK1 Kinase Activity-Mediated Hepatocyte Apoptosis. Cancer Cell *28*, 582–598.

Kumar, H., Koyama, S., Ishii, K.J., Kawai, T., and Akira, S. (2008). Cutting edge: cooperation of IPS-1- and TRIF-dependent pathways in poly IC-enhanced antibody production and cytotoxic T cell responses. J. Immunol. Baltim. Md 1950 *180*, 683–687.

Künstle, G., Hentze, H., Germann, P.-G., Tiegs, G., Meergans, T., and Wendel, A. (1999). Concanavalin A hepatotoxicity in mice: Tumor necrosis factor-mediated organ failure independent of caspase-3-like protease activation. Hepatology *30*, 1241–1251.

Küsters, S., Tiegs, G., Alexopoulou, L., Pasparakis, M., Douni, E., Künstle, G., Bluethmann, H., Wendel, A., Pfizenmaier, K., Kollias, G., et al. (1997). In vivo evidence for a functional role of both tumor necrosis factor (TNF) receptors and transmembrane TNF in experimental hepatitis. Eur. J. Immunol. *27*, 2870–2875.

Lacronique, V., Mignon, A., Fabre, M., Viollet, B., Rouquet, N., Molina, T., Porteu, A., Henrion, A., Bouscary, D., Varlet, P., et al. (1996). Bcl-2 protects from lethal hepatic apoptosis induced by an anti-Fas antibody in mice. Nat. Med. *2*, 80–86.

Lamontagne, L.M., and Dupuy, J.M. (1984). Persistent infection with mouse hepatitis virus 3 in mouse lymphoid cell lines. Infect. Immun. *44*, 716–723.

Lamontagne, L., Descoteaux, J.P., and Jolicoeur, P. (1989). Mouse hepatitis virus 3 replication in T and B lymphocytes correlate with viral pathogenicity. J. Immunol. Baltim. Md 1950 *142*, 4458–4465.

Lautier, D., Lagueux, J., Thibodeau, J., Ménard, L., and Poirier, G.G. (1993). Molecular and biochemical features of poly (ADP-ribose) metabolism. Mol. Cell. Biochem. *122*, 171–193.

Lauwerys, B.R., Garot, N., Renauld, J.C., and Houssiau, F.A. (2000). Cytokine production and killer activity of NK/T-NK cells derived with IL-2, IL-15, or the combination of IL-12 and IL-18. J. Immunol. Baltim. Md 1950 *165*, 1847–1853.

LeBlanc, H.N., and Ashkenazi, A. (2003). Apo2L/TRAIL and its death and decoy receptors. Cell Death Differ. *10*, 66–75.

Leist, M., Gantner, F., Künstle, G., Bohlinger, I., Tiegs, G., Bluethmann, H., and Wendel, A. (1996). The 55-kD tumor necrosis factor receptor and CD95 independently signal murine hepatocyte apoptosis and subsequent liver failure. Mol. Med. Camb. Mass *2*, 109–124.

Liang, X., Liu, Y., Zhang, Q., Gao, L., Han, L., Ma, C., Zhang, L., Chen, Y.H., and Sun, W. (2007). Hepatitis B virus sensitizes hepatocytes to TRAIL-induced apoptosis through Bax. J. Immunol. Baltim. Md 1950 *178*, 503–510.

Liedtke, C., and Trautwein, C. (2012). The role of TNF and Fas dependent signaling in animal models of inflammatory liver injury and liver cancer. Eur. J. Cell Biol. *91*, 582–589.

Liedtke, C., Bangen, J.-M., Freimuth, J., Beraza, N., Lambertz, D., Cubero, F.J., Hatting, M., Karlmark, K.R., Streetz, K.L., Krombach, G.A., et al. (2011). Loss of caspase-8 protects mice against inflammation-related hepatocarcinogenesis but induces non-apoptotic liver injury. Gastroenterology *141*, 2176–2187.

Lin, Y., Devin, A., Cook, A., Keane, M.M., Kelliher, M., Lipkowitz, S., and Liu, Z.G. (2000). The death domain kinase RIP is essential for TRAIL (Apo2L)-induced activation of IkappaB kinase and c-Jun N-terminal kinase. Mol. Cell. Biol. *20*, 6638–6645.

Liu, X., Shi, F., Li, Y., Yu, X., Peng, S., Li, W., Luo, X., and Cao, Y. (2016). Post-translational modifications as key regulators of TNF-induced necroptosis. Cell Death Dis. *7*, e2293.

Liu, Y.-G., Liu, S.-X., Liang, X.-H., Zhang, Q., Gao, L.-F., Han, L.-H., Cao, Y.-L., Hou, N., Du, J., and Sun, W.-S. (2007). Blockade of TRAIL pathway ameliorates HBV-induced hepatocyte apoptosis in an acute hepatitis model. Biochem. Biophys. Res. Commun. *352*, 329–334.

Louvet, A., and Mathurin, P. (2015). Alcoholic liver disease: mechanisms of injury and targeted treatment. Nat. Rev. Gastroenterol. Hepatol. *12*, 231–242.

Luedde, T., Liedtke, C., Manns, M.P., and Trautwein, C. (2002). Losing balance: cytokine signaling and cell death in the context of hepatocyte injury and hepatic failure. Eur. Cytokine Netw. *13*, 377–383.

Luedde, T., Beraza, N., Kotsikoris, V., van Loo, G., Nenci, A., De Vos, R., Roskams, T., Trautwein, C., and Pasparakis, M. (2007). Deletion of NEMO/IKKgamma in liver parenchymal cells causes steatohepatitis and hepatocellular carcinoma. Cancer Cell *11*, 119–132.

Luedde, T., Kaplowitz, N., and Schwabe, R.F. (2014). Cell death and cell death responses in liver disease: mechanisms and clinical relevance. Gastroenterology *147*, 765–783.e4.

MacSween, R.N.M., Anthony, P.P., Scheuer, P.J., Burt, A.D., and Portmann, B.C. (1994). Pathology of the Liver (Churchill Livingstone).

Maeda, S., Chang, L., Li, Z.-W., Luo, J.-L., Leffert, H., and Karin, M. (2003). IKKbeta is required for prevention of apoptosis mediated by cell-bound but not by circulating TNFalpha. Immunity *19*, 725–737.

Malhi, H., Guicciardi, M.E., and Gores, G.J. (2010). Hepatocyte death: a clear and present danger. Physiol. Rev. *90*, 1165–1194.

Marinos, G., Naoumov, N.V., Rossol, S., Torre, F., Wong, P.Y., Gallati, H., Portmann, B., and Williams, R. (1995). Tumor necrosis factor receptors in patients with chronic hepatitis B virus infection. Gastroenterology *108*, 1453–1463.

Martin, J.P., Chen, W., Koehren, F., and Pereira, C.A. (1994). The virulence of mouse hepatitis virus 3, as evidenced by permissivity of cultured hepatic cells toward escape mutants. Res. Virol. *145*, 297–302.

McVicker, B.L., Tuma, D.J., and Casey, C.A. (2007). Effect of ethanol on pro-apoptotic mechanisms in polarized hepatic cells. World J. Gastroenterol. *13*, 4960–4966.

Meylan, E., Burns, K., Hofmann, K., Blancheteau, V., Martinon, F., Kelliher, M., and Tschopp, J. (2004). RIP1 is an essential mediator of Toll-like receptor 3-induced NF-kappa B activation. Nat. Immunol. *5*, 503–507.

Minagawa, M., Deng, Q., Liu, Z.-X., Tsukamoto, H., and Dennert, G. (2004). Activated natural killer T cells induce liver injury by Fas and tumor necrosis factor-alpha during alcohol consumption. Gastroenterology *126*, 1387–1399.

Mitchell, J.R., Jollow, D.J., Potter, W.Z., Davis, D.C., Gillette, J.R., and Brodie, B.B. (1973). Acetaminophen-induced hepatic necrosis. I. Role of drug metabolism. J. Pharmacol. Exp. Ther. *187*, 185–194.

Mizuhara, H., O'Neill, E., Seki, N., Ogawa, T., Kusunoki, C., Otsuka, K., Satoh, S., Niwa, M., Senoh, H., and Fujiwara, H. (1994). T cell activation-associated hepatic injury: mediation by tumor necrosis factors and protection by interleukin 6. J. Exp. Med. *179*, 1529–1537.

Mundt, B., Kühnel, F., Zender, L., Paul, Y., Tillmann, H., Trautwein, C., Manns, M.P., and Kubicka, S. (2003). Involvement of TRAIL and its receptors in viral hepatitis. FASEB J. Off. Publ. Fed. Am. Soc. Exp. Biol. *17*, 94–96.

Nagaki, M., Naiki, T., Brenner, D.A., Osawa, Y., Imose, M., Hayashi, H., Banno, Y., Nakashima, S., and Moriwaki, H. (2000). Tumor necrosis factor alpha prevents tumor necrosis factor receptor-mediated mouse hepatocyte apoptosis, but not fas-mediated apoptosis: role of nuclear factor-kappaB. Hepatol. Baltim. Md *32*, 1272–1279.

Nakashima, H., Kinoshita, M., Nakashima, M., Habu, Y., Shono, S., Uchida, T., Shinomiya, N., and Seki, S. (2008). Superoxide produced by Kupffer cells is an essential effector in concanavalin A-induced hepatitis in mice. Hepatol. Baltim. Md *48*, 1979–1988.

Natori, T., Koezuka, Y., and Higa, T. (1993). Agelasphins, novel α-galactosylceramides from the marine sponge Agelas mauritianus. Tetrahedron Lett. *34*, 5591–5592.

Noel, G., Arshad, M.I., Filliol, A., Genet, V., Rauch, M., Lucas-Clerc, C., Lehuen, A., Girard, J.-P., Piquet-Pellorce, C., and Samson, M. (2016). Ablation of interaction between IL-33 and ST2+ regulatory T cells increases immune cell-mediated hepatitis and activated NK cell liver infiltration. Am. J. Physiol. Gastrointest. Liver Physiol. *311*, G313-323.

O'Donnell, M.A., Legarda-Addison, D., Skountzos, P., Yeh, W.C., and Ting, A.T. (2007). Ubiquitination of RIP1 regulates an NF-kappaB-independent cell-death switch in TNF signaling. Curr. Biol. CB *17*, 418–424.

Ofengeim, D., and Yuan, J. (2013). Regulation of RIP1 kinase signalling at the crossroads of inflammation and cell death. Nat. Rev. Mol. Cell Biol. *14*, 727–736.

Ogasawara, J., Watanabe-Fukunaga, R., Adachi, M., Matsuzawa, A., Kasugai, T., Kitamura, Y., Itoh, N., Suda, T., and Nagata, S. (1993). Lethal effect of the anti-Fas antibody in mice. Nature *364*, 806–809.

Oliver, A.W., Amé, J.-C., Roe, S.M., Good, V., de Murcia, G., and Pearl, L.H. (2004). Crystal structure of the catalytic fragment of murine poly(ADP-ribose) polymerase-2. Nucleic Acids Res. *32*, 456–464.

Oppenheim, J.J. (2001). Cytokines: past, present, and future. Int. J. Hematol. *74*, 3–8.

Osman, Y., Kawamura, T., Naito, T., Takeda, K., Van Kaer, L., Okumura, K., and Abo, T. (2000). Activation of hepatic NKT cells and subsequent liver injury following administration of alpha-galactosylceramide. Eur. J. Immunol. *30*, 1919–1928.

Panaro, F., Andorno, E., Morelli, N., Casaccia, M., Bottino, G., Ravazzoni, F., Centanaro, M., Ornis, S., and Valente, U. (2006). Liver transplantation represents the optimal treatment for fulminant hepatic failure from Amanita phalloides poisoning. Transpl. Int. Off. J. Eur. Soc. Organ Transplant. *19*, 344–345.

Patil, M., Sheth, K.A., Krishnamurthy, A.C., and Devarbhavi, H. (2013). A review and current perspective on Wilson disease. J. Clin. Exp. Hepatol. *3*, 321–336.

Peng, H., and Tian, Z. (2015). Re-examining the origin and function of liver-resident NK cells. Trends Immunol. *36*, 293–299.

Powell, L.W., Seckington, R.C., and Deugnier, Y. (2016). Haemochromatosis. Lancet Lond. Engl. *388*, 706–716.

Prévost, C.L., Virelizier, J.L., and Dupuy, J.M. (1975). Immunopathology of mouse hepatitis virus type 3 infection. III. Clinical and virologic observation of a persistent viral infection. J. Immunol. Baltim. Md 1950 *115*, 640–643.

Racanelli, V., and Rehermann, B. (2006). The liver as an immunological organ. Hepatol. Baltim. Md *43*, S54-62.

Ram, D.R., Ilyukha, V., Volkova, T., Buzdin, A., Tai, A., Smirnova, I., and Poltorak, A. (2016). Balance between short and long isoforms of cFLIP regulates Fas-mediated apoptosis in vivo. Proc. Natl. Acad. Sci. U. S. A. *113*, 1606–1611.

Ramachandran, A., McGill, M.R., Xie, Y., Ni, H.-M., Ding, W.-X., and Jaeschke, H. (2013). Receptor interacting protein kinase 3 is a critical early mediator of acetaminophen-induced hepatocyte necrosis in mice. Hepatol. Baltim. Md *58*, 2099–2108.

Rehm, J., Mathers, C., Popova, S., Thavorncharoensap, M., Teerawattananon, Y., and Patra, J. (2009). Global burden of disease and injury and economic cost attributable to alcohol use and alcohol-use disorders. Lancet Lond. Engl. *373*, 2223–2233.

Rickard, J.A., O'Donnell, J.A., Evans, J.M., Lalaoui, N., Poh, A.R., Rogers, T., Vince, J.E., Lawlor, K.E., Ninnis, R.L., Anderton, H., et al. (2014). RIPK1 Regulates RIPK3-MLKL-Driven Systemic Inflammation and Emergency Hematopoiesis. Cell *157*, 1175–1188.

Rivera, C.A., Adegboyega, P., van Rooijen, N., Tagalicud, A., Allman, M., and Wallace, M. (2007). Toll-like receptor-4 signaling and Kupffer cells play pivotal roles in the pathogenesis of non-alcoholic steatohepatitis. J. Hepatol. *47*, 571–579.

Robinson, M.W., Harmon, C., and O'Farrelly, C. (2016). Liver immunology and its role in inflammation and homeostasis. Cell. Mol. Immunol. *13*, 267–276.

Roderick, J.E., Hermance, N., Zelic, M., Simmons, M.J., Polykratis, A., Pasparakis, M., and Kelliher, M.A. (2014). Hematopoietic RIPK1 deficiency results in bone marrow failure caused by apoptosis and RIPK3-mediated necroptosis. Proc. Natl. Acad. Sci. U. S. A. *111*, 14436–14441.

Rodriguez, I., Matsuura, K., Khatib, K., Reed, J.C., Nagata, S., and Vassalli, P. (1996). A bcl-2 transgene expressed in hepatocytes protects mice from fulminant liver destruction but not from rapid death induced by anti-Fas antibody injection. J. Exp. Med. *183*, 1031–1036.

Roychowdhury, S., Chiang, D.J., Mandal, P., McMullen, M.R., Liu, X., Cohen, J.I., Pollard, J., Feldstein, A.E., and Nagy, L.E. (2012). Inhibition of apoptosis protects mice from ethanol-mediated acceleration of early markers of CCl4 -induced fibrosis but not steatosis or inflammation. Alcohol. Clin. Exp. Res. *36*, 1139–1147.

Roychowdhury, S., McMullen, M.R., Pisano, S.G., Liu, X., and Nagy, L.E. (2013). Absence of receptor interacting protein kinase 3 prevents ethanol-induced liver injury. Hepatol. Baltim. Md *57*, 1773–1783.

Saitou, Y., Shiraki, K., Fuke, H., Inoue, T., Miyashita, K., Yamanaka, Y., Yamaguchi, Y., Yamamoto, N., Ito, K., Sugimoto, K., et al. (2005). Involvement of tumor necrosis factor-related apoptosis-inducing ligand and tumor necrosis factor-related apoptosis-inducing ligand receptors in viral hepatic diseases. Hum. Pathol. *36*, 1066–1073.

Saliba, F., and Samuel, D. (2013). Acute liver failure: current trends. J. Hepatol. *59*, 6–8.

Sarin, S.K., and Choudhury, A. (2016). Acute-on-chronic liver failure: terminology, mechanisms and management. Nat. Rev. Gastroenterol. Hepatol. *13*, 131–149.

Sato, A., Nakashima, H., Nakashima, M., Ikarashi, M., Nishiyama, K., Kinoshita, M., and Seki, S. (2014). Involvement of the TNF and FasL produced by CD11b Kupffer cells/macrophages in CCl4-induced acute hepatic injury. PloS One *9*, e92515.

Schattenberg, J.M., Zimmermann, T., Wörns, M., Sprinzl, M.F., Kreft, A., Kohl, T., Nagel, M., Siebler, J., Schulze-Bergkamen, H., He, Y.-W., et al. (2011). Ablation of c-FLIP in hepatocytes enhances death-receptor mediated apoptosis and toxic liver injury in vivo. J. Hepatol. *55*, 1272–1280.

Schindler, L., Brücher, J., and Kirchner, H. (1984). Protection of mice against infection with mouse hepatitis virus type 3 by injection of silica. Immunobiology *166*, 62–71.

Schneider, A.T., Gautheron, J., Tacke, F., Vucur, M., and Luedde, T. (2016). Receptor interacting protein kinase 1 (RIPK1) in hepatocytes does not mediate murine acetaminophen toxicity. Hepatol. Baltim. Md *64*, 306–308.

Schneider, P., Holler, N., Bodmer, J.L., Hahne, M., Frei, K., Fontana, A., and Tschopp, J. (1998). Conversion of membrane-bound Fas(CD95) ligand to its soluble form is associated with downregulation of its proapoptotic activity and loss of liver toxicity. J. Exp. Med. *187*, 1205–1213.

Schüngel, S., Buitrago-Molina, L.E., Nalapareddy, P. devi, Lebofsky, M., Manns, M.P., Jaeschke, H., Gross, A., and Vogel, A. (2009). The strength of the Fas ligand signal determines whether hepatocytes act as type 1 or type 2 cells in murine livers. Hepatol. Baltim. Md *50*, 1558–1566.

Schwabe, R.F., and Brenner, D.A. (2006). Mechanisms of Liver Injury. I. TNF-alpha-induced liver injury: role of IKK, JNK, and ROS pathways. Am. J. Physiol. Gastrointest. Liver Physiol. *290*, G583-589.

Schwabe, R.F., Seki, E., and Brenner, D.A. (2006). Toll-like receptor signaling in the liver. Gastroenterology *130*, 1886–1900.

Seino, K., Kayagaki, N., Takeda, K., Fukao, K., Okumura, K., and Yagita, H. (1997). Contribution of Fas ligand to T cell-mediated hepatic injury in mice. Gastroenterology *113*, 1315–1322.

Sekiguchi, S., Kimura, K., Chiyo, T., Ohtsuki, T., Tobita, Y., Tokunaga, Y., Yasui, F., Tsukiyama-Kohara, K., Wakita, T., Tanaka, T., et al. (2012). Immunization with a recombinant vaccinia virus that encodes nonstructural proteins of the hepatitis C virus suppresses viral protein levels in mouse liver. PloS One *7*, e51656.

Shalini, S., Dorstyn, L., Dawar, S., and Kumar, S. (2015). Old, new and emerging functions of caspases. Cell Death Differ. *22*, 526–539.

Shepard, B.D., and Badley, A.D. (2009). The Biology of TRAIL and the Role of TRAIL-Based Therapeutics in Infectious Diseases. Anti-Infect. Agents Med. Chem. *8*, 87–101.

Shieh, W.M., Amé, J.C., Wilson, M.V., Wang, Z.Q., Koh, D.W., Jacobson, M.K., and Jacobson, E.L. (1998). Poly(ADP-ribose) polymerase null mouse cells synthesize ADP-ribose polymers. J. Biol. Chem. *273*, 30069–30072.

Shutinoski, B., Alturki, N.A., Rijal, D., Bertin, J., Gough, P.J., Schlossmacher, M.G., and Sad, S. (2016). K45A mutation of RIPK1 results in poor necroptosis and cytokine signaling in macrophages, which impacts inflammatory responses in vivo. Cell Death Differ. *23*, 1628–1637.

Silke, J., Rickard, J.A., and Gerlic, M. (2015). The diverse role of RIP kinases in necroptosis and inflammation. Nat. Immunol. *16*, 689–697.

Si-Tayeb, K., Lemaigre, F.P., and Duncan, S.A. (2010). Organogenesis and development of the liver. Dev. Cell *18*, 175–189.

Slauenwhite, D., and Johnston, B. (2015). Regulation of NKT Cell Localization in Homeostasis and Infection. Front. Immunol. *6*, 255.

Spruss, A., Kanuri, G., Wagnerberger, S., Haub, S., Bischoff, S.C., and Bergheim, I. (2009). Toll-like receptor 4 is involved in the development of fructose-induced hepatic steatosis in mice. Hepatol. Baltim. Md *50*, 1094–1104.

Stanger, B.Z., Leder, P., Lee, T.H., Kim, E., and Seed, B. (1995). RIP: a novel protein containing a death domain that interacts with Fas/APO-1 (CD95) in yeast and causes cell death. Cell *81*, 513–523.

Sturman, L.S., Ricard, C.S., and Holmes, K.V. (1985). Proteolytic cleavage of the E2 glycoprotein of murine coronavirus: activation of cell-fusing activity of virions by trypsin and separation of two different 90K cleavage fragments. J. Virol. *56*, 904–911.

Subramanian, M., Kini, R., Madasu, M., Ohta, A., Nowak, M., Exley, M., Sitkovsky, M., and Ohta, A. (2014). Extracellular adenosine controls NKT-cell-dependent hepatitis induction. Eur. J. Immunol. *44*, 1119–1129.

Swain, M.G. (2008). Hepatic NKT cells: friend or foe? Clin. Sci. Lond. Engl. 1979 *114*, 457–466.

Szántó, M., Brunyánszki, A., Márton, J., Vámosi, G., Nagy, L., Fodor, T., Kiss, B., Virág, L., Gergely, P., and Bai, P. (2014). Deletion of PARP-2 induces hepatic cholesterol accumulation and decrease in HDL levels. Biochim. Biophys. Acta BBA - Mol. Basis Dis. *1842*, 594–602.

Tacke, F., and Zimmermann, H.W. (2014). Macrophage heterogeneity in liver injury and fibrosis. J. Hepatol. *60*, 1090–1096.

Tagawa, Y., Sekikawa, K., and Iwakura, Y. (1997). Suppression of concanavalin A-induced hepatitis in IFN-gamma(-/-) mice, but not in TNF-alpha(-/-) mice: role for IFN-gamma in activating apoptosis of hepatocytes. J. Immunol. Baltim. Md 1950 *159*, 1418–1428.

Takahashi, N., Duprez, L., Grootjans, S., Cauwels, A., Nerinckx, W., DuHadaway, J.B., Goossens, V., Roelandt, R., Van Hauwermeiren, F., Libert, C., et al. (2012). Necrostatin-1 analogues: critical issues on the specificity, activity and in vivo use in experimental disease models. Cell Death Dis. *3*, e437.

Takahashi, N., Vereecke, L., Bertrand, M.J.M., Duprez, L., Berger, S.B., Divert, T., Gonçalves, A., Sze, M., Gilbert, B., Kourula, S., et al. (2014). RIPK1 ensures intestinal homeostasis by protecting the epithelium against apoptosis. Nature *513*, 95–99.

Takeda, K., Hayakawa, Y., Van Kaer, L., Matsuda, H., Yagita, H., and Okumura, K. (2000). Critical contribution of liver natural killer T cells to a murine model of hepatitis. Proc. Natl. Acad. Sci. U. S. A. *97*, 5498–5503.

Takemoto, K., Hatano, E., Iwaisako, K., Takeiri, M., Noma, N., Ohmae, S., Toriguchi, K., Tanabe, K., Tanaka, H., Seo, S., et al. (2014). Necrostatin-1 protects against reactive oxygen species (ROS)-induced hepatotoxicity in acetaminophen-induced acute liver failure. FEBS Open Bio *4*, 777–787.

Teng, X., Degterev, A., Jagtap, P., Xing, X., Choi, S., Denu, R., Yuan, J., and Cuny, G.D. (2005). Structure-activity relationship study of novel necroptosis inhibitors. Bioorg. Med. Chem. Lett. *15*, 5039–5044.

Thomson, A.W., and Knolle, P.A. (2010). Antigen-presenting cell function in the tolerogenic liver environment. Nat. Rev. Immunol. *10*, 753–766.

Tiegs, G., Hentschel, J., and Wendel, A. (1992). A T cell-dependent experimental liver injury in mice inducible by concanavalin A. J. Clin. Invest. *90*, 196–203.

Ting, A.T., and Bertrand, M.J.M. (2016). More to Life than NF-κB in TNFR1 Signaling. Trends Immunol. *37*, 535–545.

Tokushige, K., Yamaguchi, N., Ikeda, I., Hashimoto, E., Yamauchi, K., and Hayashi, N. (2000). Significance of soluble TNF receptor-I in acute-type fulminant hepatitis. Am. J. Gastroenterol. *95*, 2040–2046.

Trautwein, C., Rakemann, T., Malek, N.P., Plümpe, J., Tiegs, G., and Manns, M.P. (1998). Concanavalin A-induced liver injury triggers hepatocyte proliferation. J. Clin. Invest. *101*, 1960–1969.

Trebicka, J., Krag, A., Gansweid, S., Appenrodt, B., Schiedermaier, P., Sauerbruch, T., and Spengler, U. (2011). Endotoxin and tumor necrosis factor-receptor levels in portal and hepatic vein

of patients with alcoholic liver cirrhosis receiving elective transjugular intrahepatic portosystemic shunt. Eur. J. Gastroenterol. Hepatol. *23*, 1218–1225.

Troiani, S., Lupi, R., Perego, R., Depaolini, S.R., Thieffine, S., Bosotti, R., and Rusconi, L. (2011). Identification of candidate substrates for poly(ADP-ribose) polymerase-2 (PARP2) in the absence of DNA damage using high-density protein microarrays. FEBS J. *278*, 3676–3687.

Tsuchiya, Y., Nakabayashi, O., and Nakano, H. (2015). FLIP the Switch: Regulation of Apoptosis and Necroptosis by cFLIP. Int. J. Mol. Sci. *16*, 30321–30341.

Uesugi, T., Froh, M., Arteel, G.E., Bradford, B.U., and Thurman, R.G. (2001). Toll-like receptor 4 is involved in the mechanism of early alcohol-induced liver injury in mice. Hepatol. Baltim. Md *34*, 101–108.

Van Kaer, L. (2005). alpha-Galactosylceramide therapy for autoimmune diseases: prospects and obstacles. Nat. Rev. Immunol. *5*, 31–42.

Vanden Berghe, T., Linkermann, A., Jouan-Lanhouet, S., Walczak, H., and Vandenabeele, P. (2014). Regulated necrosis: the expanding network of non-apoptotic cell death pathways. Nat. Rev. Mol. Cell Biol. *15*, 135–147.

Vanden Berghe, T., Kaiser, W.J., Bertrand, M.J., and Vandenabeele, P. (2015). Molecular crosstalk between apoptosis, necroptosis, and survival signaling. Mol. Cell. Oncol. *2*, e975093.

Vanlangenakker, N., Bertrand, M.J.M., Bogaert, P., Vandenabeele, P., and Vanden Berghe, T. (2011). TNF-induced necroptosis in L929 cells is tightly regulated by multiple TNFR1 complex I and II members. Cell Death Dis. *2*, e230.

Vick, B., Weber, A., Urbanik, T., Maass, T., Teufel, A., Krammer, P.H., Opferman, J.T., Schuchmann, M., Galle, P.R., and Schulze-Bergkamen, H. (2009). Knockout of myeloid cell leukemia-1 induces liver damage and increases apoptosis susceptibility of murine hepatocytes. Hepatol. Baltim. Md *49*, 627–636.

Vilcek, J., and Feldmann, M. (2004). Historical review: Cytokines as therapeutics and targets of therapeutics. Trends Pharmacol. Sci. *25*, 201–209.

Vince, J.E., Pantaki, D., Feltham, R., Mace, P.D., Cordier, S.M., Schmukle, A.C., Davidson, A.J., Callus, B.A., Wong, W.W.-L., Gentle, I.E., et al. (2009). TRAF2 must bind to cellular inhibitors of apoptosis for tumor necrosis factor (tnf) to efficiently activate nf-{kappa}b and to prevent tnf-induced apoptosis. J. Biol. Chem. *284*, 35906–35915.

Virág, L., Robaszkiewicz, A., Rodriguez-Vargas, J.M., and Oliver, F.J. (2013). Poly(ADP-ribose) signaling in cell death. Mol. Aspects Med. *34*, 1153–1167.

Virelizier, J.L., Dayan, A.D., and Allison, A.C. (1975). Neuropathological effects of persistent infection of mice by mouse hepatitis virus. Infect. Immun. *12*, 1127–1140.

Volarevic, V., Mitrovic, M., Milovanovic, M., Zelen, I., Nikolic, I., Mitrovic, S., Pejnovic, N., Arsenijevic, N., and Lukic, M.L. (2012). Protective role of IL-33/ST2 axis in Con A-induced hepatitis. J. Hepatol. *56*, 26–33.

Wajant, H., Pfizenmaier, K., and Scheurich, P. (2003). Tumor necrosis factor signaling. Cell Death Differ. *10*, 45–65.

Walczak, H., Miller, R.E., Ariail, K., Gliniak, B., Griffith, T.S., Kubin, M., Chin, W., Jones, J., Woodward, A., Le, T., et al. (1999). Tumoricidal activity of tumor necrosis factor−related apoptosis−inducing ligand in vivo. Nat. Med. *5*, 157–163.

Wang, H., Sun, L., Su, L., Rizo, J., Liu, L., Wang, L.-F., Wang, F.-S., and Wang, X. (2014). Mixed lineage kinase domain-like protein MLKL causes necrotic membrane disruption upon phosphorylation by RIP3. Mol. Cell *54*, 133–146.

Wang, L., Du, F., and Wang, X. (2008). TNF-alpha induces two distinct caspase-8 activation pathways. Cell *133*, 693–703.

Wang, S., Ni, H.-M., Dorko, K., Kumer, S.C., Schmitt, T.M., Nawabi, A., Komatsu, M., Huang, H., and Ding, W.-X. (2016). Increased hepatic receptor interacting protein kinase 3 expression due to impaired proteasomal functions contributes to alcohol-induced steatosis and liver injury. Oncotarget *7*, 17681–17698.

Wanner, G.A., Mica, L., Wanner-Schmid, E., Kolb, S.A., Hentze, H., Trentz, O., and Ertel, W. (1999). Inhibition of caspase activity prevents CD95-mediated hepatic microvascular perfusion failure and restores Kupffer cell clearance capacity. FASEB J. Off. Publ. Fed. Am. Soc. Exp. Biol. *13*, 1239–1248.

Watanabe, Y., Morita, M., and Akaike, T. (1996). Concanavalin A induces perforin-mediated but not Fas-mediated hepatic injury. Hepatology *24*, 702–710.

Weber, L.W.D., Boll, M., and Stampfl, A. (2003). Hepatotoxicity and mechanism of action of haloalkanes: carbon tetrachloride as a toxicological model. Crit. Rev. Toxicol. *33*, 105–136.

Weinlich, R., Oberst, A., Dillon, C.P., Janke, L.J., Milasta, S., Lukens, J.R., Rodriguez, D.A., Gurung, P., Savage, C., Kanneganti, T.D., et al. (2013). Protective roles for caspase-8 and cFLIP in adult homeostasis. Cell Rep. *5*, 340–348.

Weltin, D., Picard, V., Aupeix, K., Varin, M., Oth, D., Marchal, J., Dufour, P., and Bischoff, P. (1995). Immunosuppressive activities of 6(5H)-phenanthridinone, a new poly(ADP-ribose)polymerase inhibitor. Int. J. Immunopharmacol. *17*, 265–271.

Wolf, D., Hallmann, R., Sass, G., Sixt, M., Küsters, S., Fregien, B., Trautwein, C., and Tiegs, G. (2001). TNF-alpha-induced expression of adhesion molecules in the liver is under the control of TNFR1--relevance for concanavalin A-induced hepatitis. J. Immunol. Baltim. Md 1950 *166*, 1300–1307.

Wong, W.W.-L., Gentle, I.E., Nachbur, U., Anderton, H., Vaux, D.L., and Silke, J. (2010). RIPK1 is not essential for TNFR1-induced activation of NF-κB. Cell Death Differ. *17*, 482–487.

Wree, A., Mehal, W., and Feldstein, A. (2016). Targeting Cell Death and Sterile Inflammation Loop for the Treatment of Nonalcoholic Steatohepatitis. Semin. Liver Dis. *36*, 027–036.

Wroblewski, R., Armaka, M., Kondylis, V., Pasparakis, M., Walczak, H., Mittrücker, H.-W., Schramm, C., Lohse, A.W., Kollias, G., and Ehlken, H. (2016). Opposing role of tumor necrosis factor receptor 1 signaling in T cell-mediated hepatitis and bacterial infection in mice. Hepatol. Baltim. Md *64*, 508–521.

Wu, G.S., Burns, T.F., Zhan, Y., Alnemri, E.S., and El-Deiry, W.S. (1999). Molecular cloning and functional analysis of the mouse homologue of the KILLER/DR5 tumor necrosis factor-related apoptosis-inducing ligand (TRAIL) death receptor. Cancer Res. *59*, 2770–2775.

Xu, H., Li, H., Cao, D., Wu, Y., and Chen, Y. (2014). Tumor necrosis factor α (TNF-α) receptor-I is required for TNF-α-mediated fulminant virus hepatitis caused by murine hepatitis virus strain-3 infection. Immunol. Lett. *158*, 25–32.

Yang, C., Chen, Y., Guo, G., Li, H., Cao, D., Xu, H., Guo, S., Fei, L., Yan, W., Ning, Q., et al. (2013). Expression of B and T lymphocyte attenuator (BTLA) in macrophages contributes to the fulminant hepatitis caused by murine hepatitis virus strain-3. Gut *62*, 1204–1213.

Yélamos, J., Monreal, Y., Saenz, L., Aguado, E., Schreiber, V., Mota, R., Fuente, T., Minguela, A., Parrilla, P., de Murcia, G., et al. (2006). PARP-2 deficiency affects the survival of CD4+CD8+ double-positive thymocytes. EMBO J. *25*, 4350–4360.

Yélamos, J., Schreiber, V., and Dantzer, F. (2008). Toward specific functions of poly(ADP-ribose) polymerase-2. Trends Mol. Med. *14*, 169–178.

Yin, M., Wheeler, M.D., Kono, H., Bradford, B.U., Gallucci, R.M., Luster, M.I., and Thurman, R.G. (1999). Essential role of tumor necrosis factor alpha in alcohol-induced liver injury in mice. Gastroenterology *117*, 942–952.

Yoneyama, M., Kikuchi, M., Natsukawa, T., Shinobu, N., Imaizumi, T., Miyagishi, M., Taira, K., Akira, S., and Fujita, T. (2004). The RNA helicase RIG-I has an essential function in double-stranded RNA-induced innate antiviral responses. Nat. Immunol. *5*, 730–737.

Youn, H.S., Lee, J.Y., Fitzgerald, K.A., Young, H.A., Akira, S., and Hwang, D.H. (2005). Specific inhibition of MyD88-independent signaling pathways of TLR3 and TLR4 by resveratrol: molecular targets are TBK1 and RIP1 in TRIF complex. J. Immunol. Baltim. Md 1950 *175*, 3339–3346.

Zhang, D., Lin, J., and Han, J. (2010). Receptor-interacting protein (RIP) kinase family. Cell. Mol. Immunol. *7*, 243–249.

Zhang, H., Huang, C., Wang, Y., Lu, Z., Zhuang, N., Zhao, D., He, J., and Shi, L. (2015). Hepatitis B Virus X Protein Sensitizes TRAIL-Induced Hepatocyte Apoptosis by Inhibiting the E3 Ubiquitin Ligase A20. PloS One *10*, e0127329.

Zhang, Y.-F., He, W., Zhang, C., Liu, X.-J., Lu, Y., Wang, H., Zhang, Z.-H., Chen, X., and Xu, D.-X. (2014). Role of receptor interacting protein (RIP)1 on apoptosis-inducing factor-mediated necroptosis during acetaminophen-evoked acute liver failure in mice. Toxicol. Lett. *225*, 445–453.

Zheng, S.-J., Wang, P., Tsabary, G., and Chen, Y.H. (2004). Critical roles of TRAIL in hepatic cell death and hepatic inflammation. J. Clin. Invest. *113*, 58–64.

Zhou, Y., Dai, W., Lin, C., Wang, F., He, L., Shen, M., Chen, P., Wang, C., Lu, J., Xu, L., et al. (2013a). Protective Effects of Necrostatin-1 against Concanavalin A-Induced Acute Hepatic Injury in Mice. Mediators Inflamm. *2013*, 1–15.

Zhou, Y., Dai, W., Lin, C., Wang, F., He, L., Shen, M., Chen, P., Wang, C., Lu, J., Xu, L., et al. (2013b). Protective Effects of Necrostatin-1 against Concanavalin A-Induced Acute Hepatic Injury in Mice. Mediators Inflamm. *2013*, 1–15.

Ziegler, U., and Groscurth, P. (2004). Morphological features of cell death. News Physiol. Sci. Int. J. Physiol. Prod. Jointly Int. Union Physiol. Sci. Am. Physiol. Soc. *19*, 124–128.

VI. ANNEXES

VI.1. ANNEXE 1 : Le Toll-like Receptor-2 aggrave l'hépatite aiguë induite par le virus de l'hépatite murine.

Christian Bleau, Mélanie Burnette, Aveline Filliol, Claire Piquet-Pellorce, Michel Samson, et Lucie Lamontagne.

Article publié dans *Immunology*. 2016 Oct;149(2):204-24.

Résumé de l'article.

Dans le foie, la réplication virale est généralement détectée par des senseurs cytoplasmiques tels que les Toll like receptors (TLRs) localisés sur la membrane des endosomes cellulaires et les hélicases cytosoliques qui déclenchent une réponse inflammatoire antivirale. Des études récentes suggèrent que le TLR2 membranaire pourrait reconnaitre des protéines virales d'enveloppe et contribuer à la détection d'une infection. Cependant, son rôle sur les conséquences de l'infection virale aiguë reste inconnu. Dans cette étude, nous examinons, *in vivo*, le rôle du TLR2 dans des infections aiguës induites par le sérotype 3 du virus de l'hépatite murine de type 3 (MHV3) et le sérotype MHV-A59, qui sont respectivement fortement et faiblement hépatotropes. Nnous avons infecté des souris C57BL/6 (WT) et TLR2 knockout (KO) avec le MHV3 ou le MHV-A59. Nous avons montré que : *i)* les souris TLR2 KO infectées par le MHV3 avaient une hépatite nettement moins sévère que les souris WT qui elles présentaient une hépatite fulminante caractérisée par une mortalité précoce, des niveaux de transaminases sériques élevés, des lésions hépatiques et une forte réplication virale ; *ii)* l'infection par le MHV-A59 provoquait une hépatite bénigne et faiblement symptomatique comparable entre les souris WT et TLR2 KO ; *iii)* l'hépatite fulminante induite par le MHV3 chez les souris WT corrélait avec une forte expression intrahépatique de cytokines et chimiokines inflammatoires ainsi qu'une diminution des cellules inflammatoires par rapport à celle induite par le MHV-A59 chez les souris WT ou induite par le MHV3 chez les souris TLR2 KO ; et *iv)* ces observations *in vivo* pouvaient dépendre en partie de effets viraux dans les macrophages puisque l'infection *in vitro* de ces cellules par le MHV3, contrairement au MHV-A59, induisait une rapide et forte réplication virale, une induction d'IL-6 et dépendait de l'activation du TLR2 et de la "mitogen activated protein kinase" p38. En conclusion, ces résultats démontrent un nouveau rôle inflammatoire du TLR2 dans l'aggravation de l'hépatite fulminante induite par le MHV3.

Immunology
The Journal of cells, molecules, systems and technologies

British Society for immunology

IMMUNOLOGY ORIGINAL ARTICLE

Toll-like receptor-2 exacerbates murine acute viral hepatitis

Christian Bleau,[1] Mélanie Burnette,[1] Aveline Filliol,[2] Claire Piquet-Pellorce,[2] Michel Samson[2] and Lucie Lamontagne[1]

[1]*Department of Biological Sciences, Université du Québec à Montréal, Montreal, Canada, and* [2]*U.1085 Inserm, IRSET, Institute of Research in Environmental and Occupational Health, Université de Rennes 1, Rennes, France*

doi:10.1111/imm.12627
Received 18 February 2016; revised 31 May 2016; accepted 5 June 2016.
Correspondence: Lucie Lamontagne, Department of Biological Sciences, Université du Québec à Montréal, Montreal H3C 3P8, Canada. Email: lamontagne.lucie@uqam.ca
Senior author: Lucie Lamontagne

Summary

Viral replication in the liver is generally detected by cellular endosomal Toll-like receptors (TLRs) and cytosolic helicase sensors that trigger antiviral inflammatory responses. Recent evidence suggests that surface TLR2 may also contribute to viral detection through recognition of viral coat proteins but its role in the outcome of acute viral infection remains elusive. In this study, we examined *in vivo* the role of TLR2 in acute infections induced by the highly hepatotrophic mouse hepatitis virus (MHV) type 3 and weakly hepatotrophic MHV-A59 serotype. To address this, C57BL/6 (wild-type; WT) and TLR2 knockout (KO) groups of mice were intraperitoneally infected with MHV3 or MHV-A59. MHV3 infection provoked a fulminant hepatitis in WT mice, characterized by early mortality and high alanine and aspartate transaminase levels, histopathological lesions and viral replication whereas infection of TLR2 KO mice was markedly less severe. MHV-A59 provoked a comparable mild and subclinical hepatitis in WT and TLR2 KO mice. MHV3-induced fulminant hepatitis in WT mice correlated with higher hepatic expression of interferon-β, interleukin-6, tumour necrosis factor-α, CXCL1, CCL2, CXCL10 and alarmin (interleukin-33) than in MHV-A59-infected WT mice and in MHV3-infected TLR2 KO mice. Intrahepatic recruited neutrophils, natural killer cells, natural killer T cells or macrophages rapidly decreased in MHV3-infected WT mice whereas they were sustained in MHV-A59-infected WT mice and MHV3-infected TLR2 KO. MHV3 *in vitro* infection of macrophagic cells induced rapid and higher viral replication and/or interleukin-6 induction in comparison to MHV-A59, and depended on viral activation of TLR2 and p38 mitogen-activated protein kinase. Taken together, these results support a new aggravating inflammatory role for TLR2 in MHV3-induced acute fulminant hepatitis.

Keywords: coronavirus; inflammation; Toll-like receptor-2; viral hepatitis.

Introduction

Surface or endosomal toll-like receptors (TLR) are key pattern recognition receptors (PRRs) of infectious microorganisms in innate immunity. Host immune recognition of viruses during infections relies mainly on a combination of endosomal Toll-like receptors (TLR3, -7/8, -9) and cytosolic helicases retinoic acid inducible gene (RIG-1) and melanoma differentiation-associated protein (MDA-5) that sense viral RNA or DNA and trigger signalling pathways leading to inflammatory cytokines,

Abbreviations: ALT, alanine transaminase; AST, aspartate transaminase; CCL, chemokines CXCL; Fgl-2, fibrinogen-like protein; FHF, fulminant hepatic failure; HBC, hepatitis B virus; HCV, hepatitis C virus; HIV, human immunodeficiency virus; HPRT, hypoxanthine ribosyltransferase; IFN-α/β, interferon-α/β; IL, interleukin; i.p., intraperitoneally; KO, knockout; LSECs, liver sinusoidal endothelial cells; MAPK, mitogen-activated protein kinase; MDA-5, melanoma differentiation-associated protein; MHV, mouse hepatitis virus; MNCs, mononuclear cells; m.o.i., multiplicity of infection; NK cells, natural killer cells; NK-T cells, natural killer-T cells; p.i., post-infection; PRR, pattern recognition receptor; RIG-1, retinoic acid inducible gene; siRNA, small interfering RNA; TGF-β, transforming growth factor β; TLR, Toll-like receptor; TNF-α, tumour necrosis factor α; WT, wild-type

chemokines and antiviral type 1 interferon (IFN-α/β) production (reviewed in ref. 1).

Increasing evidence has shown that surface TLRs, such as TLR2 or TLR4, may also trigger acute inflammatory responses against viral infections through recognition of viral coat or core proteins.[2–5] Activation of surface TLR-dependent signalling pathways leads to the production of various chemokines involved in the recruitment of natural killer (NK) cells, macrophages, neutrophils and B- and T-cell subsets (reviewed in ref. 5). Higher expression of TLR2 and/or TLR4 and up-regulation of inflammatory factors have been observed in macrophages *in vitro* infected by some viruses such as human immunodeficiency virus (HIV),[6–8] influenza virus,[9] hepatitis C virus (HCV),[4] hepatitis B virus (HBV),[10] severe acute respiratory syndrome virus[11] and several herpes viruses.[12–14] TLR2 and/or TLR4 have also been involved in the induction of high inflammatory responses during acute viral infections. Indeed, TLR2 and TLR4 increase the susceptibility to rotavirus infections in infants[15] and TLR2 was suggested as an aggravating inflammatory factor in herpes virus infections.[12,14]

Recent studies have also reported an over-expression of TLR2 in the liver and on monocytes from HCV- or HCV/HIV-infected patients correlating with hepatic inflammation and damages, suggesting a role for TLR2 in hepatitis-associated inflammation.[16,17] HCV and HBV infections present subclinical to severe acute-phase patterns that may lead to viral clearance or evolve towards chronic infections (reviewed in ref. 18). For reasons that are not well understood, few cases of acute infections progress into fulminant hepatic failure, characterized by extensive necrosis and hepatocellular dysfunction, exacerbated inflammation and high mortality rate.[19] Hepatic lesions occurring during viral infections are primarily related to virally triggered host inflammatory responses (reviewed in ref. 20) and depend on a poorly elucidated balance between innate immune cell–virus interactions and the control of viral replication that is critical in the outcome of hepatitis. The contribution of TLR2 in antiviral defences and inflammatory responses during acute hepatic viral infections is unknown and needs investigation.

The mouse hepatitis viruses (MHV), belonging to the coronavirus group, induce acute or subclinical hepatitis, neurological, respiratory or/and enteric diseases in mice according to serotypes.[21] The highly hepatotrophic MHV3 serotype is a relevant model for studying virus-induced inflammatory disorders during acute hepatic infections as it induces fulminant lethal hepatitis in C57BL/6 mice within 4 days post-infection (p.i.)[22] whereas the weakly hepatotrophic MHV-A59 serotype induces a subclinical hepatitis and is rapidly cleared in the liver.[23] Within 72 hr of infection, liver dysfunction in MHV3-infected mice results from several foci of extensive necrosis[24] in contrast to that observed in the liver of mice infected with the MHV-A59 serotype.[25] All MHV serotypes use the CEACAM1a molecule as viral receptor for infection of host cells through interaction with their viral surface (S) protein.[26] It was previously demonstrated that the differential levels of viral replication and hepatitis induced by the MHV serotypes were largely related to the viral S protein,[27] suggesting that interactions of the S protein with molecules other than CEACAM1a may reflect their virulence for liver.

Peritoneal macrophages are the first viral cell target during MHV infection, followed by liver cells such as hepatocytes, macrophages, liver sinusoidal endothelial cells (LSECs) and Ito cells.[26,28] Intrahepatic macrophages, LSECs as well as NK and NK T cells are considered as major contributors to antiviral responses and release of cytokines/chemokines in the liver upon viral infection.[29] During MHV3 acute infection, inflammatory mediators such as tumour necrosis factor-α (TNF-α), interleukin-1 (IL-1), transforming growth factor-β (TGF-β), leukotriene B4 and mouse fibrinogen-like 2 (Fgl-2) protein are strongly produced by infected macrophages, correlating with the severity of hepatitis.[30] Accordingly, depletion of macrophages was reported to protect against the fulminance of hepatitis,[31] suggesting that exacerbated inflammatory responses are an aggravating factor during MHV3 infection. In addition, the intrahepatic tolerance sustained by IL-4, IL-10, TGF-β and prostaglandin E_2 is also disturbed.[32] In contrast, it has been suggested that macrophages would rather contribute to the lower gravity of hepatitis and viral clearance during MHV-A59 infection, presumably through a rapid type 1 IFN-dependent suppression of viral replication.[33] It was demonstrated that the induction of IL-6 and TNF-α in peritoneal macrophages infected by MHV3 depended on the fixation of the viral surface (S) protein to TLR2.[34] Previous *in vivo* studies also revealed higher levels of IL-6 and TNF-α in livers from MHV3-infected C57BL/6 mice than TLR2 knockout (KO) mice, suggesting an inflammatory role for TLR2 in MHV3 infection.[34] Hence, the ability of MHVs to ligate and activate TLR2-dependent inflammatory pathways in the liver may represent one determining and differential factor involved in their virulence.

In this study, we demonstrated that the severe acute hepatitis provoked by the highly hepatotrophic MHV3 but not by the weakly hepatotrophic MHV-A59 serotype, is aggravated by TLR2 in the liver, as demonstrated by significantly higher mortality, liver injury, viral replication, levels of inflammatory cytokines and chemokines as well as disturbances in intrahepatic neutrophils, macrophages, NK and NK T-cell recruitment in MHV3-infected wild-type (WT) but not infected TLR2 KO mice or MHV-A59-infected WT mice. Through *in vitro* infection of macrophagic cells, we showed that rapid and higher viral replication and/or IL-6 induction by MHV3, in

comparison to MHV-A59, depended on activation of TLR2 and p38 mitogen-activated protein kinase (MAPK), pointing out macrophages as one source of TLR2-dependent inflammatory responses in MHV3 infection.

Material and methods

Mice

Female C57BL/6 (Charles River, St Constant, Qc, Canada) and TLR2 KO (C57BL/6 background, Jackson Laboratory, Bar Harbor, MA) mice were housed in a HEPA-filtered air environment. All experiments were conducted with mice between 8 and 10 weeks of age in compliance with the regulations of the Animal Committee of the University of Quebec at Montreal (CIPA-no.641).

Viruses and cells

Highly hepatotrophic MHV3 is a cloned substrain isolated from the liver of MHV3-infected DBA2 mice.[35] Weakly hepatotrophic MHV-A59 serotype was obtained from the American Type Culture Collection (Rockville, MD). Both viruses were produced in L2 cells as previously described[34] and used within three passages. Pathogenic properties of MHV3 were assessed routinely. The mouse fibroblastic L2 cell line used for virus production and titration was grown in RPMI-1640 supplemented with 10% fetal calf serum (GIBCO Laboratories, Grand Island, NY) and antibiotics. Murine macrophagic cells J774A.1 (TIB-67TM) were grown in RPMI-1640 supplemented with L-glutamine, antibiotics (GIBCO Laboratories) and 5% fetal bovine serum (Gemini Bio-Products, Woodland, CA). All cells were passaged before reaching 85% confluence.

In vivo viral infections

Groups of six or seven WT C57BL/6 and TLR2 KO mice were infected intraperitoneally (i.p.) with 10^3 $TCID_{50}$ of MHV3 or MHV-A59. Mock-infected mice received a similar volume of PBS. Clinical signs and survival percentages were recorded and mice were killed when clinical signs reached limit points as determined by CIPA regulations. In other experiments, mice were killed by CO_2 anoxia at 24, 48 and 72 hr p.i. without regard for clinical signs. Liver and blood samples were collected and processed for further analyses.

Histopathological, transaminase activity and immunohistochemical analyses

The histopathological analysis of liver was performed using haematoxylin & eosin–safran staining. Levels of serum alanine and aspartate transaminases (ALT and AST) were assessed according to the IFCC primary reference procedures using Olympus AU2700 Autoanalyser® (Olympus Optical, Tokyo, Japan). Immunolocalization of IL-33 or CXCL10 was performed by histochemical staining using primary goat anti-mouse-IL-33 and anti-CXCL10 (R&D Systems, Minneapolis, MN) and secondary horseradish peroxidase-conjugated rabbit anti-goat antibody for IL-33 (Dako, Markham, Ont., Canada) and OmniMap anti-Rabbit-horseradish peroxidase (RUO) for CXCL-10 followed by haematoxylin counterstaining in a Ventana machine (Ventana Medical Systems, Inc. Tucson, AZ), as previously described.[36] Counting of necrotic areas and inflammatory foci was carried out on liver areas of 15–30 mm^2 using the NDP.2 VIEW image analysis software (Hamamatsu Photonics K.K., Japan).

In vitro viral infections

J774A.1 cells were infected with MHV-A59 or MHV3 at a multiplicity of infection (m.o.i.) of 0·1–1 or treated with the synthetic bacterial ligand for TLR1/2 (Pam_3CSK4) (InvivoGen, San Diego, CA). Infections were conducted in a minimal volume of fresh complete medium for the first 2 hr and then incubated at 37° in 5% CO_2 atmosphere for various times p.i. according to experiments. Supernatants were collected and kept at −80° for subsequent viral titration and/or ELISA tests. Total cell RNA was extracted from cell culture and prepared for subsequent RT-PCR analysis.

RNA interference treatments

J774A.1 cells were plated in 24-well plates at 6×10^4 cells per well and transfected with 25 nM of mouse CEACAM1 small interfering RNA (siRNA) FlexiTube premix (Qiagen, Cambridge, MA) (Mm_Ceacam1_3: CACACTCATGCATTCACTCTA) and/or mouse TLR2 (Mm_Tlr2_4: CTCGTTCTCCAGCATTTAAA) for at least 24 hr before infection. Negative and positive siRNA controls (AllStars Negative Control siRNA and Ctrl_AllStars_3,respectively, Qiagen), were added to all transfection experiments. Synthetic bacterial ligand for TLR1/2 (Pam_3CSK4) (InvivoGen San Diego, CA) was used as TLR2-positive control for cytokine production.

RNA isolation and quantitative RT-PCR

Total RNA from frozen liver samples of C57BL/6 and TLR2 KO mice was extracted using TRIzol reagent (Invitrogen, Burlington, Ont., Canada) and residual genomic DNA was removed with the Turbo DNA-free kit (Ambion, Austin, TX). Cell culture RNA was extracted with the NucleoSpin® RNA II kit (Macherey-Nagel GmbH & Co. KG, Düren, Germany). One microgram of RNA was retro-transcribed into cDNA using the high-capacity cDNA reverse transcription kit (Applied

Biosystems, Foster City, CA). Real-time PCR amplification was carried out on 25 ng cDNA using the HotStart-IT™ SYBR® Green qPCR Master Mix (USB Corporation, Cleveland, OH) on an ABI 7300 system (Applied Biosystems). Threshold cycle values (Ct) were collected and used for 'ΔΔCt' analysis. Specific primers for hypoxanthine phosphoribosyltransferase (HPRT), MHV-nucleocapsid, TLR2, TLR3, TLR4, TLR7, MDA-5, RIG-1, IFN-β, IL-6, TNF-α, IL-33, Fgl-2, CXCL1, CXCL10 and CCL2 were used (Table 1). The relative gene expression was normalized to HPRT as endogenous control and expressed as a ratio to gene expression in mock-infected mice livers (arbitrarily taken as 1). The specificity of the PCR products was confirmed by melting curve analyses.

ELISAs

Frozen liver samples from C57BL/6 and TLR2 KO mice were weighted and homogenized in Nonidet-P40 lysis buffer (Invitrogen) completed with a protease inhibitor cocktail and 1 mM PMSF (Sigma Aldrich, St Louis, MA) for protein extraction. Liver suspension was kept on ice for 30 min and centrifuged for 10 min at 1000g. Determination of IFN-β (PBL, Piscataway, NJ), IL-6, TNF-α (BD Biosciences, Mississauga, Ont., Canada), and CXCL1, CXCL10, CCL2 (eBiosciences, San Diego, CA) levels in liver lysates or cell culture supernatants was carried out according to the manufacturers' procedures.

p38 MAPK assay

The p38 MAPK activity has been evaluated in J774A.1 cells plated in 24-well plates at 3×10^4 cells per well 24 hr before infections with MHV-A59 or L2-MHV3 at an m.o.i. of 5. At 5, 15, 30, 45 or 60 min p.i., supernatants were collected and frozen at −80°, and the cells were washed three times with cold PBS once before RNA and protein extraction. Activity of p38 MAPK in *in vitro* infected cells was evaluated by phosphorylation (T180/Y182) levels with the ELISA ONE™ kit (TGR BioSciences, Thebarton, Australia) according to the manufacturer's indications. Values are expressed as percentage of phosphorylated p38/ total p38 relative to cellular control.

Virus titration

Frozen liver samples from 24-hr and 72-hr MHV3- or MHV-A59-infected C57BL/6 or TLR2 KO mice were weighted and homogenized in cold PBS. Suspension was then centrifuged at 1000g for 30 min, 10-fold serial-diluted and tested for viral detection on L2 cells cultured in 96-well plates. Cytopathic effects were recorded at 72 hr p.i. and virus titres were determined according to the Reed–Muench method and expressed as $\log_{10}$ $TCID_{50}$.

Cytofluorometric studies

Livers were perfused with PBS through the portal vein to remove blood cell contamination before dissection. After homogenization of liver tissue and elimination of hepatocytes by sedimentation, immune cells were purified using 35% Percoll gradient (Sigma Aldrich) and red blood cells were lysed with a Tris-buffered ammonium chloride solution. Mononuclear cells (MNCs; 10^6 cells) were incubated with anti-CD16/32 antibodies (BD Biosciences) to block non-specific binding. Cells were then incubated with optimal dilutions of anti-CD3-V500, anti-Gr1-V450, anti-CD11b-phycoerythrin-Cy7, anti-CD19-allophycocyanin, anti-CD4-FITC, anti-NK1.1-Peridinin chlorophyll

Table 1. Primer sets used for quantitative RT-PCR

Gene	Forward primer	Reverse primer
HPRT	5′-GAAAGACTTGCTCGAGATGTCATG-3′	5′-CACACAGAGGGCCACAATGT-3′
IFN-β	5′-CGGACTTCAAGATCCCTATGGA-3′	5′-TGGCAAAGGCAGTGTAACTCTTC-3′
IL-6	5′-TCGGAGGCTTAATTACACATGTTC-3′	5′-TGCCATTGCACAACTCTTTTCT-3′
TNF-α	5′-TCCCAGGTTCTCTTCAAGGGA-3′	5′-GGTGAGGAGCACGTAGTCGG-3′
CCL2	5′-GCAGCAGGTGTCCCAAAGAA-3′	5′GGTCAGCACAGACCTCTCTCTTG-3′
CXCL10	5′-GGCCATAGGGAAGCTTGAAAT-3′	5′-TCGTGGCAATGATCTCAACAC-3′
TLR2	5′-CCCTGTGCCACCATTTCC-3′	5′-CCACGCCCACATCATTCTC-3′
TLR3	5′-TGGGCTGAAGTGGACAAATCT-3′	5′-TGCCGACATCATGGAGGTT-3′
TLR4	AGCTTCAATGGTGCCATCATT	CCAGGTGCTGCAGCTCTTCT
TLR7	5′-CAGTGAACTCTGGCCGTTGA-3′	5′-CAAGCCGGTTGTTGGAGAA-3′
MHV-N	5′-TGGAAGGTCTGCACCTGCTA-3′	5′-TTTGGCCCACGGGATTG-3′
RIG-I	5′-GCCAGAGTGTCAGAATCTCAGTCAG-3′	5′-GAGAACACAGTTGCCTGCTGCTCA-3′
MDA-5	5′-GCCCTCTCCTTCCTCTGAGACT-3′	5′-GCTGGAGGAGGGTCAGCAA-3′
IL-33	5′-GCTGCGTCTGTTGACACATTG-3′	5′-GGGAGGCAGGAGACTGTGTTAA-3′
Fgl-2	5′- CGTTGTGGTCAACAGTTTGGA-3′	5′- GATGTTGAACCGGCTGTGACT-3′
CXCL1	5′-CCGAAGTCATAGCCACACTCAA-3′	5′-CAAGGGAGCTTCAGGGTCAA-3′

protein-Cy-5.5 and anti-CD8-allophycocyanin-Cy7 antibodies (BD Biosciences) and fixed in PBS containing 2% fetal calf serum, 0·01 M sodium azide and 2% formaldehyde. Stained cells were analysed on a FACS Aria II® flow cytometer using BD FACS DIVA software (BD Bioscience) and the data were processed using CXP software (Beckman Coulter, Mississauga, Ont, Canada). Dead cells and doublet cells were excluded on the basis of forward and side scatter and analyses were performed on 10 000 events recorded. Myeloid cells, gated by high side scatter, were assessed for CD11b and Gr1 to enumerate macrophages ($CD11b^+$ $Gr1^{inter}$) and neutrophils ($CD11b^+$ $Gr1^{high}$). Lymphoid cells were gated according to forward and side scatter and first assessed for NK1.1 and CD3 expression to discriminate NK from NKT cells. $CD3^+$ $NK1.1^-$ T cells were further gated to allow determination of $CD4^+$ and $CD8^+$ subpopulations. B lymphocytes were determined by $CD19^+$ $CD3^-$ expression (see Supplementary material, Fig. S1).

Statistical analyses

Data obtained from *in vivo* experiments were expressed as means ± SEM. Multiple group analyses for PCR, ELISA and viral titres data were evaluated by one-way analyses of variance test with post-hoc Tukey test using PASW STATISTICS software (PASW version 18, IBM SPSS Inc. Chicago, IL). Survival curve comparisons were performed using the Log Rank test. Analysis of *in vitro* results was performed using Student's *t*-test to evaluate the statistical significance of differences between infected or treated cells and uninfected or untreated cells. All results are shown as means ± standard error. Values of $P \leq 0{\cdot}05$ were considered as significant.

Results

Higher hepatic damage and viral replication in the liver of MHV3-infected than MHV-A59-infected mice

To confirm that the highly hepatotrophic MHV3 induces more dramatic hepatic lesions than the weakly virulent MHV-A59 serotype following i.p. inoculation, groups of C57BL/6 mice were infected with both viruses, livers were collected at 24–72 hr p.i. and histopathological analysis, viral replication and IFN-β production levels were recorded. Histopathological analysis of livers from MHV3-infected mice revealed few inflammatory cells surrounding necrotic foci as soon as 24 hr p.i. [Fig. 1a (i)]. Presence of inflammatory cells, however, was reduced from 48 hr p.i. whereas necrotic foci extended until 72 hr p.i. [Fig. 1a (ii, iii)]. No inflammatory foci were observed in livers from mock-infected mice (results not shown). Larger inflammatory foci, however, were observed in liver from MHV-A59-infected mice up to 48 hr p.i. without extensive necrosis areas as seen in MHV3-infected mice ($P \leq 0{\cdot}01$) [Fig. 1a (iv–vii)]. Extensive hepatic lesions in mice infected by MHV3 correlated with higher levels of AST and ALT at 72 hr p.i. than in MHV-A59-infected mice [Fig. 1b (i, ii)] ($P \leq 0{\cdot}001$).

Viral replication, as evidenced by nucleocapsid RNA levels and viral titres, increased more in the liver of MHV3-infected mice when compared with mice infected with MHV-A59 ($P \leq 0{\cdot}05$ to $P \leq 0{\cdot}001$) [Fig. 1b (iii, iv)]. MHV3 replication in the liver increased throughout infection despite higher IFN-β production ($P \leq 0{\cdot}001$) [Fig. 1b (v, vi)]. Such lower viral replication of MHV-A59, however, did not result from an increase in IFN-β, since lower mRNA levels and production of IFN-β were detected in the liver of MHV-A59-infected. No increase in IFN-α transcription has been observed in both MHV3- and MHV-A59-infected mice (results not shown).

Higher expression of TLR2 over other TLRs and helicases in the liver of MHV3- than MHV-A59-infected mice

Several endosomal TLRs and helicases are simultaneously activated and up-regulated upon viral infection, triggering inflammatory responses (reviewed in ref. 1). We explored the hypothesis that MHV3 infection may induce higher expression of TLRs or helicase genes in the liver than MHV-A59. Hence, kinetics of transcription levels of surface TLR2 and TLR4, endosomal TLR3 and TLR7, and helicase RIG-1 and MDA-5 genes have been assessed by quantitative RT-PCR in the liver of infected mice from 24 to 72 hr p.i. and expressed as mRNA fold changes relative to levels in mock-infected mice. As shown in Fig. 2(a), TLR2 gene expression steadily increased over the course of infection

Figure 1. Mortality, hepatic damages and viral replication during murine hepatitis virus 3 (MHV3) and MHV-A59-induced hepatitis in C57BL/6 mice. Groups of six or seven C57BL/6 mice were intraperitoneally (i.p.) infected with 1000 $TCID_{50}$ of MHV3 or MHV-A59. Percentages of surviving mice were recorded at various times post-infection (p.i.). (a) (i–vi) Histopathological analysis was conducted on livers at 24, 48 and 72 hr p.i. (vii) Histological analysis of inflammatory foci in liver from MHV3- or MHV-A59 infected C57BL/6 mice. (b) Serum samples from infected mice were assayed for aspartate transaminase (AST) and alanine transaminase (ALT) activity from 24 to 72 hr p.i. (i, ii). MHV3 or MHV-A59 replication in livers of infected mice was determined by analysis of the nucleoprotein (MHV-N) RNA expression from 24 to 72 hr p.i. by quantitative RT-PCR, and values represent fold change in gene expression relative to mock-infected mice after normalization with HPRT expression (iii). Viral titration ($TCID_{50}$) in liver was assayed at 24 and 72 hr p.i. (iv). mRNA fold increases for interferon-β (IFN-β) were evaluated by quantitative RT-PCR in livers of MHV3- or MHV-A59 infected mice. Values represent fold change in gene expression relative to mock-infected mice (arbitrary value of 1) after normalization with HPRT expression (v). Production levels of IFN-β were quantified by ELISA test at 72 hr p.i. in livers (vi). Results are representative of two different experiments. (*$P < 0{\cdot}05$; **$P < 0{\cdot}01$; ***$P < 0{\cdot}001$).

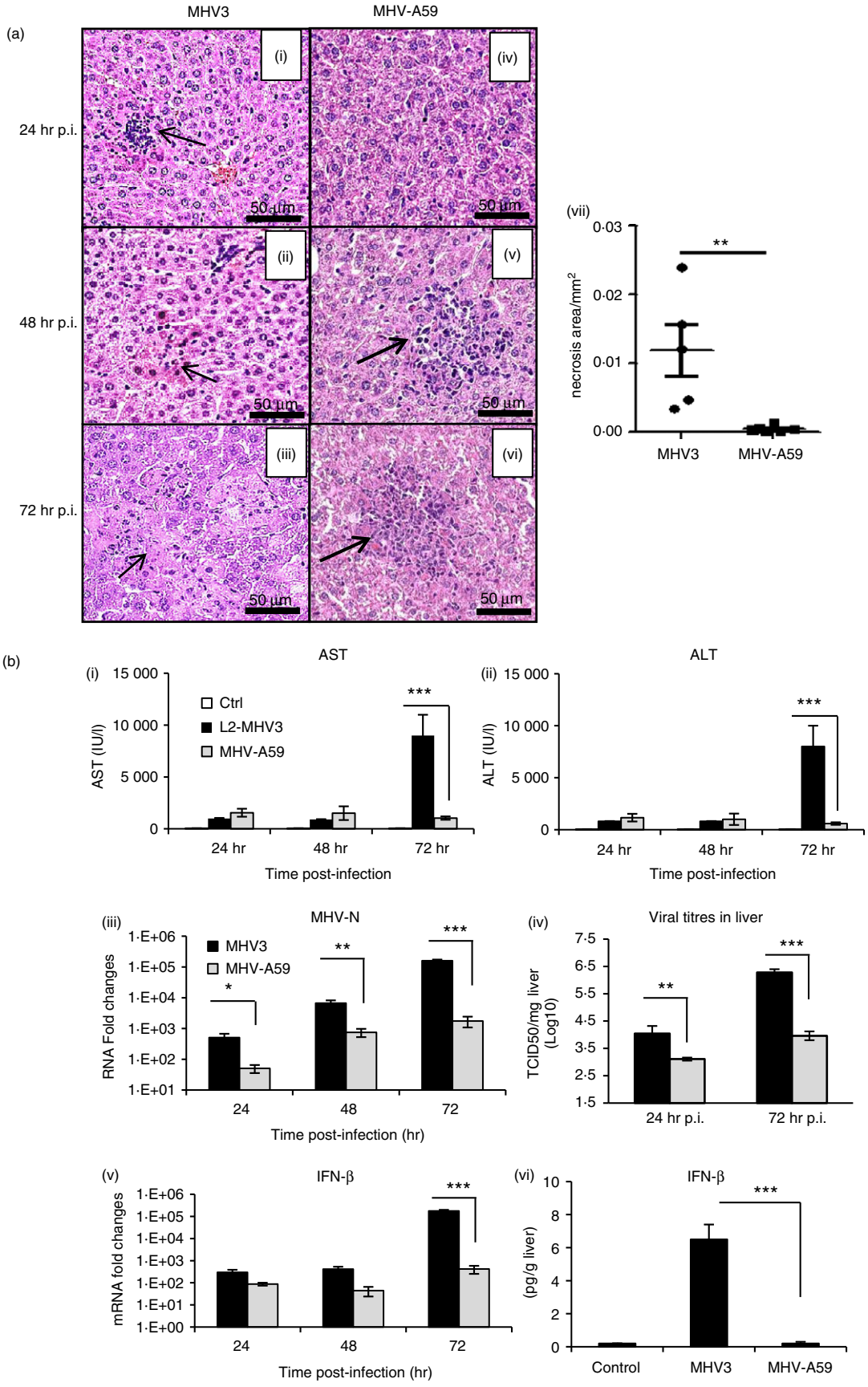
(a)
MHV3
MHV-A59
24 hr p.i.
48 hr p.i.
72 hr p.i.
(i)
(ii)
(iii)
(iv)
(v)
(vi)
50 μm
(vii)
necrosis area/mm2
0·03
0·02
0·01
0·00
**
MHV3
MHV-A59
(b)
AST
ALT
(i)
(ii)
15 000
10 000
5 000
0
AST (IU/l)
ALT (IU/l)
Ctrl
L2-MHV3
MHV-A59
***
24 hr
48 hr
72 hr
Time post-infection
(iii)
MHV-N
RNA Fold changes
1·E+06
1·E+05
1·E+04
1·E+03
1·E+02
1·E+01
MHV3
MHV-A59
*
**
***
24
48
72
Time post-infection (hr)
(iv)
Viral titres in liver
TCID50/mg liver (Log10)
7·5
6·5
5·5
4·5
3·5
2·5
1·5
24 hr p.i.
72 hr p.i.
(v)
IFN-β
mRNA fold changes
1·E+00
(vi)
(pg/g liver)
10
8
6
4
2
0
Control
MHV3
MHV-A59

with MHV3 reaching over 120-fold the expression in mock-infected mice at 72 hr p.i. whereas it remained barely increased and drastically lower in MHV-A59-infected mice ($P \leq 0{\cdot}05$ to $P \leq 0{\cdot}001$). Levels of TLR4 and TLR7 mRNA expression were not affected by either MHV3 or MHV-A59 infections (Fig. 2b,c). Endosomal TLR3 or RIG-1 and MDA-5 gene expression levels also increased in MHV3-infected mice, albeit markedly less than TLR2, and were similarly lower or not induced in mice infected with MHV-A59 ($P \leq 0{\cdot}05$ to $P \leq 0{\cdot}001$) (Fig. 2d–f).

These data suggest that MHV3 but not MHV-A59 infection strongly induces expression of TLR2, over other TLRs and helicases, in the liver of infected mice.

Higher expression of inflammatory cytokines, IL-33 (alarmin) and Fgl-2 in the liver of MHV3-infected than MHV-A59-infected mice

Activation of TLRs, mainly surface TLR2, is involved in the release of pro-inflammatory cytokines such as TNF-α and IL-6 (reviewed in ref. 1). Higher induction of hepatic TLR2 expression by MHV3 than MHV-A59 infection suggests that higher levels of TNF-α or IL-6 may occur in the liver of MHV3-infected mice. To investigate this hypothesis, levels of TNF-α and IL-6 expression were evaluated by quantitative RT-PCR and ELISA tests in livers from infected mice. As shown in Fig. 3(a,b), IL-6 mRNA and secretion levels increased only in MHV3-infected mice ($P \leq 0{\cdot}05$ and $P \leq 0{\cdot}001$). Higher expression of TNF-α was also found in the liver of MHV3- than MHV-A59-infected mice ($P \leq 0{\cdot}01$ to $P \leq 0{\cdot}001$) (Fig. 3c) and correlated with higher secretion at 72 hr p.i. ($P \leq 0{\cdot}001$) (Fig. 3d).

We have previously demonstrated that expression of IL-33, a new alarmin, was up-regulated in the liver of MHV3-infected C57BL/6 mice correlating with an increase of inflammatory cytokines.[36] Messenger RNA levels and immunolocalization for IL-33 were assayed in the livers of MHV3-infected and/or MHV-A59-infected mice. As shown in Fig. 3(e), gene expression of IL-33 increased only in the liver of MHV3-infected mice ($P \leq 0{\cdot}001$) and IL-33 was localized mainly in cells lining sinusoids and to a lesser extent in hepatocytes at 24 and 72 hr p.i. in MHV3-infected mice (Fig. 3g).

It was previously demonstrated that fulminance of MHV3-induced hepatitis correlated with levels of Fgl-2 produced by liver sinusoidal endothelial cells.[37,38] As expected, Fgl-2 expression increased sooner, at 48 hr p.i., in the liver of MHV3-infected mice than MHV-A59-infected mice ($P \leq 0{\cdot}05$ and $P \leq 0{\cdot}01$).

Activation of TLR2, as other TLRs, is also involved in chemokine production in acute and chronic liver diseases[39] (reviewed in ref. 1). We hypothesized that MHV3 infection may favour greater release of chemokines in the liver than MHV-A59 infection. Hence, mRNA and protein levels of CCL2, CXCL1 and CXCL10 were evaluated

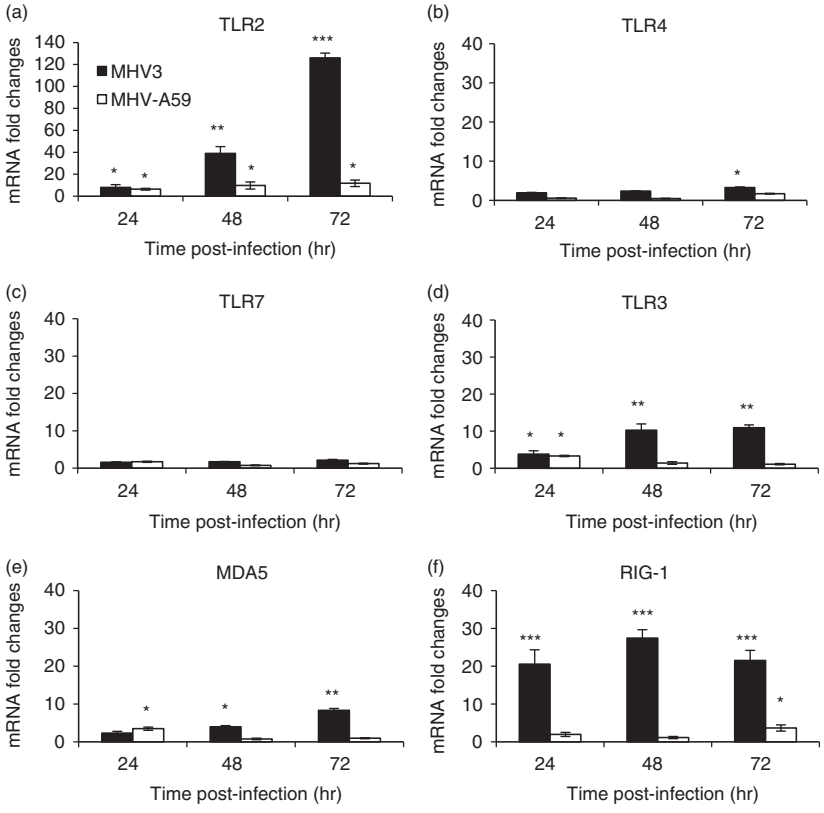

Figure 2. Messenger RNA levels of Toll-like receptor 2 (TLR2), TLR4, TLR3, TLR7 and helicases retinoic acid inducible gene (RIG-1) and melanoma differentiation-associated protein (MDA-5) genes in the liver of murine hepatitis virus (MHV) 3- and MHV-A59-infected mice. Groups of six or seven C57BL/6 (wild-type; WT) mice were intraperitoneally (i.p.) infected with 1000 $TCID_{50}$ of MHV3 or MHV-A59. At 24, 48 or 72 hr post-infection (p.i.), livers from each group were collected and Toll-like receptors (TLR2, -3, -4, -7) (a–d) and helicases (MDA-5 and RIG-1) (e and f) mRNA fold changes were analysed by quantitative RT-PCR. Values represent fold change in gene expression relative to mock-infected mice (arbitrary value of 1) after normalization with HPRT expression. Results are representative of two different experiments. ($*P < 0{\cdot}05$; $**P < 0{\cdot}01$; $***P < 0{\cdot}001$).

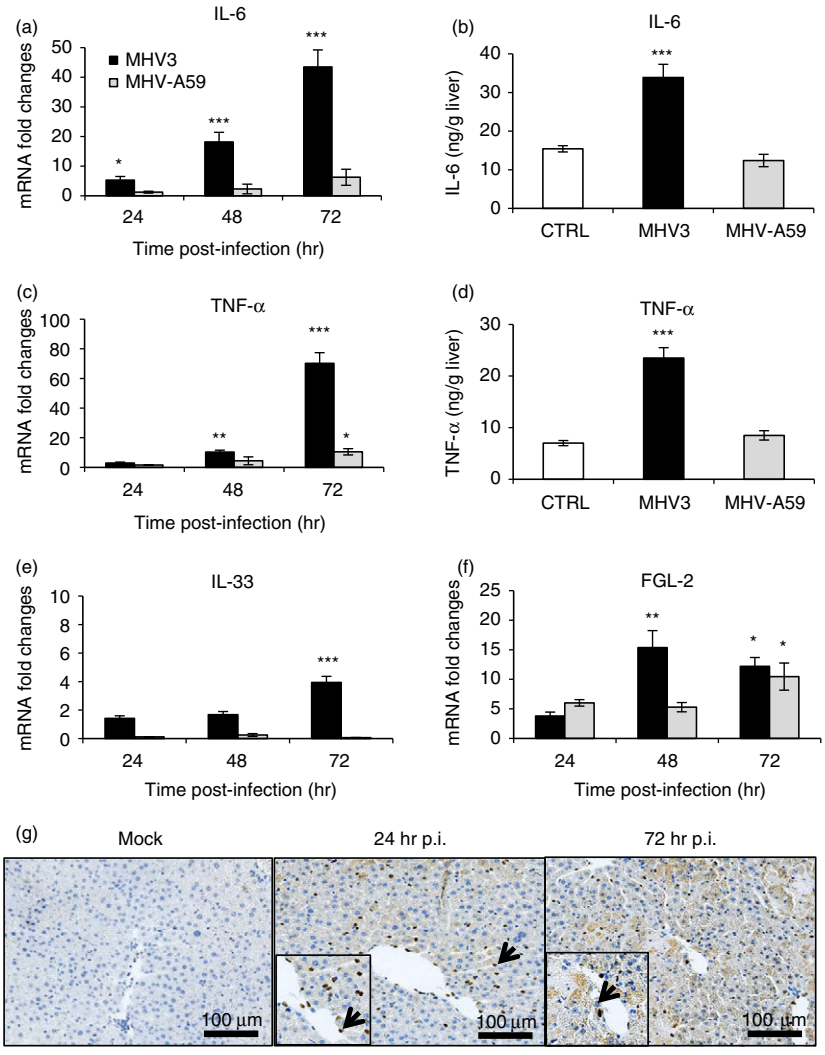

Figure 3. Messenger RNA levels and production of inflammatory cytokines, interleukin-33 (IL-33) and fibrinogen-like 2 (Fgl-2) in the liver of murine hepatitis virus (MHV) 3- and MHV-A59-infected mice. Groups of six or seven C57BL/6 mice were intraperitoneally (i.p.) infected with 1000 $TCID_{50}$ of MHV3 or MHV-A59. At 24, 48 or 72 hr post-infection (p.i.), livers from each group were collected and mRNA fold increases for interleukin-6 (IL-6) (a), tumour necrosis factor-α (TNF-α) (c), IL-33 (e) and Fgl-2 (f) were evaluated by quantitative RT-PCR in livers of infected mice. Values represent fold change in gene expression relative to mock-infected mice (arbitrary value of 1) after normalization with HPRT expression. Production levels of IL-6 (b) and TNF-α (d) were quantified by ELISA test at 72 hr p.i. in livers. Expression of IL-33 determined by immunohistochemistry in livers from mock-infected and MHV3-infected WT mice at 24 and 72 hr p.i. (g). Some positive IL-33 cells are indicated by arrows. Results are representative of two different experiments. (*$P < 0{\cdot}05$; **$P < 0{\cdot}01$; ***$P < 0{\cdot}001$).

by quantitative RT-PCR and ELISA tests, respectively, in the livers of infected mice. As shown in Fig. 4, transcription levels of CCL2 and CXCL10 genes increased over infection time in MHV3-infected mice and reached higher levels at 72 hr p.i. than in MHV-A59-infected mice ($P \leq 0{\cdot}05$ to $P \leq 0{\cdot}001$) (Fig. 4a,c). CCL2 was highly produced in liver from MHV3-infected mice ($P \leq 0{\cdot}01$ and $P \leq 0{\cdot}001$) (Fig. 4b). Production of CXCL10, however, was higher in the liver of MHV-A59-infected than MHV3-infected mice although gene expression was lower ($P \leq 0{\cdot}01$ and $P \leq 0{\cdot}001$) (Fig. 4d). Levels of mRNA and protein for CXCL1 were more increased in the liver of MHV3-infected mice than in MHV-A59-infected mice ($P \leq 0{\cdot}05$ to $P \leq 0{\cdot}001$) (Fig. 4e,f).

Transient and lower recruitment of neutrophils, NK cells and macrophages in the livers of MHV3- and MHV-A59-infected mice

Higher CXCL1, CCL2 and lower CXCL10 levels in the livers of MHV3-infected mice suggest higher recruitment of neutrophils, macrophages, NK and NK T cells rather than lymphoid cells (reviewed in ref. 40). Smaller or lower inflammatory foci, however, were observed in the livers of MHV3-infected mice compared with MHV-A59-infected mice [Fig. 1a (ii–vi)] suggesting that inflammatory cell subsets are differentially recruited during MHV3 and MHV-A59 infections. To verify this hypothesis, intrahepatic MNCs were isolated from the livers of MHV3- and MHV-A59-infected mice at 24 and 48 hr p.i., immunolabelled and then phenotyped by cytofluorometric analysis. Percentages and numbers of NK-T ($NK1.1^+$ $CD3^+$) and NK ($NK1.1^+$ $CD3^-$) cells, neutrophils ($CD11b^{hi}$ $Gr1^{hi}$), macrophages ($CD11b^+$ $Gr1^{int}$) as well as B ($CD19^+$), CD4 ($CD3^+$ $CD4^+$) and CD8 ($CD3^+$ $CD8^+$) lymphocyte subsets were compared between groups of mice. As shown in Fig. 5(a), percentages of neutrophils ($CD11b^{hi}$ $Gr1^{hi}$) and macrophages ($CD11b^+$ $Gr1^{int}$) rapidly increased at 24 hr p.i. in MHV3-infected mice in spite of high individual variation for neutrophils ($P \leq 0{\cdot}05$ to $P \leq 0{\cdot}001$). Percentages of NK cells ($NK1.1^+$ $CD3^-$) increased only at

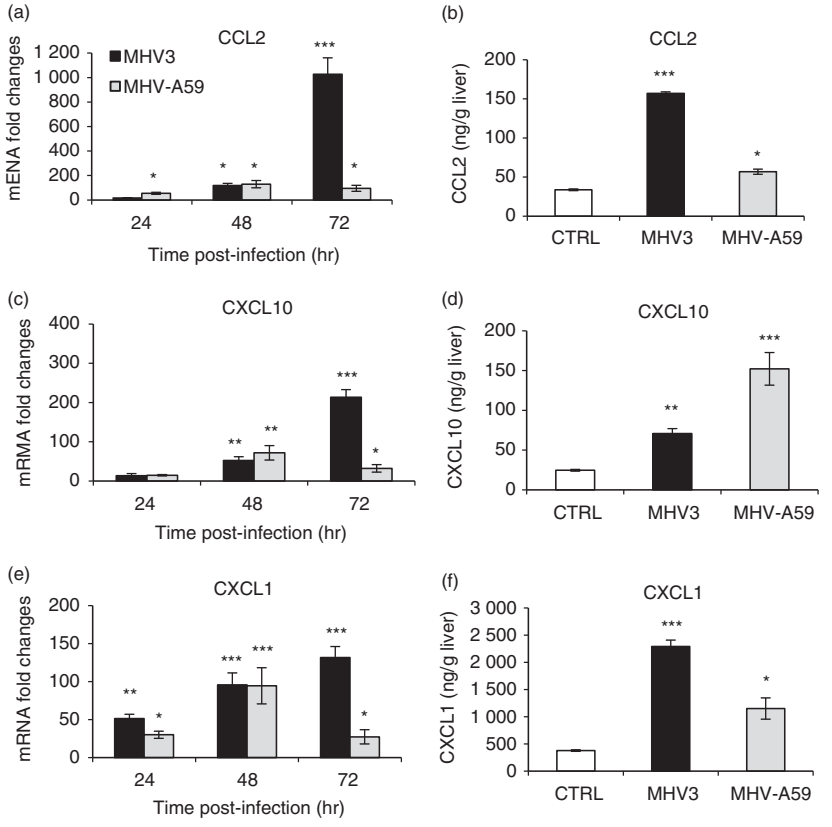

Figure 4. Messenger RNA expression and production of chemokines CCL2, CXCL1 and CXCL10 in the livers of murine hepatitis virus (MHV) 3- and MHV-A59-infected mice. Groups of six or seven C57BL/6 mice were intraperitoneally (i.p.) infected with 1000 $TCID_{50}$ of MHV3 or MHV-A59. At 24, 48 or 72 hr post-infection (p.i.), livers from each group were collected. mRNA expression levels for CCL2 (a), CXCL10 (c) and CXCL1 (e) were evaluated by quantitative RT-PCR at 24, 48 and 72 hr p.i in livers from MHV3- or MHV-A59-infected mice. Values represent fold change in gene expression relative to mock-infected mice (arbitrary value of 1) after normalization with HPRT expression. Protein levels of CCL2 (b), CXCL10 (d) and CXCL1 (f) were quantified in livers by ELISA tests at 72 hr p.i. (*$P < 0{\cdot}05$; **$P < 0{\cdot}01$; ***$P < 0{\cdot}001$).

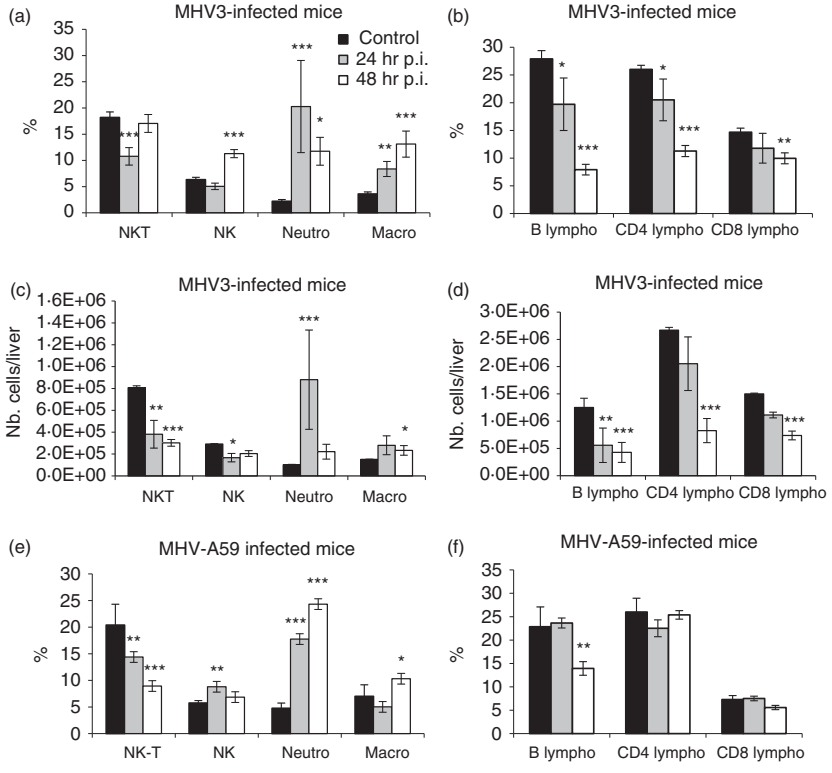

Figure 5. Analysis of intrahepatic mononuclear cells (MNCs) in the liver of murine hepatitis virus (MHV) 3- and MHV-A59-infected C57BL/6 mice. Intrahepatic MNCs were isolated from groups of six mock-infected, MHV3- and MHV-A59-infected C57BL/6 mice at 24 and 48 hr p.i., immunolabelled with NK1.1, CD3, Gr1, CD11b, CD19, CD4 and CD8 monoclonal antibodies and analysed by cytofluorometry. Percentages of natural killer T (NK-T) ($NK1.1^+$ $CD3^+$), natural killer (NK) ($NK1.1^+$ $CD3^-$), neutrophils ($Gr1^{hi}$ $CD11b^{hi}$) and macrophages ($Gr1^+$ $CD11b^{int}$) cells were evaluated in the livers of MHV3 (a) and MHV-A59 (e) -infected mice. Percentages of b ($CD19^+$) and CD4 ($CD3^+$ $CD4^+$) and CD8 ($CD3^+$ $CD8^+$) subpopulations of $CD3^+$ $NK1.1^-$ cells were similarly analysed (b and f). Absolute numbers for each cell subset were calculated in using respective percentages reported to total number of isolated MNC in the liver of MHV3- (c and d). (*$P < 0{\cdot}05$; **$P < 0{\cdot}01$; ***$P < 0{\cdot}001$).

48 hr p.i ($P \leq 0{\cdot}001$) and NK-T ($NK1.1^+$ $CD3^+$) cell percentage decreased at 24 hr p.i. only ($P \leq 0{\cdot}001$). Percentages of CD4, CD8 and B lymphocytes decreased in the livers of MHV3-infected mice at 24 and/or 48 hr p.i. ($P \leq 0{\cdot}05$ to $P \leq 0{\cdot}001$) (Fig. 5b), as previously reported.[41]

Analyses of cell-subset percentages, however, are not fully representative of recruited inflammatory cells because total number of isolated MNCs strongly decreased with time in the liver of MHV3-infected mice.[41] To properly reflect the evolution of cell recruitment in infected mice, absolute numbers of each inflammatory cell subset have been calculated using the percentage of each cell subset reported to total number of isolated MNCs. As shown in Fig. 5(c), the transient increase of neutrophil percentage observed in the liver of MHV3-infected mice was in accordance with the increase in neutrophil numbers at 24 hr p.i. only ($P \leq 0{\cdot}001$). However, low increase of absolute number of macrophages occurred at 48 hr p.i. only ($P \leq 0{\cdot}05$). In addition, both NK-T and NK cell numbers decreased ($P \leq 0{\cdot}05$ to $P \leq 0{\cdot}001$) in contrast to that seen in percentages. The decreases in numbers of CD4, CD8 and B cells were magnified when compared with percentages ($P \leq 0{\cdot}01$ and $P \leq 0{\cdot}001$) (Fig. 5b,d). The extensive cell necrosis in the liver of MHV3-infected mice at 72 hr p.i., however, did not allow us to isolate sufficient numbers of MNCs for accurate immunolabellings and cytofluorometric analysis.

In livers from MHV-A59-infected mice, however, percentages of neutrophils strongly increased as soon as 24 hr p.i. ($P \leq 0{\cdot}001$) whereas NK cells transiently increased ($P \leq 0{\cdot}05$) and NK-T cells decreased ($P \leq 0{\cdot}01$ and $P \leq 0{\cdot}001$) (Fig. 5e). Macrophage percentage slightly increased at 48 hr p.i. only ($P \leq 0{\cdot}05$). In contrast to that seen in the liver of MHV3-infected mice, only the B-cell percentage decreased slightly at 48 hr p.i. ($P \leq 0{\cdot}01$) whereas CD4 and CD8 lymphocyte percentages remained unchanged (Fig. 5f). The number of MNCs isolated in the liver of MHV-A59-infected mice did not significantly differ that in from mock-infected mice, in contrast with that seen in MHV3-infected mice. In consequence, variations in absolute numbers of cell subsets did not differ from percentages (results not shown).

Lower liver damage and viral replication in MHV3-infected TLR2 KO mice

We have previously observed that MHV3-induced acute hepatitis was less severe in TLR2 KO mice.[34] The comparative study between MHV3 and MHV-A59 infections regarding severity of hepatitis, TLR2 expression level, and inflammatory cytokines and chemokines in liver from infected mice support this hypothesis and suggest that higher virulence of MHV3 may be related to TLR2-dependent exacerbated inflammatory responses. To verify whether TLR2 is involved in aggravated hepatic damages and viral replication during acute MHV3 infection, groups of WT C57BL/6 and TLR2 KO mice were i.p. infected with MHV3 or MHV-A59 and survival rates, liver injury and viral load in the liver were monitored from 24 to 72 hr p.i. As shown in Fig. 6(a), mortality rate of MHV3-infected TLR2 KO mice was delayed when compared with infected WT mice as it occurred from only 96 to 120 hr p.i. in contrast to WT mice, for which mortality reached more than 70% of mice at 72 hr p.i. ($P \leq 0{\cdot}001$). Considering the fulminance of hepatitis, such a statistically significant delay can support a role for TLR2 in the pathogenic processes of hepatitis. As expected, no mortality was observed in WT and TLR2 KO mice infected with MHV-A59 (see Supplementary material, Fig. S2A). Histopathological analysis of livers from MHV3-infected TLR2 KO revealed inflammatory foci only by 48 hr p.i. and fewer necrotic foci at 72 hr p.i. when compared with liver from MHV3-infected WT mice (Fig. 6b compared with Fig. 1a). In livers from MHV-A59-infected TLR2 KO mice, however, few large inflammatory foci, similar to those observed in MHV-A59-infected WT mice, were noted (see Supplementary material, Fig. S2B). Accordingly, serum AST and ALT levels were lower in MHV3-infected TLR2 KO than in infected WT mice (Fig. 6c,d) ($P \leq 0{\cdot}05$ and $P \leq 0{\cdot}001$). Hepatic lesions, comparable to those seen in livers from MHV3-infected WT mice, occurred later in infected TLR2 KO mice (results not shown), leading to a delayed mortality of mice.

Viral replication of MHV3 in the liver of infected TLR2 KO, as determined by the expression of the viral nucleoprotein RNA (quantitative RT-PCR) and viral titres, was also lower and delayed when compared with replication in MHV3-infected WT mice (Fig. 6e,f) ($P \leq 0{\cdot}05$ to $P \leq 0{\cdot}001$). MHV-A59 replication in livers from TLR2 KO mice, however, was not altered (see Supplementary material, Fig. S2C) when compared with infected WT mice.

Dietrich *et al.*[42] have previously reported that TLR2 signalling may lead to IFN-α/β production when TLR2 is internalized in endosomes. As shown in Fig. 6(g,h), transcription and production of IFN-β occurred later and reached lower levels in MHV3-infected TLR2 KO mice than in WT mice ($P \leq 0{\cdot}001$). No significant increase of IFN-α transcription has been observed in both MHV3-infected mouse strains (results not shown).

TLR2 is involved in aggravation of MHV3-induced hepatitis instead of other TLRs or helicase genes

To support the hypothesis that severity of MHV3-induced hepatitis mainly involves TLR2 rather than other PRRs, kinetics of transcription levels of surface TLR2 and TLR4, endosomal TLR3 and TLR7, as well as helicase RIG-1 and MDA-5, genes were compared in livers from MHV3-infected WT and TLR2 KO mice. As observed above, an increase of surface TLR2 but not TLR4 gene expression levels over the course of infection by MHV3 was confirmed in the liver of WT mice ($P \leq 0{\cdot}05$ to $P \leq 0{\cdot}001$) (Fig. 7a,b) whereas absence of TLR2 induction was validated in infected TLR2 KO mice. Endosomal TLR3 or

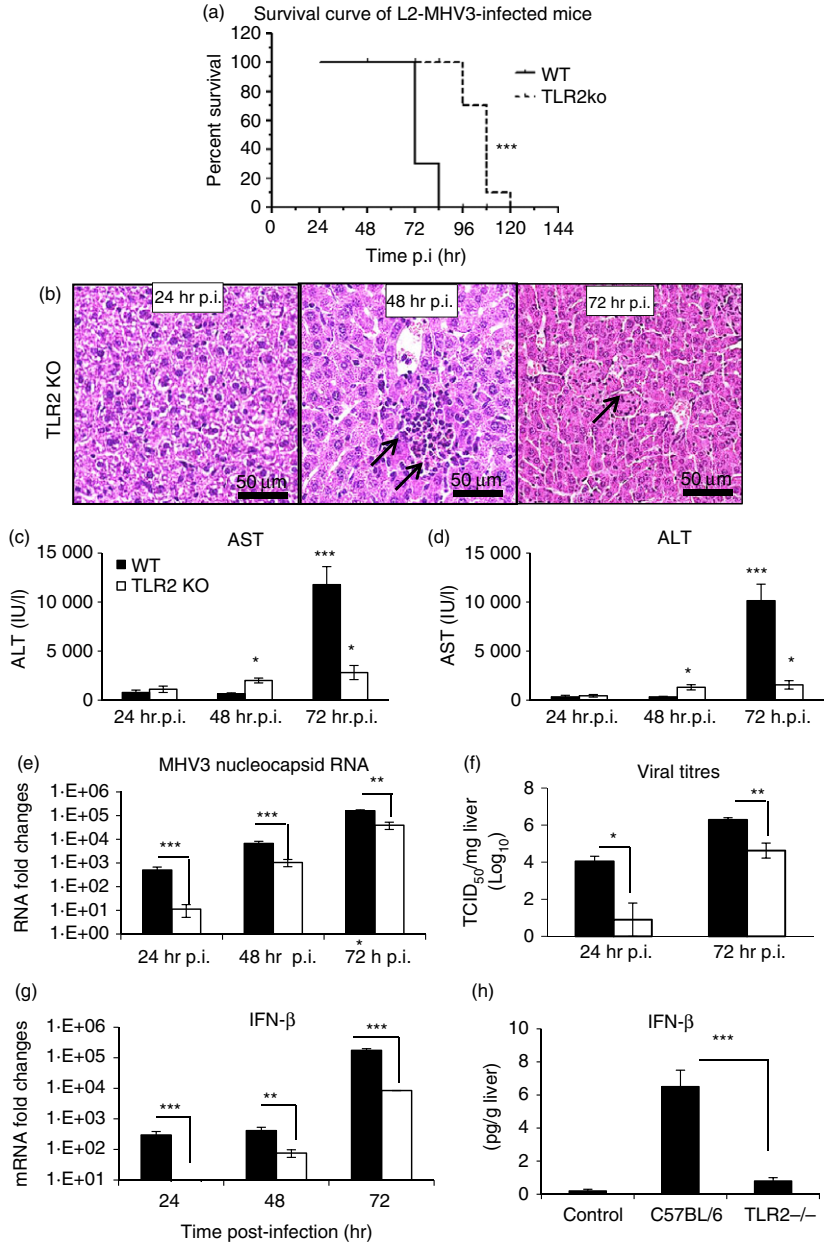

Figure 6. Hepatic damages, viral replication and interferon-β (IFN-β) production in the liver of murine hepatitis virus (MHV) 3-infected wild-type (WT) and Toll-like receptor 2 knockout (TLR2 KO) mice. Groups of six to seven C57BL/6 (WT) and TLR2 KO mice were intraperitoneally (i.p.) infected with 1000 $TCID_{50}$ of MHV3. Survival curve of MHV3-infected WT and TLR2 KO mice (a). Histopathological analysis was conducted on livers from MHV3-infected TLR2 KO at 24, 48 and 72 hr post-infection (p.i.) (b). Serum samples from MHV3-infected WT and TLR2 KO mice were assayed for aspartate transaminase (AST) (c) and alanine transaminase (ALT) (d) activity at 24–72 hr p.i. Replication of MHV3 in livers of infected mice was determined by analysis of the nucleoprotein (MHV-N) RNA expression at 24, 48 and 72 hr p.i. by quantitative RT-PCR, and by viral titration ($TCID_{50}$) at 24 and 72 hr p.i. (e, f). Messenger RNA fold increases for IFN-β were analysed in livers from MHV3-infected mice by quantitative RT-PCR at 24, 48 and 72 hr p.i. (g). Values represent fold change in gene expression relative to mock-infected mice (arbitrary value of 1) after normalization with HPRT expression. Protein levels of IFN-β in the liver were quantified by ELISA test at 72 hr p.i. (h). (*$P < 0{\cdot}05$; **$P < 0{\cdot}01$; ***$P < 0{\cdot}001$).

RIG-1 and MDA-5, but not TLR7, gene expression levels similarly increased in livers from both WT and TLR2 KO mice infected with MHV3 ($P \leq 0{\cdot}05$ to $P \leq 0{\cdot}001$) (Fig. 7c–f). These data support that MHV3 infection specifically increases the expression of TLR2 in the liver of WT mice because other TLRs and helicases are similarly expressed in infected WT and TLR2 KO mice.

Decreases of inflammatory cytokines, alarmin IL-33 but not Fgl-2 gene expression in the liver of MHV3-infected TLR2 KO mice

We have previously reported that IL-6 and TNF-α production by peritoneal macrophages *in vitro* infected with MHV3 depends on TLR2 activation by the viral glycoprotein S.[34] In order to verify whether TLR2 is specifically involved in the exacerbation of the inflammatory cytokine response during MHV3 infection, as previously observed in Fig. 3, levels of TNF-α and IL-6 expression were compared by quantitative RT-PCR and ELISA tests in MHV3-infected WT and TLR2 KO mice. As shown in Fig. 8(a), mRNA levels of IL-6 increased throughout MHV3 infection in WT mice ($P \leq 0{\cdot}01$ and $P \leq 0{\cdot}001$) but were impaired in infected TLR2 KO mice as demonstrated by fourfold lower levels at 72 hr p.i. ($P \leq 0{\cdot}05$). Interleukin-6 secretion increased only in the liver of MHV3-infected WT mice ($P \leq 0{\cdot}001$) (Fig. 8b). Similarly, lower expression of TNF-α was found in the livers of MHV3-infected

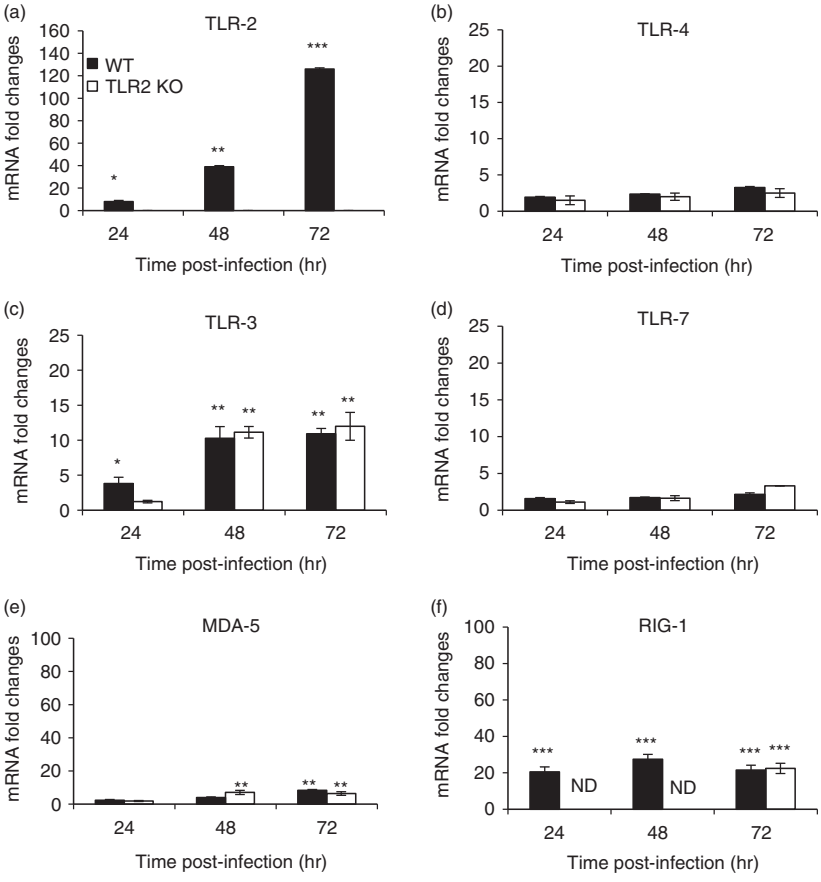

Figure 7. Messenger RNA levels of Toll-like receptors (TLRs) and helicases in the livers of murine hepatitis virus (MHV) 3-infected wild-type (WT) and TLR2 knockout (KO) mice. Groups of six or seven C57BL/6 (WT) and TLR2 KO mice were intraperitoneally (i.p.) infected with 1000 $TCID_{50}$ of MHV3. At 24, 48 or 72 hr post-infection (p.i.), livers from each group were collected and Toll-like receptors (TLR2, -3, -4, -7) (a–d) and helicases [retinoic acid inducible gene (RIG-1) and melanoma differentiation-associated protein (MDA-5)] (e and f) mRNA fold changes were analysed by quantitative RT-PCR. Values represent fold change in gene expression relative to mock-infected mice (arbitrary value of 1) after normalization with HPRT expression. (*$P < 0{\cdot}05$; **$P < 0{\cdot}01$; ***$P < 0{\cdot}001$). N.D. not done.

TLR2 KO mice than WT mice ($P \leq 0{\cdot}05$ and $P \leq 0{\cdot}001$) (Fig. 8c). Such defects in TNF-α mRNA expression correlated with lower production at 72 hr p.i. ($P \leq 0{\cdot}001$) (Fig. 8d).

The IL-33 gene expression level was delayed to 72 hr p.i. in MHV3-infected TLR2 KO mice whereas it was induced as early as 24 hr p.i. in WT mice ($P \leq 0{\cdot}01$) (Fig. 8e). mRNA levels for Fgl-2, however, increased similarly up to 48 hr p.i. in the livers of both WT and TLR2 KO infected mice ($P \leq 0{\cdot}05$ and $P \leq 0{\cdot}01$) (Fig. 8f).

Decreases in CXCL1, CCL2 and CXCL10 levels in the livers of MHV3-infected TLR2 KO mice

It was recently shown that the TLR2 signalling network is essential for inflammatory cell recruitment in acute liver injury.[39] Accordingly, we hypothesized that TLR2 activation may be involved in the induction of the high chemokine levels observed during MHV3 infection (Fig. 4) but expected that it would be decreased in liver from infected TLR2 KO mice. As shown in Fig. 9(a,b), mRNA and protein levels of CXCL1 increased sooner and higher in the liver of MHV3-infected WT mice than TLR2 KO mice ($P \leq 0{\cdot}05$ to $P \leq 0{\cdot}001$). Transcription and production levels of CCL2 and CXCL10 also increased over infection time in infected WT mice but were dramatically impaired and delayed in infected TLR2 KO mice ($P \leq 0{\cdot}05$ to $P \leq 0{\cdot}001$) (Fig. 9c–f). Immunolocalization of CXCL10 showed lower expression in hepatocytes of MHV3-infected TLR2 KO than WT mice at 72 hr p.i. (Fig. 9g).

Delayed recruitment of neutrophils, NK cells and macrophages in the liver of MHV3-infected TLR2 KO mice

To verify whether the reduced production of CXCL1, CCL2 and/or CXCL10 in the liver of MHV3-infected TLR2 KO mice involved lower recruitment of inflammatory cells, intrahepatic MNCs were isolated from the livers of mock-infected and MHV3-infected WT and TLR2 KO mice at 24 and 48 hr p.i., immunolabelled and then phenotyped by cytofluorometric analysis, as indicated above. As shown in the Supplementary material (Fig. S3A), percentages of neutrophils and macrophages increased at 48 hr p.i. only in the liver of MHV3-infected TLR2 KO mice ($P \leq 0{\cdot}001$) whereas NK and NKT cell percentages remained unchanged. Both B and CD8 cell percentages, however, decreased in the liver of infected TLR2 KO mice ($P \leq 0{\cdot}01$ and $P \leq 0{\cdot}001$) (see Supplementary material, Fig. S3B). As no major reduction in total isolated MNCs was observed over time in livers from MHV3-infected TLR2 KO mice in contrast to that

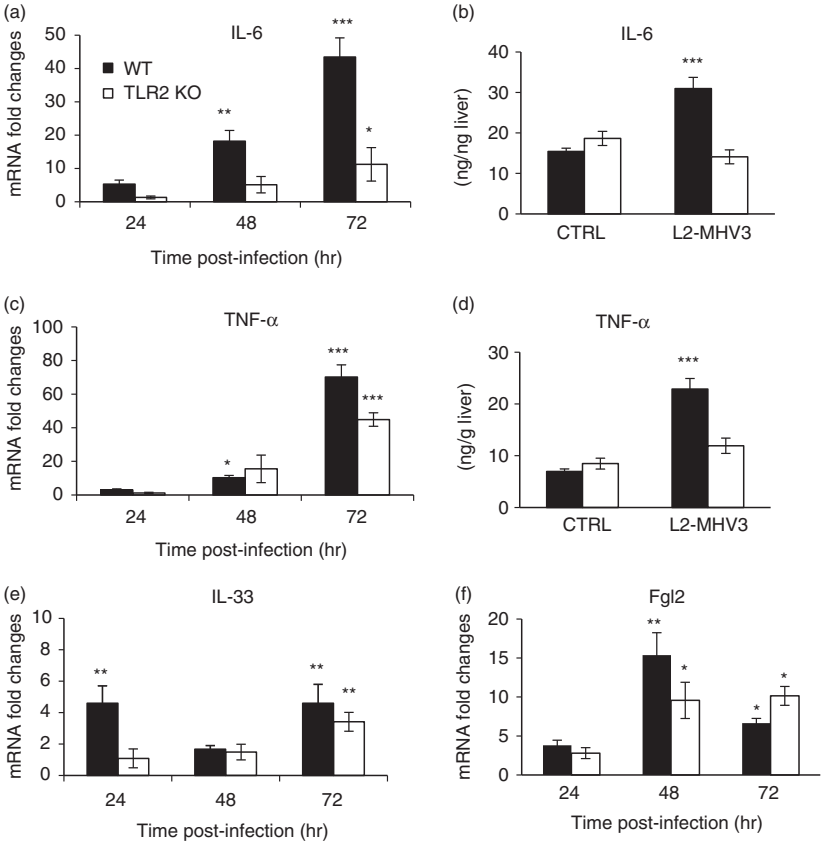

Figure 8. Expression levels of cytokines, interleukin-33 (IL-33) and fibrinogen-like 2 (Fgl-2) gene in the liver of murine hepatitis virus (MHV) 3-infected wild-type (WT) and Toll-like receptor 2 (TLR2) knockout (KO) mice. Groups of six or seven C57BL/6 (WT) and TLR2 KO mice were intraperitoneally (i.p.) infected with 1000 $TCID_{50}$ of MHV3. At 24, 48 or 72 hr p.i., livers from each group were collected. mRNA fold increases for IL-6 (a), tumour necrosis factor-α (TNF-α) (c), IL-33 (e), and the Fgl-2 (f) were evaluated by quantitative RT-PCR in livers of infected mice. Values represent fold change in gene expression relative to mock-infected mice (arbitrary value of 1) after normalization with HPRT expression. Production levels of IL-6 (b) and TNF-α (d) were quantified in livers by ELISA tests at 72 hr p.i. (*$P < 0{\cdot}05$; **$P < 0{\cdot}01$; ***$P < 0{\cdot}001$).

seen in MHV3-infected WT mice, changes in percentages for each cell subset reflect similar changes in cell numbers (results not shown).

Taken together, these results suggest that TLR2 favours greater hepatic damage, more viral replication and a stronger inflammatory response as well as the transient increase in inflammatory cells and losses of NK and NKT cells in the liver only in MHV3-infected WT mice, not in MHV-A59-infected WT mice or MHV3-infected TLR2 KO mice, supporting an aggravating role for TLR2 in acute hepatitis.

TLR2-dependent viral replication and inflammatory responses in *in vitro* MHV3-infected macrophages

We aimed to identify the cells involved in the exacerbated TLR2-dependent inflammatory responses in the liver of MHV3-infected mice. We first investigated whether TLR2 expression was increased in *in vitro* infected macrophages, hepatocytes and LSECs. Preliminary data revealed that both LSECs (Bleau *et al.* manuscript in revision) and macrophages expressed higher TLR2 expression levels upon MHV3 infection. It has been previously demonstrated that macrophages are the first target cells following MHV infection and that lower virulence of MHV-A59 is due to suppression of viral replication by these cells.[22,33] In addition, induction of TNF-α and IL-6 in peritoneal macrophages infected with MHV3 was shown to depend on surface (S) viral protein fixation to TLR2 and heparan sulphate[34] in contrast to MHV-A59.[43] These observations suggest that macrophages may be one cellular source participating in TLR2-dependent inflammatory responses during MHV3 infection.

We first verified whether MHV-A59 and MHV3 differentially replicate and induce cytokine production in macrophages. J774A.1 macrophages were infected with both viruses at 0·1–1 m.o.i. for 4–24 hr p.i. and MHV nucleoprotein (N-MHV) and IL-6 expression were then evaluated. As shown in Fig. 10(a), the nucleoprotein RNA expression occurred sooner and reached higher levels in cells infected by MHV3 than MHV-A59 ($P \leq 0{\cdot}01$ to $P \leq 0{\cdot}001$). In accordance, viral titres were also higher in MHV3-infected cells (results not shown). Rapid and higher IL-6 transcription levels occurred in MHV3-infected cells (Fig. 10b) except at 24 hr p.i. ($P \leq 0{\cdot}001$) and correlated with higher production levels (MHV3: 430 ± 45 pg/ml; MHV-A59: 82 ± 15 pg/ml; $P \leq 0{\cdot}001$). To verify whether higher replication of MHV3 in macrophages was associated with faster viral entry into cells, immediate-early levels (within 60 min p.i.) of N-MHV RNA levels were evaluated in MHV3 and MHV-A59-infected J774.1 cells. Higher levels of N-MHV mRNA were detected in MHV3-infected cells than in MHV-A59-infected cells, from 5 min p.i. until 60 min p.i. ($P \leq 0{\cdot}05$ to $P \leq 0{\cdot}001$) (Fig. 10c).

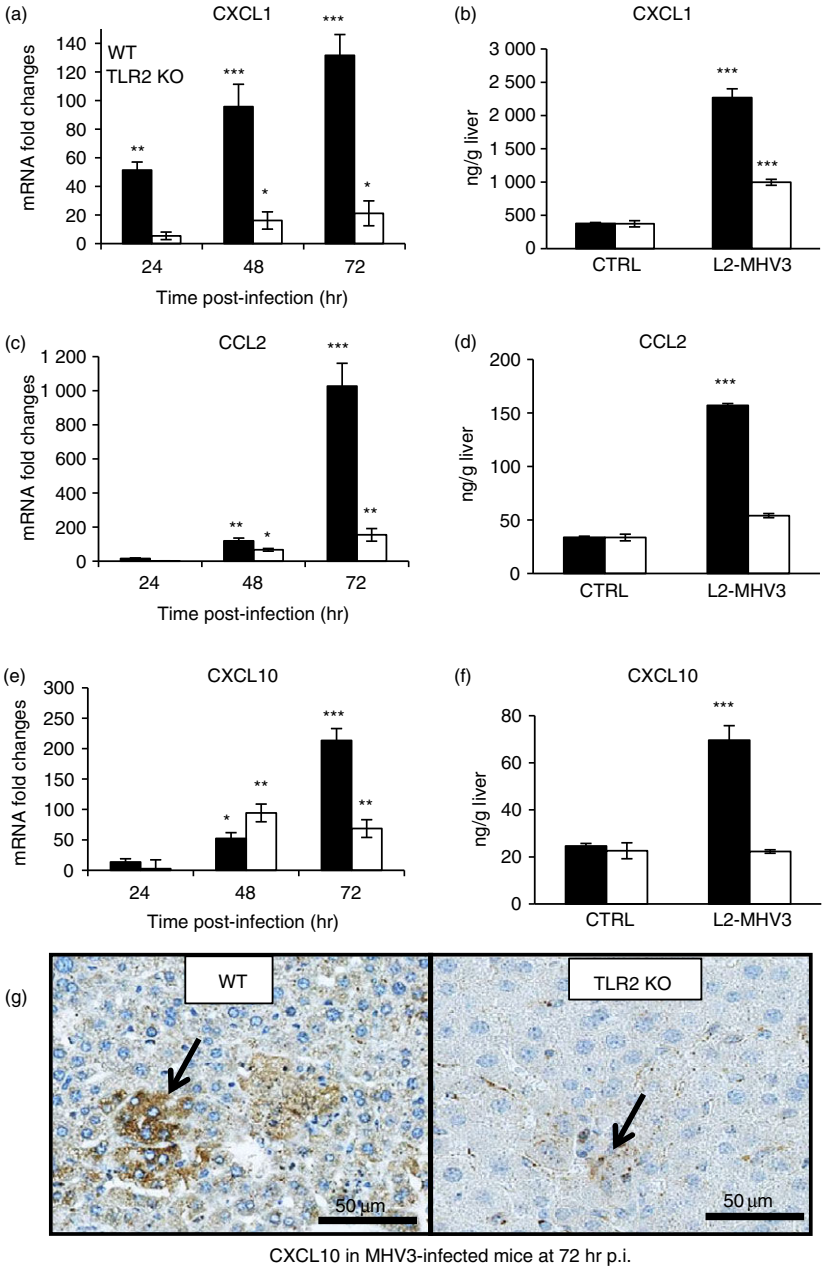

CXCL10 in MHV3-infected mice at 72 hr p.i.

Figure 9. Messenger RNA expression levels and production of CCL2, CXCL1 and CXCL10 in the livers of murine hepatitis virus (MHV) 3-infected wild-type (WT) and Toll-like receptor knockout (TLR2 KO) mice. Groups of six or seven C57BL/6 (WT) and TLR2 KO mice were intraperitoneally (i.p.) infected with 1000 $TCID_{50}$ of MHV3. At 24, 48 or 72 hr post-infection (p.i.), livers from each group were collected. mRNA expression for CXCL1 (a), CCL2 (c) and CXCL10 (e) genes was evaluated by quantitative RT-PCR in livers from MHV3-infected WT and TLR2 KO mice. Values represent fold change in gene expression relative to mock-infected mice (arbitrary value of 1) after normalization with HPRT expression. Protein levels of CXCL1 (b), CCL2 (d) and CXCL10 (f) in the liver were quantified by ELISA test at 72 hr p.i. Immunolocalization of CXCL10 in the liver determined by histochemistry staining in MHV3-infected WT and TLR2 KO mice (g). (*$P < 0{\cdot}05$; **$P < 0{\cdot}01$; ***$P < 0{\cdot}001$).

Since early p38 MAPK activation is involved in early secretion of IL-6 in MHV3-infected peritoneal macrophages,[34] the kinetics of p38 MAPK phosphorylation was evaluated within the first 60 min p.i. by ELISA test. A TLR2 agonist (Pam3C5K4) was used as positive control for TLR2-dependent induction of the p38 MAPK signalling pathway. Results shown in Fig. 10(d) indicate that phosphorylated p38 MAPK rapidly increased in cells treated with TLR2 agonist and peaked within 30 min ($P \leq 0{\cdot}001$). Similar increase, peaking at 30 min, also occurred in MHV3 infected cells ($P \leq 0{\cdot}05$ to $P \leq 0{\cdot}01$) whereas no increase of phosphorylated p38 MAPK was detected in MHV-A59-infected cells. These results suggest that TLR2 may be involved in rapid and higher viral replication and IL-6 secretion in MHV3-infected cells.

To verify this hypothesis, J774.1 cells were next treated with siRNAs for TLR2 and/or CEACAM1a genes before infection with MHV3 at an m.o.i of 0·1–1·0 for 22 hr. MHV RNA, TLR2 and CEACAM1a fold changes were then evaluated by quantitative RT-PCR and infectious viruses were titrated. Results indicate that MHV-RNA expression decreased in MHV3-infected cells treated with siRNA for CEACAM1a and/or TLR2 ($P \leq 0{\cdot}01$) (Fig. 10e). Similarly to N-MHV RNA levels, infectious MHV3 virus titres in supernatants of infected J774.1 cells decreased in siCEACAM1a- or siTLR2- or both

siCEACAM1a/siTLR2-treated J774.1 cells when compared with untreated infected cells ($1{\cdot}2 \times 10^6 \pm 0{\cdot}3 \times 10^6$; $4{\cdot}5 \times 10^5 \pm 0{\cdot}3 \times 10^5$ and $1{\cdot}5 \times 10^4 \pm 0{\cdot}3 \times 10^4$ compared with $2{\cdot}5 \times 10^6 \pm 0{\cdot}8 \times 10^6$ $TCID_{50}$/ml, respectively; $P \leq 0{\cdot}05$ to $P \leq 0{\cdot}01$). MHV-A59 RNA, however, decreased only in cells treated with siRNA for CEACAM1a (alone or in combination with siRNA for TLR2) ($P \leq 0{\cdot}01$)(Fig. 10e). As expected, TLR2 expression levels increased higher in MHV3-infected macrophages, and such an increase was also inhibited following knockdown of one or both CEACAM1a and TLR2 genes ($P \leq 0{\cdot}001$) (Fig. 10f).

To confirm the role of TLR2 in the early induction of the IL-6 response by MHV3, IL-6 mRNA fold changes and secretion were assessed in macrophages treated with siRNA for TLR2 and/or CEACAM1a and infected for 5 or 22 hr p.i. As shown in Fig. 10(g,h), knockdown of CEACAM1a and/or TLR2 genes strongly decreased IL-6 transcription and secretion levels by MHV3-infected macrophages, as also shown at 5 hr p.i. ($P \leq 0{\cdot}001$), indicating that IL-6 production depends on both CEACAM1a and TLR2 molecules. The efficiency of siTLR2 treatment and the involvement of TLR2 in IL-6 induction was confirmed by significant decreases of IL-6 expression in cells activated by the TLR2 agonist Pam_3CSK4 ($P \leq 0{\cdot}01$) (Fig. 10g).

Discussion

In this work, we demonstrated for the first time an aggravating role for TLR2 in the acute phase of hepatitis in comparing the fulminant MHV3-induced hepatitis to milder hepatitis induced by the closely related MHV-A59 infection in mice. The involvement for TLR2 in the fulminance of MHV3-induced acute hepatitis was shown by earlier mortality and higher hepatic lesions and viral replication in infected WT mice than TLR2 KO mice whereas subclinical hepatitis induced by MHV-A59 infection was not influenced by TLR2 as mortality rate, hepatic damages and viral titres were comparable in both infected WT and TLR2 KO mice. The severity of hepatitis in MHV3-infected WT mice correlated with higher expression of TLR2, IFN-b inflammatory cytokines and chemokines and alarmin IL-33 in the liver. Despite higher chemokine levels, neutrophils, NK, NK-T cells or macrophages were only transiently or weakly recruited in the liver of MHV3-infected WT mice in contrast to delayed but sustained inflammatory cells recruitment in MHV3-infected TLR2 KO or MHV-A59-infected WT mice.

It is the first report showing higher TLR2 expression over other PRRs in acute viral hepatitis during the first days of infection. Many PRRs are activated after exposure to hepatotrophic viruses, such as endosomal TLR3 or TLR7 and intracytoplasmic helicases RIG-1 or MDA-5, to activate IFN type 1 and inflammatory factors. In the livers from MHV3- but not MHV-A59-infected WT mice, we have observed greater expression of TLR2 over other PRRs such as TLR3, RIG-1, MDA-5 or TLR4 and TR7, suggesting that MHV3 preferentially activates TLR2 transcription. Higher expression of TLR2 has been recently associated with disease progression of hepatitis C.[44] Levels of hepatic inflammation in HCV- and HCV/HIV-infected patients, also correlated with higher transcription of TLR2 and TLR4 genes in the liver[17] suggesting a pro-inflammatory role for TLR2 in hepatitis. Accordingly, blocking of TLR2 was recently shown to attenuate Concanavalin A-induced experimental hepatitis in mice.[45] We have observed fewer hepatic lesions, less viral replication and lower inflammatory responses in MHV3-infected TLR2 KO mice, indicating that TLR2 may act as an aggravating factor in fulminant hepatitis. However, TLR2 KO mice were not protected from MHV3-induced lethal hepatitis, but survival was significantly improved due to delayed occurrence of hepatic necrosis (observations not shown), supporting that other TLR2-independent mechanisms are also involved in the outcome of MHV3 infection. Unlike MHV3, the weakly hepatotrophic MHV-A59 showed no ability to increase TLR2 expression in the liver and induced comparable mild hepatitis in WT or TLR2 KO mice, strengthening the importance of TLR2 in MHV3-induced hepatitis.

Activation of TLR2 through the MyD88 /nuclear factor-κB-dependent pathway leads to up-regulation of numerous genes involved in innate host defence such as TNF-α, IL-1β, IL-6, IFN-γ, chemokines and TLR expression (reviewed in ref. 46). We have observed that TNF-α and IL-6 increased sooner and more in the liver of MHV3-infected WT mice than in TLR2 KO or MHV-A59-infected mice. It was previously reported that TNF-α

Figure 10. *In vitro* murine hepatitis virus (MHV) 3 and MHV-A59 infections of macrophages untreated or treated with small interfering (si) RNA for Toll-like receptor 2 (TLR2) and CEACAM1a. J774A.1 macrophages were infected with 0·1–1 multiplicity of infection (m.o.i.) of MHV3 or MHV-A59 and incubated for various times post-infection (p.i.) according to experiments (a–d). Cells were also transfected with mouse CEACAM1 and/or TLR2 siRNA for at least 24 hr before infections in other experiments (e and f). Nucleocapsid RNA (a, c and e), TLR2 (f), and interleukin-6 (IL-6) (b and g) mRNA fold changes were analysed by quantitative RT-PCR at various times p.i. Values represent fold change in gene expression relative to mock-infected mice (arbitrary value of 1) after normalization with HPRT expression. Phosphorylated p38 mitogen-activated protein kinase (MAPK) levels were evaluated by ELISA test and expressed as percentages of total p38 MAPK (d). The synthetic bacterial ligand for TLR2–TLR1 (Pam_3CSK4) was used as TLR2 positive control for the detection of phosphorylated p38 MAPK and IL-6 expression (d and g). IL-6 secretion was quantified by ELISA test in MHV3-infected cells at 5 hr p.i. (h). Results are representative of two different experiments. (*$P < 0{\cdot}05$; **$P < 0{\cdot}01$; ***$P < 0{\cdot}001$). N.D. Not done.

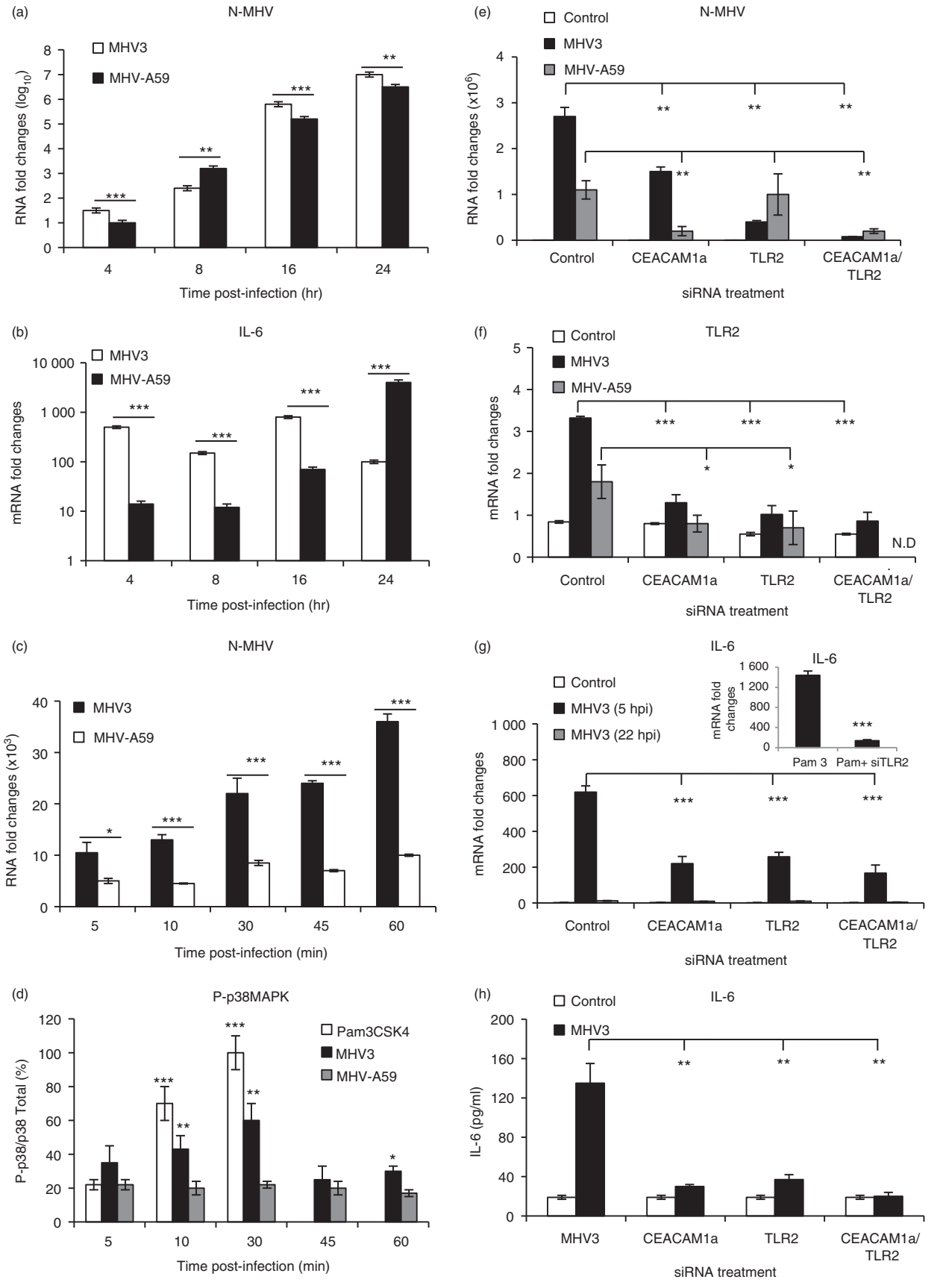
(a)
N-MHV
MHV3
MHV-A59
RNA fold changes (log10)
Time post-infection (hr)
(b)
IL-6
mRNA fold changes
Time post-infection (hr)
(c)
N-MHV
RNA fold changes (x10³)
Time post-infection (min)
(d)
P-p38MAPK
Pam3CSK4
P-p38/p38 Total (%)
Time post-infection (min)
(e)
N-MHV
Control
RNA fold changes (x10⁶)
Control
CEACAM1a
TLR2
CEACAM1a/ TLR2
siRNA treatment
(f)
TLR2
mRNA fold changes
N.D
siRNA treatment
(g)
IL-6
MHV3 (5 hpi)
MHV3 (22 hpi)
mRNA fold changes
Pam 3
Pam+ siTLR2
siRNA treatment
(h)
IL-6
IL-6 (pg/ml)
siRNA treatment

activity significantly increases as soon as 24 hr p.i. during MHV3 infection, even before the virus is detectable in the liver,[47] supporting an early activation through an unidentified signalling pathway. Following i.p. infection, MHV3 primarily replicates in peritoneal macrophages and then within liver Kupffer cells and LSECs.[48,49] A role for macrophages in MHV3-induced TLR2-dependent inflammatory responses is supported by *in vitro* infections. Our results indicate that both CEACAM1a and TLR2 are involved in viral replication and early IL-6 expression (as soon as 5 hr p.i.) in macrophages. Jacques *et al.*[34] have previously demonstrated that TLR2 and heparan sulphate were involved in the induction of inflammatory cytokines in MHV3-infected macrophages. Our results suggest that higher and earlier TLR2-dependent IL-6 induction by MHV3 may be related to higher and earlier activation of the p38 MAPK pathway by the virus. In addition, since a very early role for the p38 MAPK pathway (within 30 min) was reported in viral replication of MHV3 in J774.1 macrophages,[50] higher and earlier replication of MHV3 than MHV-A59 may also result from differential activation of this pathway by the viruses. No role for TLR2, however, was reported in viral replication and induction of IL-6 by MHV-A59.[43,51] Such a difference may explain the lower viral load and inflammatory responses in the liver of MHV-A59-infected mice. In addition, preliminary data have shown that UV-inactivated MHV3 viral particles bound more rapidly to macrophage surface (<10 min) than UV-inactivated MHV-A59, suggesting that S protein from MHV3 may express higher affinity for TLR2 than MHV-A59.

Hepatocytes and non-parenchymal hepatic cells were also reported to express both the viral receptor CEACAM1a[26] and TLR2.[52,53] *In vitro* MHV3 infection in hepatocytes leads to rapid cell death (less than 24 hr p.i.) and low viral infectious titres and inflammatory cytokine levels, which are barely influenced by siTLR2 treatments (results not shown), suggesting that the exacerbated inflammatory response in the liver of MHV3-infected mice does not mostly depend on infected hepatocytes, in spite of extensive necrosis foci. Vascular and tolerant properties of LSECs, however, were disturbed when *in vitro* infected with MHV3 (Bleau *et al*. manuscript in revision). Hence, we can hypothesize that TLR2 fixation of viral infectious particles or free viral S proteins on MHV3 permissive cells, such as Kupffer cells and LSECs, may favour both viral replication and exacerbated inflammatory responses that may contribute to higher liver injury in MHV3-infected mice. Indeed, high levels of TNF-α in the liver are generally associated with extensive necrosis,[54] and absence of TNF-α, but not IL-6, was recently shown to significantly reduce hepatic lesions (AST/ALT) and increase the survival of MHV3-infected mice.[55]

Following viral replication in macrophages and LSECs, viruses reach hepatocytes leading to rapid extensive syncytia and cell lysis.[28] The fulminance of liver lesions indicates that innate antiviral mechanisms cannot control viral infection and inflammatory responses. Type I IFN production by infected cells is the most important antiviral mechanism acting in the first days of infection. Higher IFN-β production, however, was found in the liver of MHV3-infected WT mice than TLR2 KO mice or MHV-A59-infected WT mice. The positive correlation between IFN-β production and viral replication levels may reflect the spreading of viral replication in the liver rather than the efficiency of antiviral effects. Indeed, it was already reported that higher levels of type I IFN were produced simultaneously with higher MHV3 titres by peritoneal macrophages from C57BL/6 mice,[56] supporting a negligible role of type I IFN in the control of MHV3 replication. Such explanation is also supported by a positive correlation between low levels of IFN-β and low viral replication in MHV3-infected TLR2 KO mice or MHV-A59-infected WT mice, indicating that lower viral replication does not result from higher production of antiviral IFN-β. In addition, no significant IFN-α expression was induced in the liver of all infected groups of mice (results not shown), indicating no major role for type I IFN in the control of MHV replication and hepatitis. In addition, type I IFN response in mouse coronavirus infections depends mainly on TLR3 and helicases RIG-1 or MDA-5 engagement by viral RNAs.[57–59] Transcription levels of TLR3, RIG-1 and MDA-5 were comparable in livers from both MHV3-infected WT and TLR2 KO mice and less transcribed in MHV-A59-infected WT mice, suggesting that higher induction of IFN-β by MHV3 infection did not depend on these PRRs. We can therefore postulate that higher levels of IFN-β in the livers of MHV3-infected WT mice may result from extensive hepatic infection and/or TLR2 engagement by MHV3. Indeed, Dietrich *et al.*[42] have demonstrated that translocation of TLR2 in endolysosomal compartments following ligand engagement can trigger IFN-β production via the MyD88/interferon regulatory factor (IRF)-1/IRF-7-dependent pathway in macrophages. Preliminary data revealed increased expression of IRF-7 in livers from MHV3-infected WT mice, suggesting activation of this signalling pathway in some hepatic cells. Future work should address this hypothesis. Nevertheless, such an interesting potential new role for TLR2 in IFN-β regulation may not be of major importance in MHV3 infection as no protection against hepatitis seems to be provided by high IFN-β levels.

TLR2 activation also leads to production of chemokines involved in inflammatory cell recruitment. Earlier and higher production of CXCL1, CCL2 and CXCL10, as seen in the liver of MHV3-infected WT mice, may involve rapid recruitment of neutrophils, macrophages and NK or T-cell subsets, respectively (reviewed in ref. 40). As expected, CXCL1 production and concomitant neutrophil recruitment occurred sooner in the liver of

MHV3-infected WT mice, suggesting that increase in neutrophils may result from early CXCL1 release, as demonstrated by Moles *et al.*[39] The subsequent loss of neutrophils at 48 hr p.i., however, did not depend on a decrease of CXCL1 production because levels increased up to 72 hr p.i. We can hypothesize that recruited neutrophils may serve as a new cell target for viral infection leading to cell apoptosis, such as previously demonstrated for NK cells.[60] Work is in progress to clarify the loss of these cells during MHV3 infection. Our data regarding neutrophils slightly differ from those of Xu *et al.*[61] who reported percentage increases of neutrophils up to 48 hr p.i in the liver of MHV3-infected mice. Such apparent discrepancy results from the dramatic decrease in total intrahepatic MNCs, including NK, B and CD4 cells, leading to an apparent increase in neutrophil percentages in spite of a reduction in their absolute number, such as is demonstrated in the present work. These authors also linked neutrophil infiltration to a TNF-α-dependent Fgl-2 production. Our results do not support this hypothesis as chemokine production and neutrophil infiltration in the liver occurred earlier than Fgl-2 induction in MHV3-infected WT mice. Total counts of MNCs in the livers of both MHV3-infected TLR2 KO mice and MHV-A59-infected WT mice were not highly altered over infection time and neutrophil numbers steadily increased up to 48 hr p.i. supporting a recruitment of these cells despite lower levels of CXCL1. The delayed and preserved neutrophil pool may therefore favour viral clearance and contribute to controlling acute hepatitis, as suggested by lower viral titres, inflammation and damages in these mice. Recent work regarding the respiratory rat coronavirus infection showed that neutrophils were required for an effective antiviral response but could also contribute to lung pathology.[62] On the other hand, we cannot exclude that higher levels of chemokines in the liver of MHV3-infected WT mice may also contribute to hepatotoxicity without respect to neutrophil infiltration.[63]

We have similarly observed lower macrophage recruitment in the livers of MHV3-infected WT mice than MHV3-infected TLR2 KO and MHV-A59-infected WT mice despite higher production of CCL2. It was previously demonstrated that macrophage expansion in the liver is related to influx of peripheral monocytes facilitated by high levels of CCL2 rather than to increase of Kupffer cells[64] (reviewed in ref. 65). However, resident and recruited macrophages are permissive to MHV3 infection[48,49] and we have shown that viral replication in macrophages is increased by TLR2, suggesting that low number of macrophages in the livers of MHV3-infected WT mice result from higher viral replication and subsequent cell lysis. Accordingly, the low presence of inflammatory cells in necrosis foci observed in livers from MHV3-infected WT mice may result from virus-induced cell lysis of recruited MNCs. Lower levels of CXCL-1 and CCL2 in the livers of MHV3-infected TLR2 KO and MHV-A59-infected WT mice involved lower but sustained recruitment of neutrophils and macrophages, suggesting that these cells might be protective rather than deleterious in acute hepatitis process. In agreement, depletion of macrophages in MHV-A59-infected mice has been shown to promote lethal fulminant hepatitis within 4 days p.i.[23]

In addition, NK, NK-T, B and T lymphocytes decreased only in the liver of MHV3-infected WT mice despite higher levels of CXCL10. Such a reduction may result directly from permissivity of NK and B cells to viral infection, and indirectly from virally induced lysis of thymic dendritic cells, as was previously reported.[60,66,67] The larger inflammatory foci observed in the livers of MHV-A59-infected WT mice and MHV3-infected TLR2 KO mice may therefore reflect the sustained recruitment of MNCs. On the other hand, high amounts of CXCL10 in the liver have already been associated with apoptosis of human and murine hepatocytes,[68] suggesting that high levels of CXCL10 induced by MHV3 may also contribute to hepatic lesions.

Some other inflammatory factors induced by MHV3 infection were less dependent, or not dependent, on TLR2. Indeed, we have observed that IL-33 release was less influenced by TLR2 and rather reflected the severity of liver damage, as was previously reported.[69,70] We have recently shown that IL-33 expression was up-regulated in the liver of MHV3-infected C57BL/6 mice, mainly in LSECs, vascular endothelial cells and hepatocytes in the first 24–32 hr p.i.[36] This study also demonstrated that TLR3 was involved in the up-regulation of IL-33 in poly(I:C)-treated mice. However, IL-33 expression was more strongly induced in the livers of MHV3-infected WT mice than in poly(I:C)-treated mice, suggesting that other PRRs might be involved in IL-33 release during MHV3 infection. Our observations suggest that TLR2 might be another candidate involved in early IL-33 induction. The mechanism(s) by which MHV3 favour(s) IL-33 secretion is pending and need(s) further investigation. The induction of the vascular factor Fgl-2, a pro-thrombinase promoting microvascular thrombosis and hepatocyte necrosis during MHV3 infection,[37,38] was comparable in WT and TLR2 KO mice and remained low or delayed in MHV-A59-infected WT mice, indicating that this factor is not regulated by TLR2 and not involved in TLR2-exacerbated hepatic damage, in spite of its worsening role in hepatitis outcome.

The present work with animal models of viral hepatitis induced by two closely related serotypes of MHVs, highlights the complex interactions between surface TLR2 and intracellular PRRs in the recognition of viral infections and the induction of protective or worsening inflammatory responses during acute infections. The use of the MHV3 model provided new insights into the aggravating role of surface TLR2 in acute viral diseases. Activation of surface TLR signalling pathways has been recently

associated with pathogenic processes in several viral infections. Indeed, TLR2 and/or TLR4 are involved in the induction of inflammatory response in severe acute respiratory syndrome virus, several herpesviruses (herpes simplex virus 1, varicella virus, cytomegalovirus), influenza, HIV, HBV and HCV infections.[6–14] In most cases, TLR2-promoted inflammatory TNF-α, IL-6 or chemokine IL-8 responses are mediated by macrophages.[6,7,12,13,17] The viral mechanisms involved in the activation of TLR2 inflammatory pathways are not clearly elucidated. The ability of MHV3 viral proteins to bind and activate TLR2 signalling is not unique to coronaviruses. Indeed, HBV and HCV core proteins were reported to induce TLR2-dependent activation of nuclear factor-κB and p38 MAPK and subsequent production of TNF-α, IL-6 and IL-12 in macrophages.[3,71] Hence, one could presume that activation of TLR2 by HCV/HBV core proteins could aggravate hepatic inflammation and damage. In agreement with this hypothesis, an up-regulation of TLR2 in the liver and on monocytes, correlating with higher TNF-α levels and necroinflammatory activity in the liver, was reported in patients with hepatitis C.[16,17] Our data demonstrate for the first time that up-regulating the inflammatory activity of TLR2 in the acute phase of viral hepatitis favours fulminant hepatitis. In humans, fulminant hepatic failure (FHF) is an uncommon clinical condition characterized by extensive hepatic necrosis, severe impairment of liver function and a high mortality rate.[19] The most recognized causal agents of FHF are hepatitis viruses (especially HBV) but several non-hepatic herpesviruses (herpes simplex virus, cytomegalovirus and varicella virus) and drugs were also associated with FHF.[19] The pathophysiology of FHF is unclear but increasing evidence suggests that regardless of the aetiological cause of FHF, the host's inflammatory response contributes to liver microcirculatory disorders and injury. Accordingly, macrophage activation and inflammatory cytokines were shown to play a key role in FHF.[72,73] Moreover, the core protein from HBV was suggested as a potential initiating factor in patients with fulminant hepatitis B but mechanisms are still elusive.[74,75] Hence, we can propose that strong TLR2-dependent activation of macrophages in the liver by viral proteins from hepatitis or non-hepatitis viruses during acute infection may predispose to FHF induction.

Work is in progress to further determine the mechanisms involved in TLR2-dependent increase of inflammatory responses and viral replication in infected intrahepatic resident and recruited cell populations.

Acknowledgements

The authors want to acknowledge Pascale Bellaud and Eric Massicotte for their technical assistance within histochemistry and cytofluorometry analyses, and Dr Anthony Karelis for revising the manuscript. This work was funded by a grant from NSERC from Government of Canada (no. 2895-2009). Christian Bleau and Melanie Burnette were supported by NSERC fellowships.

Author contributions

C. Bleau, M. Burnette, and A. Filliol performed the experiments. C. Piquet-Pellorce has designed cytofluorometric experiments. L. Lamontagne and C. Bleau have designed the study. C. Bleau and L. Lamontagne have written the paper and all authors contributed to revision and corrections of the manuscript.

Disclosures

The authors indicated no financial or commercial conflict of interest.

References

1 Broering R, Lu M, Schlaak JF. Role of Toll-like receptors in liver health and disease. *Clin Sci (Lond)* 2011; **121**:415–26.
2 Villalba M, Hott M, Martin C, Aguila B, Valdivia S, Quezada C *et al.* Herpes simplex virus type 1 induces simultaneous activation of Toll-like receptors 2 and 4 and expression of the endogenous ligand serum amyloid A in astrocytes. *Med Microbiol Immunol* 2012; **201**:371–9.
3 Dolganiuc A, Oak S, Kodys K, Golenbock DT, Finberg RW, Kurt-Jones E *et al.* Hepatitis C core and nonstructural 3 proteins trigger toll-like receptor 2-mediated pathways and inflammatory activation. *Gastroenterology* 2004; **127**:1513–24.
4 Hoffmann M, Zeisel MB, Jilg N, Paranhos-Baccalà G, Stoll-Keller F, Wakita T *et al.* Toll-like receptor 2 senses hepatitis C virus core protein but not infectious viral particles. *J Innate Immun* 2009; **1**:446–54.
5 Mercin A, Kluwe J, Schwabe RF. Toll-like receptors as target on chronic liver disease. *Gut* 2009; **58**:704–20.
6 Heggelund L, Müller F, Lien E, Yndestad A, Ueland T, Kristiansen KI *et al.* Frøland SS Increased expression of toll-like receptor 2 on monocytes in HIV infection: possible roles in inflammation and viral replication. *Clin Infect Dis* 2004; **39**:264–9.
7 Heggelund L, Damås JK, Yndestad A, Holm AM, Müller F, Lien E *et al.* Stimulation of toll-like receptor 2 in mononuclear cells from HIV-infected patients induces chemokine responses: possible pathogenic consequences. *Clin Exp Immunol* 2004; **138**:116–21.
8 Gekonge B, Giri MS, Kossenkov AV, Nebozyhn M, Yousef M, Mounzer K *et al.* Constitutive gene expression in monocytes from chronic HIV-1 infection overlaps with acute Toll-like receptor induced monocyte activation profiles. *PLoS ONE* 2012; **7**:e41153.
9 Karlström A, Heston SM, Boyd KL, Tuomanen EI, McCullers JA. Toll-like receptor 2 mediates fatal immunopathology in mice during treatment of secondary pneumococcal pneumonia following influenza. *J Infect Dis* 2011; **204**:1358–6.
10 Zhao RR, Yang XF, Dong J, Zhao YY, Wei X, Huang CX *et al.* Toll-like receptor 2 promotes T helper 17 cells response in hepatitis B virus infection. *Int J Clin Exp Med* 2015; **8**:7315–23.
11 Dosch SF, Mahajan SD. Collins ARSARS coronavirus spike protein-induced innate immune response occurs via activation of the NF-κB pathway in human monocyte macrophages *in vitro*. *Virus Res* 2009; **142**:19–27.
12 Kurt-Jones EA, Chan M, Zhou S, Wang J, Reed G, Bronson R *et al.* Herpes simplex virus 1 interaction with Toll-like receptor 2 contributes to lethal encephalitis. *Proc Natl Acad Sci U S A* 2004; **101**:1315–20.
13 Wang JP, Kurt-Jones EA, Shin OS, Manchak MD, Levin MJ, Finberg RW. Varicella-zoster virus activates inflammatory cytokines in human monocytes and macrophages via Toll-like receptor 2. *J Virol* 2005; **79**:12658–66.
14 Boehme KW, Guerrero M, Compton T. Human cytomegalovirus envelope glycoproteins B and H are necessary for TLR2 activation in permissive cells. *J Immunol* 2006; **177**:7094–102.
15 Xu J, Yang Y, Sun J, Ding Y, Su L, Shao C *et al.* Expression of Toll-like receptors and their association with cytokine responses in peripheral blood mononuclear cells of children with acute rotavirus diarrhoea. *Clin Exp Immunol* 2006; **144**:376–81.
16 Riordan SM, Skinner NA, Kurtovic J, Locarnini S, McIver CJ, Williams R *et al.* Toll-like receptor expression in chronic hepatitis C: correlation with pro-inflammatory cytokine levels and liver injury. *Inflamm Res* 2006; **55**:279–85.

17 Berzsenyi MD, Roberts SK, Preiss S, Woollard DJ, Beard MR, Skinner NA *et al.* Hepatic TLR2 & TLR4 expression correlates with hepatic inflammation and TNF-α in HCV & HCV/HIV infection. *J Viral Hepat* 2011; **18**:852–60.

18 Rehermann B, Nascimbeni M. Immunology of hepatitis B virus and hepatitis C virus infection. *Nat Rev Immunol* 2005; **5**:215–29.

19 Liu M, Chan WY, McGilvray I, Ning Q, Levy GA. Fulminant viral hepatitis: molecular and cellular basis, and clinical implications. *Expert Rev Mol Med* 2001; **3**:1–19.

20 Ramadori G, Moriconi F, Malik I, Dudas J. Physiology and pathophysiology of liver inflammation, damage and repair. *J Physiol Pharmacol* 2008; **59**:107–17. 21.

21 Weiss SR, Leibowitz JL. Coronavirus pathogenesis. *Adv Virus Res* 2011; **81**:85–164.

22 Le Prevost C, Levy-Leblond E, Virelizier JL, Dupuy JM. Immunopathology of mouse hepatitis virus type 3 infection. Role of humoral and cell-mediated immunity in resistance mechanisms. *J Immunol* 1975; **114**:221–5.

23 Wijburg OL, Heemskerk MH, Boog CJ, Van Rooijen N. Role of spleen macrophages in innate and acquired immune reponses against mouse hepatitis virus strain A59. *Immunology* 1997; **92**:252–8.

24 Lamontagne L, Descoteaux JP, Jolicoeur P. Mouse hepatitis virus 3 replication in T and B lymphocytes correlate with viral pathogenicity. *J Immunol* 1989; **142**:4458–65.

25 Lavi E, Gilden DH, Highkin MK, Weiss SR. The organ tropism of mouse hepatitis virus A59 in mice is dependent on dose and route of inoculation. *Lab Anim Sci* 1986; **36**:130–5.

26 Godfraind C, Coutelier JP. Morphological analysis of mouse hepatitis virus A-59-induced pathology with regard to viral receptor expression. *Histol Histopathol* 1998; **13**:181–9.

27 Navas S, Seo SH, Chua MM, Das Sarma J, Lavi E, Hingley ST *et al.* Murine coronavirus spike protein determines the ability of the virus to replicate in the liver and cause hepatitis. *J Virol* 2001; **5**:2452–7.

28 Martin JP, Chen W, Koehren F, Pereira CA. The virulence of mouse hepatitis virus 3, as evidenced by permissivity of cultured hepatic cells toward escape mutants. *Res Virol* 1994; **145**:297–302.

29 Tacke F, Luedde T, Trautwein C. Inflammatory pathways in liver homeostasis and liver injury. *Clin Rev Allergy Immunol* 2009; **36**:4–12.

30 Pope M, Rotstein O, Cole E, Sinclair S, Parr R, Cruz B *et al.* Pattern of disease after murine hepatitis virus strain 3 infection correlates with macrophage activation and not viral replication. *J Virol* 1995; **69**:5252–60.

31 Schindler L, Brücher J, Kirchner H. Protection of mice against infection with mouse hepatitis virus type 3 by injection of silica. *Immunobiology* 1984; **166**:62–71.

32 Jacques A, Bleau C, Martin JP, Lamontagne L. Intrahepatic endothelial and Kupffer cells involved in immunosuppressive cytokines and natural killer (NK)/NK T cell disorders in viral acute hepatitis. *Clin Exp Immunol* 2008; **152**:298–310.

33 Cervantes-Barragán L, Kalinke U, Züst R, König M, Reizis B, López-Macías C *et al.* Type I IFN-mediated protection of macrophages and dendritic cells secures control of murine coronavirus infection. *J Immunol* 2009; **182**:1099–106.

34 Jacques A, Bleau C, Turbide C, Beauchemin N, Lamontagne L. Macrophage interleukin-6 and tumour necrosis factor-α are induced by coronavirus fixation to Toll-like receptor 2/heparan sulphate receptors but not carcinoembryonic cell adhesion antigen 1a. *Immunology* 2009; **128**:e181–92.

35 Dupuy JM, Rodrigue D. Heterogeneity in evolutive patterns of inbred mice infected with a cloned substrain of mouse hepatitis virus type 3. *Intervirology* 1981; **16**:114–7.

36 Arshad MI, Patrat-Delon S, Piquet-Pellorce C, L'helgoualc'h A, Rauch M, Genet V *et al.* Pathogenic mouse hepatitis virus or poly(I:C) induce IL-33 in hepatocytes in murine models of hepatitis. *PLoS ONE* 2013; **8**:e74278.

37 Ding JW, Ning Q, Liu MF, Lai A, Leibowitz J, Peltekian KM *et al.* Fulminant hepatic failure in murine hepatitis virus strain 3 infection: tissue-specific expression of a novel fgl2 prothrombinase. *J Virol* 1997; **71**:9223–30.

38 Marsden PA, Ning Q, Fung LS, Luo X, Chen Y, Mendicino M *et al.* The Fgl2/ fibroleukin prothrombinase contributes to immunologically mediated thrombosis in experimental and human viral hepatitis. *J Clin Invest* 2003; **112**:58–66.

39 Moles A, Murphy L, Wilson CL, Chakraborty JB, Fox C, Park EJ *et al.* A tlr2/S100a9/Cxcl-2 signaling network is necessary for neutrophil recruitment in acute and chronic liver injury in the mouse. *J Hepatol* 2014; **60**:782–91.

40 Oo YH, Shetty S, Adams DH. The role of chemokines in the recruitment of lymphocytes to the liver. *Dig Dis* 2010; **28**:31–44.

41 Lamontagne L, Lusignan S, Page C. Recovery from mouse hepatitis virus infection depends on recruitment of $CD8^+$ cells rather than activation of intrahepatic $CD4^+$ αβ-TCR^{inter} or NK-T cells. *Clin Immunol* 2001; **101**:345–56.

42 Dietrich N, Lienenklaus S, Weiss S, Gekara NO. Murine Toll-like receptor 2 activation induces type I interferon responses from endolysosomal compartments. *PLoS ONE* 2010; **5**:e10250.

43 Zhou H, Zhao J, Perlman S. Autocrine interferon priming in macrophages but not in dendritic cells results in enhanced cytokine and chemokine production after coronavirus infection. *MBio* 2010; **1**:e00219–10.

44 Tarantino G, Di Cristina A, Pipitone R, Almasio PL, Di Vita G, Craxi A *et al. In vivo* liver expression of TLR2, TLR3 and TLR7 in chronic hepatitis C. *J Biol Regul Homeost Agents* 2013; **27**:233–9.

45 Zhou M, Zhu X, Ye S, Zhou B. Blocking TLR2 *in vivo* attenuates experimental hepatitis induced by concanavalin A in mice. *Int Immunopharmacol* 2014; **21**:241–6.

46 Melchjorsen J. Learning from the messengers: Innate sensing of viruses and cytokine regulation of immunity — clues for treatments and vaccines. *Viruses* 2013; **5**:470–527.

47 Devictor D, Décimo D, Sebire G, Tardieu M, Haddchouel M. Enhanced tumor necrosis factor α in coronavirus but not in paracetamol-induced acute hepatic necrosis in mice. *Liver* 1992; **12**:205–8.

48 Décimo D, Boespflug O, Meunier-Rotival M, Hadchouel M, Tardieu M. Genetic restriction of murine hepatitis virus type 3 expression in liver and brain: comparative study in BALB/c and C3H mice by immunochemistry and hybridization *in situ*. *Arch Virol* 1993; **130**:269–77.

49 Pereira CA, Steffan AM, Kirn A. Interaction between mouse hepatitis viruses and primary cultures of Kupffer and endothelial liver cells from resistant and susceptible inbred mouse strains. *J Gen Virol* 1984; **65**:1617–20.

50 McGilvray ID, Lu Z, Wei AC, Dackiw AP, Marshall JC, Kapus A *et al.* Murine hepatitis virus strain 3 induces the macrophage prothrombinase fgl-2 through p38 mitogen-activated protein kinase activation. *J Biol Chem* 1998; **273**:32222–9.

51 Mazaleuskaya L, Veltrop R, Ikpeze N, Martin-Garcia J, Navas-Martin S. Protective role of Toll-like Receptor 3-induced type I interferon in murine coronavirus infection of macrophages. *Viruses* 2012; **4**:901–23.

52 Schwabe RF, Seki E, Brenner DA. Toll-like receptor signaling in the liver. *Gastroenterology* 2006; **130**:1886–1900.

53 Matsumura T, Ito A, Takii T, Hayashi H, Onozaki K. Endotoxin and cytokine regulation of toll like receptor (TLR) 2 and TLR4 gene expression in murine liver and hepatocytes. *J Interferon Cytokine Res* 2000; **20**:915–21.

54 Schümann J, Wolf D, Pahl A, Brune K, Papadopoulos T, van Rooijen N *et al.* Importance of Kupffer cells for T-cell-dependent liver injury in mice. *Am J Pathol* 2000; **157**:1671–83.

55 Liu J, Tan Y, Zhang J, Zou L, Deng G, Xu X *et al.* C5aR, TNF-α, and FGL2 contribute to coagulation and complement activation in virus-induced fulminant hepatitis. *J Hepatol* 2015; **62**:354–62.

56 Schindler L, Engler H, Kirchner H. Activation of natural killer cells and induction of interferon after injection of mouse hepatitis virus type 3 in mice. *Infect Immun* 1982; **35**:869–73.

57 Zhao L, Rose KM, Elliott R, Van Rooijen N, Weiss SR. Cell-type-specific type I interferon antagonism influences organ tropism of murine coronavirus. *J Virol* 2011; **85**:10058–68.

58 Roth-Cross JK, Bender SJ, Weiss SR. Murine coronavirus mouse hepatitis virus is recognized by MDA5 and induces type I interferon in brain macrophages/microglia. *J Virol* 2008; **82**:9829–38.

59 Ireland DD, Stohlman SA, Hinton DR, Atkinson R, Bergmann CC. Type I interferons are essential in controlling neurotropic coronavirus infection irrespective of functional CD8 T cells. *J Virol* 2008; **82**:300–10.

60 Lehoux M, Jacques A, Lusignan S, Lamontagne L. Murine viral hepatitis involves NK cell depletion associated with virus-induced apoptosis. *Clin Exp Immunol* 2004; **137**:41–51.

61 Xu H, Li H, Cao D, Wu Y, Chen Y. Tumor necrosis factor α (TNF-α) receptor-I is required for TNF-α-mediated fulminant virus hepatitis caused by murine hepatitis virus strain-3 infection. *Immunol Lett* 2014; **158**:25–32.

62 Haick AK, Rzepka JP, Brandon E, Balemba OB, Miura TA. Neutrophils are needed for an effective immune response against pulmonary rat coronavirus infection, but also contribute to pathology. *J Gen Virol* 2014; **95**:578–90.

63 Stefanovic L, Brenner DA, Stefanovic B. Direct hepatotoxic effect of KC chemokine in the liver without infiltration of neutrophils. *Exp Biol Med* 2005; **230**:573–86.

64 Zimmermann HW, Seidler S, Nattermann J, Gassler N, Hellerbrand C, Zernecke A *et al.* Functional contribution of elevated circulating and hepatic non-classical CD14CD16 monocytes to inflammation and human liver fibrosis. *PLoS ONE* 2010; **5**:e11049.

65 Karlmark KR, Wasmuth HE, Trautwein C, Tacke F. Chemokine-directed immune cell infiltration in acute and chronic liver disease. *Expert Rev Gastroenterol Hepatol* 2008; **2**:233–42.

66 Jolicoeur P, Lamontagne L. Mouse hepatitis virus 3 pathogenicity expressed by a lytic viral infection in bone marrow 14.8^+ mu^+ B lymphocyte subpopulations. *J Immunol* 1989; **143**:3722–30.

67 Lamontagne L, Jolicoeur P. Mouse hepatitis virus 3-thymic cell interactions correlating with viral pathogenicity. *J Immunol* 1991; **146**:3152–9.

68 Sahin H, Borkham-Kamphorst E, Doo NT, Berres ML, Kaldenbach M, Schmitz P *et al.* Proapoptotic effects of the chemokine, CXCL 10 are mediated by the noncognate receptor TLR4 in hepatocytes. *Hepatology* 2013; **57**:797–805.

69 Wang J, Zhao P, Guo H, Sun X, Jiang Z, Xu L *et al.* Serum IL-33 levels are associated with liver damage in patients with chronic hepatitis C. *Mediators Inflamm* 2012;**2012**:819636.

70 Wang J, Cai Y, Ji H, Feng J, Ayana DA, Niu J *et al.* Serum IL-33 levels are associated with liver damage in patients with chronic hepatitis B. *J Interferon Cytokine Res* 2012; **32**:248–53.

71 Cooper A, Tal G, Lider O, Shaul Y. Cytokine induction by the hepatitis B virus capsid in macrophages is facilitated by membrane heparan sulfate and involves TLR2. *J Immunol* 2005; **175**:3165–76.

72 Ando K, Moriyama T, Guidotti LG, Wirth S, Schreiber RD, Schlicht HJ *et al.* Mechanisms of class I restricted immunopathology. A transgenic mouse model of fulminant hepatitis. *J Exp Med* 1993; **178**:1541–1554.

73 de la Mata M, Meager A, Rolando N, Daniels HM, Nouri-Aria KT, Goka AK *et al.* Tumour necrosis factor production in fulminant hepatic failure: relation to aetiology and superimposed microbial infection. *Clin Exp Immunol* 1990; **82**:479–48.

74 Mondelli M, Eddleston AL. Mechanisms of liver cell injury in acute and chronic hepatitis B. *Semin Liver Dis* 1984; **4**:47–58.

75 Aritomi T, Yatsuhashi H, Fujino T, Yamasaki K, Inoue O, Koga M *et al.* Association of mutations inthe core promoter and precore region of hepatitis virus with fulminant and severe acute hepatitis in Japan. *J Gastroenterol Hepatol* 1998; **13**:1125–32.

Supporting Information

Additional Supporting Information may be found in the online version of this article:

Figure S1. Gating strategies used for cytofluorometric studies.

Figure S2. Mortality, hepatic damages and viral replication in murine hepatitis virus (MHV) -A59-infected Toll-like receptor 2 knockout mice.

Figure S3. Analysis of intrahepatic mononuclear cells in the liver of murine hepatitis virus 3-infected Toll-like receptor 2 knockout mice.

VI.2. ANNEXE 2 : L'infection par le virus de l'hépatite murine induit l'activation de fonctions inflammatoires dans les cellules endothéliales sinusoïdales hépatiques dépendantes du Toll Like Receptor 2 pendant l'hépatite aiguë.

Christian Bleau, Aveline Filliol, Michel Samson et Lucie Lamontagne.

Article publié dans *J Virol.* 2016 Sep 29;90(20):9096-113.

Résumé de l'article.

Dans des conditions physiologiques, les cellules endothéliales sinusoïdales hépatiques (LSECs) participent à la tolérance immunitaire du foie par l'expression de médiateurs anti-inflammatoires. En revanche, lors d'une infection virale ou d'une activation du Toll Like Receptor 2 (TLR2), les LSECs peuvent avoir des fonctions pro-inflammatoires. Cependant, leur rôle dans l'inflammation hépatique au cours de l'hépatite virale aiguë est inconnu. Par l'utilisation du virus de l'hépatite murine de type 3 (MHV3) hautement virulent, et de ses variants atténués, les 51.6-MHV3 et YAC-MHV3, qui présentent tous les deux un faible tropisme pour les LSECs, nous avons étudié *in vivo* et *in vitro* les conséquences de l'infection des LSECs sur leur profil inflammatoire et sur l'aggravation de l'hépatite aiguë. Nous avons montré, qu'en comparaison à l'infection des souris avec les variants atténués, celle induite par le MHV3 conduisait à une hépatite fulminante associée à des hauts niveaux de charge virale, des plages de nécrose, l'expression de médiateurs inflammatoires et un recrutement précoce de cellules inflammatoires. Ce désordre hépatique corrélait avec une production perturbée de l'IL-10 et de facteurs vasculaires par les LSECs. Nous avons ensuite montré que l'infection par le MHV3 des LSECs en culture primaire altérait leur production de cytokines anti-inflammatoires et conduisait à une libération importante de facteurs pro-inflammatoires et pro-coagulants ainsi qu'un dommage précoce des cellules par rapport à l'infection induite avec les variants atténués du MHV3. La forte réplication virale et le profil pro-inflammatoire des LSECs infectées par le MHV3 étaient associés à une activation spécifique de la voie du TLR2 par le virus. Nous démontrons donc ici que l'activation du TLR2 des LSECs par le MHV3 est un facteur aggravant de l'inflammation hépatique et corrèle avec la sévérité de l'hépatite. En conclusion, nos résultats confirment que la conservation des propriétés immunotolérantes des LSECs au cours de l'hépatite virale aiguë est impérative pour limiter l'inflammation et le dommage hépatique.

AMERICAN SOCIETY FOR MICROBIOLOGY | Journal of Virology

Mouse Hepatitis Virus Infection Induces a Toll-Like Receptor 2-Dependent Activation of Inflammatory Functions in Liver Sinusoidal Endothelial Cells during Acute Hepatitis

Christian Bleau,[a] Aveline Filliol,[b] Michel Samson,[b] Lucie Lamontagne[a]

Département des Sciences Biologiques, Université du Québec à Montréal, Montreal, Canada[a]; U.1085 Inserm, Institut de Recherche en Santé-Environnement-Travail, Université de Rennes 1, Rennes, France[b]

ABSTRACT

Under physiological conditions, the liver sinusoidal endothelial cells (LSECs) mediate hepatic immune tolerance toward self or foreign antigens through constitutive expression of anti-inflammatory mediators. However, upon viral infection or Toll-like receptor 2 (TLR2) activation, LSECs can achieve proinflammatory functions, but their role in hepatic inflammation during acute viral hepatitis is unknown. Using the highly virulent mouse hepatitis virus type 3 (MHV3) and the attenuated variants 51.6-MHV3 and YAC-MHV3, exhibiting lower tropism for LSECs, we investigated *in vivo* and *in vitro* the consequence of LSEC infection on their proinflammatory profiles and the aggravation of acute hepatitis process. *In vivo* infection with virulent MHV3, in comparison to attenuated strains, resulted in fulminant hepatitis associated with higher hepatic viral load, tissue necrosis, and levels of inflammatory mediators and earlier recruitment of inflammatory cells. Such hepatic inflammatory disorders correlated with disturbed production of interleukin-10 (IL-10) and vascular factors by LSECs. We next showed *in vitro* that infection of LSECs by the virulent MHV3 strain altered their production of anti-inflammatory cytokines and promoted higher release of proinflammatory and procoagulant factors and earlier cell damage than infection by attenuated strains. This higher replication and proinflammatory activation in LSECs by the virulent MHV3 strain was associated with a specific activation of TLR2 signaling by the virus. We provide evidence that TLR2 activation of LSCEs by MHV3 is an aggravating factor of hepatic inflammation and correlates with the severity of hepatitis. Taken together, these results indicate that preservation of the immunotolerant properties of LSECs during acute viral hepatitis is imperative in order to limit hepatic inflammation and damage.

IMPORTANCE

Viral hepatitis B and C infections are serious health problems affecting over 350 million and 170 million people worldwide, respectively. It has been suggested that a balance between protection and liver damage mediated by the host's immune response during the acute phase of infection would be determinant in hepatitis outcome. Thus, it appears crucial to identify the factors that predispose in exacerbating liver inflammation to limit hepatocyte injury. Liver sinusoidal endothelial cells (LSECs) can express both anti- and proinflammatory functions, but their role in acute viral hepatitis has never been investigated. Using mouse hepatitis virus (MHV) infections as animal models of viral hepatitis, we report for the first time that *in vitro* and *in vivo* infection of LSECs by the pathogenic MHV3 serotype leads to a reversion of their intrinsic anti-inflammatory phenotype toward a proinflammatory profile as well to as disorders in vascular factors, correlating with the severity of hepatitis. These results highlight a new virus-promoted mechanism of exacerbation of liver inflammatory response during acute hepatitis.

Under physiological conditions, the liver adopts mechanisms of immune tolerance toward innocuous gut-derived food and microbial antigens (such as lipopolysaccharide [LPS]) to prevent undesired inflammatory responses. The induction of tolerance in the liver is mediated by several resident hepatic cell types, such as the endothelial cells (ECs) lining the hepatic sinusoids (liver sinusoidal endothelial cells [LSECs]), the Kupffer cells (KCs), and to a lesser extent the hepatocytes (1). However, the tolerizing and anti-inflammatory functions of LSECs were recently shown to be more efficient than those of KCs (2). Given their anatomical situation, LSECs are first in contact with portal-delivered antigens and thus act as a sieving barrier in expressing highly efficient sentinel and scavenger functions that contribute to clearance of microbial products (3). They also tightly control blood-parenchyma exchanges via a dynamic regulation of the sinusoidal blood flow in releasing vasoactive factors such as NO (reviewed in reference 4). LSECs play a major role in liver tolerance in displaying a restricted Toll-like receptor (TLR)-mediated activation profile to microbial products (5, 6) and producing large amounts of anti-inflammatory cytokines, such as transforming growth factor β (TGF-β) and interleukin-10 (IL-10) (7, 8). However, upon viral infection or stimulation by TLR1/2 ligands, LSECs can switch toward an inflammatory and immunogenic state and induce recruitment of leukocytes and virus-specific $CD8^+$ T cell immunity (5, 9). The role of LSECs in inflammatory

Received 1 June 2016 **Accepted** 23 July 2016

Accepted manuscript posted online 3 August 2016

Citation Bleau C, Filliol A, Samson M, Lamontagne L. 2016. Mouse hepatitis virus infection induces a Toll-like receptor 2-dependent activation of inflammatory functions in liver sinusoidal endothelial cells during acute hepatitis. J Virol 90:9096–9113. doi:10.1128/JVI.01069-16.

Editor: S. Perlman, University of Iowa

Address correspondence to Lucie Lamontagne, lamontagne.lucie@uqam.ca.

liver diseases is poorly understood, but as these cells can express both anti- and proinflammatory functions, they could act as either moderators or exacerbators of liver inflammation.

Hepatitis B virus (HBV) and hepatitis C virus (HCV) infections are serious health problems affecting over 350 million and 170 million people worldwide, respectively (10). Most liver damage in HBV/HCV infections is attributed primarily to an exuberant immunopathological response triggered by viral infection rather than direct injury caused by viral replication (11, 12). It has been suggested that the balance between protection and liver damage mediated by the host's immune response during the acute phase of infection would be critical in the outcome of hepatitis (13). Evidence suggests that an exacerbated hepatic inflammatory response during acute infection may predispose to the development of a fulminant hepatic failure characterized by extensive hepatocellular dysfunctions and high mortality (14). The role of LSECs in viral hepatitis is largely unknown, and data are somewhat contradictory. Indeed, LSECs were suggested to contribute to the clearance of HCV and HBV from the bloodstream (15, 16) and to control HCV replication (17) or instead to promote its transmission to hepatocytes by acting as a viral reservoir (18). A few data suggest that LSECs may also participate in hepatic inflammation, since fibrinogen-like factor 2 (Fgl2), promoting vascular thrombosis and hepatic inflammation, and the proinflammatory alarmin IL-33, both produced by LSECs, are upregulated in acute or chronic hepatitis (19–22). A better understanding of the role of LSECs during the acute phase of viral hepatitis may help to identify new mechanisms that predispose to inflammation-driven hepatocyte injury and liver failure.

Mouse hepatitis virus type 3 (MHV3), belonging to the coronavirus family, is a relevant murine model to unravel the role of LSECs in acute viral hepatitis. MHV3 infects LSECs, hepatocytes, Kupffer cells (KCs), and Ito cells, all of which express the carcinoembryonic antigen 1a (CEACAM1a) viral receptor, and induces fulminant hepatitis leading to death of susceptible C57BL/6 mice within 3 to 4 days (23–25). LSECs are thought to play an important role in the resistance of A/J mice to MHV3 infection by controlling viral replication and delaying the transmission of the viral progeny to hepatocytes (26). Previous studies have reported early structural and vascular disorders in LSECs during MHV3 infection in susceptible C57BL/6 mice. Indeed, a reduced number of fenestrations in liver sinusoids and a correlation between the fulminance of hepatitis and the induction of Fgl2 in LSECs have been described (27, 28). We have also shown that MHV3 infection was associated with early release of IL-33 by LSECs (29) and a reduction in the intrahepatic levels of immunosuppressive IL-10, prostaglandin E_2 (PGE_2), and TGF-β cytokines, suggesting virus-induced disturbances in LSEC-mediated liver tolerance (30). Several attenuated MHV3 variants, such as the 51.6- and YAC-MHV3 viruses, have been *in vitro* generated to study the role of specific hepatic cell types in the hepatitis process. Compared to the parental MHV3, the major difference of the 51.6-MHV3 variant is its inefficiency of replication in LSECs (24). This difference is reflected by induction of milder hepatitis and higher hepatic levels of IL-10 and TGF-β (30). The YAC-MHV3 variant, showing lower tropism for LSECs and macrophages, induces a subclinical hepatitis characterized by few perivascular inflammatory foci (31) and higher induction of anti-inflammatory cytokines in the liver than with 51.6-MHV3 (30). The absence of vascular thrombosis combined with efficient recruitment of mononuclear cells favors hepatic clearance of YAC-MHV3 and full recovery of infected mice within 15 days (32). These improved clinical outcomes in mice infected by the attenuated variants support the hypothesis that preservation of the structural and functional integrity of LSECs may be one determining factor in the severity of hepatitis.

In this study, we report that robust infection of LSECs by the highly virulent MHV3, in contrast to the attenuated 51.6- and YAC-MHV3 variants, promotes disturbances in their anti-inflammatory functions and secretion of vascular factors, resulting in high release of inflammatory mediators and procoagulant Fgl2 simultaneously with decrease in NO and IL-10 levels. Such MHV3-induced LSEC disorders correlated *in vivo* with higher hepatic inflammation, damage, and viral replication as well as disturbances in leukocyte recruitment in mice infected by MHV3. We provide evidence that higher infection and proinflammatory activation of LSECs by MHV3 was related to a specific viral induction of TLR2 signaling. The aggravating role for TLR2 in hepatic inflammation and LSEC disorders was confirmed in MHV3-infected TLR2 knockout (KO) mice, in which hepatic damage, the pro- versus anti-inflammatory cytokine ratio, and LSEC-derived IL-10 production were significantly improved.

MATERIALS AND METHODS

Mice. Female C57BL/6 (Charles River, St-Constant, Quebec, Canada) and TLR2 KO (C57BL/6-129 $Tlr^{tm/Kir}$/J; Jackson Laboratory, Bar Harbor, ME) mice were housed in a HEPA-filtered air environment. All experiments were conducted with mice between 8 and 10 weeks of age in compliance with the regulations of the Animal Committee of the University of Quebec in Montreal (CIPA).

Viruses. MHV3 is a cloned pathogenic substrain isolated from the livers of infected DBA2 mice. MHV3 induces a rapid mortality in C57BL/6 mice within 3 to 4 days postinfection (p.i.) (23). The escape mutant 51.6-MHV3 was selected from the pathogenic MHV3 virus cultured into L2 cells in the presence of S protein-specific A51 monoclonal antibodies (24). This variant induces a delayed mortality (5 to 9 days p.i.) and expresses low tropism for LSECs but retains ability to infect Kupffer cells (KCs) (24). The nonpathogenic YAC-MHV3 variant is a cloned substrain produced in persistently infected YAC-1 cells, showing lower ability to replicate in LSECs and macrophages. Compared to the attenuated 51.6-MHV3 strain, this variant causes no mortality and induces efficient recruitment of innate immune cells, allowing viral clearance from the liver within 2 weeks p.i. (31). All viruses were passaged fewer than three times onto L2 cells, and their pathogenic properties were assessed routinely.

Isolation and purification of LSECs. Mice were euthanized, and the portal vein was isolated and injected with 3 ml of Hanks balanced salt solution (HBSS)–10 nM HEPES followed by 3 ml of digestion buffer consisting of 0.2% (wt/vol) collagenase A in HBSS–10 nM HEPES (Sigma-Aldrich, St. Louis, MO). The liver was then excised, injected several times with digestion buffer, and dissociated by a 30-min incubation in 10 ml of digestion buffer at 37°C on a shaking plate (200 rpm). The resulting cell suspension was passed through sterile 70-μm and 40-μm nylon mesh filters successively (Falcon; BD Biosciences, Mississauga, Ontario, Canada) and centrifuged at 400 × *g* for 10 min. The cell pellet was resuspended in 3 ml of RPMI 1640, layered at the top of a discontinuous 50%/25% Percoll gradient (Sigma-Aldrich), and centrifuged at 800 × *g* for 20 min without brakes. The interphase between the two density cushions, containing enriched nonparenchymal cells, was collected and washed with phosphate-buffered saline (PBS). LSECs were then purified using the positive-selection phycoerythrin (PE) kit (Stemcell, Vancouver, Canada) with an anti-CD146 monoclonal antibody, a specific marker of endothelial cells in liver (33), according to the manufacturer's procedure. LSEC purity was analyzed by cytometry before each experiment and reached over 90%.

TABLE 1 Primers used for quantitative reverse transcription-PCR

Gene	Forward primer	Reverse primer
HPRT	5′-GAAAGACTTGCTCGAGATGTCATG-3′	5′-CACACAGAGGGCCACAATGT-3′
IL-6	5′-TCGGAGGCTTAATTACACATGTTC-3′	5′-TGCCATTGCACAACTCTTTTCT-3′
TNF-α	5′-TCCCAGGTTCTCTTCAAGGGA-3′	5′-GGTGAGGAGCACGTAGTCGG-3′
CCL2	5′-GCAGCAGGTGTCCCAAAGAA-3′	5′-GGTCAGCACAGACCTCTCTCTTG-3′
CXCL10	5′-GGCCATAGGGAAGCTTGAAAT-3′	5′-TCGTGGCAATGATCTCAACAC-3′
ICAM-1	5′-GTCCGCTGTGCTTTGAGAACT-3′	5′-CGGAAACGAATACACGGTGAT-3′
TLR3	5′-TGGGCTGAAGTGGACAAATCT-3′	5′-TGCCGACATCATGGAGGTT-3′
CAV-1	5′-GCGCACACCAAGGAGATTG-3′	5′-CACGTCGTCGTTGAGATGCT-3′
TLR7	5′-CAGTGAACTCTGGCCGTTGA-3′	5′-CAAGCCGGTTGTTGGAGAA-3′
MHV-N	5′-TGGAAGGTCTGCACCTGCTA-3′	5′-TTTGGCCCACGGGATTG-3′
RIG-I	5′-GCCAGAGTGTCAGAATCTCAGTCAG-3′	5′-GAGAACACAGTTGCCTGCTGCTCA-3′
MDA-5	5′-GCCCTCTCCTTCCTCTGAGACT-3′	5′-GCTGGAGGAGGGTCAGCAA-3′
IL-33	5′-GCTGCGTCTGTTGACACATTG-3′	5′-GGGAGGCAGGAGACTGTGTTAA-3′
Fgl2	5′-CGTTGTGGTCAACAGTTTGGA-3′	5′-GATGTTGAACCGGCTGTGACT-3′
CXCL1	5′-CCGAAGTCATAGCCACACTCAA-3′	5′-CAAGGGAGCTTCAGGGTCAA-3′
IL-10	5′-GATGCCCCAGGCAGAGAA-3′	5′-CACCCAGGGAATTCAAATGC-3′
TGF-β	5′-AGCGCTCACTGCTCTTGTGA-3′	5′-GCTGATCCCGTTGATTTCCA-3′

***In vivo* viral infections.** Groups of 6 or 7 wild-type (WT) C57BL/6 or TLR2 KO mice were intraperitoneally (i.p.) infected with 10^3 50% tissue culture infective doses ($TCID_{50}$) of MHV3, 51.6-MHV3, or YAC-MHV3. Mock-infected mice received a similar volume of PBS. Mice were sacrificed by CO_2 anoxia at 24, 48, or 72 h postinfection (p.i.). Liver and blood samples were collected and frozen for further analyses.

Histopathological and immunohistochemical (IHC) analyses and determination of transaminase levels. The histopathological analysis of liver was done by hematoxylin-eosin-safranin staining. Determination of serum alanine transaminase (ALT) and aspartate transaminase (AST) was performed according to the IFCC primary reference procedures using an Olympus AU2700 Autoanalyser (Olympus Optical, Tokyo, Japan). Immunolocalization of IL-33 and caveolin-1 (CAV-1) was performed on liver sections fixed in paraformaldehyde and embedded in paraffin incubated with primary goat anti-mouse IL-33 (R&D Systems Inc., Minneapolis, MN) or rabbit anti-mouse CAV-1 (LSBio, Seattle, WA) for 1 h in a Ventana automated machine (Ventana Medical Systems, Inc., Tucson, AZ) and secondary horseradish peroxidase (HRP)-conjugated rabbit anti-goat antibody (Dako, Markham, Ontario, Canada) or OmniMap anti-rabbit–HRP (RUO) for 16 min. Double-immunofluorescence stainings of IL-10 or IL-33 and CAV-1 were conducted on liver cryosections fixed in paraformaldehyde and incubated overnight with primary goat anti-mouse IL-10 (R&D Systems Inc., Minneapolis, MN) or primary goat anti-mouse IL-33 (R&D Systems) and rabbit anti-mouse CAV-1 (LSBio) and then with DyLight-649 anti-goat Cy3 anti-rabbit secondary antibodies (Jackson ImmunoResearch, West Grove, PA) and Hoechst counterstain (Invitrogen, Ontario, Canada). Slides were mounted (mounting medium; Invitrogen, Ontario, Canada), imaged with a Nikon Eclipse Ni-E Z1 microscope, and analyzed using SpotAdvance software.

Virus titration. Frozen liver samples from mice infected with MHV for 24 or 72 h were weighed and homogenized in cold PBS. The suspension was then centrifuged at 13,000 rpm for 30 min and analyzed for viral detection. Viral titration was also performed on LSEC culture supernatants. Liver suspension and cell culture supernatants were 10-fold serially diluted and tested for viral presence on L2 cells cultured in 96-well plates. Cytopathic effects (CPE), characterized by the occurrence of large syncytia and cell lysis, were recorded at 72 h p.i., and virus titers were determined according to the Reed-Muench method and expressed as $\log_{10}$ $TCID_{50}$.

***In vitro* viral infections.** Freshly isolated LSECs were seeded in 24-well plates at a density of 7.5×10^5 cells/ml in RPMI 1640 supplemented with 10% fetal calf serum (FCS) and antibiotics (Wysent, St-Bruno, Quebec, Canada). Cells were then infected with infectious MHV3, YAC-MHV3, or 51.6-MHV3 at a multiplicity of infection (MOI) of 0.1 and incubated at 37°C under 5% CO_2 for 24 to 72 h depending on the experiment. Cell culture supernatants were collected for enzyme-linked immunosorbent assays (ELISAs), and total RNA was extracted for quantitative reverse transcription-PCR (qRT-PCR) analysis.

siRNA transfection. LSECs were seeded in 24-well plates at 60 000 cells/ml and transfected with 25 nM small interfering RNA (siRNA) Flexitude premix (Qiagen, Cambridge, MA) targeting TLR2 mRNA (target sequence, CTCGTTCTCCAGCATTTAAA) and with the AllStars negative-control siRNA as a nonsilencing transfection control for 36 h prior to infection for 24 h.

RNA isolation and qRT-PCR. RNA from *in vitro*-infected LSECs was extracted using the NucleoSpin RNA II kit (Macherey-Nagel, Bethlehem, PA) according to the manufacturer's procedure. Total RNA from frozen liver samples was extracted using TRIzol reagent (Invitrogen, Burlington, Ontario, Canada), and, residual genomic DNA was removed with the Turbo DNA-free kit (Ambion, Austin, TX). One microgram of RNA was reverse transcribed into cDNA using a high-capacity cDNA reverse transcription kit (Applied Biosystems, Foster City, CA). Real-time PCR amplification was carried out on 25 ng cDNA using the HotStart-IT SYBR green qPCR master mix (USB Corporation, Cleveland, OH) on an ABI 7300 system (Applied Biosystems). The primer sets used are listed in Table 1. Threshold cycle (C_T) values were collected and used for $\Delta\Delta C_T$ analysis. The gene expression was normalized to that of hypoxanthine phosphoribosyltransferase (HPRT) as an endogenous control and expressed as a ratio to gene expression in mock-infected mice livers or control (uninfected) LSECs in *in vitro* experiments (level arbitrarily taken as 1). The specificity of the PCR products was confirmed by melting curve analyses, and all qPCR assays were run in duplicate.

ELISA and nitric oxide assay. Frozen liver samples were weighed and homogenized in NP-40 lysis buffer (Invitrogen) with a protease inhibitor cocktail (Sigma-Aldrich, St. Louis, MO) and 1 mM phenylmethylsulfonyl fluoride (PMSF) for protein extraction. The liver suspension was kept on ice for 30 min and centrifuged for 10 min at 13,000 rpm. Determination of IL-6 and tumor necrosis factor alpha (TNF-α) (BD BioSciences, San Jose, CA), CXCL10 and CCL2 (eBioscience, San Diego, CA), and CXCL1 and IL-33 (R&D Systems, Minneapolis, MN) in liver lysates and/or LSEC culture supernatants was carried out by ELISAs. Levels of nitric oxide (NO) were quantified using the Griess reagent assay (Invitrogen) according to the manufacturer's procedure.

Cytofluorometric studies. Livers were perfused with PBS through the portal vein to remove blood cell contamination prior to dissection. Liver tissues were then homogenized, and hepatocytes were removed by sedi-

mentation. Inflammatory cells were enriched using 35% Percoll gradient (Sigma-Aldrich), and red blood cells were lysed with a Tris-buffered ammonium chloride solution. One million (10^6) leukocytes were incubated with anti-CD16/32 antibodies (BD Biosciences) to block nonspecific binding. Cells were incubated with optimal dilutions of anti-CD3–V500, anti-Gr1–V450, anti-CD11b–PE-Cy7, anti-CD19–allophycocyanin (APC), anti-CD4–fluorescein isothiocyanate (FITC), anti-NK1.1–peridinin chlorophyll protein (PerCP)-Cy-5.5, and anti-CD8–APC-Cy7 antibodies (BD Biosciences) and fixed in PBS containing 2% FCS, 0.01 M sodium azide, and 2% formaldehyde. Stained cells were analyzed on a FACSAria II flow cytometer using BD FACS Diva software (BD Bioscience), and the data were processed using CXP software (Beckman Coulter, Mississauga, Ontario, Canada). Dead cells and doublet cells were excluded on the basis of forward scatter (FSC) and side scatter (SCC), and analyses were performed on 10,000 events recorded. Myeloid cells, gated by high side scatter, were assessed for CD11b and Gr1 to enumerate macrophages ($CD11b^+$ $Gr1^{inter}$) and neutrophils ($CD11b^+$ $Gr1^{high}$). Lymphoid cells were gated according to FSC/SCC and first assessed for NK1.1 and CD3 expression to discriminate NK from NK-T cells. $CD3^+$ $NK1.1^-$ T cells were further gated to allow determination of $CD4^+$ and $CD8^+$ subpopulations. B lymphocytes were determined by $CD19^+$ $CD3^-$ expression.

Statistical analyses. Data are expressed as mean ± standard error of the mean. Statistical analyses for *in vitro* studies were performed with Student's *t* test comparing uninfected (control) to virus-infected cells or virulent to attenuated MHV3 infections. Multiple-group analyses were conducted for *in vivo* studies, and data obtained by qPCR, ELISA, and viral titration were evaluated by one-way analysis of variance (ANOVA) with *post hoc* Tukey test using PASW Statistics software (PASW version 18; IBM SPSS Inc., Chicago, IL). *P* values of ≤0.05 were considered significant.

RESULTS

Lower tropism of attenuated MHV3 variants for LSECs is associated with less severe damage and less viral replication in the liver. Previous studies have shown that acute infections by the attenuated 51.6- and YAC-MHV3 variants resulted in milder or subclinical hepatitis, respectively, in comparison to the fulminant hepatitis induced by the parental virulent MHV3 strain (24, 31). We first aimed to compare the evolution of damage, inflammatory infiltrates, and viral replication in the livers of mice infected by virulent and attenuated MHV3 strains. C57BL/6 mice were i.p. infected with either MHV3 or attenuated viruses for 24 to 72 h, and blood and liver samples were collected for clinical, histopathology, and viral titer analyses. Liver histopathology for virulent MHV3-infected mice showed inflammatory foci surrounding necrotic cells at 24 h and 48 h p.i.; these disappeared at 72 h p.i., while hepatocyte necrosis became extensive (Fig. 1A and B). Infection with 51.6-MHV3 revealed a delayed occurrence of inflammatory foci at 48 h p.i. with barely detectable hepatic damage, while YAC-MHV3 induced few small inflammatory infiltrates with no observable hepatic necrosis areas even at 72 h p.i. (Fig. 1A and B). Extensive hepatic damage in virulent MHV3-infected mice correlated with high levels of blood ALT and AST at 72 h p.i. ($P \leq 0.001$) (Fig. 1C and D) and sooner and higher viral replication than in mice infected with the attenuated 51.6- and YAC-MHV3 variants ($P \leq 0.01$ to 0.001) (Fig. 1E and F).

Attenuated MHV3 strains induce lower Fgl2, CAV-1, and IL-33 expression in the liver than virulent MHV3. Vascular and structural disorders in LSECs were reported in viral hepatitis, correlating with hepatic damage (19, 27, 29). Indeed, previous studies have demonstrated that induction of Fgl2, a prothrombinase expressed by LSECs and promoting vascular thrombosis and hepatic inflammation, correlated with MHV3-induced fulminant hepatitis (28). Moreover, a direct association between capillarization (lack of fenestrations) of LSECs in livers from HCV-infected patients and overexpression of caveolin-1 (CAV-1), a key component of LSEC fenestrations, was recently reported (34). To verify whether the lower severity of hepatitis induced by the attenuated MHV3 strains was associated with less dysfunction in LSECs, mRNA levels for CAV-1 and Fgl2 in livers from all infected groups of mice were quantified by qRT-PCR. Intrahepatic expression of CAV-1 in MHV3- and 51.6-MHV3-infected mice was also localized by immunohistochemical staining. As shown in Fig. 2A, greater increases of CAV-1 mRNA levels were observed at 48 h p.i. in the livers of MHV3-infected mice while less or no induction was noted in 51.6- and YAC-MHV3-infected mice ($P \leq 0.001$ and 0.05, respectively). Immunolocalization of CAV-1 revealed specific expression in LSECs and confirmed higher induction in the livers of MHV3-infected mice than in those of 51.6-MHV3-infected mice (Fig. 2B). Fgl2 gene expression increased as soon as 24 h p.i. in mice infected with MHV3, while it was delayed and lower in 51.6-MHV3 infection and not induced in YAC-MHV3-infected mice ($P \leq 0.05$ to 0.001) (Fig. 2C). In addition, Fgl2 mRNA reached higher levels in the livers of mice infected with virulent MHV3 than in those infected with attenuated viruses ($P \leq 0.001$).

We have recently reported that MHV3 infection was associated with early release of IL-33, an alarmin secreted mainly by injured LSECs (29). We aimed to verify whether lower tropism of attenuated MHV3 strains for LSECs may be associated with lower expression of IL-33. To test this hypothesis, mRNA expression, production, and localization of IL-33 in livers from MHV3- and 51.6-MHV3-infected groups of mice were assessed by qRT-PCR, ELISA, and IHC, respectively. As shown in Fig. 2D and E, gene expression and release of IL-33 increased only in the livers of MHV3-infected mice ($P \leq 0.001$), while IL-33 was not induced or was inhibited in mice infected with 51.6- or YAC-MHV3 ($P \leq 0.05$ to 0.01). IHC stainings indicated that expression of IL-33 was induced only in the liver of MHV3-infected mice and was localized mostly in LSECs and to a lesser extent in hepatocyte nuclei (Fig. 2F). Induction of IL-33 in LSECs in livers from MHV3-infected mice at 48 h p.i. and to a lesser extent at 72 h p.i. was confirmed by double immunostaining of IL-33 and caveolin-1 (Fig. 2G).

Virulent MHV3 infection leads to an imbalance of pro- over anti-inflammatory mediators in the liver, in contrast to infection by attenuated MHV3 strains. Given the crucial role of LSECs in the control of liver inflammation through production of anti-inflammatory cytokines, we presumed that dysfunction of LSECs in MHV3-infected mice may favor the induction of a proinflammatory state in the liver. To verify this hypothesis, levels of anti-inflammatory cytokines (IL-10 and TGF-β) and proinflammatory cytokines (IL-6 and TNF-α) and chemokines (CCL2, CXCL1, and CXCL10) were assayed by qRT-PCR (from 24 to 72 h p.i.) and ELISA (72 h p.i.) in the livers of all groups of infected mice. As indicated in Fig. 3IA and B, mRNA expression levels and production of IL-10 were markedly increased in the livers of 51.6-MHV3- and YAC-MHV3-infected mice compared to MHV3-infected mice ($P \leq 0.05$ to 0.001). To a lesser extent, TGF-β mRNA and production levels were also more induced in the livers of 51.6-MHV3-infected mice, especially at 24 and 48 h p.i. ($P \leq 0.05$ to 0.001) (Fig. 3IC and D). To determine whether IL-10 induction in the livers of 51.6-MHV3-infected mice occurred in endothelial cells (ECs), immunohistochemistry staining using specific anti-

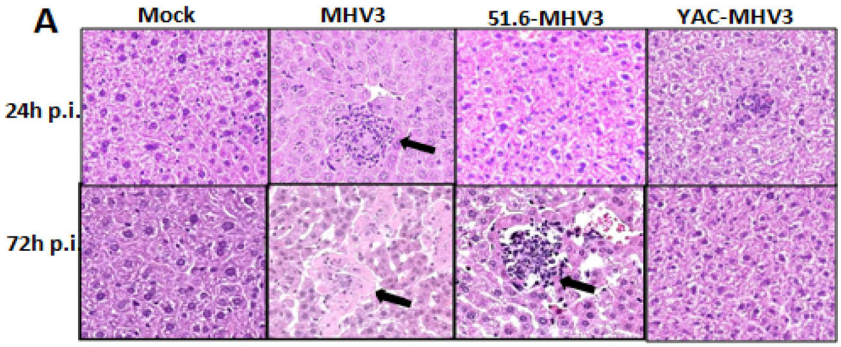

B

Virus	Time p.i. (hrs)	Inflammatory foci	Hepatic necrosis foci
MHV3	24	++	-
	48	++	++
	72	+	++++
51.6-MHV3	24	-	-
	48	+	+
	72	++	+
YAC-MHV3	24	+	-
	48	+	-
	72	+	-

+ (scarce foci); ++ (10% of hepatic tissue); +++ (20-30% of hepatic tissue); ++++ (up to 40% of hepatic tissue)

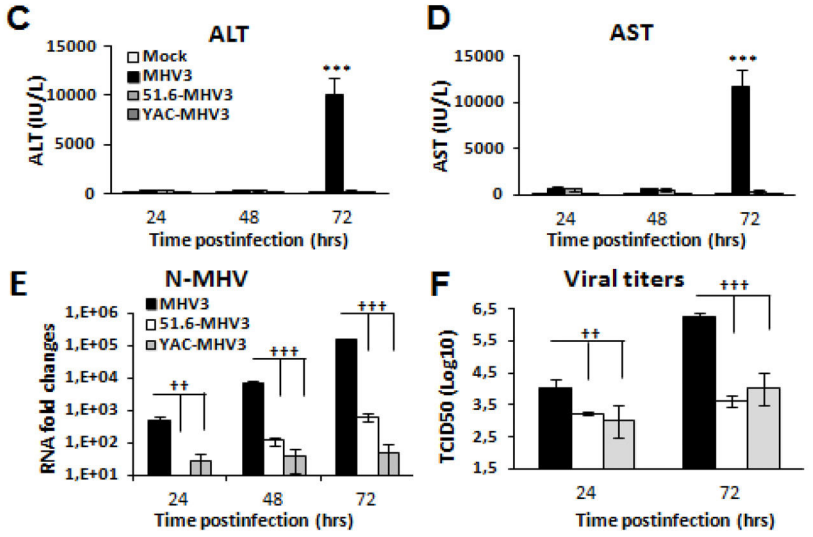

FIG 1 Hepatic damage and viral replication in highly hepatotropic MHV3- and attenuated 51.6- and YAC-MHV3-infected mice. Groups of 5 or 6 C57BL/6 mice were intraperitoneally infected with 1,000 $TCID_{50}$ of MHV3, 51.6-MHV3, or YAC-MHV3. (A) Histopathological analysis was conducted on livers from mock- and virus-infected mice from each group at 24 and 72 h p.i. Inflammatory and necrotic foci are indicated by arrows. (B) Summary of occurrence of necrotic and inflammatory foci in livers from infected mice at 24, 48, and 72 h p.i. (C and D) ALT (C) and AST (D) activities were assayed in serum samples from mock- and virus-infected mice at 24, 48, and 72 h p.i. ***, $P < 0.001$ (compared with mock-infected mice). (E and F) MHV3 replication in livers from each group of infected mice was determined by analysis of the nucleoprotein (NP) RNA expression at 24, 48, and 72 h p.i. by qRT-PCR (E) and by viral titration ($TCID_{50}$) (F) at 24 h and 72 h p.i. Values represent fold change in gene expression relative to that in mock-infected mice after normalization to HPRT expression. Values are means and standard errors of the means. ††, $P < 0.01$; †††, $P < 0.001$ (compared with MHV3-infected mice).

bodies to IL-10 and CAV-1 (an EC marker) was conducted on liver sections. In comparison to results for mock-infected mice, IL-10 expression in livers from 51.6-MHV3-infected mice was induced in the parenchyma and in venous and sinusoidal ECs, whereas the occurrence and intensity of IL-10 staining were weaker in MHV3-infected mice (Fig. 3II).

On the other hand, intrahepatic IL-6 and TNF-α mRNA expression and production levels were more upregulated in MHV3-infected mice than in 51.6- or YAC-MHV3-infected mice ($P \leq 0.05$ to 0.001) (Fig. 3IE to H). Along the same line, chemokine CXCL1, CCL2, and CXCL10 transcription and production levels increased throughout infection by MHV3 but were delayed or dramatically reduced in 51.6- or YAC-MHV3-infected mice ($P \leq 0.05$ to 0.001) (Fig. 3IIIA to F).

Virulent MHV3 induces higher expression of TLRs and helicases in the liver than attenuated MHV3 strains. Induction of the

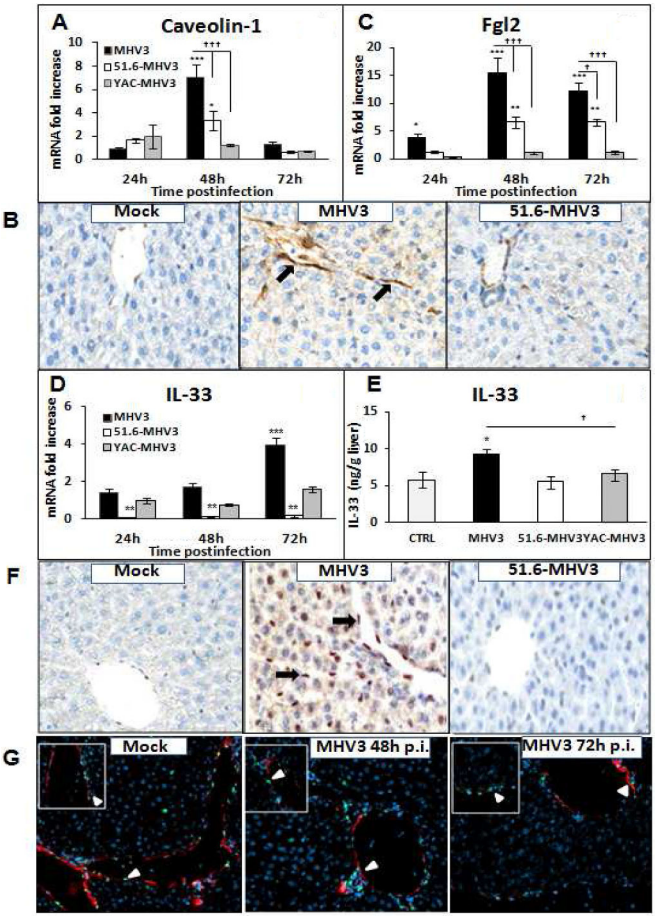

FIG 2 Gene expression and production of caveolin-1, Fgl2, and IL-33 in the livers of MHV3-, 51.6-MHV3-, and YAC-MHV3-infected mice. Groups of 5 or 6 C57BL/6 (WT) mice were intraperitoneally infected with 1,000 $TCID_{50}$ of MHV3, 51.6-MHV3, and YAC-MHV3. At 24, 48, or 72 h p.i., livers were collected from mock- and virus-infected mice of each group. (A, C, and D) mRNA expression for caveolin-1 (A), Fgl2 (C), and IL-33 (D) genes was evaluated by qRT-PCR. Values represent fold change in gene expression relative to that in mock-infected mice (arbitrarily taken as 1) after normalization to HPRT expression. (B and F) *In situ* expression of caveolin-1 (B) and IL-33 (F) in livers from mock-, MHV3-, and 51.6-MHV3-infected mice at 48 h p.i. was determined by immunohistochemistry. Caveolin-1- and IL-33-positive cells are indicated by arrows. (E) Levels of production of IL-33 at 72 h p.i. in the liver of each mouse were quantified by ELISA. (G) Immunolocalization of IL-33 in LSECs was confirmed by double immunostaining of IL-33 (green) and CAV-1 (red) in livers from mock- and MHV3-infected mice at 48 and 72 h p.i. Cell nuclei were counterstained with Hoechst (blue). Values are means and standard errors of the means. *, $P < 0.05$; **, $P < 0.01$; ***, $P < 0.001$ (compared with mock-infected mice). †, $P < 0.05$; ††, $P < 0.01$; †††, $P < 0.001$ (compared with MHV3-infected mice).

inflammatory response during viral infection is triggered upon activation of pattern recognition receptors (PRRs), such as TLRs and helicases, by viral products. Several studies have reported increased TLR expression in viral hepatitis, correlating with liver inflammation (reviewed in reference 17). We explored the hypothesis that higher release of inflammatory mediators in MHV3 infection may be related to increased expression of TLRs or helicases in the liver. Thus, the kinetics of surface TLR2 and -4, endosomal TLR3 and -7, and helicase RIG-1 and MDA-5 gene expression in the livers of infected mice were compared by qRT-PCR from 24 to 72 h p.i. As shown in Fig. 4A, TLR2 expression steadily increased over the course of infection with MHV3, while its induction was drastically reduced in mice infected with the attenuated variants ($P \leq 0.01$ to 0.001). Expression levels of the TLR3, TLR4, RIG-1, and MDA-5 genes were increased equally or more during MHV3 infection than during 51.6- or YAC-MHV3 infection, albeit markedly less so than TLR2 ($P \leq 0.05$ to 0.001) (Fig. 4B, C, E, and F), whereas levels of TLR7 were unaffected by any of the viruses (Fig. 4D).

These data suggest that higher levels of inflammatory mediators in the livers of MHV3-infected mice may be associated with preferential and higher induction of PRRs, especially TLR2, by the virulent MHV3.

The hepatic proinflammatory state in virulent MHV3-infected mice leads to rapid but transient intrahepatic recruitment of inflammatory cells and decreases of B, CD4, and CD8 lymphocyte subsets. LSECs are responsible for the recruitment and transmigration of leukocytes during liver inflammation (35). We postulated that higher production of chemokines in the livers of MHV3-infected mice induced higher recruitment of inflammatory cells than in mice infected with attenuated virus strains. This hypothesis was supported by higher occurrence of inflammatory infiltrates in the livers of MHV3-infected mice at 24 h p.i. (Fig. 1A). To determine leukocyte subsets recruited into the liver, intrahepatic mononuclear cells were isolated at 24 and 48 h p.i. from all groups of mice and immunolabeled, and the percentages of NK-T ($NK1.1^+$ $CD3^+$) and NK ($NK1.1^+$ $CD3^-$) cells, neutrophils ($CD11b^{hi}$ $Gr1^{hi}$), macrophages ($CD11b^+$ $Gr1^{int}$), B cells ($CD19^+$), and T cells ($CD8^+$ and $CD4^+$) were analyzed by cytofluorometry and compared to those in cells from mock-infected mice. As shown in Fig. 5IA, the percentages of NK-T cells transiently decreased in the livers of MHV3-infected mice ($P \leq 0.001$), differently from what was seen in livers from 51.6- and YAC-MHV3 infected mice ($P \leq 0.05$ to 0.01). NK cell percentages increased more in MHV3- than in 51.6-MHV3-infected mice, while they decreased in YAC-MHV3-infected mice ($P \leq 0.05$ to 0.001) (Fig. 5IB). Neutrophils, however, were recruited earlier and to higher levels into the livers of MHV3- than into those of 51.6- and YAC-MHV3-infected mice ($P \leq 0.05$ and 0.001, respectively) (Fig. 5IC). Percentages of intrahepatic macrophages increased more in MHV3-infected mice ($P \leq 0.05$ to 0.001) (Fig. 5ID). Regarding lymphocyte subsets, B and $CD4^+$ cell percentages decreased more strongly in the livers of MHV3-infected mice ($P \leq 0.05$ and 0.001, respectively) (Fig. 5IE and F), while $CD8^+$ cells were reduced more by 51.6- or YAC-MHV3 infection ($P \leq 0.05$ to 0.001) (Fig. 5IG).

Since a substantial decrease in the total number of isolated intrahepatic cells was noted over infection time with MHV3 only, the analysis of absolute numbers of each cell subset rather than the relative percentages better reflects the recruitment of inflammatory cells. Cell numbers were then determined, using the percentage of each subset with respect to the total number of isolated cells in the livers of the mice. As shown in Fig. 5IIA and B, NK-T cells decreased only in the livers of MHV3-infected mice ($P \leq 0.01$ and 0.001), while total NK cells were not altered in all infected groups. The number of neutrophils, however, earlier but transiently increased at 24 h p.i. in MHV3-infected mice, while they were delayed or recruited less in livers from 51.6- and YAC-MHV3-infected mice, respectively, compared to MHV3 infection ($P \leq 0.05$ to 0.001) (Fig. 5IIC). In contrast to what was observed with per-

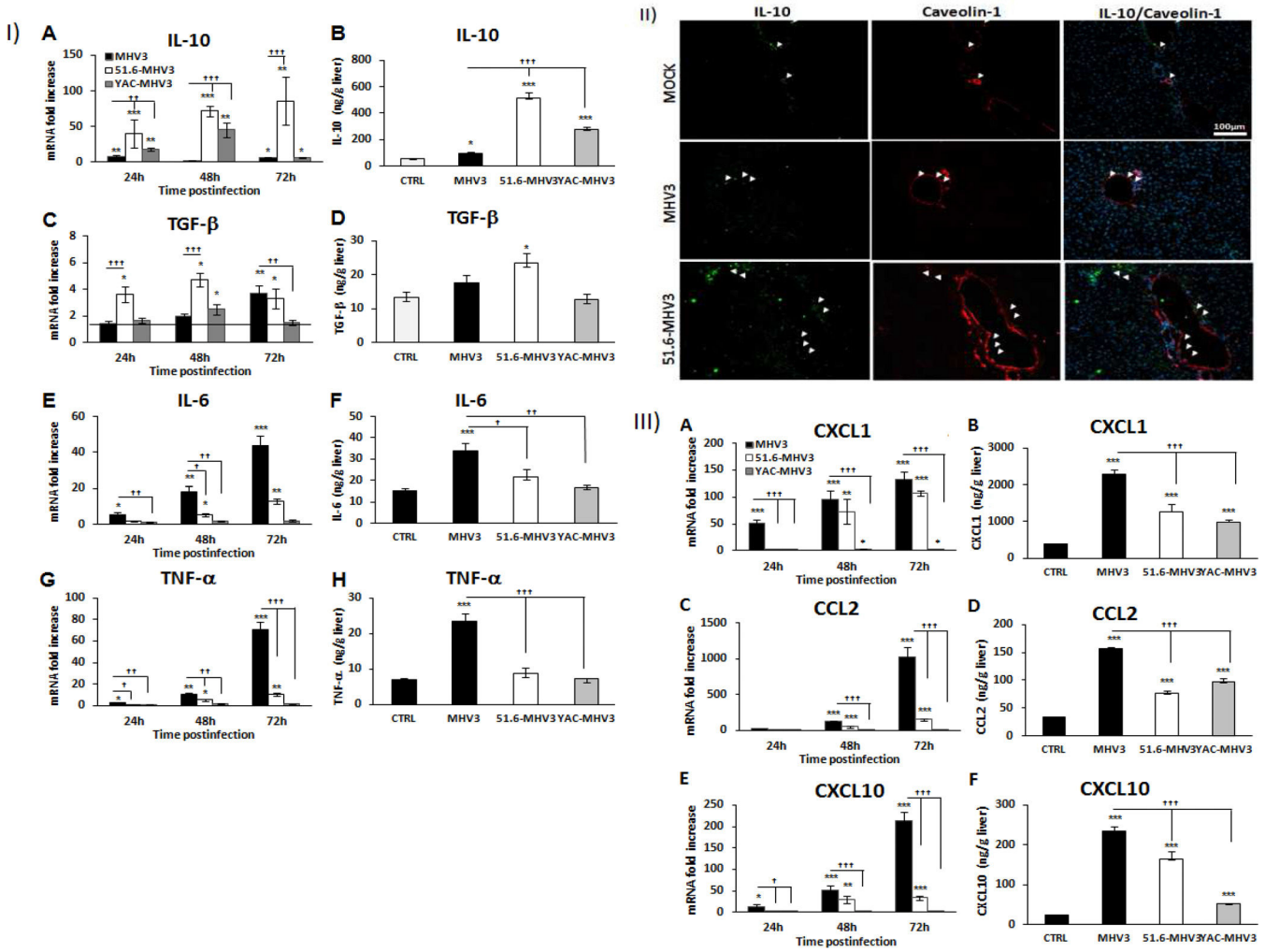

FIG 3 Gene expression and production of IL-10, TGF-β, IL-6, TNF-α, CXCL1, CCL2, and CXCL10 in the livers of MHV3-, 51.6-MHV3-, and YAC-MHV3-infected mice. Groups of 5 or 6 C57BL/6 mice were intraperitoneally infected with 1,000 $TCID_{50}$ of MHV3, 51.6-MHV3, and YAC-MHV3. At 24, 48, or 72 h p.i., livers were collected from mock- and virus-infected mice of each group. (I) Fold changes in mRNAs of IL-10 (A), TGF-β (C), IL-6 (E), and TNF-α (G) were analyzed by qRT-PCR. Values represent fold change in gene expression relative to those in mock-infected mice (arbitrarily taken as 1) after normalization to HPRT expression. Production levels of IL-10 (B), TGF-β (D), IL-6 (F), and TNF-α (H) at 72 h p.i. in the liver of each mouse were quantified by ELISA. (II) *In situ* expression of IL-10 and caveolin-1 was assayed by immunohistochemistry in livers of mock-, MHV3-, and 51.6-MHV3-infected mice at 48 h p.i. (arrows show IL-10- and caveolin-1-expressing endothelial cells). (III) Fold changes in mRNAs of CXCL1 (A), CCL2 (C), and CXCL10 (E) were analyzed by qRT-PCR. Values represent fold change in gene expression relative to that in mock-infected mice (arbitrarily taken as 1) after normalization to HPRT expression. Production levels of CXCL1 (B), CCL2 (D), and CXCL10 (F) at 72 h p.i. in the liver of each mouse were quantified by ELISA. Values are means and standard errors of the means. *, $P < 0.05$; **, $P < 0.01$; ***, $P < 0.001$ (compared with mock-infected mice). †, $P < 0.05$; ††, $P < 0.01$; †††, $P < 0.001$ (compared with MHV3-infected mice).

centages, the numbers of intrahepatic macrophages increased in the livers of mice infected with the attenuated YAC- and 51.6-MHV3 strains ($P \leq 0.01$ and 0.001) but not in those infected with MHV3, but such increases were not statistically significant compared to MHV3 infection (Fig. 5IID). The numbers of B and T (CD4 and CD8) cells were also dramatically impaired over the course of infection by MHV3 but were less or not altered by 51.6- or YAC-MHV3 infections or transiently increased at 24 h p.i. in YAC-MHV3-infected mice ($P \leq 0.05$ to 0.001) (Fig. 5IIE and G).

Permissivity of LSECs to MHV3 strains correlates with virulence. We next attempted to characterize the effect of virulent and attenuated MHV3 infection on the functional and structural integrity of LSECs *in vitro*. LSECs were isolated from the livers of C57BL/6 mice and purified by Percoll gradients followed by immunomagnetism using anti-CD146 antibodies. As shown in Fig. 6A, 87 to 91% of isolated cells expressed the endothelial markers CD146, CD54 (ICAM-1), and CD31 (PECAM-1) but not the macrophage marker F4/80. Isolated LSECs were then infected by the MHV3 strains, and viral replication as well as CPE were monitored from 24 to 120 h p.i. The CPE in LSECs were characterized by cell lysis and rounded cells instead of typical MHV-induced giant syncytial cells (usually observed in L2 cells) and occurred sooner in virulent MHV3-infected culture, as cells were totally lysed by 72 h p.i. In contrast, CPE in cells infected by attenuated strains were delayed to 72 h p.i. and increased up to 120 h p.i. (Fig. 6B) ($P \leq 0.001$ compared with MHV3-infected cells). Infectious viruses in supernatants from MHV3-infected LSECs were

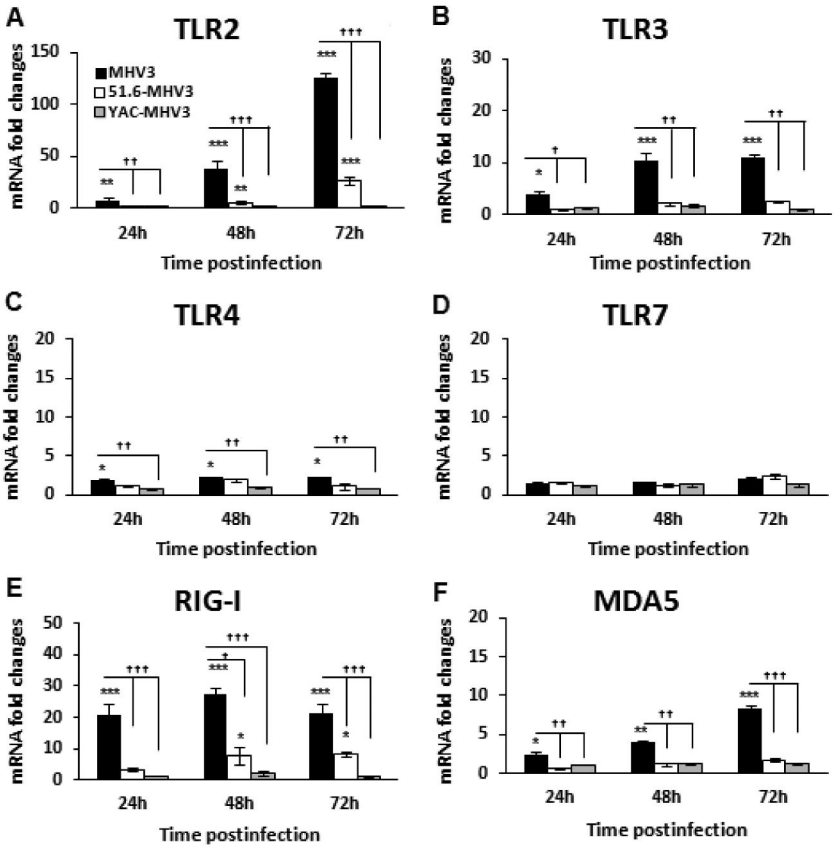

FIG 4 Gene expression of TLR2, -3, -4, and -7 and helicases RIG-I and MDA5 in the livers of MHV3-, 51.6-MHV3-, and YAC-MHV3-infected mice. Groups of 5 or 6 C57BL/6 (WT) mice were intraperitoneally infected with 1,000 $TCID_{50}$ of MHV3, 51.6-MHV3, and YAC-MHV3. At 24, 48, or 72 h p.i., livers were collected from mock- and virus-infected mice of each group. mRNA expression for the TLR2 (A), TLR3 (B), TLR4 (C), TLR7 (D), RIG-I (E), and MDA5 (F) genes was evaluated by qRT-PCR. Values represent fold change in gene expression relative to that in mock-infected mice (arbitrarily taken as 1) after normalization to HPRT expression. Values are means and standard errors of the means. *, $P < 0.05$; **, $P < 0.01$; ***, $P < 0.001$ (compared with mock-infected mice). †, $P < 0.05$; ††, $P < 0.01$; †††, $P < 0.001$ (compared with MHV3-infected mice).

detected at 48 h p.i. and then started to decrease as cell damage became extensive, whereas titers of 51.6- and YAC-MHV3 were detected only after 96 or 120 h p.i. (Fig. 6C) ($P \leq 0.001$ compared with MHV3-infected cells).

Virulent, but not attenuated, strain MHV3 induces Fgl2, IL-33, and caveolin-1 expression and alters NO production by LSECs. To confirm that attenuated MHV3 variants, in contrast to MHV3 virus, do not disturb LSEC integrity and vascular factors, as observed *in vivo*, the expression levels of the alarmin IL-33 and the prothrombinase Fgl2 in infected LSECs were evaluated. As expected and as shown in Fig. 7A to C, gene expression and release of IL-33 increased throughout infection only in MHV3-infected cells ($P \leq 0.05$ to 0.001), while Fgl2 expression was upregulated at 48 h p.i. only in MHV3-infected cells ($P \leq 0.05$ to 0.001). Lower levels of Fgl2 mRNA at 72 h p.i. ($P \leq 0.05$) reflected total cell lysis in MHV3-infected LSECs.

MHV3 replication was already shown to be controlled *in vitro* by nitric oxide (NO) (36). Since LSECs constitutively release NO, a vasodilator factor regulating sinusoidal blood flow (37), we examined whether higher replication of MHV3 in LSECs may result from a defect in NO production by quantifying NO levels in culture supernatants. As shown in Fig. 7D, release of NO was reduced only in MHV3-infected cells and not in 51.6-MHV3- or YAC-MHV3-infected cells ($P \leq 0.01$) (Fig. 7B). Since NO production was reported to be negatively regulated by CAV-1 through inhibition of endothelial nitric oxide synthase (eNOS) activity (38), we investigated whether NO alteration by MHV3 infection was associated with upregulation of CAV-1 expression in infected LSECs, as seen in the livers of MHV3-infected mice. In agreement with our *in vivo* observations, the CAV-1 mRNA expression level increased only in MHV3-infected LSECs at 24 and 48 h p.i. (Fig. 7E) ($P \leq 0.05$ to 0.001).

Virulent MHV3, in contrast to attenuated strains, promotes LSEC conversion to a proinflammatory profile. MHV3-infected mice exhibited a higher inflammatory response in the liver than mice infected by attenuated strains, suggesting a defect in the control of inflammation by LSECs. LSECs were already reported to produce IL-6 upon infection by mouse cytomegalovirus (MCMV) (5), indicating a possible switch from an anti- to a proinflammatory phenotype once infected. We thus speculated that LSECs infected by MHV3, in comparison to attenuated strains, may adopt a preponderant proinflammatory profile. To address this, mRNA expression and production levels of anti-inflammatory (IL-10 and TGF-β) and proinflammatory (IL-6 and TNF-α) cytokines produced by infected LSECs were determined by qRT-PCR and ELISAs. As shown in Fig. 8IA and B, IL-10 mRNA expression and

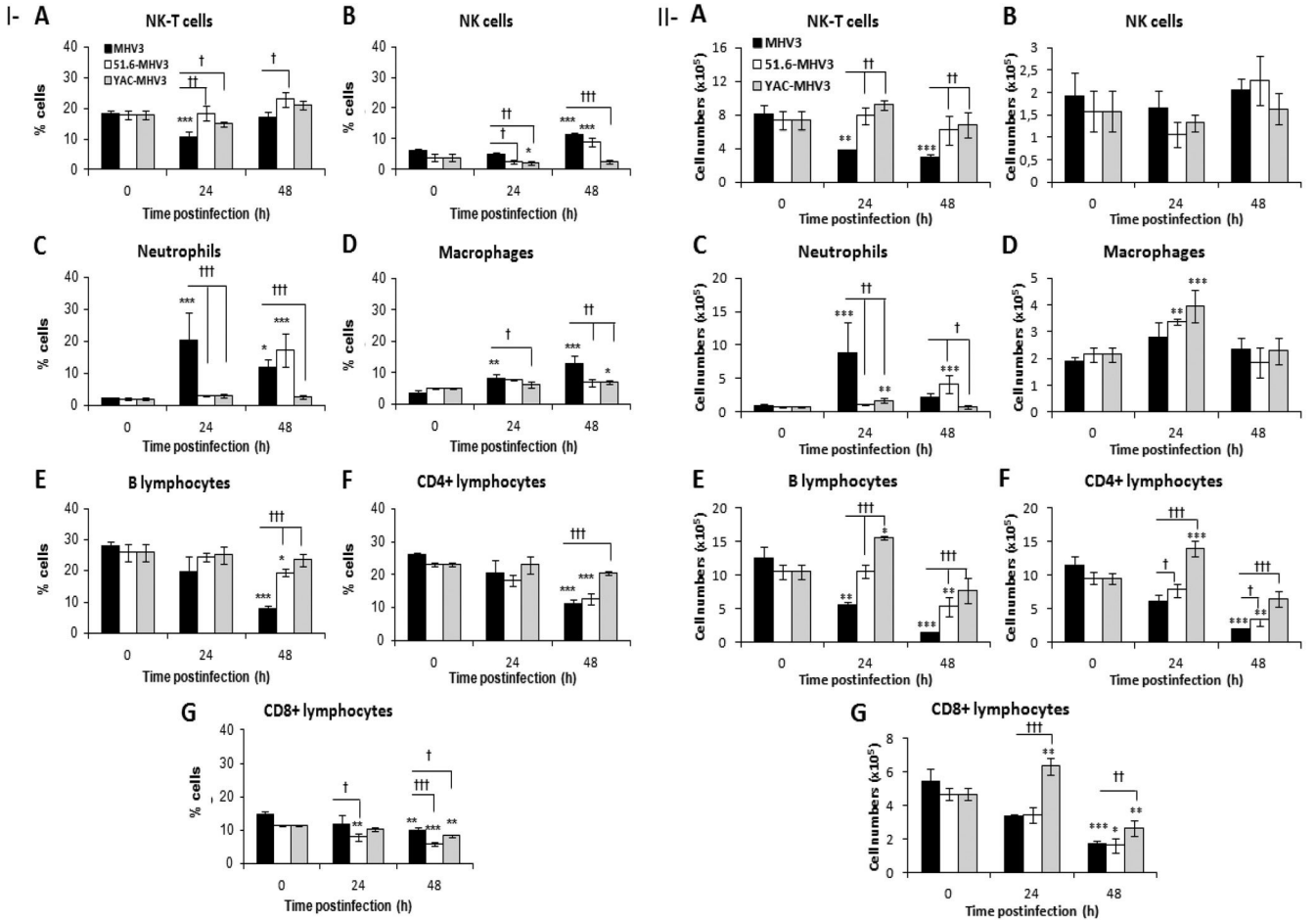

FIG 5 Percentages and numbers of intrahepatic mononuclear cell subsets in livers from MHV3-, 51.6-MHV3-, and YAC-MHV3-infected mice. Intrahepatic mononuclear cells were isolated from groups of 5 or 6 mock-infected or MHV3-, 51.6-MHV3-, or YAC-MHV3-infected C57BL/6 mice at 24 and 48 h p.i., immunolabeled with NK1.1, CD3, Gr1, CD11b, CD19, CD4, and CD8 monoclonal antibodies, and analyzed by cytofluorometry. (I) Percentages of NK-T cells ($NK1.1^+$ $CD3^+$) (A), NK cells ($NK1.1^+$ CD3) (B), neutrophils ($Gr1^{hi}$ $CD11b^{hi}$) (C), macrophages ($Gr1^+$ $CD11b^{int}$) (D), B lymphocytes ($CD19^+$) (E), CD4 cells ($CD3^+$ $CD4^+$) (F), and CD8 cells ($CD3^+$ $CD8^+$) (G) were evaluated in livers from each group of infected mice. (II) Absolute numbers for each cell subset (calculated by using respective percentages reported with respect to the total number of isolated mononuclear cells) were similarly recorded in livers of respective groups. Values are means and standard errors of the means. *, $P < 0.05$; **, $P < 0.01$; ***, $P < 0.001$ (compared with mock-infected mice). †, $P < 0.05$; ††, $P < 0.01$; †††, $P < 0.001$ (compared with MHV3-infected mice).

production slightly increased at 24 h p.i. in MHV3-infected LSECs but decreased thereafter below the basal level in uninfected cells ($P \leq 0.05$ and 0.001). Consistent with the upregulation of IL-10 in the livers of mice infected with attenuated MHV3 strains, IL-10 levels increased rapidly or progressively higher in 51.6-MHV3- and YAC-MHV3-infected LSECs than in MHV3-infected LSECs up to 72 h p.i. ($P \leq 0.05$ to 0.001). TGF-β expression, however, was not induced or was slightly induced in cells infected by the attenuated strains ($P \leq 0.05$) but was less inhibited in attenuated-virus-infected cells than in virulent MHV3-infected cells ($P \leq 0.05$ and 0.01) (Fig. 8IC and D). These results suggest that MHV3 infection suppresses the anti-inflammatory function of LSECs whereas attenuated strains promote it.

TNF-α mRNA levels, however, transiently increased only in MHV3-infected LSECs at 24 h p.i. ($P \leq 0.01$) (Fig. 3IE) and were completely inhibited at 72 h p.i. by all MHV3 strains ($P \leq 0.01$). The amounts of TNF-α released in supernatants of infected LSECs, however, increased in all infected cells ($P \leq 0.001$) but remained higher in MHV3- and YAC-MHV3-infected cells than in 51.6-MHV3-infected cells ($P \leq 0.05$) (Fig. 8IF). The IL-6 mRNA expression reached higher levels in cells infected by virulent MHV3 than in those infected by attenuated strains only at 24 h p.i. ($P \leq 0.05$ to 0.001) (Fig. 8IG), correlating with higher release in supernatants of MHV3-infected cells ($P \leq 0.01$) (Fig. 8IH).

LSECs were also reported to secrete chemokines upon infection by dengue virus and to enhance their production in chronic inflammatory liver disease (39, 40). Thus, we presumed that MHV3-infected LSECs may produce higher levels of chemokines. As shown in Fig. 3IIA to D, CXCL1 and CCL2 expression was higher upregulated in MHV3-infected LSECs than in 51.6- and YAC-MHV3-infected cells at 24 and 48 h p.i., leading to larger amounts released in cell supernatants ($P \leq 0.05$ to 0.001). CXCL10 gene expression and production levels increased only in MHV3-infected LSECs ($P \leq 0.05$ to 0.001) (Fig. 8IIE and F).

Proinflammatory activation of LSECs by MHV3 depends on TLR2 signaling. We have previously shown that induction of in-

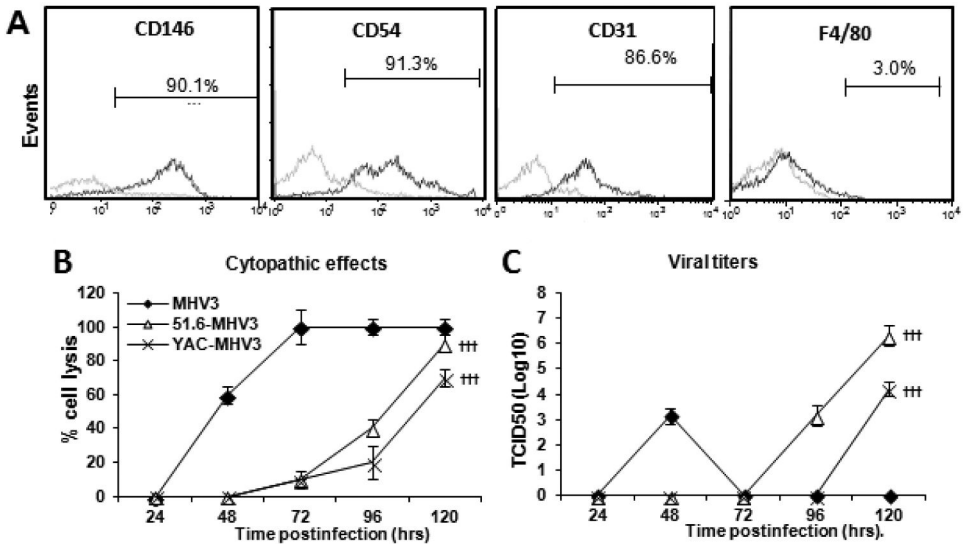

FIG 6 Permissivity of LSECs to MHV3, 51.6-MHV3, and YAC-MHV3 infection. Mouse LSECs were isolated with Percoll gradients and enriched by immunomagnetism with anti-CD146 antibodies. (A) LSECs were characterized by immunolabeling with antibodies for CD146, CD54, CD31, and F4/80 cell markers and cytofluorometric analysis. (B and C) LSECs were infected at an MOI of 0.1 with MHV3, 51.6-MHV3, and YAC-MHV3. The evolution of cytopathic effects in LSEC cultures was noted up to 5 days p.i. (B), and the kinetics of MHV infections were monitored by quantifying viral titers in supernatants of infected LSECs (C). All experiments were conducted in triplicate. Results are representative of two independent experiments. Values are means for each point. †††, $P < 0.001$ compared with MHV3-infected cells.

flammatory cytokines by MHV3 in *in vitro*-infected macrophages depended on TLR2 signaling (37). In addition, Liu et al. (9) recently demonstrated that TLR2 activation on LSECs reversed their anti-inflammatory functions. Since TLR2 was strongly upregulated in livers from MHV3-infected mice, we aimed to investigate whether TLR2 was involved in the conversion of LSECs toward a proinflammatory profile. We first sought to determine whether MHV3 increased TLR2 expression on LSECs. As shown in Fig. 9A, levels of TLR2 mRNAs were significantly higher in cells infected by MHV3 than in those infected by attenuated strains at 24 h p.i. ($P \leq$ 0.05 to 0.01). To address whether TLR2 was involved in the cytokine response and viral replication in infected LSECs, TLR2 expression was abrogated by siRNAs prior to infection, and IL-6 and CXCL1 mRNA levels were determined by qRT-PCR at 24 h p.i. Viral replication of MHV3, but that of not 51.6- and YAC-MHV3, was significantly reduced following TLR2 knockdown ($P \leq 0.001$) (Fig. 9B). A markedly decreased expression of IL-6 and CXCL1 levels and an upregulation of IL-10 levels were also observed in MHV3-infected cells rendered defective for TLR2, while no difference was noted in cells infected with the attenuated variants ($P \leq 0.001$) (Fig. 9C to E). These results suggest that the higher tropism and proinflammatory induction capacities of MHV3 in LSECs reflect its unique ability to activate TLR2 signaling.

TLR2 exacerbates liver damage and increases viral replication in mice infected by virulent but not attenuated MHV3 strains. We already reported that MHV3-induced acute hepatitis was less severe in TLR2 KO mice (41). To verify whether TLR2 is differentially involved in the evolution of hepatitis induced by virulent and attenuated MHV3 strains, groups of wild-type (WT) C57BL/6 and TLR2 knockout (KO) mice were i.p. infected with MHV3 or 51.6-MHV3. The survival rate was monitored, and liver damage and viral load were evaluated at 72 h p.i. As shown in Fig. 10A and B, survival of TLR2 KO mice infected by MHV3, but not 51.6-MHV3, was prolonged compared to that of the respective infected WT mice ($P \leq 0.001$). Accordingly, histopathological analysis of the liver revealed fewer and smaller necrotic foci in MHV3-infected TLR2 KO mice than in WT mice, whereas comparable and barely detectable hepatic damage was noted in TLR2 KO and WT mice infected with 51.6-MHV3 (Fig. 10C).

In addition, viral replication of MHV3 at 72 h p.i. was lower in the livers of infected TLR2 KO mice than in those of WT mice, whereas 51.6-MHV3 replication was similar in both mouse strains (Fig. 10D) ($P \leq 0.001$). Taken together, these results suggest that TLR2 aggravates hepatic damage and viral replication in mice infected by virulent but not attenuated MHV3 strains.

TLR2 activation by virulent MHV3 decreases IL-10 and increases inflammatory cytokine and chemokine expression. It was previously reported that hepatic levels of IL-6 and TNF-α were reduced in MHV3-infected TLR2 KO mice in comparison to C57BL/6 mice, suggesting a role for TLR2 in MHV3-induced release of inflammatory factors (41). Thus, we speculated that MHV3, in contrast to 51.6-MHV3, may promote a proinflammatory cytokine profile in the liver through TLR2 activation, such as observed in *in vitro*-infected LSECs. To test this hypothesis, expression levels of several inflammatory and anti-inflammatory factors were compared between livers from TLR2 KO and wild-type (WT) mice infected with both viruses. As shown in Table 2, lower TNF-α, IL-6, CXCL1, CCL2, and CXCL10 mRNA expression and higher IL-10 levels occurred in the livers of MHV3-infected TLR2 KO mice compared to those of WT mice ($P \leq 0.001$), whereas levels of Fgl2 and IL-33 were similar in both mouse strains. In contrast, no difference was observed between cytokine profile in 51.6-MHV3-infected WT and TLR2 KO mice, albeit a slight reduction of CXCL10 expression was noted in TLR2 KO mice ($P \leq 0.05$). Given the importance of IL-10 in the control of hepatic inflammation, we aimed to determine whether higher lev-

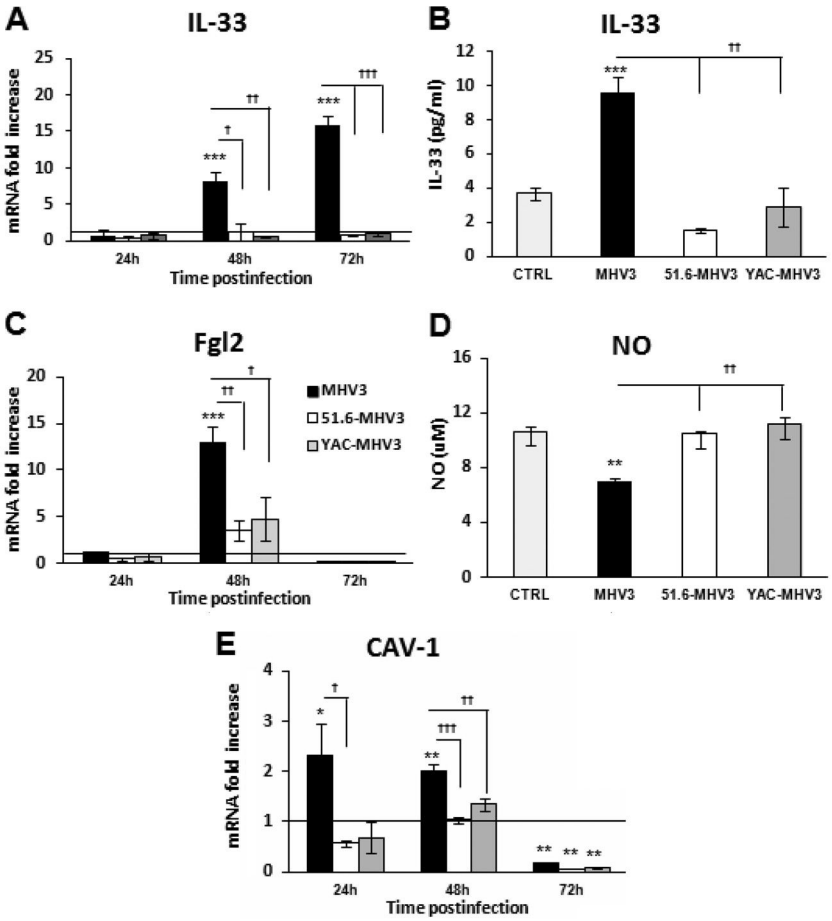

FIG 7 Expression levels of Fgl2, IL-33, and caveolin-1 and production of NO in *in vitro* MHV3-, 51.6-MHV3-, and YAC-MHV3-infected LSECs. LSECs were infected at an MOI of 0.1 with MHV3, 51.6-MHV3, and YAC-MHV3, and RNA and supernatant from LSECs infected with each viral strain were collected at 24, 48, or 72 h p.i. (A, C, and E) IL-33 (A), Fgl2 (C), and caveolin-1 (E) mRNA fold changes were analyzed by qRT-PCR. Values represent fold change in gene expression relative to that in uninfected LSECs (control arbitrarily taken as 1) after normalization to HPRT expression. All samples were run in duplicate. (B and D) Production levels of IL-33 were quantified by ELISA (B) and NO levels were assayed by the Griess reaction (D) in supernatants at 48 h p.i. All experiments were run in duplicate, and results are representative of two independent experiments. Values are means and standard errors of the means. *, $P < 0.05$; **, $P < 0.01$; ***, $P < 0.001$ (compared with mock-infected cells). †, $P < 0.05$; ††, $P < 0.01$; †††, $P < 0.001$ (compared with MHV3-infected cells).

els in livers from MHV3-infected TLR2 KO mice reflected higher production by ECs. A double immunohistochemistry staining of IL-10 and CAV-1 on liver sections revealed that expression of IL-10 in ECs was effectively higher in livers from MHV3-infected TLR2 KO mice than in those from WT mice (Fig. 11; compare Fig. 3II).

DISCUSSION

In this work, we investigated the role of LSECs in hepatic inflammation during the acute viral hepatitis process using the MHV3 model of infection. We demonstrated that the severity of hepatitis, viral replication, and hepatic inflammation correlated with permissivity of LSECs for MHV3 strains and subsequent structural and functional disturbances. We showed that *in vitro* infection of LSECs by the virulent MHV3, in contrast to the attenuated 51.6- and YAC-MHV3 variants, resulted in earlier cell damage and disorders in inflammatory and vascular factors, as reflected by a high release of inflammatory cytokines/chemokines and procoagulant Fgl2 and a decrease in NO and IL-10 levels. We showed that the higher replication rate and proinflammatory activity of MHV3 in LSECs was associated with its specific activation of TLR2 signaling in LSECs and that TLR2 is a key factor of hepatic inflammation and LSEC-derived IL-10 disorders in MHV3-induced fulminant hepatitis.

LSECs, lining the hepatic sinusoids, mediate liver tolerance under physiological conditions (reviewed in reference 1), but these cells are the target of many hepatotropic viruses. The consequence of LSEC infection in inflammatory liver diseases such as viral hepatitis has never been investigated. We have shown that MHV3 infection induced differential structural and functional disorders in LSECs according to strain virulence. Indeed, the highly virulent MHV3 replicated faster and to higher levels in LSECs, leading to occurrence of CPE such as a change in morphology (rounded cells) and cell lysis from 48 h p.i. Previous reports have already shown that *in vivo* and *in vitro* infections of LSECs by MHV3 are associated with cell damage and loss of fenestrations (27), but no syncytial cells were observed. However, MHV3 did not replicate in LSECs as fast as it usually does

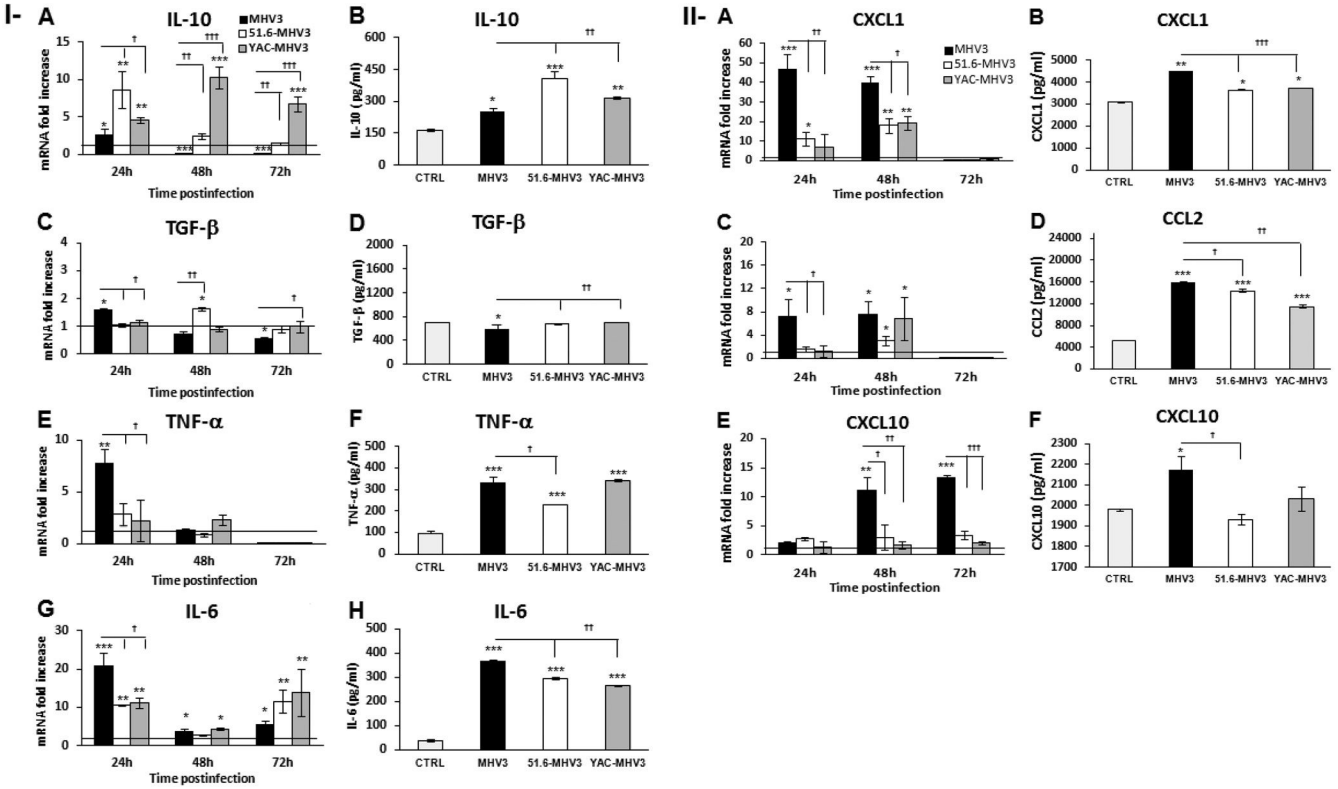

FIG 8 Gene expression and production of IL-10, TGF-β, IL-6, TNF-α, CXCL1, CCL2, and CXCL10 in *in vitro* MHV3-, 51.6-MHV3-, and YAC-MHV3-infected LSECs. LSECs were infected at an MOI of 0.1 with MHV3, 51.6-MHV3, and YAC-MHV3, and RNA and supernatant from LSECs infected with each viral strain were collected at 24, 48, or 72 h p.i. (I) Fold changes in IL-10 (A), TGF-β (C), IL-6 (E), and TNF-α (G) mRNA were analyzed by qRT-PCR. Values represent fold change in gene expression relative to that in uninfected LSECs (control arbitrarily taken as 1) after normalization to HPRT expression. All samples were run in duplicate. Production levels of IL-10 (B), TGF-β (D), IL-6 (F), and TNF-α (H) in supernatants were quantified by ELISA at 24 h p.i. (II) Fold changes in CXCL1 (A), CCL2 (C), and CXCL10 (E) mRNA were analyzed by qRT-PCR. Values represent fold change in gene expression relative to that in control (uninfected) LSECs after normalization to HPRT expression. All samples were run in duplicate. Production levels of CXCL1 (B), CCL2 (D), and CXCL10 (F) in supernatants were quantified by ELISA at 24 h p.i. All experiments were conducted in duplicate, and results are representative of two independent experiments. Values are means and standard errors of the means. *, $P < 0.05$; **, $P < 0.01$; ***, $P < 0.001$ (compared with mock-infected cells). †, $P < 0.05$; ††, $P < 0.01$; †††, $P < 0.001$ (compared with MHV3-infected cells).

in *in vitro*-cultured cells, since no viral burden was detected until 48 h p.i. while MHV3 titers are detectable within 24 h p.i. in macrophages (24, 41). Our results are nevertheless in accordance with those of Pereira et al. (26), who have shown that MHV3 replicates more rapidly in Kupffer cells (KCs) than in LSECs *in vitro*, suggesting that LSECs may transiently control the viral replication.

In agreement, replication of the attenuated 51.6- and YAC-MHV3 variants was delayed to 96 or 120 h p.i. and was associated with barely detectable CPE, reflecting their weaker tropism for LSECs. It was recently reported that LSECs exhibit a high capacity for clearance of circulating viruses (42, 43), suggesting that they may have a high ability to sequester attenuated but not virulent MHV3 particles. However, the fact that replication of MHV3 variants in LSECs was delayed but not aborted suggests, rather, a host cell-dependent mechanism of control of viral replication. Indeed, preliminary results showed a higher antiviral IFN-β response in LSECs infected by attenuated MHV3 strains (results not shown). The low IFN-β response in virulent MHV3-infected LSECs may be related to specific viral evasion mechanisms from host viral sensors or interference with downstream signaling pathways. We have observed that MHV3, in contrast to attenuated strains, induced neither TLR3 nor RIG-I expression in LSECs (results not shown), suggesting lower detection by these viral sensors. Further work should address whether viral products or evasion strategies are involved in MHV3-induced impairment of the IFN-β response in LSECs.

The inability of attenuated MHV3 variants to establish a rapid infection in LSECs correlated with a less severe hepatitis. Indeed, 51.6-MHV3 infection resulted in lower viral replication, transaminase levels, and liver damage than MHV3 infection. The 51.6-MHV3 variant differs from the pathogenic MHV3 only by its weaker tropism for LSECs but retains its virulence for hepatocytes, KCs, and Ito cells (24), suggesting that resistance of LSECs to viral replication may protect against fulminant hepatitis. Similarly, the nonpathogenic YAC-MHV3, also with a low ability to replicate in LSECs, induced light and transient hepatic lesions, reinforcing the importance of functional integrity of LSECs in the evolution of viral hepatitis. Indeed, less severe hepatic damage and viral load in mice infected with the attenuated variants may possibly result from a better early control of viral replication by LSECs, leading to reduced transmission of viral progeny to the hepatic parenchyma. In agreement, a delayed replication of MHV3 in LSECs was suggested as a crucial step in the resistance of various strains of mice

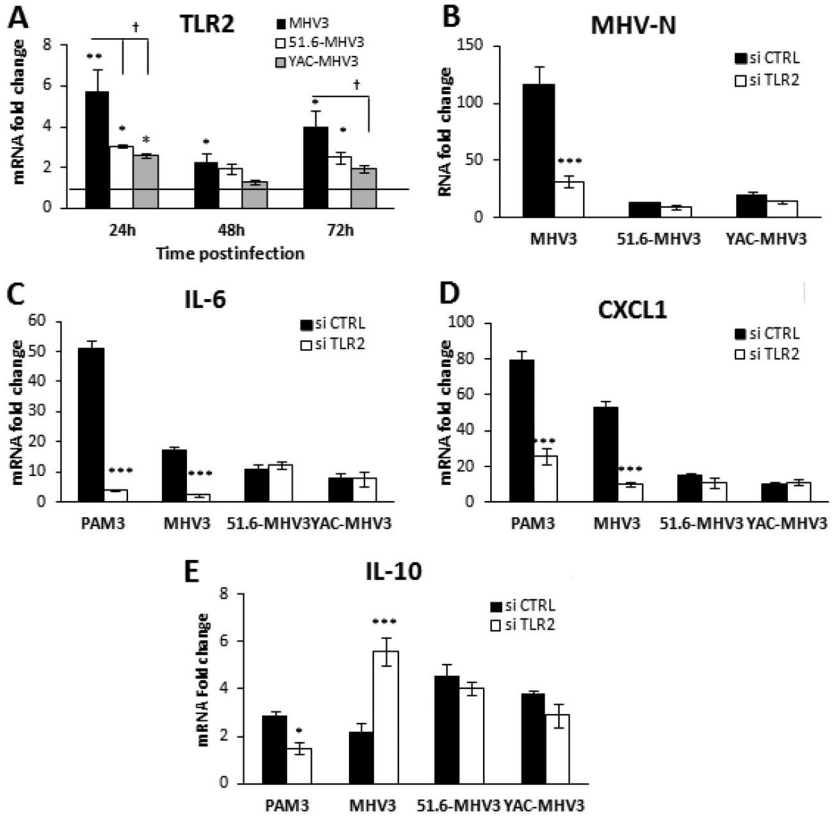

FIG 9 Role of TLR2 in viral replication and expression of IL-6 and CXCL1 in MHV3-, 51.6-MHV3-, and YAC-MHV3-infected LSECs. (A) LSECs were infected at an MOI of 0.1 with MHV3, 51.6-MHV3, and YAC-MHV3. At 24, 48, and 72 h p.i., RNA from infected LSECs was extracted and mRNA expression levels for the TLR2 gene were determined by qRT-PCR. (B to D) LSECs were treated with a specific siRNA against TLR2 prior to infection with viruses or treatment with the specific TLR2 agonist Pam3Cys (as a positive control) for 24 h. mRNA expression levels of MHV nucleoprotein (MHV-N) (B), IL-6 (C), and CXCL1 (D) were determined by qRT-PCR. Values represent fold change in gene expression relative to that in control (uninfected) LSECs after normalization to HPRT expression. All samples were run in duplicate, and results are representative of two independent experiments. *, $P < 0.05$; **, $P < 0.01$; ***, $P < 0.001$ (compared with control cells). †, $P < 0.05$ (compared with MHV3-infected cells).

to MHV3 infection by allowing time for the local and systemic responses to clear the infective particles (26).

We report here for the first time that *in vitro* MHV3 infection promotes a proinflammatory activation of LSECs. Indeed, MHV3 induced higher levels of IL-6, TNF-α, and chemokines in LSECs than attenuated strains and inhibited their basal release of IL-10, while attenuated strains enhanced it. These inflammatory disorders in LSECs correlated with higher ratios of intrahepatic inflammatory to anti-inflammatory mediators in the livers of MHV3-infected mice, suggesting that LSECs may have lost their ability to control inflammation. In agreement, IL-10 staining was significantly lower in ECs from the livers of mice infected by MHV3 than in those of mice infected by attenuated strains. The importance of IL-10 production by LSECs in the suppression of proinflammatory cytokine release by Th1 and Th17 cells was recently shown by Carambia et al. (44). In addition, LSECs were recently shown to be more efficient than KCs in tolerizing autoreactive Th1 cells via IL-10 (2). The lower inflammatory profiles in livers from 51.6- and YAC-MHV3-infected mice are in line with our previous observations (30). The highly attenuated YAC-MHV3 infection correlated with lower induction of inflammatory mediators than 51.6-MHV3 infection. Higher levels of anti-inflammatory IL-10 and immunosuppressive PGE_2 in the livers of YAC-MHV3- than in those of 51.6-MHV3-infected mice were reported previously (30), suggesting that the highly attenuated phenotype of YAC-MHV3 may reflect the preservation of integrity of LSECs and other, yet-unidentified hepatic cells. Since YAC-MHV3, unlike 51.6-MHV3, was shown to replicate less in macrophages *in vitro* (45), it is plausible that preservation of KC tolerance functions may further contribute to lower inflammatory responses during YAC-MHV3 infection. Altogether, the results from YAC-MHV3 and 51.6-MHV3 infections strengthen the importance of LSEC structural and functional integrity in restricting the hepatic inflammatory response and subsequent damage. In agreement, activation of LSECs toward a proinflammatory profile was pointed out as a critical component of intrahepatic inflammation in hepatic fibrosis (40).

Differences in the LSEC cytokine profile according to infection by pathogenic or attenuated MHV3 strains may reflect differential PRR induction and activation by viral fixation and/or replication. We have already demonstrated that IL-6 and TNF-α production by MHV3-infected macrophages resulted from TLR2 activation by the surface (S) viral protein (41). The production of TNF-α by LSECs is known to depend on TLR1 to -4, -6, and -8, while IL-6 is produced following activation of TLR1 to -4 only (4, 17). It has been recently demonstrated that TLR1/2 ligand (PamC3), but not

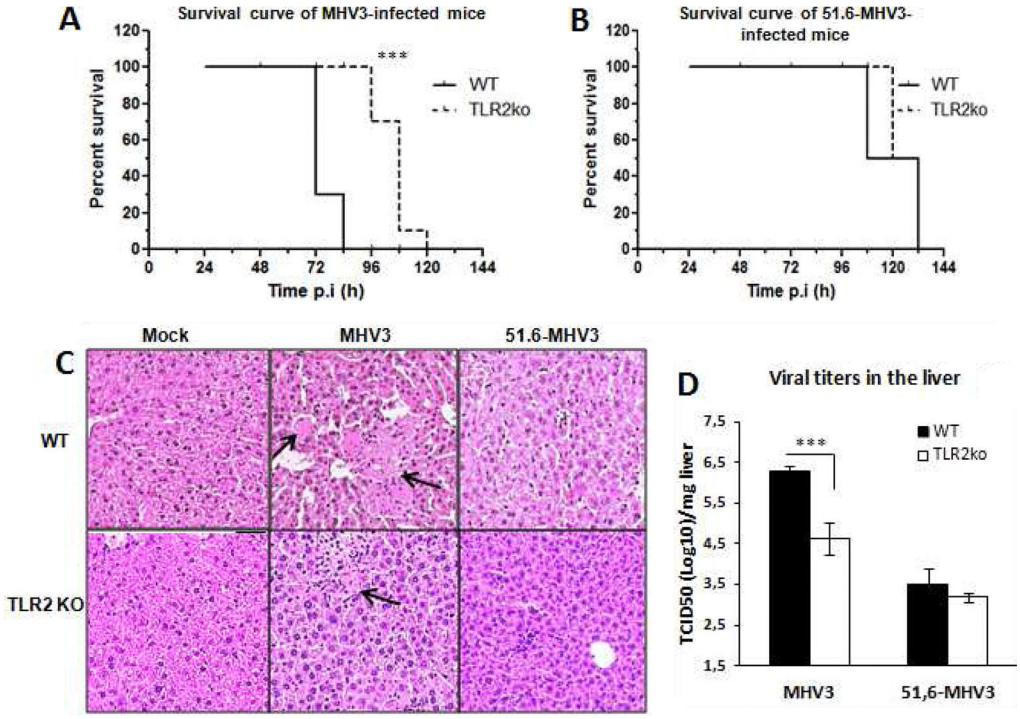

FIG 10 Mortality, hepatic damage, and viral replication in MHV3- and 51.6-MHV3-infected C57BL/6 (WT) and TLR2 KO mice. Groups of 6 or 7 C57BL/6 (WT) and TLR2 KO mice were intraperitoneally (i.p.) infected with 1,000 $TCID_{50}$ of MHV3 and 51.6-MHV3. (A and B) Percentages of MHV3-infected (A) and 51.6-MHV3-infected (B) surviving mice were recorded at various times postinfection (p.i.). (C) Histopathological analysis was conducted on livers from mock-, MHV3-, and 51.6-MHV3-infected WT and TLR2 KO mice at 72 h p.i. Necrotic foci are indicated by arrows. (D) MHV3 and 51.6-MHV3 replication in livers from infected WT and TLR2 KO mice was determined by viral titration ($TCID_{50}$) at 24 h and 72 h p.i. Values are means and standard errors of the means. Results are representative of two different experiments. ***, $P < 0.001$ compared with WT mice.

TLR3 ligand [poly(I·C)] or LPS, reverted the suppressive properties of LSECs (9). We have shown that the virulent MHV3 strain highly induced TLR2 expression on cultured LSECs and that TLR2 knockdown abrogated IL-6 and CXCL1 induction only in LSECs infected by MHV3. Indeed, the proinflammatory activity of MHV3 may be related to its unique ability to induce TLR2 signaling. In agreement, lower levels of inflammatory cytokines and chemokines were observed in the livers of MHV3-infected TLR2 KO mice, correlating with milder hepatic damage and delayed mortality of mice. Thus, TLR2 activation may represent one determining and differential factor involved in the severity of virulent versus attenuated MHV3-induced hepatitis. In line with this hypothesis, the survival rate, inflammatory response, and liver damage were similar in TLR2 KO and WT mice infected by 51.6-MHV3 and were comparable to those observed in MHV3-infected TLR2 KO mice. Furthermore, IL-10 levels were significantly higher in MHV3-infected TLR2 KO mice, with increased expression on ECs and also on some CAV-1 negative cells, suggesting that specific activation of TLR2 by the virus could be one mechanism by which MHV3 reverts the anti-inflammatory phenotype, at least in LSECs. Supporting this assumption, IL-10 expression was significantly upregulated in *in vitro*-MHV3-infected LSECs treated with siTLR2, suggesting an inhibitory effect for TLR2 on IL-10 induction by MHV3. Accordingly, TLR2 activation has already been shown to temporarily reverse Treg suppressive functions (46, 47). Further work will be done to identify other IL-10-producing CAV-1-negative cells during MHV3 infection.

TLR2 may also potentiate MHV3 infection, as viral replication was significantly reduced in the livers of TLR2 KO mice and in cultured LSECs rendered defective for TLR2. In addition, activation of TLR2 by MHV3 may account for its higher replication rate

TABLE 2 Transcription levels of several genes in livers from MHV3- and 51.6-MHV3-infected C57BL/6 (WT) and TLR2 KO mice at 72 h p.i.[a]

	Fold change (mean ± SEM)[b]			
	MHV3 infection		51.6-MHV3 infection	
Gene	WT	TLR2 KO	WT	TLR2 KO
TNF-α	70.2 ± 7.2	44.9 ± 4.0***	10.5 ± 1.03	7.1 ± 2.8
IL-6	43.5 ± 5.7	11.2 ± 5.0***	13 ± 1.4	14 ± 7.4
IL-10	5.8 ± 1.4	44 ± 11.7***	54.5 ± 17.4	41.4 ± 3.8
CXCL1	131 ± 15	21.1 ± 8.7***	107 ± 4.9	91 ± 11.9
CCL2	1,027 ± 134	155 ± 37***	147 ± 14.8	120.4 ± 39.1
CXCL10	213 ± 20	69 ± 15***	33.7 ± 7.4	17.5 ± 4.8*
Fgl2	6.65 ± 0.70	10.1 ± 1.2	6.7 ± 0.7	4.7 ± 1.7
IL-33	4.5 ± 0.4	3.7 ± 0.3	ND	ND

[a] Groups of 5 or 6 C57BL/6 (WT) or TLR2 KO mice were intraperitoneally infected with 1,000 $TCID_{50}$ of MHV3 or 51.6-MHV3. At 72 h p.i., livers were collected from mock- and virus-infected mice from each group, and mRNA fold changes for several genes were analyzed by qRT-PCR.

[b] Values represent fold change in gene expression relative to that in mock-infected mice after normalization to HPRT expression. Samples from each mouse were run in duplicate. Values that are significantly different between MHV3-infected TLR2 KO and C57BL/6 (WT) mice or between 51.6-MHV3-infected TLR2 KO and C57BL/6 (WT) mice are indicated by asterisks as follows: ***, $P < 0.01$; *, $P < 0.5$. ND not detectable.

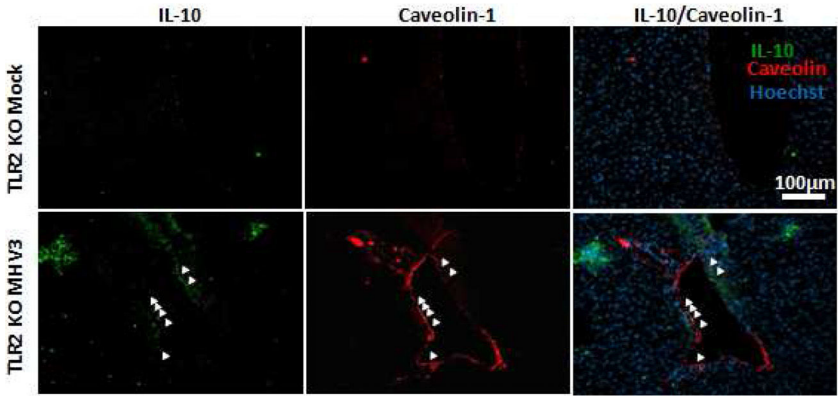

FIG 11 Expression of IL-10 and caveolin-1 in livers from MHV3-infected TLR2 KO mice. Groups of 6 TLR2 KO mice were intraperitoneally (i.p.) infected with 1,000 $TCID_{50}$ of MHV3, and immunolocalization of IL-10 in the livers and ECs of mock- and MHV3-infected TLR2 KO mice was determined by double immunostaining of IL-10 (green) and caveolin-1 (red) at 48 h p.i. Cell nuclei were counterstained with Hoechst stain (blue). *In situ* expression of IL-10 and caveolin-1 by endothelial cells is indicated by arrows.

in LSECs, since the replication of 51.6-MHV3 was not influenced by TLR2 in infected LSECs or mice. It has been demonstrated that MHV replication depends on the activation of the P38 mitogen-activated protein kinase (MAPK) at the beginning of the replicative cycle (48). Thus, it is conceivable that activation of TLR2 by MHV3 on LSECs optimizes P38 MAPK activation, predisposing to more efficient viral replication. Since TLR2 is also expressed, though to a lesser extent, by other resident or recruited cells in the liver, such as KCs, neutrophils, and hepatocytes, as observed in preliminary experiments, we can hypothesize that several $TLR2^+$ cell types permissive to MHV3 infection may act synergistically in promoting viral replication and hepatic inflammation. Indeed, preliminary *in vitro* results revealed that production of inflammatory mediators and viral replication in MHV3-infected hepatocytes and macrophages were enhanced by TLR2. Further work is in progress to clarify the mechanistic implications of TLR2 in MHV3 replication and the role of recruited and resident $TLR2^+$ inflammatory cells in hepatic inflammation and damage.

The differences in chemokine levels induced by the pathogenic and attenuated MHV3 strains may explain the differences in recruited intrahepatic leukocyte subsets. Indeed, lower levels of CXCL1 and CCL2 in livers from 51.6- and YAC-MHV3-infected mice correlated with delayed or lower intrahepatic recruitment of neutrophils and macrophages, thus explaining the smaller inflammatory foci without extensive necrosis areas seen in livers from these mice. Unexpectedly, neutrophils were only transiently recruited, and the numbers of NK-T, T, and B lymphocytes progressively decreased throughout MHV3 infection, despite high induction of chemokines. We have previously demonstrated that intrahepatic NK and NK-T cells undergo higher apoptosis and that B and T cells are more strongly depleted in lymphoid organs during MHV3 infection than during YAC-MHV3 infection (30, 31, 49), thus altering lymphocyte recruitment or turnover into the liver. The highly attenuated YAC-MHV3 infection, compared to MHV3, was also related to effective activation of $CD8^+$ cells (32).

In addition, impairment of intrahepatic leukocyte populations and severe liver injury in MHV3-infected mice may also be connected to disturbances in LSEC-derived vascular factors. We have demonstrated that MHV3, unlike attenuated variants, significantly altered NO release by LSECs. Susceptibility of mice to MHV3 infection has already been inversely correlated with NO levels in the liver, but the mechanism was not elucidated (50). The constitutive expression of NO by LSECs is essential for the regulation of intrahepatic sinusoidal blood flow and protects against liver diseases. Indeed, impairment of NO release by LSECs has been associated with hepatic microvascular dysfunction and portal hypertension in pathological liver conditions such as fibrosis and cirrhosis (37). In cirrhotic livers, an NO defect has been linked to overexpression of CAV-1, a negative regulator of the endothelial NO synthase activity, on LSECs (38). We have observed that reduced NO levels in LSECs correlated with a concomitant upregulation of CAV-1, supporting that MHV3-induced NO impairment is indirectly related to CAV-1 induction. Furthermore, we have demonstrated that expression of the procoagulant Fgl2 increased only in LSECs infected by MHV3. MHV3-induced expression of Fgl2 has already been reported in endothelium of intrahepatic veins and sinusoids and was associated with severe intravascular coagulation, ischemia, and liver necrosis in MHV3-infected mice (28). In agreement, liver histopathological analysis revealed vascular thrombosis and fibrin deposition in hepatic veins and sinusoids from 48 h p.i. in MHV3-infected mice only (results not shown). No difference in Fgl2 levels was observed between MHV3-infected WT and TLR2 KO mice, indicating that induction of Fgl2 in LSECs is TLR2 independent. Since Fgl2 expression in LSECs was reported to be promoted by the MHV nucleocapsid protein and TNF-α (51, 52), we can assume that higher induction of Fgl2 in the livers of MHV3-infected mice may reflect higher hepatic TNF-α levels and viral replication rate in LSECs. Thus, the combined effect of CAV-1/NO imbalance and Fgl2 induction during MHV3 infection may contribute to alter leukocyte recruitment and aggravate hepatitis in disturbing hepatic microcirculation.

The alarmin IL-33 was shown to be upregulated in LSECs during chronic HBV and HCV infections and acute liver failure, but the mechanism is elusive (21, 22). In agreement with our previous report, MHV3 infection increased IL-33 production in both LSECs and hepatocytes (29). Our results showed that IL-33 expression in LSECs was increased only by virulent

MHV3 and was not modulated by TLR2, suggesting that IL-33 release is rather a consequence of MHV3-induced cell damage, as necrotic cells in the liver were shown to secrete alarmins such as HMGB-1 and IL-33 (53). In addition, a high IL-33 serum level was associated with liver damage in HBV and HCV infections, indicating that IL-33 could be considered a predictive indicator of viral hepatitis evolution, as previously suggested (54, 55).

Using the MHV3 animal model of viral acute hepatitis, this work suggests a novel virus-promoted mechanism of hepatic inflammation and damage involving disorders in LSEC-derived inflammatory and vascular factors. The use of MHV3 variants expressing weak tropism for LSECs allowed us to better discriminate the importance of LSECs, over that of other hepatic cells, in tolerance/inflammation imbalance during acute viral infection. Our results support that induction of TLR2-dependent reversion of LSEC anti-inflammatory functions by MHV3 may participate in the pathological inflammatory response that predisposes to fulminant hepatitis. Unlike MHV3, HCV and HBV do not productively infect LSECs, but RNA from HCV was recently shown to induce the expression of inflammatory cytokines and chemokines in human microvascular endothelial cells via TLR3 activation (56), indicating that LSECs can be activated through PRR engagement by HCV-derived products. The "core" protein of HCV and HBV was reported to bind to TLR2 and induce a TLR2-dependent inflammatory cytokine response in monocytes and macrophages (57, 58). Thus, one could presume that core proteins could also promote proinflammatory activation of LSECs via TLR2, aggravating hepatic inflammation. In this regard, a high correlation between TLR2 expression and hepatic inflammation and necrosis was demonstrated in the livers of HCV-infected patients (59).

ACKNOWLEDGMENTS

We acknowledge Corentine Lux, Pascale Bellaud, and Eric Massicotte for their technical assistance.

FUNDING INFORMATION

This work was funded by the government of Canada through NSERC grant 2895-2009 to Lucie Lamontagne. Christian Bleau was supported by an NSERC fellowship. The funders had no role in study design, data collection and interpretation, or the decision to submit the work for publication.

REFERENCES

1. **Tiegs G, Lohse AW.** 2010. Immune tolerance: what is unique about the liver. J Autoimmun **34:**1–6. http://dx.doi.org/10.1016/j.jaut.2009.08.008.
2. **Xu X, Jin R, Li M, Wang K, Zhang S, Hao J, Sun X, Zhang Y, Wu H, Zhang J, Ge Q.** 2016. Liver sinusoidal endothelial cells induce tolerance of autoreactive CD4(+) recent thymic emigrants. Sci Rep **6:**19861. http://dx.doi.org/10.1038/srep19861.
3. **Thomson AW, Knolle PA.** 2010. Antigen-presenting cell function in the tolerogenic liver environment. Nat Rev Immunol **10:**753–766. http://dx.doi.org/10.1038/nri2858.
4. **Oda M, Yokomori H, Han JY.** 2003. Regulatory mechanisms of hepatic microcirculation. Clin Hemorheol Microcirc **29:**167–182.
5. **Kern M, Popov A, Scholz K, Schumak B, Djandji D, Limmer A, Eggle D, Sacher T, Zawatzky R, Holtappels R, Reddehase MJ, Hartmann G, Debey-Pascher S, Diehl L, Kalinke U, Koszinowski U, Schultze J, Knolle PA.** 2010. Virally infected mouse liver endothelial cells trigger CD8+ T-cell immunity. Gastroenterology **138:**336–346. http://dx.doi.org/10.1053/j.gastro.2009.08.057.
6. **Wu J, Meng Z, Jiang M, Zhang E, Trippler M, Broering R, Bucchi A, Krux F, Dittmer U, Yang D, Roggendorf M, Gerken G, Lu M, Schlaak JF.** 2010. Toll-like receptor-induced innate immune responses in non-parenchymal liver cells are cell type-specific. Immunology **129:**363–374. http://dx.doi.org/10.1111/j.1365-2567.2009.03179.x.
7. **Bissell DM, Wang SS, Jarnagin WR, Roll FJ.** 1995. Cell-specific expression of transforming growth factor-beta in rat liver. Evidence for autocrine regulation of hepatocyte proliferation. J Clin Invest **96:**447–455.
8. **Knolle PA, Uhrig A, Hegenbarth Löser S E, Schmitt E, Gerken G, Lohse AW.** 1998. IL-10 down-regulates T cell activation by antigen-presenting liver sinusoidal endothelial cells through decreased antigen uptake via the mannose receptor and lowered surface expression of accessory molecules. Clin Exp Immunol **114:**427–433. http://dx.doi.org/10.1046/j.1365-2249.1998.00713.x.
9. **Liu J, Jiang M, Ma Z, Dietze KK, Zelinskyy G, Yang D, Dittmer U, Schlaak JF, R oggendorf, Lu MM.** 2013. TLR1/2 ligand-stimulated mouse liver endothelial cells secrete IL-12 and trigger CD8+ T cell immunity in vitro. J Immunol **191:**6178–6190. http://dx.doi.org/10.4049/jimmunol.1301262.
10. **Lavanchy D.** 2009. The global burden of hepatitis C. Liver Int **29:**74–81. http://dx.doi.org/10.1111/j.1478-3231.2008.01934.x.
11. **Yang Q, Shi Y, Yang Y, Lou G, Chen Z.** 2015. The sterile inflammation in the exacerbation of HBV-associated liver injury. Mediators Inflamm **2015:**508681. http://dx.doi.org/10.1155/2015/508681.
12. **Bortolami M, Kotsafti A, Cardin R, Farinati F.** 2008. Fas/FasL system, IL-1beta expression and apoptosis in chronic HBV and HCV liver disease. J Viral Hepat **15:**515–522. http://dx.doi.org/10.1111/j.1365-2893.2008.00974.x.
13. **Barnaba V.** 2010. Hepatitis C virus infection: a "liaison a trois" amongst the virus, the host, and chronic low-level inflammation for human survival. J Hepatol **53:**752–761. http://dx.doi.org/10.1016/j.jhep.2010.06.003.
14. **Liu M, Chan WY, McGilvray I, Ning Q, Levy GA.** 2001. Fulminant viral hepatitis: molecular and cellular basis, and clinical implications. Exp Rev Mol Med **3:**1–19. http://dx.doi.org/10.1017/S1462399401002575.
15. **Breiner KM, Schaller H, Knolle PA.** 2001. Endothelial cell-mediated uptake of a hepatitis B virus: a new concept of liver targeting of hepatotropic microorganisms. Hepatology **34:**803–808. http://dx.doi.org/10.1053/jhep.2001.27810.
16. **Pöhlmann S, Zhang J, Baribaud F, Chen K, Leslie GJ, Lin G, Granelli Piperno A, Doms RW, Rice CM, McKeating JA.** 2003. Hepatitis C virus glycoproteins interact with DC-SIGN and DC-SIGNR. J Virol **77:**4070–4080. http://dx.doi.org/10.1128/JVI.77.7.4070-4080.2003.
17. **Broering R, Wu J, Meng Z, Hilgard P, Lu M, Trippler M, Szczeponek A, Gerken G, Schlaak JF.** 2008. Toll-like receptor-stimulated non-parenchymal liver cells can regulate hepatitis C virus replication. J Hepatol **48:**914–922. http://dx.doi.org/10.1016/j.jhep.2008.01.028.
18. **Ludwig IS, Lekkerkerker AN, Depla E, Bosman F, Musters RJ, Depraetere S, van Kooyk Y, Geijtenbeek TB.** 2004. Hepatitis C virus targets DC SIGN and LSIGN to escape lysosomal degradation. J Virol **78:**8322–8332. http://dx.doi.org/10.1128/JVI.78.15.8322-8332.2004.
19. **Zhu CL, Yan WM, Zhu F, Zhu YF, Xi D, Tian DY, Levy G, Luo XP, Ning Q.** 2005. Fibrinogen-like protein 2 fibroleukin expression and its correlation with disease progression in murine hepatitis virus type 3-induced fulminant hepatitis and in patients with severe viral hepatitis B. World J Gastroenterol **11:**6936–6940. http://dx.doi.org/10.3748/wjg.v11.i44.6936.
20. **Foerster K, Helmy A, Zhu Y, Khattar R, Adeyi OA, Wong KM, Shalev I, Clark DA, Wong PY, Heathcote EJ, Phillips MJ, Grant DR, Renner EL, Levy GA, Selzner N.** 2010. The novel immunoregulatory molecule FGL2a potential biomarker for severity chronic hepatitis C virus infection. J Hepatol **53:**608–615. http://dx.doi.org/10.1016/j.jhep.2010.04.020.
21. **Marvie P, Lisbonne M, L'Helgoualc'h A, Rauch M, Turlin B, Preisser L, Bourd-Boittin K, Théret N, Gascan H, Piquet-Pellorce C, Samson M.** 2010. Interleukin-33 overexpression is associated with liver fibrosis in mice and humans. J Cell Mol Med **14:**1726–1739. http://dx.doi.org/10.1111/j.1582-4934.2009.00801.x.
22. **Roth GA, Zimmermann M, Lubsczyk BA, Pilz J, Faybik P, Hetz H, Hacker S, Mangold A, Bacher A, Krenn CG, Ankersmit HJ.** 2010. Up-regulation of interleukin 33 and soluble ST2 serum levels in liver failure. J Surg Res **163:**e79–e83. http://dx.doi.org/10.1016/j.jss.2010.04.004.
23. **Le Prevost C, Virelizier JL, Dupuy JM.** 1975. Immunopathology of mouse hepatitis virus type 3 infection. III. Clinical and virologic observation of a persistent viral infection. J Immunol **115:**640–645.

24. **Martin JP, Chen Koehren WF, Pereira CA.** 1994. The virulence of mouse hepatitis virus 3, as evidenced by permissivity of cultured hepatic cells toward escaped mutants. Res Virol **145:**297–302. http://dx.doi.org/10.1016/S0923-2516(07)80034-3.
25. **Belouzard S, Millet JK, Licitra BN, Whittaker GR.** 2012. Mechanisms of coronavirus cell entry mediated by the viral spike protein. Viruses **4:**1011–1033. http://dx.doi.org/10.3390/v4061011.
26. **Pereira CA, Steffan AM, Kirn A.** 1984. Interaction between mouse hepatitis viruses and primary cultures of Kupffer and endothelial liver cells from resistant and susceptible inbred mouse strains. J Gen Virol **65:**1617–1620. http://dx.doi.org/10.1099/0022-1317-65-9-1617.
27. **Steffan AM, Pereira CA, Bingen A, Valle M, Martin JP, Koehren F, Royer C, Gendrault JL, Kirn A.** 1995. Mouse hepatitis virus type 3 infection provokes a decrease in the number of sinusoidal endothelial cell fenestrae both in vivo and in vitro. Hepatology **22:**395–401.
28. **Marsden PA, Ning Q, Fung S, Luo X, Chen Y, Mendicino M, Ghanekar A, Scott JA, Miller T, Chan CW, Chan MW, He W, Gorczynski RM, Grant DR, Clark DA, Phillips MJ, Levy GA.** 2003. The Fgl2/fibroleukin prothrombinase contributes to immunologically mediated thrombosis in experimental and human viral hepatitis. J Clin Invest **112:**58–6626. http://dx.doi.org/10.1172/JCI18114.
29. **Arshad MI, Patrat-Delon S, Piquet-Pellorce C, L'helgoualc'h A, Rauch M, Genet V, Lucas-Clerc C, Bleau C, Lamontagne L, Samson M.** 2013. Pathogenic mouse hepatitis virus or poly(I:C) induce IL-33 in hepatocytes in murine models of hepatitis. PLoS One **8:**e74278. http://dx.doi.org/10.1371/journal.pone.0074278.
30. **Jacques A, Bleau C, Martin JP, Lamontagne L.** 2008. Intrahepatic endothelial and Kupffer cells involved in immunosuppressive cytokines and natural killer (NK)/NK T cell disorders in viral acute hepatitis. Clin Exp Immunol **152:**298–310. http://dx.doi.org/10.1111/j.1365-2249.2008.03628.x.
31. **Lehoux M, Jacques A, Lusignan S, Lamontagne L.** 2004. Murine viral hepatitis involves NK cell depletion associated with virus-induced apoptosis. Clin Exp Immunol **137:**41–51. http://dx.doi.org/10.1111/j.1365-2249.2004.02501.x.
32. **Lamontagne L, Lusignan S, Page C.** 2001. Recovery from mouse hepatitis virus infection depends on recruitment of CD8(+) cells rather than activation of intrahepatic CD4(+)alphabeta(−)TCR(inter) or NK-T cells. Clin Immunol **101:**345–356. http://dx.doi.org/10.1006/clim.2001.5131.
33. **Schrage A, Loddenkemper C, Erben U, Lauer U, Hausdorf G, Jungblut PR, Johnson J, Knolle PA, Zeitz M, Hamann A, Klugewitz K.** 2008. Murine CD146 is widely expressed on endothelial cells and is recognized by the monoclonal antibody ME-9F1. Histochem Cell Biol **129:**441–451. http://dx.doi.org/10.1007/s00418-008-0379-x.
34. **Yamazaki H, Oda M, Takahashi Y, Iguchi H, Yoshimura K, Okada N, Yokomori H.** 2013. Relation between ultrastructural localization, changes in caveolin-1, and capillarization of liver sinusoidal endothelial cells in human hepatitis C-related cirrhotic liver. J Histochem Cytochem **61:**169–176. http://dx.doi.org/10.1369/0022155412468590.
35. **Neumann K, Erben U, Kruse N, Wechsung K, Schumann M, Klugewitz K, Scheffold A, Kühl AA.** 2015. Chemokine transfer by liver sinusoidal endothelial cells contributes to the recruitment of CD4+ T cells into the murine liver. PLoS One **10:**e0123867. http://dx.doi.org/10.1371/journal.pone.0123867.
36. **Pope M, Marsden PA, Cole E, Sloan S, Fung LS, Ning Q, Ding JW, Leibowitz JL, Phillips MJ, Levy GA.** 1998. Resistance to murine hepatitis virus strain 3 is dependent on production of nitric oxide. J Virol **72:**7084–7090.
37. **Iwakiri Y, Kim MY.** 2015. Nitric oxide in liver diseases. Trends Pharmacol Sci **36:**524–536. http://dx.doi.org/10.1016/j.tips.2015.05.001.
38. **Yokomori H, Oda M, Yoshimura K, Nomura M, Wakabayashi G, Kitajima M, Ishii H.** 2003. Elevated expression of caveolin-1 at protein and mRNA level in human cirrhotic liver: relation with nitric oxide. J Gastroenterol **38:**854–860. http://dx.doi.org/10.1007/s00535-003-1161-4.
39. **Peyrefitte CN, Pastorino B, Grau GE, Lou J, Tolou H, Couissinier-Paris P.** 2006. Dengue virus infection of human microvascular endothelial cells from different vascular beds promotes both common and specific functional changes. J Med Virol **78:**229–242. http://dx.doi.org/10.1002/jmv.20532.
40. **Connolly MK, Bedrosian AS, Malhotra A, Henning JR, Ibrahim J, Vera V, Cieza-Rubio NE, Hassan BU, Pachter HL, Cohen S, Frey AB, Miller G.** 2010. In hepatic fibrosis, liver sinusoidal endothelial cells acquire enhanced immunogenicity. J Immunol **185:**2200–2208. http://dx.doi.org/10.4049/jimmunol.1000332.
41. **Jacques A, Bleau C, Turbide C, Beauchemin N, Lamontagne L.** 2009. Macrophage interleukin-6 and tumour necrosis factor-alpha are induced by coronavirus fixation to Toll-like receptor 2/heparan sulphate receptors but not carcinoembryonic cell adhesion antigen 1a. Immunology **128:**e181–192. http://dx.doi.org/10.1111/j.1365-2567.2008.02946.x.
42. **Ganesan LP, Mohanty S, Kim J, Clark KR, Robinson JM, Anderson CL.** 2011. Rapid and efficient clearance of blood-borne virus by liver sinusoidal endothelium. PLoS Pathog **7:**e1002281. http://dx.doi.org/10.1371/journal.ppat.1002281.
43. **Simon-Santamaria J, Rinaldo CH, Kardas P, Li R, Malovic I, Elvevold K, McCourt P, Smedsrød B, Hirsch HH, Sørensen KK.** 2014. Efficient uptake of blood-borne BK and JC polyomavirus-like particles in endothelial cells of liver sinusoids and renal vasa recta. PLoS One **9:**e111762. http://dx.doi.org/10.1371/journal.pone.0111762.
44. **Carambia A, Frenzel C, Bruns OT, Schwinge D, Reimer R, Hohenberg H, Huber S, Tiegs G, Schramm C, Lohse AW, Herkel J.** 2013. Inhibition of inflammatory CD4 T cell activity by murine liver sinusoidal endothelial cells. J Hepatol **58:**112–118. http://dx.doi.org/10.1016/j.jhep.2012.09.008.
45. **Lamontagne L, Dupuy JM.** 1987. Characterization of a non pathogenic MHV3 variant derived from a persistently infected lymphoid cell line. Adv Exp Med Biol **218:**255–263. http://dx.doi.org/10.1007/978-1-4684-1280-2_30.
46. **Sutmuller RP, den Brok MH, Kramer M, Bennink EJ, Toonen LW, Kullberg BJ, Joosten LA, Akira S, Netea MG, Adema GJ.** 2006. Toll-like receptor 2 controls expansion and function of regulatory T cells. J Clin Invest **116:**485–494. http://dx.doi.org/10.1172/JCI25439.
47. **Liu G, Zhao Y.** 2007. Toll-like receptors and immune regulation: their direct and indirect modulation on regulatory CD4+ CD25+ T cells. Immunology **122:**149–156. http://dx.doi.org/10.1111/j.1365-2567.2007.02651.x.
48. **Banerjee S, Narayanan K, Mizutani T, Makino S.** 2002. Murine coronavirus replication-induced p38 mitogen-activated protein kinase activation promotes interleukin-6 production and virus replication in cultured cells. J Virol **76:**5937–5948. http://dx.doi.org/10.1128/JVI.76.12.5937-5948.2002.
49. **Lamontagne L, Descoteaux JP, Jolicoeur P.** 1989. Mouse hepatitis virus 3 replication in T and B lymphocytes correlate with viral pathogenicity. J Immunol **142:**4458–4465.
50. **Tsuhako MH, Augusto O, Linares E, Dagli ML, Pereira CA.** 2006. Association between nitric oxide synthesis and vaccination-acquired resistance to murine hepatitis virus by SPF mice. Free Radic Biol Med **41:**1534–1541. http://dx.doi.org/10.1016/j.freeradbiomed.2006.08.011.
51. **Ning Q, Liu M, Kongkham P, Lai MM, Marsden PA, Tseng J, Pereira B, Belyavskyi M, Leibowitz J, Phillips MJ, Levy G.** 1999. The nucleocapsid protein of murine hepatitis virus type 3 induces transcription of the novel fgl2 prothrombinase gene. J Biol Chem **274:**9930–9936. http://dx.doi.org/10.1074/jbc.274.15.9930.
52. **Liu J, Tan Y, Zhang J, Zou L, Deng G, Xu X, Wang F, Ma Z, Zhang J, Zhao T, Liu Y, Li Y, Zhu B, Guo B.** 2015. C5aR, TNF-α, and FGL2 contribute to coagulation and complement activation in virus-induced fulminant hepatitis. J Hepatol **62:**354–362. http://dx.doi.org/10.1016/j.jhep.2014.08.050.
53. **Arshad MI, Piquet-Pellorce C, Samson M.** 2012. IL-33 and HMGB1 alarmins: sensors of cellular death and their involvement in liver pathology. Liver Int **32:**1200–1210. http://dx.doi.org/10.1111/j.1478-3231.2012.02802.x.
54. **Wang J, Zhao P, Guo H, Sun X, Jiang Z, Xu L, Feng J, Niu J, Jiang Y.** 2012. Serum IL-33 levels are associated with liver damage in patients with chronic hepatitis C. Mediat Inflam **2012:**819636.
55. **Wang J, Cai Y, Ji H, Feng J, Ayana DA, Niu J, Jiang Y.** 2012. Serum IL-33 levels are associated with liver damage in patients with chronic hepatitis B. J Interferon Cytokine Res **32:**248–253. http://dx.doi.org/10.1089/jir.2011.0109.
56. **Pircher J, Czermak T, Merkle M, Mannell H, Krötz F, Ribeiro A, Vielhauer V, Nadjiri J, Gaitzsch E, Niemeyer M, Porubsky S, Gröne HJ, Wörnle M.** 2014. Hepatitis C virus induced endothelial inflammatory response depends on the functional expression of TNFα receptor subtype 2. PLoS One **9:**e113351. http://dx.doi.org/10.1371/journal.pone.0113351.

57. **Cooper A, Tal G, Lider O, Shaul Y.** 2005. Cytokine induction by the hepatitis B virus capsid in macrophages is facilitated by membrane heparan sulfate and involves TLR2. J Immunol **175:**3165–3176. http://dx.doi.org/10.4049/jimmunol.175.5.3165.
58. **Dolganiuc A, Oak S, Kodys K, Golenbock DT, Finberg RW, Kurt-Jones E, Szabo G.** 2004. Hepatitis C core and nonstructural 3 proteins trigger Toll-like receptor 2-mediated pathways and inflammatory activation. Gastroenterology **127:**1513–1524. http://dx.doi.org/10.1053/j.gastro.2004.08.067.
59. **Berzsenyi MD, Roberts SK, Preiss S, Woollard DJ, Beard MR, Skinner NA, Bowden DS, Visvanathan K.** 2011. Hepatic TLR2 and TLR4 expression correlates with hepatic inflammation and TNF-α in HCV and HCV/HIV infection. J Viral Hepat **18:**852–860. http://dx.doi.org/10.1111/j.1365-2893.2010.01390.x.

VI.3. ANNEXE 3 : L'invasion cérébrale par le virus de l'hépatite murine dépend d'une détérioration des jonctions serrées et de la production d'interféron béta dans les cellules endothéliales microvasculaires.

Christian Bleau, Aveline Filliol, Michel Samson et Lucie Lamontagne.

Article publié dans *J Virol.* 2015 Oct;89(19):9896-908.

Résumé de l'article.

Les coronavirus présentent des propriétés neuro-invasives chez l'Homme et l'animal suite à leur réplication dans des organes périphériques. Cependant, le mécanisme de cette invasion cérébrale est inconnu. Le but principal de ce travail a été d'évaluer la capacité des coronavirus à traverser la barrière hémato-encéphalique (BBB pour "Blood Brain Barrier") et infecter le système nerveux central. L'utilisation de différentes souches virales de coronavirus murin possédant un neurotropisme et un hépatotropisme: le virus de l'hépatite murine de type 3 (MHV3), neurotrope et hautement hépatotrope, son variant atténué, le MHV3-51.6, qui présente un faible tropisme pour les cellules endothéliales et la souche MHV-A59, neurotrope mais faiblement hépatotrope, nous a permis d'étudier l'intégrité de la BBB lors de l'infection par ces virus *in vivo* chez la souris et *in vitro* dans des cellules endothéliales microvasculaires cérébrales (BMECs pour "Brain Microvascular Endothelial Cells"). Nous rapportons ici la capacité spécifique du MHV3, et non pas du 51.6-MHV3 et du MHV-A59 à traverser la BBB au cours de l'infection aigüe suite à l'infection par voie intrapéritonéale. L'invasion cérébrale a donc été observée uniquement chez les souris infectées par le MHV3. Celle-ci corrélait avec l'augmentation de la perméabilité de la BBB et était associée à une diminution de l'expression des protéines de jonctions: Zona occludens-1 (ZO-1), VE-cadherine et occludine, mais pas de la claudine-5, dans le cerveau des souris infectées et dans les cellules BMECs en culture. La rupture de la BBB au cours de l'infection par le MHV3 n'était pas reliée à une production de cytokines ou chimiokines inflammatoires par les BMECs infectées. En revanche, nous avons montré que, contrairement au variant MHV3-51.6 et à la souche MHV-A59, l'infection des BMECs par le MHV3 entraînait une diminution de la production d'IFN-β normalement impliquée dans le contrôle des protéines de jonctions de la BBB. Nos résultats mettent donc en évidence l'importance de la production d'IFN-β par les BMECs infectées, dans la préservation des fonctions de la BBB qui prévient l'accès des virus infectieux hématogènes au parenchyme cérébral.

JVI Journals.ASM.org

Brain Invasion by Mouse Hepatitis Virus Depends on Impairment of Tight Junctions and Beta Interferon Production in Brain Microvascular Endothelial Cells

Christian Bleau,[a] Aveline Filliol,[b] Michel Samson,[b] Lucie Lamontagne[a]

Département des Sciences Biologiques, Université du Québec à Montréal, Montréal, Québec, Canada[a]; Institut de Recherche en Santé-Environnement-Travail, Université de Rennes 1, Rennes, France[b]

ABSTRACT

Coronaviruses (CoVs) have shown neuroinvasive properties in humans and animals secondary to replication in peripheral organs, but the mechanism of neuroinvasion is unknown. The major aim of our work was to evaluate the ability of CoVs to enter the central nervous system (CNS) through the blood-brain barrier (BBB). Using the highly hepatotropic mouse hepatitis virus type 3 (MHV3), its attenuated variant, 51.6-MHV3, which shows low tropism for endothelial cells, and the weakly hepatotropic MHV-A59 strain from the murine coronavirus group, we investigated the virus-induced dysfunctions of BBB *in vivo* and in brain microvascular endothelial cells (BMECs) *in vitro*. We report here a MHV strain-specific ability to cross the BBB during acute infection according to their virulence for liver. Brain invasion was observed only in MHV3-infected mice and correlated with enhanced BBB permeability associated with decreased expression of zona occludens protein 1 (ZO-1), VE-cadherin, and occludin, but not claudin-5, in the brain or in cultured BMECs. BBB breakdown in MHV3 infection was not related to production of barrier-dysregulating inflammatory cytokines or chemokines by infected BMECs but rather to a downregulation of barrier protective beta interferon (IFN-β) production. Our findings highlight the importance of IFN-β production by infected BMECs in preserving BBB function and preventing access of blood-borne infectious viruses to the brain.

IMPORTANCE

Coronaviruses (CoVs) infect several mammals, including humans, and are associated with respiratory, gastrointestinal, and/or neurological diseases. There is some evidence that suggest that human respiratory CoVs may show neuroinvasive properties. Indeed, the severe acute respiratory syndrome coronavirus (SARS-CoV), causing severe acute respiratory syndrome, and the CoVs OC43 and 229E were found in the brains of SARS patients and multiple sclerosis patients, respectively. These findings suggest that hematogenously spread CoVs may gain access to the CNS at the BBB level. Herein we report for the first time that CoVs exhibit the ability to cross the BBB according to strain virulence. BBB invasion by CoVs correlates with virus-induced disruption of tight junctions on BMECs, leading to BBB dysfunction and enhanced permeability. We provide evidence that production of IFN-β by BMECs during CoV infection may prevent BBB breakdown and brain viral invasion.

The blood-brain barrier (BBB) is a highly selective barrier critical for central nervous system (CNS) homeostasis in controlling peripheral blood-brain exchange and preventing neurotoxins and pathogens from access to the CNS. The functional and structural integrity of the BBB mainly relies on specific features of the brain microvascular endothelial cells (BMECs) lining the brain capillaries. These cells are tightly connected by a unique assembly of adherens junctions composed of transmembrane cadherin and tight-junction complexes (e.g., claudins and occludin) anchored to actin filaments via adaptor molecules, such as zona occludens (ZO) (1).

The BBB is known to provide significant protection against hematogenously spread viruses, as several viruses inoculated in periphery were shown to induce neuropathology only after mechanically or chemically mediated disruption of the BBB (2–4). However, some infectious blood-borne viruses primarily targeting peripheral organs have evolved strategies to thwart the BBB, including direct infection of BMECs, "Trojan horse" invasion via the traffic of infected immune cells in the CNS or paracellular entry through alteration of tight junctions (1). Disruption of tight junctions, resulting from either viral products or host immune factors (5–8), may lead to an increase in extravasation of immune cells and poorly regulated flux of molecules as well as ions across the BBB, which are critical events in neuropathogenesis (9).

Coronaviruses (CoVs) are enveloped, positive-sense, single-stranded RNA viruses that infect several mammals, including humans. There is some evidence that suggests that respiratory CoVs may show neuroinvasive properties. The severe acute respiratory syndrome coronavirus (SARS-CoV), which causes severe acute respiratory syndrome in humans, and the human CoVs OC43 and 229E were found in the brains of SARS patients and multiple scle-

Received 9 June 2015 **Accepted** 13 July 2015

Accepted manuscript posted online 22 July 2015

Citation Bleau C, Filliol A, Samson M, Lamontagne L. 2015. Brain invasion by mouse hepatitis virus depends on impairment of tight junctions and beta interferon production in brain microvascular endothelial cells. J Virol 89:9896–9908. doi:10.1128/JVI.01501-15.

Editor: S. Perlman

Address correspondence to Lucie Lamontagne, lamontagne.lucie@uqam.ca.

doi:10.1128/JVI.01501-15

rosis patients, respectively (10–13). However, the mechanism of neuroinvasion by hematogenously spread CoVs is elusive.

The different serotypes of viruses in the mouse hepatitis virus (MHV) coronavirus group induce hepatic, respiratory, or enteric diseases, followed by neurological disorders (14), and thus, the mouse is a relevant animal model for the study of neuroinvasion by CoVs. The highly hepatotropic mouse hepatitis virus type 3 (MHV3) is known as the most virulent MHV strain, causing fulminant hepatitis and death of susceptible C57BL/6 mice within 3 to 5 days postinfection (p.i.) (15) and neurological disease following nonlethal hepatitis in semisusceptible C3H mice characterized by meningitis, ependymitis, and encephalitis beginning 3 to 4 weeks p.i. after intraperitoneal (i.p.) infection (15, 16). This suggests brain invasion by MHV3 through the BBB endothelium in the acute phase of infection. The attenuated 51.6-MHV3 variant has lost the ability to replicate in liver endothelial cells (17) and induces acute hepatitis and death of susceptible C57BL/6 mice within 5 to 9 days p.i. (18), suggesting an important role for endothelial cells in disease outcome. The weakly hepatotropic MHV-A59 causes no mortality and moderate hepatitis without neurological disease in C57BL/6 mice when i.p. inoculated (19). Brain invasion and disease by the MHV-A59 serotype is however enabled following intranasal infection and depends on the olfactory nerve, instead of the BBB, as the portal of viral entry into the CNS (19–21) suggesting a restriction of CNS invasion at the BBB level (19, 22).

BMECs have already been reported as potential cell targets for MHVs, as they express the MHV receptor, carcinoembryonic antigen 1a (CEACAM1a) (23). Primary mouse BMECs were shown to support MHV3 replication *in vitro* (24), but conflicting results regarding viral replication of MHV-A59 in BMECs have been reported (22, 25, 26). Since all MHV strains use the same cell receptor (CEACAM1a), and both MHV3 and MHV-A59 can bind to BMECs (22, 24), another factor(s) might be involved in BBB invasion according to MHV serotype.

We demonstrated here that the highly hepatotropic MHV3 strain, but not the MHV-A59 or 51.6-MHV3 variant, elicited an *in vivo* and *in vitro* breakdown of functional and structural integrity of the BBB, enabling viral invasion of the brain. The MHV strain-specific ability to cross the BBB during acute liver infection correlated with enhanced BBB permeability due to alteration of tight junctions zona occludens protein 1 (ZO-1), VE-cadherin, and occludin but not claudin-5 expression on BMECs. Barrier disruption in MHV3 infection was not related to the release of inflammatory cytokines or chemokines by infected BMECs but rather to a downregulation of barrier protective beta interferon (IFN-β) production.

MATERIALS AND METHODS

Mice. Female C57BL/6 (Charles River, St. Constant, Quebec, Canada) mice were housed in a HEPA-filtered air environment. All experiments were conducted with mice between 8 to 10 weeks of age in compliance with the regulations of the Animal Committee of the University of Quebec at Montreal, Canada.

Viruses. Highly pathogenic MHV3 is a cloned substrain isolated from the liver of an infected DBA2 mouse and maintained in L2 cells for less than three passages, as described previously (27). The mildly virulent MHV-A59 strain was obtained from the American Type Culture Collection (ATCC) (Rockville, MD, USA). The lower-virulence 51.6-MHV3 is an escape mutant, selected from the pathogenic MHV3 virus in the presence of S protein-specific A51 and A37 monoclonal antibodies, having lost tropism for liver sinusoidal endothelial cells (17). All viruses were produced in L2 cells, and their pathogenic properties were assessed routinely.

Cells. bEnd.3 (ATCC CRL-2390), an immortalized mouse brain endothelial cell line, was cultured in RPMI 1640 medium supplemented with 10% heat-inactivated fetal calf serum (FCS) and antibiotics (Wysent, St. Bruno, Quebec, Canada). Freshly trypsinized bEnd.3 cells were seeded in collagen-treated 24-well plates at 6×10^4 cells/cm^2 or collagen-treated 6.5-mm-diameter Transwell polycarbonate membrane inserts (Fisher Scientific, Ontario, Canada) and incubated until they reached confluence. The cells were then infected with MHV3, MHV-A59, or 51.6-MHV3 at a multiplicity of infection (MOI) of 0.1 for 24 to 72 h or up to 8 days according to the particular experiment. In some experiments, cells were concomitantly treated with IFN-β (100 pg/ml) or anti-IFN-β (1 μg/ml) (R&D Systems, Minneapolis, MN). Cell culture supernatant was collected for enzyme-linked immunosorbent assays (ELISAs) and virus titration, and total RNA was extracted for quantitative reverse transcription-PCR (qRT-PCR) analyses. *In vitro* studies were conducted in triplicate.

***In vivo* viral infections.** Groups of six wild-type C57BL/6 mice were infected intraperitoneally (i.p.) with 10^3 50% tissue culture infective doses ($TCID_{50}$) of MHV3, MHV-A59, or 51.6-MHV3. Mock-infected mice received a similar volume of phosphate-buffered saline (PBS) (Wysent, St. Bruno, Quebec, Canada). Mice were sacrificed by CO_2 anoxia 72 h postinfection (p.i.). The brain and liver were collected and frozen at −80°C for further analyses.

RNA isolation and qRT-PCR. Total RNA from frozen brain samples was extracted using TRIzol reagent (Invitrogen, Burlington, Ontario, Canada), and residual genomic DNA was removed with the Turbo DNA-free kit (Ambion, Austin, TX). RNA from bEnd.3 cells was extracted using a NucleoSpin RNA II kit (Macherey-Nagel, Bethlehem, PA) according to the manufacturer's instructions. One microgram of RNA was reverse transcribed into cDNA using the high-capacity cDNA reverse transcription kit (Applied Biosystems, Foster City, CA). Real-time PCR amplification was carried out on 25 ng cDNA using the HotStart-IT SYBR green qPCR master mix (USB Corporation, Cleveland, OH) on an ABI 7300 system (Applied Biosystems, Foster City, CA). Primer sets used are listed in Table 1. Threshold cycle (C_T) values were collected and used for $\Delta\Delta C_T$ analysis. Gene expression was normalized to expression of the hypoxanthine phosphoribosyltransferase (HPRT) gene as an endogenous control and expressed as a ratio of gene expression in mock-infected mice or bEnd.3 cells. The specificity of the PCR products was confirmed by melting curve analyses. All qPCR analyses of samples from *in vitro* and *in vivo* experiments were run in duplicate.

ELISAs. Determination of the levels of IFN-β (PBL, Piscataway, NJ), interleukin 6 (IL-6), tumor necrosis factor alpha (TNF-α) (BD, Mississauga, Ontario, Canada), CXC chemokine ligand 10 (CXCL10), CC chemokine ligand 2 (CCL2) (eBiosciences, San Diego, CA), and CXCL1 (R&D Systems, Minneapolis, MN) in bEnd.3 cell culture supernatants was carried out according to the manufacturer's instructions.

Virus titration. Virus titration was performed on brain lysates from infected mice and infected bEnd.3 cell culture supernatants by 10-fold serial dilutions on L2 cell monolayers cultured in 96-well plates. Cytopathic effects, characterized by syncytia and cell lysis, were recorded at 72 h p.i., and virus titers were determined according to the Reed-Muench method and expressed as $\log_{10}$ $TCID_{50}$.

***In vivo* assessment of BBB integrity.** Changes in blood-brain barrier permeability were assessed using sodium fluorescein (NaF) (Sigma-Aldrich) as previously described (28). Briefly, mice were infected for 72 h and i.p. injected with 100 μl of 10% NaF in PBS 1 h prior to euthanasia. Cardiac blood was collected, transcardial perfusion with 15 ml PBS was performed, and brains were removed, weighed, and homogenized in PBS (1:10 [wt/vol]). NaF content was measured on a Synergy 4 microplate fluorometer (Biotek, Winooski, VT) with excitation at 485 nm and emission at 530 nm using standards ranging from 0.78 μg/ml to 5 μg/ml. The NaF concentration in the brain was normalized to serum NaF concentrations for each mouse to allow comparisons among mice and calculated as

TABLE 1 Primer sets used for quantitative reverse transcription-PCR

Gene	Primer sequence	
	Forward primer	Reverse primer
HPRT	5′-GAAAGACTTGCTCGAGATGTCATG-3′	5′-CACACAGAGGGCCACAATGT-3′
IFN-β	5′-CGGACTTCAAGATCCCTATGGA-3′	5′-TGGCAAAGGCAGTGTAACTCTTC-3′
IL-6	5′-TCGGAGGCTTAATTACACATGTTC-3′	5′-TGCCATTGCACAACTCTTTTCT-3′
TNF-α	5′-TCCCAGGTTCTCTTCAAGGGA-3′	5′-GGTGAGGAGCACGTAGTCGG-3′
CCL2	5′-GCAGCAGGTGTCCCAAAGAA-3′	5′-GGTCAGCACAGACCTCTCTCTTG-3′
CXCL10	5′-GGCCATAGGGAAGCTTGAAAT-3′	5′-TCGTGGCAATGATCTCAACAC-3′
Occludin	5′-TGTGGGATAAGGAACACATTTATGA-3′	5′-CAGACACATTTTTAACCCACTCTTCA-3′
Claudin-5	5′-TCTGCTGGTTCGCCAACAT-3′	5′-CGGCACCGTCGGATCA-3′
ZO-1	5′-TGAACGCTCTCATAAGCTTCGTAA-3′	5′-ACCGTACCAACCATCATTCATTG-3′
VE-cadherin	5′-GCGCAGCATCGGGTACTC-3′	5′-GCTTGGTTATTCGGAAGAATTGG-3′
MHV N	5′-TGGAAGGTCTGCACCTGCTA-3′	5′-TTTGGCCCACGGGATTG-3′

follows: (microgram of NaF in the brain/milligram of brain)/(microgram of NaF in sera/microliter of blood). Data are expressed as fold increase in fluorescence compared to the levels in uninfected mice.

siRNA transfections. bEnd.3 cells were seeded in collagen-treated 24-well plates at 60,000 cells/ml and transfected with 25 nM small interfering RNA (siRNA) Flexitube premix (Qiagen, Cambridge, MA) targeting Toll-like receptor 2 (TLR2) mRNA (target sequence, CTCGTTCTCCAGCATTTAAA), CEACAM1a mRNA (target sequence, CACACTCATGCATTCACTCTA), caveolin-1 mRNA (target sequence, ATGGTTTGTCTTGATCAAGAA), or clathrin mRNA (target sequence, CACGTGTTATGGAGTATATTA) or transfected with the AllStars negative-control siRNA (Qiagen, Cambridge, MA) as a nonsilencing transfection control for 36 h prior to infections.

Transendothelial electrical resistance and *in vitro* permeability assays. bEnd3 cell monolayers were grown on collagen-treated 6.5-mm-diameter Transwell polycarbonate membrane inserts (6×10^4 cells/cm^2) (0.4-μm pore size; Costar, Corning, Tewksbury, MA) assembled into 24-well plates and infected for 24 to 72 h. Transendothelial electrical resistance (TEER) (ohms per square centimeter), reflecting barrier integrity, was recorded using an EVOM volt ohmmeter (World Precision Instruments, Sarasota, FL) and calculated by subtracting the resistance of blank inserts from that of the inserts with cells and multiplying the subtracted values by the area of the insert. Barrier function was further analyzed by measuring the permeability of the cell monolayer to sodium fluorescein (molecular mass of 376 Da) and Evans blue (EVB)-labeled albumin (molecular mass of 67 kDa) (Sigma-Aldrich, St. Louis, MO). Ringer-HEPES was added to the abluminal side, while the luminal side was loaded with Ringer-HEPES containing 200 μg/ml NaF, 170 μg/ml EVB, and 10 mg/ml bovine serum albumin (BSA). The cells were incubated at 37°C for 30 min, and the levels of NaF and EVB in the abluminal side were measured using a fluorometer (Biotek, Winooski, VT) with an excitation/emission wavelength ratio of 485/530 nm for NaF and an excitation/emission wavelength ratio of 540/680 nm for EVB. NaF and EVB concentrations were determined using a standard curve.

Immunochemistry. bEnd.3 cells were seeded in collagen-treated two-well Labtek chamber slides and infected for 48 h. The cells were fixed with 3.7% paraformaldehyde (PFA) for 10 min at room temperature, permeabilized with 0.3% Triton X-100, and blocked with 3% BSA. The cells were incubated with primary antibodies (ZO-1, occludin, and VE-cadherin antibodies diluted 1:100; all antibodies from LSBio, Seattle, WA) overnight at 4°C, then incubated with fluorescein isothiocyanate (FITC)-labeled goat anti-rabbit secondary antibody (1:500) (1 h at room temperature), and mounted in antifade medium containing 4′,6′-diamidino-2-phenylindole (DAPI) counterstain (Invitrogen, Ontario, Canada). Fixed cells were imaged with a Zeiss LSM700 static Observer Z1 confocal microscope (63×) (Zeiss, Toronto, Ontario, Canada) and analyzed using ZEN 2009 software. For brain immunolocalization of ZO-1, VE-cadherin, and occludin, mouse brain sections (5 μm) were fixed in paraformaldehyde and embedded in paraffin and the antigens were retrieved by incubating the sections with primary antibodies (1, 2.5, and 10 μg/ml, respectively; all antibodies from LSBio, Seattle, WA) for 1 h in a Ventana automated machine (Ventana Medical Systems, Tucson, AZ), and OmniMap anti-rabbit secondary antibodies conjugated to horseradish peroxidase (HRP) (RUO) for 16 min. The sections were then counterstained with hematoxylin.

Statistical analyses. Data are expressed as means ± standard errors of means. *In vitro* statistical analyses were performed with Student's *t* test comparing the values for mock-infected cells to the values for MHV-infected cells; for experiments with siRNAs, the values for treated MHV-infected cells were compared to the values for untreated MHV-infected cells. *In vivo* statistical analyses were conducted with a one-way analysis of variance (ANOVA) test followed by a *posthoc* Tukey analysis using software program PASW version 18 (IBM SPSS Inc., Chicago, IL). MHV-infected mice were compared to mock-infected mice or MHV3-infected mice were compared to MHV-A59- and 51.6-MHV3-infected mice according to experiments. *P* values of ≤0.05 were considered significant.

RESULTS

Brain invasion by hematogenously spread MHVs correlates with strain virulence and tropism for liver. The discrepancies regarding brain invasion by the highly hepatotropic MHV3 or the weakly hepatotropic MHV-A59 following hematogenous spread of viruses (i.p. inoculation) suggest strain-specific abilities to traffic across the BBB (15, 16, 22, 25, 29). To verify this hypothesis, C57BL/6 mice were i.p. infected for 72 h with MHV3, its attenuated 51.6-MHV3 variant or MHV-A59, and the brains were harvested, stained for histopathological analyses, and assayed for viral detection. Examination of hematoxylin-eosin (HE)-stained brain sections revealed the low-level presence of inflammatory cells in the meninges, microvasculature, and ependymal tissue lining the ventricles in the brains of MHV3-infected mice (Fig. 1A). No inflammatory cells or abnormalities in the neural tissue and choroid plexus were detected in the brains of 51.6-MHV3- or MHV-A59-infected mice. In addition, no multinucleate or rounding cells usually observed in the livers of MHV-infected mice were noted in the brains of all infected mice. Histopathological analysis of the liver was also done from 24 to 72 h p.i. to confirm that viral infection first occurred in the liver following i.p. inoculation in all groups of mice. Multiple foci of inflammatory infiltrations and hepatocyte necrosis were noted as soon as 24 h p.i. and extended until 72 h p.i. in the livers of MHV3-infected mice, while only a few localized foci of necrotic cells were present in the livers of MHV-A59- or 51.6-MHV3-infected mice (results not shown).

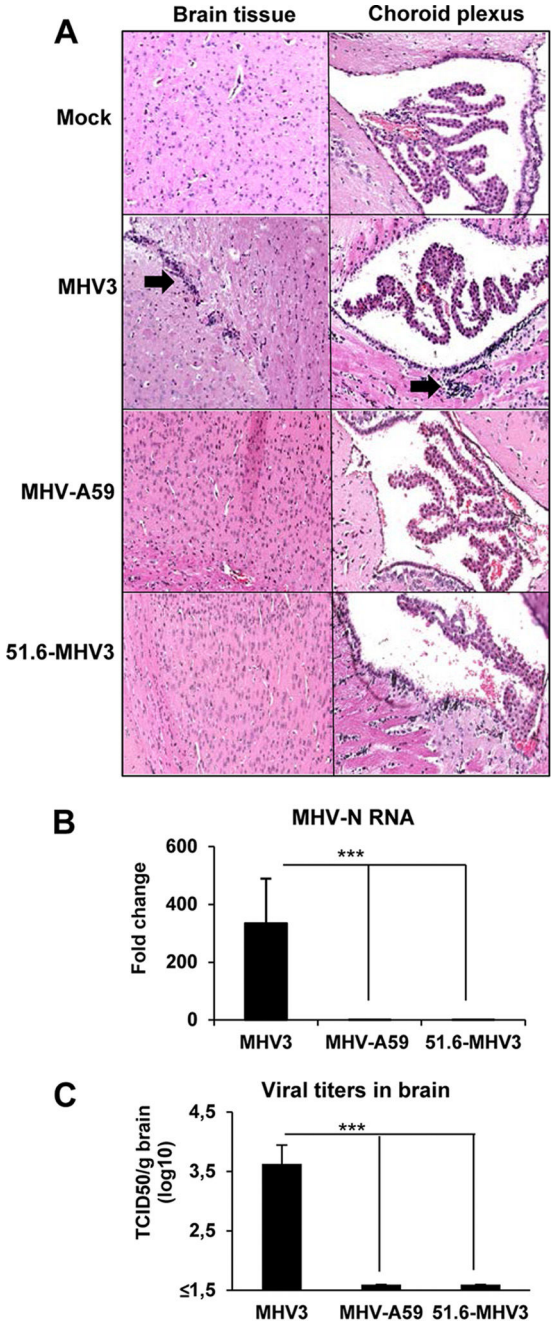

FIG 1 Brain invasion by hematogenously spread MHVs correlates with virulence. (A) Groups of six or seven mice were i.p. mock infected (PBS) or infected with 1,000 $TCID_{50}$ (50% tissue culture infective doses) of MHV3, MHV-A59, and 51.6-MHV3 for 72 h, and harvested brains were subjected to hematoxylin-eosin-safranin staining for histopathological analyses. (B) Viral detection of MHV3, MHV-A59, and 51.6-MHV3 at 72 h p.i. in brain samples of infected mice determined by qRT-PCR analysis of the viral nucleoprotein (N) expression and viral titration ($TCID_{50}$). The viral detection threshold is 1.6 $TCID_{50}$/ml. Values are means plus standard errors of means (error bars). Values that are significantly different ($P < 0.001$) are indicated (***).

Trafficking of virus to the brain was assessed by detection of MHV nucleoprotein (N) RNAs and titration of infectious particles. Viral RNAs and virus titers were detected only in the brains of highly hepatotropic MHV3-infected mice, while no evidence of replication of MHV-A59 and 51.6-MHV3 was noted (Fig. 1B and C). Viral replication level in the brain after 72 h p.i., was, however, too low to permit significant immunolabeling of virally infected cells. Similarly, infectious viruses were titrated at 72 h p.i. in the livers of all groups of mice and demonstrated that MHV3 replicated higher (6.3 ± 0.1 $\log_{10}$ $TCID_{50}$/g liver) than MHV-A59 (3.9 ± 0.16 $\log_{10}$ $TCID_{50}$/g liver) and 51.6-MHV3 (3.6 ± 0.17 $\log_{10}$ $TCID_{50}$/g liver). These results suggest that only the highly hepatotropic MHV3 may have the ability to invade the brain by hematogenous spread and to cross the BBB.

Breakdown of the BBB and alteration of tight junctions occur only in the brains of highly hepatotropic MHV3-infected mice. To further investigate whether MHV3 but not 51.6-MHV3 or MHV-A59 viral replication in the brain following liver infection was due to a breakdown of the BBB, assessment of BBB permeability was performed in mice infected for 72 h with each virus and injected i.p. with 10% NaF dye 1 h prior to euthanasia. The leakage of NaF from the peripheral circulation into the brain is allowed only when the BBB is compromised (30). As shown in Fig. 2A, NaF levels increased in the brains of MHV3-infected mice, indicating a breakdown of the BBB ($P \leq 0.05$). No significant difference in NaF uptake was observed in mice infected with MHV-A59 and 51.6-MHV3.

Since the integrity of the tight junctions is crucial for maintaining the function of the BBB, we asked whether breakdown of the BBB following MHV3 infection resulted from decrease in tight-junction proteins. To assess this, mRNA expression of tight-junction proteins (claudin-5, VE-cadherin, occludin, and ZO-1) was evaluated in the brains of infected mice at 72 h p.i. by qRT-PCR. Compared to brains from mock-infected mice, the level of expression of occludin mRNA was significantly reduced by about 50% in the brains of MHV3-infected mice, but not MHV-A59- or 51.6-MHV3-infected mice ($P \leq 0.01$) (Fig. 2B). The levels of expression of ZO-1 and VE-cadherin mRNA were also impaired in the brains of MHV3-infected mice and to a lesser extent in MHV-A59-infected mice ($P \leq 0.05$ to 0.01), but not in 51.6-MHV3-infected mice (Fig. 2C and D). No significant change in claudin-5 expression was evidenced in mice infected with either virus (Fig. 2E).

To confirm that reduction in tight-junction mRNA expression in the brain was in accordance with a concomitant decrease in protein expression, immunohistochemistry (IHC) stainings using specific antibodies to each protein were conducted on brain tissue. VE-cadherin, occludin, and ZO-1 staining intensities were lower in brain microvessels from MHV3-infected mice than in brain microvessels from mock-infected mice, as shown by the black arrows (Fig. 2F). Lower reduced expression of VE-cadherin and ZO-1 was also detected in the brains of MHV-A59-infected mice, while no change in tight-junction protein expression was induced by 51.6-MHV3 infection.

BMECs (bEnd.3 cell line) are more permissive to MHV3 replication than to 51.6-MHV3 and MHV-A59 replication. Decrease in tight-junction protein expression may result from direct permissivity of BMECs to viral replication and subsequent virus-induced cell damage (31). To determine whether specific MHV3-induced breakdown of the BBB and alteration of tight-junction expression resulted from a differential permissivity of BMECs to MHV infections, *in vitro* infections with MHV3, 51.6-MHV3, and MHV-A59 at an MOI of 0.1 were conducted on a BMEC cell line (bEnd.3 cells) known to exhibit properties similar to those of pri-

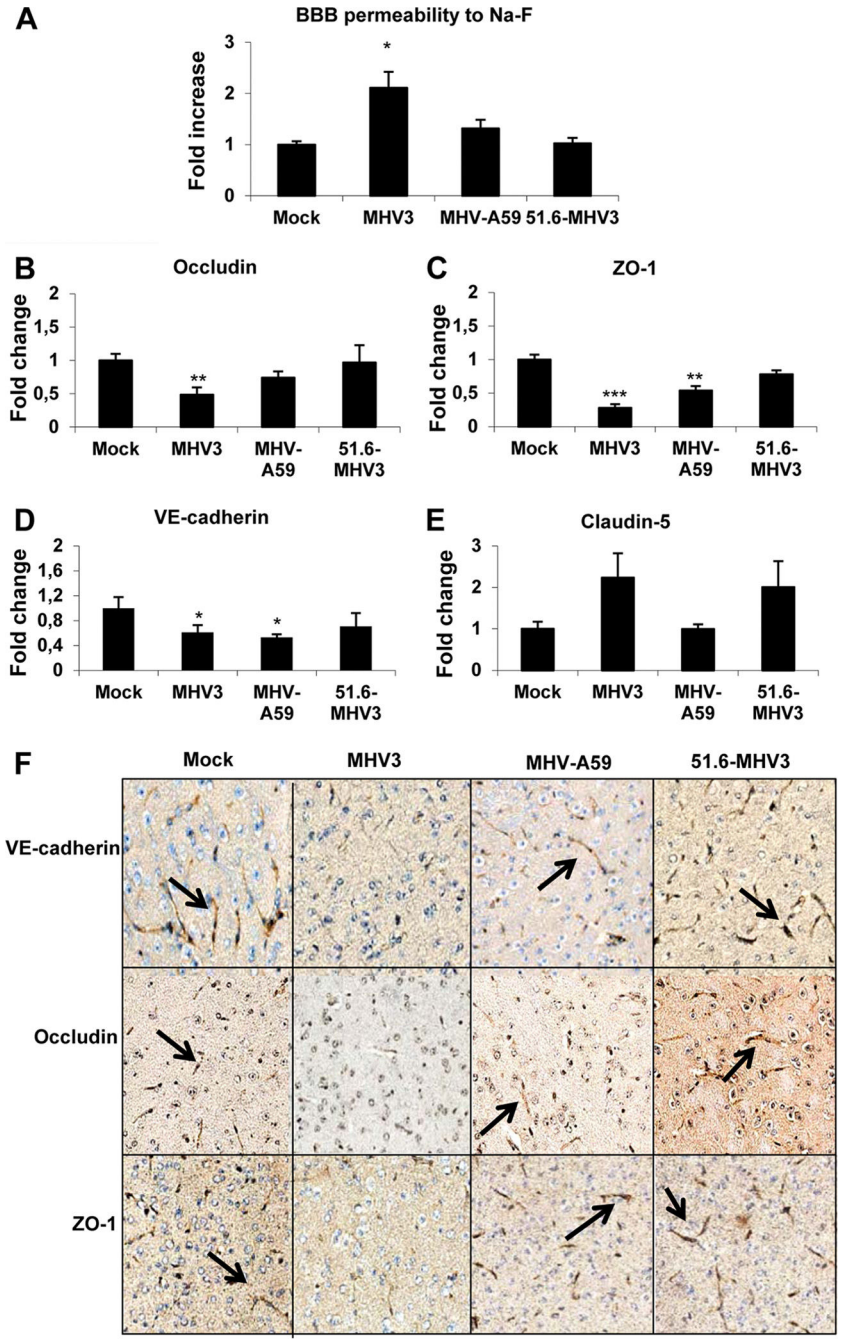

FIG 2 MHV3, but not MHV-A59 and 51.6-MHV3, induces BBB breakdown. Groups of six or seven mice were i.p. mock infected (PBS) or infected with 1,000 $TCID_{50}$ of MHV3, MHV-A59, and 51.6-MHV3 for 72 h. (A) Determination of BBB permeability assessed by sodium fluorescein (NaF) uptake 1 h prior to euthanasia. (B to E) mRNA expression of occludin (B), ZO-1 (C), VE-cadherin (D), and claudin-5 (E) was evaluated in brain samples by qRT-PCR. Values represent fold change in gene expression relative to mock-infected mice after normalization with HPRT expression. All samples were run in duplicate. Values that are significantly different from the value for mock-infected mice are indicated by asterisks as follows: *, $P < 0.05$; **, $P < 0.01$; ***, $P < 0.001$. (F) Immunohistochemistry stainings of VE-cadherin, occludin, and ZO-1 on brain sections of MHV3-, MHV-A59- and 51.6-MHV3-infected mice.

mary BMECs (32, 33). The kinetics of viral replication showed that production of infectious MHV3 increased from day 2 to day 3 p.i. and then stabilized up to day 8 p.i. (Fig. 3A). Viral titers of MHV-A59, unlike MHV3, steadily decreased over time after a rapid increase in the first 3 days ($P \leq 0.01$). As expected, the 51.6-MHV3 variant, expressing low tropism for liver endothelial cells (17), showed a delayed replication in bEnd.3 cells, as evidenced by the absence of infectious virus production until day 3 p.i., followed by a lower viral replication level ($P \leq 0.01$). Occurrence of few foci of cytopathic effects, characterized by rounded cells instead of typical "cobblestone" morphology, were noted in MHV3- and MHV-A59-infected cell cultures, but no typical MHV-induced giant syncytial cells or cell lysis was observed (not shown).

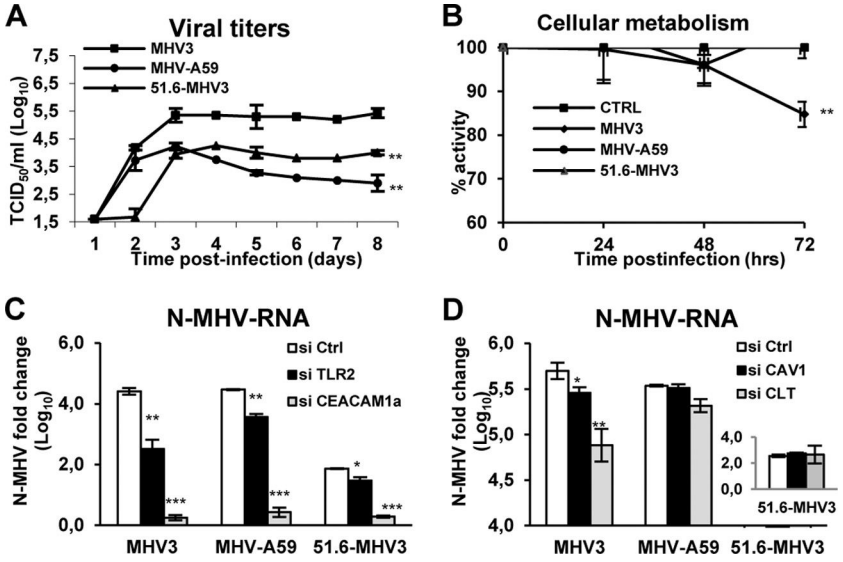

FIG 3 MHV3 exhibits higher tropism for BMECs than MHV-A59 and 51.6-MHV3 do. Mouse bEnd.3 immortalized brain microvascular endothelial cells (BMECs) were infected with MHV3, MHV-A59, or 51.6-MHV3 at an MOI of 0.1. (A) Kinetics of MHV infections up to 8 days p.i. (B) Metabolic activity of infected BMECs as determined by MTS-PMS colorimetric assay from 24 h to 72 h p.i. (C) Roles of CEACAM1a and TLR2 in MHV entry into BMECs. (D) Roles of caveolin-1 (CAV-1) and clathrin (CLT) in MHV endocytosis by BMECs. bEnd.3 cells were treated with specific siRNA to each molecule prior to infection for 24 h, and MHV nucleoprotein (N) mRNA expression was determined by qRT-PCR. All experiments were conducted in triplicate. Results are representative of two or three independent experiments. Values are means ± standard errors of means (error bars). Values that are significantly different are indicated by asterisks as follows: *, $P < 0.05$; **, $P < 0.01$; ***, $P < 0.001$. CTRL and Ctrl, control (uninfected cells).

In order to confirm low or no major changes in cellular metabolism in the first 72 h of infection in MHV3-, MHV-A59-, or 51.6-MHV3-infected BMECs, the metabolic activity of infected bEnd.3 cells was evaluated using the 3-(4,5-dimethylthiazol-2-yl)-5-(3-carboxymethoxyphenyl)-2-(4-sulfophenyl)-2H-tetrazolium inner salt) (MTS)-phenazine methosulfate (PMS) colorimetric assay from 24 h to 72 h p.i. and compared to uninfected control cells. The percentage of optical density (OD), compared with control cells, slowly decreased (about 15%) in the first 72 h p.i. only in MHV3-infected bEnd.3 cells ($P \leq 0.01$) (Fig. 3B). In addition, the loss of cell activity did not increase when cells were infected with a higher MOI (MOIs of 1 and 5) (results not shown).

Higher permissivity of BMECs to MHV3 depends on CEACAM1a and TLR2 ligation and on both clathrin- and caveolin-dependent endocytosis for entry, in contrast to 51.6-MHV3 and MHV-A59. It was previously shown that the protective role of the BBB against brain invasion by blood-borne MHV-A59 was related to a specific blockade of viral entry in BMECs (22). Fixation and entry of MHVs in target cells generally depend on fixation of viral S protein to the common MHV receptor CEACAM1a and further endocytosis or fusion with the host cell (23). However, we have also previously demonstrated that S protein from MHV3 can ligate to TLR2 on the macrophage cell surface (34). To provide insight into how MHV3 exhibits differential viral fixation and/or entry into BMECs compared to MHV-A59 and 51.6-MHV3, the levels of MHV nucleoprotein (N) RNA, as an indicator of viral entry and/or subsequent replication, were evaluated in bEnd.3 cells following abrogation of CEACAM1a or TLR2 expression by specific siRNAs. As shown in Fig. 3C, abrogation of the CEACAM1a expression resulted in a substantial decrease of MHV N RNA expression in BMECs infected with all viruses ($P \leq 0.001$). Knockdown of TLR2 expression, however, provoked a higher decrease of viral replication in MHV3-infected cells ($P \leq 0.01$) than in MHV-A59- and 51.6-MHV3-infected cells ($P \leq 0.01$ and $P \leq 0.05$, respectively), suggesting a more important role for TLR2 in the fixation or entry of MHV3 in BMECs.

It has already been demonstrated that restriction of the BBB to weakly hepatotropic MHV-A59 virus entry was abrogated by SDS detergent treatment (22), suggesting that restriction of MHV-A59 entry in BMECs occurred at the endocytosis step (35). It is thus proposed that MHV3, in contrast to MHV-A59, takes advantage of caveolin- and/or clathrin-dependent endocytic pathways to infect BMECs. To address this, bEnd.3 cells were treated with siRNAs for clathrin or caveolin-1 prior to infection by all MHV strains. As shown in Fig. 3D, MHV N RNA levels decreased in MHV3-infected cells when clathrin or caveolin-1 expression was abrogated ($P \leq 0.05$ to 0.01), while MHV N RNA levels of MHV-A59 were altered only in clathrin-deficient, infected cells ($P \leq 0.05$), suggesting that MHV3, in contrast to MHV-A59, may use both endocytic pathways for viral entry into BMECs. No significant effect was observed in 51.6-MHV3-infected cells, due to no or low viral RNA level.

MHV3, but not MHV-A59 and 51.6-MHV3, enhances *in vitro* permeability of BMECs, leading to viral transendothelial migration. We further investigated whether MHV3 infection might affect *in vitro* the barrier functions of BMECs, such as observed *in vivo* above. To address this, an *in vitro* model of BBB was constructed using bEnd.3 cell monolayers growing on Transwell inserts as previously described (32, 33). First, cells were infected with MHV strains for 24 to 72 h, and transendothelial electrical resistance (TEER), reflecting BBB integrity, was monitored. TEER decreased at 48 and 72 h p.i. in MHV3-infected BMECs ($P \leq 0.05$ to 0.01), while it was weakly affected at 72 h p.i. only in MHV-A59-infected cells ($P \leq 0.05$) (Fig. 4A). The 51.6-MHV3 infection did not alter the TEER.

Thereafter, to determine whether such alteration of TEER in

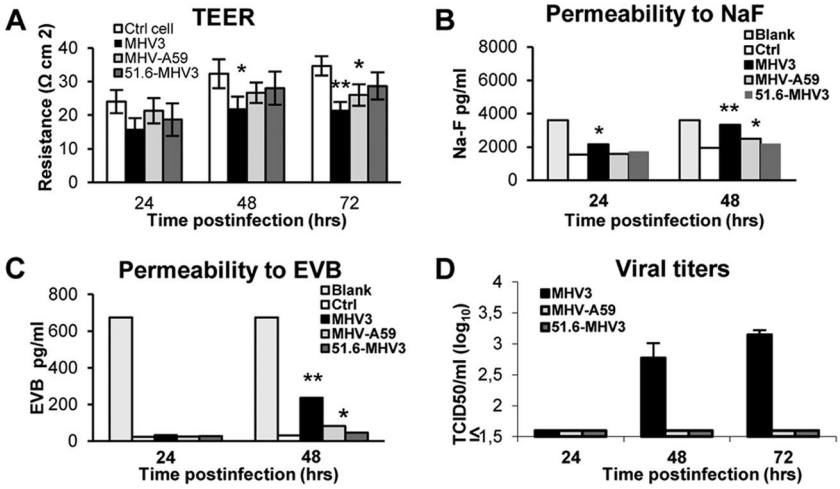

FIG 4 MHV3, but not MHV-A59 and 51.6-MHV3, alters *in vitro* BMEC barrier integrity. An *in vitro* model of BBB was constructed using bEnd.3 cell monolayers grown on Transwell inserts, and cells were infected with MHV3, MHV-A59, or 51.6-MHV3 at an MOI of 0.1. (A) Transendothelial electrical resistance (TEER), reflecting barrier integrity, was monitored from 24 to 72 h. (B and C) Evaluation of the paracellular permeability of bEnd.3 monolayers to NaF (B) or Evans blue (C) dye at 24 and 48 h p.i. Blank corresponds to maximal permeability (insert without cells). (D) Determination of viral transmigration across the bEnd.3 monolayer. Viral titers were recorded in the basolateral chamber from 24 to 72 h p.i. The Viral detection threshold is 1.6 $TCID_{50}$. All experiments were conducted in triplicate. Results are representative of two independent experiments. Values that are significantly different are indicated by asterisks as follows: *, $P < 0.05$; **, $P < 0.01$.

MHV3-infected bEnd3 cells correlated with enhanced paracellular permeability, extravasation of the fluorescent NaF dye through infected bEnd.3 cell monolayers was evaluated in the basolateral chamber. NaF uptake was significantly increased in MHV3-infected monolayers as soon as 24 h p.i. and extended to 48 h p.i., indicating considerable effects on BBB paracellular permeability ($P \leq 0.05$ to 0.01) (Fig. 4B). MHV-A59 infection, however, induced a slight increase of NaF uptake at 48 h p.i. only ($P \leq 0.05$). To further characterize the extent of damage induced by MHV3 infection on BMEC permeability, extravasation of the high-molecular-weight Evans blue (EVB) dye was assessed. Albeit to a lesser extent than NaF, a higher uptake of EVB was found in MHV3-infected bEnd.3 monolayers ($P \leq 0.01$) than in MHV-A59-infected bEnd.3 monolayers ($P \leq 0.05$) (Fig. 4C). No effect on the permeability to either dye was noted in 51.6-MHV3-infected cells. Finally, we postulated that MHV3-induced enhancement of permeability would allow the virus to transmigrate across the bEnd.3 monolayer, so we assessed infectious virus titers in the basolateral chamber. As shown in Fig. 4D, MHV3 viral titers (more than 1.6 $\log_{10}$ units), but not MHV-A59 or 51.6-MHV3 viral titers, were detected at 48 and 72 h p.i. in the basolateral chamber, indicating that only MHV3 exhibited the ability to cross the *in vitro* BMEC barrier.

Breakdown of the *in vitro* BMEC barrier by MHV3 results from decreased expression of occludin, VE-cadherin, and ZO-1 tight-junction proteins. To further determine whether MHV3-induced impairment of barrier function of BMECs was associated with alteration of tight junctions in BMECs, such as observed above in the brains of infected mice, the levels of expression of claudin-5, ZO-1, VE-cadherin, and occludin mRNA were evaluated in infected bEnd.3 cells by qRT-PCR at 48 h p.i. Significant reduction of occludin, VE-cadherin, and ZO-1 mRNA expression occurred in MHV3-infected BMECs only ($P \leq 0.05$) (Fig. 5A, B, and C). Claudin-5 mRNA expression in BMECs, however, was not affected by MHV3 or other virus strains (Fig. 5D).

To confirm that such reduction in mRNA expression of tight junctions was consistent with a reduction in protein expression, immunofluorescence staining was performed on infected cells. In comparison to uninfected cells (control), the intensity of surface staining of VE-cadherin and ZO-1 as well as cytoplasmic and nuclear staining of occludin decreased in MHV3-infected BMECs, while no apparent difference was noted in either MHV-A59- or 51.6-MHV3-infected cells (Fig. 5E).

MHV3-induced breakdown of the *in vitro* BMEC barrier does not depend on inflammatory factors. BBB disruption during viral infection may be indirectly provoked by virus-induced inflammatory mediators, such as the cytokines TNF-α and IL-6 or chemokines CCL2 and CXCL10 (1, 5–8). Accordingly, we hypothesized that MHV3 infection, but not MHV-A59 and 51.6-MHV3 infections, may increase the production of autocrine inflammatory factors by BMECs that might subsequently compromise BBB integrity. To address this, the levels of TNF-α, IL-6, CCL2, and CXCL10 were evaluated in MHV-infected bEnd.3 cells by qRT-PCR and ELISAs at 24 h p.i. As shown in Fig. 6A and B, mRNA levels of TNF-α did not increase in MHV3-infected cells, in contrast to 51.6-MHV3- and MHV-A59-infected cells ($P \leq 0.05$), although protein expression was not detected by ELISA. Transcription and production of IL-6, however, increased in 51.6-MHV3- and MHV-A59-infected cells ($P \leq 0.05$ to 0.001) (Fig. 6C and D), but not MHV3-infected cells. The production of CCL2 increased only in 51.6-MHV3-infected cells ($P \leq 0.01$ to 0.001) (Fig. 6E and F), while CXCL10 levels were not induced in any MHV-infected cells (Fig. 6G and H). Taken together, these results suggest that barrier breakdown by MHV3 infection does not correlate with induction of inflammatory factors, which are instead produced by 51.6-MHV3- and MHV-A59-infected cells.

MHV3-induced breakdown of *in vitro* BMEC barrier is related to impaired production of IFN-β by infected cells. It was demonstrated that IFN-β promotes BBB integrity and prevents virus-induced barrier breakdown (36, 37). Accordingly, we hy-

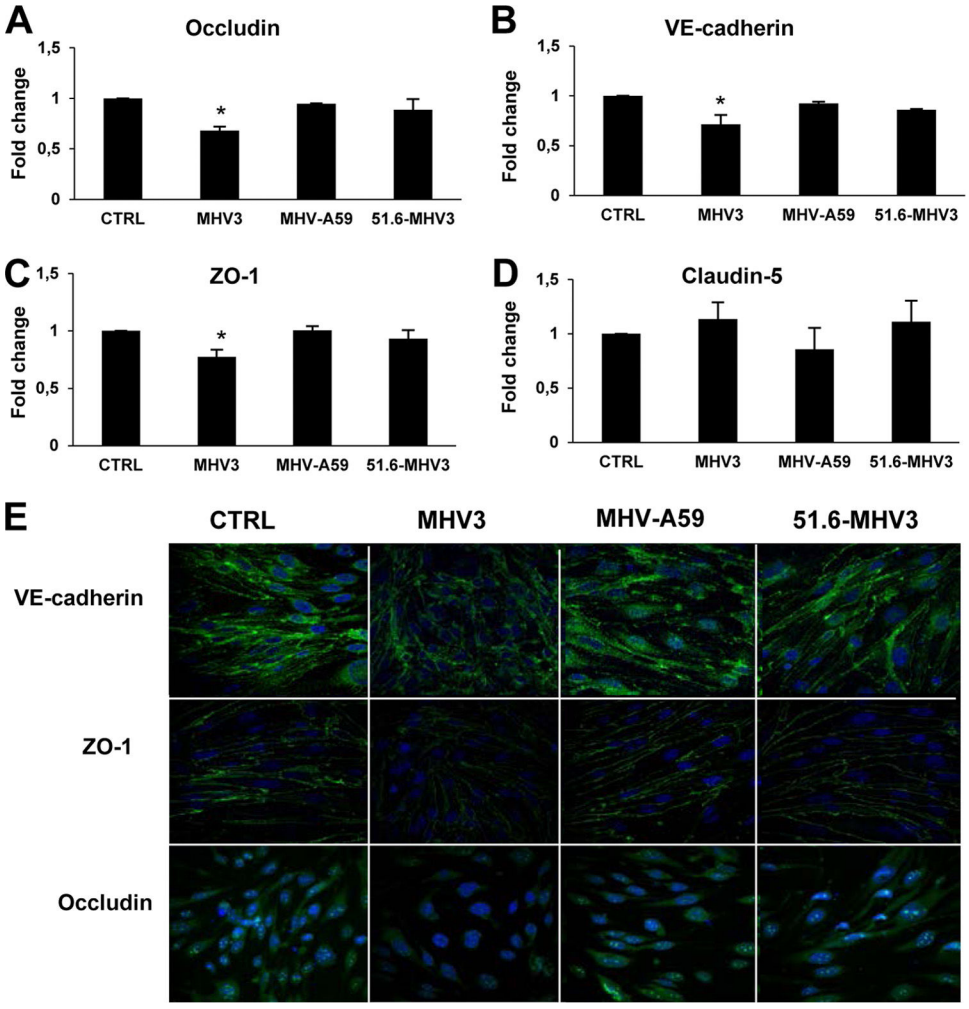

FIG 5 MHV3, but not MHV-A59 and 51.6-MHV3, alters tight-junction expression on BMECs. (A to D) bEnd.3 cells were infected for 48 h with MHV3, MHV-A59, and 51.6-MHV3 at an MOI of 0.1, and the levels of expression of occludin (A), VE-cadherin (B), ZO-1 (C), and claudin-5 (D) mRNA were evaluated by qRT-PCR. Values represent fold change in gene expression relative to uninfected cells (control [CTRL]) after normalization with HPRT expression. All samples were run in duplicate. All experiments were conducted in triplicate. Results are representative of two independent experiments. Values that are significantly different ($P < 0.05$) are indicated (*). (E) Immunofluorescence stainings of the tight-junction (green) VE-cadherin, occludin, and ZO-1 and the nucleus (blue) in uninfected (CTRL) and infected bEnd.3 cells. Images presented are from one representative experiment out of three independent experiments.

pothesized that MHV-A59 or 51.6-MHV3, but not MHV3, induced barrier protective IFN-β production by BMECs. As expected, higher levels of mRNA and secreted IFN-β were detected in 51.6-MHV3- and MHV-A59-infected cells ($P \leq 0.05$ to 0.001) than in MHV3-infected cells ($P \leq 0.05$) (Fig. 7A and B).

To confirm that barrier disruption during MHV3 infection results from the absence of IFN-β production, we evaluated the barrier properties of bEnd.3 cell monolayers upon MHV infections in the presence of IFN-β (100 pg/ml) or anti-IFN-β antibodies (1 μg/ml) at 48 h p.i. As observed in Fig. 7C, addition of IFN-β increased the TEER both in control (uninfected) and MHV-infected cultures, which is in concordance with its barrier enhancing properties ($P \leq 0.05$ to 0.01). TEER decreased only in MHV3-infected cells but was completely restored by IFN-β treatment ($P \leq 0.01$) (Fig. 7C). However, addition of anti-IFN-β antibodies did not decrease TEER in spite of a nonsignificant decrease in 51.6-MHV3-infected cells. Moreover, previously observed enhancement of paracellular permeability to NaF and EVB in MHV3-infected cells and to a lesser extent in MHV-A59-infected cells at 72 h p.i. was abolished following the addition of IFN-β ($P \leq 0.01$ and $P \leq 0.05$, respectively) (Fig. 7D and E), while anti-IFN-β treatment increased paracellular permeability in weakly hepatotropic MHV-A59- and 51.6-MHV3-infected BMECs compared with untreated infected cells ($P \leq 0.01$ and $P \leq 0.05$, respectively).

In order to confirm that the rescued barrier properties of infected bEnd.3 cells following IFN-β treatment result from preservation of tight-junction protein expression, the levels of expression of occludin, ZO-1, and VE-cadherin mRNA were analyzed by qRT-PCR. As shown in Fig. 7F to H, the addition of IFN-β to MHV3-infected cells abolished the decreases in expression of occludin, ZO-1, and VE-cadherin genes ($P \leq 0.05$ to 0.01) and blocked MHV3 trafficking across the bEnd.3 monolayer, as no infectious viruses were detected in the basolateral chamber (not shown).

On the other hand, neutralization of IFN-β potentially pro-

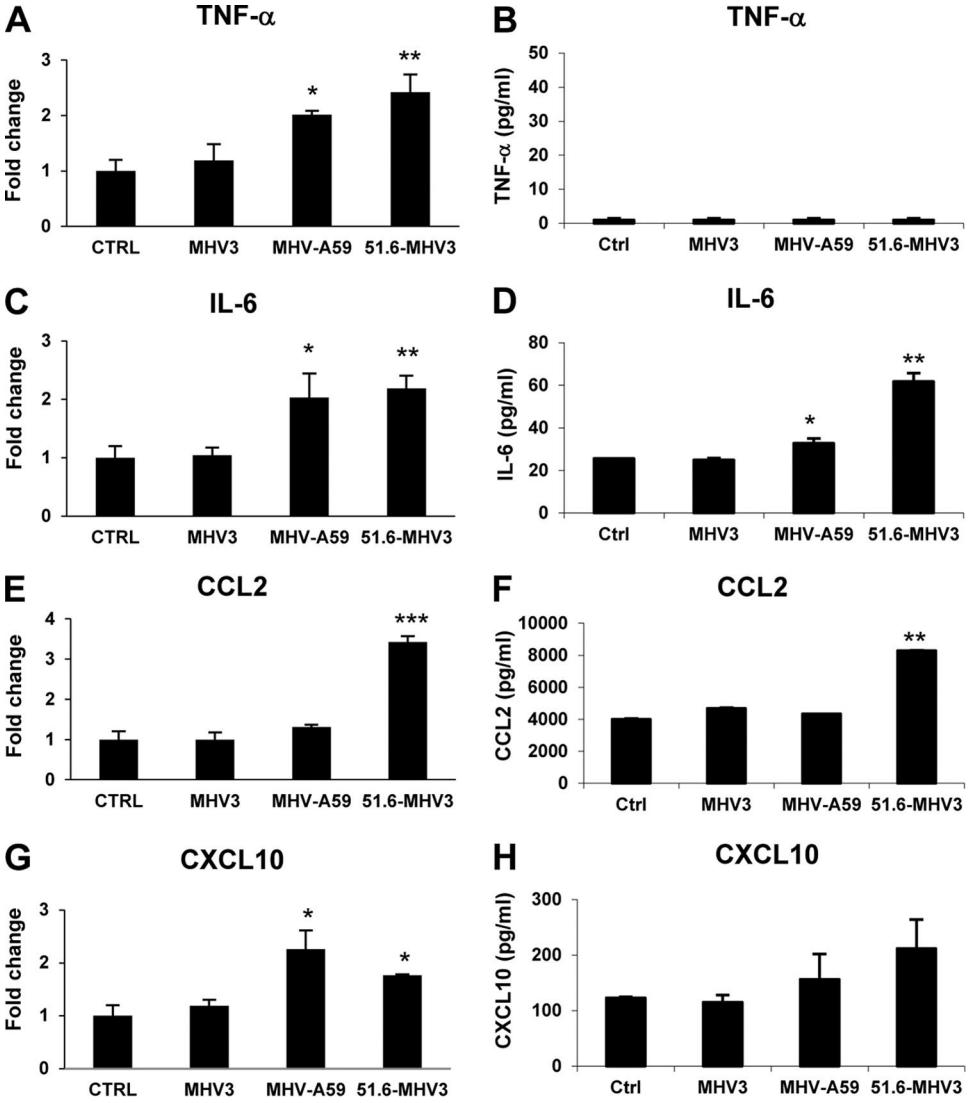

FIG 6 MHV3-induced breakdown of BMEC barrier does not depend on inflammatory factors. (A to H) bEnd.3 cells were infected with MHV3, MHV-A59, and 51.6-MHV3 at an MOI of 0.1, and mRNA expression (A, C, E, and G) and protein levels (B, D, F, and H) of TNF-α, IL-6, CCL2, and CXCL10 were evaluated by qRT-PCR and ELISAs, respectively, at 24 h p.i. All samples were run in duplicate. All experiments were conducted in triplicate. Results are representative of two independent experiments. Values that are significantly different are indicated by asterisks as follows: *, $P < 0.05$; **, $P < 0.01$; ***, $P < 0.001$.

duced in MHV3-infected culture did not worsen virus-induced barrier permeability or reduction of tight junctions (Fig. 7D to H), which is in accordance with the low levels of IFN-β produced by MHV3-infected cells. However, as shown in MHV-A59- and 51.6-MHV3-infected cultures, neutralization of IFN-β increased barrier permeability to NaF and EVB ($P \leq 0.05$ to 0.01), correlating with concomitant reduction of TEER ($P \leq 0.05$) (Fig. 7C to E) and decreased expression of occludin and VE-cadherin in 51.6-MHV3-infected cells, but not in MHV-A59-infected cells ($P \leq 0.05$) (Fig. 7F to H).

To verify whether such improvement of barrier integrity by IFN-β might indirectly result from its antiviral rather than its barrier protective properties, virus titers were assessed in both IFN-β-treated and untreated MHV-infected cells. Viral replication of MHV3 was not blocked by IFN-β treatment, since viral titers remained similar in untreated and IFN-β-treated infected cells (4.6 ± 0.3 and 4.3 ± 0.3 $\log_{10}$ $TCID_{50}$/ml, respectively), while MHV-A59 replication was completely abolished in IFN-β-treated cells (from 3.9 ± 0.33 to <1.6 $\log_{10}$ $TCID_{50}$/ml). Moreover, neutralization of IFN-β increased viral titers in MHV-A59- and 51.6-MHV3-infected cells (from 3.9 ± 0.33 to 5 ± 0.04 $\log_{10}$ $TCID_{50}$/ml and from <1.6 to 4 ± 0.1 $\log_{10}$ $TCID_{50}$/ml, respectively). In addition, neutralization of IFN-β allowed transit of MHV-A59, but not 51.6-MHV3, across the cell monolayer as evidenced by titers in the basolateral chamber (3.175 ± 0.25 $\log_{10}$ $TCID_{50}$/ml). These results suggest that the amount of IFN-β produced by BMECs upon infection with MHV-A59 and 51.6-MHV3, but not MHV3, may both control viral replication in these cells and prevent induction of BBB breakdown.

DISCUSSION

In this work, we report for the first time that BBB integrity can be impaired during acute liver infection by highly hepatotropic MHV3, but not by weakly hepatotropic MHV-59 and attenuated

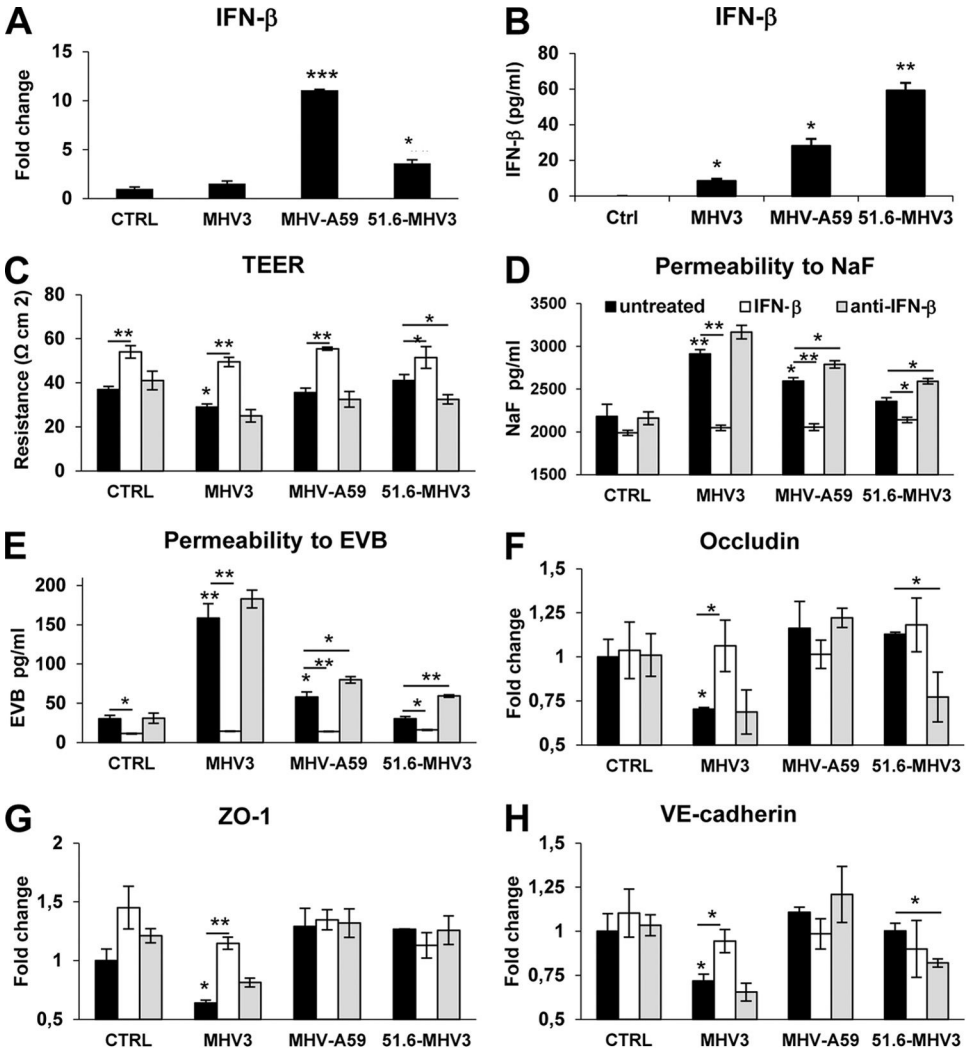

FIG 7 MHV3-induced breakdown of BMEC barrier is related to downregulation of barrier protective IFN-β production by infected BMECs. (A and B) bEnd.3 cells were infected with MHV3, MHV-A59, and 51.6-MHV3 at an MOI of 0.1, and mRNA expression (A) and protein expression (B) of IFN-β was evaluated at 24 h p.i. by qRT-PCR and ELISAs, respectively. All samples were run in duplicate. All experiments were conducted in triplicate. (C to H) Evaluation of barrier integrity of bEnd.3 monolayers infected for 48 h with MHV3, MHV-A59, and 51.6-MHV3 at an MOI of 0.1 in the presence of recombinant IFN-β (100 pg/ml) or anti-IFN-β monoclonal antibodies (1 μg/ml). (C) Recordings of TEER in infected bEnd.3 cultures. (D and E) Evaluation of the paracellular permeability of infected bEnd.3 monolayers to NaF (D) or Evans blue (E) dyes. (F to H) mRNA expression levels of occludin (F), ZO-1 (G), and VE-cadherin (H) in bEnd.3 cells evaluated by qRT-PCR. Values represent fold change in gene expression relative to uninfected cells (control [CTRL]) after normalization with HPRT expression. Results are representative of two independent experiments. Values that are significantly different are indicated by asterisks as follows: *, $P < 0.05$; **, $P < 0.01$; ***, $P < 0.001$.

51.6-MHV3 strains, enabling MHV3 invasion of the CNS. We demonstrated here that MHV strain-specific ability to cross the BBB during acute liver infection correlated with enhanced BBB permeability as evidenced *in vivo* and *in vitro*. Enhanced BBB permeability in MHV3 infection only is associated with higher viral tropism for BMECs and disruption of ZO-1, VE-cadherin, and occludin tight junctions. Such impairment of tight-junction expression was independent of virus-induced barrier-dysregulating TNF-α, IL-6, CCL2, and CXCL10 but rather related to inhibition of barrier protective IFN-β production by BMECs.

Some human respiratory strains of CoVs have shown neuroinvasive properties and were proposed as potential etiological agents for multiple sclerosis (10–12), but their mechanism of neuroinvasion is unclear. The major aim of our work was to investigate the ability of CoVs to enter the CNS through the BBB during the acute phase of infection in peripheral organs. We provide evidence that brain invasion by blood-borne MHVs correlate with strain virulence and peripheral replication in the liver. As previous studies reported the inability of the weakly hepatotropic MHV-A59 strain to induce neurological disease following i.p. infection in contrast to the highly hepatotropic MHV3 (16, 22), we presumed a strain-specific restriction of CNS invasion at the BBB level according to virulence. In agreement, brain examination of i.p. acutely infected mice revealed that viral replication occurred only in the brains of MHV3-infected mice, indicating a specific ability of this strain to enter the CNS by the hematogenous route. Moreover, no replication in the brain of the 51.6-MHV3 variant, having no tropism for endothelial cells (17), suggested that permissivity of cerebral en-

dothelial cells to MHV3 infection played a major role in brain invasion. This strain-specific ability of MHV3 to cross the BBB *in vivo* has been confirmed *in vitro* on a modeled BBB of a bEnd.3 cell monolayer grown on a Transwell system. As expected, only MHV3 transmigrated across the bEnd-3 cell monolayer and reached the basolateral chamber. BBB invasion by MHV3 during acute infection results from enhanced barrier permeability, as evidenced by a higher decrease of TEER and leakage of both the low-molecular-weight NaF and the high-molecular-weight Evans blue dyes in the brains of infected mice and/or BMECs. We would reasonably assume that virus-induced BBB impairment preceded viral brain invasion *in vivo*, since no virus titers were found until 72 h p.i. in the brains, while infectious viruses were detected as soon as 24 h p.i. in the livers of MHV3-infected mice (results not shown). Taken together, these results demonstrate the strain-specific ability of the highly hepatotropic MHV3 to cross the BBB, but not the attenuated 51.6-MHV3 or weakly hepatotropic MHV-A59.

BBB disruption by blood-borne viruses after primary replication in peripheral organs is a common feature of several acute viral infections, but the mechanisms involved have not yet been completely elucidated. Several of these acute viral infections, including murine adenovirus type 1 (MAV-1), human immunodeficiency virus type 1 (HIV-1), West Nile virus (WNV), and lymphocytic choriomeningitis mouse virus (LCMV) infections were reported to trigger increases in BBB permeability through disruption of tight junctions (1, 31, 36). We showed here for the first time that a coronavirus, MHV3, can increase BBB permeability in impairing tight-junction ZO-1, VE-cadherin, and occludin expression in BMECs and the brain. The MHV-A59 or 51.6-MHV3 strain, however, induced no or a slight reduction of ZO-1 and VE-cadherin expression that may reflect their weak tropism for BMECs. No decrease of claudin-5 expression was observed, suggesting that either claudin was not specifically altered by viral infection or that a small decrease in claudin-5 might be masked by the higher number of other claudin family members (38).

Viral replication and/or viral products are rarely directly implicated in BBB disruption (1), but MAV-1 infection itself and the gp120 from HIV were shown to disrupt tight junctions on BMECs (31, 39). Replication of MHV3 in BMECs did not reach high titers and was associated with low cell damage and loss of activity. As expected, ligation to CEACAM1a viral receptor was essential for infection of BMECs by all MHVs, but MHV3 exhibited an additional ability to take advantage of both caveolin- and clathrin-dependent endocytic pathways for entry into BMECs. MHV-A59 entry via clathrin-dependent endocytosis, but not caveolin-dependent endocytosis, has also been previously reported in other cell types (40, 41). TLR2 is located in enriched caveolin-1-associated lipid raft microdomains at the cell surface (42). We have shown that TLR2 engagement by MHV3 on BMECs favored viral replication, which is in agreement with our previous findings that viral S protein of MHV3 can ligate to both CEACAM1a and TLR2 on macrophages (34), in contrast to MHV-A59 (43). Interestingly, as TLR2 activation was shown to increase permeability and downregulate tight-junction protein expression on BMECs (44), TLR2 ligation by viruses or soluble viral coat proteins may represent a new mechanism of BBB disruption by viruses.

Viral fixation and endocytosis pathways also trigger activation of inflammatory cytokines, chemokines, and type 1 interferon according to TLR and/or helicase-dependent downstream signaling pathways (5, 34, 36). Loss of tight junctions in several viral infections can indirectly result from virus-induced barrier-dysregulating cytokines or chemokines, such as IL-6, TNF-α, CCL2, or CXCL10 by BMECs themselves or other CNS cell types (1, 5–8). It was previously shown that MHV3 fixation to TLR2 in macrophages increased TNF-α and IL-6 production (34), but herein, no induction of cytokine and chemokine production by MHV3-infected BMECs was observed. However, cytokine and chemokine production was noted instead in BMECs infected with 51.6-MHV3 and MHV-A59, indicating that BBB breakdown cannot result from virus-induced host inflammatory factors, since BBB was not significantly altered by these two strains. Nevertheless, we cannot rule out the possibility that cytokines and chemokines may be produced *in vivo* by recruited inflammatory cells in the CNS during MHV3 infection and thus contribute to BBB disruption. However, only a few inflammatory cells have been evidenced by hematoxylin-eosin-safranin (HES) staining at 72 h p.i. in the brains of MHV3-infected mice, and the levels of IL-6, TNF-α, CCL2, and CXCL10 were lower in the brains of MHV3-infected mice than in the brains of MHV-A59- and 51.6-MHV3-infected mice (results not shown), thus minimizing the role of inflammatory factors in BBB breakdown.

Postinfection BBB breakdown has already been observed following intracerebral infection of mice with the strictly neurotropic MHV-JHM strain and has been primarily associated with matrix metalloproteinase 9 (MMP-9) produced by infiltrating neutrophils (45). However, in this study, *in vivo* enhancement of BBB permeability was observed only by day 4 p.i. Such discrepancies with our data may result from differences in the route of inoculation and the MHV strain used. It is possible that intracerebral inoculation, which bypasses BBB transit, may have not been conducive to infection of the endothelium by the virus. Herein, we report that MHV3 infection of BMECs can directly alter BBB integrity without assistance of neutrophils and MMPs. We cannot, however, rule out the possibility that later recruited neutrophils may further affect BBB integrity by MMP production once it has been first compromised by viral infection of BMECs. Preliminary data, however, revealed that expression of MMP1a and MMP3 by BMECs was not affected by *in vitro* infection with MHV3, 51.6-MHV3, or MHV-A59 strain.

Unlike inflammatory mediators, IFN-β is known to promote tight-junction formation and stability (37). The differential IFN-β production by BMECs upon infection by MHVs may possibly represent one key factor in MHV strain specificity to induce BBB breakdown. We have shown that 51.6-MHV3 and, to a lesser extent MHV-A59, compared to MHV3, elicited IFN-β production by BMECs, supporting the hypothesis that IFN-β could act as a protective factor in preventing barrier damage and brain invasion by these strains. The lower IFN-β production by cells infected with MHV-A59 may reflect posttranscriptional inhibitory mechanisms of IFN-β production by viral factors (reviewed in reference 46). Induction of IFN-β by WNV has already been reported to prevent its trafficking across a BBB model *in vitro* (36). The specific mechanism of barrier protection by IFN-β is unknown, but Daniels et al. (36) recently reported that IFN-β was able to rescue barrier dysfunction elicited by inflammatory cytokines. Thus, one could speculate that IFN-β production by MHV-A59- and 51.6-MHV3-infected BMECs may counteract cytokine-mediated barrier damage or that low levels of inflammatory cytokines produced by infected BMECs may not be sufficient to induce BBB

breakdown. In accordance, activation of type I IFNs by dengue virus was reported to ameliorate inflammatory cytokine-driven barrier dysfunction in peripheral endothelium (47). The importance of IFN-β downregulation in MHV3-induced BBB breakdown is supported by our results showing that the addition of IFN-β antagonized MHV3-mediated permeability and disruption of tight junctions in BMECs independently of its antiviral properties, as viral replication was not altered. Resistance of MHV3 to antiviral properties of type I IFN *in vitro* has already been observed (48). On the other hand, barrier integrity in MHV-A59- and 51.6-MHV3-infected BMEC monolayers was lost when IFN-β was neutralized with monoclonal antibodies, confirming that prevention of BBB breakdown during MHV-A59 and 51.6-MHV3 infection is due at least partly to IFN-β production. Moreover, in contrast to MHV3, replication of MHV-A59 and 51.6-MHV3 was lowered by IFN-β, suggesting that BMECs can control replication of these viral strains through IFN-β production. This is in agreement with previous findings showing no appearance of productive replication of MHV-A59 in BMECs *in vivo* (22, 25).

Hence, the results of this study show for the first time that hematogenously spread mouse coronaviruses can invade the CNS at the BBB level following peripheral primary replication. Earlier and higher replication of MHV3 in the liver (not shown), combined with higher permissivity of BMECs to MHV3 infection, may potentiate BBB breakdown and further brain invasion. On the other hand, preservation of BBB integrity in MHV-A59 and 51.6-MHV3 infection prevents their trafficking from the periphery to the CNS. This hypothesis is supported by a previous report showing that MHV-A59 spread to the brain is allowed only after intravenous (i.v.) injection of sodium dodecyl sulfate detergent into the mice, which is presumed to alter BBB integrity (22).

In human infections, the mechanism involved in CNS invasion by CoVs following primary infection in the upper respiratory tract is unclear. The CoV 229E strain was previously reported to infect BMECs (49), suggesting that BBB invasion by human CoVs is probable.

The mechanism(s) used by MHV3 to block the production of IFN-β by BMECs is not yet known. The absence of cytokine and chemokine production by MHV3-infected BMECs, in contrast to MHV-A59- and 51.6-MHV3-infected BMECs, suggests that MHV3 may specifically evade detection by TLRs or helicases and/or signaling downstream pathways in BMECs. Accordingly, Mazaleuskaya et al. (50) have recently shown that stimulation of TLR-2, TLR-4, and TLR-7 by specific agonists had no effect on MHV3 replication. Further research is needed to confirm viral evasion mechanisms used by MHV3 in BMECs and their effects on BBB disruption.

ACKNOWLEDGMENTS

We thank Dominic Fillion and Pascale Bellaud for technical assistance with confocal microscopy and histochemistry, respectively, and Antony Karelis for revision of the manuscript.

This work was funded by grants from NSERC, which is funded by the Government of Canada. Christian Bleau was supported by an NSERC fellowship.

REFERENCES

1. **Spindler KR, Hsu TH.** 2012. Viral disruption of the blood-brain barrier. Trends Microbiol **20:**282–290. http://dx.doi.org/10.1016/j.tim.2012.03.009.
2. **Hase T, Dubois DR, Summers PL.** 1990. Comparative study of mouse brains infected with Japanese encephalitis virus by intracerebral or intraperitoneal inoculation. Int J Exp Pathol **71:**857–869.
3. **Kobiler D, Lustig S, Gozes Y, Ben-Nathan D, Akov Y.** 1989. Sodium dodecylsulphate induces a breach in the blood-brain-barrier and enables a West Nile virus variant to penetrate into mouse brain. Brain Res **496:**314–316. http://dx.doi.org/10.1016/0006-8993(89)91079-2.
4. **Lustig S, Danenberg HD, Kafri Y, Kobiler D, Ben-Nathan D.** 1992. Viral neuroinvasion and encephalitis induced by lipopolysaccharide and its mediators. J Exp Med **176:**707–712. http://dx.doi.org/10.1084/jem.176.3.707.
5. **Wang T, Town T, Alexopoulou L, Anderson JF, Fikrig E, Flavell RA.** 2004. Toll-like receptor 3 mediates West Nile virus entry into the brain causing lethal encephalitis. Nat Med **10:**1366–1373. http://dx.doi.org/10.1038/nm1140.
6. **Afonso PV, Ozden S, Prevost MC, Schmitt C, Seilhean D, Weksler B, Couraud PO, Gessain A, Romero IA, Ceccaldi PE.** 2007. Human blood-brain barrier disruption by retroviral-infected lymphocytes: role of myosin light chain kinase in endothelial tight-junction disorganization. J Immunol **179:**2576–2583. http://dx.doi.org/10.4049/jimmunol.179.4.2576.
7. **Chen CJ, Ou YC, Li JR, Chang CY, Pan HC, Lai CY, Liao SL, Raung SL, Chang CJ.** 2014. Infection of pericytes in vitro by Japanese encephalitis virus disrupts the integrity of the endothelial barrier. J Virol **88:**1150–1161. http://dx.doi.org/10.1128/JVI.02738-13.
8. **Chai Q, She R, Huang Y, Fu ZF.** 2015. Expression of neuronal CXCL10 induced by rabies virus infection initiates infiltration of inflammatory cells, production of chemokines and cytokines, and enhancement of blood-brain barrier permeability. J Virol **89:**870–876. http://dx.doi.org/10.1128/JVI.02154-14.
9. **Obermeier B, Daneman R, Ransohoff RM.** 2013. Development, maintenance and disruption of the blood-brain barrier. Nat Med **19:**1584–1596. http://dx.doi.org/10.1038/nm.3407.
10. **Arbour N, Day R, Newcombe J, Talbot PJ.** 2000. Neuroinvasion by human respiratory coronaviruses. J Virol **74:**8913–8921. http://dx.doi.org/10.1128/JVI.74.19.8913-8921.2000.
11. **Murray RS, Brown B, Brian D, Cabirac GF.** 1992. Detection of coronavirus RNA and antigen in multiple sclerosis brain. Ann Neurol **31:**525–533. http://dx.doi.org/10.1002/ana.410310511.
12. **Stewart JN, Mounir S, Talbot PJ.** 1992. Human coronavirus gene expression in the brains of multiple sclerosis patients. Virology **191:**502–505. http://dx.doi.org/10.1016/0042-6822(92)90220-J.
13. **Gu J, Gong E, Zhang B, Zheng J, Gao Z, Zhong Y, Zou W, Zhan J, Wang S, Xie Z, Zhuang H, Wu B, Zhong H, Shao H, Fang W, Gao D, Pei F, Li X, He Z, Xu D, Shi X, Anderson VM, Leong AS.** 2005. Multiple organ infection and the pathogenesis of SARS. J Exp Med **202:**415–424. http://dx.doi.org/10.1084/jem.20050828.
14. **Cowley TJ, Weiss SR.** 2010. Murine coronavirus neuropathogenesis: determinants of virulence. J Neurovirol **16:**427–434. http://dx.doi.org/10.1007/BF03210848.
15. **Virelizier JL, Dayan AD, Allison AC.** 1975. Neuropathological effects of persistent infection of mice by mouse hepatitis virus. Infect Immun **12:**1127–1140.
16. **Tardieu M, Goffinet A, Harmant-van Rijckevorsel G, Lyon G.** 1982. Ependymitis, leukoencephalitis, hydrocephalus, and thrombotic vasculitis following chronic infection by mouse hepatitis virus 3 (MHV3). Acta Neuropathol **58:**168–176. http://dx.doi.org/10.1007/BF00690797.
17. **Martin JP, Chen W, Koehren F, Pereira CA.** 1994. The virulence of mouse hepatitis virus 3, as evidenced by permissivity of cultured hepatic cells toward escaped mutants. Res Virol **145:**297–302. http://dx.doi.org/10.1016/S0923-2516(07)80034-3.
18. **Jacques A, Bleau C, Martin JP, Lamontagne L.** 2008. Intrahepatic endothelial and Kupffer cells involved in immunosuppressive cytokines and natural killer (NK)/NK T cell disorders in viral acute hepatitis. Clin Exp Immunol **152:**298–310. http://dx.doi.org/10.1111/j.1365-2249.2008.03628.x.
19. **Lavi E, Gilden DH, Highkin MK, Weiss SR.** 1986. The organ tropism of mouse hepatitis virus A59 in mice is dependent on dose and route of inoculation. Lab Anim Sci **36:**130–135.
20. **Netland J, Meyerholz DK, Moore S, Cassell M, Perlman S.** 2008. Severe acute respiratory syndrome coronavirus infection causes neuronal death in the absence of encephalitis in mice transgenic for human ACE2. J Virol **82:**7264–7275. http://dx.doi.org/10.1128/JVI.00737-08.
21. **Barnett EM, Perlman S.** 1993. The olfactory nerve and not the trigeminal nerve is the major site of CNS entry for mouse hepatitis virus, strain JHM. Virology **194:**185–191. http://dx.doi.org/10.1006/viro.1993.1248.

22. **Godfraind C, Havaux N, Holmes KV, Coutelier JP.** 1997. Role of virus receptor-bearing endothelial cells of the blood-brain barrier in preventing the spread of mouse hepatitis virus-A59 into the central nervous system. J Neurovirol **3:**428–434. http://dx.doi.org/10.3109/13550289709031188.
23. **Belouzard S, Millet JK, Licitra BN, Whittaker GR.** 2012. Mechanisms of coronavirus cell entry mediated by the viral spike protein. Viruses **4:**1011–1033. http://dx.doi.org/10.3390/v4061011.
24. **Joseph J, Kim R, Siebert K, Lublin FD, Offenbach C, Knobler RL.** 1995. Organ specific endothelial cell heterogeneity influences differential replication and cytopathogenicity of MHV-3 and MHV-4. Adv Exp Med Biol **380:**43–50. http://dx.doi.org/10.1007/978-1-4615-1899-0_6.
25. **Lavi E, Das Sarma J, Weiss SR.** 1999. Cellular reservoirs for coronavirus infection of the brain in beta2-microglobulin knockout mice. Pathobiology **67:**75–83. http://dx.doi.org/10.1159/000028054.
26. **Godfraind C, Coutelier JP.** 1998. Morphological analysis of mouse hepatitis virus A59-induced pathology with regard to viral receptor expression. Histol Histopathol **13:**181–199.
27. **Dupuy JM, Rodrigue D.** 1981. Heterogeneity in evolutive patterns of inbred mice infected with a cloned substrain of mouse hepatitis virus type 3. Intervirology **16:**114–117. http://dx.doi.org/10.1159/000149255.
28. **Phares TW, Kean RB, Mikheeva T, Hooper DC.** 2006. Regional differences in blood-brain barrier permeability changes and inflammation in the apathogenic clearance of virus from the central nervous system. J Immunol **176:**7666–7675. http://dx.doi.org/10.4049/jimmunol.176.12.7666.
29. **Tardieu M, Boespflug O, Barbé T.** 1986. Selective tropism of a neurotropic coronavirus for ependymal cells, neurons, and meningeal cells. J Virol **60:**574–582.
30. **Yen LF, Wei VC, Kuo EY, Lai TW.** 2013. Distinct patterns of cerebral extravasation by Evans blue and sodium fluorescein in rats. PLoS One **8:**e68595. http://dx.doi.org/10.1371/journal.pone.0068595.
31. **Gralinski LE, Ashley SL, Dixon SD, Spindler KR.** 2009. Mouse adenovirus type 1-induced breakdown of the blood-brain barrier. J Virol **83:**9398–9410. http://dx.doi.org/10.1128/JVI.00954-09.
32. **Watanabe T, Dohgu S, Takata F, Nishioku T, Nakashima A, Futagami K, Yamauchi A, Kataoka Y.** 2013. Paracellular barrier and tight junction protein expression in the immortalized brain endothelial cell lines bEND.3, bEND.5 and mouse brain endothelial cell 4. Biol Pharm Bull **36:**492–495. http://dx.doi.org/10.1248/bpb.b12-00915.
33. **Brown RC, Morris AP, O'Neil RG.** 2007. Tight junction protein expression and barrier properties of immortalized mouse brain microvessel endothelial cells. Brain Res **1130:**17–30. http://dx.doi.org/10.1016/j.brainres.2006.10.083.
34. **Jacques A, Bleau C, Turbide C, Beauchemin N, Lamontagne L.** 2009. Macrophage interleukin-6 and tumour necrosis factor-alpha are induced by coronavirus fixation to Toll-like receptor 2/heparan sulphate receptors but not carcinoembryonic cell adhesion antigen 1a. Immunology **128**(Suppl 1)**:**e181–e192. http://dx.doi.org/10.1111/j.1365-2567.2008.02946.x.
35. **Fine M, Llaguno MC, Lariccia V, Lin MJ, Yaradanakul A, Hilgemann DW.** 2011. Massive endocytosis driven by lipidic forces originating in the outer plasmalemmal monolayer: a new approach to membrane recycling and lipid domains. J Gen Physiol **137:**137–154. http://dx.doi.org/10.1085/jgp.201010469.
36. **Daniels BP, Holman DW, Cruz-Orengo L, Jujjavarapu H, Durrant DM, Klein RS.** 2014. Viral pathogen-associated molecular patterns regulate blood-brain barrier integrity via competing innate cytokine signals. mBio **5**(5)**:**e01476-14. http://dx.doi.org/10.1128/mBio.01476-14.
37. **Kraus J, Ling AK, Hamm S, Voigt K, Oschmann P, Engelhardt B.** 2004. Interferon-beta stabilizes barrier characteristics of brain endothelial cells in vitro. Ann Neurol **56:**192–205. http://dx.doi.org/10.1002/ana.20161.
38. **Mineta K, Yamamoto Y, Yamazaki Y, Tanaka H, Tada Y, Saito K, Tamura A, Igarashi M, Endo T, Takeuchi K, Tsukita S.** 2011. Predicted expansion of the claudin multigene family. FEBS Lett **585:**606–612. http://dx.doi.org/10.1016/j.febslet.2011.01.028.
39. **Nakamuta S, Endo H, Higashi Y, Kousaka A, Yamada H, Yano M, Kido H.** 2008. Human immunodeficiency virus type 1 gp120-mediated disruption of tight junction proteins by induction of proteasome-mediated degradation of zonula occludens-1 and -2 in human brain microvascular endothelial cells. J Neurovirol **14:**186–195. http://dx.doi.org/10.1080/13550280801993630.
40. **Eifart P, Ludwig K, Böttcher C, de Haan CA, Rottier PJ, Korte T, Herrmann AJ.** 2007. Role of endocytosis and low pH in murine hepatitis virus strain A59 cell entry. Virology **81:**10758–10768. http://dx.doi.org/10.1128/JVI.00725-07.
41. **Burkard C, Verheije MH, Wicht O, van Kasteren SI, van Kuppeveld FJ, Haagmans BL, Pelkmans L, Rottier PJ, Bosch BJ, de Haan CA.** 2014. Coronavirus cell entry occurs through the endo-/lysosomal pathway in a proteolysis-dependent manner. PLoS Pathog **10:**e1004502. http://dx.doi.org/10.1371/journal.ppat.1004502.
42. **Soong G, Reddy B, Sokol S, Adama R, Prince A.** 2004. TLR2 is mobilized into an apical lipid raft receptor complex to signal infection in airway epithelial cells. J Clin Invest **113:**1482–1489. http://dx.doi.org/10.1172/JCI200420773.
43. **Zhou H, Zhao J, Perlman S.** 2010. Autocrine interferon priming in macrophages but not dendritic cells results in enhanced cytokine and chemokine production after coronavirus infection. mBio **1**(4)**:**e00219-10. http://dx.doi.org/10.1128/mBio.00219-10.
44. **Nagyoszi P, Wilhelm I, Farkas AE, Fazakas C, Dung NT, Hasko J, Krizbbai IA.** 2010. Expression and regulation of Toll-like receptors in cerebral endothelial cells. Neurochem Int **57:**556–564. http://dx.doi.org/10.1016/j.neuint.2010.07.002.
45. **Zhou J, Stohlman SA, Hinton DR, Marten NW.** 2003. Neutrophils promote mononuclear cell infiltration during viral-induced encephalitis. J Immunol **170:**3331–3336. http://dx.doi.org/10.4049/jimmunol.170.6.3331.
46. **Rose KM, Weiss SR.** 2009. Murine coronavirus cell type dependent interaction with the type I interferon response. Viruses **1:**689–712. http://dx.doi.org/10.3390/v1030689.
47. **Patkar C, Giaya K, Libraty DH.** 2013. Dengue virus type 2 modulates endothelial barrier function through CD73. Am J Trop Med Hyg **88:**89–94. http://dx.doi.org/10.4269/ajtmh.2012.12-0474.
48. **Vassão RC, Mello IG, Pereira CA.** 1994. Role of macrophages, interferon gamma and procoagulant activity in the resistance of genetic heterogeneous mouse populations to mouse hepatitis virus infection. Arch Virol **137:**277–288. http://dx.doi.org/10.1007/BF01309475.
49. **Cabirac GF, Murray RS, McLaughlin LB, Skolnick DM, Hogue B, Dorovini-Zis K, Didier PJ.** 1995. In vitro interaction of coronaviruses with primate and human brain microvascular endothelial cells. Adv Exp Med Biol **380:**79–88. http://dx.doi.org/10.1007/978-1-4615-1899-0_11.
50. **Mazaleuskaya L, Veltrop R, Ikpeze N, Martin-Garcia J, Navas-Martin S.** 2012. Protective role of Toll-like receptor 3-induced type I interferon in murine coronavirus infection of macrophages. Viruses **4:**901–923. http://dx.doi.org/10.3390/v4050901.

SUMMARY

Study of hepatolysis induced by immune cells in murine hepatitis models: roles of RIPK1 and PARP1/2

Hepatocyte death is a starting point of liver disease progression by promoting inflammatory and regenerative processes. These events are beneficial at the beginning of the pathology for the restoration of hepatic homeostasis. However when they are unregulated, they lead to the development of fibrosis, cirrhosis or hepatocellular carcinoma. Thus, it is important to study the signaling pathways leading to the hepatocyte death as their inhibition is a potential therapeutic approach to reduce liver diseases progression. Innate and acquired immune cells play key roles in the induction or amplification of hepatolysis, mainly mediated by expression and release of death ligands belonging to the TNF-superfamily including TNF-α, FasL and TRAIL.

Some studies had already suggested the role of RIPK1 and PARP1/2 proteins in the induction of hepatocyte death during hepatitis induced by Concanavalin A (ConA) in mice. Through chemical and genetic approaches, we studied the role of these proteins in the hepatocyte death process during hepatitis.

First, we were interested in the dual role of RIPK1 protein that controls the cell fate by promoting survival or death. By blocking its kinase activity, we confirme its role in the induction of liver injury induced by ConA. However, using specific conditional mice deficient in RIPK1 only in liver parenchymal cells (LPC) (*Ripk1*$^{LPC\text{-}KO}$), we reveale its necessary function in the protection of hepatocyte during hepatitis. These works demonstrate that deletion of RIPK1 sensitizes hepatocytes to TNF-α-induced apoptosis by TRAF2 destabilization. Thus RIPK1 plays a key role in the protection of hepatocytes during hepatitis induced by ConA, lipopolysaccharide (LPS), DNA-CpG, or recombinant IFN-γ and TRAIL co-administration.

In addition, we demonstrate that RIPK1 partially protects from hepatitis and hepatocyte death induced by the activation of Fas.

Finally, we showe that PARP2 deficiency leads to a systemic decrease of the number of the invariant NKT-subpopulation of lymphocytes, including in the liver, which prevente hepatocyte death during ConA hepatitis.

To conclude, this work helps to clarify the roles of RIPK1 and PARP2 during acute hepatitis. The ability of RIPK1 to control hepatocyte death and survival suggests its involvement during chronic hepatitis and opens the door to its investigation into human liver diseases.

RESUME

Etude de l'hépatolyse induite par les cellules immunitaires dans des modèles murins d'hépatites : rôles des protéines RIPK1 et PARP1/2

La mort des hépatocytes est un des éléments initiateurs de la progression des maladies hépatiques par l'induction de processus inflammatoires et de régénération. Ces événements, bénéfiques à court terme pour le rétablissement de l'homéostasie hépatique sont parfois dérégulés et peuvent conduire au développement de la fibrose, de la cirrhose, voire d'un carcinome hépatocellulaire. Ainsi, les voies conduisant à la mort des hépatocytes et leur blocage comme une potentielle approche thérapeutique sont aujourd'hui étudiées. Les cellules de l'immunité innée et acquise sont responsables de l'induction ou de l'amplification de cette hépatolyse, principalement via l'expression et la libération de ligands de mort appartenant à la superfamille du TNF-α, dont TNF-α, FasL et TRAIL.

Des travaux suggèrent le rôle des protéines RIPK1 et PARP1/2 dans l'induction de l'hépatolyse dans l'hépatite induite par la Concanavaline A (ConA) chez la souris. Par l'utilisation de modèles chimiques et génétiques, nous avons étudié l'implication de ces protéines dans le processus de mort des hépatocytes.

Tout d'abord, nous nous sommes intéressés au double rôle de la protéine RIPK1 dans le contrôle de la vie et la mort de l'hépatocyte. En bloquant son activité kinase nous avons confirmé son rôle dans l'induction de l'hépatolyse dans l'hépatite induite par la ConA. Cependant, en utilisant des souris conditionnellement déficientes pour RIPK1 dans les cellules parenchymateuses hépatiques (LPC) ($Ripk1^{LPC\text{-}KO}$) nous avons révélé sa fonction nécessaire à la survie des hépatocytes et au maintien de l'homéostasie hépatique au cours de l'hépatite. Ces travaux démontrent que l'absence de RIPK1 sensibilise les hépatocytes à l'apoptose induite par le TNF-α en déstabilisant la protéine TRAF2. Ainsi RIPK1 joue un rôle clef dans la protection des hépatocytes au cours des hépatites induites par la ConA, le lipopolysaccharide (LPS), les motifs CpG ou induite par une co-administration d'IFN-γ et de TRAIL recombinantes.

De plus, nous avons mis en évidence que RIPK1 protège partiellement de l'hépatolyse et de l'hépatite induite par l'activation de Fas.

Enfin, nous avons montré que l'absence de la protéine PARP2 conduisait à une diminution du nombre de NKT invariants systémiques, dont hépatiques, conduisant à une inhibition de la mort des hépatocytes induite par l'administration de ConA.

Ces travaux ont permis de préciser le rôle de RIPK1 et de PARP2 dans les hépatites aiguës. La capacité de RIPK1 à contrôler la mort et la survie de la cellule suggère son implication au cours des hépatites chroniques et ouvre la porte à son investigation dans les maladies hépatiques humaines.